

Investigation of CHO cell surface glycosylation using lectin probes



Thesis submitted for the degree of
Doctor of Philosophy

by

Jonathan Cawley, B.Sc.

Supervised by

Brendan O'Connor, B.Sc., Ph.D.

Dermot Walls, B.Sc., Ph.D.

School of Biotechnology

Dublin City University

September 2017

Declaration

I hereby certify that this material, which I now submit for assessment on the programme of study leading to the award of Doctor of Philosophy is entirely my own work, and that I have exercised reasonable care to ensure that the work is original, and does not to the best of my knowledge breach any law of copyright, and has not been taken from the work of others save and to the extent that such work has been cited and acknowledged within the text of my work.

Signed: _____

ID No.: 59378201

Date: _____

To my parents Michael & Delia

Acknowledgements

I would like to take this opportunity to thank...

My supervisors, Brendan and Dermot – for giving me the opportunity to complete a PhD and for all the encouragement, input and guidance the past few years.

Donal – for sharing this journey with me from day 1 in S201. You are someone I've always looked up to.

Tríona, Ruth, Colm and Paul – for your helping hand and advice.

Disha and Dave – for all the chats in the office over a cup of tea/coffee.

My parents – for supporting me and giving me every opportunity in life. I would never have completed this without both of you helping me along the way. You have inspired me to be hardworking and to put my all into everything I do. Also, thank you for insisting that I stayed in school until I completed the Leaving Cert.

Paul, Emma and Davey baby – for always being there for me and for listening, or at least pretending to listen, to my 'boring' science talk. Ye are a great bunch, thank you for everything.

Ellen – for all the support, love, food and encouragement the past few years. You are amazing and I would not have been able to finish this without you.

Waters family in Ballynooney – for always making me feel welcome and at home away from home. I really appreciate all your well wishes during my PhD and job search.

Padraig, Niall and Brendan – for helping me unwind and take my mind off all things science related whenever I'm back home.

Fred – for keeping me sane and reducing my stress level.

Phil and Chris – for inspiring and motivating me through the medium of music, you are both greatly missed.

Table of Contents

Declaration	i
Dedication	ii
Acknowledgements	iii
List of Figures	xi
List of Tables	xix
List of Abbreviations, Units and Prefixes	xxiii
Abstract	xxvii
Chapter 1 <i>Introduction</i>	1
1.1 Glycobiology	2
1.2 Glycosylation	2
1.2.1 Eukaryotic glycosylation	7
1.2.1.1 Eukaryotic N-linked glycosylation	8
1.2.1.2 Eukaryotic O-linked glycosylation	14
1.2.1.3 Other types of linked glycans	18
1.2.2 Prokaryotic glycosylation	19
1.3 Biological roles of glycans	21
1.3.1 Protein structure and folding regulation	21
1.3.2 Cell adhesion and cell signalling	23
1.3.3 Immune functions of glycans	23
1.3.4 Cell surface glycosylation	24
1.3.5 Glycosylation and disease	26
1.4 Therapeutic glycoproteins	28
1.5 Glycan analysis	30
1.5.1 Glycan analysis using antibodies	32
1.5.2 Glycan analysis using CE, MS and HPLC	33
1.5.3 Glycan analysis using lectins	35
1.5.3.1 Enzyme-linked lectin assay (ELLA)	36
1.5.3.2 Lectin microarray	37

1.5.3.3	Lab in a Trench	39
1.6	Fluorescence microscopy	40
1.6.1	Fluorescence microscopy for glycan analysis	42
1.7	Flow cytometry	43
1.7.1	Flow cytometry for glycan analysis	47
1.8	Lectins	49
1.8.1	The functions of lectins	52
1.8.2	Recombinant lectins	53
1.8.3	<i>Agrocybe aegerita</i> lectin 2	54
1.8.4	GafD from <i>Escherichia coli</i>	56
1.8.5	PA-IL and PA-IIL lectins from <i>Pseudomonas aeruginosa</i>	57
1.9	The biopharmaceutical industry	59
1.10	Chinese hamster ovary cells	62
1.10.1	CHO DP-12	64
1.10.2	Immunoglobulin G1	64
1.11	Bioprocess conditions affecting glycosylation	66
1.11.1	Physical conditions	67
1.11.2	Chemical conditions	68
1.12	Aims and objectives of this study	70
Chapter 2 <i>Materials and Methods</i>		74
2.1	Bacterial strains, vectors, constructs and primers	73
2.2	CHO DP-12	79
2.3	Microbiological media	80
2.4	Cell culture growth media	81
2.5	Buffers and solutions	82
2.6	Antibiotics	87
2.7	Storing and culturing of bacteria	88
2.8	Isolation and purification of DNA	88
2.8.1	Isolation of plasmid DNA	88
2.8.2	Isolation of DNA from PCR mixtures and agarose gels	89
2.9	Agarose gel electrophoresis	89

2.10	Transformations	91
2.10.1	Preparation of competent cells - The rubidium chloride method	91
2.10.2	Transformation of competent cells	91
2.11	Enzymatic reactions	92
2.12	Site-directed mutagenesis	93
2.13	DNA sequencing	95
2.14	In silico analysis of DNA and protein sequences	95
2.15	Standard expression culture	96
2.16	Preparation of cleared lysate for protein purification	96
2.16.1	Cell lysis by cell disruption	96
2.16.2	Preparation of lysate for IMAC column loading	97
2.17	Purification of recombinant lectins	97
2.17.1	Standard IMAC procedure	98
2.17.2	Stripping and recharging the IMAC resin	98
2.18	Purification of IgG1	98
2.19	Sodium dodecyl sulfate polyacrylamide gel electrophoresis (SDS-PAGE)	100
2.19.1	Preparation of SDS gels	100
2.19.2	Sample preparation and application	101
2.19.3	Visualising SDS-PAGE gels	103
2.20	Screening for protein expression	103
2.21	Western blot analysis	104
2.21.1	Protein transfer to nitrocellulose membrane	104
2.21.2	Staining of proteins immobilised on nitrocellulose membrane	105
2.21.3	Protein probing and visualisation	105
2.22	Concentrating and buffer exchanging recombinant protein	105
2.23	Protein quantification	106
2.23.1	Protein quantification using the BCA assay	107
2.23.2	Protein quantification using 280 nm readings	107
2.24	Biotinylation of recombinant proteins	108
2.25	Enzyme-linked lectin assay	109
2.26	Enzyme-linked immunosorbent assay	112

2.27	Cell culture techniques	114
2.27.1	General consumables	114
2.27.2	Cell culture cabinet and incubators	114
2.27.3	CHO DP-12 cultures	114
2.27.4	Trypan blue cell counts	116
2.27.5	ADAM™ cell counter	117
2.27.6	Cryopreservation of cells	118
2.27.7	Thawing cells	118
2.28	Probing cells with commercial and recombinant lectins	119
2.28.1	Determining lectin cytotoxicity	119
2.28.2	Fluorescent microscopy	122
2.28.3	Flow cytometry	123
2.28.3.1	Flow cytometer sample preparation	123
2.28.3.2	Flow cytometer use and data acquisition	124
2.28.3.3	Flow cytometer data analysis and gating strategy	124
Chapter 3 <i>The expression, characterisation and labelling of non-plant lectins from <i>Agrocybe aegerita</i>, <i>Escherichia coli</i> and <i>Pseudomonas aeruginosa</i></i>		129
3.1	Overview	130
3.2	Cloning and expression of recombinant lectins	130
3.3	<i>Agrocybe aegerita</i> lectin 2	131
3.3.1	The AAL-2 coding sequence and protein sequence	131
3.3.2	Expression and IMAC purification of AAL-2	132
3.3.3	Cloning and expression of AAL-2 variants to enhance IMAC purification	134
3.3.4	Optimising the IMAC purification of AAL-2	141
3.3.5	AAL-2 quantification, biotinylation and western blot analysis	142
3.3.6	Enzyme-linked lectin assay analysis of AAL-2	144
3.3.7	ELLA analysis of AAL-2, WGA and GSL II with specific and non-specific monosaccharides	147
3.3.8	Mutagenesis of AAL-2	151

3.4	G(F17) fimbrial lectin, GafD1-178, from <i>E. coli</i>	151
3.4.1	The GafD1-178 coding sequence	151
3.4.2	Expression, IMAC purification and biotinylation of GafD1-178	152
3.4.3	ELLA analysis of GafD1-178	155
3.5	PA-IL (LecA) from <i>Pseudomonas aeruginosa</i>	156
3.5.1	LecA coding sequence and protein sequence	156
3.5.2	Expression, IMAC purification and biotinylation of LecA	157
3.5.3	LecA cloning strategy to generate EGFP fusion	161
3.5.4	EGFP-LecA expression and purification	162
3.5.5	Optimising the LecA probe for biotinylation and labelling	164
3.5.6	ELLA analysis of LecA5K and RCA I with specific and non-specific monosaccharides	171
3.6	Confirmation of recombinant lectin biotinylation	174
3.7	Discussion	175
Chapter 4 <i>Investigating CHO DP-12 lectin cytotoxicity and cell surface glycosylation using lectins and fluorescent microscopy</i>		179
4.1	Overview	180
4.2	Determining lectin toxicity	180
4.3	CHO DP-12 cell surface glycoanalysis using lectins and fluorescent microscopy	183
4.4	Discussion	193
Chapter 5 <i>Investigating CHO DP-12 cell surface and IgG1 product glycosylation using lectin probes and flow cytometry</i>		198
5.1	Overview	199
5.2	Adapting adherent CHO DP-12 cells to serum-free suspension culture	199
5.3	Determining an appropriate lectin probing concentration	202
5.4	Determining an appropriate cell number to probe	204
5.5	Determining an appropriate temperature for probing cells with lectins	205
5.6	Detaching adherent CHO DP-12 cells from tissue culture flasks	207

5.7	Lectin binding differences between adherent and suspension CHO DP-12 cell surfaces	209
5.8	Comparison of LecA variants binding to the CHO DP-12 cell surface	210
5.9	Assessing the specificity of lectin binding to live CHO DP-12 cells	212
5.10	Effect of spent medium on CHO DP-12 cell surface glycosylation	221
5.11	Effect of reduced L-glutamine on CHO DP-12 cell surface glycosylation	227
5.12	Effect of ammonia on CHO DP-12 cell surface glycosylation	233
5.13	Effect of sodium butyrate on CHO DP-12 cell surface glycosylation	238
5.14	Purification and glycoanalysis of recombinant IgG1 from an untreated CHO DP-12 culture	244
5.15	Purification and glycoanalysis of recombinant IgG1 from CHO DP-12 cultures treated with spent medium, reduced L-glut, NH ₄ Cl or NaBu	248
5.16	Discussion	252
Chapter 6 <i>General Discussion</i>		262
6.1	Discussion	263
References		270
 Appendices		
A	Nucleotide and protein sequences for AAL-2 with an <i>N</i> -terminal His ₆ tag, <i>N</i> -terminal His ₆ tag with linker, <i>C</i> -terminal His ₆ tag and EGFP fusion	A1
B	Mutagenesis of AAL-2	B1
C	IMAC resin saturation	C1
D	Nucleotide and protein sequences for EGFP-LecA fusion, LecA and LecA with additional lysine residues	D1
E	Flow cytometry data for optimising cell preparation for lectin probing	E1
F	Flow cytometry data for CHO DP-12 adherent and suspension culture comparison	F1
G	Flow cytometry data for lectin inhibition checks	G1
H	Flow cytometry data for spent medium treated cells	H1

I	Flow cytometry data for cells treated with L-glut free medium	I1
J	Flow cytometry data for cells treated with 10 mM NH ₄ Cl	J1
K	Flow cytometry data for cells treated with 3 mM NaBu	K1

List of Figures

Chapter 1

Fig. 1.1:	Complexity and diversity of the glycome	4
Fig. 1.2:	Haworth projection of monosaccharide building blocks for animal glycans	5
Fig. 1.3:	Linear and branched glycans at the cell surface	6
Fig. 1.4:	ABO blood group antigens: H(O), A and B	7
Fig. 1.5:	The synthesis and transfer of the Glc ₃ Man ₉ GlcNAc ₂ oligosaccharide to an asparagine residue on a nascent polypeptide	9
Fig. 1.6:	Processing and maturation of an <i>N</i> -glycan through the ER and Golgi	11
Fig. 1.7:	Types of <i>N</i> -glycans	13
Fig. 1.8:	Four of the core structures of mucin type <i>O</i> -glycans	15
Fig. 1.9:	Cell wall of a Gram-negative bacterium	20
Fig. 1.10:	Glycan transfer and glycoprotein processing in the endoplasmic reticulum	22
Fig. 1.11:	Biosynthesis of monosaccharides and human glycosylation disorders	27
Fig. 1.12:	Methods for glycan analysis of therapeutic glycoproteins	31
Fig. 1.13:	MALDI-TOF MS profiles of the <i>N</i> -glycans released from lysed wild type sCHO cells	34
Fig. 1.14:	Schematic of an ELLA	36
Fig. 1.15:	Schematic of a lectin microarray	38
Fig. 1.16:	Lab in a Trench platform	39
Fig. 1.17:	Schematic of fluorescence microscopy	41
Fig. 1.18:	Excitation and emission spectra of common fluorochromes	41
Fig. 1.19:	Fluorescent microscope images of CHO cells probed with MAL II	42
Fig. 1.20:	Light scattering and detection in a flow cytometer	44
Fig. 1.21:	Electrostatic cell sorting	47
Fig. 1.22:	A breakdown of the search results for 'lectin' in the Protein Data Bank archive	51
Fig. 1.23:	Structure of AAL-2	56
Fig. 1.24:	3D view of GafD1-178	57
Fig. 1.25:	Tetramer and monomer structures of PA-IL(LecA) and PA-IIL(LecB)	58

Fig. 1.26: IgG1 structure	64
Fig. 1.27: Modification of IgG <i>N</i> -glycans	66

Chapter 2

Fig. 2.1: The pQE-30 vector (Qiagen)	77
Fig. 2.2: The pQE-60 vector (Qiagen)	78
Fig. 2.3: 1kb DNA ladder (New England Biolabs N3232)	90
Fig. 2.4: Site-directed mutagenesis	94
Fig. 2.5: Protein markers	102
Fig. 2.6: Semi-dry Western blot transfer stack	104
Fig. 2.7: Schematic of an ELLA	110
Fig. 2.8: Schematic of direct and indirect ELISA	112
Fig. 2.9: Orbital shaker for maintaining CHO DP-12 suspension cultures	116
Fig. 2.10: Haemocytometer grid layout	117
Fig. 2.11: Resazurin reduction	120
Fig. 2.12: Flow cytometry data gating strategy	125
Fig. 2.13: Flow cytometry data gating strategy – the importance of removing doublets	126
Fig. 2.14: Sample data for the comparison of AAL and GSL I B4 binding patterns	128

Chapter 3

Fig. 3.1: AAL-2 coding sequence	131
Fig. 3.2: AAL-2 protein sequence	132
Fig. 3.3: IMAC purification of AAL-2 with an <i>N</i> -terminus His ₆ tag	133
Fig. 3.4: IMAC purification of AAL-2 with an <i>N</i> -terminus His ₆ tag with additional wash steps	134
Fig. 3.5: The construction of pAAL-2_NL, a pQE-30 plasmid containing AAL-2 with a 90 nucleotide <i>N</i> -terminus linker	135
Fig. 3.6: The construction of pEGFP_AAL-2, a pQE-30 plasmid containing an EGFP-AAL-2 fusion with a His ₆ tag at the EGFP <i>N</i> -terminus	136
Fig. 3.7: The construction of pAAL-2_CT, a pQE-60 plasmid containing AAL-2 with a <i>C</i> -terminus His ₆ tag	137

Fig. 3.8:	Agarose gel analysis of plasmid constructs containing AAL-2	137
Fig. 3.9:	The purification of AAL-2 with a linker, a C-terminus His ₆ tag and fused to EGFP	138
Fig. 3.10:	Horizontal and vertical views of the putative 3D structures of AAL-2 variants represented in cartoon format	140
Fig. 3.11:	The purification of AAL-2 using two IMAC resins	141
Fig. 3.12:	BCA assay standard curve and sample results	142
Fig. 3.13:	Western blot analysis of IMAC purification fractions and buffer exchanged AAL-2	143
Fig. 3.14:	ELLA analysis of AAL-2 storage conditions	145
Fig. 3.15:	ELLA analysis of AAL-2 and two GlcNAc binding plant lectins, GSL II and WGA	146
Fig. 3.16:	ELLA analysis of AAL-2 with GlcNAc and GalNAc monosaccharides	148
Fig. 3.17:	ELLA analysis of WGA with GlcNAc and GalNAc monosaccharides	149
Fig. 3.18:	ELLA analysis of GSL II with GlcNAc and GalNAc monosaccharides	150
Fig. 3.19:	GafD1-178 coding sequence and translated protein sequence	152
Fig. 3.20:	IMAC purification of GafD1-178 with an N-terminus His ₆ tag	153
Fig. 3.21:	ELLA analysis of GafD1-178 and GSL II with GlcNAc	154
Fig. 3.22:	ELLA analysis of GafD1-178 with GlcNAc and GalNAc monosaccharides	155
Fig. 3.23:	LecA coding sequence and translated protein sequence	157
Fig. 3.24:	IMAC purification of LecA	158
Fig. 3.25:	ELLA analysis of LecA with galactose	159
Fig. 3.26:	Monomer structure of LecA with highlighted lysine residues	160
Fig. 3.27:	The construction of pEGFP_LecA, a pQE-30 plasmid containing an EGFP-LecA fusion with a His ₆ tag at the EGFP N-terminus	161
Fig. 3.28:	Expression check for EGFP-LecA fusion	162
Fig. 3.29:	Plasmid restriction analysis using AccI	163
Fig. 3.30:	IMAC purification of EGFP-LecA	164
Fig. 3.31:	Multiple protein sequence alignment of LecA variants	166
Fig. 3.32:	Expression check and purification of LecA5K	167

Fig. 3.33:	Two horizontal views of the 3D structure of LecA5K represented in cartoon format	168
Fig. 3.34:	SDS-PAGE analysis of purified and biotinylated LecA variants with broad and low range protein markers	169
Fig. 3.35:	ELLA analysis of LecA and biotinylated LecA variants	170
Fig. 3.36:	ELLA analysis of LecA5K with Gal and Glc monosaccharides	172
Fig. 3.37:	ELLA analysis of RCA I with Gal and Glc monosaccharides	173
Fig. 3.38:	SDS-PAGE and western blot analysis of biotinylated recombinant lectins	174

Chapter 4

Fig. 4.1:	Determining optimum seeding concentration	181
Fig. 4.2:	CHO DP-12 cell lectin toxicity	182
Fig. 4.3:	Brightfield image of CHO DP-12 cells	186
Fig. 4.4:	CHO DP-12 cells probed with AAL	186
Fig. 4.5:	CHO DP-12 cells probed with recombinant AAL-2	187
Fig. 4.6:	CHO DP-12 cells probed with Con A	188
Fig. 4.7:	CHO DP-12 cells probed with LCA	188
Fig. 4.8:	CHO DP-12 cells probed with MAL II	189
Fig. 4.9:	CHO DP-12 cells probed with recombinant LecB	189
Fig. 4.10:	CHO DP-12 cells probed with recombinant EGFP-LecA	190
Fig. 4.11:	CHO DP-12 cells probed with recombinant LecA5K	190
Fig. 4.12:	CHO DP-12 cells probed with RCA I	191
Fig. 4.13:	CHO DP-12 cells probed with WGA	191
Fig. 4.14:	CHO DP-12 cells probed with UEA I	192
Fig. 4.15:	CHO DP-12 cells probed with GSL II	192
Fig. 4.16:	CHO DP-12 cells probed with recombinant GafD1-178	193

Chapter 5

Fig. 5.1:	Adapting CHO DP-12 cells from adherent serum-supplemented culture to suspension serum-free culture	201
Fig. 5.2:	Determining an appropriate lectin probing concentration	202
Fig. 5.3:	Dotplots of suspension CHO DP-12 cells probed with lectins	203

Fig. 5.4:	Determining an appropriate cell number per sample	205
Fig. 5.5:	Determining an appropriate cell lectin probing temperature	206
Fig. 5.6:	Comparison of cell detachment methods using AAL-2 and MAL II	208
Fig. 5.7:	FSC-A and SSC-A comparison of adherent and suspension adapted CHO DP-12 cells	210
Fig. 5.8:	Comparison of LecA and LecA variants binding suspension adapted CHO DP-12 cells	211
Fig. 5.9:	AAL-2 inhibition check with competitive/non-competitive monosaccharide gradient	212
Fig. 5.10:	AAL-2 inhibition check with competitive/non-competitive BSA-linked monosaccharide gradient	212
Fig. 5.11:	GafD1-178 inhibition check with competitive/non-competitive monosaccharides	213
Fig. 5.12:	LecA5K inhibition check with competitive/non-competitive monosaccharides	214
Fig. 5.13:	AAL inhibition check with competitive/non-competitive monosaccharides	215
Fig. 5.14:	DSL inhibition check with competitive/non-competitive monosaccharides	215
Fig. 5.15:	ECL inhibition check with competitive/non-competitive monosaccharides	216
Fig. 5.16:	GNL inhibition check with competitive/non-competitive monosaccharides	216
Fig. 5.17:	Jacalin inhibition check with competitive/non-competitive monosaccharides	217
Fig. 5.18:	LCA inhibition check with competitive/non-competitive monosaccharides	217
Fig. 5.19:	LecB inhibition check with competitive/non-competitive monosaccharides	218
Fig. 5.20:	MAL II inhibition check with non-competitive monosaccharide	218
Fig. 5.21:	NPL inhibition check with competitive/non-competitive monosaccharides	219
Fig. 5.22:	RCA I inhibition check with competitive/non-competitive monosaccharides	219
Fig. 5.23:	WGA inhibition check with competitive/non-competitive monosaccharides	220

Fig. 5.24: CHO DP-12 cells probed with AAL-2 following spent medium treatment	223
Fig. 5.25: CHO DP-12 cells probed with AAL-2 after spent medium and fresh medium treatments	223
Fig. 5.26: CHO DP-12 cells probed with LecA5K following spent medium treatment	224
Fig. 5.27: CHO DP-12 cells probed with LecA5K after spent medium and fresh medium treatments	224
Fig. 5.28: CHO DP-12 cells probed with MAL II following spent medium treatment	225
Fig. 5.29: CHO DP-12 cells probed with MAL II after spent medium and fresh medium treatments	225
Fig. 5.30: CHO DP-12 cells probed with PNA following spent medium treatment	226
Fig. 5.31: CHO DP-12 cells probed with PNA after spent medium and fresh medium treatments	226
Fig. 5.32: CHO DP-12 cells probed with LecA5K following L-glutamine free medium treatment	229
Fig. 5.33: CHO DP-12 cells probed with LecA5K following L-glutamine free medium and fresh medium treatments	229
Fig. 5.34: CHO DP-12 cells probed with MAL II following L-glutamine free medium treatment	230
Fig. 5.35: CHO DP-12 cells probed with MAL II following L-glutamine free medium and fresh medium treatments	230
Fig. 5.36: CHO DP-12 cells probed with PNA following L-glutamine free medium treatment	231
Fig. 5.37: CHO DP-12 cells probed with PNA following L-glutamine free medium and fresh medium treatments	231
Fig. 5.38: CHO DP-12 cells probed with RCA I following L-glutamine free medium treatment	232
Fig. 5.39: CHO DP-12 cells probed with RCA I following L-glutamine free medium and fresh medium treatments	232
Fig. 5.40: CHO DP-12 cells probed with AAL-2 following NH ₄ Cl treatment	235
Fig. 5.41: CHO DP-12 cells probed with AAL-2 following NH ₄ Cl and fresh medium treatments	235
Fig. 5.42: CHO DP-12 cells probed with LCA following NH ₄ Cl treatment	236

Fig. 5.43: CHO DP-12 cells probed with LCA following NH ₄ Cl and fresh medium treatments	236
Fig. 5.44: CHO DP-12 cells probed with LecA5K following NH ₄ Cl treatment	237
Fig. 5.45: CHO DP-12 cells probed with LecA5K following NH ₄ Cl and fresh medium treatments	237
Fig. 5.46: CHO DP-12 cells probed with AAL-2 following NaBu treatment	240
Fig. 5.47: CHO DP-12 cells probed with AAL-2 following NaBu and fresh medium treatments	240
Fig. 5.48: CHO DP-12 cells probed with LecA5K following NaBu treatment	241
Fig. 5.49: CHO DP-12 cells probed with LecA5K following NaBu and fresh medium treatments	241
Fig. 5.50: CHO DP-12 cells probed with MAL II following NaBu treatment	242
Fig. 5.51: CHO DP-12 cells probed with MAL II following NaBu and fresh medium treatments	242
Fig. 5.52: CHO DP-12 cells probed with RCA I following NaBu treatment	243
Fig. 5.53: CHO DP-12 cells probed with RCA I following NaBu and fresh medium treatments	243
Fig. 5.54: Purification of recombinant IgG1 using Protein A/G	245
Fig. 5.55: SDS-PAGE and western blot analysis of purified IgG1	246
Fig. 5.56: ELISA analysis of purified IgG1	247
Fig. 5.57: ELLA and ELISA analysis of heat treated IgG1	248
Fig. 5.58: Purification of recombinant IgG1 from 12 treated CHO DP-12 cultures	249
Fig. 5.59: ELLA and ELISA analysis of purified IgG1 from treated cultures	250
Fig. 5.60: ELLA and ELISA analysis of purified IgG1 from treated cultures	251

Appendices

Fig. B.1: The alignment of AAL-2 and PVL protein sequences	B2
Fig. B.2: Whole vector amplification strategy for the generation of pAAL-2_MT	B3
Fig. B.3: AAL-2 and AAL-2 _{mut} protein sequence alignment	B4
Fig. B.4: IMAC purification of AAL-2 _{mut}	B5
Fig. B.5: The six GlcNAc binding pockets of AAL-2	B6
Fig. C.1: IMAC purification of LecA	C1

Fig. F.1: Gated and ungated dotplots of adherent and suspension adapted CHO DP-12 cells

F3

List of Tables

Chapter 1

Table 1.1: Monosaccharides common in eukaryotes	5
Table 1.2: Therapeutic glycoproteins	29
Table 1.3: Source and specificity of common lectins	51
Table 1.4: Biopharmaceutical products produced in CHO	63

Chapter 2

Table 2.1: <i>E. coli</i> strains	73
Table 2.2: Plasmid vectors	74
Table 2.3: Plasmid constructs	75
Table 2.4: Primer sequences (Synthesised by IDT, Belgium)	76
Table 2.5: CHO DP-12	79
Table 2.6: PCR programme cycle	92
Table 2.7: SDS-PAGE gel recipes	100
Table 2.8: Biotinylated lectins from Vector Laboratories Ltd UK	111
Table 2.9: Flow cytometry sample data	127

Chapter 3

Table 3.1: Primer sequences for increasing LecA lysine content (Synthesised by IDT, Belgium)	165
--	-----

Chapter 4

Table 4.1: Lectin panel for fluorescent microscopic analysis of CHO DP-12 cells	185
---	-----

Chapter 5

Table 5.1: Comparison of MFI from trypsinised cells with cells removed using a scraper, CDS and EDTA	207
Table 5.2: Comparison of MFI from lectins probing adherent and suspension adapted CHO DP-12 cells	209

Table 5.3: Comparison of MFI from lectin binding suspension adapted CHO DP-12 cells treated and untreated with spent medium	222
Table 5.4: Comparison of MFI from lectin binding suspension adapted CHO DP-12 cells treated and untreated with L-glutamine free medium	228
Table 5.5: Comparison of MFI from lectin binding suspension adapted CHO DP-12 cells treated and untreated with 10 mM NH ₄ Cl	234
Table 5.6: Comparison of MFI from lectin binding suspension adapted CHO DP-12 cells treated and untreated with 3 mM NaBu	239
Table 5.7: Purified recombinant IgG1 samples and corresponding flow cytometry sections and treatments	249

Appendices

Table E.1: Flow cytometry data for determining an appropriate lectin probing concentration, see Fig. 5.2 and Fig. 5.3	E1
Table E.2: Flow cytometry data for determining an appropriate cell number per sample, see Fig. 5.4	E1
Table E.3: Flow cytometry data for determining an appropriate cell lectin probing temperature, see Fig. 5.5	E2
Table E.4: Flow cytometry data for comparing trypsin and cell scraper for cell detachment, see Fig. 5.6	E2
Table E.5: Flow cytometry data for comparing trypsin and cell dissociation solution for cell detachment, see Fig. 5.6	E3
Table E.6: Flow cytometry data for comparing trypsin and 10 mM EDTA solution for cell detachment, see Fig. 5.6	E3
Table F.1: Flow cytometry data for adherent CHO DP-12 cells probed with lectin panel, summarised in Table 5.2	F1
Table F.2: Flow cytometry data for suspension adapted CHO DP-12 cells probed with lectin panel, summarised in Table 5.2	F2
Table F.3: Flow cytometry data for unstained adherent and suspension adapted CHO DP-12, corresponding to Fig. 5.7 and Fig. H.1	F3
Table F.4: Flow cytometry data for assessing LecA and LecA variants, corresponding to Fig. 5.8	F3
Table G.1: Flow cytometry data for suspension CHO DP-12 cells probed with recombinant AAL-2 and GafD1-178, corresponding to Fig. 5.9, Fig. 5.10 and Fig. 5.11	G1

Table G.2: Flow cytometry data for suspension CHO DP-12 cells probed with recombinant LecA5K, AAL, DSL, ECL, GNL, and Jacalin corresponding to Fig. 5.12 to Fig. 5.17	G2
Table G.3: Flow cytometry data for suspension CHO DP-12 cells probed with LCA, LecB, MAL II, NPL, RCA I, and WGA corresponding to Fig. 5.18 to Fig. 5.23	G3
Table H.1: Flow cytometry data for suspension CHO DP-12 cells untreated (24 h) and probed with lectin panel, corresponding to Table 5.3 and Fig. 5.24 to Fig. 5.31	H1
Table H.2: Flow cytometry data for suspension CHO DP-12 cells spent medium treated (24 h) and probed with lectin panel, corresponding to Table 5.3 and Fig. 5.24 to Fig. 5.31	H2
Table H.3: Flow cytometry data for suspension CHO DP-12 cells spent medium treated (T) and untreated (U) for 24 h followed by 72 h fresh medium and probed with lectin panel, corresponding to Table 5.3 and Fig. 5.24 to Fig. 5.31	H3
Table I.1: Flow cytometry data for suspension CHO DP-12 cells untreated (48 h) and probed with lectin panel, corresponding to Table 5.4 and Fig. 5.32 to Fig. 5.39	I1
Table I.2: Flow cytometry data for suspension CHO DP-12 cells treated (0 mM L-glut 48 h) and probed with lectin panel, corresponding to Table 5.4 and Fig. 5.32 to Fig. 5.39	I2
Table I.3: Flow cytometry data for suspension CHO DP-12 cells untreated (48 h + 72 h) and probed with lectin panel, corresponding to Table 5.4 and Fig. 5.32 to Fig. 5.39	I3
Table I.4: Flow cytometry data for suspension CHO DP-12 cells treated (0 mM L-glut 48 h + 4 mM L-glut 72 h) and probed with lectin panel, corresponding to Table 5.4 and Fig. 5.32 to Fig. 5.39	I4
Table J.1: Flow cytometry data for suspension CHO DP-12 cells untreated (48 h) and probed with lectin panel, corresponding to Table 5.5 and Fig. 5.40 to Fig. 5.45	J1
Table J.2: Flow cytometry data for suspension CHO DP-12 cells treated (10 mM NH ₄ Cl 48 h) and probed with lectin panel, corresponding to Table 5.5 and Fig. 5.40 to Fig. 5.45	J2
Table J.3: Flow cytometry data for suspension CHO DP-12 cells untreated (48 h + 72 h) and probed with lectin panel, corresponding to Table 5.5 and Fig. 5.40 to Fig. 5.45	J3

Table J.4: Flow cytometry data for suspension CHO DP-12 cells treated (10 mM NH ₄ Cl 48 h + 0 mM NH ₄ Cl 72 h) and probed with lectin panel, corresponding to Table 5.5 and Fig. 5.40 to Fig. 5.45	J4
Table K.1: Flow cytometry data for suspension CHO DP-12 cells untreated (96 h) and probed with lectin panel, corresponding to Table 5.6 and Fig. 5.46 to Fig. 5.53	K1
Table K.2: Flow cytometry data for suspension CHO DP-12 cells treated (3 mM NaBu 96 h) and probed with lectin panel, corresponding to Table 5.6 and Fig. 5.46 to Fig. 5.53	K2
Table K.3: Flow cytometry data for suspension CHO DP-12 cells untreated (96 h + 96 h) and probed with lectin panel, corresponding to Table 5.6 and Fig. 5.46 to Fig. 5.53	K3
Table K.4: Flow cytometry data for suspension CHO DP-12 cells treated (3 mM NaBu 96 h + 0 mM NaBu 96 h) and probed with lectin panel, corresponding to Table 5.6 and Fig. 5.46 to Fig. 5.53	K4
Table K.5: Comparison of MFI from lectin binding suspension adapted CHO DP-12 cells fed 4 days and 9 days previously and probed with lectin panel	K5

List of Abbreviations, Units and Prefixes

Abbreviations

A	Adenine
aa	amino acid
AAL	<i>Aleuria aurantia</i> lectin
AAL-2	<i>Agrocybe aegerita</i> lectin 2
ACS	American chemical society
AE	Anion-exchange
Amp ^R	Ampicillin resistant
APS	Ammonium persulphate
Asn	Asparagine
BCA	Bicinchoninic acid
β-IFN	beta-interferon
BLAST	Basic local alignment search tool
BSA	Bovine serum albumin
BSC	Biological safety cabinet
bp	Base pairs
C	Cytosine
C	Carbon
CDG	Congenital disorders of glycosylation
CHO	Chinese hamster ovary
CRD	Carbohydrate-recognition domain
CV	Column volume
Cys	Cysteine
dam	DNA adenine methyltransferase
DAPI	4',6-diamidino-2-phenylindole
DCs	Dendritic cells
dH ₂ O	distilled H ₂ O
DMSO	Dimethyl sulfoxide
Dol	Dolichol
DSL	<i>Datura stramonium</i> lectin
DTT	Dithiothreitol
EDTA	Ethylenediaminetetraacetic acid
EGF	Epidermal growth factor
EGFP	Enhanced green fluorescent protein
ELLA	Enzyme-linked lectin assay

ELISA	Enzyme-linked immunisorbent assay
ER	Endoplasmic reticulum
F	Phenylalanine
Fc	Crystallisable fragment
FBS	Foetal bovine serum
FITC	Fluorescein isothiocyanate
Fuc	Fucose
G	Guanine
GAG	Glycosaminoglycans
Gal	Galactose
GalCer	Galactosyl ceramide
GDP	Guanosine diphosphate
GlcA	Glucuronic acid
GlcCer	Glucosyl ceramide
GalNAc	<i>N</i> -acetylgalactosamine
GFP	Green fluorescent protein
GlcNAc	<i>N</i> -acetylglucosamine
Glu	Glucose
GNL	<i>Galanthus nivalis</i> lectin
GSL	Glycosphingolipids
HPA	<i>Helix pomatia</i> agglutinin
HRP	Horseradish peroxidase
HI	Heat inactivated
IdoA	Iduronic acid
IDT	Intergrated DNA Technologies
IgG1	Immunoglobulin G class 1
IMAC	Immobilised metal affinity chromatography
IMS	Industrial methylated spirits
IPTG	Isopropyl β -D-1-thiogalactopyranoside
K	Lysine
K	Guanine or threonine
Lac	Lactose
LAC	Lectin affinity chromatography
LB	Lysogeny broth
LPS	Lipopolysaccharide
M	Adenine or cytosine
mAb	Monoclonal antibody
Man	Mannose
MBL	Mannose binding lectin

MCS	Multiple cloning site
MurNAc	<i>N</i> -acetylmuramic acid
MWCO	Molecular weight cut-off
Na	Sodium
NA	Neuraminic acid
NaBu	Sodium butyrate
Neu5Ac	<i>N</i> -acetylneuraminic acid
Neu5Gc	<i>N</i> -glycolylneuraminic acid
NHS	<i>N</i> -hydroxysuccinimide
Ni	Nickel
NPL	<i>Narcissus pseudonarcissus</i> lectin
Nt	nucleotide
NTA	Nitrilotriacetic acid
OGA	<i>O</i> -GlcNAcase
OGT	<i>O</i> -GlcNAc transferase
ORF	Open reading frame
OST	Oligosaccharyltransferase
P	Phosphate
PCR	Polymerase chain reaction
PE	Phycoerythrin
PEG	Polyethylene glycol
PI	Propidium iodide
PNA	Peanut agglutinin lectin
PS	Phosphatidylserine
PTM	Post-translational modification
PVA	Polyvinyl alcohol
PVL	<i>Psathyrella velutina</i> lectin
RCA I	<i>Ricinus communis</i> agglutinin I
RMFI	Relative mean fluorescence intensity
Ser	Serine
SDS	Sodium dodecyl sulphate
SDS-PAGE	Sodium dodecyl sulfate polyacrylamide gel electrophoresis
SDTB	Semi-dry transfer buffer
SLe ^A	Sialyl-lewis antigen
T	Threonine
TAE	Tris-acetate-EDTA
TB	Tris-borate
Thr	Threonine
T _m	Melting temperature

TMB	3,3',5,5'-Tetramethylbenzidine
TBST	Tris-buffered saline and Tween 20
UEA I	<i>Ulex europaeus</i> agglutinin
UDP/UTP	Uridine diphosphate/triphosphate
UPR	Unfolded protein response
UV	Ultraviolet
v/v	Volume per volume
W	Tryptophan
WGA	Wheatgerm agglutinin
w/v	Weight per volume
Xyl	Xylose

Units

A	Ampere
A	Absorbance units
Da	Dalton
g	Gram
g	Gravitational force
h	Hour
L	Litre
M	Molar
min	Minute
pH	Potential hydrogen
psi	Pounds per square inch
RCF	Relative centrifugal force
rpm	Revolutions per minute
s	Second
V	Volt

Prefixes

k	Kilo 10^3
m	Milli 10^{-3}
μ	Micro 10^{-6}
n	Nano 10^{-9}

Abstract

Investigation of CHO cell surface glycosylation using lectin probes

Jonathan Cawley

Chinese hamster ovary (CHO) cells are extensively used for the production of therapeutic proteins which frequently undergo post-translational modifications (PTM), including glycosylation. This process can alter the function, stability, immunogenicity and efficacy of the glycoprotein. There are many culture conditions that may affect glycosylation. The CHO glycocalyx, carbohydrate coat surrounding the cell membrane, may be informative to cell health and the glycosylation state of the product. It is therefore of great interest to understand how the CHO glycocalyx changes in different culture conditions. Fluorescent microscopy and flow cytometry were used to glycoanalyse CHO DP-12 cells. Novel recombinant lectins were mutated for optimum fluorescent labelling and purified using immobilized metal affinity chromatography (IMAC). Lectins from non-plant sources are perfect glycan probes as they are generally non-toxic but also superior to other binding proteins such as antibodies whose specificities for glycans are ill-defined.

In this study a eukaryotic lectin, *Agrocybe aegerita* lectin 2 (AAL-2), and prokaryotic lectins from *Pseudomonas aeruginosa* (LecA) and *Escherichia coli* (GafD1-178) were modified, recombinantly produced, purified and characterised. LecA was modified to optimise its labelling (biotinylation) for subsequent use as a fluorescently labelled lectin probe. CHO DP-12 cells underwent various culture media treatments, e.g. spent medium, 0 mM L-glutamine, 10 mM NH₄Cl or 3 mM NaBu, and the glycocalyx was investigated with a panel of lectins. Lectin binding changed significantly after culture conditions were altered. MAL II binding (sialic acid) decreased 43.79 % following spent medium treatment. A simultaneous 229 % increase in recombinant LecA, a galactophilic lectin, binding was observed which dropped to 32.24 % when the cells were reseeded in fresh medium. Recombinant IgG1 was also purified from treated CHO DP-12 cultures and glycoanalysed by an optimised enzyme-linked lectin assay (ELLA). The recombinant lectins produced were highly appropriate for investigating the glycocalyx of live CHO DP-12 cells.

Chapter 1

Introduction

1.1 Glycobiology

Glycobiology is the study of the structure, biochemistry and biological functions of oligosaccharides (linked sugars or glycans). Prof. R. Dwek coined the term in 1988 to recognise a new field encompassing the studies of carbohydrate chemistry and biochemistry (Rademacher et al. 1988). More specifically this field includes the study of glycoconjugates (glycans attached to proteins and lipids), glycosyltransferases (enzymes which catalyse glycan biosynthesis) and lectins and glycosidases which are glycan recognising proteins. The study of all the free sugars and glycan structures of a particular organism is called glycomics and is a subcategory of glycobiology. Glycobiology is a rapidly emerging field within the biological sciences as it is of vital importance to complex cell to cell interactions, in particular cell surface recognition, where glycans are key mediators. Glycobiology is of great importance for the biopharmaceutical industry where glycans are pivotal in determining the properties of biological therapeutics (Berg et al. 2002). The rapid growth of the release of therapeutic glycoproteins including biosimilars, as many patents are expiring, is now putting greater emphasis on the glycan characterisation of glycoproteins in order to demonstrate both safety and efficacy (Planinc et al. 2016).

1.2 Glycosylation

All cells and many macromolecules throughout all domains of life are decorated with sugars or sugar chains (oligosaccharides), referred to as glycans, which may be attached to lipids or proteins via a covalent glycosidic linkage. The attaching of these glycans is an enzymatic process called glycosylation. Glycosylation is a type of post-translational modification (PTM) which is more diverse than other covalent PTMs, such as acetylation, phosphorylation and succinylation (Schäffer and Messner 2017). Protein glycosylation is not only one of the most common PTMs but also one of the most important.

The glycome is the complete set of glycans in a cell or an organism. The glycomes of any two cell types will not be identical due to variation in the expression of specific glycotransferases. The glycome of a cell or organism may be much more complex than

its proteome (Taylor and Drickamer 2006). Unlike proteins whose sequences are encoded on a nucleic acid template, glycan structures are encoded indirectly in the genome. They are assembled without a template through a series of sequentially catalysed reactions which is dependent on the enzymes and substrates present. The enzymes involved in glycosylation are expressed in a tissue-specific manner permitting a cell to alter its 'glycoprofile' based on the cellular environment (Behr and Sasisekharan 2007). This environment is not constant but changes with the different stages of cell growth and substrate availability thus adding to glycan diversification. Proteins that differ considerably can have the same or similar glycans attached as the nature of the glycans is hugely influenced by the physiological state of the cell (Eklund and Freeze 2005).

Proteins and nucleotides are both assembled in a linear fashion, i.e. polymers are formed by joining monomers with one type of linkage. Glycan assembly is the antithesis of this. Monosaccharides can be linked at multiple positions to each other with an α or β glycosidic bond. This variation in bonding can lead to a vast array of saccharides with only a small number of monosaccharides. Four different nucleotides or amino acids could only generate 24 unique tetramers, whereas four different monosaccharides could theoretically generate 4.194×10^6 unique tetrasaccharides (Laine 1997). Glycan, and therefore glycoprotein, diversity is vast, see Fig. 1.1. Glycoproteins can be modified with both homogeneous and heterogeneous glycans. Glycoproteins which differ only by their glycans are called glycoforms. Glycoforms can have, as a result of their glycans, distinct properties and characteristics (Taylor and Drickamer 2006).

The sequencing of the human genome along with algorithms for predicting gene function have estimated that 2 % of human genes are involved in glycosylation and that approximately 50 % of human proteins are glycosylated (Campbell and Yarema 2005, Walsh and Jefferis 2006). Glycans may alter protein conformation and modify their activity. Multiple glycans can also interact with different affinities with the same protein. As glycoproteins are found throughout the extracellular space, both on cell surface and secreted proteins, they are essential for numerous other biological processes including molecular recognition, intra/inter- cellular signalling, immunity,

inflammation, and interactions with carbohydrate specific proteins, lectins (Geyer and Geyer 2006).

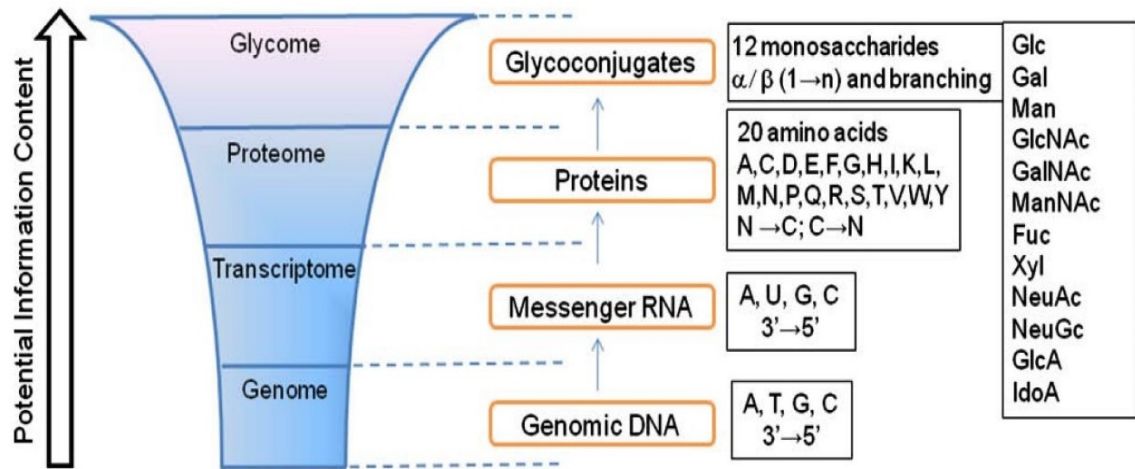


Fig. 1.1: Complexity and diversity of the glycome. The glycome is comprised of the largest group of post-translationally modified molecules. There is an exponential increase in information content from genome to glycome. The genome, transcriptome and proteome are generated by template driven processes whereas the glycome is governed by complex biological pathways which are influenced by carbohydrate availability, expression levels, enzyme activity and monosaccharide transporters (Gupta et al. 2010).

Protein glycosylation was first demonstrated, in proteins other than mucins, in the 1930s where the carbohydrate component of egg albumin was investigated. It was widely thought that glycosylation was unique to eukaryotic organisms (Nothaft and Szymanski 2010). However, 40 years later Sleytr and Thorne (1976) discovered glycoproteins on the surface layers (S-layers) of hyperthermophilic *Clostridium* species. *Bacteria* and *Archaea* have the greatest diversity regarding glycan building blocks as they contain approximately one hundred different monosaccharides. Eukaryotes possess a more limited amount with plants being the most diverse with 25 distinct monosaccharides. In contrast only 11 different monosaccharides are found in animals, see Fig. 1.2 and Table 1.1 (Varki et al. 2009).

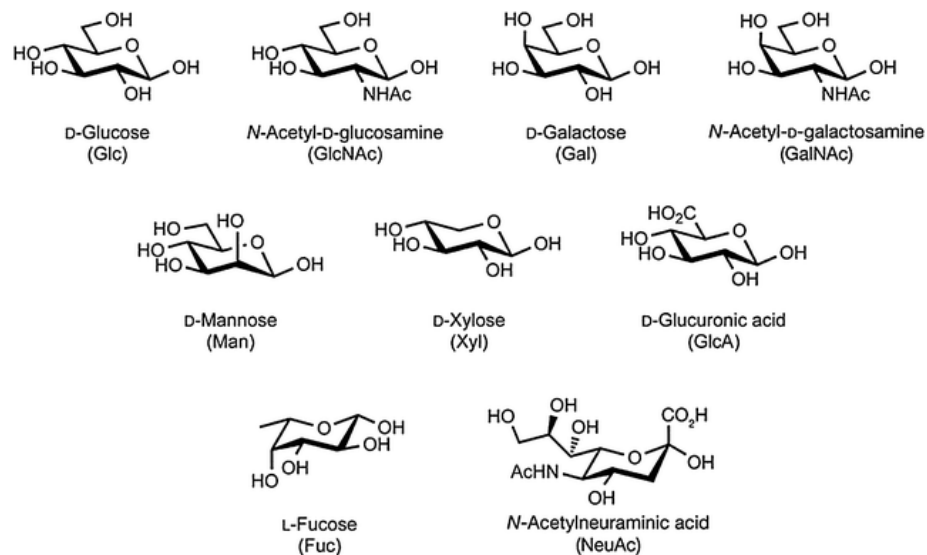


Fig. 1.2: Haworth projection of monosaccharide building blocks for animal glycans. Monosaccharides found in animals, with the exemption of fucose, are principally D-stereoisomers. Iduronic acid, not shown above, is not synthesized directly from a nucleotide sugar donor. Glucuronic acid is added to the growing glycosaminoglycan (GAG) chain where it is then epimerized to iduronic acid (Varki et al. 2009; Reuel et al. 2012).

Table 1.1: Monosaccharides common in eukaryotes

Type	Description	Example	Abbreviation
Pentoses	Five-carbon neutral sugars	D-xylose	Xyl
Hexoses	Six-carbon neutral sugars	D-glucose	Glc
		D-galactose	Gal
		D-mannose	Man
Hexosamines	Hexoses with an amino group at the 2-position, which can be free or N-acetylated	<i>N</i> -acetyl-D-glucosamine <i>N</i> -acetyl-D-galactosamine	GlcNAc GalNAc
Deoxyhexoses	Six-carbon neutral sugars without the hydroxyl group at the 6-position	L-fucose	Fuc
Uronic acids	Hexoses with a negatively charged carboxylate at the 6-position	D-glucuronic acid	GlcA
		L-iduronic	IdoA
Sialic acids	Nine-carbon acidic sugars	<i>N</i> -acetylneuraminic acid	Neu5Ac/NANA
		<i>N</i> -glycolylneuraminic acid	Neu5Gc/NGNA

The broadest glycan subcategories are linear and branched. Linear glycans are comprised mainly of glycosaminoglycans (GAGs) of which there are four types. All four types of GAGs are formed of repeating disaccharide units, uronic acids linked to hexosamines, and are O-linked to a core protein. Branched glycans can be O-linked or N-linked to a glycoprotein or glycolipid, Fig 1.3. This branching structure allows the monosaccharide building blocks to be assembled in thousands of possible combinations resulting in information dense glycans (Behr and Sasisekharan 2007). The glycocalyx is a collective term for the glycoproteins and glycolipids at the extracellular surface of the plasma membrane. All glycan categories have been well studied. However, N-linked glycans which are attached to secreted proteins are best understood due to the availability of serum glycoproteins for glycoanalysis (Taylor and Drickamer 2006).

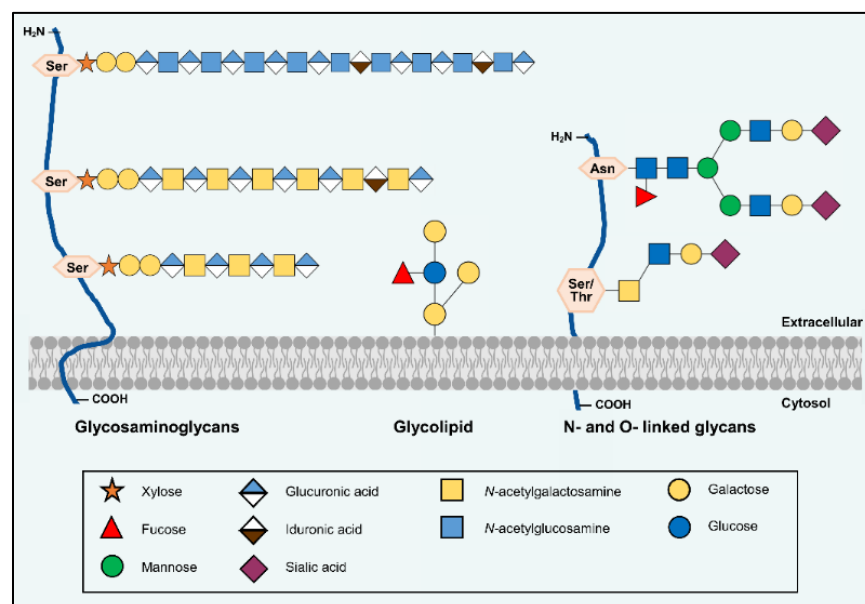


Fig. 1.3: Linear and branched glycans at the cell surface. Examples of glycans attached to membrane proteins and lipids. Image created using Microsoft Publisher 15.0.

The extent of glycans at the cell surface provides an opportunity for immense information storage which leads to, and enhances, cell-cell communication and cell matrix interaction. Sialic acids at the cell surface are present on the non-reducing end of glycans on glycoproteins and glycolipids which are important for modulating ligand-receptor interaction due to their negative charges (Azuma et al. 2000). Additionally, their absence increases cell membrane adhesiveness which, when coupled with decreased surface charge, can facilitate recognition by phagocytes (Sarter 2007). The

glycocalyx is useful for mediating symbiotic relationships with commensal bacteria in the lumen of the gut (Varki et al. 2009).

1.2.1 Eukaryotic glycosylation

Glycoprotein synthesis in eukaryotes occurs in the endoplasmic reticulum (ER) and in the Golgi apparatus of the cell. This enzymatic process is dependent on the presence of specific glycotransferases, the availability of monosaccharides and the current metabolic state of the cell (Taylor and Drickamer 2006). The synthesis of both N- and O-linked glycans have been well defined and are discussed below in greater detail. Over 70 % of the eukaryotic proteome is glycosylated and of this 90 % are *N*-glycosylated, which modulate glycoprotein stability, cellular interactions, transport and signalling (Dell et al. 2010; Lombard 2016).

The ABO blood-group antigens demonstrate the importance of specific glycotransferases. On each erythrocyte there are approximately 2 million ABH(O) glycan antigen sites (Cohen et al. 2009). These glycan motifs, also present on glycolipids and on other cells, can trigger immune reactions. The ABO antigens are extremely similar and differ by only one monosaccharide, see Fig. 1.4.

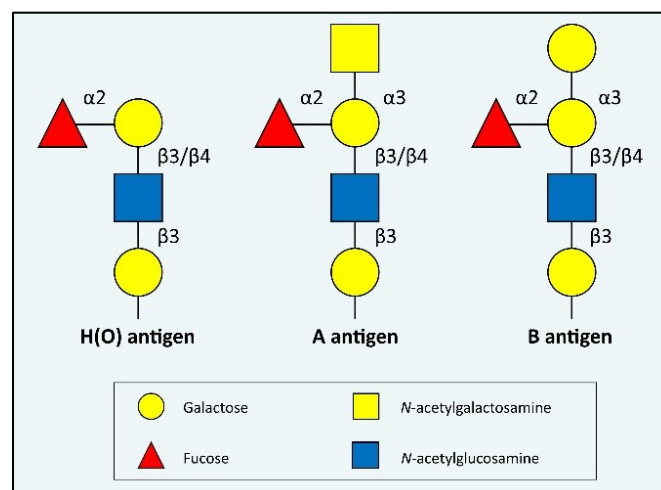


Fig. 1.4: ABO blood group antigens: H(O), A and B. The terminal monosaccharide distinguishes the three antigens, thus determining an individual's blood type. Image created using Microsoft Publisher 15.0.

The enzymes required for O antigen synthesis are present in everyone. People with type A and type B blood have an additional transferase, GalNAc transferase and Gal transferase respectively. Individuals with AB blood have both transferases and therefore display both A and B antigens (Varki et al. 2009). The genes encoding both these transferases are remarkably similar and evolved from a common ancestor as the resulting proteins differ by just three amino acids (Lodish et al. 2000).

1.2.1.1 Eukaryotic N-linked glycosylation

The attachment of glycans to the amide nitrogen on asparagine side chains is called N-linked glycosylation. This type of glycosylation occurs on secreted proteins and on membrane bound proteins. N-linked glycosylation occurs throughout all domains of life but the emphasis here will be on the mechanism and processes involved in eukaryotic N-linked glycosylation. The sequence required for N-linked glycosylation is Asn-X-Thr/Ser where X can be any amino acid except proline. Threonine (Thr) is more frequent than serine (Ser) and in some extremely rare cases cysteine has been incorporated to produce an Asn-X-Cys sequence for N-linked glycosylation. Approximately 30 % of possible N-linked glycan sites are actually glycosylated (Geyer and Geyer 2006, Varki et al. 2009). N-linked glycans mainly contain GlcNAc, Man, Gal, Fuc and sialic acids (Reuter and Gabius 1999).

The production of N-linked glycans can be broken down into three steps. First, the basic glycan structure is initially assembled attached to a dolichol lipid which is then transferred to the polypeptide, and finally the *N*-glycan is folded and processed. It is this last step which results in the huge diversity that is found within completed *N*-glycans. The oligosaccharide is synthesized and bound to the dolichol lipid via 2 phosphates, dolichol phosphate (Dol-P). The dolichol lipid is found in several cellular compartments including the endoplasmic reticulum (ER) and it is primarily used for the formation of the cellular membrane. However, if the cellular level of Dol-P is low then *N*-glycan synthesis is drastically reduced. The structure of Dol-P has been preserved across all eukaryotes (Varki et al. 2009).

The initial additions to Dol-P occur on the cytosolic side of the ER membrane. The first two monosaccharide donors are uridine diphosphate *N*-acetylglucosamine (UDP-GlcNAc) and guanosine diphosphate mannose (GDP-Man) which deliver two *N*-acetylglucosamine (GlcNAc) and five mannose (Man) residues (Taylor and Drickamer 2006). The resulting structure, Man₅GlcNAc₂-Dol-P-P, is then, by means that are not completely known, flipped across the membrane to the lumen side of the ER. Fig 1.5 shows this process and the attachment of additional monosaccharides on the lumen side of the ER. Four mannose residues are added by Dol-P-Man donors then three glucose residues by Dol-P-Glc which forms Glc₃Man₉GlcNAc₂-P-P-Dol. This oligosaccharide can now be transferred to an asparagine residue on a nascent polypeptide (Varki et al. 2009).

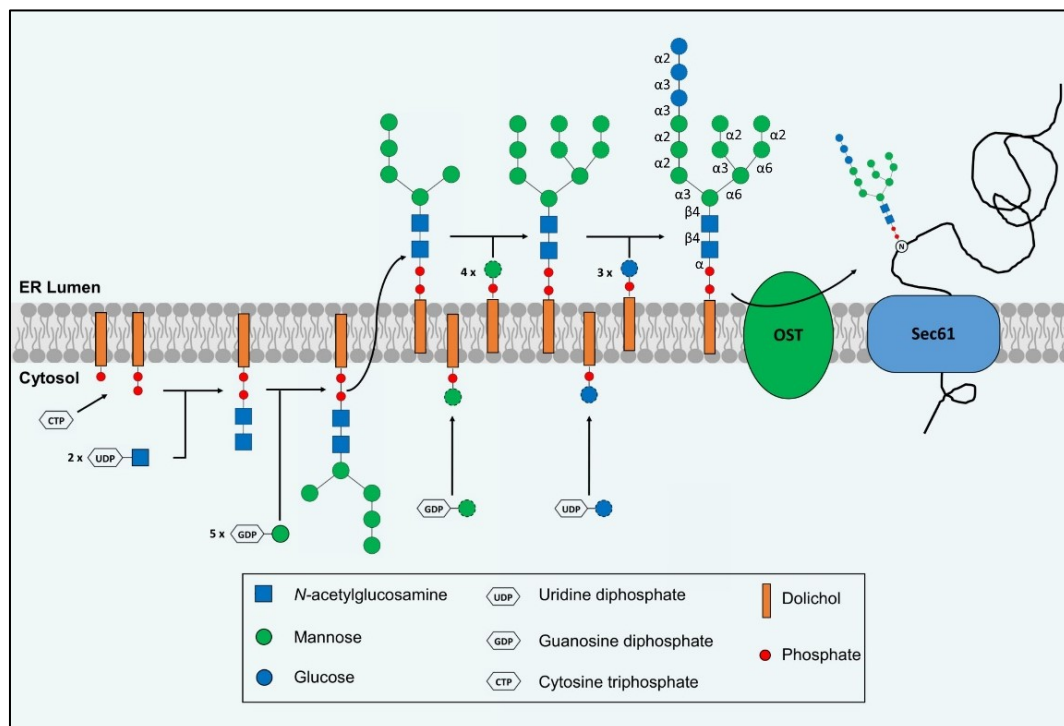


Fig. 1.5: The synthesis and transfer of the Glc₃Man₉GlcNAc₂ oligosaccharide to an asparagine residue on a nascent polypeptide. Monosaccharides are assembled on a dolichol lipid anchor which is then re-orientated from the cytosol to the ER lumen where the glycan is further extended by additional monosaccharides. The oligosaccharyltransferase (OST) catalyses the transfer of the assembled glycan to the asparagine side chain of a polypeptide which is transported from the cytosol to the ER lumen via the Sec61 translocon. Image created using Microsoft Publisher 15.0.

In complex eukaryotes the OST is a multi-protein complex consisting of up to 8 proteins. The multi-protein OST has subunits that influence the nature of the glycosylation that occurs. In complex eukaryotes the OST subunit Ost1p promotes a specific type of glycosylation while subunits Ost3p/6p confer oxido-reductase activity (Schwarz and Aebi 2011). There are multiple processing reactions that can occur when $\text{Glc}_3\text{Man}_9\text{GlcNAc}_2$ has been covalently attached to the asparagine residues of polypeptides. These reactions are initially involved with controlling protein folding followed by processes that lead to *N*-glycan diversification.

Firstly, monosaccharides are removed at the non-reducing end of the glycan by exoglycosidases. This glucose residue trimming is completed by glucosidase I, removes terminal α 1,2-linked glucose, and glucosidase II which individually removes the final two glucose residues that are α 1,3-linked (Taylor and Drickamer 2006). The glucose residue trimming occurs in the ER lumen and it precedes protein folding. When the glycan is deglycosylated it folds into a protein and it moves from the ER into the Golgi for additional *N*-glycan processing. If the protein has folded incorrectly it is subject to reglycosylation by an enzyme, α -glucosyltransferase, located in the lumen of the ER. After reglycosylation the protein will be degraded if it does not refold into the correct protein conformation (Varki et al. 2009).

Prior to glycoprotein secretion there are lectins which play an important role in insuring correct folding. Calnexin and calreticulin are two lectins that are involved in this protein folding quality control system. These lectins can both bind to the monoglucosylated form of the *N*-glycan, $\text{Glc}_1\text{Man}_9\text{GlcNAc}_2\text{-Asn}$. When they are bound to the glycoprotein they prevent unwanted protein oligomerization and support correct protein folding. Calnexin and calreticulin also associate with a protein, ERp57, which promotes the formation of disulphide bonds as the protein is folding (Taylor and Drickamer 2006; Varki et al. 2009). The final glucose is removed causing the lectin to release the correctly folded glycoprotein or the glucose can be removed as the glycoprotein dissociates from the lectin (Taylor and Drickamer 2006). This control mechanism ensures that incorrectly folded glycoproteins, including those that have been refolded, will be degraded and will not be secreted thus allowing only correctly folded

glycoproteins to be released into to Golgi for further modification, see Fig. 1.6 (Eklund and Freeze 2005).

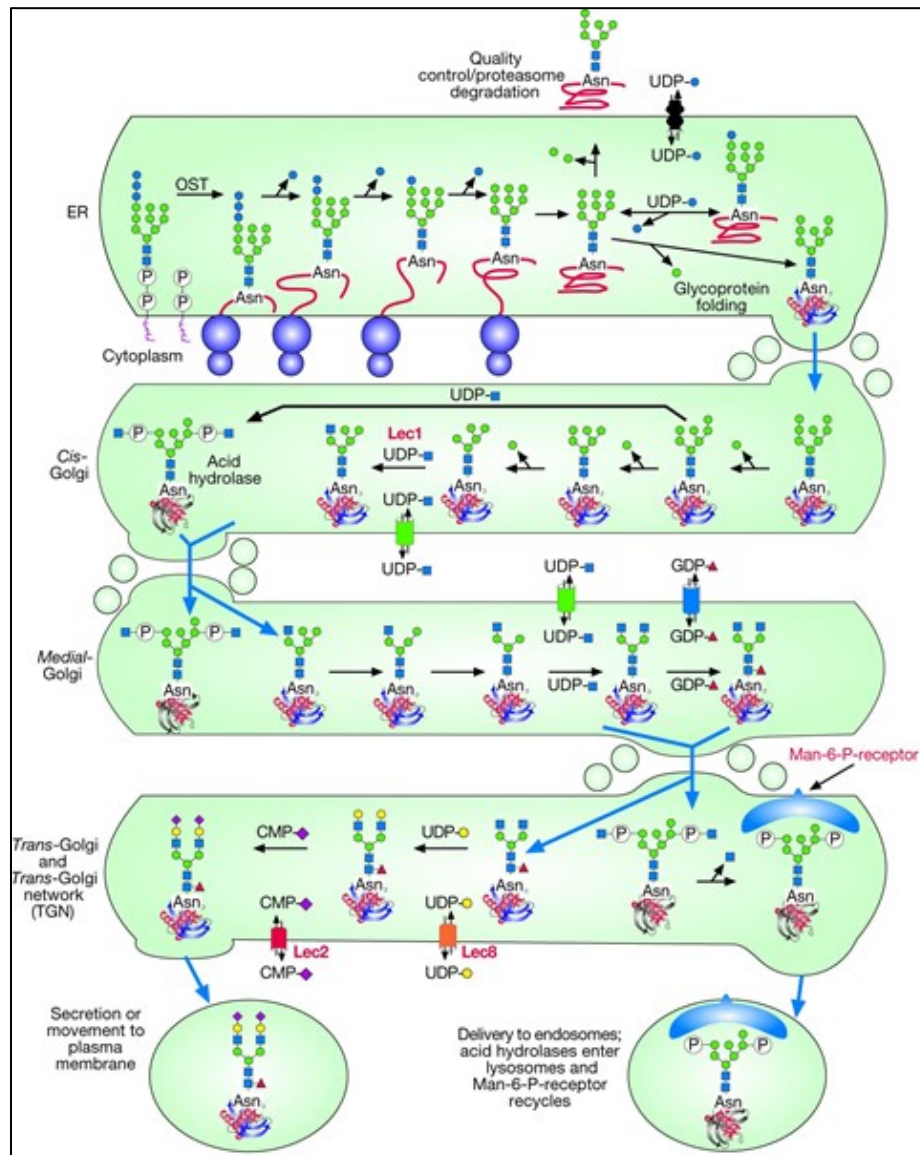


Fig. 1.6: Processing and maturation of an N-glycan through the ER and Golgi. The three glucose residues are removed from the 14-sugar $\text{Glc}_3\text{Man}_9\text{GlcNAc}_2$ glycan, which was transferred to Asn-X-Ser/Thr sequons by glucosidases in the ER. ER mannosidase also removes a mannose residue. The removal of these sugars are closely associated with glycoprotein folding assisted by the lectins calnexin and calreticulin. Another lectin, termed EDEM (ER degradation-enhancing α -mannosidase I-like protein), binds to mannose residues on glycoproteins that have folded incorrectly and chaperones them via retrotranslocation into the cytoplasm for degradation. In the *cis* compartment of the Golgi the $\text{Man}_5\text{GlcNAc}_2$ glycan is generated by the removal of mannose residues. This

removal can be blocked by deoxymannojirimycin, a mannosidase inhibitor, leaving the $\text{Man}_8\text{GlcNAc}_2$ glycan which is not processed further. GlcNAcT-1 acts on the $\text{Man}_5\text{GlcNAc}_2$ glycan in the *medial*-Golgi which initiates the first branch of an *N*-glycan. α -Mannosidase II removes two terminal mannose residues in a reaction that is blocked by the inhibitor swainsonine. The substrate for GlcNAcT-II is generated by α -mannosidase II. The biantennary *N*-glycan generated is further extended by the addition of fucose, galactose, and sialic acid to generate a complex *N*-glycan with two branches. Complex *N*-glycans can have many more sugars than shown here, including additional residues attached to the core, additional branches and branches extended with poly-*N*-acetyllactosamine units (Varki et al. 2009).

There are many *N*-glycan processes that can take place in the Golgi apparatus. GlcNAc-phosphotransferase can add GlcNAc-phosphate, GlcNAc is then removed, yielding a $\text{Man}_8\text{GlcNAc}_2\text{-Asn}$ *N*-glycan that contains an added phosphate. This type of glycan modification is used to send defective glycoproteins to the lysosome (Varki et al. 2009). The removal of mannose residues by α -mannosidase I, which acts specifically on α 1,2- linked mannose, is a more routine glycan modification (Liebminger et al. 2009). This is extremely common in vertebrates and the end product is the $\text{Man}_5\text{GlcNAc}_2\text{-Asn}$ glycan. This *N*-glycan is the basis for further diversification and from it, high mannose, hybrid and complex glycans can be produced, see Fig 1.7 (Wang 2016).

High mannose glycans are glycans containing five to nine mannose residues. The important step in complex glycan synthesis is the attachment of GlcNAc at the α 1-3-linked D-mannose residue. The further addition of GlcNAc monosaccharides results in multi-antennary complex glycan structures (Reuter and Gabius 1999). Complex glycans contain the three core mannose residues with added GlcNAc residues at the α 3 and α 6 mannose sites. In hybrid glycans only one of the α 3 and α 6 mannose sites is occupied by a GlcNAc residue. The core *N*-glycan structure, $\text{Man}_5\text{GlcNAc}_2\text{-Asn}$, can undergo a huge change in the Golgi due to the removal of mannose residues, by mannosidases I and II, and the addition of GlcNAc residues by GlcNAc-transferase I and II.

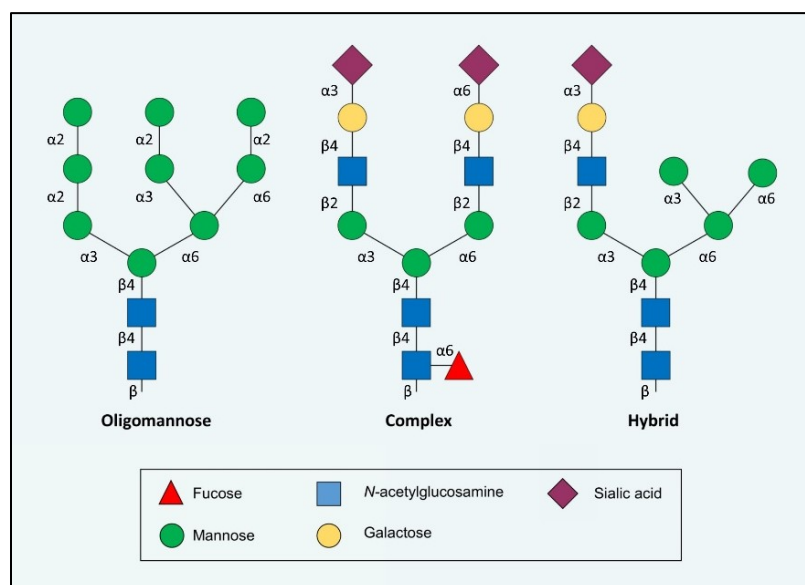


Fig. 1.7: Types of *N*-glycans. The *N*-glycans added to a protein at the Asn-X-Ser/Thr sequence are of three types in a mature glycoprotein: oligomannose, complex and hybrid, all containing the common Man₃GlcNAc₂-Asn core. Image created using Microsoft Publisher 15.0.

The capping units on complex and hybrid *N*-glycans are an important modification. A galactose residue is added to all GlcNAc residues and subsequently a sialic acid, *N*-acetylneuraminic acid (NeuNAc), residue is added to the galactose (Taylor and Drickamer 2006). This sialic acid addition is essential for a functional glycoprotein post secretion as nonsialylated glycoproteins have exposed galactose residues that are recognized by asialo-glycoprotein receptors and are removed from the serum (Bork et al. 2009). Fucosylation is a common modification found in eukaryotic *N*-glycans. Fucosyltransferase adds a fucose to the GlcNAc residue, which is directly attached to the Asn. This occurs on hybrid and complex *N*-glycans and can control the biological function of growth factor receptors (Miyoshi et al. 2008).

In mammals this fucose is added with an α 1-6 linkage, whereas in plants it is added with an α 1,3- linkage. In insect cells difucosylation occurs. During this process separate enzymes add α 1,6-linked fucose first before adding the α 1,3-linked fucose. The α 1,3-linked fucose is immunogenic which results in insect and plants cells being suboptimal for the production of therapeutic glycoproteins (Reuter and Gabius 1999).

The range of possible *N*-glycans is vast which is due to the multiple processing pathways and reactions that can occur. Over 500 different *N*-glycans have been identified and characterised but it is expected that there are over 1000 different *N*-glycans on mammalian glycoproteins alone (Taylor and Drickamer 2006).

1.2.1.2 Eukaryotic O-linked glycosylation.

O-linked glycosylation is the addition of a glycan to the oxygen atom of an amino acid in a polypeptide. Unlike N-linked glycosylation, a consensus sequence is not required. *O*-glycans are generally biantennary structures which are relatively compact unlike *N*-glycans which can have multiple branch points. There are two major types of O-linked glycosylation namely (i) Mucin type *O*-glycans and (ii) Non-mucin type *O*-glycans.

(i) Mucin type *O*-glycans

Mucins are a type of glycoprotein that are produced by epithelial cells and are heavily glycosylated with O-linked glycans. Interacting mucins can form disulphide bonds resulting in a gelatin-like substance that can retain water and act as an additional barrier and help protect from invading microbes (Taylor and Drickamer 2006). *N*-acetylgalactosamine (GalNAc) is added to the oxygen atom in serine and threonine residues to produce mucin type *O*-glycans. Branching can occur from this first GalNAc residue. GlcNAc can also be added to these residues although the most common type found in humans is the mucin type *O*-glycan (Varki et al. 2009). The different mucin *O*-glycans have been categorised into 8 groups based on their core structure. Fig 1.8 shows 4 of these core structures. Mucins, like N-linked glycoproteins, can be secreted or membrane bound.

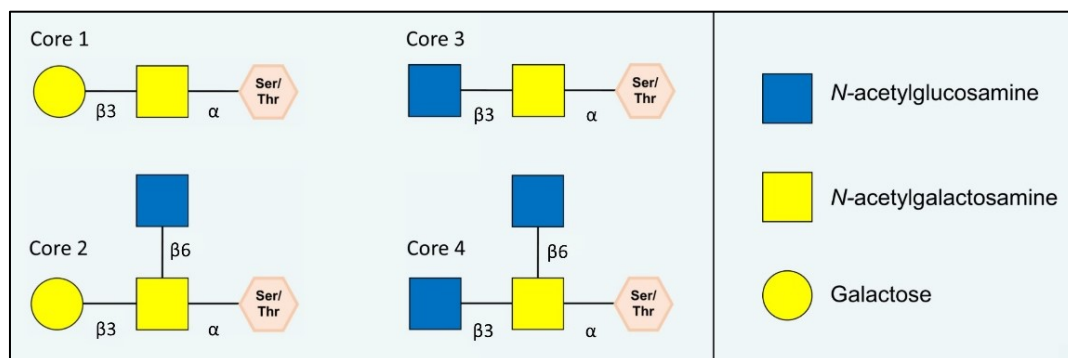


Fig. 1.8: Four of the core structures of mucin type *O*-glycans. These structure all contain GalNAc attached to serine or threonine and other Gal and/or GlcNAc residues. Image created using Microsoft Publisher 15.0.

The oligosaccharide is not assembled on a precursor molecule like dolichol, in *N*-linked glycosylation, but rather it is assembled in a stepwise fashion. GalNAc transferase adds a single GalNAc monosaccharide to a serine or threonine residue to initiate the synthesis of mucin type *O*-glycans. The synthesis of *O*-glycans occurs in the Golgi and it does not begin until the protein is fully synthesized and correctly folded (Stanley 2011). There are numerous different GalNAc-transferase genes that have been found in mammalian species. *O*-linked glycosylation does not require a consensus sequence and this variation in the amino acid sequence is thought to affect the activity of certain GalNAc-transferase isozymes. This influencing factor along with the tissue specificity of the GalNAc-transferases and other modifications, including sialylation, is thought to determine the diversification of mucin type *O*-glycans (Varki et al. 2009). The number of known *O*-glycan structures is thought to be far greater than of *N*-glycans, e.g. in human lung mucin alone there are over 100 different *O*-glycans (Reuter and Gabius 1999).

The glycans on erythrocyte membranes that determine blood type are *N*-linked and *O*-linked. The key factor that causes an individual's blood group type is determined by the presence or absence of specific glycosyltransferases. The *O*-type antigen differs from the A-type and the B-type antigens by the addition of one GalNAc residue and one galactose residue respectively (Taylor and Drickamer 2006). Mucin type *O*-glycans are the most common *O*-glycan found in humans. However there are numerous other

O-glycans that are present and are involved in a wide variety of functions. *O*-linked glycans are found in the hinge region of IgA and this is thought to help increase protease resistance (Taylor and Drickamer 2006). Other locations include *O*-linked GlcNAc glycans which are found in cytoplasmic proteins, *O*-linked mannose glycans are found in brain glycoproteins, *O*-linked fucose glycans are found in epidermal growth factor-like domains and *O*-linked galactose glycans found attached to lysine residues in collagen (Geyer and Geyer 2006).

(ii) Non-mucin type *O*-glycans

O-GlcNAcylation

O-linked β -*N*-acetylglucosamine (*O*-GlcNAc) is a common post-translational modification attached to serine and threonine residues on nuclear and cytoplasmic proteins. It is an important PTM first discovered in the 1980s and is involved in many biological processes including epigenetic regulation, transcription, translation, homeostasis and protein signalling and trafficking (Ma and Hart 2014; Harwood and Hanover 2014). No exact consensus sequence for *O*-GlcNAcylation has been identified although there is a high occurrence of proline, valine and other serine or threonine residues near the accepting serine or threonine (Julenius et al. 2009).

O-GlcNAcylation is extremely common and has been found in all eukaryotic cells including yeast (Taylor and Drickamer 2006). *O*-GlcNAcylation is often considered more similar to protein phosphorylation than to other types of glycosylation, e.g. *N*-glycans or mucin type *O*-glycans. This is because only a single monosaccharide is transferred to the protein. The glycan is not elongated and branching does not occur. Phosphate can be added or removed from a protein by a variety of kinases and phosphatases whereas GlcNAc is only added by *O*-GlcNAc transferase (OGT) or removed by *O*-GlcNAcase (OGA). OGT and OGA are expressed in all tissue types (Harwood and Hanover 2014). The precise function of this GlcNAc modification to intracellular proteins has not been completely identified. It is thought that *O*-GlcNAc is involved in regulating protein phosphorylation as GlcNAc attached to serine and threonine residues prevents them being phosphorylated. In excess of 3,000 *O*-GlcNAcylated proteins have been identified and almost all of which are involved in

cellular metabolism (Groves et al. 2013). *O*-GlcNAcylation is so prevalent that up to 5 % of all cellular glucose is used to generate its donor, UDP-GlcNAc (Hart et al. 2007).

O-Fucosylation

The addition of a fucose residue to the hydroxyl group on serine or threonine amino acids is called *O*-fucosylation. This type of O-linked glycan was first identified in 1975 from a glycopeptide isolated from human urine but it was another 15 years before a protein was found with O-linked fucose, namely urokinase (Hallgren et al. 1975; Kentzer et al. 1990). A consensus sequence for *O*-fucosylation was suggested as proteins with this modification also have a cysteine-rich motif at the same position. Two such cysteine-rich motifs were identified which subsequently confirmed two independent *O*-fucosylation pathways (Vasudevan and Haltiwanger 2014).

One cysteine-rich sequence called an Epidermal Growth Factor-like repeat (EGR repeat) is approximately 40 amino acids long and found on many cell surface and secreted proteins. There are 6 cysteines forming three disulphide bonds in the EGF repeat and the consensus sequence for *O*-fucosylation here is C²-X₍₄₋₅₎-(S/T)-C³ where C² and C³ are the second and third cysteines and X is any other amino acid (Lira-Navarrete et al. 2011).

O-Mannosylation

The addition of mannose residues to serine and threonine amino acids called *O*-mannosylation and is initiated at the ER. Unlike *N*-glycosylation and *O*-fucosylation, a consensus sequence is not required. This monosaccharide transfer, from dolichol-phosphate, is completed by a family of protein *O*-mannosyltransferases. While the newly synthesised glycoprotein moves out of the ER and through the Golgi further additions can be made resulting in diverse and branched glycans. *Saccharomyces cerevisiae* has been utilised to understand and characterise *O*-mannosyl glycans. It is the only type of *O*-glycosylation which occurs in yeast making it an ideal candidate to study to better understand their synthesis (Neubert and Strahl 2016). However, this

post-translational modification is prevalent in higher organisms and accounts for a third of all O-linked glycans in the brain (Varki et al. 2009).

Recent studies have revealed that there are at least 23 distinct *O*-mannosyl glycans playing crucial roles in congenital muscular dystrophies and cancers (Praisman and Wells 2014). Dystroglycan is an extracellular matrix receptor in epithelial tissues where it mediates cell-matrix interactions and it crucial for tissue morphology. Dystroglycan is heavily glycosylated with one *O*-mannosyl glycan, essential for ligand binding. Mutations disrupting the *O*-mannosylation pathway impairs dystroglycan function and can result in muscular dystrophies (Wells 2013). In prostate cancer dystroglycan has loss of function as it is hypoglycosylated, due to down-regulation of glycotransferases (Esser et al. 2012; Hara et al. 2011).

1.2.1.3 Other types of linked glycans

Glycans are divided into different classes according to how they are linked to the polypeptide chain or lipid. N- and O- linked glycans are best understood and other types such as carbon linked (*C*-mannosylation) and glycolipids are often overlooked. *C*-mannosylation is the addition of a mannose sugar to the C2 carbon atom of a tryptophan (W) residue via a C-C bond. This modification occurs at the first tryptophan residue in the W-X-X-W/F consensus sequence where X is any amino acid and the last amino acid can be tryptophan or another aromatic amino acid like phenylalanine. This modification is unique as it is carbon linked but also because after the attachment of α -mannose there is no further extension. It is thought that *C*-mannosylation is involved in acceptor protein regulation but this has yet to be confirmed (Ihara et al. 2014).

Glycosphingolipids (GSLs) are the most common type of glycolipid in vertebrates. They are a heterogeneous group of membrane lipids formed by a ceramide backbone linked, β -glycosidic, to a glycan. Numerous glycans can be linked to a variety of ceramide molecules giving rise to diverse compounds with different structures and biological functions (D'Angelo et al. 2013). GSL biosynthesis is initiated when a monosaccharide, glucose or galactose, is added to ceramide. Glucosyl ceramide (GlcCer) is the precursor for 90 % of mammalian GSLs. Galactosyl ceramide (GalCer)

is the precursor for the remainder. GlcCer is synthesized at the cytosolic side of the ER after which it is flipped to the lumen side and is elongated by glycosyltransferases (Lingwood 2011). These glycolipids mediate cell-to-cell recognition and are essential for growth and development and have been implicated in a number of diseases.

1.2.2 Prokaryotic glycosylation

Bacteria and archaea can post-translationally modify proteins with N- and O- linked glycans. In *Eukarya* it is estimated that over two-thirds of all proteins are glycosylated. However, an estimate for the same in *Prokarya* is not available. Prokaryotic glycosylation is not understood to the same degree, as it is in eukaryotes, due to the enormous variability in both glycan structure and synthesis (Schäffer and Messner 2017). Protein glycosylation was once thought to be restricted to eukaryotes as prokaryotes have a comparatively short life span and they lack cellular organelles, such as ER and Golgi apparatus, which are required for eukaryotic glycan synthesis (Upreti et al. 2003). Carbohydrates were not considered part of prokaryotic proteins until Mescher and Strominger (1976) purified a glycoprotein from the surface (S-) layer of the halophile archaea *Halobacterium salinarium* which had glycans accounting for 10 to 12 % of the protein's molecular weight. Bacteria and archaea can have N- or O-linked glycans, however O-linked glycans are the predominant type in bacteria and N-linked glycans are the predominant type in archaea.

Prokaryotic glycans are far more diverse, structurally, than eukaryotic glycans as they can be assembled from many more monosaccharide building blocks. However, they do have some similarities. Many bacterial N-linked glycans do require a consensus sequence, e.g. Asp-Ser and Asp-Thr in *Chryseobacterium meningosepticum*, although it can differ from species to species. Prokaryotic glycans are classified into 5 types depending on their location; surface-layer glycoproteins, membrane-associated glycoproteins, cell-surface glycoproteins (associated with the pili and flagella), cellular glycoproteins and secreted glycoproteins (Upreti et al. 2003).

Glycoproteins in eukaryotes are essential for many biological processes including protein function and stability, intracellular signalling and cell adhesion to name but a

few. It is thought that glycoproteins in prokaryotes have similar functions although much has yet to be confirmed (Upreti et al. 2003).

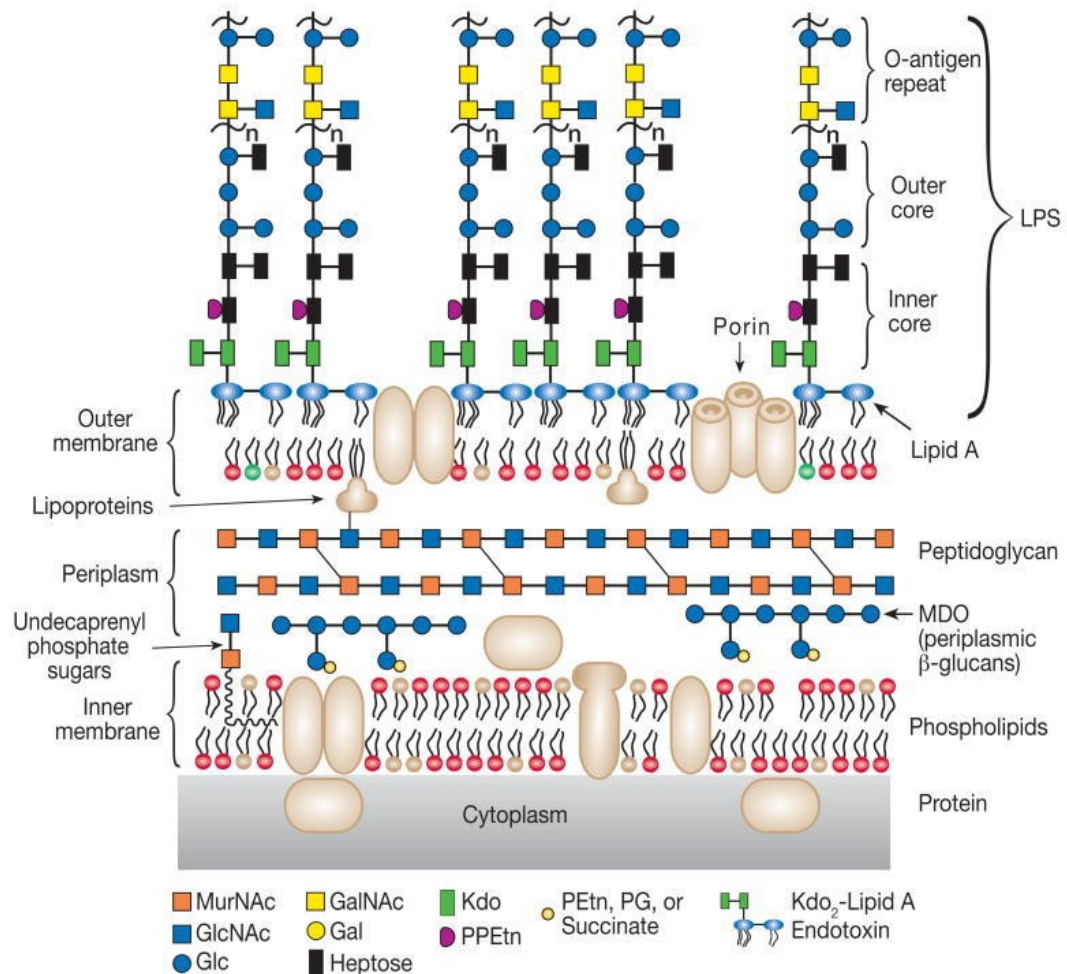


Fig. 1.9: Cell wall of a Gram-negative bacterium. Between the outer and inner membrane is the periplasm which is occupied by peptidoglycan (GlcNAc and MurNAc copolymer) and β -glucans. The outer membrane is covered in lipopolysaccharide (LPS) which contains multiple *O*-antigen repeats (Varki et al. 2009).

The pili of Gram negative bacterium *Neisseria meningitidis* are coated with glycans and when these glycans are sialylated there is an increase in its virulence. The level of serum resistance among *N. meningitidis* strains has been shown to correlate with their strain specific LPS sialylation (Kugelberg et al. 2008). Similarly the increase of LPS sialylation of *Neisseria gonorrhoea* is related to a corresponding increase in its complement resistance. Sialic acid residues are important for infectious bacteria as they camouflage the bacterium. The immune system of the host identifies the sialic acid

coated LPS as self-antigen. Many studies have shown that the glycosylation of proteins are key facets of the virulence and immunogenicity of infectious pathogens (Upreti et al. 2003; Gasparini et al. 2015).

1.3 Biological roles of glycans

The various glycosylation pathways in eukaryotes yield an enormous quantity of glycan structures and due to their prevalence in all cells, over 70 % of the eukaryotic proteome is thought to be glycosylated, their functions are probably therefore vast (Dell et al. 2010). The importance of glycans and their biological roles has been previously stated, however, some of their key functions are discussed below including deficiencies in glycosylation and the resulting maladies.

1.3.1 Protein structure and folding regulation

N-linked glycosylation has a direct role in protein folding. During *N*-glycan synthesis, in the ER, two chaperones, calnexin (CNX) and calreticulin (CRT), bind to the monoglucosylated *N*-glycan and keep it in the ER until it is correctly folded. Proteins that do not oligomerise or fold correctly are tagged by these chaperones where they are translocated to the cytoplasm and destroyed by proteases in a process termed ER-associated degradation (ERAD). The most common destruction tag is ubiquitin, a small protein which is attached to lysine residues (Ellgaard and Helenius 2003). Misfolded proteins can accumulate if glycosylation is inhibited or suppressed. CNX and CRT are 65 kDa and 46 kDa proteins, respectively, and have 45 % sequence similarity. During cell stress and ER stress, e.g. heat shock and amino acid deprivation, their expression is induced. Although they bind identical glycans, where they bind glycans differs. CRT binds glycans when they are located away from the ER inner membrane, whereas CNX will bind glycans close to it. CRT is found in the lumen of the ER, cytosol, nucleus and plasma membrane and is a chaperone of glycoprotein folding but also an integral part of the ER calcium buffer system. CRT is thought to be responsible for about half of the calcium in the ER and is kept in the ER as it contains KDEL sequence at its *C*-terminal (Caramelo and Armando 2015).

The glycans on a glycoprotein are bound by CNX and CRT during the protein folding process, see Fig 1.10. Their presence on folded proteins contributes to maintaining a correctly folded state by increasing the thermodynamic stability of the protein. The sugars in the attached glycan can form new interactions, hydrogen bonds, with the amino acid side chains thus maintaining protein structure (Mitra et al. 2003; Shental-Bechor and Levy 2008).

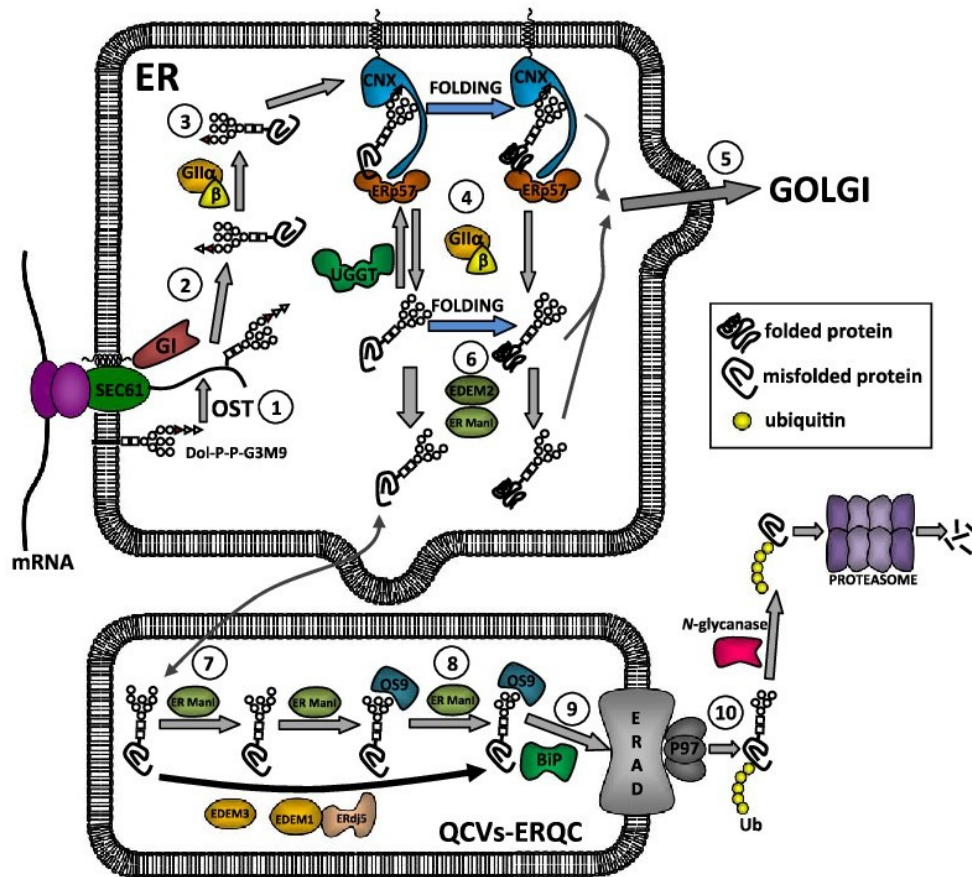


Fig. 1.10: Glycan transfer and glycoprotein processing in the endoplasmic reticulum. Oligosaccharyltransferase (OST) complex transfers the glycan from Dol-P to a nascent protein (1) and glucose trimming occurs (2) and (3) before CNX or CRT (not shown) bind and retain the glycoprotein in the ER while folding occurs. The remaining glucose residue is cleaved (4) and properly folded proteins can leave the ER (5). A mannose residue can also be trimmed before the glycoprotein leaves the ER (6) but if the protein is misfolded additional mannose residues are cleaved (7), disulphide residues are reduced (8) and the misfolded glycoprotein is labelled with ubiquitin and exported from the ER-derived quality control vesicle (9) to the cytosol for further glycan removal (10) and finally complete protein annihilation by proteasomes (Caramelo and Armando 2015)

1.3.2 Cell adhesion and cell signalling

Numerous secreted proteins, e.g. hormones and cytokines, are decorated with glycans which can alter their activity when binding to receptors. Glycan changes will therefore alter how these secreted proteins interact with and activate signalling proteins such as G proteins. Glycosylation is directly involved with the cellular response to external factors by regulating signalling pathways (Arey 2012). The insulin receptor, a type of tyrosine kinase, is glycosylated with numerous N- and O- linked glycans. A decrease in the availability of glucose has been shown to affect the O-glycans on this receptor but not the N-glycans. Mutational studies on the O-glycan sites on the insulin receptor have identified significant functions as the level of O-glycosylation is directly linked with its level of phosphorylation. An increase in O-glycosylation in pancreas β -cells leads to an increase in β -cell apoptosis. The glycaemic state of a cell can control the glycans displayed on the receptor thereby regulating its function (D'Alessandris et al. 2004; Arey 2012).

Cell-cell communication and cell adhesion is essential for the formation of three-dimensional tissues in multicellular organisms. There are three broad classes of proteins involved in cell adhesion; cell adhesion receptors, extra-cellular matrix (ECM) proteins and cytoplasmic membrane proteins, most of which are glycosylated (Gu et al. 2012). N-glycosylation has been identified as a key component of cell adhesion and N-glycan changes has been shown to affect cell-cell interaction thus affecting cell-cell communication, cell differentiation, migration and ultimately tumour invasion (Gu et al. 2009). Research by Guo et al. (2002) showed that the overexpression of a glycosyltransferase, N-acetylglucosaminyltransferase V (GnT-V), in human fibrosarcoma HT1080 cells resulted in increased cell migration and invasion due to N-glycan changes on $\alpha 5\beta 1$ integrin.

1.3.3 Immune functions of glycans

There are many glycan-dependant interactions that are essential components of the innate and adaptive immune system; immune cell trafficking and activation, T-cell/B-cell receptor signalling, antibody function and pathogen recognition, to name but a few

(van Kooyk et al. 2013). Dendritic cells (DCs) are the central link between the innate and adaptive immune responses. They have a role in antigen screening and the subsequent uptake and antigen presentation to T cells. DC surface sialylation is involved in this antigen uptake and presentation to activate T cells. The degree of sialic acid at the DC surface changes during DC differentiation and activation although this isn't completely understood. During DC differentiation sialyltransferase is tightly regulated (Crespo et al. 2008). Sialic acid residues covering host cells prevent autoimmune reactions, i.e. pathogen recognition of self-cells. It has been extensively shown that during the initial inflammation period cell surface sialic acid increases both to protect cells from pathogens but also to assist the immune system distinguishing between self and non-self cells and antigens (Crespo et al. 2013; Yasukawa et al. 2015).

Mannose-binding lectin (MBL also known as mannose-binding protein) binds to glycans displayed at the cell surface of microorganisms. It is synthesised in the liver and predominantly circulates in serum but is also detected in other fluids, e.g. synovial and amniotic (Taylor and Drickamer 2006). It provides a type of innate immunity by distinguishing between the glycan patterns on host cells and those on pathogens. MBL, despite its name, binds mannose, fucose and GlcNAc but does not bind galactose or sialic acid. MBL is a multimer of identical 32 kDa polypeptide chains, ideal for binding repeating glycan patterns that are found on the surface of microbes. MBL can activate the complement system and also mediate phagocytosis (Ip et al. 2009). It is an important component of innate immunity as reduced or loss of MBL activity is associated with severe recurring infections in infants as they are at a critical time when the maternally-derived antibodies are declining and their own immune system is immature (Auriti et al. 2017).

1.3.4 Cell surface glycosylation

All living cells are covered with a complex glycocalyx. Even enveloped viruses are coated with glycans from their budding cells. A glycocalyx seems to be a universal requirement for cellular life. Glycans offer increased complexity at the cell surface. If the cell surface was decorated solely with proteins it would be difficult for a host to evade a pathogen that had evolved to bind a cell surface protein, i.e. subtle amino acid

changes can severely alter protein structure and function (Varki 2011). Proteins at the cell surface, membrane proteins, mediate cell–cell interactions, adhesion, ion transfer, and the transmission of signals into and out of the cell. Glycans on membrane proteins can drastically impact their structure and therefore impede their cell surface function (Chandler and Costello 2016).

The variation in glycans at the cell surface can have many functions, e.g. to display a recognised pattern or conversely to mask a specific glycan pattern. Numerous glycan biomarkers can be displayed at the cell surface which may correlate with cell health, differentiation and disease (Ohtsubo and Marth 2006). An increase in shortened *O*-glycans, Tn antigen, on the cell surface can predict reduced survival rates of certain cancer patients (Kabata and Amano 2005). Glycans at the cell surface are not recognised the same way by glycan-binding proteins in glycan arrays. The cell surface is composed of complex glycan mixtures which can interact with both each other, glycan-glycan interactions, and with proteins. Whether a glycan is detected at the cell surface depends on the composition of other glycans on the same cell surface, three different glycan-binding proteins that recognise α 2,6-sialic acid bind identically on glycan arrays but have different binding patterns at the cell surface of erythrocytes (NRC 2012).

Cell surface glycans are directly involved in many interactions with both other cells and proteins. The glycocalyx is not a defined set of glycans at the surface but rather the glycans displayed at the cell surface at any given time. This carbohydrate coat is not fixed but changes with cell growth, stress and death which fluctuate depending on the cellular environment, e.g. nutrient availability and pH. Cell surface glycosylation can therefore be used as an indicator of cell health and even reveal the nature of glycosylation on secreted proteins. Research by Davies (2012) tested the variability of cell surface glycosylation using Chinese hamster ovary (CHO) clones. Their work indicates that the glycan core is conserved among all clones, as it is essential for cellular function. Con A binding, which binds the α -mannose residues that form the core glycan structure, was conserved across all clones and correlated with cell proliferation. However, clones did exhibit considerable differences in glycan residues which are not part of the core glycan structure. Binding of RCA I, β 1-4-galactose binder, was highly variable among the clones, differed by up to 3.2 fold, and did not correlate with cell

proliferation. Similar work by Grainger and James (2013) showed that enhanced feeding strategies for CHO cell lines resulted in significant changes to cell surface RCA I binding. The RCA I cell surface binding also correlated strongly with the galactose content on the mAb being expressed. This interesting examples demonstrates how the glycans at the cell surface may provide information on the glycans on the product.

Franz et al. (2006) probed the cell surfaces of peripheral blood mononuclear cells with a panel of lectins to differentiate between healthy and dying cells. They assessed lectin binding using a flow cytometer and found that certain lectins, *Griffonia simplicifolia* II (GSL II), *Narcissus pseudonarcissus* (NPL), and *Ulex europaeus* I (UEA I), bound preferentially to dying cells. They demonstrated that the glycocalyx changes with cell health, i.e. certain glycan epitopes become more or less frequent, and that these changes can be detected with lectins and subsequently measured using flow cytometry.

1.3.5 Glycosylation and disease

Glycosylation is a vital cellular process and complications with glycan synthesis or transfer can lead to diseases which can affect nearly every organ system (Freeze 2013). The recent advances in genetics, particularly next generation sequencing, has helped identify glycosylation disorders. There are over 100 different Congenital Disorders of Glycosylation (CDG) currently known of which more than 80 % impact neurological function (Freeze et al. 2015). As up to 2 % of human genes are thought to be involved in glycosylation, there are many opportunities for mutations to arise resulting in disease, see Fig. 1.11 (Campbell and Yarema 2005; Freeze 2013).

CDG patients are identified by their irregular glycosylation, particularly the under sialylation of serum glycoproteins, predominantly serum transferrin (Leroy 2006). CDG are grouped broadly depending on whether the assembly of the lipid linked oligosaccharide is disrupted, CDG Type I (CDG-I), or whether further glycan processing and trimming in the ER and Golgi is disrupted, CDG Type II (CDG-II) (Hennet 2012). Recent work by Timal et al. (2012) utilized whole-exome sequencing to identify genes for 6 previously unsolved CDG-I patients. Their results also included

the first CDG-I linked to a sex chromosome, mutation in *ALG13* on chromosome X. *ALG13* encodes a UDP-*N*-acetylglucosaminyltransferase subunit which heterodimerises with asparagine-linked glycosylation 14 homolog forming a UDP-GlcNAc glycosyltransferase. This glycosyltransferase catalyses the addition of the second sugar in *N*-glycan biosynthesis (NCBI 2017). The *ALG13*-CDG disorder results in several phenotypes including; hydrocephalus, epilepsy, dysfunction of the liver, microcephaly, recurring infections and early death (Freeze 2013).

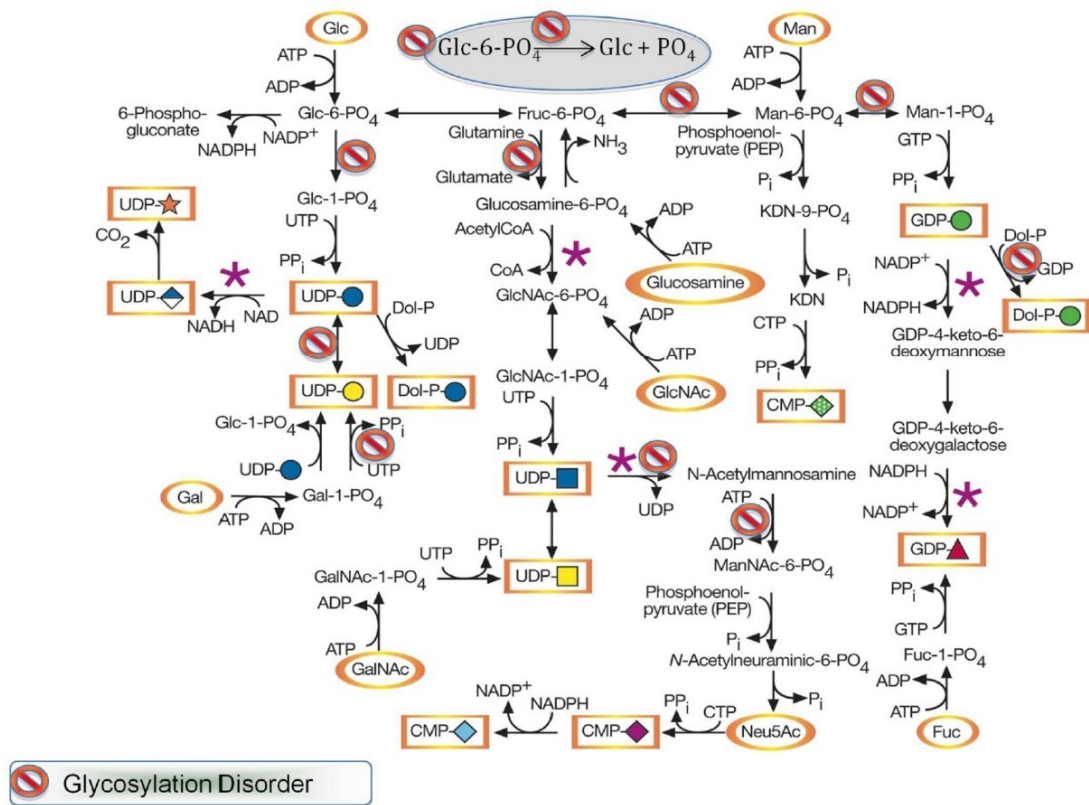


Fig. 1.11: Biosynthesis of monosaccharides and human glycosylation disorders. The reactions within in the ER are shown by the grey oval on top and all other reactions are presumed to occur in the cytoplasm. Known instances of metabolic regulation are identified with purple asterisks (Freeze 2013).

Aberrant glycosylation is also associated strongly with cancer. Cell surface glycans are essential for cell-cell communication and immature *O*-glycans at the cell surface, exposing Tn antigen (GalNAc-O-Ser/Thr), are associated with metastatic cancer due to increased cell adhesion to endothelium (Bapu et al. 2016; Radhakrishnan et al. 2014). Similarly, an increase in sialylation at the cell surface is associated with malignancy

and poor prognosis in cancer patients. Cell-cell adhesion is interrupted which leads to cell detachment from the tumour by electrostatic repulsion due to increased negative charges (Seidenfaden et al. 2003; Munkley and Elliott 2016). Other glycosylation disorders include glycosphingolipid (GSL) storage diseases. GSLs accumulate in the lysosomes which is primarily caused by mutations in glycosidases. Gaucher's disease, the most common GSL storage disease, is a rare autosomal recessive genetic disease caused by a mutation in β -glucocerebrosidase resulting in the accumulation of GlcCer in macrophages. These cells, termed Gaucher cells, then begin to infiltrate the bone marrow, spleen and liver causing a variety of symptoms; severe pain, osteoporosis and skin pigmentation changes (Varki et al. 2009; Stirnemann et al. 2017).

1.4 Therapeutics glycoproteins

Therapeutic glycoproteins are the fastest growing class of products within the biotechnology industry. These products are important for the treatment of diseases and they include protein class products, i.e. hormones, cytokines, enzymes, enzyme inhibitors, fusion-proteins, blood clotting factors, and monoclonal antibodies (mAb) (Zhang et al. 2015). Global therapeutic protein sales have been rapidly increasing the past few decades and in 2013 they were approximately \$140 billion (Walsh 2014). Table 1.2 shows the variety of glycosylated biopharmaceuticals and the broad range of illnesses they treat.

Table 1.2: Therapeutic glycoproteins

Class	Brand (Drug) name	Description	Medical use
<i>Antibodies</i>	Avastin (bevacizumab)	Inhibits VEGF	Colorectal and other cancers
	Heceptin (trastuzumab)	EGFR inhibitor	Breast Cancer
	Humira (adalimumab)	TNF α inhibitor	Rheumatoid arthritis
	Remicade (infliximab)	TNF α inhibitor	Rheumatoid arthritis
	Opdivo (nivolumab)	Human anti-PD-1	Stage 2, 3 and 4 melanoma
	Yervoy (ipilimumab)	Human anti-CTLA-4	Stage 2, 3 and 4 melanoma
<i>Hormones</i>	Luveris (lutropin alfa)	Rh luteinizing hormone	Female fertility issues
	Thyrogen (human TSH)	Thyroid-stimulating hormone	Thyroid cancer
<i>Blood factors</i>	Advate (factor VIII)	Human FVIII	Hemophilia
	NovoSeven (factor VIIa)	Human FVIIa	Hemophilia
<i>Other</i>	Elelyso (Taliglucerase alfa)	Taliglucerase	Gaucher disease
	Epogen (epoetin alfa)	Human erythropoietin	Anemia
	Enbrel (etanercept)	TNF inhibitor fusion protein	Rheumatoid arthritis
	Rebif (IFN β 1a)	Human INF β 1a	Multiple sclerosis

Glycoproteins can be highly glycosylated and the glycans can contribute to a significant portion of the glycoprotein size and mass. The presence of glycans can alter glycoprotein properties such as stability, plasma residence time, activity and provide steric protection from proteases e.g. O-linked glycans at the hinge region of IgA increase protease resistance and hypersialylated glycans mask galactose residues and reduce immunogenicity (Byrne et al. 2007; Taylor and Drickamer 2006). There have been many studies to determine the exact effect that glycans have on protein properties. A common method of analysis is to compare a glycoprotein with its deglycosylated form i.e. a glycoprotein treated with PNGaseF (Skropeta 2009). The effect that glycans

have on protein function can vary for every protein. The presence of glycans might alter protein function and not its stability *in vivo* and vice versa.

Immunoglobulin G (IgG) is a glycoprotein consisting of two identical heavy chains and light chains, see Section 1.10.2 for additional information. There is one glycan on each of the two heavy chains at Asn-297. This glycan has a heptapolysaccharide core containing GlcNAc and mannose. Fucose, GlcNAc, galactose and sialic acid residues are also found on this glycan but only 5 % of serum IgG contains this fully completed complex *N*-glycan with sialic acid terminals (Kaneko et al. 2006). The sialylated glycans on IgG doesn't affect its pharmacokinetic profile but the anti-inflammatory properties of IgG are entirely dependent on this terminal sialylation (Anthony et al. 2008). By assigning certain regulatory functions to specific glycan epitopes, evolution has created a mechanism by which protein function can be altered significantly without the requirement of a change in the protein amino acid sequence, i.e. a modification to a gene encoding a specific protein (Lauc et al. 2014).

Human EPO has 3 *N*-linked glycans and an *O*-linked glycan which can contribute up to 40 % of its molecular mass. These glycans are essential for the *in vivo* potency of EPO. Deglycosylated EPO has no *in vivo* potency but it is threefold more potent *in vitro* (Bork et al. 2009). The glycans on EPO are not required for protein function but are essential for stability and *in vivo* biological activity. Glycans can alter various parameters of a protein differently e.g. a modified form of EPO with two additional *N*-glycans has an extended serum half-life but reduced receptor binding affinity (Sethuraman and Stadheim 2006). The glycosylation of proteins generally improves their stability, thermodynamic properties, secretion, potency and serum half-life (Byrne et al. 2007). There are exceptions to this rule and improvements to these properties might not only be caused by the presence of glycans but also by their position on the protein.

1.5 Glycan analysis

It is of great interest to analyse glycans attached to glycoproteins as they can alter protein function, bioactivity, serum half-life and immunogenicity. Glycan analysis is becoming increasingly more important as the release of glycoprotein biosimilars is

further emphasising the need for robust means to interrogate glycans to demonstrate glycoprotein efficacy and safety at the product evaluation stage (Planinc et al. 2016). Glycan structure and composition is complex due to linkages and branching between monosaccharides. This, coupled with the fact that glycan building blocks are extremely similar, i.e. galactose is an epimer of glucose, which makes their analysis unsurprisingly difficult. There are many glycan analysis methods, see Fig 1.12, which are broadly grouped depending on the unit of interrogation, i.e. whole glycoproteins, released whole glycans or released monosaccharides.

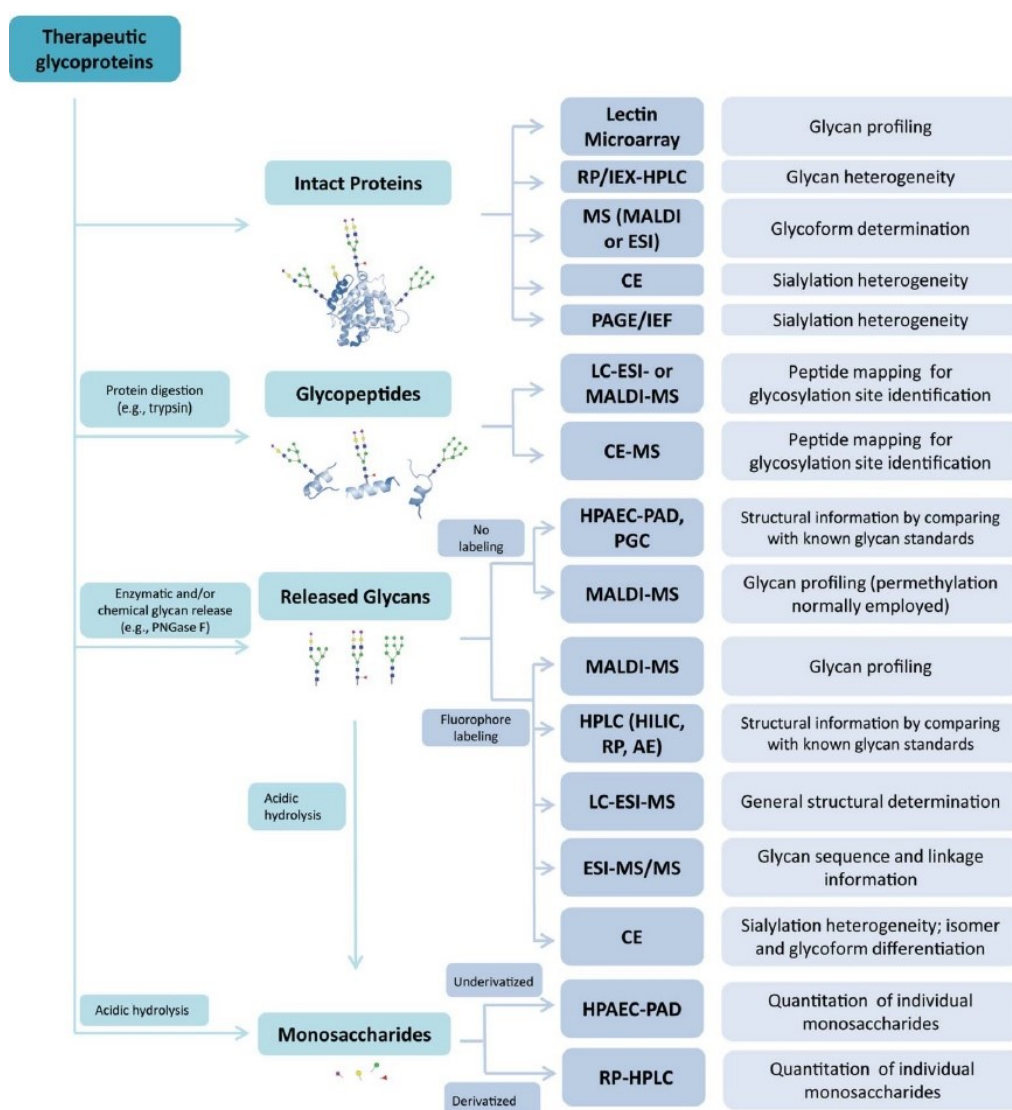


Fig. 1.12: Methods for glycan analysis of therapeutic glycoproteins. Glycans can be assessed in multiple ways; as whole glycans on whole proteins or peptides, whole glycans removed from proteins or monosaccharides removed from glycans (Zhang et al. 2015).

The biopharmaceutical industry utilises many mammalian and non-mammalian hosts to produce therapeutic glycoproteins both of which may contain non-human type glycans, e.g. *N*-glycolylneuraminic acid in mammalian hosts and terminal α -Gal or xylose in plant hosts. The glycoprotein Eprex (Taliglucerase alfa), see Table 1.2, for the treatment of Gaucher disease is produced in carrot cells and its glycans, all possessing terminal mannose residues, account for 7 % of its molecular weight (EMA 2017; Fox 2012). Glycosylation is implicated in many biological functions and diseases, see Section 1.3, making glycan analysis of vital importance in clinical and diagnostic settings as well as clone selection in upstream biopharmaceutical environments.

1.5.1 Glycan analysis using antibodies

There are many anti-glycan antibodies that are used as part of the innate immune system. These include antibodies against sialoglycans, blood group antigens A and B and anti-Gal antibodies which account for approximately 1 % of all human serum IgG (Shilova et al. 2015; Galili 2013; Dotan et al. 2006). Antibodies can bind glycans with greater affinity than lectins but not many applications using anti-glycan antibodies have so far been described (Gemeiner et al. 2009). Some highly specific anti-glycan antibodies have been produced. A mouse IgM mAb with specificity for O-linked GlcNAc was reported by Comer et al. (2001) showing no cross-reactivity with closely related glycan structures. However, this same anti-glycan antibody (CTD110.6 mAb) was more recently shown by Tashima and Stanley (2014) to bind not only O-linked GlcNAc but also terminal GlcNAc on N-linked glycans. Anti-glycan antibodies are superior probes in a clinical situation where a specific glycan epitope is to be detected which relates to a disease state, e.g. there is no lectin specific for binding the sialyl-lewis antigen (SLe^A) which is a tumour marker expressed in advanced epithelial cells. However, anti-glycan antibodies, generally, cannot distinguish whether they are binding a glycan antigen that is N-linked, O-linked or on a glycolipid (Varki et al. 2009). There are numerous other limitations of anti-glycan antibodies including their inability to differentiate between specific monosaccharide linkages, e.g. α 2,3-linked and α 2,6-linked sialic acid, and the difficulties with their production, i.e. it can be difficult for a host to generate antibodies against common glycan determinants which includes self-antigens (Gemeiner et al. 2009).

1.5.2 Glycan analysis using CE, MS and HPLC

Capillary electrophoresis (CE) is a high-resolution separation technique using submillimeter diameter capillaries which can be applied to many biological molecules separating them according to their charge-to-mass ratios. CE can nearly completely resolve whole glycoproteins. Kinoshita et al. (2000) reported the successful separation of serum α_1 -acid glycoprotein into its constituent glycoforms. However, they encountered problems when trying to resolve recombinant EPO due to non-specific adsorption of the glycoprotein to the capillary cell wall. This is a common problem with CE during glycoprotein separation. CE is a useful technique for the separation of glycoforms however, it is not informative regarding the type of glycans attached to the proteins. Other analytical techniques such as mass spectrometry (MS) and high-performance liquid chromatography (HPLC) are more powerful which can provide a greater separation of glycoforms, a characterisation of the glycans and their relative quantification (Geyer and Geyer 2006).

Mass spectrometry is used extensively for the analysis of biological samples. More specifically it is routinely used to analyse the exact nature of glycosylation on biomolecules. During MS the sample is ionised in the gas-phase and injected into an electric field for analysis. The sample is then separated according to its mass-to-charge ratio. The protein sample can be prepared in solution or embedded in a matrix. The two main MS methods that correspond to these preparations are electrospray ionisation (ESI) and matrix-assisted laser desorption/ionisation (MALDI) respectively. The analysis of glycoproteins using MS may be difficult to perform due to the extent of the glycan heterogeneity. Certain MS formats, such as MALDI-time-of-flight (MALDI-TOF), are able to resolve small glycoforms, typically up to 40 kDa. However, Dillon et al. 2004 were able to successfully resolve whole IgG1 glycoforms, 146 kDa, using a combination of RP-HPLC and ESI-MS. Large glycoproteins with many glycans attached generally result in unresolved broad peaks (Geyer and Geyer 2006). This can be solved by releasing glycans from proteins, analysing them using HPLC and/or MS and comparing their mass to that of known glycans. However the release of glycans can be problematic. Enzymes, such as peptide *N*-Glycosidase F (PNGaseF) and endoglycosidase (EndoF), can cleave whole *N*-glycans from proteins but all *N*-glycans may not be accessible due to steric hindrance. The denaturation of the glycoprotein is

required for complete *N*-glycan release. The release of *O*-glycans is more difficult as they are a more diverse class of glycan and there aren't glycosidases available which are broad enough to remove all of them. They can be removed however, using chemical treatments such as alkaline β -elimination. During this process ammonium hydroxide or sodium hydroxide hydrolyse the β -hydroxyl groups of serine or threonine releasing the *O*-linked glycans. This is not a simple release as it takes between 8-16 h to complete during which the glycan can be further degraded at the reducing end in what is known as 'peeling' reactions – although this can be lessened with a reducing agent such as sodium borohydride (Sigma 2017). In addition to unwanted glycan degradation, other protein modifications can be removed during the release of *O*-glycans, such as methylation and sulfation. This along with the complete destruction of the protein backbone can lead to the loss of biologically important information about the sample (Geyer and Geyer 2006; Morelle and Michalski 2007). Fig. 1.13 displays the range of highly similar glycans that can be separated using mass spectrometry.

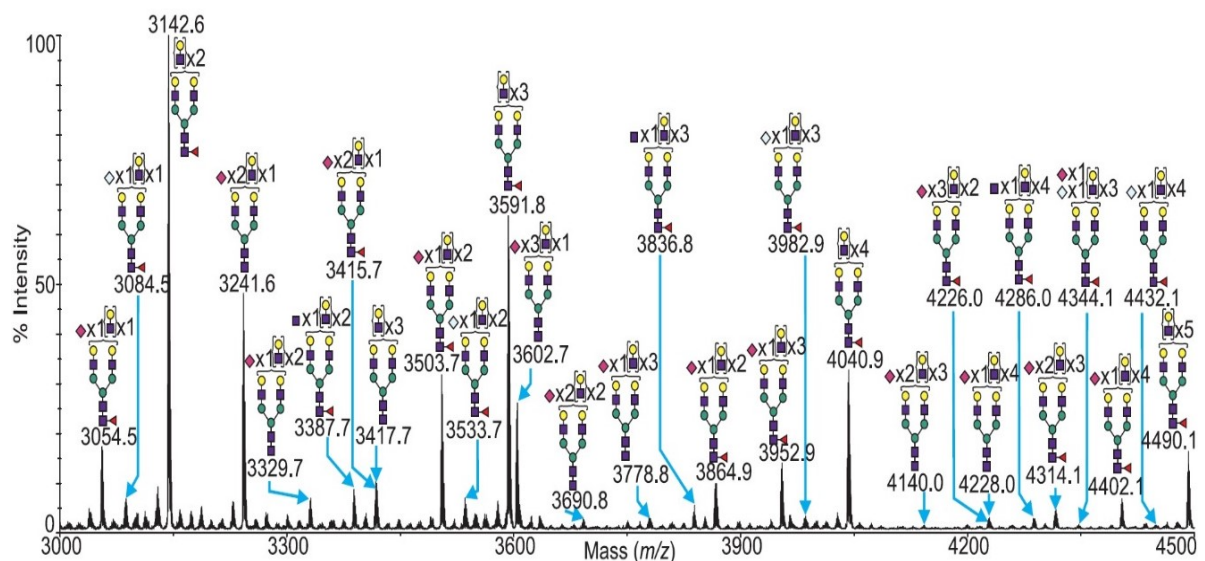


Fig. 1.13: MALDI-TOF MS profiles of the *N*-glycans released from lysed wild type sCHO cells. CHO cells were disrupted by sonication and *N*-glycans were release using PNGaseF (North et al. 2009).

High-performance liquid chromatography (HPLC) is a type of column chromatography where a sample in a solvent (mobile phase) is pumped at high pressure through a packed column (stationary phase). Sample components with greater interaction with the stationary phase, e.g. hydrogen bonding, will migrate more slowly through the column.

There are many HPLC techniques; size exclusion (SE), anion exchange (AE), normal-phase (NP) and reverse phase (RP), which are widely used, typically in combination, to separate complex glycoforms. Normal-phase HPLC can be used for the separation of most *N*-glycans resulting in high resolution. Other HPLC formats such as high pH AE are preferred for the separation of negatively charged glycans, e.g. highly sialylated glycans. The strong base conditions (pH 13.0) can finely resolve glycans. In this environment the glycans are present as oxyanions and can interact with the amino groups in the stationary phase. There is a downside to the increased separation achieved in basic conditions. This environment can cause the epimerisation of GlcNAc to ManNAc (Gohlke 2002). HPLC methods can accurately resolve heterogeneous glycan mixtures but the identification of said glycans cannot be determined using HPLC retention times. Similarly conventional MS separation methods struggle to distinguish certain stereoisomers, e.g. mannose, glucose and galactose, due to identical masses (Yang et al. 2016). Sample fragmentation analysis using MS can infer glycan structural information but high-end equipment as well as experienced users are required. Alternatively, sequential trimming of glycan/glycoprotein samples using a defined order of glycosidases can be used to elucidate additional glycan structural information (Sheridan 2007). However, this technique also has limitations, i.e. insufficient glycosidases specific for every glycosidic linkage. For the separation of specific glycoforms, glycans differing in only one glycosidic linkage for example, nature's glycan binding proteins, lectins, can be employed.

1.5.3 Glycan analysis using lectins

Lectins are proteins that can recognise and bind reversibly to specific glycan structures. They can discriminate the positions of the glycosidic linkages between monosaccharides subunits and are therefore extremely useful tools for glycan analysis. Their history, sources and purification are detailed in Section 1.6. Lectins are commonly used to pull out or pre-concentrate a glycoprotein prior to investigation by MS using lectin affinity chromatography (LAC). During LAC, lectins have been immobilized onto silica and Sepharose beads producing a lectin affinity resin which can reversibly bind to glycoproteins. The separation of glycoforms can be achieved with a gradient elution of a specific free sugar (O'Connor 2017). A purified glycoprotein can be

characterised using a plate based assay called enzyme-linked lectin assay (ELLA). Large numbers of lectins can be used together in a lectin microarray to provide detailed information about glycoproteins and cell surface glycans. Other methods to investigate the cell surface include Lab in a trench (LiaT) (see Section 1.5.3.3), fluorescence microscopy (see Section 1.6) and flow cytometry (see Section 1.7). All three of these techniques are extremely compatible with the lectin based analysis of glycans.

1.5.3.1 Enzyme-linked lectin assay (ELLA)

The ELLA is a multiwell plate assay which is analogous to the common ELISA. This assay can be used to analyse glycoproteins and study lectin-glycan interactions. During the development and production of novel recombinant lectins it is a useful tool for assessing their specificity and activity. The ELLA was first described by McCoy et al. (1983) to detect glycoproteins bearing specific carbohydrate residues. The assay was later developed, particularly optimisation of the blocking step, by researchers here at DCU (Thompson et al. 2011). Recombinantly produced lectins and commercial plant and fungal lectins, which are biotinylated, can be used in the ELLA, Fig 1.14.

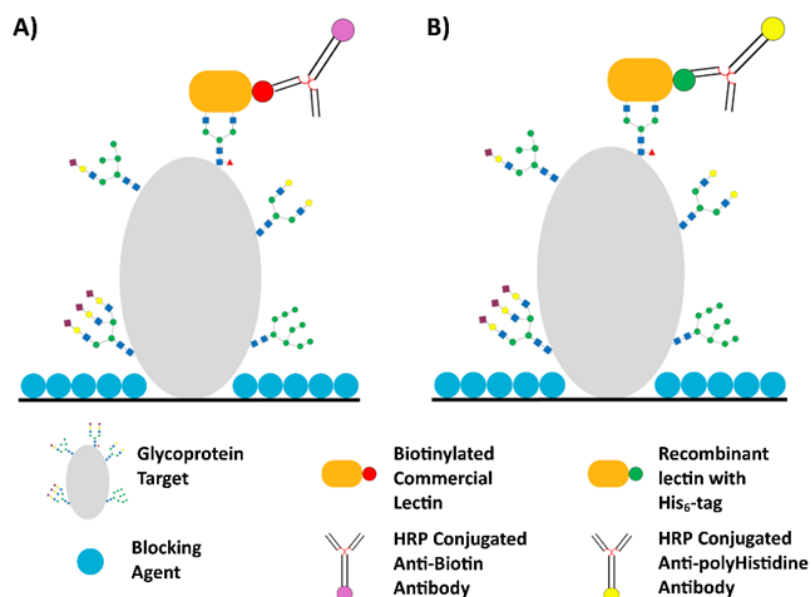


Fig. 1.14: Schematic of an ELLA. A glycoprotein target is immobilised on the plate surface after which the plate is blocked with 0.5 % PVA in TBS. Lectins are added to probe the glycoproteins which are subsequently detected by antibodies. **A)** Probing glycoproteins with biotinylated commercial lectins. **B)** Probing glycoproteins with His₆-tagged recombinant lectins. Image created using Microsoft Publisher 15.0.

This assay is versatile and can be easily modified to best suit a particular analytical need. The ELLA was optimised by Westgeest et al. (2015) for the rapid analysis of human influenza viruses. They coated a plate with fetuin, a glycoprotein with sialic acid capped glycans, and added wild-type influenza A virus. Neuraminidase (NA), an enzyme which can cleave sialic acids, is the second most prevalent surface protein of the influenza virus. NA activity reveals terminal galactose residues which can then be detected using peanut agglutinin lectin (PNA). This modified ELLA is useful for testing antibodies for NA and also for monitoring antigenic drift of the human influenza virus.

Similarly, Kim et al. (2008) used a modified ELLA, antibody-based enzyme-linked lectin assay (ABELLA), for the analysis of glycans on recombinantly produced EPO. This assay is akin to a sandwich ELISA. An anti-EPO mAb was added to the plate to capture EPO from diluted cell culture supernatant which was then probed with lectins, MAL II and SNA, to identify the nature of EPO sialylation, i.e. α 2,3- or α 2,6-terminal sialic acid. Non-lectin based analysis of glycoprotein sialylation requires the purification of the glycoprotein from cell culture supernatant, a greater amount of the glycoprotein and the release of glycans for analysis using HPLC and/or MS, all of which requires increased time and labour (Kim et al. 2008).

1.5.3.2 Lectin microarray

A lectin microarray is the immobilisation of multiple lectins on a solid support for high-throughput glycan analysis. Glycans from a variety of samples, e.g. glycoproteins, cell membranes, mammalian cells, bacteria and viruses, can be glycoprofiled using this technique, see Fig. 1.15 (Krishnamoorthy and Mahal 2009). It is a powerful rapid diagnostic tool useful in both clinical and research settings. Lectin microarrays have been used to glycoprofile cancer samples. Matsuda et al. (2008) presented an optimised lectin microarray for the glycoanalysis of tissue sections, consisting of approximately 500 cells, of adenocarcinoma and normal epithelia. This lectin microarray, particularly the lectin *Wisteria floribunda* agglutinin (WFA) was able to discriminate between cancerous and non-cancerous epithelial cells. Similarly a lectin microarray was used by Tateno et al. (2007) to investigate the cell surface glycosylation of CHO and its glycosylation-defective cell lines. They used a panel of 43 lectins to investigate cell

surface glycans of CHO, CHO-Lec1 (*N*-acetylglucosaminyltransferase I deficient) and CHO-Lec2 (CMP-sialic acid transporter deficient) cell lines. They observed, as expected, an increase in mannose specific lectins binding to CHO-Lec1 cells and a decrease in sialic acid specific lectin binding to CHO-Lec2 cells.

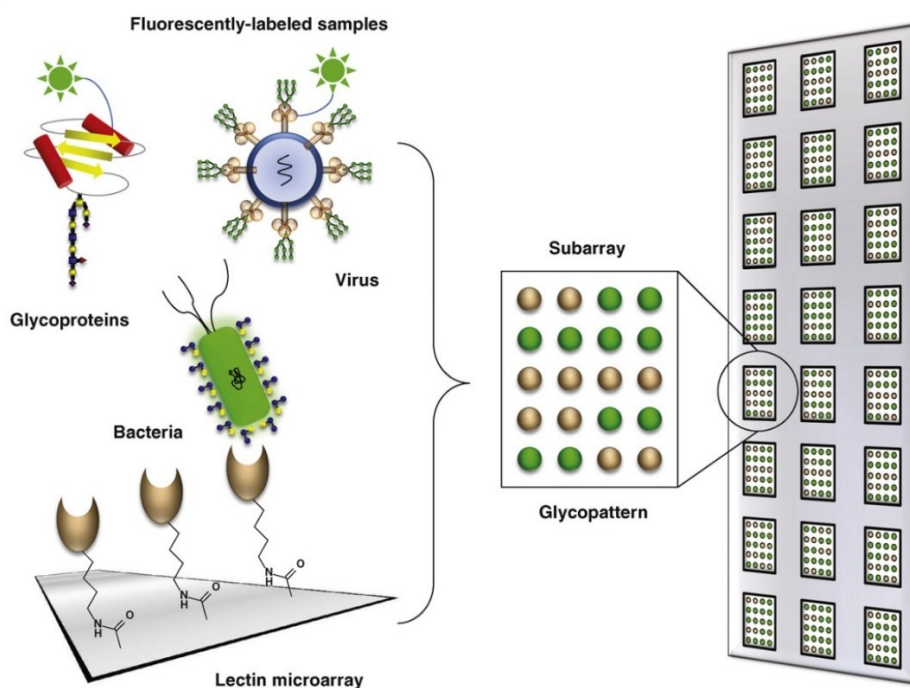


Fig. 1.15: Schematic of a lectin microarray. Lectins are immobilized onto glass slides which are *N*-hydroxysuccinimide (NHS)-activated. Glycan containing samples (shown as mammalian glycoproteins, bacteria, and HIV virus) are fluorescently labelled and added to the lectin microarray. Lectins will bind to the sample if it contains its specific glycan epitope. The binding pattern across the whole microarray provides an elaborate profile of the glycans in the sample. Many samples can be analysed simultaneously (Hsu and Mahal 2009).

The lectin microarray is a highly effective, cheap, rapid and versatile method of glycan analysis of both purified glycoproteins and whole cells without the need for the release of glycans which is a requirement of other analytical methods (Yue and Haab 2009). Multiple lectins can be used simultaneously to probe a biological sample generating a detailed and unique glycoprofile. Additionally the number of available lectins to immobilise on a microarray is ever increasing. This is largely due to the production of lectins using recombinant methods which allows for precise tailoring of lectin specificities (Gemeiner et al. 2009). Lectin microarrays are ideal for an initial screening

step to determine if there are biologically relevant glycosylation changes on cell samples. However, there are some disadvantages to using this approach. Certain glycan changes may go undetected if they are infrequent in a biological sample. The binding profile generated is typically only semi-quantitative, i.e. cells that are not captured by lectins are washed away and it is therefore difficult to determine what percentage of the sample is not accounted for.

1.5.3.3 Lab in a Trench

Lab in a Trench (LiaT) is a microfluidic platform in which cells are trapped in a shear-free environment by gravity settling where they can be observed and probed, Fig. 1.16. It is an ideal system for probing live cells with fluorescently labelled lectins (O'Connell et al. 2014). The trapped cells are probed with a fluorescently labelled lectin and viewed under a microscope. The bound lectin is eluted with the addition of a specific free monosaccharide and the same cells can be probed with a different lectin repeatedly.

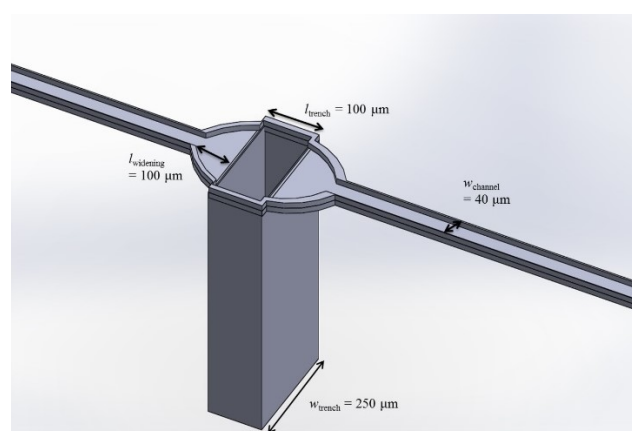


Fig. 1.16: Lab in a Trench platform. 3-D diagram of the cell capturing trench (O'Connell 2016).

The LiaT platform has many advantages over other more conventional methods for cell surface glycan analysis. Firstly, LiaT requires only small volumes of reagents to be used which reduces cost and helps with lectin/monosaccharide diffusion in the system. Secondly, the same cells are probed sequentially which allows for the approximate location of certain glycans to be determined by overlaying multiple fluorescent images.

Thirdly, cell surface glycans are not removed from the cells which again both decreases analysis times and cost as cells can be removed directly from culture, quickly washed and probed with lectins. Fourthly, cells are probed in a shear-free environment as they are captured due to gravity (O'Connell et al. 2014).

1.6 Fluorescence microscopy

Fluorescence microscopy is a powerful imaging technique which can be applied to any biological research setting and many clinical environments, e.g. cardiovascular, oncology, ophthalmology and urology (Nikon 2017). Fluorescence microscopy is based upon the excitation and emission of fluorescent molecules, called fluorochromes, in a sample. Fluorescence of this nature was first described by George G. Stokes in 1852 when he observed the mineral fluor spar, mineral form of calcium fluoride (CaF_2), emitting red light when it was excited by ultraviolet light. Stokes also observed that fluorescence emission always had a longer wavelength than the excitation light (Spring and Davidson 2016). The fluorescent molecules in the sample absorb light/photons and the electrons in the sample are excited to a higher energy level. When the excited electrons return to their ground-state, energy is lost in the form of vibration which results in the emission spectrum shifting towards longer wavelengths. This shifting of light between excitation and emission is referred to as Stokes' Shift. The discovery of a naturally occurring fluorescent protein, green fluorescent protein (GFP), has completely transformed cell biology (Snapp 2005). GFP and its many variants are commonly fused to non-fluorescent proteins, as they generally retain their ability to fold correctly and fluoresce, and viewed using fluorescence microscopy. The protein of interest can be studied in great detail and information regarding its cellular distribution and interaction with other proteins can be obtained (Snapp 2005; Johnson and Criss 2013).

Multiple fluorochromes can be combined in a sample to stain specific molecules or structures within the biological sample. For example, an antibody or lectin conjugated to a fluorochrome can target cell surface receptors or glycans and a different fluorochrome can stain DNA or the ER thus identifying cellular components. Several light filters are required in the microscope to ensure the desired excitation wavelength is applied to the sample and that the emission wavelength is detected in the appropriate

filter, see Fig. 1.17. When choosing fluorochromes it is important to check their excitation and emission spectra so that they can be clearly separated from each other and from the auto-fluorescence of the sample, see Fig. 1.18.

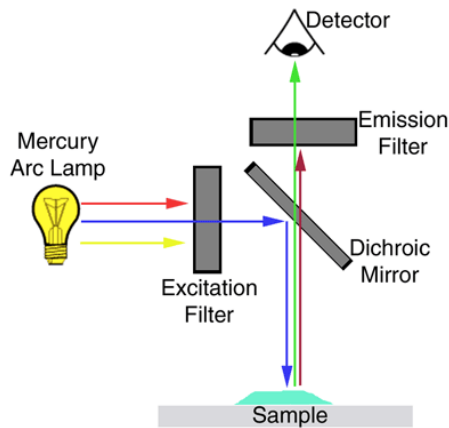


Fig. 1.17: Schematic of fluorescence microscopy. The excitation filter permits only a specific wavelength of light to pass. The dichroic beam splitter (mirror) reflects shorter wavelengths of light and allows longer wavelengths to pass. The emission filter ensures that only light emitted by a certain fluorochrome is detected (JIC 2017).

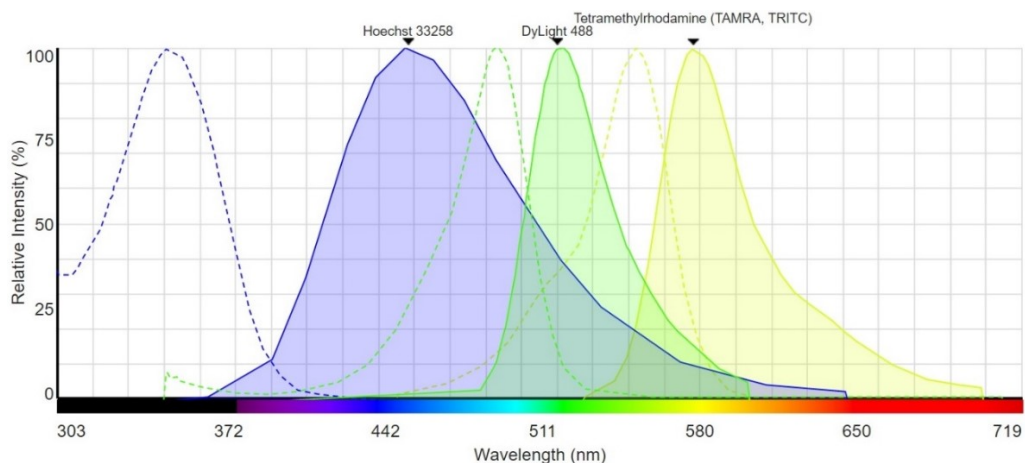


Fig. 1.18: Excitation and emission spectra of common fluorochromes. The excitation (dashed) and emission (solid) plots of Hoechst 33258 (Blue), DyLight 488 (Green) and TRITC (yellow/orange) are shown. Hoechst 33258 is a DNA binding fluorescent dye. DyLight 488 and tetramethylrhodamine isothiocyanate (TRITC) are flexible fluorochromes which are often conjugated to streptavidin for use with any biotinylated probes. Image generated using the online Fluorescence SpectraViewer provided by Thermo Fisher Scientific.

1.6.1 Fluorescence microscopy for glycan analysis

Fluorescence microscopy is a useful tool for investigating the cell glycocalyx. The sample preparation is simple compared to other glycan analytical methods which often require glycan release. A carefully designed panel of fluorochromes paired to lectins and additional probes, e.g. antibodies, and other cellular stains (DNA/ER specific), can elucidate much information about a cell sample, see Fig. 1.19.

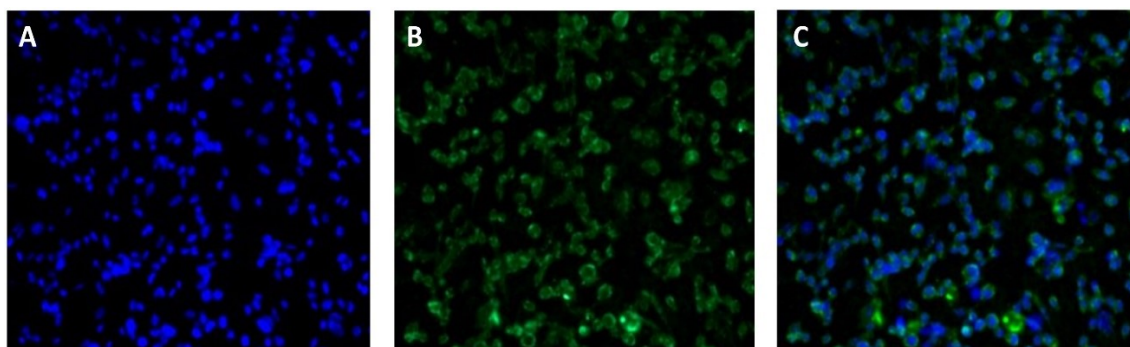


Fig. 1.19: Fluorescent microscope images of CHO cells probed with MAL II. CHO DP-12 cells were probed with the α 2,3-NeuNAc specific *Maackia amurensis* lectin (MAL II) lectin for 30 minutes and viewed with the Nikon Eclipse Ti inverted fluorescent microscope at 100x magnification. **A)** DNA is stained with Hoechst 33258 and viewed in the DAPI channel. **B)** MAL II (5 μ g/mL) was premixed with DyLight 488 and the cells viewed in the FITC channel. **C)** A merged image was created in ImageJ 1.49 (<http://imagej.nih.gov/ij/download.html>).

Fluorescence microscopy was used by Meesmann et al. (2010) to examine the sialic acid content of surface glycans of apoptotic lymphocytes. They observed a decrease in both α 2,6-linked and α 2,3-linked sialic acids at the cell surface after apoptosis induction in lymphoblasts with UV-B irradiation. Cells were probed with fluorescein isothiocyanate (FITC) labelled lectins and an ER stain, conjugated to phycoerythrin (PE), was used to identify cells irrespective of lectin binding. Fluorescence microscopy was also employed by Peiris et al. (2012) in developing a cancer biosensor. Metastatic, SW620, and non-metastatic, SW480, colorectal cancer cells were grown on biosensor chips and the binding kinetics of a range of lectins was determined using quartz crystal microbalance (QCM) analysis. This lectin binding data was then compared with data obtained using fluorescence microscopy. The panel of lectins were FITC labelled and a

blue DNA counterstain was used to colocalise the binding observed. They detected changes in the lectin binding profile, particularly UEA I and HPA, between the non-metastatic and metastatic colorectal cancer cell lines.

Fluorescence microscopy is often used to produce qualitative data only; where images are visually compared. However, quantitative data can also be obtained which can discriminate between seemingly indistinguishable images by using sophisticated software such as AutoQuant X3 (Lee et al. 2014). There are drawbacks to quantifying fluorescence intensity. The excitation light from a mercury lamp can vary by up to 10 % over the timescale of milliseconds to seconds, which worsens as the lamp ages, and fluorescence loss can occur due to photo-bleaching both of which are problematic when quantifying fluorescence. However, there are many similar fluorochromes with different characteristics which can be selected depending on the application, e.g. FITC is one of the most commonly used fluorochromes however it has a relatively high rate of photo-bleaching and is pH sensitive but alternative fluorochromes with similar excitation/emission spectra such as Alexa Fluor 488 and DyLight 488 can be used over a wide pH range and have increased photostability (Thermo 2017).

Other drawbacks to using fluorescence microscopy for cell surface glycan analysis include the large volumes of reagents required compared to other methods such as LiaT and flow cytometry, the relatively small number of cells that are investigated and fluorescence from lectins binding to non-cellular structures, e.g. cell debris or serum proteins attached to the bottom of the plate. The latter can however be partly resolved by counterstaining with cell specific fluorochromes, e.g. Hoechst 33258, a DNA stain.

1.7 Flow cytometry

Flow cytometry is a laser based technology where multiple characteristics of a single cell such as size, granularity and relative amounts of cell components like DNA and mRNA are measured when a cell suspension flows through a laser and the resulting scattered light, which is information rich, is received by multiple detectors, see Fig. 1.20. It is also capable of detecting light emitted simultaneously from multiple fluorochromes attached to lectins or antibodies bound to various cell structures. The

first fluorescent based flow cytometry technology was developed in 1968 at the University of Münster and was called ‘pulse cytophotometry’ (German: Impulszytophotometrie). However, the term ‘flow cytometry’ has been the accepted name for this technology since 1976 (Sack et al. 2006).

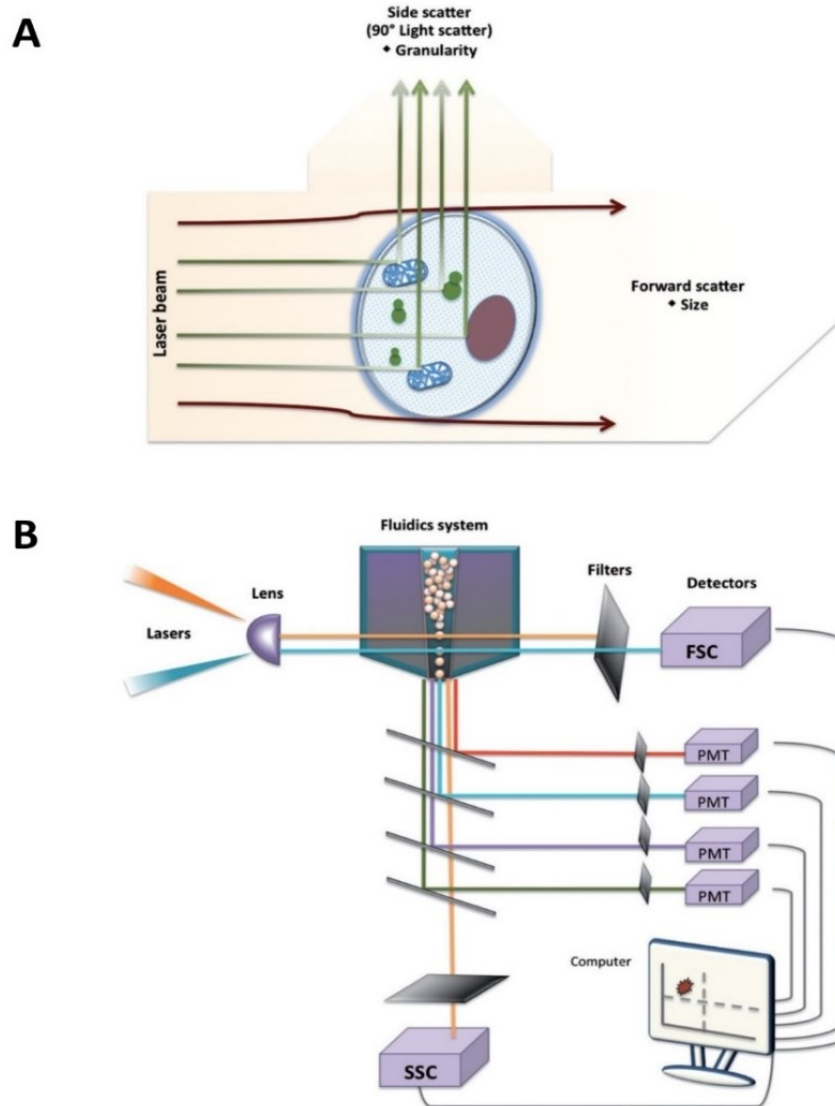


Fig. 1.20: Light scattering and detection in a flow cytometer. A) Schematic of light scattering. The light scattered in the forward direction is proportional to the cell size and side scattered light is proportional to cell granularity and internal complexity. **B)** Schematic of signal detection in a flow cytometer. The scattered light and fluorescence from cells interrogated with a laser is converted to voltages by photodetectors, photomultiplier tubes (PMT). A series of dichroic mirrors and filters are positioned in the path of the fluorescence and scattered light to partition it so each detector measures a specific spectral band and the resulting data is viewed and further analysed using flow cytometry software. Images were modified from Adan et al. 2017.

The main components of a flow cytometer are the fluidics, optics, the electronic detectors and the computer. The fluidic system takes up the cell suspension sample and transports it through the instrument. Prior to laser-cell interaction the cell sample enters the flow chamber where it is surrounded by a stream of sheath fluid, typically PBS. The cell sample pressure is greater than that of the sheath fluid which helps align the cells in single file, hydrodynamic focusing, before passing through the laser beam (Wilkerson 2012). This flow rate can be altered depending on the resolution required, e.g. a slow flow rate is more appropriate for DNA analysis where it reduces the size of the sample stream and improves accuracy. It is essential that the fluidic system is thoroughly rinsed after every use to remove cell debris which could interfere with the next user's cell samples.

The flowing cells pass through a carefully positioned laser beam and light is scattered in the forward direction, forward scatter (FSC), and to the side, side scatter (SSC). The cell components affecting light scatter are the membrane, nucleus, other organelles, cell granularity, cell size and topology. The FSC light is light diffracted along the same plane as the laser beam and it is proportional to the cell surface area, i.e. size. The SSC light is both refracted and reflected light collected at 90 ° to the laser beam and is proportional to the internal complexity and granularity of the cell (Adan et al. 2017). Fluorescent light from fluorescently labelled lectins and antibodies is reflected at the same angle as SSC, see Fig. 1.20 B).

Fluorescent probes are used to identify a wide variety of cell characteristics in flow cytometry. The excitation and subsequent emission of light at a larger wavelength is referred to as Stokes' Shift, see Section 1.6 and Fig. 1.18. A cell sample can be probed with multiple fluorochromes providing the panel is carefully designed, i.e. fluorochromes are picked which are suitable for the lasers and filters/detectors in the cytometer, and are chosen appropriately, e.g. certain fluorochromes are brighter and should be paired with less frequent antigens/targets and conversely highly expressed antigens/targets should be paired with dimmer fluorochromes (Bushnell 2015). There are many online tools providing assistance in designing a fluorochrome panel, which include Thermo Fisher Scientific's Fluorescence SpectraViewer (see Fig. 1.18),

Biolegend's Multicolor Panel Selector and BD Biosciences' Fluorescence Spectrum Viewer.

The optical system of a flow cytometer consists of lens to shape and focus the laser beam and multiple dichroic mirrors and filters to separate the fluorescence and scattered light and direct it to a detector to measure a specific spectral band. Photomultiplier tubes (PMT) are sensitive and the preferred detector for weak SSC light. The light captured by the PMT is converted proportionally to electrons creating an electric current which is converted to a voltage pulse by the amplifier. This signal is then converted to digital data by analog to digital converters and can be displayed as a dot plot or histogram by the computer. Flow cytometry is a high throughput technology where multiple cellular parameters and fluorescent signals can be obtained from cells at rates in the 1000's per second. Usually a minimum of 10,000 events are recorded per sample which provides a comprehensive assessment of a cell population. However, millions of cells can be analysed when rare cellular events are to be detected, e.g. measuring vaccine-induced T cell responses which can be as little as 0.1 % of a cell population (Precopio et al. 2007).

A fluorescence-activated cell sorter (FACS) is a type of flow cytometer capable of sorting cells depending on their light scattering and fluorescence characteristics. This provides cells for downstream applications after data acquisition. Two or three way sorting is common although it is possible to perform up to 6-way cell sorting with Beckman Coulters cell sorter MoFlo Astrios EQ (Beckman 2017). A single or multiple parameters can be used for sorting cells. Droplets containing cells pass through laser beams where light is scattered and at the same time they are charged by a charging electrode. As these charged droplets fall between positively and negatively charged plates they are deflected into separate tubes, see Fig. 1.21. The user can select the fluorescent cells of interest using the accompanying FACS software and the droplets are charged accordingly.

The recorded data is exported and then gated and analysed using flow cytometry software which can generate various plots, e.g. dot plots and histograms, to best

visualise and interpret the probed cells. A typical flow cytometry data analysis and gating strategy is outlined in Section 2.28.3.3.

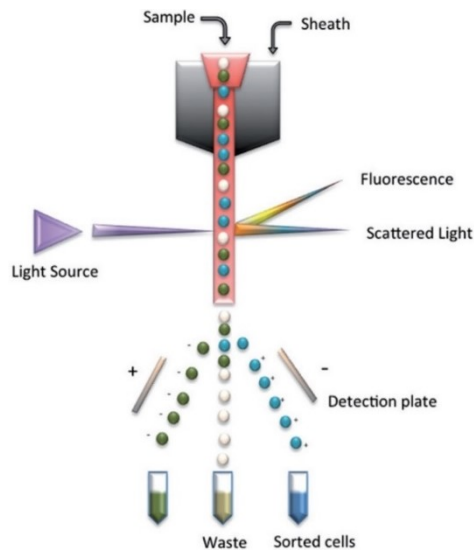


Fig. 1.21: Electrostatic cell sorting. Droplets containing cells are charged by an electrode and are deflected from the mainstream by positively and negatively charged plates. Image from Adan et al. 2017.

There are numerous applications of flow cytometry, which include, phenotyping blood cells, investigating apoptotic markers, detecting mitochondrial proteins, detecting receptor/membrane protein changes at the cell surface, detecting intracellular cytokines, sorting cells, cell cycle analysis, cell viability studies and cell surface glycosylation analysis.

1.7.1 Flow cytometry for glycan analysis

Investigating the cell surface is the most common type of flow cytometry staining experiment. All protein and glycan structures at the cell surface are easily accessible to fluorescently labelled lectins or antibodies. Lectins are ideal glycan probes in a flow cytometry setting. Much work has been published regarding the use of lectins in apoptosis studies as there are well documented cell surface glycan changes when cells are stressed and transitioning between early and late stage apoptosis (Beer et al. 2008; Batisse et al. 2004; Heyder et al. 2003). Additionally some lectins, particularly plant lectins, are themselves cytotoxic and can induce apoptosis so this must be considered when using lectins for the analysis of cell surface glycans (Stanley and Sundaram 2014).

A fluorescently labelled protein, annexin V- FITC, and a fluorescent DNA stain, propidium iodide (PI), are routinely used to distinguish between apoptotic/non-apoptotic and viable/non-viable cells respectively. Loss of plasma membrane integrity is an early hallmark of apoptosis during which the phospholipid phosphatidylserine (PS) flips from the cytosolic side to the extracellular side of the plasma membrane. Exposed PS can be detected by annexin V and thereby differentiate between apoptotic and non-apoptotic cells. Cell viability can be determined by the exclusion of PI which is a DNA stain that cannot cross the plasma membrane of live cells. Early stage apoptotic cells are both annexin-V positive and PI negative whereas late apoptotic and dead cells are both annexin-V positive and PI positive (BD 2017).

Human galectins, lectins which bind galactose residues, were used by Beer et al. (2008) to detect apoptosis by binding to surface glycans of granulocytes and lymphocytes. The galectins were produced recombinantly, purified using affinity chromatography and biotinylated. They observed an increase in galectin binding with apoptosis progression. Similar cell surface glycan changes were detected by Heyder et al. (2003) when they assessed a panel of human cell lines with a mannose specific lectin from the daffodil plant, *Narcissus pseudonarcissus* lectin (NPL) after a short acid treatment. Stanley and Sundaram (2014) described an assay for determining the cytotoxic effects of lectins on a panel of CHO cells lines, CHO-K1 cells and lectin resistance CHO cells. They also completed a glycan binding assay using lectins and a flow cytometer where they observed cell surface glycan differences between the CHO cell lines, demonstrating the suitability of flow cytometry for glycan analysis.

The connection between aberrant glycosylation and disease was previously stated, see Section 1.3.5. Flow cytometry analysis of cell surface glycans using fluorescently labelled lectins is an ideal method to investigate altered glycosylation and associate it with both the state of the cells, using additional stains, and its biological function. Suzuki et al. (2015) modified the surface glycosylation of human malignant lymphoma cell lines using *O*-glycan and *N*-glycan inhibitors, benzyl- α -GalNAc (BZ) and tunicamycin (TM). Lectin binding, analysed by flow cytometry, was significantly altered after BZ and TM treatments. Their work showed the biological role of glycans in the adhesion to and invasion of the ECM by cancer cell lines.

The analysis of surface glycans on live cells using fluorescently labelled lectins is an established and robust method. It is also more straight forward and less problematic than fixing cells although time constraints on the day of analysis are to be considered. The use of a multicolour panel of lectin probes and other dyes can elucidate a plethora of cellular information which would otherwise not be obtained using glycan analytical methods such as, fluorescent microscopy, lectin microarrays and MS. The high number of cells that can be processed, 10,000 per sample in 1-2 minutes, increases the validity of the data acquired as a significant portion of the cell population are analysed. Additionally, a more rapid and simple method using only single lectin probes is sufficient to obtain lectin binding information and detailed cellular information, FSC and SSC data. Furthermore the specificity of lectin binding can easily be demonstrated using a flow cytometer with the addition of a specific or non-specific monosaccharide.

1.8 Lectins

Proteins that agglutinate cells have been known to exist since the 19th century. The first agglutinating protein was discovered by Peter Stillmark in 1888 from the seeds of *Ricinus communis*, the castor oil plant. This extremely toxic protein is named ricin (Sharon and Lis 2004). However, it wasn't until the 1960s that the vast range of cell types these proteins bind to and their sugar specificity became known. William Boyd coined the term lectin in 1954, from the Latin *lectus* meaning to choose or select, and it is defined as a carbohydrate binding protein other than an enzyme, antibody or transport protein for free sugars (Solís et al. 2015, Barondes 1988).

In 1960 Peter Nowell discovered that the PHA lectin (phytohemagglutinin) from *Phaseolus vulgaris* (red kidney bean) can stimulate lymphocytes to undergo mitosis. This was a massive immunological discovery and it disproved the commonly held view at the time that lymphocytes are incapable of division or further differentiation. Other lectins were also proven to be mitogenic and in the 1970s the T cell growth factor, interleukin-2, was discovered using lymphocytes stimulated by PHA. These discoveries gave lectins great exposure and with emerging purification techniques, immobilized dextran (Sephadex®) in 1965, the number of purified lectins increased greatly (Sharon and Lis 2004). Lectins quickly became an irreplaceable tool for histochemistry and for detecting, purifying and characterising glycoproteins. Most lectins were initially

isolated from plant and fungi with eel, snail and horseshoe crab providing the odd exception but today lectins are known to occur throughout nature (Varki et al. 2009). A galactose specific liver asialoglycoprotein receptor from a rabbit was the first mammalian lectin to be isolated and characterised (Hudgin et al. 1974).

The binding property of lectins arises from a region of their polypeptide sequence, which is termed the carbohydrate-recognition domain (CRD). Lectins have been classified structurally, depending on the type of protein folding, but more generally they are classified in five groups according to their binding specificity (i) Glucose/Mannose; (ii) Galactose and *N*-acetyl-Dgalactosamine; (iii) *N*-acetylglucosamine; (iv) L-fucose, and (v) Sialic acid (Nicolson 1974). The specificity and source of some common lectins is presented in Table 1.3. Lectin binding is non-covalent and reversible with both free sugars and glycoproteins in solution or displayed on the cell surface. Lectins possess a minimum of two carbohydrate binding sites in order for them to agglutinate cells and/or bind complex multi branched oligosaccharides whereas proteins with one carbohydrate binding region are referred to as selectins. Lectin binding is generally weak but high avidity can be reached by multivalent binding. The low avidity of a single carbohydrate binding site is thought to improve lectin function in nature. “A multivalent carbohydrate-binding protein that is not an antibody” was a traditional definition for a lectin (Varki et al. 2009). Lectin binding specificity is determined using the Hapten inhibition test. In this assay, carbohydrates are tested for their ability to inhibit lectin agglutinating cells or lectins inducing glycoprotein precipitation. From this assay it has been shown that lectins can interact with more than one carbohydrate (Singh and Sarathi 2012). Concanavalin A was the first lectin whose amino acid sequence was identified and also whose 3-D structure was solved by x-ray crystallography. The former was completed by Edelman et al. (1972), the latter was also completed by Edelman but also independently by Hardman and Ainsworth (1972). Once sequence data was available many homologs were identified in related species. The 3-D structures and additional protein information of over 100,000 proteins are currently available online in the Protein Data Bank (PDB) archive. There are currently over 1500 lectin entries in the PDB, see Fig. 1.22.

Table 1.3: Source and specificity of common lectins

Lectin Name (Abbreviation)	Lectin Source	Common name	Specificity
Concanavalin A (Con A)	<i>Canavalia ensiformis</i>	Jack Bean	Man
<i>Griffonia simplicifolia</i> lectin II (GSL II)	<i>Griffonia simplicifolia</i>	Griffonia	GlcNAc
<i>Ricinus communis</i> agglutinin II (RCA II)	<i>Ricinus communis</i>	Castor oil plant	Gal, Lac & GalNAc
<i>Aleuria aurantia</i> lectin (AAL)	<i>Aleuria aurantia</i>	Orange Peel Fungus	Fuc
Phytohaemagglutinin (PHA)	<i>Phaseolus vulgaris</i>	Common bean	Gal, Man & GlcNAc

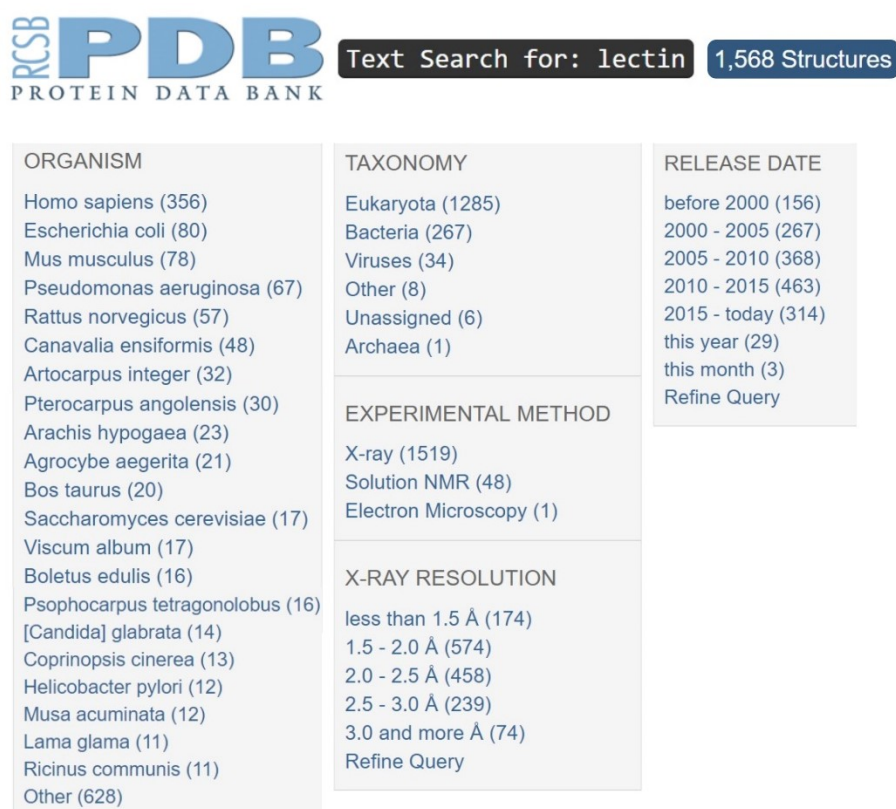


Fig. 1.22: A breakdown of the search results for 'lectin' in the Protein Data Bank archive. There are 1,568 lectin structure entries in the PDB as of 5th April 2017. The release date figures shows a gradual increase in the number of lectin entries over each 5 year period. The PDB, established in 1971, is the single worldwide repository for information on the 3-D structure of proteins. The PDB can be accessed at <http://www.rcsb.org/pdb/home/home.do>. Image generated by modifying a screenshot of the webpage.

1.8.1 The functions of lectins

The biological roles of lectins are diverse but the primary function of lectins in animals is to mediate cell-cell contact. Lectins at the cell surface will bind, temporarily, to displayed carbohydrates on another cell. Cells are connected by many specific lectin-carbohydrate interactions which are individually relatively weak but collectively strong. Lectins also play a significant role in the innate immune system. The human mannose-binding lectin (MBL) is important for the first-line host defence against a wide variety of infectious agents including gram-positive bacteria, gram-negative bacteria, yeasts, mycobacteria, and viruses. MBL has the ability to distinguish between normal host cells, non-self cells and infected host cells due to the special geometry of carbohydrates at the cell surface. MBP can activate the complement and increase phagocytosis of infected cells (Takahashi and Ezekowitz 2005).

The precise role of lectins in plants is not known but some functions such as plant defence are certain. The lectin in castor beans, ricin, is toxic to most animals and serves as a strong insecticide. Many plant lectins bind sugars such as galactose, glucose and mannose. However, they often have greater affinity for oligosaccharides that are not commonly found in plants or are completely absent suggesting a role in defence. Examples of this are the lectins from *Maackia amurensis* (MAL II) and *Sambucus nigra* (EBL) which bind *N*-acetylneuraminic acid (sialic acid) which is not found in plants but is a large component of animal glycoproteins (Peumans and Van Damme 1995).

As lectins bind glycoconjugates at the cell surface, it is logical to deduce that this can be exploited by pathogens. *Escherichia coli* bacteria are able to infect the gastrointestinal tract using lectins, located on fimbriae, to attach to target epithelial cells (Berg et al. 2002). Multiple lectins on the hairy-like fimbriae appendages results in high avidity multivalent interactions with the host cell. Bacterial lectins binding mammalian host cells is not always pathogenic as they also play an essential role in maintaining a symbiotic relationship. For example, a glycosphingolipid, Gal α 1-4Gal β 1-4Glc β -ceramide, is found on columnar epithelium in the large intestine but not in the small intestine. This cell surface moiety allows many bacterial species, e.g. *Clostridium*, *E. coli*, and *Lactobacillus*, to colonise the large intestine only (Varki et al. 2009).

The first lectin isolated from a microorganism, the influenza virus hemagglutinin, binds to the internal sequences found in complex glycans. This results in a highly specific lectin-glycan interaction. The human influenza viruses bind mainly to cells containing α 2,6-linked sialic acid whereas influenza viruses of other animals and birds bind preferentially to α 2,3-linked sialic acid (Varki et al. 1999).

1.8.2 Recombinant lectins

The purification of lectins before 1965, prior to the breakthrough of cross-linked dextran gels (Sephadex®), involved conventional techniques, primarily a series of precipitations with salts and solvents (Nascimento et al. 2012). Since this breakthrough the most commonly used purification strategy for lectins from crude extracts is affinity chromatography followed by lectin precipitation. The main problem with this non-recombinant method is that the final purified product is often a heterogeneous mixture of several isoforms which may have differing biological activities. This batch to batch variation is not ideal and can lead to varying results when using lectins as probes (Oliveira et al. 2014). Additionally purifying lectins from raw materials is a time consuming process, requires large amounts of starting biological material and the lectin yield is often low. Producing lectins by recombinant means resolves many of these issues and allows for greater control of the production and purification processes (Gemeiner et al. 2009).

High product yields with a defined amino acid sequence can be achieved easily and consistently using recombinant technology. Other major advantages include the ability to tailor/modify the lectin properties, namely

- (i) site-directed mutagenesis to alter/enhance binding properties (see Section 2.12)
- (ii) direct lectin labelling - creating a lectin fusion protein by joining a lectin to a fluorescent protein, e.g. green fluorescent protein.
- (iii) lectin modification enhancing its application, e.g. inserting additional lysine residues to the lectin will provide additional primary amines (NH_3) which will help lectin coupling to *N*-hydroxysuccinimide (NHS)-activated columns. This will also improve the indirect labelling of the lectin with NHS-activated biotins for example.

The expression host of choice for producing recombinant proteins is *E. coli*. High cell density cultures can be achieved using *E. coli* which has a theoretical density limit of approximately 200 g dry cell mass/L or 1×10^{13} viable cells/mL (Rosano and Ceccarelli 2014). This host also has a high growth rate ($\sim 2.0 \text{ h}^{-1}$), is cultivated cheaply, can produce a large quantity of protein, over 200 mg/L can be easily achieved, and it is well understood as it is the host in which recombinant DNA technology was created (Wingfield 2015; Lam and Ng 2011; Oliveira et al. 2013; Cohen et al. 1973).

The main drawback with this host is the inability to perform certain eukaryotic post-translational modifications, primarily glycosylation. This can affect the way the protein is processed, disulphide bond formation and protein folding. These factors therefore influence the protein stability and need to be considered before expressing a protein in a bacterial host. The B chain of the ricin lectin is an example of this drawback. When it is produced recombinantly in *E. coli* it is less stable than the glycosylated native lectin (Oliveira et al. 2013, Ferrini et al. 1995). Plant lectins often form multimers and are glycosylated and therefore they are not suited to recombinant production in bacterial hosts. However, this is not a major concern as the recombinant lectins used in this work are from non-mammalian/non-plant sources and are not glycosylated proteins. Recombinant prokaryotic lectins can also have increased specificity when compared to their plant counterparts. Many lectins have a primary carbohydrate binding site with adjacent satellite sites that allows for interaction with additional residues of an oligosaccharide. This is particularly evident in the legume lectin family where mannose-specific lectins can also recognise and tolerate glucose almost equally well (Loris et al. 2003). This is not ideal when specific glycan binding is desired. The lectins produced in this work are described in the following 3 sections.

1.8.3 *Agrocybe aegerita* lectin 2

Agrocybe aegerita lectin 2 (AAL-2) is an *N*-acetylglucosamine specific lectin from *Agrocybe aegerita* (poplar mushroom). It consists of 407 amino acids residues and has a molecular weight of 43.17 kDa. It was recently isolated (UniProt accession No. H6CS64 [2012]) and shown to bind to terminal non-reducing GlcNAc with a greater affinity than that of other well-known GlcNAc binding lectins such as GSL II (*Griffonia simplicifolia* Lectin II) and WGA (wheatgerm agglutinin). Jiang et al. (2012) tested

AAL-2 against 465 glycan candidates and found that it was specific for non-reducing GlcNAc and where GlcNAc was linked to galactose (GlcNAc-Gal or *N*-acetyl-lacosamine [LacNAc]) binding affinity increased. AAL-2 is capable of binding α or β linked GlcNAc. AAL-2 binding was greatest for [GlcNAc-Gal]_n-GlcNAc where n is 1, 2 or 3.

AAL-2 is a useful probe for detecting *O*-GlcNAc, a protein post-translational modification where GlcNAc is added to Ser/Thr residues. *O*-GlcNAcylation is a PTM important for many cellular processes including regulating transcription and protein expression and it is thought to be a process more similar to protein phosphorylation than to classical protein glycosylation (Varki et al. 1999). Over 1000 *O*-GlcNAcylated proteins, nearly exclusively in the cytoplasm and nucleoplasm, have been identified (Hart et al. 2011). However, the recent discovery of an extracellular *O*-GlcNAc transferase (EOGT), which is localised to the lumen of the ER and conserved from *Caenorhabditis elegans* to *Homo sapiens*, is responsible for adding *O*-GlcNAc onto cell surface proteins and secreted proteins (Ogawa et al. 2014). AAL-2 has also been identified as a probe for 'classical' *O*-glycans terminating in GlcNAc.

AAL-2 is from the same lectin family, seven-blade β -propeller fungal lectins, as previously characterised *Psathyrella velutina* Lectin (PVL) whose structure is known, since 2006, and shares 60 % sequence similarity with AAL-2, see Appendix B. In 2015 the AAL-2 structure was first reported. It comprises of seven blades in a single domain each of which are approximately 56 residues and form four anti-parallel β -strands arranged in a W-like shape, see Fig. 1.23 (Ren et al. 2015). The seven W-motifs form a doughnut shape with a central pore and the first β -strand in each motif is orientated in the same direction, entrance to exit direction as shown in Fig. 1.23.

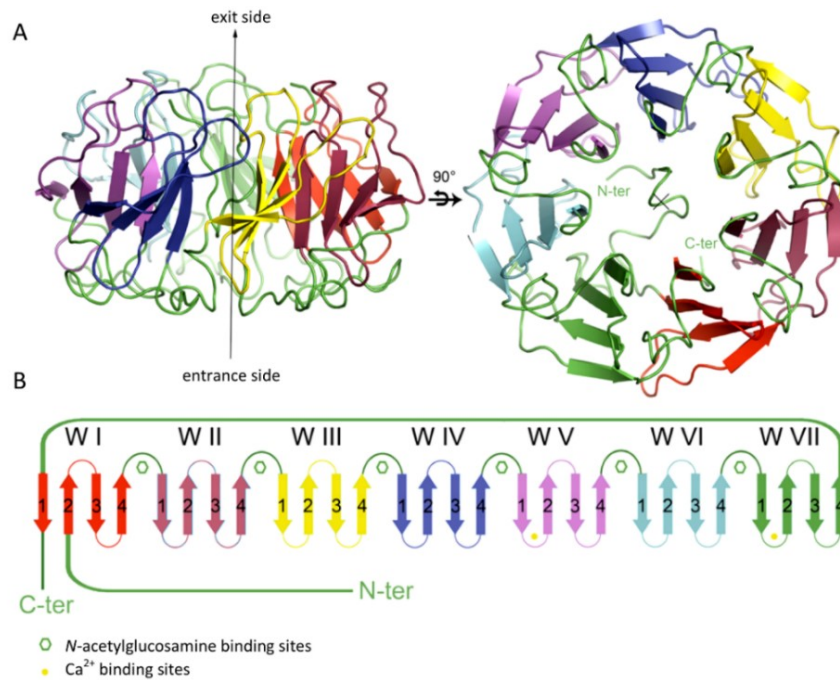


Fig. 1.23: Structure of AAL-2. **A)** Two orthogonal views of the AAL-2 structure. **B)** AAL-2 schematic showing the direction of the β -strands in each of the W-motifs and where the 6 GlcNAc and 2 Ca^{2+} binding sites are located (Ren et al. 2015).

1.8.4 GafD from *Escherichia coli*

The *gafD* gene encodes a terminal β *N*-acetylglucosamine specific lectin. This G(F17) fimbrial lectin is from enterotoxigenic *E. coli* which is associated with diarrhoea and urinary tract infections. Neonatal ruminants are particularly vulnerable to infection, and the subsequent intestinal colonisation, by *E. coli* expressing this fimbrial lectin (Boraston et al. 2011). The mature GafD lectin is 321 amino acids but other smaller C-terminally truncated peptides are also expressed by *E. coli* (Tanskanen et al. 2000). GafD1-178 is one of these peptides which consists of 178 amino acids residues and is 19.1 kDa, see Fig. 1.24. This lectin is obviously easily expressed in *E. coli* but its purification is also straightforward as it is a fimbrial protein that is translocated out of the cytoplasm so cell lysis is not required for its release after expression.

GafD1-178 is a more specific GlcNAc binding probe than AAL-2 as it will only bind β terminal *N*-acetylglucosamine residues. GafD1-178 has the most affinity for GlcNAc- β 1-3Gal. It is approximately 2 fold greater than that of free GlcNAc. It also has high affinity for GlcNAc β 1-4Gal and GlcNAc β 1-6Gal residues. The 3-D structure of its

GlcNAc binding region was solved by Merckel et al. (2003). GafD1-178 consists of 16 β -strands and one helix structure forming a β -barrel structure. Two other *E. coli* fimbrial lectins, FimH and PapG, have a similar β -barrel structure but their disulphide-bond patterns are different and therefore they have different ligand binding specificities (Westerlund-Wikström and Korhonen 2005). GafD1-178 is a useful glycan probe. Its binding to glycoproteins on cell surfaces is a marker for apoptosis (Batisse et al. 2004). This recombinant lectin had been previously utilised by O'Connell (2016) where it was shown to bind preferentially to late apoptotic B-lymphocytes. Here, GafD1-178 was expressed, purified, assessed by ELLA and biotinylated for subsequent use on the fluorescent microscope and flow cytometer as it may bind preferentially to stressed CHO cells.

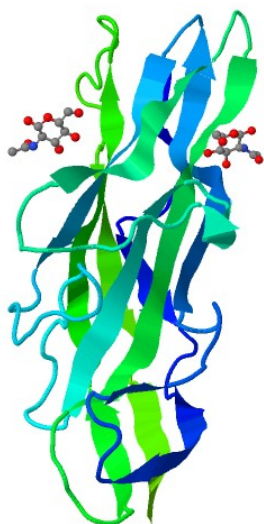


Fig. 1.24: 3D view of GafD1-178. The secondary structure of GafD1-178 with two *N*-acetylglucosamine ligands represented in ball and stick form. Image generated using the JSmol viewer on the PDB website, PDB code 1OIO.

1.8.5 PA-IL and PA-IIL lectins from *Pseudomonas aeruginosa*

Pseudomonas aeruginosa is a gram negative bacterium capable of infecting plants and animals. It is an opportunistic pathogen that is of particular concern for immunocompromised and cystic fibrosis patients. The success of *P. aeruginosa* as an infectant is due to it being a multidrug resistant pathogen but also its ability to adhere to tissues and form biofilms via recognition of host glycans. This attachment capacity is partly mediated by two lectins, the galactose-specific PA-IL lectin and the fucose-specific PA-IIL lectin (Kadam et al. 2013).

The PA-IL and PA-IIL lectins are more commonly known as LecA and LecB respectively. Both lectins form tetrameric structures and are dependent on divalent cations for binding activity, see Fig. 1.25. LecA is a 12.7 kDa protein consisting of 121 amino acids residues and binds galactose. The specificity of LecA binding has been extensively examined using a 241 glycan epitope glycan array (Blanchard et al. 2008). LecA is highly specific for α 1-4 linked terminal galactose but also recognises, to a lesser degree, α 1-3 and α 1-6 linked terminal galactose. The glycan array detected no significant binding to β -linked galactose residues. LecB is an 11.7 kDa protein consisting of 114 amino acids residues and is specific for fucose and its derivatives (Imberty et al. 2004). LecB is abundant in the outer membrane of *P. aeruginosa* and is a key virulence factor as a LecB-deficient strain is considerably hindered in its ability to form biofilms (Loris et al. 2003). LecA and LecB are both amenable to production in *E. coli* where gram quantities can be easily achieved. Additionally their binding regions can be altered by random or site-directed mutagenesis generating novel lectins with diverse glycan binding specificities (Keogh et al. 2014).

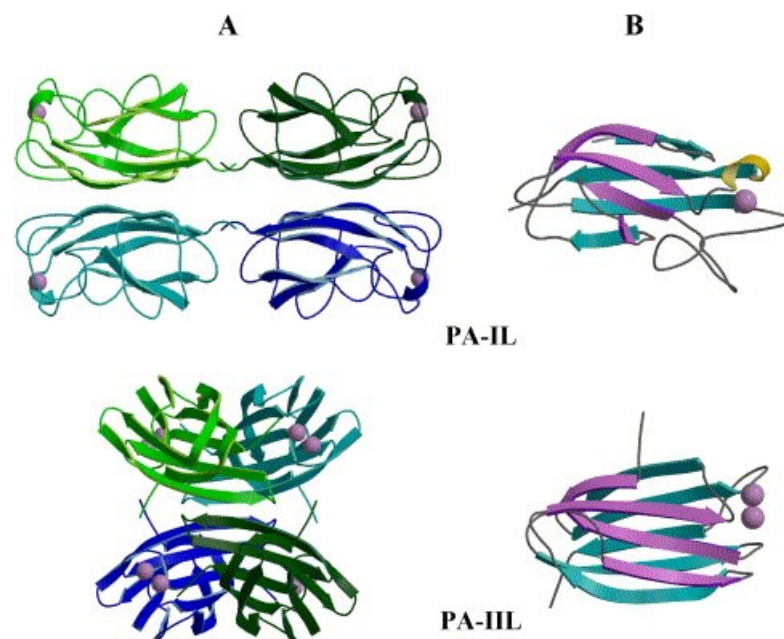


Fig. 1.25: Tetramer and monomer structures of PA-IL(LecA) and PA-IIL(LecB). A) Tetramers of LecA and LecB are shown with a different colour representing each subunit and space-filling spheres representing calcium ions. B) Monomers of LecA and LecB are shown with a different colour representing each β sheet (Imberty et al. 2004).

1.9 The biopharmaceutical industry

The first therapeutic proteins produced were purified from human sources. Plasma is a source for blood clotting factors and albumin, and the pancreas is a source for insulin (Sethuraman and Stadheim 2006). This method of obtaining proteins has numerous drawbacks and it is far from ideal. This method raises concerns over the product consistency, possibility of contamination from viruses or prions and it limits the quantity that can be produced (Swiech et al. 2012). Therapeutic protein production naturally shifted towards cell-culture expression systems where many if not all of the mentioned problems are addressed. The biopharmaceutical industry has grown rapidly since the first recombinant product, Humulin (recombinant human insulin), was released in 1982. By 2000 there were 50 different recombinant proteins approved for use with a global market value of \$12 billion and strong growth was predicted for the following decade (Walsh 2000, Kelley 2001). The prediction of strong growth was accurate and in 2009 there were over 165 recombinant biopharmaceuticals approved for human use with an additional 500 proteins in clinical development of which 70 % were glycoproteins (Durocher and Butler 2009). Due to the approval and release of new biopharmaceuticals the global market value rose to an estimated \$140 billion in 2013 (Walsh 2014). The U.S. Food and Drug Administration (FDA) and the Center for Biologics Evaluation and Review (CBER) combined have approved 62 recombinant therapeutics proteins in the 5 and a half year period from January 2011 to August 2016, 45 % of which were monoclonal antibodies, bringing the total of approved biotherapeutics in U.S. and E.U. markets to over 200 (Mahajan 2016; Lagassé et al. 2017). The completion of the human genome project in 2003 strongly influenced this growth. This completion caused a change from the study of genomics towards proteomics with a goal to identify functional proteins to help identify potential targets for therapeutic proteins (Laken and Leonard 2001). For a list of glycosylated biopharmaceuticals and the broad range of illnesses they treat see Table 1.2 Therapeutic Glycoproteins in Section 1.4.

It is expected that the number of approved biotherapeutics will continue to rise over the next decade with the release of both new therapeutic products but also the release of biosimilars. There will be a substantial market for biosimilars, estimated to be greater than \$50 billion annually, as more than 20 of the best-selling biopharmaceuticals will

be off-patent by 2020 (Banga 2015). As of August 2016 the FDA has approved 3 biosimilars (Lagassé et al. 2017). Once a biotherapeutic product is off-patent, the manufacturer of the biosimilar does not get direct access to detailed data, e.g. DNA sequences and cell lines used, of the original product. Much of this information has to be retrieved by reverse-engineering the process. This is particularly difficult as there can be over 5,000 critical process steps during the production of a biotherapeutic protein. Additionally the FDA does not require the exact same manufacturing process for the original and the biosimilar product (Lagassé et al. 2017). It is expected that certain aspects of the biotherapeutic, e.g. post-translational modifications including glycosylation, will be different. Therefore, it is important that complete analysis, including glycoanalysis, of the biosimilar product is completed to demonstrate similarity, safety and comparable efficacy. However, there are many reasons why differences between the original product and the biosimilar product may actually be desired. Some of the products coming off-patent were first released in the 1980s when recombinant DNA technology was still in its infancy and since then it has greatly advanced. Similarly, the manufacturers of biosimilar products can use the latest technologies in all process steps which is something that originators were unable to do due to the financial consequences of having to continually regain regulatory approval (Schellekens and Moors 2010).

The quantity of proteins required for research/clinical applications is rather small but proteins for therapeutic applications are required in quantities that are approaching the metric ton scale (Andersen and Krummen 2002). Genetically engineered expression systems offer major benefits and allow for the design of more advanced glycoproteins that have enhanced therapeutic properties e.g. increased bioavailability and serum half-life (Swiech et al. 2012). Chinese hamster ovary (CHO) cells are the current expression system of choice as no undesirable immunogenic effects have been observed and they have a history of regulatory approval (Durocher and Butler 2009). Non-mammalian systems do have advantages, such as reducing costs and increasing quantities, but other problems arise relating to the immunogenic profile of the glycoprotein e.g. glycans produced in yeast are hyper-mannosylated and therefore not suitable for human use although advances in the glycoengineering of yeast, especially *Pichia pastoris*, are rectifying this (Hamilton and Gerngross 2007). The baculovirus-insect cell system is an

expression system that has been used for the production of recombinant proteins. However, the glycosylation pathways in this eukaryote are much simpler than those in higher eukaryotes. Insect cell systems can synthesise *N*-glycans although they are not the complex type with sialic acids caps that are found in their mammalian counterparts. Furthermore, insect cells systems can produce *N*-glycans containing core α 1,3-fucose which is known to be allergenic thus limiting their use for producing therapeutic glycoproteins in biopharmaceutical settings (Jenkins et al. 1996; Shi and Jarvis 2007).

Glycoprotein function, stability and efficacy is strongly influenced by the nature of the glycans attached to the protein. The complete understanding of glycosylation, from glycan assembly to *in vivo* effects, is therefore paramount for producing novel therapeutic glycoproteins. The various bioprocess conditions that can alter cell health and therefore influence glycosylation need to be considered, see Section 1.11. It is important that cell health is monitored throughout a bioreactor campaign. This can be done, crudely, using basic measurements such as cell concentration and viability from off-line trypan blue counts. Additionally more sophisticated techniques can be implemented to measure other bioprocess parameters such as pH, dissolved oxygen, glucose and lactate concentrations which can inform the operator about nutrient consumption and therefore the status of the culture (Weichert and Becker 2013). Glucose and lactate levels have been shown to correlate with both the cell density, by Tsao et al. (2005), and with the rate of recombinant protein production, by Chen et al. (2012). However, obtaining detailed cellular information and product glycosylation data is difficult. Lectins can be utilized to address both these issues. The former can be completed by either probing a cell sample with a panel of fluorescently labelled lectins followed by flow cytometry analysis or by using a lectin microarray. The latter could be completed by using ELLA to analyse a crudely purified glycoprotein, e.g. IgG can be rapidly purified (< 20 minutes) from a small cell suspension volume using a mini Protein A/G column. There are also automated systems which can directly pull out a product from culture supernatant, using Protein A coated tips, and analyse its glycans. The Pall FortéBio OctetRED96 is one such system which can quantitatively assess the binding kinetics of protein-protein and protein-small molecule interactions (PALL 2017). These methods utilise the specificity of lectins to provide rapid and detailed information about cell health and glycoprotein quality. Furthermore, the analysis of cell

surface glycans may be sufficient for detecting glycan changes on the product as Grainger and James (2013) demonstrated that they are strongly correlated.

1.10 Chinese hamster ovary cells

Chinese hamster ovary (CHO) cells have been used extensively over the past three decades for the expression of recombinant therapeutic proteins establishing them as the industry standard, as approximately 70 % of all therapeutic proteins are produced in CHO cells (Kim et al. 2012). Chinese hamsters, *Cricetulus griseus*, have been used for research purposes since 1919 when they were used to type pneumococci. The CHO cell line was established in 1957 when Dr. T. Puck, University of Colorado, isolated ovary cells from a Chinese hamster which grew strongly *in vitro* (Jayapal et al. 2007). A recombinant tissue plasminogen activator (Activase), produced in CHO cells, was approved for use in 1987. This was also the first recombinant therapeutic protein produced in mammalian cells (Walsh 2009). CHO cells possess many of the characteristics of an ideal expression system. CHO cells are capable of producing human-like glycans and the downstream processing of products produced in CHO cells has developed to a level of high purity i.e. only picogram levels of CHO DNA is present per product dose (Jayapal et al. 2007). The product titer in CHO cells has also increased considerably since the 1980s from 1-100 mg/L to nearly 1 g/L a decade ago and to the current 5 g/L (Huang et al. 2010; Gronemeyer et al. 2014). Additionally product titers in excess of 10 g/L have also been reported in CHO from extended fed-batch and perfusion cultures (Kelley 2009; Li et al. 2010). CHO is the most widely used mammalian expression system and the bestselling biopharmaceuticals of the last decade, include Avastin, Herceptin, Humira, Enbrel, Epogen, are nearly exclusively produced in CHO, see Table 1.4. CHO is the longest established mammalian expression system with no adverse effects documented which makes it an attractive choice for biopharmaceutical companies.

Improving the bioprocess performance of CHO and enhancing product characteristics is a priority for the biopharmaceutical industry. The publication of the CHO-K1 genome, <http://www.chogenome.org/>, has allowed for a better understanding of the genotype-phenotype relationship in CHO. Assessing the glycosylation capabilities of CHO is important when considering glycoprotein therapeutics. There are 300 genes in

humans that are involved in glycan synthesis and degradation and all of these but three, *ALG13* (UDP-*N*-acetylglucosamine transferase), *CHST7* (carbohydrate sulfotransferase 7) and *CHST13* (carbohydrate sulfotransferase 13), have homologs in the CHO-K1 genome. However, RNA data from exponentially growing CHO-K1 was used to determine that only approximately half of these genes are actually expressed (Xu et al. 2011).

Table 1.4: Biopharmaceutical products produced in CHO

Brand name (Drug; description)	Manufacturer	Year approved	EU Patent expiry^a	2016 Sales^b (\$ billions)
Avastin (bevacizumab; anti VEGF-A)	Genentech/Roche	2004	2019	6.88
Advate (factor VIII; human FVIII)	Baxter	2003	2019	2.11
Humira (adalimumab; TNF α inhibitor)	Abbott	2002	2018	16.52
Orencia (abatacept; IgG1-CTLA-4 fusion)	BMS	2005	2017	1.15
Aranesp (darbepoetin alfa; erythropoietin)	Amgen	2001	Expired 2016	2.09
Avonex (IFN β 1a; human IFN β 1a)	Biogen Idec	1996	Expired 2015	2.31
Enbrel (etanercept; TNF inhibitor fusion)	Amgen, Pfizer	1998	Expired 2015	9.24
Herceptin (trastuzumab; EGF inhibitor)	Genentech/Roche	1998	Expired 2014	6.88
Epogen (epoetin alfa; erythropoietin)	Amgen	1989	Expired 2013	1.28
Rituxan (rituximab; anti CD20)	Roche	1997	Expired 2013	7.24
Remicade (infliximab; anti TNF)*	Johnson & Johnson	1998	Expired 2015	8.05
Flixabi (infliximab; anti TNF)	Samsung Bioepis	2016	-	-

^a Patent data from Walsh 2014. ^b Sales data from www.evaluategroup.com

* Remicade is actually produced in murine myeloma cells, SP2/0, however its biosimilar Flixabi is produced in CHO cells (EMA 1999; EMA 2016).

1.10.1 CHO DP-12

A cell line was chosen for this work that is representative of those used by the biopharmaceutical industry. CHO cell lines are undoubtedly the standout workhorse for therapeutic protein production (Jayapal et al. 2007). The CHO DP-12 cell line, derived from the CHO-K1 cell line, was selected as it is a cell line used for the production of therapeutic proteins for clinical use (Shields 2002; Wong et al. 2007). These cells co-express the variable light and heavy chains of the murine 6G4.2.5 monoclonal antibody, IgG1, (ATCC HB-11722) which inhibits interleukin 8 binding, see Section 1.10.2 below. CHO DP-12 cells are the expression host for two Genentech humanised mAb products, Avastin (bevacizumab - inhibits VEGF-A for multiple cancers) and Raptiva (efalizumab - targets CD11a antigen for immunosuppression in psoriasis patients). However, Raptiva was withdrawn from the market in 2009 due to increased reactivation of latent JC virus infection (EMA 2015a; EMA 2015b).

1.10.2 Immunoglobulin G

Immunoglobulin G (IgG), approximately 150 kDa, is one of the most abundant proteins in human serum, accounting for 10-20 % of plasma protein. It is the major class of immunoglobulins in human, the others being IgM, IgD, IgA and IgE. There are four IgG subclasses named in decreasing serum concentration, IgG1 (146 kDa), IgG2 (146 kDa), IgG3 (170 kDa) and IgG4 (146 kDa), which share over 90 % amino acid sequence similarity although each subclass has unique properties such as antigen binding, cell activation and serum half-life (Vidarsson et al. 2014).

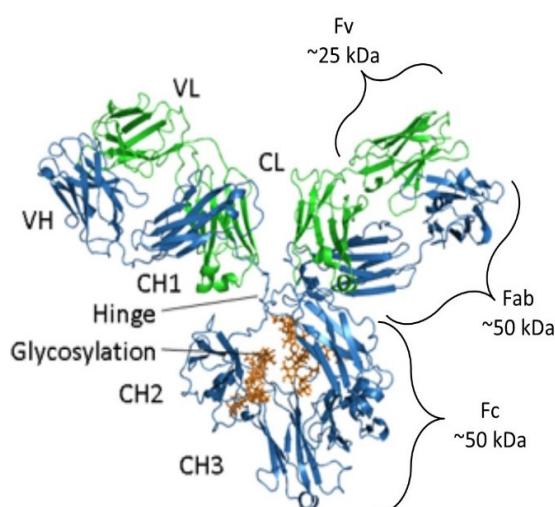


Fig. 1.26: IgG structure. The secondary structure of IgG is shown as a ribbon representation. The heavy chain is in blue and the light chain is in green. The *N*-glycan, Asn297, on the heavy chain is shown in orange. Image modified from Absolute antibody (2017).

Two heavy chains and two light chains combine to form a single ‘Y’ shaped antibody through disulphide bonds and non-covalent interactions. The heavy chain, shown in blue in Fig. 1.26, is composed of one *N*-terminal variable domain (VH) and three constant domains (CH1, CH2 and CH3). The light chain, shown in green, is composed of one *N*-terminal variable domain (VL) and one constant domain (CL). The light chain associates with two domains on the heavy chain, VH and CH1, forming the fragment of antigen binding (Fab). The VH and VL domains of the Fab bind to the antigen. The CH2 and CH3 domains form the Fc tail, fragment crystalline, which is separated from the Fabs by a hinge region. The Fc tail is responsible for antibody function as it is recognised by IgG-Fc receptors (FcγR) on innate immune cells and by C1q, a component of the C1 complex in complement activation (Vidarsson et al. 2014; Liu et al. 2017).

There is one bi-antennary N-linked glycan on each heavy chain at a highly conserved site, asparagine 297, in the CH2 domain (Lauc 2013). The IgG glycans are crucial components of the Fc tail and their monosaccharide constituents may significantly alter the IgG interaction with the IgG-Fc receptors. If the glycan is core fucosylated, fucose attached to the first GlcNAc residue, the binding of the FcγRIIIa (CD16) receptor, expressed mainly on natural killer cells, to the IgG Fc tail is greatly reduced. This receptor initiates antibody-dependant cellular cytotoxicity (ADCC) which leads to the destruction of the targeted cells. Up to 98 % of IgGs can be fucosylated which is an added safety mechanism in regulating ADCC. The misregulation of ADCC can result in autoimmune disorders and/or cancer (Scanlan et al. 2008; Pucic et al. 2011). Furthermore, the presence of sialic acid caps on the IgG *N*-glycans is directly linked with IgG function changing it from being pro-inflammatory to anti-inflammatory. Sialylated glycans reduce inflammation and maintain immune homeostasis through the T_H2 pathway (humoral immune response) (Anthony et al. 2011). Similarly the anti-inflammatory properties of IgG has been linked to the galactosylation of its *N*-glycans (Karsten et al. 2012). Glycosylation is extremely important for IgG activity, efficacy and regulation. The glycosylation of therapeutic proteins produced in CHO cells can vary depending on the clone and the bioprocessing conditions, e.g. pH, temperature, nutrient availability and ammonia accumulation (Yang and Butler 2002; Yoon et al.

2005; Hossler et al. 2009). Fig. 1.27 shows the variety of glycosyltransferases that can alter IgG *N*-glycans and therefore influence its function.

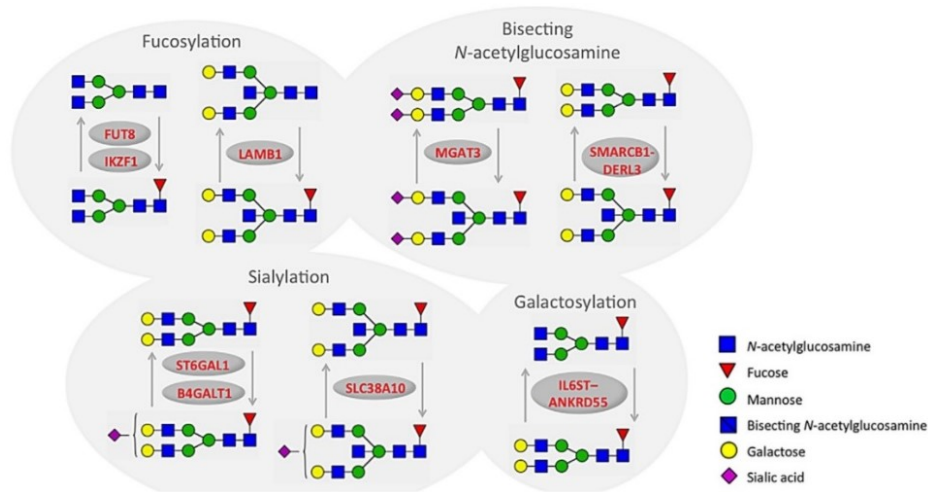


Fig. 1.27: Modification of IgG *N*-glycans. The various glycosyltransferases that can alter IgG *N*-glycans identified by a genome-wide association study (GWAS). Many of these glycosyltransferases are encoded by genes associated with autoimmune and inflammatory disorders. Image modified from Lauc et al. (2013).

1.11 Bioprocess conditions affecting glycosylation

Protein glycosylation occurs in the secretory pathway, ER and Golgi apparatus, and is influenced by many cellular factors. It is therefore not surprising that cell stress, particularly ER stress, can strongly influence the nature of glycosylation that occurs (Gerlach et al. 2012). The ER has a signalling pathway, the unfolded protein response (UPR), to cope with proteins that are folded incorrectly due to changes in homeostasis caused by chemical and physical stimuli, such as increased protein synthesis, altered calcium level, nutrient availability and altered glycosylation (Zhang and Kaufman 2006). Proteins that fold incorrectly due to high ER stress will be refolded and/or degraded but less extreme ER stress, caused by changing culture conditions, can lead to a shift in the glycosylation patterns on glycoproteins (Spearmann et al. 2007).

The choice of expression system is important when producing recombinant glycoproteins for human use. CHO cells are extensively used as a desired glycosylation profile can be achieved resulting in a safe and effective product. However, there are

numerous cell culture conditions that need to be considered and monitored throughout the production of a glycoprotein to ensure glycosylation heterogeneity is minimised and product quality does not decline. Glycosylation is complex and can be influenced by a myriad of factors, such as glycosyltransferase expression, nutrient availability, ER stress, by-product accumulation etc., which in turn are influenced by both the physical and the chemical conditions of the cell culture which are not fixed but fluctuate throughout a bioreactor campaign (Hossler et al. 2009).

1.11.1 Physical conditions

There are many process conditions that can be altered to enhance protein synthesis and achieve optimal glycosylation. Trummer et al. (2006) investigated the effects of temperature, pH and dissolved oxygen (DO) on the production and glycosylation of a recombinant erythropoietin-Fc (EPO-Fc) fusion protein expressed by CHO DUKX-B11 cells. The maximum sialic acid ratio, which is moles of *N*-acetylneuraminic acid to moles of glycoprotein, was found to be approximately 13 at pH 7.0. The ratio decreased if the pH decreased or increased slightly to pH 6.9 or pH 7.20. When the DO was at 50 % air saturation, the maximum ratio was achieved. Decreasing the culture temperature dramatically increased the protein concentration reached. A temperature drop from 37 °C to 30 °C resulted in a 2.4-fold increase in EPO-Fc. This increase can be primarily attributed to a prolonged culture as the temperature decrease suppressed cell growth. The temperature drop, while increasing specific productivity, resulted in a negative effect on EPO-Fc sialylation. There was a 40 % decrease in EPO-Fc sialylation when the culture temperature dropped from 37 °C to 30 °C. It is important that DO levels are controlled to maintain optimum metabolic conditions for the cells. However, the effects of hypoxia on protein glycosylation in CHO cell cultures is unclear. There was only a minor glycosylation change observed in oxygen deprived CHO cells producing tissue plasminogen activator (tPA), however an increase in the sialylation of recombinant follicle stimulating hormone (FSH) was reported in a CHO culture with high DO (Butler 2006; Hossler et al. 2009).

A similar study was completed by Yoon et al. (2005) where the production and glycosylation of a recombinant glycoprotein, EPO, from CHO cells was investigated. They too concluded that the pH and temperature of a cell culture drastically effect

growth, productivity and protein glycosylation. They suggested that the optimum pH for cell growth varies among CHO cell lines as their highest specific growth rate was observed at pH 7.6 at 37 °C. This indicates that the physical conditions within a bioreactor are not a ‘one size fits all’ but rather they should be tuned to best suit the cell line and the product in question thereby satisfying the manufacturer, i.e. achieving the optimum product yield without a compromise in the glycosylation of the product.

1.11.2 Chemical conditions

Mammalian cell culture medium is a complex mixture of 50 to 100 chemically defined ingredients, of which over 30 are essential, in addition to a small number of undefined components which are often supplemented. These undefined components include bovine serum which provides a plethora of macromolecules, i.e. carrier proteins, trace elements, hormones and growth factors, although for obvious regulatory reasons serum is omitted from biopharmaceutical cell culture media. The composition of culture medium, which changes by means of cellular metabolism, can drastically effect cell growth, protein synthesis and protein glycosylation (Hossler et al. 2009).

The depletion of glucose in cell culture medium has been shown to impact the type of glycosylation and its frequency, i.e. site-occupancy, on recombinant glycoproteins. Hayter et al. (1992) reported that CHO cells producing recombinant human interferon- γ (IFN- γ) produced an aglycosylated IFN- γ when glucose was limited. A similar result was also reported much more recently by Liu et al. (2014). They analysed the glycans on a chimeric heavy chain antibody produced in CHO cells when glucose availability was altered. They too observed the production of an aglycosylated protein, e.g. when the cells were deprived of glucose for 24 h, 45 % of the mAbs produced were aglycosylated. They also analysed the intracellular lipid linked oligosaccharides (LLO) which showed a decrease in the amount of complete LLO (Glc₃Man₉GlcNAc₂) when glucose was limited. Glucose is essential for the synthesis of complete glycosylation precursors, LLO (Glc₃Man₉GlcNAc₂), however high glucose concentrations results in lactate accumulation which can inhibit cell growth and production (Ahn and Antoniewicz 2012). The cultivation of cells in fed-batch mode greatly reduces the issues encountered with high or low glucose concentrations. As glucose depletion is so strongly linked with decreased glycan site-occupancy and increased glycan

heterogeneity it is vital that it is monitored throughout glycoprotein production (Fan et al. 2015a; Fan et al. 2015b; Villacres et al. 2015).

Glutamine is the most abundant extracellular amino acid *in vivo*. It is an essential component in cell culture media where it is a carbon and nitrogen source and a precursor for peptide and protein synthesis (Newsholme et al. 2003). Like glucose in cell culture media, when cells are starved of glutamine there are adverse effects to cell growth and glycosylation but a high concentration of glutamine is equally unwanted due to metabolite accumulation, principally ammonia. Glutaminolysis is the conversion of glutamine to pyruvate via the tricarboxylic acid (TCA) cycle and the malate-aspartate shuttle. Glutaminase converts glutamine to glutamate releasing ammonia. Glutamate is then converted to α -ketoglutarate by glutamate dehydrogenase, again releasing ammonia, after which it enters the TCA cycle. Metabolising one mole of glutamine to α -ketoglutarate yields one to two moles of ammonia. Ammonia accumulation occurs as glutamine is metabolised but also as glutamine degrades in liquid media. It has been known for some time that ammonia can inhibit cell growth and influence glycosylation (Ozturk et al. 1992; Andersen and Goochee 1995; Yang and Butler 2002). The typical ammonium concentrations reached in batch cultures are 2-10 mM (Altamirano et al. 2000). Street et al. (1993) showed using a nitrogen isotope that nearly all of the ammonia in CHO cell cultures is derived from the amide group of glutamine.

Sodium butyrate (NaBu) is routinely added to CHO cell cultures to enhance the expression of recombinant proteins such as EPO, by Chung et al. (2001), tPA, by Hendrick et al. (2001) and antibodies by Kim and Lee (2000). The expression of genes controlled by mammalian promoters, such as simian virus 40 (SV40) and cytomegalovirus (CMV), are increased by NaBu. This enhanced expression has been shown for both endogenous and exogenous genes in CHO cells (Mimura et al. 2001). The enhanced gene expression is thought to be caused by an increase in histone acetylation due to histone deacetylase being inhibited. Transcription factors get greater access to chromatin with increased histone acetylation (Lee et al. 1993). While increased gene expression is easily achieved with the addition of NaBu, there are also many undesirable effects which includes; reduced cell growth, increased cellular apoptosis and decreased glycoprotein quality (Sung et al. 2004; Lee and Lee 2012).

The effect of NaBu on the glycosylation of glycoproteins has been well documented. Sung et al. (2004) reported that the glycosylation of human thrombopoietin (hTPO) was considerably altered with NaBu. They expressed hTPO in CHO cells and observed a 3.3-fold increase in final hTPO concentration when 3 mM NaBu was added to the culture. However, the sialylation of hTPO decreased and glycan heterogeneity increased which effected the biological activity of hTPO, i.e. *in vivo* activity of hTPO was 72 % of that from culture without NaBu. The addition of NaBu is useful for increasing product yields however it can negatively influence glycosylation and so it should be assessed on a case by case basis as certain variables, such as the target glycoprotein, the host cell line and the culture mode, i.e. batch, fed-batch or perfusion etc., will influence its usefulness.

1.12 Aims and objectives of this study

The glycosylation of therapeutic proteins is crucial for their stability, efficacy, serum half-life and over all biological activity. Cell stress, from physical and/or chemical variables, encountered during the production of glycoproteins can alter the glycosylation profile resulting in sub-optimal therapeutics. The glycans displayed at the cell surface have been previously shown to change when cells are stressed and entering an apoptotic state and may also provide information as to the nature of the glycosylation of the product. Lectins are ideal glycan probes to examine these changes. However, many commonly used commercial lectins are purified from plant sources utilising conventional chromatography resulting in batch-to-batch variation in the resultant product. This has resulted in unwanted variation in the performance of these lectins. In addition many of these plant lectins are cytotoxic. Therefore, non-plant lectins produced recombinantly give the significant advantage of ease of production, consistent performance and reduced cytotoxicity.

Aim 1: To express, purify, characterise and label novel non-plant lectins.

Recombinant lectins are expressed in *E.coli* where relatively large quantities of soluble lectin may be achieved. The objective is to purify lectins using immobilised metal affinity chromatography (IMAC). The binding specificities of the resultant lectins are then assessed using the enzyme-linked lectin assay (ELLA). Fusing lectins to fluorescent proteins and/or altering their amino acid sequence, using site-directed

mutagenesis, are used to enhance lectin labelling, directly or indirectly, for their subsequent use on a fluorescent microscope and flow cytometer. This work is described in chapters 3 and 4.

Aim 2: To investigate CHO DP-12 cell surface and product glycan changes using lectins.

A panel of recombinant lectins, see aim 1, and commercial plant lectins are used to probe the CHO DP-12 cell surface. The objective is to determine the lectin binding profile for these cells and assess lectin binding differences when cells are cultured in altered media i.e. nutrient depleted, low glutamine, high ammonia or with sodium butyrate. This lectin binding is assessed using fluorescent microscopy and quantified using flow cytometry. In addition the glycosylated protein product from these CHO DP-12 cells, recombinant IgG1, is purified using protein A/G affinity chromatography and its glycosylation status is assessed by ELLA. This work is described in chapter 5. Ultimately, the overall aim and objective of this work is to assess the ability of a combination of lectin probes and flow cytometry to successfully interrogate the surface glycosylation state of CHO cells.

Chapter 2

Materials and Methods

2.1 Bacterial strains, vectors, constructs and primers

Table 2.1: *E. coli* strains

Strain	Use in project	Genotype	Features	Source
JM109	For competent cells and for initial small scale protein expression.	e14-(McrA-) <i>recA1</i> <i>endA1 gyrA96 thi-1</i> <i>hsdR17</i> (r_k^- , m_k^+) <i>supE44</i> <i>relA1</i> $\Delta(lac-proAB)$ [F' <i>traD36 proAB</i> <i>lacIqZ</i> Δ M15]	Enhanced for high quality miniprep DNA. The <i>recA1</i> mutation improves insert stability. Appropriate for routine cloning.	Stratagene ^a
KRX	For increased level of protein expression.	[F', <i>traD36</i> , Δ <i>ompP</i> , <i>proA</i> ⁺ <i>B</i> ⁺ , <i>lacIq</i> , $\Delta(lacZ)$ M15] Δ <i>ompT</i> , <i>endA1</i> , <i>recA1</i> , <i>gyrA96</i> (Nal ^r), <i>thi-1</i> , <i>hsdR17</i> (r_k^- , m_k^+), e14- (McrA-), <i>relA1</i> , <i>supE44</i> , $\Delta(lac-proAB)$, $\Delta(rhaBAD)::T7$ RNA polymerase	Engineered for optimised controlled protein expression. The <i>recA1</i> mutation minimizes undesirable recombination events. The <i>ompP</i> and <i>ompT</i> mutations reduce the proteolysis of overexpressed proteins.	Promega ^b

a - JM109 2016; b - KRX 2016

Table 2.2: Plasmid vectors

Plasmid	Description	Source
pQE-30	A vector for the expression of <i>N</i> -terminally-tagged (His) ₆ proteins with Amp ^R , a T5 promoter and a lac operator.	Qiagen
pQE-60	A vector for the expression of <i>C</i> -terminally-tagged (His) ₆ proteins with Amp ^R , a T5 promoter and a lac operator.	Qiagen
pQE-30_AAL-2	pQE-30 (Qiagen) derived plasmid containing fungal lectin AAL-2.	ISSC*
pQE-30_LecA	pQE-30 (Qiagen) derived plasmid containing a lectin, LecA, from the gram-negative bacterium <i>Pseudomonas aeruginosa</i> .	ISSC*
pQE-30_GafD1-178	pQE-30 (Qiagen) derived plasmid containing a fimbrial lectin, GafD, from <i>Escherichia coli</i> .	ISSC*
pQE-30_CHA-1	pQE-30 (Qiagen) derived plasmid containing a lectin, CHA-1, from <i>Cepaea hortensis</i> (Garden snail).	ISSC*
pQE-30_EGFP	pQE-30 (Qiagen) derived plasmid containing EGFP.	ISSC*

* The Irish Separation Science Cluster (ISSC) had previously inserted genes encoding carbohydrate binding proteins into Qiagen vectors. The protein FASTA sequences were obtained from the NCBI Protein Database (<https://www.ncbi.nlm.nih.gov/protein>). Prior to gene block synthesis the sequences were codon optimised for expression in *E. coli* using IDT's online Codon Optimization Tool (<https://eu.idtdna.com/CodonOpt>). The synthesised gene blocks (<https://eu.idtdna.com/pages/products/genes/>) were then inserted in frame into the multiple cloning site of Qiagen vectors.

Table 2.3: Plasmid constructs

Plasmid	Description	Source
<i>Plasmids containing AAL-2</i>		
pEGFP_AAL-2	pQE-30 containing an EGFP-AAL-2 fusion. EGFP is encoded between the <i>N</i> -terminal (His) ₆ tag and the AAL-2 coding sequence.	This Work
pAAL-2_NL	pQE-30 containing a 90 nucleotide linker between the <i>N</i> -terminal (His) ₆ tag and AAL-2.	This Work
pAAL-2_CT	pQE-60 containing AAL-2.	This Work
pAAL-2_MT	pQE-30 containing AAL-2 with G53A, G54A, W55A, G222A, G223A and W224A mutations.	This Work
<i>Plasmids containing LecA</i>		
pEGFP_LecA	pQE-30 containing an EGFP-LecA fusion. EGFP is encoded between the <i>N</i> -terminal (His) ₆ tag and LecA coding sequence.	This Work
pLecA3K	pQE-30 containing LecA with an insertion encoding 3 lysine residues at the <i>C</i> -terminus of the protein.	This Work
pLecA5K	pQE-30 containing LecA with an insertion encoding 5 lysine residues at the <i>C</i> -terminus of the protein.	This Work
pLecA3KH	pQE-30 containing LecA with an insertion encoding 3 lysine residues before at the <i>N</i> -terminal (His) ₆ tag.	This Work
pLecAH3K	pQE-30 containing LecA with an insertion encoding 3 lysine residues between the <i>N</i> -terminal (His) ₆ tag and the LecA coding sequence.	This Work

Table 2.4: Primer sequences (Synthesised by IDT, Belgium)

Name	Primer Sequence (5' → 3')	Change	T _m (°C)
<i>Primers for cloning</i>			
60AAL2_F	GTCAGT <u>CCATGGG</u> CATGACCTCTAACGTTATC	-	46.8
60AAL2_R	GTCAGT <u>AGATCT</u> TTAGTGACGAGAAGAGTC	-	49.9
<i>Primers for AAL-2 mutagenesis</i>			
AAL-2 FP1	P-GCGCTGACCACCAAACACGTTCGTCTGATCG C	W55A	65.7
AAL-2 RP1	P-AGCAGCAGCGTTCTGAGCGAAGTTTTTAACA GCC	G53A, G54A	63.1
AAL-2 FP2	P-GCTGCTGCTAAAATCGGTGACCACCCGCGT TTCGTTGC	G222A, G223A, W224A	66.9
AAL-2 RP2	P-AGCGTCAATGCAGAAGTTGTCGATAACAGAT TTAGCCG	Silent mutation	65.6
<i>Primers for lysine insertion</i>			
LecAKF	P-TAAAAGCTTAATTAGCTGAGCTTGGACTCCT GT	-	60.7
LecA3KR	P- CTTCTTCTT GGACTGATCCTTTCCAATATTG ACACT	3 lysine insertion	56.7
LecA5KR	P- CTTCTTCTTCTTCTT GGACTGATCCTTTCC AATATTGACACTGAA	5 lysine insertion	58.9
LecA3KHF	P-TCGCATCACCATCACCATCACGGATCCATG	-	64.4
LecA3KHR	P- CTTCTTCTT CATAGTTAATTTCTCCTCTTTA ATGAA	3 lysine ins/del*	50.6
LecAH3KF	P-TCCATGGCTTGGAAGGTGAGGTTCTGGC	-	65.5
LecAH3KR	P- CTTCTTCTT TCCGTGATGGTGATGGTGATG CGATCC	3 lysine insertion	65

Notes: Non-binding nucleotides are in bold.
Restriction sites are underlined.
Melting temperatures were calculated using the formula
 $T_m = 64.9 + 41 * (yG+zC-16.4) / (wA+xT+yG+zC)$

- * Insertion and deletion. 6 nucleotides before the (His)₆ tag were replaced with 9 nucleotides encoding lysine.
- P- denotes phosphorylation at the 5' end.

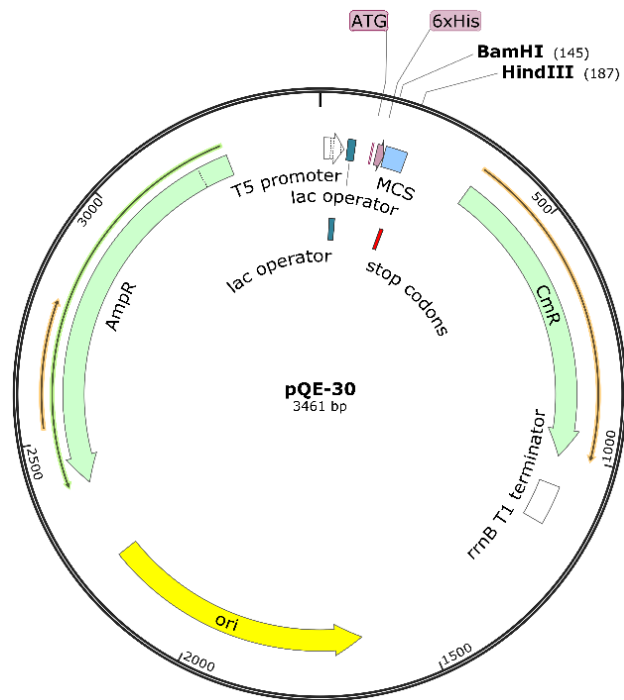


Fig. 2.1: The pQE-30 vector (Qiagen). This 3461 bp Qiagen expression vector is used for the expression of *N*-terminally-tagged His₆ proteins. This vector contains a T5 phage promoter (white), a lac operator (dark green), a His₆ tag (pink) and a MCS after the His₆ tag (blue). The *bla* and *cat* genes (light green) encode β-lactamase and chloramphenicol acetyltransferase, respectively, which confers ampicillin and chloramphenicol resistance to the bacteria. This image was generated using SnapGene® Viewer Version 3.1.4.

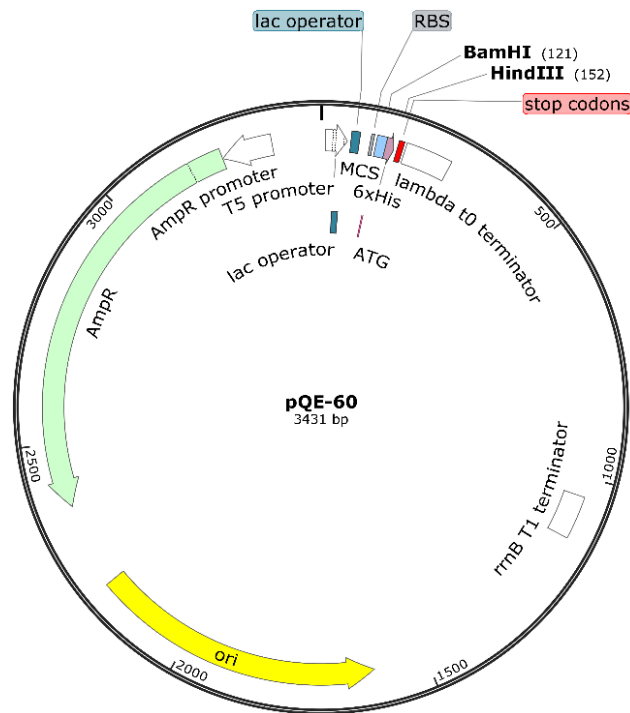
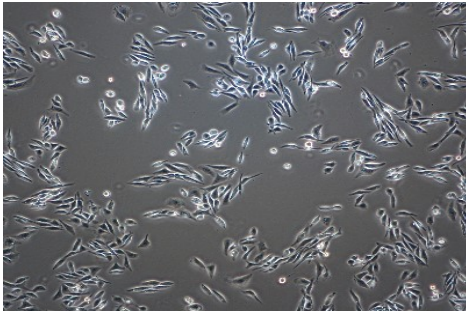


Fig. 2.2: The pQE-60 vector (Qiagen). This 3431 bp Qiagen expression vector is used for the expression of C-terminally-tagged His₆ proteins. This vector contains a T5 phage promoter (white), a lac operator (dark green), a His₆ tag (pink), a MCS before the His₆ tag (blue) and a transcription terminator, t₀, from phage lambda (white). The *bla* gene (light green) encodes β-lactamase which confers ampicillin resistance to the bacteria. This image was generated using SnapGene® Viewer Version 2.8.

2.2 CHO DP-12

Table 2.5: CHO DP-12

Organism	<i>Cricetulus griseus</i> , hamster, Chinese
Tissue	Ovary
Morphology	Fibroblast
Culture Properties	Adherent
Biosafety Level	1
Product	Co-expression of variable light and heavy chains of the murine recombinant immunoglobulin G1 (IgG1) which inhibits interleukin 8 mediated human neutrophil chemotaxis. IgG1 is a 146 kDa glycoprotein.
Low Density	
High Density	
Source	National Institute for Cellular Biotechnology, DCU

2.3 Microbiological media

The chemicals and solutions used were all ACS grade and were supplied by Sigma-Aldrich unless otherwise stated. Media was sterilised by autoclaving at 121 °C for 20 min. The distilled water (dH₂O) is from a Milli-Q® Academic system with a MILLIPAK™ 0.22 µm filter.

Lysogeny broth (LB)

Tryptone	10 g/L	(Scharlau Casein Trypsic Peptone 07-119)
NaCl	10 g/L	
Yeast extract	10 g/L	(Scharlau Yeast Extract 07-079)
pH	7.0	

The pH was adjusted to 7.0 using 0.1 M NaOH and brought to the correct volume using dH₂O. To produce solid agar plates 15 g/L of agar was added prior to sterilisation.

Terrific broth (TB)

Tryptone	12 g/L	(Scharlau Casein Trypsic Peptone 07-119)
Yeast extract	24 g/L	(Scharlau Yeast Extract 07-079)
Glycerol	4 mL/L	

Distilled H₂O was added bringing the volume to 900 mL followed by autoclaving. After cooling, 100 mL of 1M potassium phosphate buffer, Section 2.5, was added aseptically and the pH was brought to pH 7.4.

Super optimal broth (SOB)

Tryptone	20 g/L	(Scharlau Casein Trypsic Peptone 07-119)
Yeast extract	5 g/L	(Scharlau Yeast Extract 07-079)
NaCl	500 mg/L	
KCl	2.5 mM	
pH	7.0	

The solution was autoclaved and cooled to 55 °C. 1M MgCl₂ and 1M MgSO₄ were filter sterilised and added to final concentrations of 10 mM each.

Super optimal broth with catabolite repression (SOC)

SOB medium was made and a filter sterilised solution of 50 % glucose was added to a final concentration of 20 mM.

2.4 Cell culture growth media

CHO DP-12 was grown both adherently in T-75 tissue culture flasks in DME/F12 medium and in suspension in BalanCD CHO Growth A Medium. The two types of complete media are described below. Cell culture media was prepared aseptically in a biological safety cabinet (Holten Laminair HB2448) and stored at 4 °C.

Adherent serum-supplemented medium

Dulbecco's Modified Eagle's Medium/ Ham's Nutrient Mixture F-12 (D8437)	445 mL
10 % Foetal Bovine Serum (Gibco® Non-HI)	50 mL
1 % Penicillin-Streptomycin (P0781)	5 mL
200 nM Methotrexate hydrate (06563)	90.9 µL (1.1 mM stock)

Suspension serum-free medium

BalanCD CHO Growth A Medium/ (Irvine Scientific 91128)	950 mL
0.252 % Polyvinyl alcohol	20 mL (12.6 % stock in PBS)
1 % Penicillin-Streptomycin (P0781)	10 mL
200 nM Methotrexate hydrate (06563)	181.8 µL (1.1 mM stock)
4 mM L-Glutamine	20 mL (200 mM stock)

2.5 Buffers and solutions

Potassium phosphate buffer

KH ₂ PO ₄	23.1 g
K ₂ HPO ₄	125.4 g
pH	7.4

The volume was brought to 1 L with dH₂O and autoclaved.

TB buffer

PIPES	10 mM
CaCl ₂	10 mM
KCl	250 mM
pH	6.7

The pH was adjusted with 1 M KOH and MnCl₂ was added to a final concentration of 50 mM. The solution was sterilised using a syringe and a 0.22 µm filter membrane and stored at 4 °C.

TE buffer

Tris base	10 mM
Na ₂ -EDTA	1 mM
pH	8.0

The pH was adjusted with 1 M HCl.

RF1 solution

RbCl	100 mM
CaCl ₂	10 mM
Potassium acetate	30 mM
Glycerol	15 %
pH	5.8

The pH was adjusted with 1 M HCl and MnCl₂ was added to a final concentration of 50 mM. The solution was sterilised using a syringe and a 0.22 µm filter membrane and stored at 4 °C.

RF2 solution

RbCl	100 mM
CaCl ₂	75 mM
Potassium acetate	10 mM
Glycerol	15 %
pH	6.8

The solution was sterilised using a syringe and a 0.22 µm filter membrane and stored at 4 °C.

TAE buffer (50X)

Tris base	242 g/L
Glacial acetic acid	57.1 mL/L
EDTA	50 mM
pH	8.0

The pH was adjusted with 1 M HCl. The solution was diluted using dH₂O for a 1X solution.

Agarose gel

TAE Buffer (1X)	1 L
Agarose	7 g/L (0.7 %)

1 % and 1.5 % agarose gels were occasionally used. The agarose was dissolved by autoclaving and then stored at 60 °C.

PBS (10X)

Na ₂ HPO ₄	10.9 g/L
NaH ₂ PO ₄	3.2 g/L
NaCl	90 g/L

For PBST, Triton X-100 was added to PBS 1X to a concentration of 0.1 % (v/v).

TBS buffer

Tris base	20 mM
NaCl	150 mM
CaCl ₂	1 mM
MgCl ₂	1 mM
pH	7.6

The pH was adjusted with 1 M HCl and MnCl₂ is added to a final concentration of 1 mM. To make TBST, Tween 20, a detergent, was added to a final concentration of 0.1 % (v/v). To make western blot blocking buffer BSA was added to TBST to a final concentration of 5 % (w/v).

Gel loading dye

Bromophenol blue	0.25% (w/v)
Xylene cyanol	0.25 % (w/v)
Ficoll (Type 400)	15 % (w/v)

Bromophenol blue and xylene cyanol on a 1 % agarose gel migrate to approximately 300 bp and 4000 bp.

SDS solution

SDS	10 % (w/v)
-----	------------

SDS-PAGE buffer (5X)

Tris base	15 g/L
Glycine	72 g/L
SDS	5 g/L
pH	8.3

The pH was adjusted with 1 M HCl. This was diluted using dH₂O to a 1X running buffer solution.

SDS-PAGE sample buffer (10X) 8 mL

SDS	3.2 mL of 10 % stock
2-Mercaptoethanol	0.8 mL
Tris base	2.0 mL of 0.5 M stock, pH 6.8
Bromophenol Blue	0.5 % (w/v)
dH ₂ O	0.4 mL

Coomassie blue stain solution

dH ₂ O	50 % (v/v)
Methanol	40 % (v/v)
Acetic Acid	10 % (v/v)
Coomassie blue	0.25 % (w/v)

Coomassie blue destain solution

dH ₂ O	45 % (v/v)
Methanol	45 % (v/v)
Acetic Acid	10 % (v/v)

Western blot semi dry transfer buffer (SDTB)

Tris base	5.8 g
Glycine	2.9 g
Methanol	200 mL
SDS	0.37 g

The volume was brought to 1 L with dH₂O and stored at 4 °C.

Ethidium bromide solution

A stock solution, 10 mg/mL, in dH₂O was stored at 4 °C. To stain agarose gels 100 µL of stock solution was added to 1 L of dH₂O. This stain solution was kept in the dark. A de-staining bag (GeneChoice) was used to extract used ethidium bromide from the solution. The remaining solution was disposed of and the ethidium was incinerated. Ethidium bromide solution was kept covered in a designated area of the laboratory.

Lysis buffer

NaH ₂ PO ₄	50 mM
NaCl	0.5 M
Imidazole	10-250 mM
pH	8.0

The pH was adjusted with 1 M HCl.

Citrate buffer

Sodium Citrate (0.1 M)	3.63 mL
Citric Acid (0.1 M)	1.37 mL
dH ₂ O	5 mL
pH	5.5

TMB substrate

1 TMB tablet (T3406)	1 mg
Citrate Buffer	10 mL
H ₂ O ₂	2 µL

H₂O₂ is added directly before use.

Methotrexate stock solution

Methotrexate hydrate	1.1 mM
----------------------	--------

Methotrexate was dissolved in PBS. The solution was sterilised using a syringe and a 0.22 µm filter membrane. The solution was stored in 100 µL aliquots at -20 °C for up to 6 months. Typically 90.9 µL of the MTX stock solution (1.1 mM) was added to 500 mL of complete media resulting in a MTX working concentration of 200 nM.

Sodium butyrate stock solution

Sodium Butyrate	0.9 M
-----------------	-------

NaBu was dissolved in PBS. The solution was sterilised using a syringe and a 0.22 µm filter membrane. The solution was stored in 200 µL aliquots at -20 °C for up to 1 month. Typically 166.6 µL of the NaBu stock solution (0.9 M) was added to 50 mL of complete media resulting in a NaBu working concentration of 3 mM.

Ammonium chloride stock solution

NH ₄ Cl	1 M
pH	7.2

Ammonium chloride was added to dH₂O and the pH adjusted with 0.1 M NaOH. The solution was sterilised using a syringe and a 0.22 µm filter membrane and stored at 4 °C. Typically 500 µL of the ammonium chloride stock solution is added to 49.5 mL of complete media resulting in an ammonia working concentration of 10 mM.

Elution buffer for Protein A/G resin

Glycine	0.1 M
pH	2.5

The pH was adjusted with 1 M HCl. The solution was sterilised using a syringe and a 0.22 µm filter membrane and stored at 4 °C.

Neutralization buffer for Protein A/G resin

Tris base	1 M
pH	8.5

The pH was adjusted with 1 M HCl. The solution was sterilised using a syringe and a 0.22 µm filter membrane and stored at 4 °C.

EDTA cell dissociation solution

EDTA	10 mM
pH	7.5

The solution was made in PBS. The pH was adjusted with 1 M HCl. The solution was sterilised using a syringe and a 0.22 µm filter membrane and stored at 4 °C.

2.6 Antibiotics

Stock solutions of ampicillin were prepared in dH₂O at a concentration of 100 mg/L and stored at -20 °C. The working concentration of ampicillin in LB agar plates and liquid cultures was 100 µg/mL.

2.7 Storing and culturing of bacteria

All bacterial stocks were stored at -80 °C in 26.7 % glycerol. *E. coli* was cultured by inoculating a LB agar plate, see Section 2.3, with a loopful of culture from a thawed glycerol stock. Inoculated plates were incubated at 37 °C for 18-24 h. To produce a broth culture a single colony was used to inoculate 5 mL of media which was incubated at 37 °C in a shaker incubator for 18-24 h. For protein expression, 2 mL of this 5 mL culture was used to inoculate 200 mL of TB, see Section 2.3, and was incubated at 37 °C in a shaker incubator for 2-4 hours. Table 2.1 shows the bacterial strains used and their features. Glycerol stocks were made from 1 mL of LB culture plus 500 µL of an 80 % glycerol solution and stored at -80 °C.

2.8 Isolation and purification of DNA

2.8.1 Isolation of Plasmid DNA

Plasmid DNA was isolated using the Sigma GenElute Plasmid Miniprep Kit (PLN350). This kit was used according to the manufacturer's instructions. 1.5 mL of bacterial culture in a microfuge tube was centrifuged (Labnet Spectrafuge™ 24D) at 15,000 g for 2 min to pellet the cells. The supernatant was removed and the pellet was resuspended in 200 µL of resuspension solution. The RNase A solution was added to the resuspension solution prior to use and stored at 4 °C. 200 µL of lysis solution was added and the tube was gently inverted and left at room temperature for 5 min. Harsh mixing may cause the co-purification of unwanted chromosomal DNA. 350 µL of neutralisation solution was added and mixed by inversion to precipitate cell debris, lipids, proteins and chromosomal DNA. The mixture was left at room temperature for 10 min. The precipitate was collected by centrifugation at 15,000 g for 10 min. A spin column had been prepared for binding by adding 500 µL of column preparation solution and centrifuging at 15,000 g for 1 min. The supernatant was transferred to the prepared spin column and centrifuged for 30 s to bind the plasmid DNA. The flow through was discarded and 750 µL of wash solution was added and centrifuged at 15,000 g for 30 s to removed contaminants. The flow through was discarded and the matrix was dried by centrifuging at 15,000 g for 2 min. The spin column was transferred to a new microfuge

tube and 100 μL of elution solution was added. The plasmid DNA was eluted by centrifugation at 15,000 g for 30 s.

2.8.2 Isolation of DNA from PCR mixtures and agarose gels.

The illustra™ GFX™ PCR DNA and Gel Band Purification Kit (28-9034-71) from GE Healthcare was used to isolate DNA from PCR mixtures and agarose gels. This kit was used according to the manufacturer's instructions. The DNA band to be purified from the agarose gel was excised using a scalpel. Up to 300 mg of agarose gel was then transferred to a microfuge tube. 500 μL of capture buffer type 3 was added and the sample was mixed thoroughly by vortexing. The tube was incubated at 55 °C for 10-15 min until the agarose gel was fully dissolved. During this incubation the tube was inverted every 2-3 min. Alternatively, for the purification of DNA from PCR mixtures, 500 μL of capture buffer type 3 was added to 100 μL of a PCR mixture and mixed until the solution was a pale yellow. The sample was placed in a spin column and centrifuged at 15,000 g for 30 s and the flow through was discarded. 500 μL of wash buffer type 1 was added and centrifuged at 15,000 g for 30 s. The flow through was discarded and the column was dried in a new microfuge tube by centrifugation at 15,000 g for 2 min. 30 μL of DNA elution buffer was added to the centre of the column matrix and left at room temperature for 2 min. The column was then centrifuged at 15,000 g for 30 s to elute the DNA. The purified DNA was stored at -20 °C.

2.9 Agarose gel electrophoresis

DNA was analysed by agarose gel electrophoresis in a BioRad horizontal gel apparatus connected to a Labnet Power Station™ 300 power supply. Agarose was prepared by adding 0.7 % to TAE buffer and dissolving by boiling. The agarose was stored at 60 °C to prevent solidification. When required the heated agarose was poured into plastic trays and let to set containing a plastic comb to form wells. 1X TAE buffer was used as the running buffer. Typically 1.5 μL of gel loading dye, see Section 2.6, was mixed with 7 μL of sample to help the sample settle in the well. A molecular size marker was run on every gel by adding 0.5 μg of 1 kb DNA ladder (N3232L New England Biolabs®) to a well. The ladder was also loaded with gel loading dye. Gels are run at 120 V for

20-40 min on a Labnet Powerstation 300. The gel was then stained for 15 min by immersion in an ethidium bromide solution, see Section 2.5. Gels are visualized using an UV transilluminator, Pharmacia Biotech ImageMaster VDS (peak 312 nm), coupled with a Fujifilm Thermal Imaging System FT1-500 which prints gel pictures. SYBR® Safe gels are prepared for subsequent DNA band extraction. 30 mL of 0.7 % agarose was mixed with 3 µL of SYBR Safe stain (Invitrogen™ S33102) and poured into a plastic gel tray to set. These gels were visualized using a transilluminator, Dark Reader CCR (DR-46B).

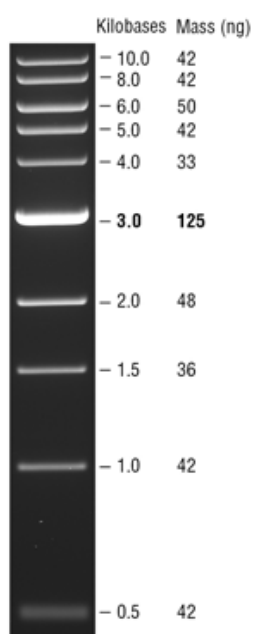


Fig. 2.3: 1kb DNA ladder (New England Biolabs N3232). The molecular marker was visualized by ethidium bromide staining on a 0.8 % TAE agarose gel. Mass values are for 0.5 µg/lane. Image obtained from <https://www.neb.com>.

2.10 Transformations

2.10.1 Preparation of competent cells - The rubidium chloride method.

Hanahan (1985) first described the following method. 5 mL of LB with the appropriate antibiotics was inoculated with a single colony of the relevant bacteria and allowed to grow overnight at 37 °C in a shaking incubator at 200 rpm. 2.5 mL of this overnight culture was added to 250 mL LB in a 1 L flask and allowed to grow to an A_{600} of 0.5 (early-mid exponential phase) at 37 °C at 200 rpm. The flask was placed on ice for 10 min to cool. All subsequent steps took place at 4 °C. The culture was centrifuged to collect the cells at 1,500 g for 5 min. The culture media was decanted and the cell pellet was resuspended very gently in 75 mL of ice-cold RF1 buffer, see Section 2.5. The suspension was then left on ice for 90 min. The cells were again collected by centrifugation as before. The culture media was again discarded and the pellet was resuspended very gently in 10 mL ice-cold RF2, see Section 2.5. The cell suspension was aliquoted (200 μ L/tube) into sterile microfuge tubes (1.5 mL) which were then flash frozen in a metal block, which was precooled to -80 °C. The competent cells were then stored at -80 °C.

2.10.2 Transformation of competent cells.

An aliquot of competent cells were taken from the -80 °C freezer and thawed on ice. 200 μ L of competent cells were mixed with plasmid DNA or ligation reaction. This mixture was kept on ice for 30 min, to allow the DNA to bind to the cells. The mixture was then heat shocked at 42 °C in a water bath for 30 s and quickly returned to ice for 2 min. 800 μ L of SOC broth, see Section 2.3, was added aseptically and incubated at 37 °C in a water bath for 1 hour. 200 μ L was spread on agar plates with the appropriate antibiotics and incubated overnight at 37 °C. The rest was concentrated by centrifugation at 15,000 g for 1 minute. The cell pellet was resuspended in 200 μ L of culture media. This was spread on an agar plate and incubated overnight at 37 °C as previously described.

2.11 Enzymatic reactions.

All enzymes and buffers used were obtained from New England Biolabs® or Promega™ and were according to the manufacturer's instructions. Polymerase chain reactions (PCR) reactions were performed in Veriti 96 well Thermal Cycler (Applied Biosciences).

Standard PCR reaction mixture

Template DNA	1 µL
dNTPs (10 mM)	1 µL
Primers (10 µM)	1 µL of each
Buffer (5X)	10 µL
dH ₂ O	35 µL
Q5® High-Fidelity DNA polymerase	1 µL

Table 2.6: PCR programme cycle

Step	Temperature (°C)	Time	Cycles
Initial denaturation	95	10 min	1
Denaturation	95	30 s	} 30
Annealing	55-70	30 s	
Extension	72	2 min	
Final extension	72	10 min	1
	4	Hold	

DpnI restriction digest

PCR product	15 µL
Buffer (10X)	2.5 µL
DpnI	1 µL
dH ₂ O	6.5 µL

The reaction mixture was incubated at 37 °C for 2 h.

Restriction digest

Purified plasmid or PCR product	15 μ L
Buffer (10X)	2.5 μ L
Restriction enzyme	1 μ L
dH ₂ O	6.5 μ L

The reaction mixture was incubated at 37 °C for 2 h.

Ligation reaction

Vector	10 μ L
Insert	5 μ L
T4 DNA Ligase	1 μ L
Ligase buffer (10X)	2.5 μ L
dH ₂ O	6.5 μ L

The reaction mixture was incubated at room temperature for 3 h or overnight at 4 °C.

2.12 Site-directed mutagenesis

Site-directed mutations were introduced into open reading frames (ORF) on plasmid constructs by PCR amplification using back to back complementary phosphorylated primers carrying the desired mutation. Insertions were also introduced using back to back complementary phosphorylated primers. Unlike conventional PCR where only a specific region of the DNA template is amplified, here whole plasmid synthesis was completed, see Fig. 2.4.

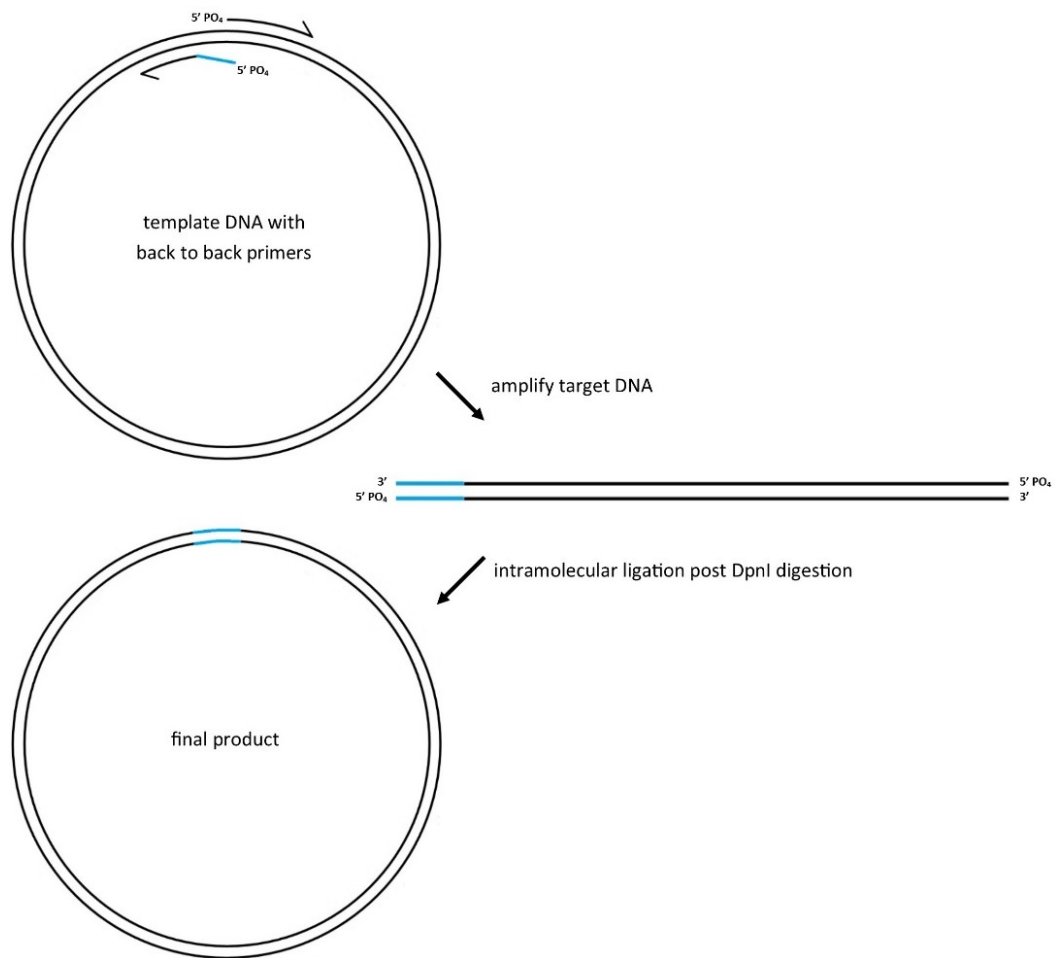


Fig. 2.4: Site-directed mutagenesis. One of the two primers contains the desired mutation or insertion (blue region) at the 5' region of the primer. Both primers are phosphorylated at the 5' end allowing for intramolecular ligation post amplification. The resulting plasmid is then transformed into competent cells.

A standard PCR reaction mixture, as described in Section 2.10.1.1, was set up. The PCR was carried out using Q5® High-Fidelity DNA polymerase. The standard program cycle for Q5® High-Fidelity DNA polymerase reactions was used, see Table 2.6. An extension time of 2 min was used to amplify plasmids of 3.5-4 kb. The template DNA was then eliminated by digestion with DpnI restriction endonuclease, Section 2.11. DpnI selectively digests the template DNA from *dam*⁺ *E. coli* strains, e.g. JM109 and KRX, over the newly synthesized DNA. DpnI will only cut the DNA when the adenine in the restriction site, GA^VTC, is methylated. The amplified plasmid, with the incorporated mutation, is circularised by ligation, see Section 2.11, which is possible as phosphorylated primers were used during the initial PCR amplification.

2.13 DNA Sequencing

Recombinant clones and mutants were verified by DNA sequencing. Commercial sequencing services were provided by MWG-Biotech/Eurofins Genomics. Eurofins use the cycle sequencing technology (dideoxy chain termination) on ABI 3730XL sequencing machines. This method is a modification of the traditional Sanger sequencing method. Plasmids were purified, see Section 2.8.1, and eluted in dH₂O. 15 µL was shipped in duplicate so forward and reverse reads could be obtained. Primers were not sent with plasmids to be sequenced as all plasmids were vectors recognised, pQE, by MWG-Biotech/Eurofins Genomics.

2.14 *In silico* analysis of DNA and protein sequences

The BLAST program, available from NCBI (<http://blast.ncbi.nlm.nih.gov/Blast.cgi>), was used to identify regions of local similarity in protein and DNA sequences deposited in GenBank. A protein BLAST search of *Agrocybe aegerita* lectin 2 (AAL-2) (AFA53122.1) identified sequence similarity with partial *Lacrymaria velutina* lectin (PVL) (ABB17278.1). DNA and protein sequences were aligned using the alignment function in BLAST and the local alignment tools provided by the European Bioinformatics Institute (<http://www.ebi.ac.uk/Tools/psa/>). Multiple Sequence Alignment was also completed using CLUSTALW (<http://www.genome.jp/tools/clustalw/>). The Protein Data Bank (<http://www.rcsb.org/pdb>) was used to identify glycan or ion binding sites and structural information (e.g. helices, turns and beta strands). Restriction sites in DNA sequences were identified using Webcutter 2.0 (<http://rna.lundberg.gu.se/cutter2/>) and SnapGene® Viewer Version 2.8. ExpASy was used to translate nucleotide sequences into protein sequences (<http://web.expasy.org/translate/>) and to compute protein parameters, molecular weight, theoretical pI, amino acid composition, extinction coefficient, etc., using the ProtParam tool (<http://web.expasy.org/protparam/>).

Protein structure was predicted using the free online I-TASSER tool (<http://zhanglab.ccmb.med.umich.edu/I-TASSER/>). This tool is provided by the Zhang Lab at the University of Michigan. I-TASSER has been ranked as the best server for

protein structure prediction in community-wide Critical Assessment of Structure Prediction (CASP) experiments (Zhang 2008). The I-TASSER tool uses the PDB and other protein sequence databases to determine the likely structure of a submitted protein sequence. The I-TASSER tool generates 5 predicted 3D models of the submitted protein sequence, each with its own C-score which estimates the quality of the model. The 3D model with the highest C-score, i.e. highest confidence model, was selected. All 3D protein structures were viewed and subsequently coloured/labelled using PyMOL Version 1.3 (<http://pymol.org/edu/?q=educational/>).

2.15 Standard expression culture

Single colonies of the bacteria containing the expression plasmid of interest were prepared on a LB agar plate, with the appropriate antibiotics, from a working glycerol stock. A single colony was selected to inoculate a sterilin containing 5 mL of LB and antibiotic. The culture was incubated overnight at 37 °C at 200 rpm. A 1 L baffled Erlenmeyer flask containing 200 mL TB media and appropriate antibiotic was inoculated with 2 mL of this overnight culture. The culture was grown at 37 °C, with shaking at 200 rpm, until an A_{600} of 0.4-0.6 was reached (mid-late exponential phase). At this point IPTG was added to a final concentration of 100 µg/mL to induce expression of the protein. The culture was then incubated at 30 °C for 18-20 h before the cells were collected by centrifugation at 4,000 g for 10 min using a Sorvall™ GSA rotor. The pellet can be stored at -20 °C and the supernatant is autoclaved and discarded.

2.16 Preparation of cleared lysate for protein purification

2.16.1 Cell lysis by cell disruption

A cell pellet from a 200 mL culture, see Section 2.15, was resuspended in 100 mL lysis buffer containing 20 mM imidazole, see Section 2.5, and 0.1 % antifoam (Sigma Antifoam SE-15). The cells were mixed in this buffer for 10-15 min using a magnetic bar and stirrer until the cell pellet was dissolved and the cells were fully homogenised. The cells were lysed using a Constant Systems Ltd cell disruptor (TS Series Bench Top). The pressure was selected according to the organism being disrupted. For *E. coli*,

the pressure selected was 15 kpsi. Prior to loading sample 100 mL of lysis buffer containing 20 mM imidazole is passed through the system to equilibrate it. The system is also cooled to keep the sample chilled as it is being disrupted. This is achieved by preparing a water bath filled with ice water and circulating this through the cooling jacket surrounding the disruption head. The sample was then loaded into the reservoir and disrupted. The disrupted sample was collected and passed through the system again to ensure complete disruption. 20 mL of lysis buffer was chased through the instrument at the selected pressure to harvest any residual sample. The system was thoroughly cleaned after each use by running 150 mL of dH₂O, 150 mL of ethanol followed by a final 150 mL of dH₂O through the machine. The disrupted sample was then spun at 15,000 g for 40 min at 4 °C to pellet any insoluble debris. The cell lysate was stored at 4 °C for protein purification.

2.16.2 Preparation of lysate for IMAC column loading

The lysate is filtered through Whatman® filter paper (Grade 1 - 11 µm) using a Nalgene® reusable vacuum filter unit (DS0320-5045) into a clean bottle. This filter step helps remove cell debris and aggregates in the lysate. The filtered lysate ready for IMAC column loading.

2.17 Purification of recombinant lectins

Immobilised metal affinity chromatography (IMAC) was used to purify recombinant proteins as they contained either an *N*- or *C*- terminal His₆ tag. The concept of protein purification by IMAC was first reported by Porath et al. (1975). Transition metal ions, Zn²⁺, Cu²⁺, Ni²⁺ and Co²⁺ have affinity for histidine in aqueous solutions. IMAC resin consists of a Sepharose bead functionalised with a chelator, e.g. nitrilotriacetic acid (NTA), which is then charged with a metal ion. Three oxygen atoms and one nitrogen atom on the NTA ligand coordinate with four of the six Ni²⁺ valencies. The remaining two interact with nitrogen atoms on adjacent histidine residues. Most untagged proteins will flow through the charged resin. Weakly bound non-target proteins, e.g. proteins with surface histidine residues, are removed with imidazole (20-100 mM) washes. Bound His₆ tagged proteins are eluted with 250 mM imidazole.

2.17.1 Standard IMAC procedure

IMAC-Sepharose FastFlow resin (GE Healthcare) and Profinity™ IMAC resin (Bio-rad) were used. 2-5 mL of resin was added to a 20 mL column. The storage buffer, 20 % industrial methylated spirits (IMS), was allowed to flow through and the resin was washed with 5-10 column volumes (CV) of dH₂O until it had settled. The column was equilibrated with 10 CV of lysis buffer containing 20 mM imidazole. The filtered cell lysate was then added to the column and a slow flow rate was set to ensure optimum capture of the protein by the resin. The resin was subsequently washed with 10 CV of lysis buffer containing a 20 mM imidazole. Additional wash steps with 5-10 CV of lysis buffer containing 50-80 mM imidazole were also used. The recombinant protein was then eluted with a high concentration of imidazole (250 mM). The initial flow through (unbound), washes and elution fraction were all collected and labelled. The column was then washed with 10 CV of dH₂O followed by 5 CV of 20 % ethanol in which the resin was then stored. Fractions taken at each step of the process are analysed by SDS-PAGE, see Section 2.19.

2.17.2 Stripping and Recharging the IMAC Resin

The resin is stripped and recharged before loading filtered cell lysate. The column is first washed with 2 CV of dH₂O followed by 2 CV of 50 % IMS. The metal ions are then stripped by washing with 2 CV of 100 mM EDTA, pH 8.0. To remove any remaining impurities the column is then washed with 2 CV of 200 mM NaCl, 2 CV of dH₂O and 10 CV of 30 % isopropanol. The resin is then washed with 10 CV of dH₂O and recharged with 1 CV of 100 mM NiSO₄. The column is again washed with 10 CV of dH₂O and stored in 20 % IMS.

2.18 Purification of IgG1

IgG1 was purified from CHO culture cultures using a Thermo Scientific Protein A/G Nab spin kit (89950). This kit was used according to the manufacturer's instructions. CHO DP-12 suspension cultures were centrifuged at 250 g for 5 min to pellet cells. The supernatant was decanted and passed through a 0.2 µm Minisart syringe filter, to

remove large debris which may clog and dirty the Protein A/G resin. This supernatant was stored at 4 °C until the day of purification.

The column, buffers and CHO supernatant were equilibrated to room temperature. A column was placed in a 2 mL collection tube and centrifuged at 5,000 g for 1 min. The flow through was discarded. The column was equilibrated with Binding Buffer (100 mM phosphate, 150 mM NaCl pH 7.2) prior to loading CHO supernatant. 400 µL of Binding Buffer was added to the column and mixed briefly before centrifugation at 5,000 g for 1 min. The flow through was discarded and this step was repeated once more. The bottom of the column was capped and 500 µL of CHO supernatant was added. The top of the column was capped and the column was incubated at room temperature for 10 min with mixing by inversion. The column was placed in a new 2 mL collection tube and centrifuged at 5,000 g for 1 min. This flow through contained the unbound sample and was kept. The column was placed in a new 2 mL collection tube. The column was washed and the resin suspended by adding 400 µL of Binding Buffer. The column was centrifuged at 5,000 g for 1 min and the flow through was kept. The column was washed two additional times for a total of three washes.

The IgG was then eluted by adding 400 µL of IgG Elution Buffer to the spin column, mixing the resin and centrifuging at 5,000 g for 1 min. 40 µL of Neutralization Buffer was added to 2 mL collection tubes prior to IgG elution. A total of three elution fractions were collected. The spin column was washed 3 times with 400 µL of Binding Buffer and the flow through was discarded. The resin was stored in 400 µL of Binding Buffer at 4 °C. The elution fractions containing the purified IgG was determined using SDS-PAGE analysis, see Section 2.19.

The Elution and Neutralization buffers with this kit were supplied in low quantities. Additional buffers were made, as described in Section 2.5, which resulted in equivalent results.

2.19 Sodium dodecyl sulfate polyacrylamide gel electrophoresis (SDS-PAGE)

The sodium dodecyl sulphate polyacrylamide gel electrophoresis (SDS-PAGE) method outlined by Laemmli (1970) was used to analyse protein samples.

2.19.1 Preparation of SDS gels

The gels were made according to Table 2.7.

Table 2.7: SDS-PAGE gel recipes

Resolving/Stacking gel	10 %	15 %	4 %
Acrylamide/Bis-acrylamide, 30 %	2.5 mL	3.75 mL	0.325 mL
dH ₂ O	3.0 mL	1.758 mL	1.54 mL
1.5 M Tris-HCl pH 8.8	1.875 mL	1.875 mL	-
0.5 M Tris-HCl pH 6.8	-	-	0.625 mL
10 % (w/v) Ammonium persulphate (APS)	37.5 µL	37.5 µL	12.5 µL
10 % (w/v) SDS	75 µL	75 µL	25 µL
TEMED (<i>N,N,N',N'</i> -Tetramethylethylenediamine)	3.5 µL	3.5 µL	2.5 µL

APS and TEMED were added last to the mix as they polymerise the acrylamide. Gels were cast, 90 x 80 x 1 mm, using ATTO mini slab glass plates. The glass plates and gasket were assembled and held with clips. The seal was checked with dH₂O before pouring the gel. The resolving gel was poured, immediately after APS and TEMED were added, to approximately 1.5 cm below the top of the plate. The resolving gel was overlaid with a layer 20 % IMS and left to polymerise at room temperature for 45-50 min. Overlaying the resolving gel is extremely important as it ensures that the top of the resolving gel is completely flat, keeps protein bands parallel to the wells, and prevents to resolving gel from drying out after it polymerises. After polymerisation the 20 % IMS overlay was removed and the top of the resolving gel was rinsed with dH₂O before adding the stacking gel. A comb was inserted diagonally, to ensure air bubbles do not

remain at the bottom of the wells, into to the top of the stacking gel to form loading wells and left at room temperature for 30 min. The gel, if not used immediately, was wrapped in damp tissue and stored at 4 °C.

2.19.2 Sample preparation and application

18 µL of sample and 2 µL of 10X SDS-PAGE sample buffer, see Section 2.5, were added to a microcentrifuge tube. This mixture was boiled at 100 °C on a heating block, Labnet Accublock™ Digital Dry Bath, for 5 min. The gel was positioned in the electrophoresis chamber, the comb was removed and 1X SDS-PAGE running buffer was added which removes unpolymerised acrylamide from the wells. 15 µL of the prepared sample was applied to each SDS-PAGE well. The first lane on each gel was loaded with 8 µL of a molecular weight marker. For coomassie staining the unstained NEB molecular weight marker (Broad Range protein marker, Fig 2.5) was loaded. For Western Blot analysis the Thermo Scientific molecular weight marker (PageRuler™ Plus Prestained Protein Ladder, Fig 2.5) was loaded. The gel was run at 30 mA for 80 min at room temperature. The ATTO AE-6500 mini-slab size electrophoresis system was used connected to a Labnet Power Station™ 300 power supply.

The NEB Broad Range protein marker (Fig 2.5 image A) consists of rabbit muscle myosin (212 kDa), MBP-β-galactosidase from *E. coli* (158 kDa), β-galactosidase from *E. coli* (116 kDa), rabbit muscle phosphorylase b (97 kDa), bovine serum albumin (66 kDa), bovine liver glutamic dehydrogenase (55.5 kDa), MBP2 from *E. coli* (42.7 kDa), thioredoxin reductase from *E. coli* (34.6 kDa), soybean trypsin inhibitor (20.040-20.167 kDa), chicken egg white lysozyme (14.3 kDa), bovine lung aproptinin (6.5 kDa), bovine pancreas insulin A chain (3.4 kDa) and bovine pancreas B chain (2.34 kDa).

Expedeon's Runblue prestained dual-colour marker (Fig. 2.5 image B) consists of two red reference bands at 71 kDa and 28 kDa. The remaining six bands are stained blue. CSTs' prestained protein marker low range (1.7-42 kDa) is a mixture of proteins coupled to blue, green or orange dyes that resolve to 6 bands when electrophoresed.

The Thermo Scientific PageRuler™ Plus Prestained Protein Ladder (Fig 2.5 image C) consists of a mixture of nine recombinant proteins ranging from 10 kDa to 250 kDa. There are two orange/red reference bands at 70 kDa and 25 kDa and a green reference band at 10 kDa to highlight the protein ladder. The remaining six bands are stained blue.

The Color-coded Prestained Protein Marker from Cell Signalling Technology (Fig. 2.5 image D) is a low range (1.7-42 kDa) protein mixture. The proteins are covalently coupled to blue, green or orange dyes, which resolve to 6 bands between 1.7 and 42 kDa when electrophoresed.

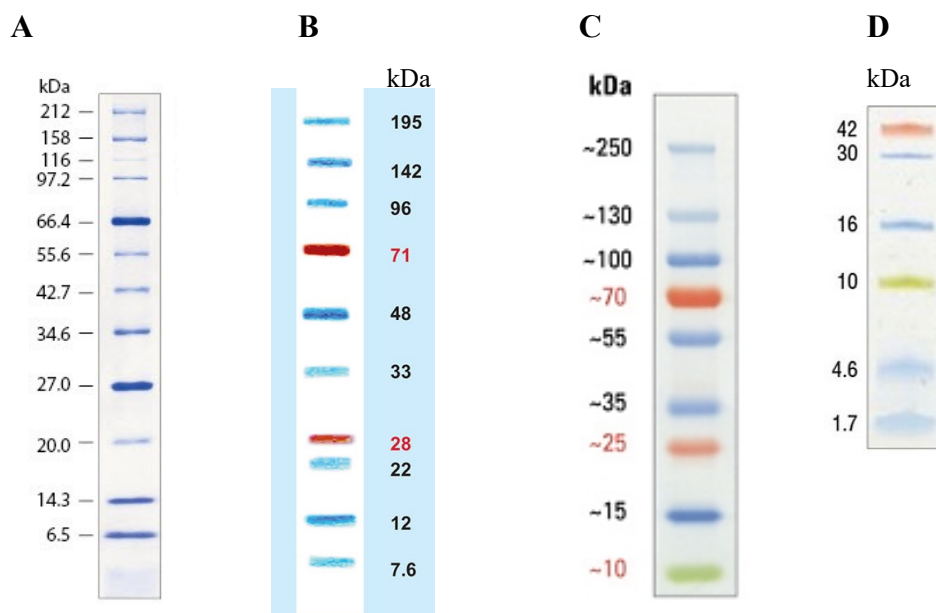


Fig. 2.5: Protein markers. **A)** NEB Broad Range protein marker (P7702S), **B)** Expedeon Runblue prestained dual-colour marker (NXA05160). **C)** Thermo Scientific PageRuler™ Plus Prestained Protein Ladder (26619). **D)** CST Prestained Protein Marker, Low Range (13070). Representative images of molecular weight marker used in this study. Images are from A; <https://www.neb.com>, B; <https://www.expedeon.com/runblue-prestained-markers>, C; <https://www.thermofisher.com/order/catalog/product/26619> and D; <https://www.cellsignal.com/products/experimental-controls/color-coded-prestained-protein-marker-low-range-1-7-42-kda/13070>.

2.19.3 Visualising SDS-PAGE gels

Polyacrylamide gels were carefully removed from between the glass plates with a spatula and rinsed with dH₂O. The gels were stained for a minimum of 2 hours with coomassie blue stain solution, see Section 2.4, in a plastic tub that was slowly rotated on an orbital shaker at room temperature. The stain was removed and the gels were rinsed with dH₂O again. Coomassie blue destain solution was added and left on the gels at room temperature for 2 hours. Additional coomassie blue destain solution was added as required until the proteins bands were visible and the gels were transparent. After destaining the gels were rinsed again with dH₂O and placed in a clean weigh boat and a digital camera was used to obtain gel images

2.20 Screening for protein expression

Competent cells were transformed, see Section 2.10.2, and 10 single colonies from the transformed plate were randomly selected and streaked onto individual LB agar plates. Following overnight incubation, single colonies from each of the individual plates were used to inoculate 8 mL TB, containing 100 µg/mL ampicillin and 100 µg/mL IPTG, and were again incubated overnight. To analyse protein expression, the cell concentration must be normalised across all 10 broth cultures, see equation 1.

$$\frac{0.7}{A_{600}} \times 300 = \text{volume } (\mu\text{L}) \text{ of culture to be harvested} \quad (1)$$

The culture volume to be harvested is centrifuged at 15,000 g for 1 minute and the resulting pellet is resuspended in 50 µL of 1X SDS-PAGE sample buffer. Samples were analysed by SDS- PAGE, see Section 2.19.2, and the gels are visualised using coomassie stain, see Section 2.19.3. The protein bands in each lane are similar but slight differences in band sizes, i.e. protein concentration, is a result of the differences in protein expression between the selected colonies. A glycerol stock was made from the streaked plate of the colony that expressed the largest amount of the inserted protein.

2.21 Western Blot analysis

Western blotting is employed to detect specific proteins in a sample. Proteins are initially separated by SDS-PAGE and then transferred to a nitrocellulose membrane (GE Healthcare X25 Protran®) and probed with antibodies that bind a specific epitope displayed by the target protein. The bound antibody is conjugated to a horseradish peroxidase (HRP) enzyme so a secondary antibody was not used.

2.21.1 Protein transfer to nitrocellulose membrane

SDS-PAGE gels were run as described in Section 2.19. However, increased prestained protein ladder was loaded, ~20 μ L. The semi-dry transfer method was employed using an electroblotter. Four pieces of filter paper (Whatman® Grade 3MM Chr Blotting Paper) and a nitrocellulose membrane were cut to the size of the SDS-PAGE gel. The filter paper and membrane were soaked in semi-dry transfer buffer (SDTB). Two pieces of filter paper and the membrane were placed on the anode plate then the SDS-PAGE gel and finally two more pieces of filter paper, see Fig 2.6. A plastic pipette was rolled over the transfer stack to push out all air bubbles. The cathode was placed on top of the transfer stack and the gels were transferred at 12 V for 30-40 min using a Bio-Rad electroblotter (Trans-Blot® SD Semi-Dry Transfer Cell) connected to a Bio-Rad Power Pac 200.

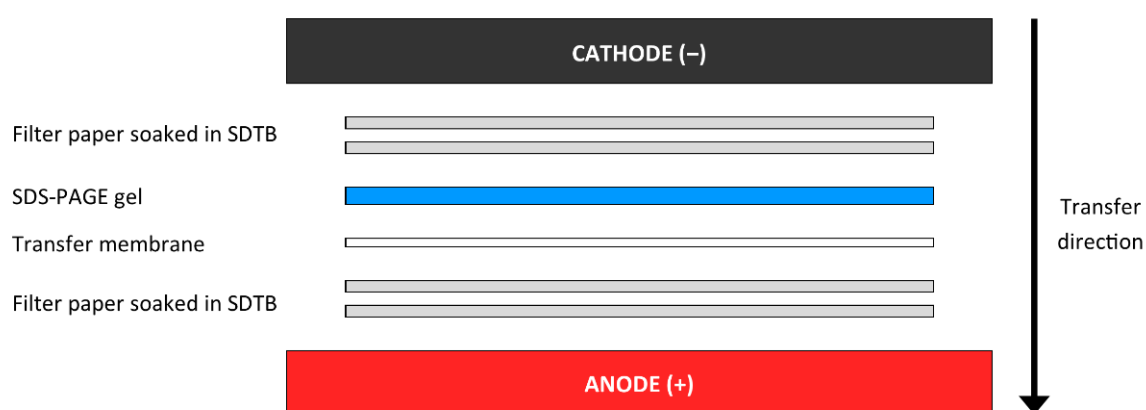


Fig. 2.6: Semi-dry Western blot transfer stack. The transfer stack is assembled from bottom to top as follows, two sheets of filter paper, transfer membrane, SDS-PAGE gel and two sheets of filter paper. Image created using Microsoft Publisher 15.0.

2.21.2 Staining of proteins immobilised on nitrocellulose membrane

The transfer of proteins from the SDS-PAGE gel to the nitrocellulose membrane is checked with Ponceau S stain. Ponceau S is a useful stain as it is easily reversed and it does not have a negative effect on subsequent probing. Transferred protein bands are stained red while the protein free background remains white. The transfer membrane was placed in a large weigh boat and covered with Ponceau S solution, approximately 15 mL, and stained for 5 min at room temperature with constant agitation. The transferred proteins were visualised and the Ponceau S stain was removed with multiple dH₂O washes. After the transfer of proteins is confirmed the membrane can be used for immunological probing.

2.21.3 Protein probing and visualisation

After Ponceau S staining the membrane is blocked for 18-20 hours with blocking buffer, 5 % BSA (w/v) in TBST, at room temperature with constant agitation. Unbound BSA was removed by washing the membrane with TBST, see Section 2.5, four times. The antibody is added in TBST (1 in 10,000) and incubated with the membrane at room temperature for 1 hour with constant agitation. The anti-polyHistidine mAb conjugated to HRP from Sigma (A7058), the anti-mouse IgG H+L peroxidase-conjugate from Jackson Immuno Reseach (115-035-062) or the anti-Biotin mAb conjugated to HRP, Sigma (A0185) were used. The membrane was washed again with TBST four times and TMB substrate (Sigma T0565) is added dropwise to develop the bands. The membrane was rinsed with dH₂O to stop the reaction and an image obtained using a digital camera.

2.22 Concentrating and buffer exchanging recombinant protein

During IMAC purification the expressed protein was eluted in lysis buffer containing 250 mM imidazole. It is desirable to remove the imidazole so the protein can be accurately quantified, remain active and stored in an optimal buffer. The elution fractions to be purified were pooled and passed through a spin column with a molecular weight cut-off (MWCO) of 10 kDa. The MWCO selected should be at least 50 % smaller than the protein of interest. For small protein samples, 1-2 mL, the Vivaspin®

500 (VS0102 - max speed 15,000 g) was used. The spin column was loaded with the pooled elution fractions and centrifuged at maximum speed for 10 min at room temperature. The flow through was collected and the retentate was topped up with PBS and the centrifugation step was repeated a further 3-5 times.

For larger protein samples, 2-20 mL, dialysis tubing (Sigma D9777) was used. This cellulose tubing has a MWCO of 14 kDa. The tubing is cut to required length and prepared by heating at 80 °C for 2 min in 30 mM EDTA. This is followed by rinsing the tubing with dH₂O before use. This preparation is required to remove glycerol and sulphur compounds present in the tubing. The tubing is tied at one end, the sample is added and the open end is then tied. The tubing is placed in 4-5 L PBS and gently stirred for 18-20 hours at 4 °C. The sample was then concentrated on polyethylene glycol flakes (MW 20,000). The protein is now suitable for quantification analysis or storage at -20 °C (short term) or -80 °C (long term).

2.23 Protein quantification

Protein quantification was completed using two different methods, the bicinchoninic acid assay (BCA assay) and by reading its absorbance at 280 nm. The BCA assay, also known as the Smith assay, was first described by Smith et al. (1985). This assay depends on the biuret reaction whereby the reduction of Cu⁺² to Cu⁺¹ by peptide bonds in the protein is proportional to the amount of protein present. Then two BCA molecules chelate with each Cu⁺¹ ion forming a purple coloured product which strongly absorbs light at 562 nm. The reaction is influenced by cysteine, tyrosine and tryptophan residues. Proteins were also quantified by reading their absorbance at 280 nm as aromatic amino acids, e.g. phenylalanine, tryptophan, histidine and tyrosine, absorb UV light. Once the extinction coefficient is known and the absorbance at 280 nm is read, the Beer-Lambert law can be used to calculate the protein concentration.

$$A = \log (I_o/I_t) \quad (2)$$

The absorbance value, A , for a given sample is a unitless expression of the light intensity before, I_0 , and after, I_t , transmission through a sample, see equation 2. Where spectrophotometry data is reported throughout this work the absorbance value at any given wavelength is referred to as $A_{450 \text{ nm}}$.

2.23.1 Protein quantification using the BCA assay

The Pierce™ BCA Protein Assay Kit (Thermo Scientific 23227) was used to quantify total protein with a working range of 20-2,000 $\mu\text{g/mL}$. The kit was used according to the manufacturer's instructions. The BCA working reagent (WR) was created by mixing reagent A with reagent B (50:1). This assay was completed in a 96-well microplate where 200 μL of WR was added to 25 μL of protein sample or BSA standard and repeated in triplicate. The 96-well plate was placed on a shaker for 30 s to mix the contents of the wells and then incubated at 37 °C for 30 min. The plate was cooled to room temperature and the absorbance was measured at 570 nm (suitable range 540-590 nm). A standard curve was created and its second order polynomial trendline equation was used to calculate the protein concentration of a sample.

2.23.2 Protein quantification using 280 nm readings

Protein samples to be quantified were centrifuged at 15,000 g for 5 min to pellet any debris in the sample that may interfere with the absorbance readings. The spectrophotometer was set to 280 nm and zeroed with a buffer identical to the buffer that the proteins samples were in. Prior to calculating the protein concentration using the Beer-Lambert law, equation 3, the extinction coefficient, ϵ , of the protein must be known. This was obtained by using the ExPASy ProtParam tool (Section 2.13).

$$A_{280} = \epsilon c \ell \quad (3)$$

Equation 3: Beer-Lambert Law relates the absorption of light to the properties and concentration of the material through which the light is travelling. A_{280} = absorbance at 280 nm (unitless), ϵ = molar extinction coefficient ($\text{M}^{-1}\text{cm}^{-1}$), c = molar concentration (M) and ℓ = pathlength (cm).

2.24 Biotinylation of recombinant proteins

Recombinant proteins were biotinylated so they can be used in activity assays and to probe live cells using a flow cytometer. The Thermo Scientific EZ-Link® Sulfo-NHS-LC-Biotin kit (21327) was used to biotinylate recombinant proteins. *N*-Hydroxysuccinimide (NHS) activated biotins react with primary amino groups, -NH₂, in pH 7-9 buffers and form stable amide bonds. Proteins, usually, have multiple primary amines in the side chains of lysine (K) residues and at the *N*-terminus of the polypeptide that are available for labelling with NHS-activated biotin. Biotin is a water soluble vitamin, B₇, which binds with high affinity to avidin and streptavidin. Biotin is a useful label as it is small, 244 Da, and can be conjugated to many proteins without altering their biological activity.

The kit was used according to the manufacturer's instructions. The biotin was removed from the freezer and a 10 mM biotin solution was prepared by adding 180 μL of dH₂O to 1 mg of biotin in a microtube. Equation 4 was used to calculate the amount of biotin to add for a 20-fold molar excess which was then used, in equation 5, to calculate the volume of biotin to add.

$$\text{mL protein} \times \frac{\text{mg protein}}{\text{mL protein}} \times \frac{\text{mmol protein}}{\text{mg protein}} \times \frac{20 \text{ mmol Biotin}}{\text{mmol protein}} = \text{mmol Biotin} \quad (4)$$

$$\text{mmol Biotin} \times \frac{1,000,000 \text{ } \mu\text{L}}{\text{L}} \times \frac{\text{L}}{10 \text{ mmol}} = \mu\text{L Biotin} \quad (5)$$

The protein to be biotinylated must be in an amine free buffer such as PBS. The appropriate volume of biotin was added to the protein and incubated on ice for 2 hours or at room temperature for 30 min. The sample was buffer exchanged, to remove excess biotin, and concentrated using a 10,000 Da MWCO spin column, see Section 2.22.

2.25 Enzyme-linked lectin assay

The enzyme-linked lectin assay (ELLA) was first described by McCoy et al. (1983) to detect glycoproteins bearing specific carbohydrate residues. The method outlined by Thompson et al. (2011) was used to characterise lectins and determine lectin binding specificities. The schematic presented in Fig. 2.7 shows two ELLA formats where biotinylated commercial lectins and recombinantly produced His₆ tagged lectins are used.

A 50 µL volume of glycoprotein at 5 µg/mL was immobilized in each well of a Nunc- Immuno™ MicroWell™ 96 well solid plate (439454) and incubated at 4 °C for 16-18 h. Each sample was assayed in triplicate. The unbound glycoprotein was removed by inverting the plate and the wells were blocked with 150 µL of 0.5% polyvinyl alcohol (PVA) in TBS for two hours at 25 °C. The solution was then removed by inverting the plate and washing with TBS supplemented with 0.1% Tween 20 four times. A 50 µL aliquot of lectin in TBS supplemented with 10 mM CaCl₂ was then added at a concentration of 5 µg/mL and incubated at 25 °C for 1 hour. This was removed by inversion and washed with TBST as before. This was followed with 50 µL of 1:10,000 murine anti-histidine (anti-polyHistidine mAb conjugated to HRP, Sigma A7058) and/or anti-biotin antibody (anti-Biotin mAb conjugated to HRP, Sigma A0185), as appropriate. The antibody was diluted fresh in TBST and was incubated for 1 hour at 25 °C. Unbound antibody was removed by inversion and washed four times with TBST, before the addition of 100 µL TMB substrate (see Section 2.4). The reaction was stopped after a specified time by the addition of 50 µL of 10 % H₂SO₄. The absorbance was measured at 450 nm using a BioTek ELx808 plate reader.

All commercial lectins used were supplied by Vector Laboratories Ltd UK, see Table 2.8. To demonstrate lectin specificity a negative control was used. The lectin was diluted to 5 µg/mL in TBS supplemented with 10 mM CaCl₂ and a defined sugar is added. The concentration of the inhibiting/eluting sugar used is that which is recommended by Vector Laboratories Ltd in the product data sheet. This lectin-sugar solution is then added to the plate as described above.

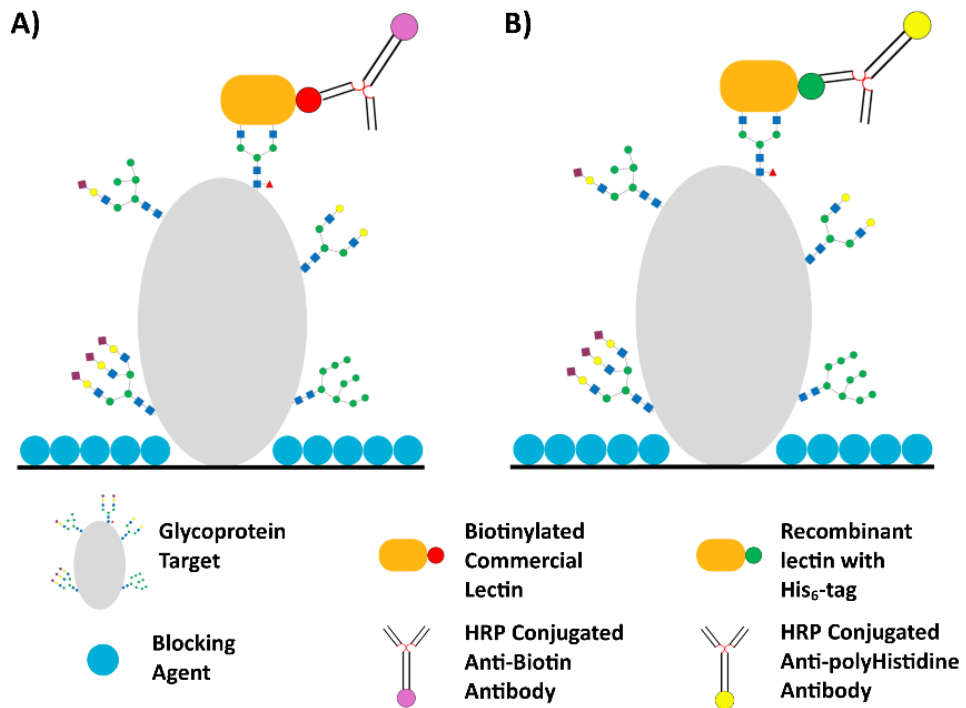


Fig. 2.7: Schematic of an ELLA. A plate is blocked, 0.5 % PVA in TBS, after a glycoprotein target is immobilised on the plate surface. Lectins are added to probe the glycoproteins and then antibodies are added to detect bound lectins. **A)** Probing glycoproteins with biotinylated commercial lectins. **B)** Probing glycoproteins with His₆-tagged recombinant lectins. Image created using Microsoft Publisher 15.0.

Table 2.8: Biotinylated lectins from Vector Laboratories Ltd UK

Lectin (Full Name)	Preferred monosaccharide
AAL (<i>Aleuria aurantia</i> lectin)	Fuc
Con A (Concanavalin A)	α Man, α Glc
DSL (<i>Datura stramonium</i> lectin)	(GlcNAc) _{2,4}
ECL (<i>Erythrina cristagalli</i> lectin)	Gal, GalNAc, Lac
GNL (<i>Galanthus nivalis</i> lectin)	α Man
GSL I (<i>Griffonia simplicifolia</i> lectin I)	α Gal, α GalNAc
GSL I B ₄ (GSL I isolectin B4)	α Gal
GSL II (<i>Griffonia simplicifolia</i> lectin II)	α GlcNAc, β GlcNAc
Jacalin	Gal
LCA (<i>Lens culinaris</i> agglutinin)	α Man, α Glc
MAL I (<i>Maackia amurensis</i> lectin I)	Gal, Lac
MAL II (<i>Maackia amurensis</i> lectin II)	α 2-3-NeuNAc
NPL (<i>Narcissus pseudonarcissus</i> lectin)	α Man
PNA (Peanut agglutinin)	Gal
RCA I (<i>Ricinus communis</i> agglutinin I)	Gal, Lac
SBA (Soybean agglutinin)	α or β GalNAc, Gal
UEA I (<i>Ulex europaeus</i> agglutinin I)	Fuc, arabinose
WGA (Wheatgerm agglutinin)	GlcNAc

2.26 Enzyme-linked immunosorbent assay

The enzyme-linked immunosorbent assay (ELISA) was first described by Perlmann and Engvall (1971) at Stockholm University where they quantitatively measured IgG in rabbit serum. This plate based assay uses antibodies to detect the presence of an antigen in a sample. It is used extensively as a diagnostic tool in medical laboratories and as a quality control assay in many industries. There are four main types of ELISA, direct, indirect, sandwich and competitive. Fig 2.8 describes the direct and indirect ELISA formats.

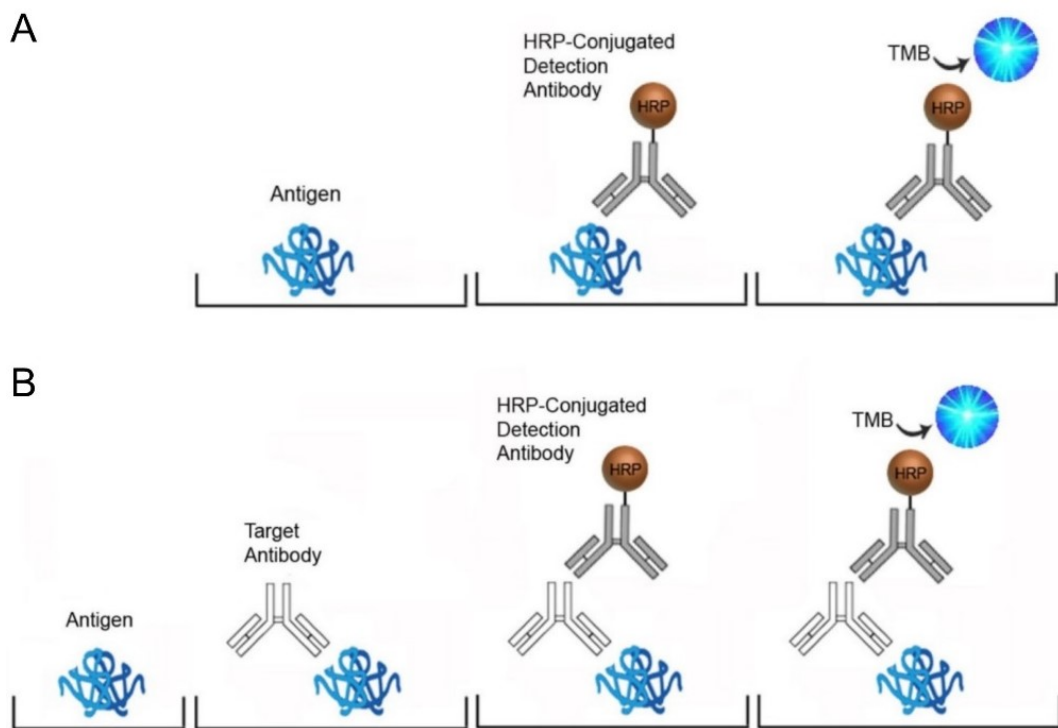


Fig. 2.8: Schematic of direct and indirect ELISA. A) Direct ELISA where the antigen to be detected is immobilised on the solid phase and probed directly with a specific antibody conjugated to HRP. **B)** Indirect ELISA where the antigen to be detected is immobilised on the solid phase and probed with an unconjugated primary antibody followed by a HRP-conjugated secondary antibody, which is specific for the primary antibody. Image modified from LSBio (2017) using Microsoft Publisher 15.0.

Protocol for Indirect ELISA

A 50 μL volume of antigen (IL-8, supplied by BioLegend # 574202) containing sample or control protein at 5 $\mu\text{g}/\text{mL}$ was immobilized in each well of a Nunc- Immuno™ MicroWell™ 96 well solid plate (439454) and incubated at 4 °C for 16-18 hours. Each sample was assayed in triplicate. The unbound protein was removed by inverting the plate and the wells were blocked with 150 μL of 0.5% polyvinyl alcohol (PVA) in TBS for one hour at 25 °C. The solution was then removed by inverting the plate and washing with TBS supplemented with 0.1% Tween 20 four times. A 50 μL aliquot of primary antibody (IgG1) in TBS supplemented with 10 mM CaCl_2 was then added at a concentration of 5 $\mu\text{g}/\text{mL}$ and incubated at 25 °C for 1 hour. This was removed by inversion and washed with TBST as before. This was followed with 50 μL of 1:10,000 caprine anti-mouse IgG (H+L) (peroxidase-conjugate, Jackson Immuno Reseach 115-035-062). The antibody was diluted fresh in TBST and was incubated for 1 hour at 25 °C. Unbound antibody was removed by inversion and washed four times with TBST, before the addition of 100 μL TMB substrate, see Section 2.5. The reaction was stopped after 3 min by the addition of 50 μL of 10 % H_2SO_4 . The absorbance was measured at 450 nm using a BioTek ELx808 plate reader.

Protocol for Direct ELISA

This protocol is a shortened version of the indirect method above. The plate was prepared identically with protein, incubated for 16-18 hours at 4 °C and blocked for 2 hours with PVA. However, only one antibody was added to the plate. 50 μL of 1:10,000 caprine anti-mouse IgG (H+L) (peroxidase-conjugate, Jackson Immuno Reseach 115-035-062) was added to each well. The antibody was diluted fresh in TBST and was incubated for 1 hour at 25 °C. Unbound antibody was removed and TMB substrate was added. The reaction was stopped with 10 % H_2SO_4 and the absorbance was measured at 450 nm using a BioTek ELx808 plate reader.

2.27 Cell culture techniques

2.27.1 General consumables

All sterile plastic tissue culture flasks, 6 well plates, flat 96 well plates, 50 mL tubes and pipette tips (10 µL – 25 mL) were supplied by Sartedt Ltd. Sterile 30 mL tubes were supplied by Thermo Scientific. Microcentrifuge tubes, supplied by Greiner Bio-One, were sterilised by autoclaving at 121 °C for 20 min.

2.27.2 Cell culture cabinet and incubators

All cell work was carried out in a Holten Laminair HB2448 cabinet and a HERAsafe KS18 class II biological safety cabinet (BSC). Strict aseptic techniques were followed at all times. The BSC was sprayed and wiped down with 70 % IMS before and after use. Everything that entered the BSC was sprayed with 70 % IMS. To reduce the risk of contamination only one cell line was worked with at a time and the BSC was left vacant for a minimum of 15 min between cell lines. RS Biotech Galaxy S and a Memmert INC 153 CO₂ incubators were used. The BSC and incubators were regularly cleaned with a broad spectrum disinfectant Virkon® (1 % w/v) followed by water and IMS.

2.27.3 CHO DP-12 cultures

Cells were maintained at 37 °C in an atmosphere with 5 % CO₂ and 95 % humidity. CHO DP- 12 cells were grown adherently in 75 cm² tissue culture flasks and subcultured every 3 to 4 days. These cells were also grown in suspension in 5 mL cultures.

Adherent culture

CHO DP- 12 cells were grown adherently in complete DMEM/Ham's F-12, see Section 2.4. Spent medium was removed from the T75 flask and 10 mL of preheated, 37 °C, PBS (Sigma D8537) was added to wash the cells. The PBS was removed and 5 mL

trypsin-EDTA (0.5 % porcine trypsin (w/v), 0.2 % EDTA (w/v) Sigma T4174) in PBS was added to the flask. The cells were incubated with trypsin at 37 °C until they were fully detached, usually 3-5 min. 5 mL of growth medium (containing 10 % FBS, see Section 2.4) was then added to the flask to inactivate the trypsin, via trypsin inhibitors present in serum. The cell solution was pipetted into a 30 mL tube and the cells were pelleted by centrifuging at 250 g for 5 min. The supernatant was poured off and the cells were resuspended in fresh preheated complete medium. An aliquot of this fresh cell suspension was removed and a cell count was performed. An appropriate volume of the cell suspension was used to seed new flasks at 2×10^5 cells/mL or to seed tubes or plates for experimental work.

Suspension culture

CHO DP-12 cells were adapted directly to suspension culture in BalanCD CHO Growth A Medium 91128, see Section 2.4. This direct adaption method was outlined and recommended in the growth medium product insert (Irvine 2015). Cells were removed from adherent culture flasks as outlined above and seeded into 5 mL suspension cultures at 3×10^5 viable cells/mL. 50 mL CELLreactor - Filter Top Tubes (#227245), supplied by Greiner Bio-One, were used for suspension cultures. The cells in suspension were grown at 37 °C in an atmosphere with 5 % CO₂ and 95 % humidity. An orbital shaker, Orbi-Shaker CO₂ (BT4000) from Benchmark Scientific, with a horizontal circular orbit of 19 mm maintained the suspension culture. This shaker had its own dedicated incubator see Fig 2.9. The cells were subcultured 1-2 times per week. During which the cells were pelleted by centrifuging at 250 g for 5 min. The supernatant was poured off and the cells are resuspended in fresh preheated medium. An aliquot of this fresh cell suspension was removed and a cell count was performed. An appropriate volume of the cell suspension was used to seed new 50 mL CELLreactor tubes at 3×10^5 cells/mL.



Fig. 2.9: Orbital shaker for maintaining CHO DP-12 suspension cultures. The orbital shaker, Orbi-Shaker CO2 BT4000 with a 19 mm orbit, is shown. Suspension cultures, 5 mL, were maintained with the shaker set at 200 rpm.

2.27.4 Trypan blue cell counts

Cell counts were completed using an Improved Neubauer haemocytometer (Hawksley BS.748). The cell viability was determined using trypan blue solution (0.4 % trypan blue, Sigma T8154). A volume of 10 μL of trypan blue was added to 100 μL of a cell suspension and mixed. A clean glass cover slip (Borosilicate glass 22 x 22 mm, VWR) was placed over the grids on the haemocytometer and 10 μL of the cell-trypan blue suspension was added. The area under the cover slip fills by capillary action and the haemocytometer is placed on a microscope. Both the Olympus CK40 inverted microscope and the Nikon Eclipse TS100 inverted microscope were used. Trypan blue stain will only enter damaged or dead cells, stained blue, whereas healthy viable cells will remain clear. A total cell count and viable cell count is completed and the % of viable cells is calculated. Cell concentrations were obtained by multiplying the average cell count (3 counts) by the dilution factor, 1.1, and by the volume fraction of the region counted on the haemocytometer. Cell concentrations were then expressed as the number of cells per mL.

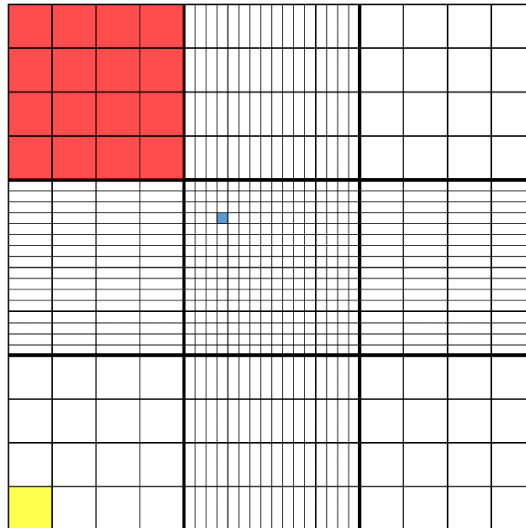


Fig. 2.10: Haemocytometer grid layout. The red, yellow and blue regions represent areas of 1 mm^2 , 0.625 mm^2 and $3.906 \times 10^{-3} \text{ mm}^2$ respectively. The depth of the haemocytometer chamber is 0.1 mm therefore the volume these regions represent are 0.1 mm^3 , 0.0625 mm^3 and $3.906 \times 10^{-4} \text{ mm}^3$ respectively. Image created using Microsoft Publisher 15.0.

2.27.5 ADAM™ cell counter

Cell counts were completed using an ADAM-MC (Advanced Detection Accurate Measurement) cell counter from NanoEnTek which is based on fluorescent dye staining and CCD camera to make cell counting and viability measuring more accurate and reliable. Cells are mixed with two propidium iodide (PI) stain solutions. The first solution contains PI which intercalates with DNA. However, viable cells are impermeable to PI so only non-viable cells will fluoresce. The second PI stain solution also contains a detergent that will disrupt viable cells allowing PI to enter and the total cell population will fluoresce. The ADAM-MC cell counter takes 22-60 images per sample and uses image analysis software to determine total and viable cell concentrations. The measuring range is $5 \times 10^4 - 4 \times 10^6$ cells/mL.

A $15 \mu\text{L}$ aliquot of cells was mixed with $15 \mu\text{L}$ of Accustain solution T (Digital Bio). A second $15 \mu\text{L}$ aliquot of cells was mixed with Accustain solution N (Digital Bio). $15 \mu\text{L}$ of each cell-stain solution is loaded into the T (total) and N (non-viable) channels

on a disposable counting slide, the Accuchip 4x. The slide is then inserted into the counter and the total and non-viable cell counts are displayed.

2.27.6 Cryopreservation of cells

To enable cells to be stored indefinitely they were cryopreserved using a cryoprotectant, dimethyl sulfoxide (DMSO) (Fisher 10293800), and stored in liquid nitrogen, -196 °C.

1. Cells to be cryopreserved were grown in 75 cm² flasks until 75- 80 % confluency was reached and they were harvested as described in Section 2.27.3.
2. Cells were pelleted by centrifugation at 250 g for 5 min and resuspended, after cell counting, in fresh medium at a concentration of 3 x 10⁶ cells/mL.
3. A 2X freezing medium was prepared containing 50 % FBS, 35 % serum free medium (Sigma D6429) and 15 % DMSO. The freezing medium was sterilised with a 0.2 µm Minisart syringe filter (Sartorius 16534-K). As DMSO is toxic to cells at room temperature, an equal volume of 2X freezing medium is slowly added to the cell suspension.
4. 1 mL aliquots of the cell suspension, containing a minimum of 1.5 x 10⁶ cells/mL, was pipetted into cryovials (Sarstedt 72.694.406) and cooled to -80 °C, -1 °C/min, using a Mr. Frosty™ freezing container (Thermo Scientific 5100-0001) filled with 100 % isopropyl alcohol. The freezing container was placed in a -80 °C freezer overnight. Following this the vials were stored in liquid nitrogen.

2.27.7 Thawing cells

1. A cryovial was removed from liquid nitrogen and quickly thawed at 37 °C.
2. The contents of the cryovial was transferred to a sterile tube containing preheated, 37 °C, complete medium.
3. The cell suspension was centrifuged at 250 g for 5 min to pellet the cells.

4. The supernatant was poured off and the cell pellet was resuspended in fresh preheated complete medium.
5. The cell suspension was pipetted into a 75 cm² flask and incubated as normal. The following day, after cells were attached to the flask, the medium was replaced to remove any trace amounts of DMSO.
6. The cells were then subcultured as normal, see Section 2.27.3, after 4 to 5 days when the flask was approximately 90 % confluent.

2.28 Probing cells with commercial and recombinant lectins

CHO DP-12 cells were probed with a panel of lectins to determine the presence of specific cell surface glycans. Cytotoxicity assays were initially completed to determine the adverse effect, if any, that lectins have on healthy cells, Section 2.28.1. Cells were prepared, probed with lectins and analysed using a fluorescent microscope, see Section 2.28.2, and a flow cytometer, see Section 2.28.3. Both techniques complement one another and they provide qualitative and quantitative data respectively.

2.28.1 Determining lectin cytotoxicity

A cell viability assay was used to determine the cytotoxic effect of lectins on CHO DP-12 cells. The FluoroFire-Blue ProViaTox assay (Molecutools - A00008), which is a resazurin-based assay, was used. Metabolically active cells can readily reduce the weak fluorescent resazurin blue dye into the highly red/pink fluorescent resorufin, see Fig. 2.11. Cells that are nonviable will not have the metabolic capacity to reduce the dye. The resazurin substrate is a cell permeable redox indicator and it is used similarly to tetrazolium compounds in other viable cell reduction assays, such as MTT and MTS. Resazurin is soluble in PBS and can be added directly to cell culture medium. The quantity of resorufin produced is directly proportional to the number of viable cells. It is reported that resazurin based reduction assays are more sensitive than their tetrazolium counterparts (Riss et al. 2013). The cytotoxicity assay was completed in a 96 well plate. The kit was used according to the supplied technical manual.

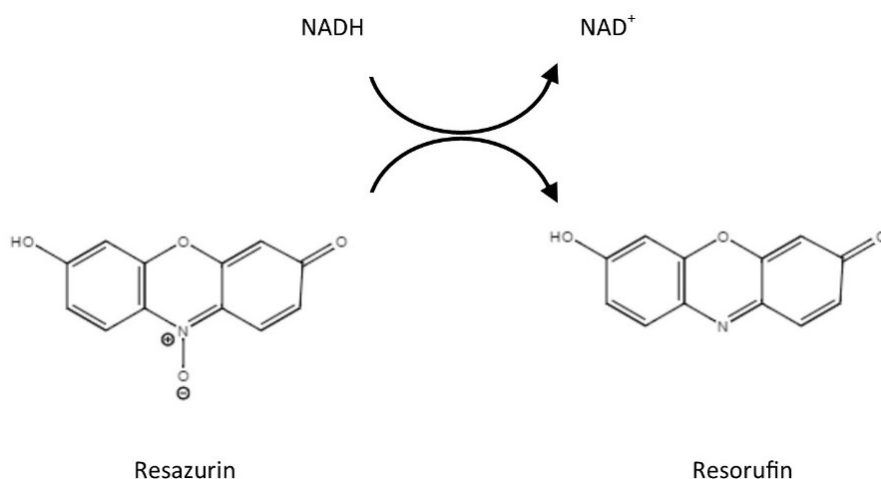


Fig. 2.11: Resazurin reduction. The structure of resazurin substrate and the pink resorufin fluorescent product from its reduction in metabolically active cells is shown. Structures generated using ChemDraw Direct.

1. CHO DP-12 cells were removed from T75 adherent flasks with trypsin, counted and seeded in clear flat-bottom 96 well plates. 100 μL of a cell suspension, 2.5×10^5 cells/mL, was added to each well. The cell concentration to use was initially determined by setting up a cell concentration 1 in 2 serial dilution (2.0×10^6 to 9.8×10^2 cells/mL) which produces an exponential S-shaped curve and the optimum seeding concentration can be selected from the linear range of the curve.
2. The lectin to be tested was added in 20 μL of PBS. A 1 in 2 serial dilution of lectin (50 - 0 $\mu\text{g/mL}$) was completed and added to cells in triplicate.
3. The FluoroFire-Blue ProViaTox reagent is equilibrated to room temperature. 10 μL of reagent is added to each well. The plate is tapped to mix cells, lectins and reagent. Incubate plate at 37 $^\circ\text{C}$ for 4 h.
4. An absorbance plate reader is used to measure absorbance at 570 nm and at 600 nm as a reference.
5. The % reagent reduced is calculated using absorbance readings and the molar extinction coefficients for the reduced and oxidised reagent, described below.

6. Lectin cytotoxicity is determined by plotting the % of the reagent reduced against lectin concentration.

Calculating reduced reagent

The 96-well plate was measured at 570 nm and 600 nm. The equation and the extinction coefficients below were used to calculate the percentage of reagent reduced.

$$\% \text{ reagent reduced} = \frac{(E_{\text{oxi}600} \times A_{570}) - (E_{\text{oxi}570} \times A_{600})}{(E_{\text{red}570} \times C_{600}) - (E_{\text{red}600} \times C_{570})} \times 100$$

$E_{\text{oxi}570}$ = molar extinction coefficient (E) of the oxidized assay reagent at 570 nm = 80586

$E_{\text{oxi}600}$ = E of oxidized assay reagent at 600 nm = 117216

A_{570} = absorbance of test wells at 570 nm

A_{600} = absorbance of test wells at 600 nm

$E_{\text{red}570}$ = E of reduced assay reagent at 570 nm = 155677

$E_{\text{red}600}$ = E of reduced assay reagent at 600 nm = 14652

C_{570} = absorbance of negative control well (media, assay reagent, no cells) at 570 nm

C_{600} = absorbance of negative control well (media, assay reagent, no cells) at 600 nm

2.28.2 Fluorescent microscopy

Fluorescent microscopy was used to observe lectin binding the CHO DP-12 cell surface. A Nikon Eclipse Ti inverted microscope with FITC and DAPI filters was used. A Hoechst nuclear stain, NucBlue® Live ReadyProbes® (ThermoFisher R37605), was used that emits blue fluorescence when bound to DNA. DyLight™ 488 streptavidin conjugate (Pierce 21832), which emits green fluorescence, was premixed with biotinylated lectins and used to probe cells.

1. CHO DP-12 cells were removed from T75 adherent flasks with trypsin, counted and seeded in 6 well plates. 3 mL of a 5×10^4 cells/mL cell suspension was added to each well. The plates were typically incubated at 37 °C for 48 hours in a 5 % CO₂ incubator.
2. Biotinylated lectins, 5 µg/mL, were premixed with DyLight488 streptavidin conjugate, 5 µg/mL, and brought to a final volume of 500 µL in TBS with 10mM CaCl₂.
3. The culture media was removed and each well was washed 3 times with 2 mL of sterile PBS.
4. 500 µL of lectin:DyLight488 mix was added to wells as appropriate. 4 different controls were used:
 - i. TBS only
 - ii. TBS with DyLight488 only
 - iii. TBS with DyLight488, lectin and inhibitory sugar.
 - iv. TBS with DyLight488, lectin and non-inhibitory sugar.

The plates were incubated in the dark at room temperature for 30 min.

5. The wells were wash again, 3 times with 2 mL TBS with 10 mM CaCl₂.
6. 500 µL TBS was added to each well to sufficiently cover the cells.
7. The NucBlue nuclear stain was then added. 1 drop from the dropper bottle(concentration not known).
8. The cells were viewed with the fluorescent microscope. Bright field images, DAPI images and FITC images were obtained.

2.28.3 Flow cytometry

A Becton Dickinson FACS Aria I was used to analyse cells. This instrument was used according to the guidelines set out by the key trainer. Biotinylated lectins were mixed with a fluorescent streptavidin conjugate, DyLight488.

2.28.3.1 Flow cytometer sample preparation

1. 7×10^5 CHO DP-12 cells were prepared for each flow cytometer sample. CHO DP-12 cells were removed from T75 adherent flasks with a cell scraper or DP-12 cells in suspension were removed from shaker tubes. Cells were counted and aliquoted into microcentrifuge tubes.
2. All samples were centrifuged at 400 g for 4 min. The supernatant was removed and the cells were washed with 500 μ L of sterile PBS, centrifuged again and the supernatant discarded.
3. A biotinylated lectin and Dylight488 streptavidin conjugate mix is prepared in 300 μ L TBS with 10 mM CaCl_2 . The lectin and Dylight488 concentration used were 5 μ g/mL and 6 μ g/mL respectively. The washed cell pellet was resuspended in this lectin-Dylight488 mix and incubated in the dark at room temperature for 30 min.
4. 4 different controls were used:
 - i. TBS only
 - ii. TBS with DyLight488 only
 - iii. TBS with DyLight488, lectin and inhibitory sugar.
 - iv. TBS with DyLight488, lectin and non-inhibitory sugar.
5. After incubation, 1 mL of TBS is added to each tube to dilute the excess lectin and Dylight488 and the cells are pelleted by centrifugation at 400 g for 4 min.
6. The cell pellet is resuspended in 200 μ L of TBS and transferred into a FACS tube. The rack holding all the FACS tubes is wrapped in tinfoil keeping the sample tubes in a dark environment.

2.28.3.2 Flow cytometer use and data acquisition

1. The flow cytometer was used in accordance with the protocol distributed by the key trainer.
2. The FACS Aria was powered on and the required lasers were turned on.
3. A new experiment was created and renamed appropriately.
4. The required dot plots and histograms were created and the sample flow rate was set to 2-3. The flow rate was adjusted so 100 to 500 events/s were recorded.
5. An unstained sample was initially loaded and the voltages for the forward scatter (FSC) and side scatter (SSC) were adjusted so that the sample was positioned correctly on the SSC-area v FSC-area dot plot i.e. the cells are plotted within the boundary of the dot plot. The voltages for the fluorophore channels were also adjusted so that the negative peaks are positioned to the left side of the histogram plot.
6. Cells probed with a lectin were then checked to ensure that the voltages set were appropriate for positive peaks. The voltages were adjusted as required.
7. Samples were loaded and a minimum of 10,000 events were recorded.
8. Data files, FCS3.0, were exported to a memory stick.
9. The flow cytometer shut down protocol was then followed.

2.28.3.3 Flow cytometer data analysis and gating strategy

Flow cytometry data, FCS3.0 files, were opened and analysed using Flowing Software 2.5.1 developed by Perttu Terho, University of Turku, Finland. This freeware is available from <http://flowingsoftware.btk.fi/index.php?page=3>. The gating strategy used is explained in Fig. 2.12.

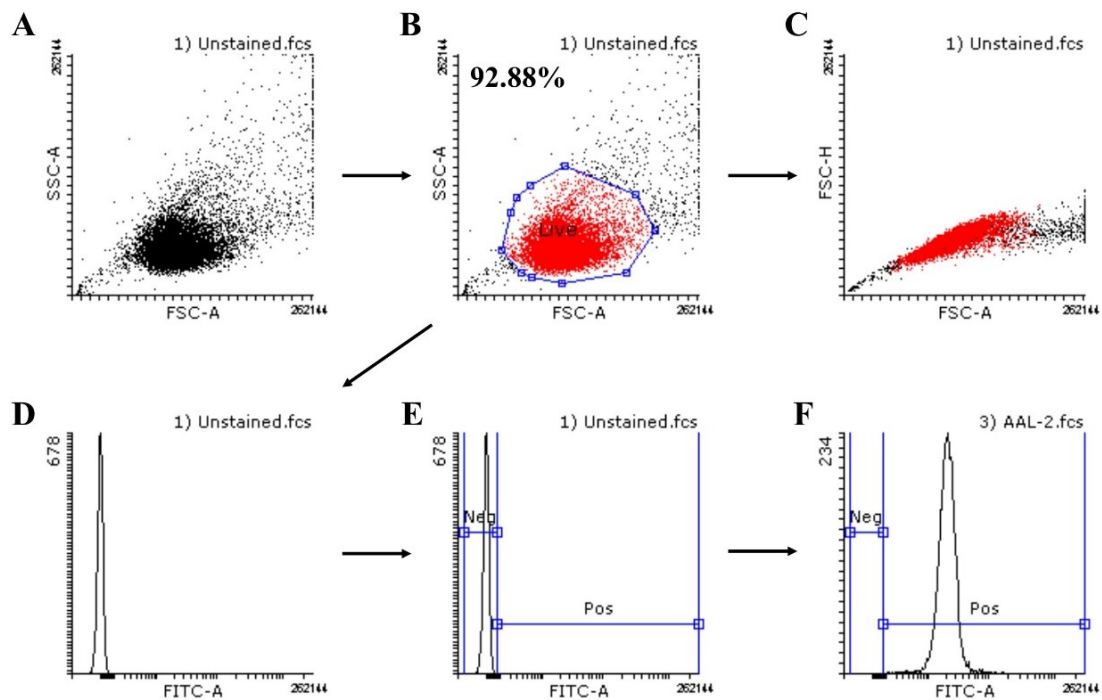


Fig. 2.12: Flow cytometry data gating strategy. **A)** Raw data, side scatter area vs. forward scatter area bivariate plot (dot plot) of unstained cells. **B)** ‘Live’ gate constructed around single cell population of unstained cells, 92.88 % of all cells in this gate. **C)** Forward scatter height vs. forward scatter area dot plot of unstained cells. **D)** Univariate plot (histogram) of fluorescence intensity (FITC-A channel) of unstained live cells. **E)** Univariate plot (histogram) of fluorescence intensity (FITC-A channel) of live cells gated negative (Neg) and positive (Pos). **F)** Negative and positive gates for fluorescence intensity applied to cells probed with AAL-2.

The gating strategy outlined in Fig. 2.12 was applied to all data. The first gate was constructed around the unstained/unprobed cells. This ‘Live’ gate excluded cell debris which registers with both low side scatter area (SSC-A) and forward scatter area (FSC-A). Events recorded with a large SSC-A and/or FSC-A are also excluded with this gate i.e. cell doublets. The exclusion of cell doublets is checked by plotting FSC-H vs FSC-A, Fig. 2.12 image C. The single cells on a FSC-H vs FSC-A plot should lie along a diagonal, as there is an increase in cell height there should be a corresponding increase in cell area. Fig. 2.12 image C shows that the Live gate has excluded cell doublets, events that fall below the diagonal which have a large FSC-A but not a correspondingly large FSC-H.

The live cell gate, constructed around unstained cells, is applied to all subsequent samples. A histogram is created showing the fluorescence intensity recorded in the FITC-A channel of unstained cells, Fig. 2.12 image D. A single peak is observed as these cells were not probed with lectin:Dylight488. Negative and positive gates are constructed on the histogram of unstained cells, Fig. 2.12 image E. The single peak is enclosed in the negative gate whereas everything to the right of this peak, i.e. recorded events with greater fluorescence intensity, fall into the positive peak. These negative and positive gates are then applied to all samples, Fig. 2.12 image F.

Fig. 2.13 illustrates the importance of removing events which are more than one cell, i.e. doublets or clumped cells. Doublet discrimination is essential for cell sorting as a doublet event may contain a positive and negative cell which registers on the cytometer as a positive event. Doublets can be equally erroneous during single staining non-cell sorting experiments where the fluorescence intensity of a doublet event can be much greater than that of single event.

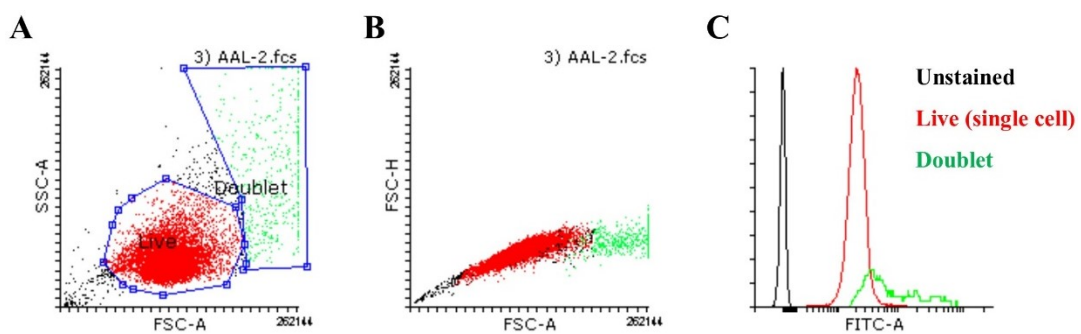


Fig. 2.13: Flow cytometry data gating strategy – the importance of removing doublets. A) ‘Live’ gate constructed around single cell population of unstained cells, applied here to cells probed with AAL-2 lectin. Also a large ‘Doublet’ gate constructed around events with high SSC-A and FSC-A. B) Forward scatter height vs. forward scatter area dot plot of cells. C) Histogram overlay of unstained cells and AAL-2 probed cells with events in both gates shown.

Once the gating strategy outlined in Fig. 2.12 is completed, a table is generated using Flowing Software to summarise the lectin binding for all cell samples, see Table 2.9. The key parameters included in the table are the percentage of cells in the live gate, the

percentage of cells in the negative and positive gates and the mean fluorescence intensity (MFI). This data can be graphed on a bar chart to complement the histogram plots.

Table 2.9: Flow cytometry sample data

10,000 events recorded for each sample in triplicate, average tabulated.

Sample	% in Live Gate	% Negative	% Positive	MFI (Neg + Pos)	MFI (Pos only)
Unstained	92.88	99.99	0.01	3.20	31.80
AAL	87.95	1.76	98.24	1154.91	1175.27
AAL-2	90.85	0.02	99.98	2308.10	2308.52
DSL	89.74	0.03	99.97	1768.60	1769.05
GSL I B4	93.00	98.54	1.46	62.81	3636.97
Jacalin	61.38	6.90	93.10	7036.02	7556.08
LCA	72.24	7.53	92.47	2883.31	3115.20
LecAK5	88.36	19.19	80.81	299.57	361.91
LecB	90.13	0.42	99.58	272.89	273.80

The percentage of events in the live gate is indicative of the cytotoxic effect that some lectins have on CHO cells. For unstained cells, there are typically 90 % of cells or greater in the live gate. Most cell samples probed with lectins are similar or have only slightly fewer cells in the live gate. However, some lectins, see Jacalin and LCA Table 2.9, are more cytotoxic and therefore a considerable decrease of cells in the live gate is observed.

The mean fluorescence intensity shown in Table 2.9 is calculated both from all negative and positives events and from positive events only. Calculating the MFI from positive events only is erroneous. This is particularly evident when the % positive events is low, see GSL I B4 Table 2.9, or if the histogram is bimodal and a large proportion of events are not considered as they fall outside the positive gate. Fig. 2.14 compares the histograms and MFIs from AAL and GSL I B4.

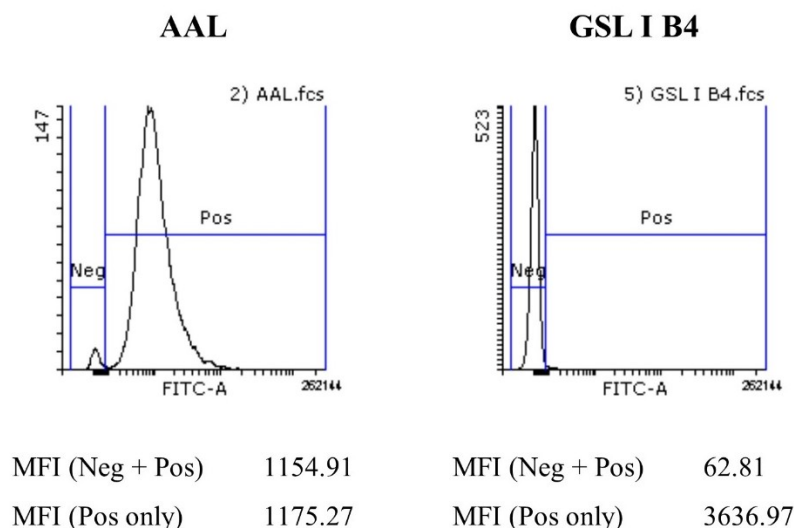


Fig. 2.14: Sample data for the comparison of AAL and GSL I B4 binding patterns. Histograms and MFIs calculated using both negative and positive events and positive events only are shown.

AAL bound to CHO DP-12 cells strongly with nearly all events, 98.24 %, in the positive gate. A small negative peak is also observed. Both methods for calculating the mean fluorescence intensity produce similar results. However, the same can't be said for GSL I B4 where only a small percent of the events, 1.46 %, are in the positive gate. MFI calculated using both negative and positive events is superior and it is also less likely for data to be misinterpreted or for low binding/outliers to be overstated.

All subsequent data presented in this work will show MFI calculated using all events in the live gate, i.e. all negative and positive events. Where relative MFI (RMFI) is mentioned it is when the MFI from lectin binding to an untreated cell sample is adjusted to 1 and the MFI from lectin binding to a treated cell sample is given as an appropriate fraction.

Chapter 3

**The expression, characterisation and labelling
of non-plant lectins from *Agrocybe aegerita*,
Escherichia coli and *Pseudomonas aeruginosa***

3.1 Overview

This chapter describes the expression, purification, mutagenesis, characterisation and labelling of non-plant lectins from *Agrocybe aegerita*, *Escherichia coli* and *Pseudomonas aeruginosa*. As previously stated in the introduction, lectins are potentially powerful glycoanalytical probes and producing them recombinantly offers many advantages, in particular, consistent performance. Producing the lectins recombinantly also offered a chance to alter their physiochemical properties, further increasing the lectin panel for glycan probing. The lectins were all expressed in *Escherichia coli* and purified using immobilised metal affinity chromatography (IMAC), see Section 2.17. The purified lectin probes were then labelled either directly, e.g. fluorescent fusion tag, or indirectly, biotin and DyLight488. Modifications were made to the coding sequences of *Agrocybe aegerita* lectin 2 (AAL-2) and *Pseudomonas aeruginosa* lectin I (PA-IL/LecA) to enhance labelling and purification. The specificity of lectin binding was determined using enzyme-linked lectin assays (ELLA), see Section 2.25. These purified lectins were then used to probe live CHO DP-12 cells which were subsequently analysed using fluorescent microscopy and flow cytometry (Chapters 4 and 5).

3.2 Cloning and expression of recombinant lectins

The bacterium *Escherichia coli* was used for expressing all lectins. It is one of the most commonly used recombinant hosts as it has many desirable characteristics (Baneyx 1999). They include; ease of cultivation, high specific growth rate ($\sim 2.0 \text{ h}^{-1}$), ability to achieve high cell density cultures and it is easily manipulated making it ideally suited to recombinant techniques. The main drawback with this host is its inability to perform certain post-translational modifications, including glycosylation. However, this is not a major concern as the recombinant lectins produced in this work are from non-mammalian/non-plant sources and are not glycosylated proteins. Two *E. coli* strains, JM109 and KRX were used for this work, see Section 2.1. *E. coli* JM109 is an ideal strain for cloning. It is *recA* negative which prevents plasmid DNA recombining with host chromosomal DNA. It is also *endA* negative which improves the quality and yield of isolated plasmid DNA. *E. coli* KRX is also suited to cloning as it too is *recA* and

endonuclease A deficient. However, this strain also contains a chromosomal copy of the T7 RNA polymerase (IPTG-inducible). This allows for tightly controlled expression of recombinant proteins. Two Qiagen pQE vectors were used for this work. Both vectors have a T5 promoter, detailed multiple cloning sites and His₆ tag regions at either the *N*- (pQE-30) or *C*- (pQE-60) termini. Ampicillin is used as the selection marker for these vectors as they both possess the β -lactamase gene. Detailed vector maps are shown in Section 2.1.

3.3 *Agrocybe aegerita* lectin 2

3.3.1 The AAL-2 coding sequence and protein sequence

A pQE vector containing AAL-2, pQE-30_AAL-2, had been previously constructed in the lab, see Table 2.2, and transformed into *E. coli* JM109. The AAL-2 sequence was checked prior to initial protein expression. A 5 mL LB broth containing ampicillin was inoculated with this *E. coli* and incubated overnight. A plasmid purification, see Section 2.8.1, was completed and confirmed by agarose gel electrophoresis, see Section 2.9. DNA sequencing was provided by Eurofins Genomics, see Section 2.13, Fig 3.1.

```

ATGAGAGGA TCGCATCAC CATCACCAT CACGGATCC ATGACCTCT AACGTTATC ACCCAGGAC
CTGCCGATC CCGGTTGCT TCTCGTGGT TTCGCTGAC ATCGTTGGT TTCGGTCTG GACGGTGT
GTTATCGGT CGTAACGCT GTTAACCTG CAGCCGTTT CTGGCTGTT AAAAACTTC GCTCAGAAC
GCTGGTGGT TGGCTGACC ACCAAACAC GTTCGTCTG ATCGCTGAC ACCACCGGT ACCGGTAAA
GGTGACATC GTTGGTTTC GGTAACGCT GGTGTTTAC GTTTCTGTT AACAACGGT AAAAAACACC
TTCGCTGAC CCGCCGAAA ATGGTTATC GCTAACTTC GGTTACGAC GCTGGTGGT TGGCGTGT
GAAAAACAC CTGCGTTAC CTGGCTGAC ATCCGTAAA ATCGGTCGT GCTGACATC ATCGGTTTC
GGTGAAAAA GGTGTTCTG GTTTCTCGT AACAACGGT GGTCTGAAC TTCGGTCCG GCTACCCTG
GTTCTGAAA GACTTCGGT TACGACGCT GGTGGTTGG CGTCTGGAC CGTCACCTG CGTTTCCTG
GCTGACGTT ACCGGTAAC GGTACCTG GACATCGTT GGTTCGGT GACAAACAC GTTTTCATC
TCTCGTAAC AACGGTGAC GGTACCTTC GTCCTGGCT AAATCTGTT ATCGACAAC TTCTGCATC
GACGCTGGT GGTTGGAAA ATCGGTGAC CACCCGCGT TTCGTTGCT GACCTGACC GGTGACGGT
ACCGCTGAC ATCATCGGT TCGGGTAAA GCTGGTTGC TGGGTTGCT CTGAACAAC GGTGGTGGT
GTTTTTCGGT CAGGTAAA CTGGTTATC AACGACTTC GGTACCGAC AAAGGTTGG CAGGCTGCT
AAACACCCG CGTTTCATC GCTGACCTG ACCGGTAAC GGTCTGGT GACGTTGTT GGTTCGGT
AACGCTGGT GTTTACGTT GCTCTGAAC AACGGTGAC GGTACCTTC CAGTCTGCT AAACGGTT
CTGAAAGAC TTCGGTGTG CAGCAGGGT TGGACCGTT TCTAAACAC CGTCGTTTC GTTGTGAC
CTGACCGGT GACGGTTGC GCTGACATC ATCGGTTTC GGTGAAAAA GAAACCCTG GTTTCTTAC
AACGACGGT AAAGGTAAC TTCGGTCCG GTTAAAGCT CTGACCAAC GACTTCTCT TTCTCTGGT
GGTAAATGG GCTCCGGAA ACCACCGTT TGCTGGATG GCTAACCTG GACTCTTCT CGTCACTAA

```

Fig. 3.1: AAL-2 coding sequence. The nucleotide sequence of AAL-2 (1,224 bp) with an *N*-terminus His₆ tag is shown (blue). The starting codon (green), the first codon in the AAL-2 sequence (underlined) and the stop codon (red) are highlighted. This

sequence is slightly different to the AAL-2 nucleotide sequence deposited in GenBank(JN001164.1) as this was codon optimised for *E. coli*. However, its translated sequence is identical, see Fig. 3.2.

```
MRGSHHHHHHGSMTSNVITQDLPIPVASRGFADIVGFGLDGVVIGRNAVNLQPFLAVKNFAQNAGGWLT  
TKHVRLIADTTGTGKGDIVGFGNAGVYVSVNNGKNTFADPPKMVIANFGYDAGGWRVEKHLRYLADIRK  
IGRADIIGFGEKGVLVSRNNGGLNFGPATLVLKDFGYDAGGWRLDRHLRFLADVTGNHGLDIVGFGDKH  
VFISRNNGDGTAFAPAKSVIDNFCIDAGGWKIGDHPRFVADLTGDGTADIIGCGKAGCWVALNNGGGVFG  
QVKLVINDFGTDKGWQAAKHPRFIADLTGNRGRDVGFGNAGVYVALNNGDGTQSAKLVLKDFGVQQG  
WTVSKHRRFVVDLTGDGCADIIGFGEKETLVSYNDGKGNFGPVKALTNDFSFSGGKWAPETTVCWMANL  
DSSRH-
```

Fig. 3.2 AAL-2 protein sequence. The protein sequence (407 amino acids) with highlighted regions corresponding to those in Fig 3.1, starting methionine, His₆ tag, starting methionine in AAL-2 sequence and the sequence terminator.

3.3.2 Expression and IMAC purification of AAL-2

The pQE-30_AAL-2 plasmid had been purified for sequence analysis as described in Section 2.8.1. A transformation was completed, see Section 2.10.2, and the purified plasmid was inserted into chemically competent *E. coli* KRX cells. A 200 mL TB medium standard expression culture, see Section 2.15, was completed. The cells were lysed by a cell disruptor and the resulting lysate was passed through a 2 mL Ni charged IMAC-Sepharose (GE Healthcare) column, see Section 2.17.1. Fig. 3.3 shows the wash and elution fractions from this purification.

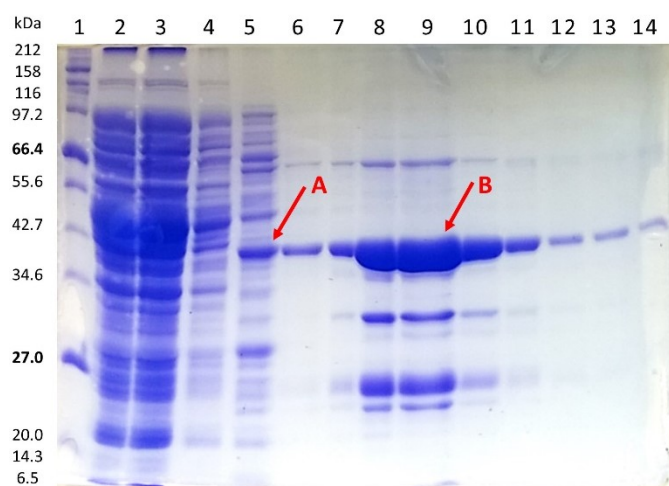


Fig. 3.3: IMAC purification of AAL-2 with an N-terminus His₆ tag. Analysis by 15 % SDS-PAGE of N-terminally His₆ tagged AAL-2 in *E. coli* KRX. Two imidazole wash steps, 20 mL of 20 mM and 10 mL of 80 mM, were completed before eluting with 250 mM imidazole. Lane 1; NEB protein ladder (Fig. 2.5), Lane 2; filtered lysate, Lane 3; unbound filtered lysate (flow through), Lane 4; Wash 1 (20 mM), Lane 5; Wash 2 (80 mM), Lanes 6 - 14; 1 mL elution fractions (250 mM).

Lanes 1 and 2 in Fig. 3.3 show the large number of proteins present in lysed *E. coli* KRX cells. The presence of large bands beside the 42.7 kDa marker in lanes 1 and 2 also indicate that AAL-2 was strongly expressed. Lanes 1 and 2 are similar as nearly all non-tagged proteins were not captured by the column. The first wash removed many unwanted proteins, lane 4. The second wash, lane 5, also removed unwanted proteins however AAL-2 was also being eluted from the column during this wash as indicated by the large band, arrow A. The bound AAL-2 was eluted by the 250 mM imidazole lysis buffer as shown by the large bands in lanes 7-11, arrow B. These lanes also show the co-purification of unwanted proteins. The expression and purification of AAL-2 was repeated with additional imidazole wash steps prior to elution, see Fig. 3.4.

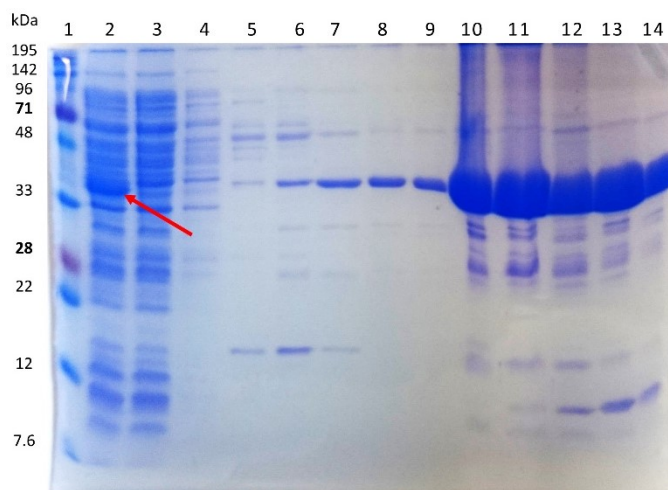


Fig. 3.4: IMAC purification of AAL-2 with an *N*-terminus His₆ tag with additional wash steps. Analysis by 15 % SDS-PAGE of *N*-terminally His₆ tagged AAL-2 in *E. coli* KRX. Four imidazole wash steps were completed, 20 mL of 20 mM, and 10 mL of 40 mM, 60 mM and 80 mM, before eluting with 250 mM imidazole. Lane 1; Expedeon prestained dual-colour marker (Fig. 2.5), Lane 2; filtered lysate, Lane 3; unbound filtered lysate, Lane 4; Wash 1 (20 mM), Lane 5; Wash 2 (40 mM), Lane 6; Wash 3 (60 mM), Lane 7; Wash 4 (80 mM), Lanes 8 - 14; 1 mL elution fractions (250 mM).

AAL-2 was strongly expressed, see arrow, and captured by the column. However, the additional wash steps did not remove the co-purified proteins as intended. Larger and smaller proteins are clearly present in the elution fractions where AAL-2 is most concentrated, lanes 10-14. These may be removed by improving the AAL-2 purification by switching the His₆ tag to the *C*-terminus or inserting a linker/spacer between the His₆ tag and the lectin, thereby improving its ability to bind the Ni charged resin.

3.3.3 Cloning and expression of AAL-2 variants to enhance IMAC purification

An alternative cloning strategy was used to enhance the purification of AAL-2. Switching the position of the His₆ tag and introducing a linker between it and AAL-2 may simplify its purification using IMAC. Three different plasmid constructs were made to enhance AAL-2 purification. These include inserting a linker (spacer) between the *N*-terminus His₆ tag and AAL-2, switching the His₆ tag to the *C*-terminus, and fusing

AAL-2 to a protein that is more easily purified. Fig. 3.5, Fig. 3.6 and Fig. 3.7 describes the cloning process. Enhanced green fluorescent protein (EGFP) was selected for the fusion as it will directly fluorescently label AAL-2. The insertion and ligation reactions were initially checked by plasmid purification and agarose gel electrophoresis following transformation into competent *E. coli* KRX cells, see Fig. 3.8, and later confirmed by plasmid sequencing analysis.

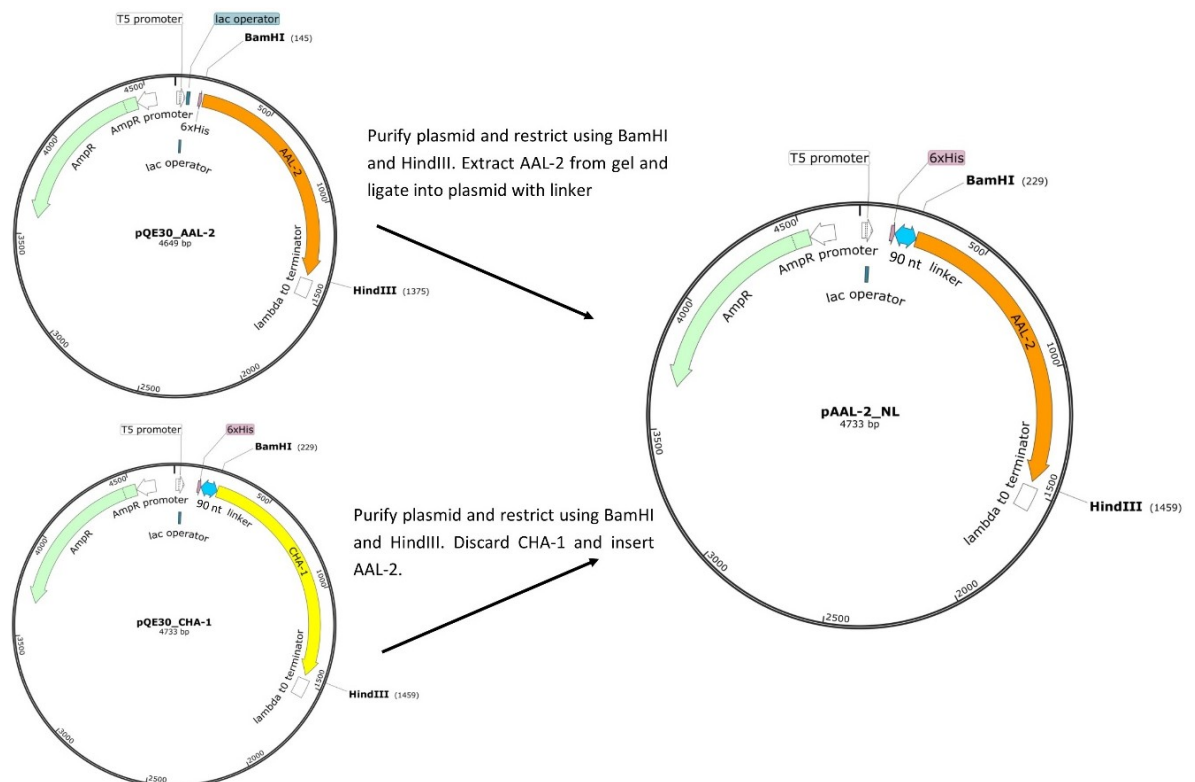


Fig. 3.5: The construction of pAAL-2_NL, a pQE-30 plasmid containing AAL-2 with a 90 nucleotide N-terminus linker. A pQE-30 vector with a 90 nt linker already existed so the insertion was completed using only BamHI and HindIII restriction digests. BamHI and HindIII are located at the N- and C- termini of AAL-2 respectively. The 90 nt linker (blue) is placed between the N-terminus His₆ tag and the start codon of AAL-2. Image generated using SnapGene Viewer Version 3.1.4.

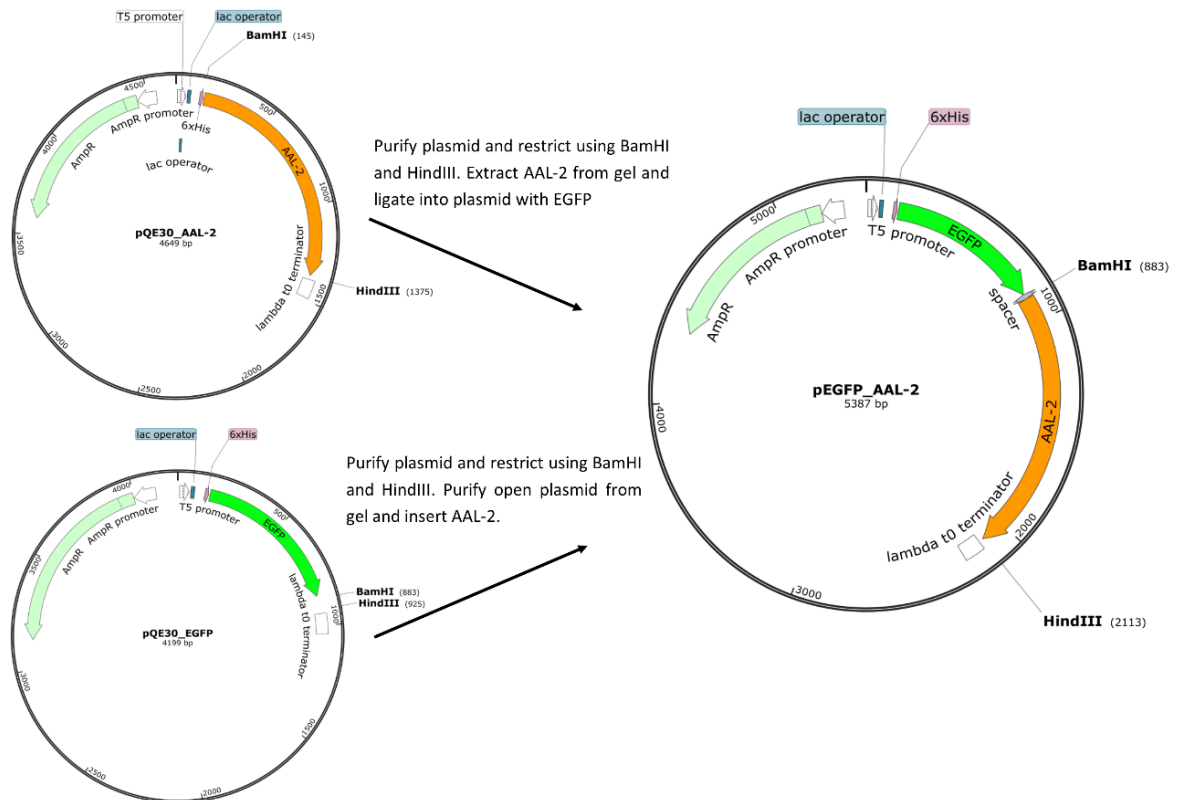


Fig. 3.6: The construction of pEGFP_AAL-2, a pQE-30 plasmid containing an EGFP-AAL-2 fusion with a His₆ tag at the EGFP *N*-terminus. This construction was completed using BamHI and HindIII restriction digests only. EGFP (green) is located between the *N*-terminus His₆ tag and the start codon of AAL-2. Image generated using SnapGene Viewer Version 3.1.4.

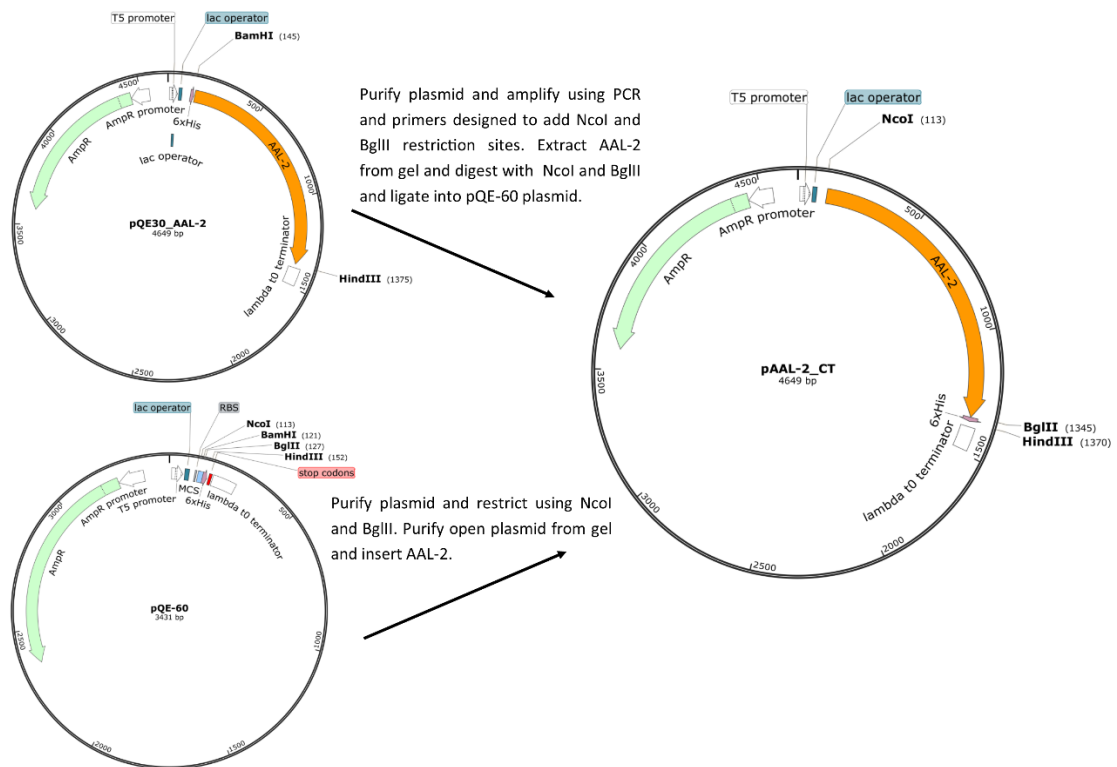


Fig. 3.7: The construction of pAAL-2_CT, a pQE-60 plasmid containing AAL-2 with a C-terminus His₆ tag. AAL- 2 was amplified by PCR where the restriction sites, NcoI and BglIII, were incorporated into the primers, 60AAL2_F and 60AAL2_R (see Table 2.4), to aid the ligation into the pQE- 60 vector. BamHI and HindIII are located on either side of the His₆ tag so they could not be used. Image generated using SnapGene Viewer Version 3.1.4.

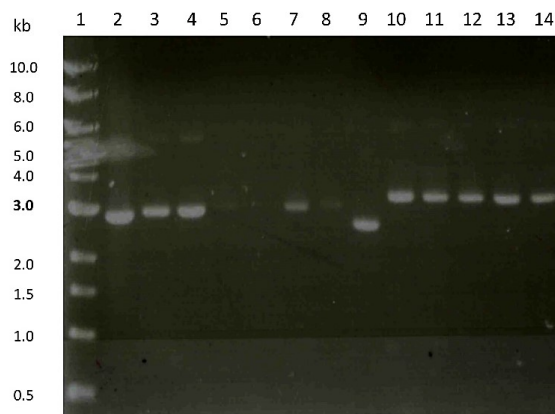


Fig 3.8: Agarose gel analysis of plasmid constructs containing AAL-2. 0.7 % agarose gel stained with EtBr. Lane 1; NEB 1kb DNA ladder, see Fig 2.3, Lane 2; pQE30_AAL-2 plasmid, Lanes 3-5; pQEAAL-2_NL plasmids from 3 transformants, Lanes 6-8; pAAL-2_CT plasmids from 3 transformants, Lane 9; pQE30_EGFP plasmid, and Lanes 10-14; pEGFP_AAL-2 plasmids from 5 transformants.

Fig. 3.8 shows a subtle size difference in the purified plasmids. The pQE30_AAL-2 plasmid in lane 2 migrated further than the pAAL-2-NL plasmids in lanes 3, 4 and 5, as they contained 90 additional nucleotides. The pAAL-2_CT plasmids, lanes 6, 7 and 8, were not as visible. The pQE30_EGFP plasmid, lane 9, migrated further than the pEGFP_AAL-2 plasmids in lanes 10-14. This migration difference was more striking as the plasmids differ in size by 1224 nucleotides. The full nucleotide and amino acid sequences of all AAL-2 variants can be found in Appendix A. The three new constructs were transformed into competent KRX cells and expressed in 200 mL TB medium. The AAL-2 variants were then purified using IMAC, see Sections 2.10, 2.15 and 2.17. Fig. 3.9 shows the protein fractions from these purifications.

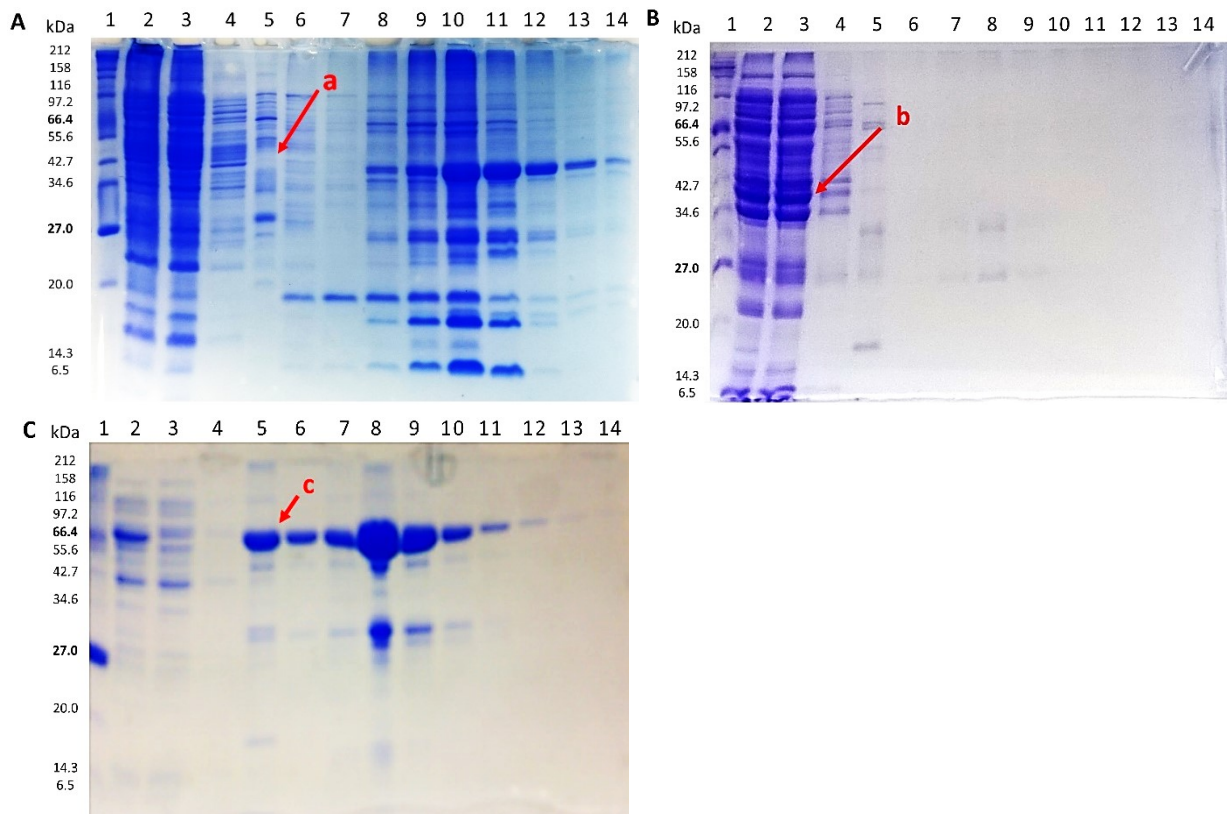


Fig. 3.9: The purification of AAL-2 with a linker, a C-terminus His₆ tag and fused to EGFP. A) AAL-2 with a 30 aa N-terminus linker, pAAL-2_NL constructed in Fig. 3.5. **B)** AAL-2 with a C-terminus His₆ tag, pAAL-2_CT constructed in Fig. 3.7 and **C)** EGFP-AAL-2 fusion, pEGFP_AAL-2 constructed in Fig. 3.6. Two imidazole wash steps, 20 mL of 20 mM and 10 mL of 80 mM, were completed before eluting with 250 mM imidazole. In all images Lane 1; NEB protein ladder (Fig. 2.5), Lane 2; filtered lysate, Lane 3; unbound filtered lysate, Lane 4; Wash 1 (20 mM), Lane 5; Wash 2 (80 mM), Lanes 6 - 14; 1 mL elution fractions (250 mM).

Fig. 3.9 compares the purification of AAL-2 using the 3 new constructs as described in Section 2.1 Table 2.3. AAL-2 with a *N*-terminal linker, gel A Fig. 3.9, is not eluted by the 80 mM imidazole wash as indicated by the absence of a band at 43 kDa in lane 5, arrow a. The elution fractions that contain the most AAL-2, lanes 9-11, also contain other proteins. AAL-2 with a *C*-terminal His₆ tag didn't bind to the column at all, gel B Fig. 3.9, as lanes 2 and 3 are identical. AAL-2 was clearly expressed but did not bind to the column, arrow b. The *C*-terminus might not be exposed and/or the addition of a His₆ tag might have influenced protein folding. The purification of the EGFP-AAL-2 fusion is shown by gel C Fig. 3.9. The expected size of the fusion is 71 kDa which is approximately the size of the large band indicated by arrow c. The second wash step and the elution fractions contained the fusion protein as large bands were visible. However, like unfused AAL-2 and AAL-2 with an *N*-terminal linker, there were a number of contaminated protein bands present.

The putative 3D structures of AAL-2 with an *N*-terminal His₆ tag (with and without a spacer) and with a *C*-terminal His₆ tag were generated using the I-TASSER online tool and are compared in Fig. 3.10.

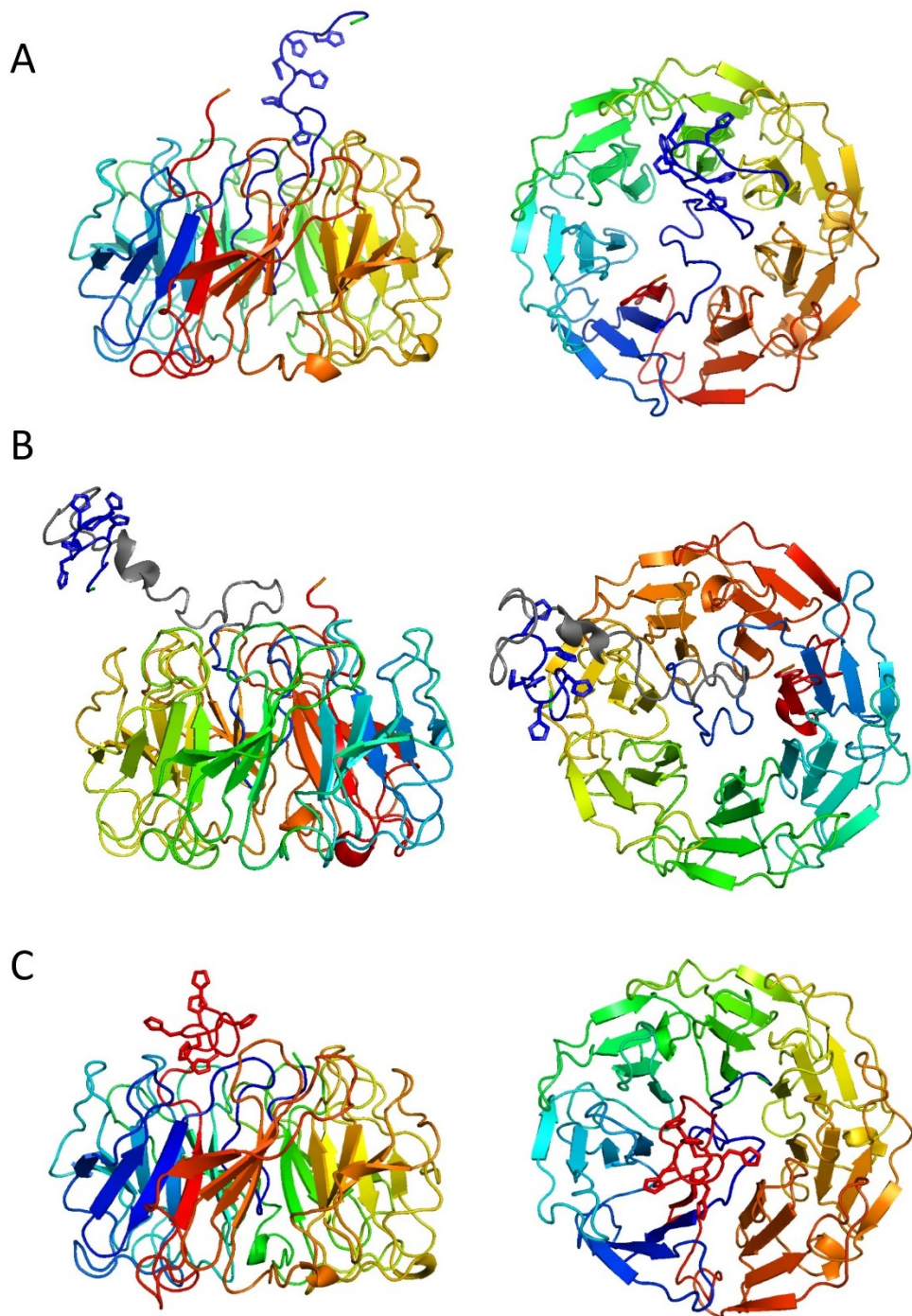


Fig. 3.10: Horizontal and vertical views of the putative 3D structures of AAL-2 variants represented in cartoon format. The *N*- and *C*- termini are green and orange respectively. **A)** AAL-2 with an *N*-terminus His₆ tag. The His₆ tag side chains are shown in blue. **B)** AAL-2 with an *N*-terminus His₆ tag and a 30 aa spacer. The His₆ tag side chains are shown in blue. The 30 aa spacer is shown in grey. **C)** AAL-2 with a *C*-terminus His₆ tag. The His₆ tag side chains are shown in red. The 3D structures were generated by the I-TASSER tool, see Section 2.14. The images were made using open-source PyMOL 1.3.

3.3.4 Optimising the IMAC purification of AAL-2

A relatively pure fraction of AAL-2 was not obtained despite altering the His₆ tag and fusing it to another protein, see Section 3.3.3. A third wash step containing imidazole (<80 mM) was added to help remove unwanted proteins. A large volume wash step, e.g. 20 mL, may help remove unwanted proteins from the column. Additionally, a second IMAC resin was used for the purification. AAL-2 was expressed from *E. coli* KRX cells containing pQE-30_AAL-2, see Table 2.2, in 400 mL TB medium. The cells were lysed by a cell disruptor and the filtered lysate divided for loading onto separate 2 mL Ni IMAC resins; IMAC-Sepharose FastFlow (GE Healthcare) and Profinity IMAC (Bio-rad). The fractions collected from these purifications were analysed by SDS-PAGE, see Fig. 3.11.

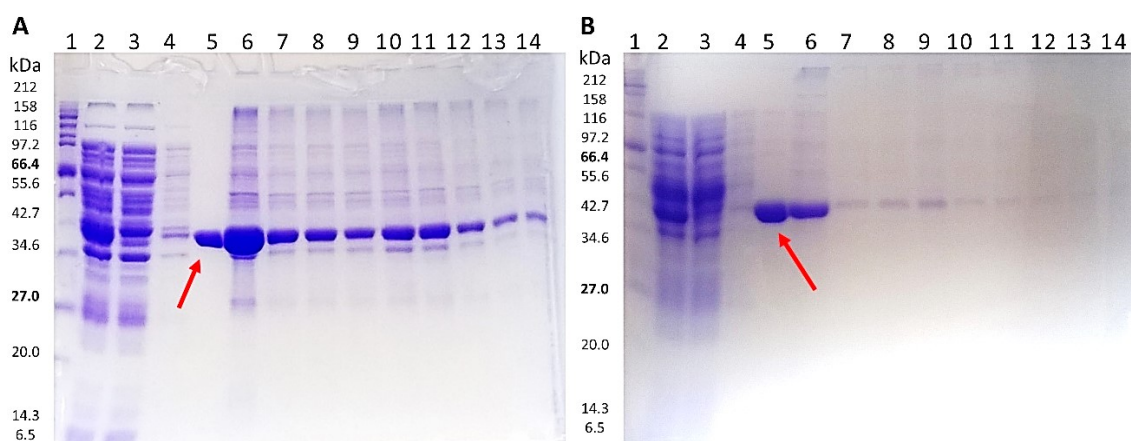


Fig. 3.11: The purification of AAL-2 using two IMAC resins. A) IMAC-Sepharose FastFlow (GE Healthcare) resin and **B)** Profinity IMAC (Bio-rad) resin. Three imidazole wash steps, 20 mL of 20 mM, 20 mL of 50 mM and 10 mL of 80 mM were completed before eluting with 250 mM imidazole. In both images Lane 1; NEB protein ladder (Fig. 2.5), Lane 2; filtered lysate, Lane 3; unbound filtered lysate, Lane 4; Wash 1 (20 mM), Lane 5; Wash 2 (50 mM), Lane 6; Wash 3 (80 mM), Lanes 7 - 14; 1 mL elution fractions (250 mM).

Incorporating a 20 mL 50 mM imidazole wash step in the IMAC purification of AAL-2 resulted in a relatively pure fraction, i.e. unwanted proteins were not visible in these lanes, lanes 5 gel A and gel B. The GE FastFlow resin captured the His₆ tagged AAL-2

with greater affinity than the Bio-rad resin. Most of the AAL-2 that was bound to the Bio-rad resin was removed prior to eluting with 250 mM imidazole. The added wash step was intended to remove contaminant proteins. However, it resulted in the elution of a large portion of the bound AAL-2 which was relatively pure, see Fig. 3.11.

3.3.5 AAL-2 quantification, biotinylation and western blot analysis

The two 50 mM imidazole wash fractions, lanes 5 in gel A and gel B in Fig. 3.9, were combined (~38 mL) as they appeared similar. The remaining fractions, which also contained AAL-2, were discarded as they contained many other proteins. A buffer exchange was completed, see Section 2.22, to remove imidazole and salt and exchange AAL-2 into a suitable buffer, PBS, for its biotinylation and storage. A bicinchoninic acid (BCA) assay, see Section 2.23, was completed to determine the protein concentration in the combined fractions before and after buffer exchange, see Fig. 3.12.

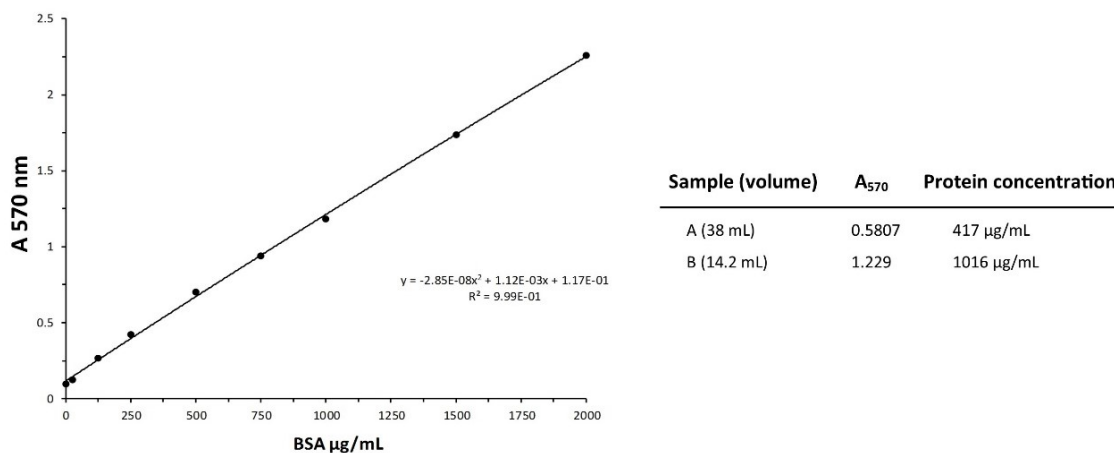


Fig. 3.12: BCA assay standard curve and sample results. A standard curve using bovine serum albumin (BSA) standards (0 - 2,000 µg/mL) was graphed and fitted with a polynomial trendline. The second order polynomial equation of the line was used to quantify the protein in samples A and B. **A)** 50 mM imidazole wash fractions pooled from Fig. 3.11. **B)** Buffer exchanged AAL-2 in PBS.

The BCA assay showed that the protein concentration increased approximately 2.5 fold after buffer exchange. 91 % of the starting protein (15.8 mg, 38 x 0.417 mL) was

recovered (14.4 mg, 14.2 x 1.016 mg). This 9 % loss could be from smaller proteins which passed through the dialysis tubing (MWCO 14 kDa). The concentration of AAL-2 in PBS was 1.016 mg/mL. The protein concentration was required to optimise the biotinylation reaction. The Thermo Scientific EZ-Link® Sulfo-NHS-LC-Biotin kit (21327) was used to biotinylate AAL-2, see Section 2.24. Following this two SDS-PAGE gels were completed, see Fig. 3.13, one for Coomassie staining and one for western blot analysis, see Section 2.21. A western blot was completed using an anti-polyHistidine mAb conjugated to HRP (Sigma A7058).

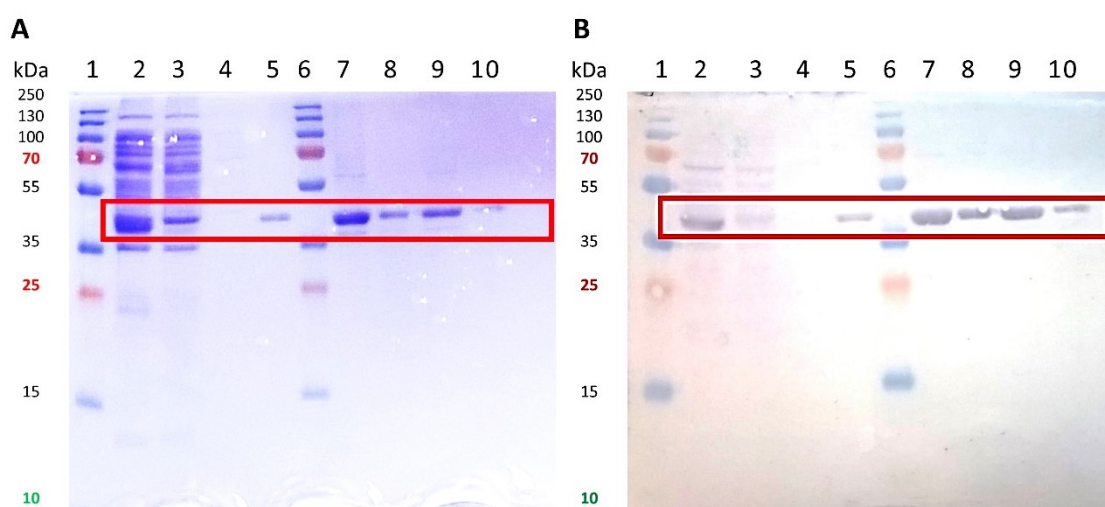


Fig. 3.13: Western blot analysis of IMAC purification fractions and buffer exchanged AAL-2. A) Coomassie stained 15 % SDS-PAGE gel and B) Western blot from a gel identical to gel A probed with anti-polyHistidine mAb. In both images Lanes 1 & 6; Thermo Scientific PageRuler Plus Prestained Protein Ladder (Fig. 2.5), Lane 2; filtered lysate, Lane 3; unbound filtered lysate, Lane 4; Wash 1 (20 mM imidazole), Lane 5; Wash 2 (50 mM imidazole), Lane 7; AAL-2 unbiotinylated (sample B from Fig. 3.12), Lane 8; AAL-2 unbiotinylated (sample B from Fig. 3.12) diluted 1 in 3, Lane 9; biotinylated AAL-2 and Lane 10; biotinylated AAL-2 diluted 1 in 3. Samples loaded in lanes 2-5 are the same samples loaded in lanes 2-5 of gel A in Fig. 3.11.

Western blot analysis of IMAC purification fractions was carried out as described in Section 2.21. This analysis demonstrated the successful purification of AAL-2. There are host proteins in *E. coli* that are similar in sized to AAL-2 however a strong signal from the anti-polyHistidine mAb confirms the presence of His₆ tagged AAL-2. The

mAb bound weakly to host proteins in lanes 2 and 3. This is most likely caused by exposed surface histidine residues which can loosely interact with the mAb. Lanes 9 and 10 show the relatively pure AAL-2 after biotinylation.

3.3.6 Enzyme-linked lectin assay analysis of AAL-2

The enzyme-linked lectin assay (ELLA), previously described in Section 2.25, was used to determine lectin activity and binding specificity. The ELLA is similar to an indirect ELISA where the antigen (glycoprotein) is attached to the solid phase (96-well plate) and the primary antibody/lectin is not labelled but detected by an enzyme-conjugated secondary antibody. Once a recombinant lectin is purified it must be stored in a suitable buffer to ensure that activity is not lost through denaturation and/or aggregation. AAL-2 was purified, biotinylated and stored in PBS. Glycerol and dithiothreitol (DTT) were added to duplicate aliquots of AAL-2 and stored at 4 °C and -20 °C. Fig. 3.14 compares the activity of AAL-2 in various storage conditions. Glycerol and DTT are two additives that can help stabilise protein folding and prevent aggregation (Bondos and Bicknell 2003). Glycerol decreases protein aggregation by promoting water-protein interaction. DTT is a strong reductant which breaks disulphide bonds leading to protein denaturation and so should generally be avoided in order to maintain a stable functioning protein. However, at a very low concentration (~ 1 mM) it may destabilise aggregates and be beneficial (Lebendiker and Danieli 2014).

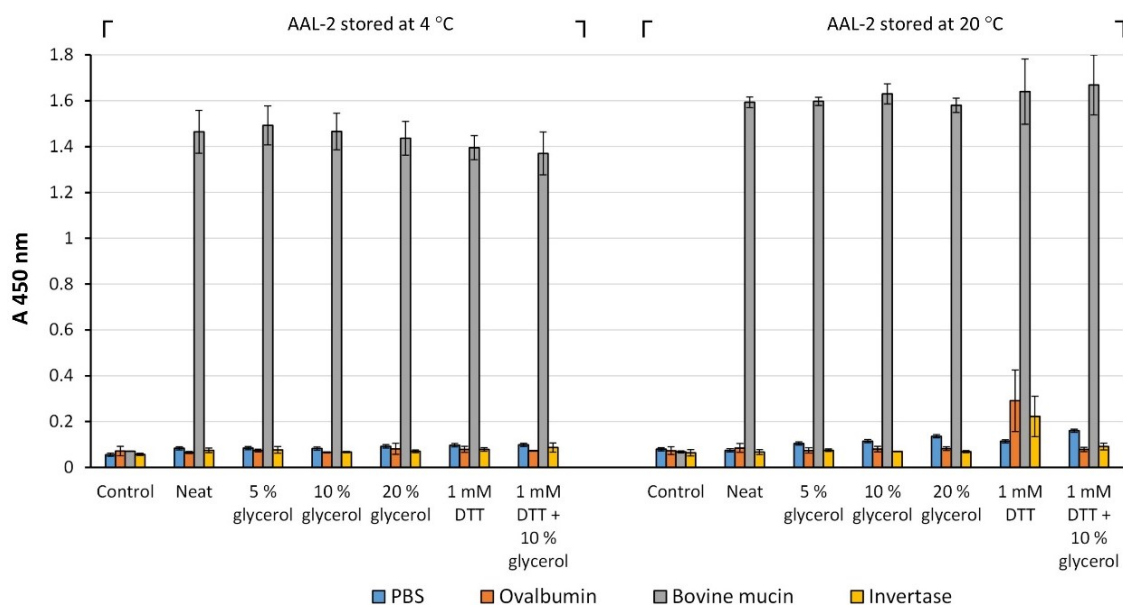


Fig. 3.14: ELLA analysis of AAL-2 storage conditions. An ELLA was completed as per Section 2.25. Duplicate aliquots of AAL-2 containing glycerol and DTT were stored at 4 °C and -20 °C for 4 weeks. The plate was blocked with 3 glycoproteins; ovalbumin, bovine mucin and invertase. An anti-polyHistidine mAb was used as a secondary probe. Error bars were calculated from the standard deviation of three replicates.

AAL-2 is expected to bind bovine mucin only as ovalbumin, from egg white, and invertase, from *Saccharomyces cerevisiae*, are two of the best studied glycoproteins both of which contain predominantly high-mannose type glycans (Harvey et al. 2000; Sigma 2013). This was observed for most AAL-2 aliquots analysed in Fig. 3.14. AAL-2 has high affinity for the GlcNAc containing glycoprotein, bovine mucin. Absorbance values were similar for AAL-2 aliquots with and without glycerol and DTT, suggesting no observed benefit from their inclusion in the buffer. However, AAL-2 binding was greater when stored at -20 °C, approximately 1.6 AU as opposed to 1.4 AU at 4 °C. This suggests that storing AAL-2 at 4 °C for a short time, 4 weeks, may result in loss of activity. This is contrary to commercial lectins, supplied by Vectors Labs (see Table 2.8), which were stored at 4 °C. It was determined that storing AAL-2 in PBS without additives at -20 °C is appropriate. ELLA analysis of AAL-2 was completed using an anti-polyHistidine mAb and an anti-biotin mAb, both conjugated to peroxidase. AAL-2 glycan binding was assessed using specific and non-specific monosaccharides and compared to two commercial plant lectins, see Fig. 3.15.

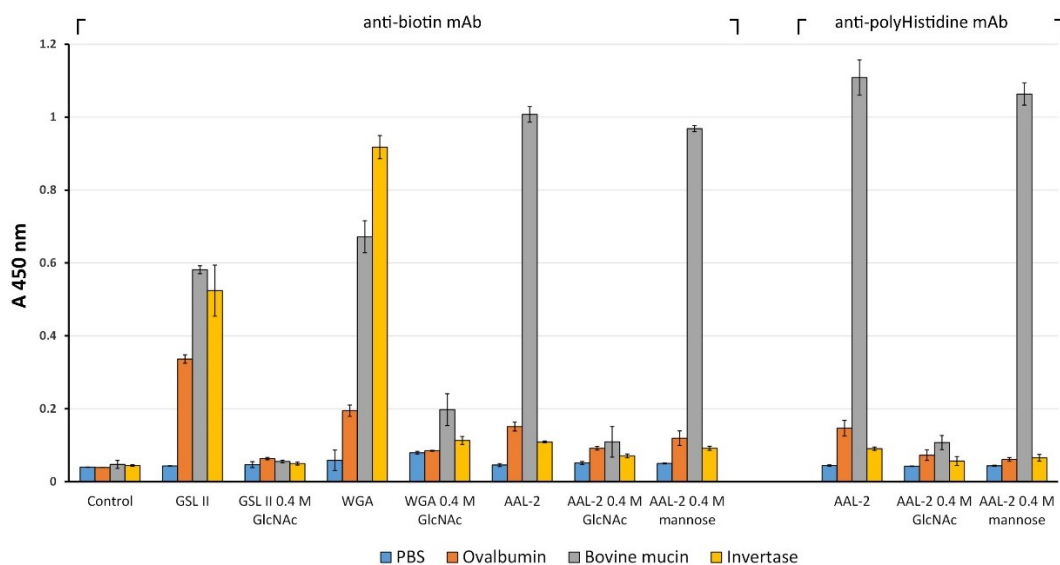


Fig. 3.15: ELLA analysis of AAL-2 and two GlcNAc binding plant lectins, GSL II and WGA. An ELLA was completed as per Section 2.25. Biotinylated plant lectins *Griffonia Simplicifolia* Lectin II (GSL II) and wheat germ agglutinin (WGA) and recombinant AAL-2 were added to the plate with and without GlcNAc, 0.4 M. AAL-2 was also premixed with a non-specific sugar, 0.4 M mannose. AAL-2 was subsequently probed with anti-biotin and anti-polyHistidine mAbs. Error bars were calculated from the standard deviation of three replicates.

The specificity of GSL II is clearly shown by the complete reduction in binding in the presence of 0.4 M GlcNAc. WGA was also inhibited but to a lesser degree. AAL-2 did not bind to all three glycoproteins like GSL II and WGA. AAL-2 binding was greatest for bovin mucin. Bovine mucin is a heavy glycosylated protein which includes core 3 *O*-glycans structures (GlcNAc β 1-3GalNAc α Ser/Thr) which AAL-2 will preferentially bind (Yamada et al. 2007). AAL-2 was inhibited in the presence of 0.4 M GlcNAc. However, 0.4 M mannose did not significantly reduce binding, demonstrating AAL-2 specificity for GlcNAc residues. Similar readings were obtained when AAL-2 was probed with the anti-polyHistidine mAb. Both the anti-polyHistidine-peroxidase mAb (A7058) and the anti-biotin-peroxidase mAb (A0185) were supplied by Sigma-Aldrich and the ratio of mAb:peroxidase during the conjugation process was 0.7:1.4 and 1.0:1.0 respectively. The slight increase detected by the anti-polyHistidine mAb could be from its increased ratio of mAb:peroxidase.

3.3.7 ELLA analysis of AAL-2, WGA and GSL II with specific and non-specific monosaccharides

Recombinant AAL-2 was premixed with its specific monosaccharide, GlcNAc, and separately with a highly similar monosaccharide, GalNAc, before being added to a plate to which glycoproteins, including BSA-GlcNAc, have been attached. The plant lectins WGA and GSL II which are also galactose binding lectins were also assessed by ELLA for comparison. GalNAc is an epimer of GlcNAc, the only difference is the orientation of the hydroxyl group on the fourth carbon, see Fig. 1.1. The inhibition of these lectins with this pair of stereoisomers was determined using ELLA, see Fig. 3.16, Fig. 3.17 and Fig. 3.18.

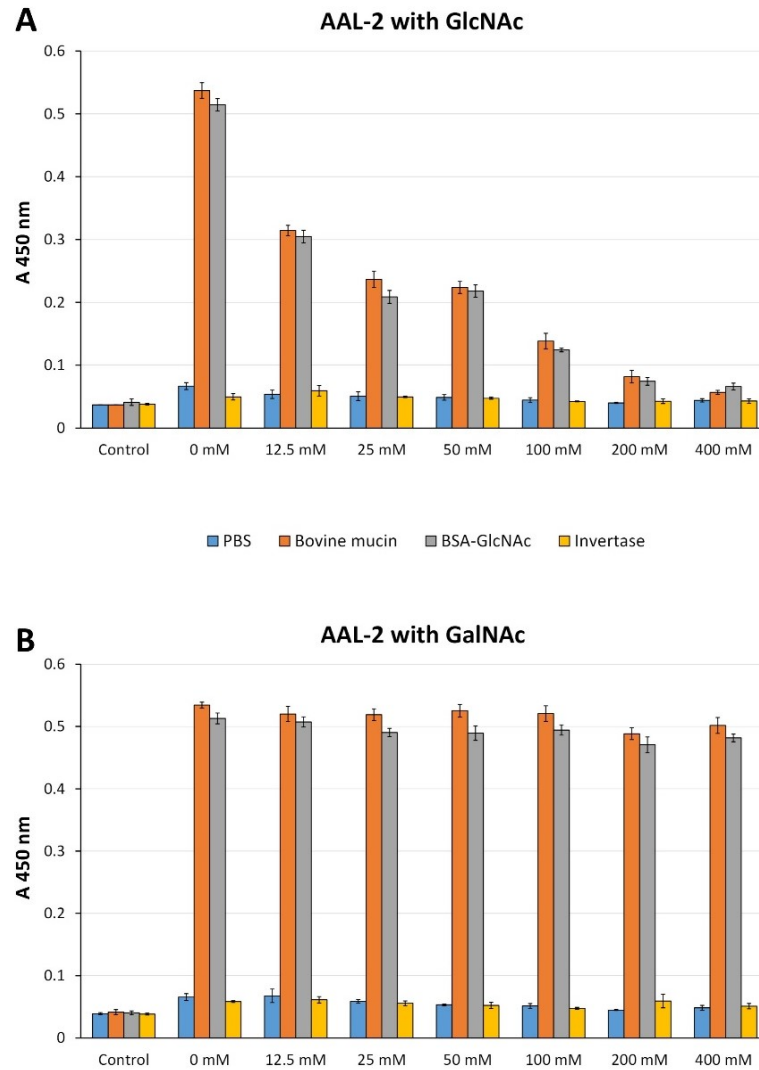


Fig. 3.16: ELLA analysis of AAL-2 with GlcNAc and GalNAc monosaccharides. An ELLA was completed as per Section 2.25 using biotinylated AAL-2. **A)** AAL-2 premixed with GlcNAc, 0 - 400 mM. **B)** AAL-2 premixed with GalNAc, 0 - 400 mM. AAL-2 binding was detected with an anti-biotin mAb. Error bars were calculated from the standard deviation of three replicates.

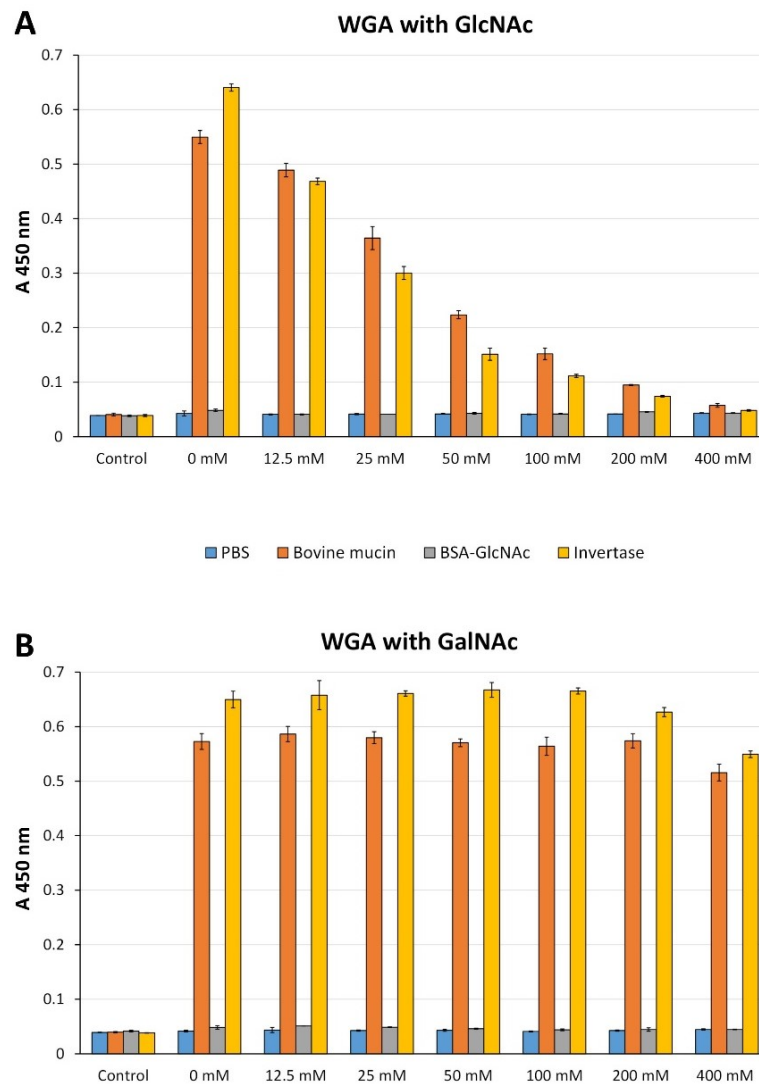


Fig. 3.17: ELLA analysis of WGA with GlcNAc and GalNAc monosaccharides. An ELLA was completed as per Section 2.25 using biotinylated WGA. **A)** WGA premixed with GlcNAc, 0 - 400 mM. **B)** WGA premixed with GalNAc, 0 - 400 mM. WGA binding was detected with an anti-biotin mAb. Error bars were calculated from the standard deviation of three replicates.

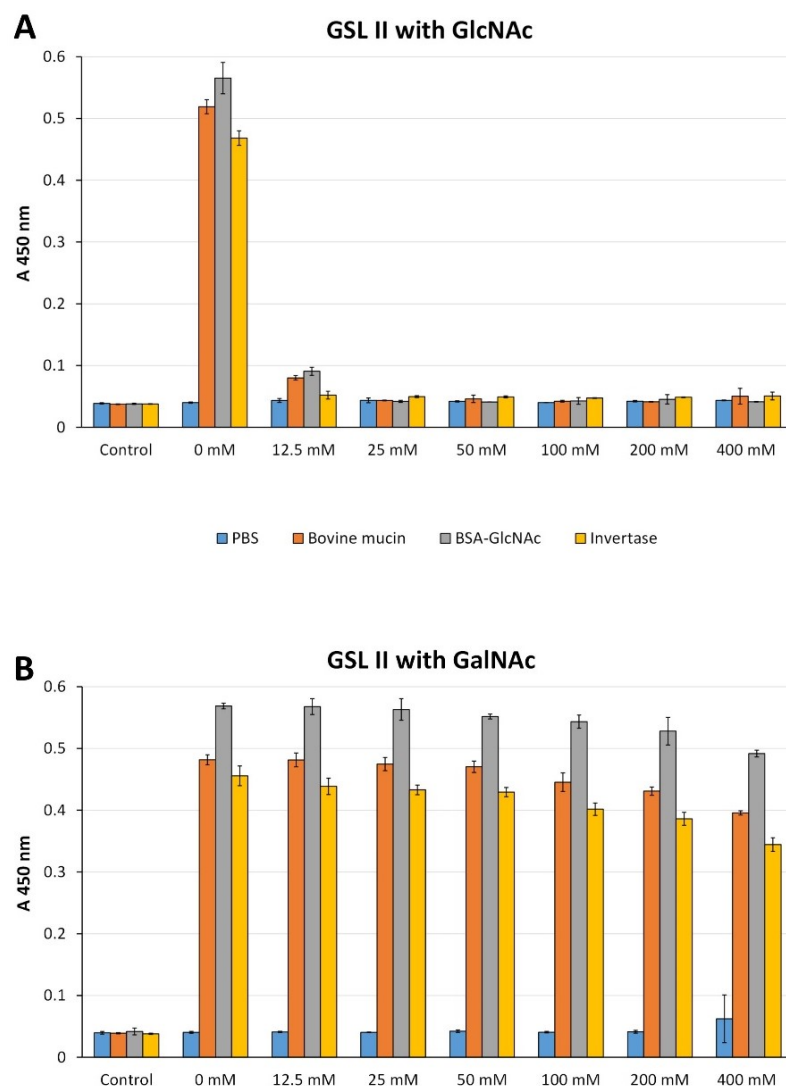


Fig. 3.18: ELLA analysis of GSL II with GlcNAc and GalNAc monosaccharides. An ELLA was completed as per Section 2.25 using biotinylated GSL II. **A)** GSL II premixed with GlcNAc, 0 - 400 mM. **B)** GSL II premixed with GalNAc, 0 - 400 mM. GSL II binding was detected with an anti-biotin mAb. Error bars were calculated from the standard deviation of three replicates.

AAL-2, WGA and GSL II were all inhibited with free GlcNAc but not with free GalNAc, even at 400 mM. The inhibition profile of AAL-2 was more similar to that of WGA. However, WGA did not bind BSA-GlcNAc at all, see Fig. 3.17. WGA binds preferentially to GlcNAc dimers and trimers and GlcNAc residues in complex *N*-glycans. BSA-GlcNAc is more akin to *O*-GlcNAc and *O*-glycans and was therefore

only bound by AAL-2 and GSL II. AAL-2 binds GlcNAc with greater affinity than GSL II as 25 mM GlcNAc was sufficient to completely inhibit GSL II binding.

3.3.8 Mutagenesis of AAL-2

Site-directed mutagenesis (SDM), as described in Section 2.12, was used to modify the AAL-2 sequence. SDM is a powerful technique which can be used to alter binding specificities through slight alterations in a protein sequence. Mutating a lectin so as to obtain a nearly identical protein but with a different binding specificity or affinity is of great use as a cellular probe. The complete loss of activity, binding knockout, is also a useful protein and is an ideal negative control. The mutation of AAL-2 to reduce/knockout GlcNAc binding was attempted. However, mutated AAL-2 was not successfully expressed and purified. This work may be found in Appendix B.

3.4 G(F17) fimbrial lectin, GafD1-178, from *E. coli*

3.4.1 The GafD1-178 coding sequence

A pQE vector containing GafD1-178, pQE-30_GafD1-178 see Table 2.2, was transformed into *E. coli* KRX. The GafD1-178 sequence was checked prior to initial protein expression. A 5 mL LB broth containing ampicillin was inoculated with this *E. coli* and incubated overnight. A plasmid purification, see Section 2.8.1, was completed and confirmed by agarose gel electrophoresis, see Section 2.9. DNA sequencing was provided by Eurofins Genomics, see Section 2.13 and Fig 3.19.

A

```
ATGAGAGGA TCGCATCAC CATCACCAT CACGGATCC ATGGCGAGTT TCATTTATT GGCAGTACG
GAGAATGAT GTTGGACCG TCTCAGGGC TCTTATTCC AGCACTCAT GCAATGGAT AACCTGCCA
TTTGTCTAT AATACCGGT TACAACATT GGATATCAG AATGCAAAT GTCTGGCGT ATTAGTGGC
GGGTTTTGT GTTGGTCTG GACGGGAAA GTGGATTTA CCCGTGGTT GGCAGTCTT GACGGGCAG
AGTATTTAT GGGCTGACG GAGGAGGTG GGACTCCTT ATATGGATG GGGGACACG AATTATTCC
AGGGGTACC GCGATGAGT GGAAACTCA TGGGAGAAT GTCTTTTCC GGATGGTGC GTGGGAAAT
TATGTATCA ACGCAGGGA CTGTCTGTT CACGTAAGA CCGTAATT TTAAAAAGA AATTCCTCT
GCGCAATAC AGTGTACAG AAAACCAGT ATCGGGAGT ATCAGAATG AGGCCCTAT AACGGTTCA
TCTGCAGGC AGTGTTTAC ACCACAGTG AATTTTACG CTGAATCCA TTTACGCTG AATGACACA
GTAACATAA
```

B

```
MRGSHHHHHHGSMAVSVFIGSTENDVGPSQGSYSSTHAMDNLPFVYNTGYNIGYQANVWRISGGFCVGL
DGKVDLPVVGSLDQSIYGLTTEEVGLLIWMGDTNYSRGTAMSGNSWENVFSGWCVGNVYSTQGLSVHVR
PVILKRNSSAQYSVQKTSIGSIRMRPYNGSSAGSVQTTVNFSLNPFTLNDTVT-
```

Fig. 3.19: GafD1-178 coding sequence and translated protein sequence. **A)** The nucleotide sequence of GafD1-178 (537 bp) with an *N*-terminus His₆ tag is shown (blue). The starting codon (green), the first codon in the GafD1-178 sequence (underlined) and the stop codon (red) are highlighted. **B)** Translated protein sequence. This sequence is identical to the binding domain of UniProtKB (Q47341).

3.4.2 Expression, IMAC purification and biotinylation of GafD1-178

As described in Section 2.15 a 200 mL TB medium standard expression culture of GafD1-178 was completed using *E. coli* KRX cells containing the pQE-30_GafD1-178 plasmid. Following induction with IPTG, 100 µg/mL, and incubation at 30 °C for 18 hours the cells were pelleted by centrifugation, 4,000 g for 10 min. Unlike other proteins which must be released from cells using cell lysis techniques, e.g. cell disruptor, the GafD1-178 protein is translocated out of the cytoplasm as it is a fimbrial protein, thus simplifying its purification. The supernatant was vacuum filtered with Whatman filter paper (Grade 1 - 11 µm) and a Nalgene reusable vacuum filter unit (DS0320-5045) into a clean duran to remove aggregates that were not pelleted. Approximately half the supernatant, 90 mL, was passed through a 2 mL Ni charged IMAC-Sepharose (GE Healthcare) column. Fig. 3.20 gel A shows the wash and elution fractions from this purification. The remaining supernatant was passed through the same column again but

an additional imidazole wash step was added to increase GafD1-178 purity in the elution fractions, see Fig. 3.20 gel B.

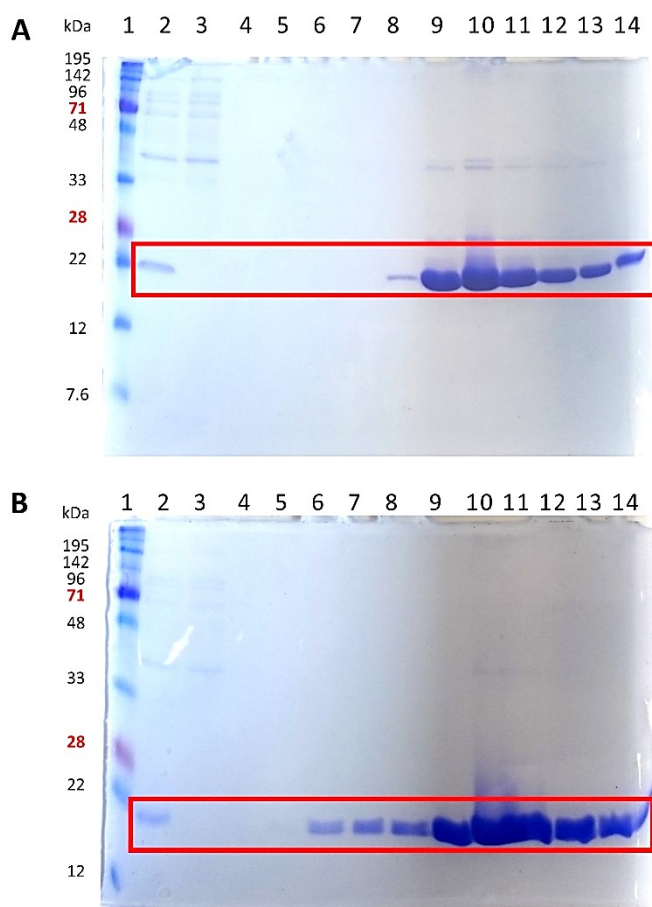


Fig. 3.20: IMAC purification of GafD1-178 with an *N*-terminus His₆ tag. Analysis by 15 % SDS-PAGE of *N*-terminally His₆ tagged GafD1-178 in *E. coli* KRX. **A)** Three imidazole wash steps, 20 mL of 20 mM, 20 mL of 40 mM and a second 20 mL of 40 mM were completed before eluting with 250 mM imidazole. **B)** The second 40 mM imidazole wash was replaced with 10 mL of 60 mM imidazole. In both gels Lane 1; Expedeon prestained dual-colour marker (Fig. 2.5), Lane 2; filtered supernatant, Lane 3; unbound filtered supernatant, Lane 4; Wash 1 (20 mM), Lane 5; Wash 2 (40 mM), Lane 6; Wash 3 (gel A 40 mM/gel B 60 mM), Lane 7 - 14; 1 mL elution fractions (250 mM).

Fig. 3.20 gel A shows the purification of GafD1-178 with light bands of unwanted proteins in the elution fractions 9 to 13. The imidazole concentration in the third wash

was increased from 40 mM to 60 mM. This greatly reduced the presence of unwanted proteins in the elution fractions. Unwanted proteins were removed by the wash steps but were not visualised in lanes 4, 5 or 6. The large wash volumes, 20 mL, and the relatively weak sensitivity of coomassie blue staining, minimum detection $\sim 2.5 \mu\text{g/ml}$, may explain the absence of bands in these lanes. The peak elution fraction in gel B, lane 10, also contained an unwanted protein, $\sim 40 \text{ kDa}$, at a low concentration. However, this protein band was not detected in the other elution fractions.

Elution fractions 7, 8, 9, 11, 12, 13 and 14 from gel B Fig. 3.20 were pooled and buffer exchanged into PBS, see Section 2.22. Following this GafD1-178 was quantified with a BCA assay and biotinylated. An ELLA was completed to assess the biotinylation of GafD1-178 and check its inhibition with GlcNAc, Fig 3.21.

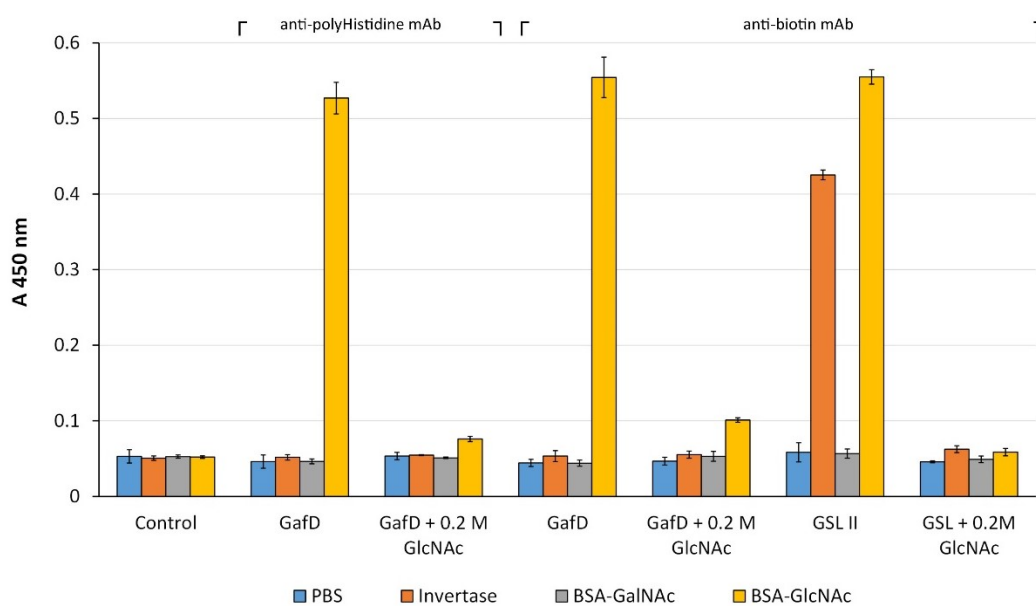


Fig. 3.21: ELLA analysis of GafD1-178 and GSL II with GlcNAc. An ELLA was completed as described in Section 2.25 using biotinylated GafD1-178 and biotinylated GSL II. GSL II and recombinant GafD1-178 were added to the plate with and without GlcNAc, 0.2 M. GSL II binding was detected with an anti-biotin mAb. GafD1-178 was subsequently probed with anti-biotin and anti-polyHistidine mAbs. Error bars were calculated from the standard deviation of three replicates.

3.4.3 ELLA analysis of GafD1-178

Recombinant GafD1-178 was premixed with its specific monosaccharide, GlcNAc, and non-specific monosaccharide, GalNAc, prior to ELLA analysis, see Fig 3.22.

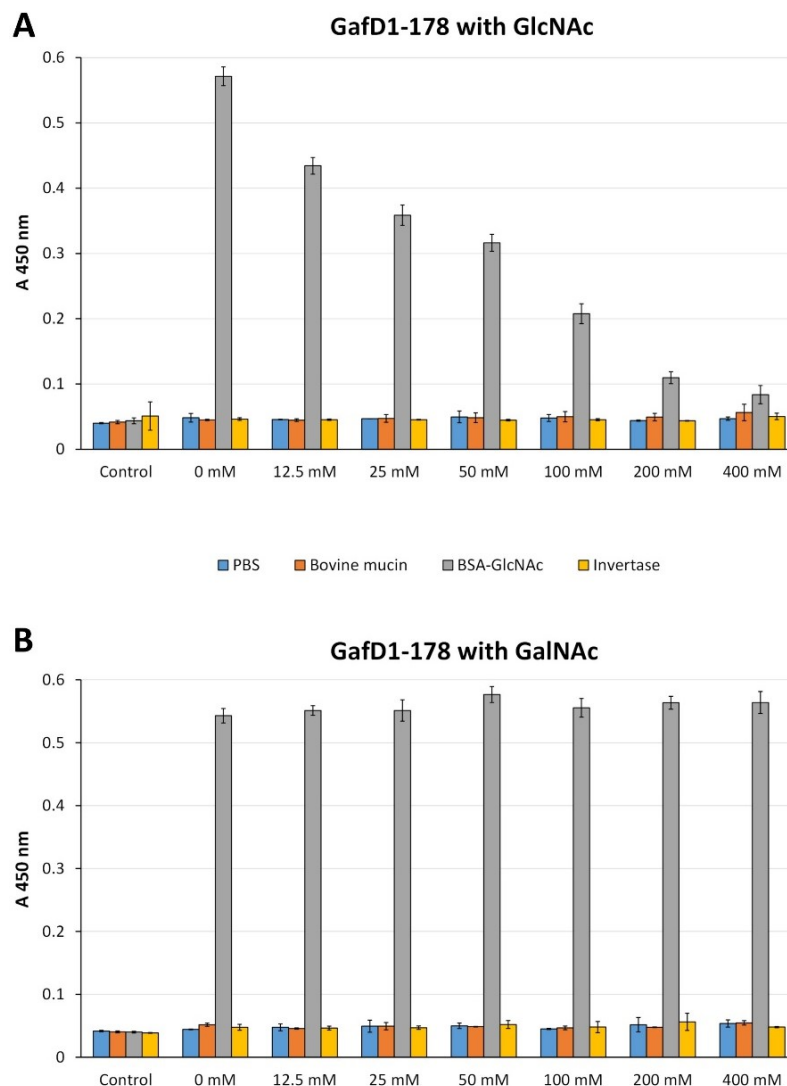


Fig. 3.22: ELLA analysis of GafD1-178 with GlcNAc and GalNAc monosaccharides. An ELLA was completed as per Section 2.25 using biotinylated GafD1-178. **A)** GafD1-178 premixed with GlcNAc, 0 - 400 mM. **B)** GafD1-178 premixed with GalNAc, 0 - 400 mM. GafD1-178 binding was detected with an anti-biotin mAb. Error bars were calculated from the standard deviation of three replicates.

The glycan binding profile of recombinant GafD1-178 was compared to that of a GlcNAc specific plant lectin, GSL II, see Fig. 3.21. GSL II bound to BSA-GlcNAc and invertase, which contains predominantly high-mannose type glycans. GafD1-178 only

bound to BSA-GlcNAc. Neither lectin bound to BSA-GalNAc. GSL II binding was inhibited with the addition of 200 mM GlcNAc. GafD1-178 binding was greatly reduced with 200 mM GlcNAc but not completely inhibited like GSL II. The binding pattern from GafD1-178 probed with anti-polyHistidine and anti-biotin antibodies was compared. A near identical binding pattern was observed indicating that the recombinant lectin was appropriately biotinylated. Fig. 3.22 shows the decrease in GafD1-178 binding BSA-GlcNAc with increasing GlcNAc. At 400 mM GlcNAc binding is nearly completely inhibited, absorbance values are less than double the PBS control. The addition of GalNAc did not reduce GafD1-178 binding which remained constant, between 0.5-0.6 AU, with GalNAc increasing from 0 mM to 400 mM.

3.5 PA-IL (LecA) from *Pseudomonas aeruginosa*

3.5.1 LecA coding sequence and protein sequence

A pQE vector containing LecA, pQE-30_LecA (see Table 2.2), was transformed into *E. coli* KRX. The LecA sequence was checked prior to initial protein expression. A 5 mL LB broth containing ampicillin was inoculated with this *E. coli* and incubated overnight. A plasmid purification, as described in Section 2.8.1, was completed and confirmed by agarose gel electrophoresis, see Section 2.9. DNA sequencing was provided by Eurofins Genomics, see Section 2.13 and Fig 3.23.

A

ATGAGAGGA TCG**CATCAC** **CATCACCAT** **CAC**GGATCC **ATG**GCTTGG AAAGGTGAG GTTCTGGCT
 AATAACGAA GCAGGGCAG GTAACGTCG ATTATCTAC AATCCGGGC GATGTCATT ACCATCGTC
 GCCGCCGGT TGGGCCAGT TACGGACCT ACCCAGAAA TGGGGGCCG CAGGGCGAT CGGGAGCAT
 CCGGACCAA GGGCTGATC TGCCACGAT GCGTTTTGT GGTGCGCTG GTCATGAAG ATTGGCAAC
 AGCGGAACC ATTCCGGTC AATACCGGG TTGTTCCGT TGGGTTGCA CCCAATAAT GTCCAGGGT
 GCAATCACT CTTATCTAC AACGACGTG CCCGGAACC TATGGCAAT AACTCCGGC TCGTTCAGT
 GTCAATATT GGAAAGGAT CAGTCC**TAA**

B

MRGSHHHHHHGSMAWKGEVLANNEAGQVTSIIYNPGDVITIVAAGWASYGPTQKWGPQGDREHPDQGLI
 CHDAFCGALVMKIGNSGTIPVNTGLFRWVAPNNVQGAITLIYNDVPGTYGNNSGFSVNIKQDS-

Fig. 3.23: LecA coding sequence and translated protein sequence. A) The nucleotide sequence of LecA (366 bp) with an *N*-terminus His₆ tag is shown (blue). The starting codon (green), the first codon in the LecA sequence (underlined) and the stop codon (red) are highlighted. **B)** Translated protein sequence. This sequence is identical to the UniProtKB (Q05097) sequence.

3.5.2 Expression, IMAC purification and biotinylation of LecA

The pQE-30_LecA plasmid had been purified for sequence analysis, see Section 3.5. A transformation was completed, see Section 2.10, and this purified plasmid was inserted into chemically competent *E. coli* KRX cells. A 200 mL TB medium standard expression culture, see Section 2.15, was completed. The cells were lysed by a cell disruptor and the resulting lysate was passed through a 2 mL Ni charged IMAC-Sepharose (GE Healthcare) column, as described in Section 2.17. Fig. 3.24 shows the wash and elution fractions from this purification. The initial purifications of LecA can be found in Appendix C.

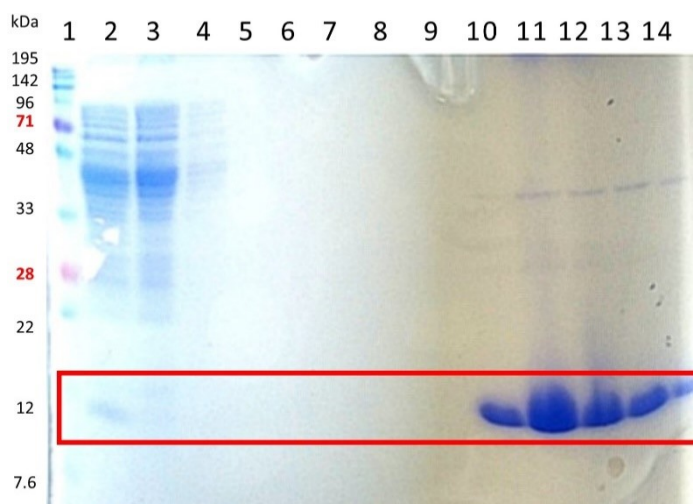


Fig. 3.24: IMAC purification of LecA. Analysis by 15 % SDS-PAGE of *N*-terminally His₆ tagged LecA in *E. coli* KRX. Three imidazole wash steps, 20 mL of 20 mM, 20 mL of 40 mM and 10 mL of 80 mM were completed before eluting with 250 mM imidazole. In Lane 1; Expedeon prestained dual-colour marker (Fig. 2.5), Lane 2; filtered lysate, Lane 3; unbound filtered lysate, Lane 4; Wash 1 (20 mM), Lane 5; Wash 2 (40 mM), Lane 6; Wash 3 (80 mM), Lane 7 - 14; 1 mL elution fractions (250 mM).

LecA was successfully purified by IMAC. A faint band was visible in the elution fractions but this was negligible compared to the large LecA band that was present. Elution fractions in lanes 10 to 14 from Fig. 3.24 were pooled and buffer exchanged into PBS, see Section 2.22. Following this LecA was quantified with a BCA assay and biotinylated. An ELLA was completed to assess the biotinylation of LecA, see Fig 3.25.

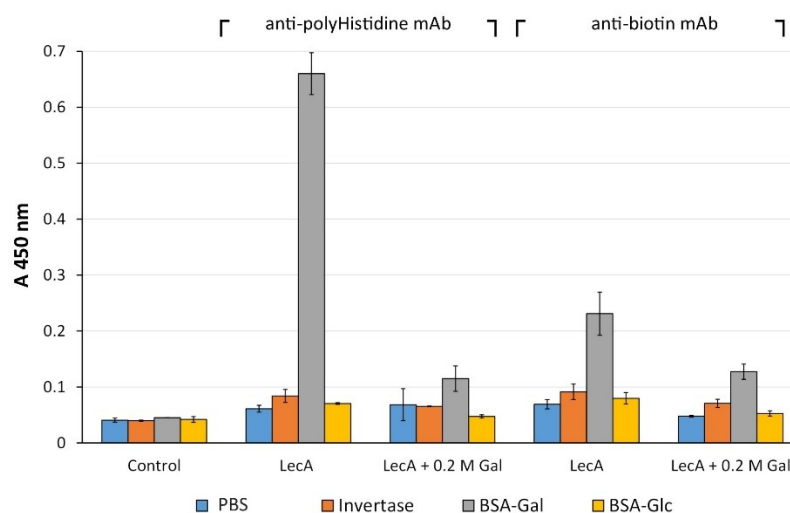


Fig. 3.25: ELLA analysis of LecA with galactose. An ELLA was completed as described in Section 2.25 using biotinylated LecA. Recombinant LecA was added to the plate with and without Gal, 0.2 M. LecA was subsequently probed with anti-biotin and anti-polyHistidine mAbs. Error bars were calculated from the standard deviation of three replicates.

This ELLA result, see Fig 3.25, shows that recombinant LecA was not appropriately biotinylated. Similar absorbance values were expected when LecA was probed with the anti-polyHistidine mAb and the anti-biotin mAb. LecA is a small protein, ~ 12.7 kDa, containing four lysine residues and so may not be biotinylated to the same extent as other larger proteins. Biotinylated LecA was also used on the flow cytometer where significant binding was not detected on the CHO cell surface. However, binding was observed with other galactose specific lectins such as RCA I and ECL, which are commercial plant lectins, which again suggests that LecA was not appropriately biotinylated. This flow cytometry data is presented in Section 5.8.

The biotinylation reaction, see Section 2.24, was completed using the Thermo Scientific EZ-Link Sulfo-NHS-LC-Biotin kit (21327). *N*-Hydroxysuccinimide (NHS) activated biotins react with primary amino groups, $-NH_2$, in pH 7-9 buffers and form stable amide bonds. Primary amines in the side chains of lysine (K) residues and at the *N*-terminus of the polypeptide may be labelled with NHS-activated biotin. However, not all lysine residues once biotinylated are accessible to streptavidin conjugates. Lysine side chains may be on the internal or the external side of the protein. Additionally, lysine side chains

on the external protein side may be less available to streptavidin, 52.6 kDa, if the side chain is not extended away from the protein, i.e. lysine residues that are located at or near pockets in the protein surface may hinder streptavidin binding. Fig. 3.26 is a cartoon representation of the LecA structure with the lysine side chains highlighted.

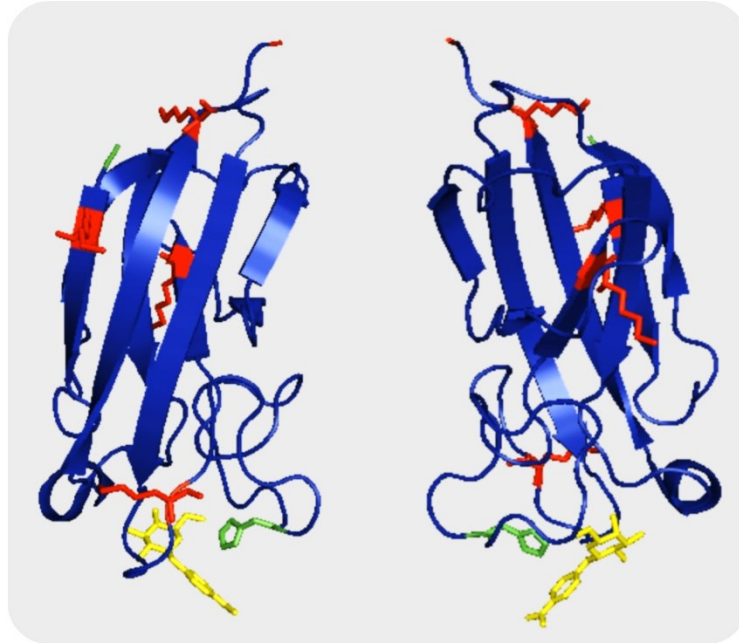


Fig. 3.26: Monomer structure of LecA with highlighted lysine residues. The 3D structure of LecA is shown from both sides in cartoon format. The *N*-terminus end of the protein is green, the *C*-terminus end is red. The side chains of the four lysine residues are shown in red. A histidine side chain is shown in green, His50, is a key residue involved in galactose binding. It forms a hydrogen bond with the hydroxyl group on carbon 6 of galactose. A ligand containing galactose, 4-nitrophenyl β -D-galactopyranoside, is shown in yellow in the LecA binding pocket. This image was generated using open-source PyMOL 1.3 and the LecA crystal structure, 3ZYF, from the Protein Data Bank.

There are four lysine residues in LecA not all of which extend outward from the protein surface. Incorporating additional lysine residues at either termini may enhance LecA biotinylation without interfering with its galactose binding ability as both termini are at the opposite end of the galactose binding site. Alternatively the LecA labelling issue, highlighted in Fig. 3.25, may be resolved by direct labelling with a fluorescent protein.

3.5.3 LecA cloning strategy to generate EGFP fusion

Enhanced green fluorescent protein (EGFP) was selected for the fusion as it will directly fluorescently label LecA. A double digest was completed on EGFP plasmid, pQE-30_EGFP, and the LecA plasmid, pQE-30_LecA, see Fig. 3.27. The insertion and ligation reactions were initially checked by plasmid purification and agarose gel electrophoresis.

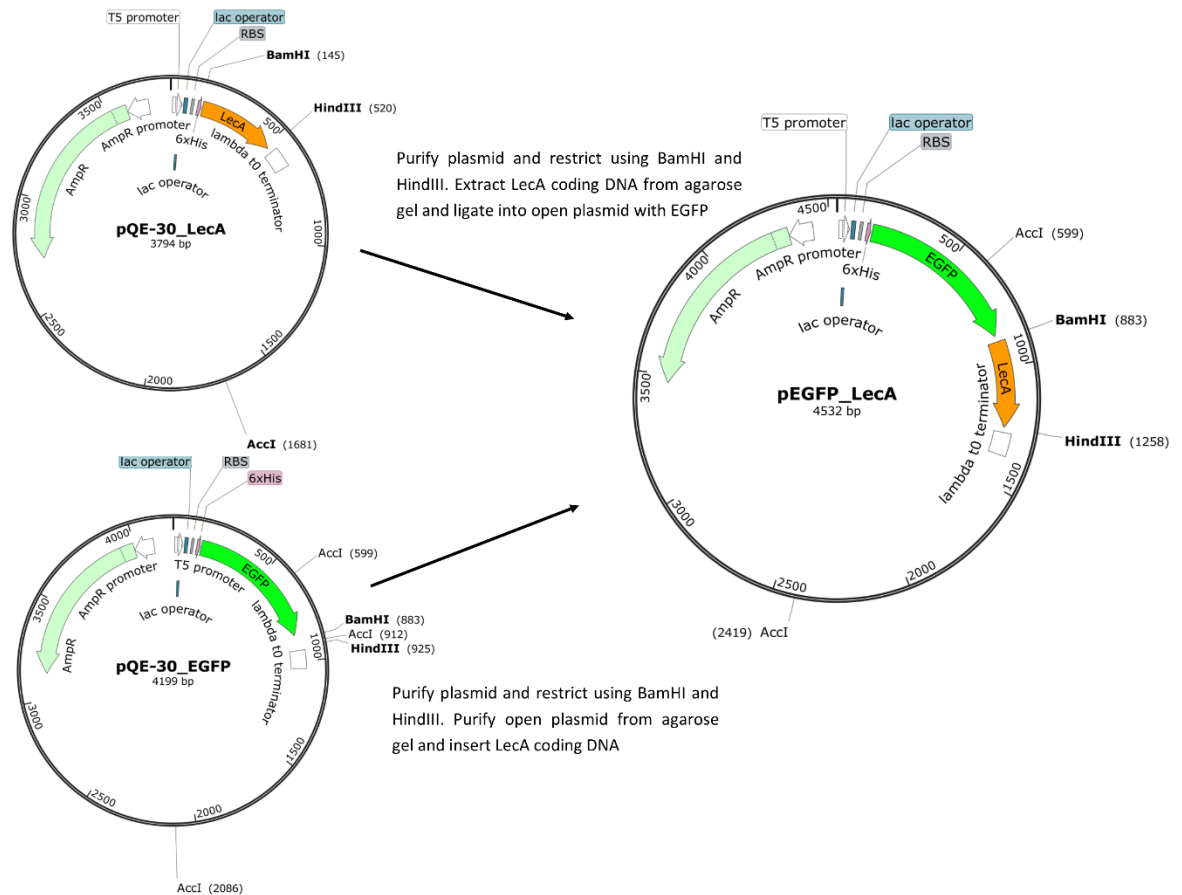


Fig. 3.27: The construction of pEGFP_LecA, a pQE-30 plasmid containing an EGFP-LecA fusion with a His₆ tag at the EGFP *N*-terminus. This construction was completed using BamHI and HindIII restriction digests only. EGFP (green) is located between the *N*-terminus His₆ tag and the start codon of LecA. Image generated using SnapGene Viewer Version 3.1.4.

3.5.4 EGFP-LecA expression and purification

The constructed pEGFP_LecA plasmid was transformed into chemically competent *E. coli* KRX cells, see Section 2.10. Following a successful transformation, an expression check was completed prior to a standard expression culture in 200 mL of TB. Nine colonies on the transformed plates were used to inoculate 8 mL of TB medium which was incubated at 37 °C for 18 hours. Glycerol stocks were made, see Section 2.7, and plasmid was purified from each culture. Protein expression in each culture was checked by normalising for cell concentration, see Section 2.20, and analysing using SDS-PAGE, see Fig. 3.28. A restriction digest was completed on each purified plasmid to confirm the correct insertion of LecA encoding DNA into the open plasmid. AccI was used for plasmid restriction analysis, see Fig. 3.29. Its restriction site is GT^VMKAC where M is adenine or cytosine and K is guanine or threonine. AccI restriction sites are labelled in Fig. 3.27. The pQE-30_LecA plasmid contains one AccI site, the pQE-30_EGFP plasmid contains three AccI sites and the newly constructed pEGFP_LecA plasmid has two AccI sites. One of the AccI sites on the pQE-30_EGFP plasmid is located between the BamHI and HindIII restriction sites and is removed after a double digest.

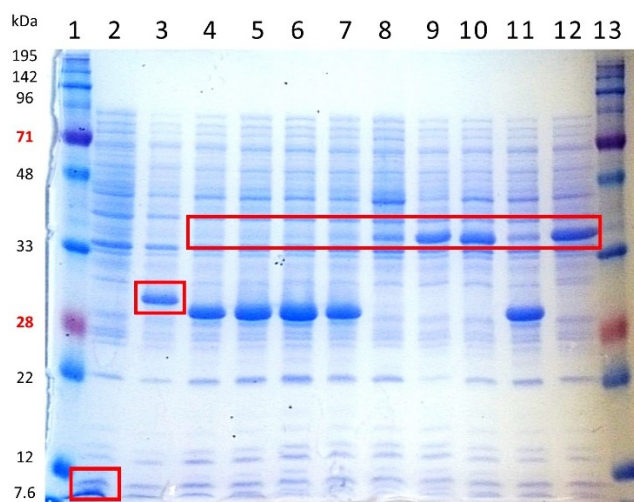


Fig. 3.28: Expression check for EGFP-LecA fusion. Analysis by 15 % SDS-PAGE of the expression of fusion protein EGFP_LecA. *E. coli* KRX cells transformed with pEGFP_LecA plasmid were grown in 8 mL TB cultures with ampicillin and IPTG both at 100 µg/mL. Culture volume harvested was determined using a spectrophotometer, see Section 2.20. In lanes 1 and 13; Expedeon prestained dual-colour marker (Fig. 2.5),

Lane 2; Cells expressing LecA only, Lane 3; Cells expressing EGFP only, Lanes 4 - 12; transformed clones 1 to 9 with pEGFP_LecA plasmid.

LecA is shown in the red box in lane 2. EGFP is shown in the red box in lane 3. The red box across lanes 4 to 12 is where the fusion protein should resolve to. Only 3 of the 9 lanes contain a band at the correct size for EGFP-LecA, lanes 9, 10 and 12. Lanes 4, 5, 6, 7 and 11 all have a similarly sized protein which is slightly smaller than EGFP suggesting that the open plasmid incorrectly self ligated to produce this. The plasmid restriction analysis that corresponds to this expression check is shown in Fig. 3.29.

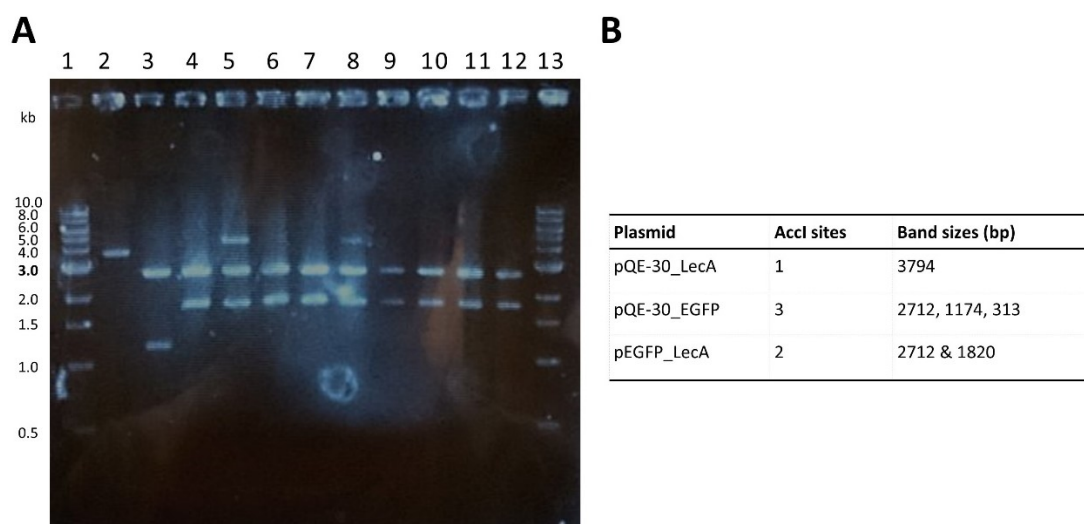


Fig. 3.29: Plasmid restriction analysis using AccI. **A)** Analysis of purified plasmids digested with AccI and separated by 1 % agarose gel electrophoresis. The lanes correspond to those in Fig. 3.28. In lanes 1 and 13; 1kb DNA ladder (Fig. 2.3), Lane 2; pQE-30_LecA plasmid, Lane 3; pQE-30_EGFP plasmid, Lanes 4-12; pEGFP_LecA plasmids from clones 1 to 9. **B)** Table displaying the expected DNA bands from the three plasmids after AccI restriction digest.

The pQE-30_LecA plasmid, lane 2, contains one AccI restriction site and was linearised resolving to one band at 3.8 kb. The pQE-30_EGFP plasmid, lane 3, contains three AccI restriction sites producing three bands, 2.7 kb, 1.2 kb and 313 bp, after digestion. The two larger bands are clearly visible at the correct position. The smaller band, 313 bp, is not visible. It is below the smallest marker in the DNA ladder, 500 bp, and its detection may be blocked by bromophenol blue in the gel loading dye which migrates to approximately 300 bp on a 1 % agarose gel. The pEGFP_LecA plasmid should yield two bands, 2.7 kb and 1.8 kb, when digested with AccI. Lanes 4, 6, 7, 9, 10, 11 and 12,

show the correctly sized bands. The clones 6, 7 and 9 which correspond to lanes 9, 10 and 12 produced the correct fusion protein, see Fig. 3.28, and the correct DNA bands after *AccI* digestion. Clone 9 in lane 12 in Fig. 3.28 and Fig 3.29 was selected for the expression of EGFP-LecA. A standard expression culture in 200 mL TB was completed. The IMAC purification from this expression is shown in Fig. 3.30.

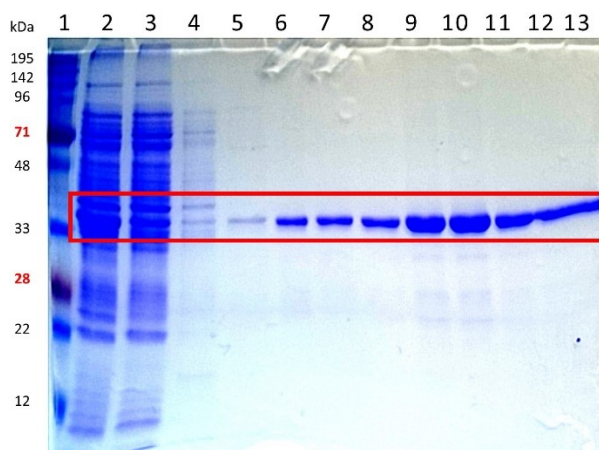


Fig. 3.30: IMAC purification of EGFP-LecA. Analysis by 15 % SDS-PAGE of *N*-terminally His₆ tagged EGFP-LecA in *E. coli* KRX. Three imidazole wash steps, 30 mL of 20 mM, 20 mL of 40 mM and 10 mL of 80 mM were completed before eluting with 250 mM imidazole. In Lane 1; Expedeon prestained dual-colour marker (Fig. 2.5), Lane 2; filtered lysate, Lane 3; unbound filtered lysate, Lane 4; Wash 1 (20 mM), Lane 5; Wash 2 (40 mM), Lane 6; Wash 3 (80 mM), Lane 7 - 13; 1 mL elution fractions (250 mM).

3.5.5 Optimising the LecA probe for biotinylation and labelling

The initial biotinylation of LecA and analysis by ELLA, Fig. 3.25, indicated that it is not optimally biotinylated, i.e. the LecA binding detected with the anti-polyHistidine mAb was significantly greater than that with the anti-biotin mAb. The LecA structure, Fig. 3.26, shows that both termini are not adjacent to the galactose binding site but at the opposite end of the protein. Therefore it may be possible to add lysine residues at either termini without affecting LecA folding and galactose binding ability. The *C*-terminus may be better suited as it is further extended away from the protein. Additionally, modifying the *N*-terminus may interfere with the His₆ tag and therefore

effect IMAC purification. The pQE-30_LecA plasmid was used as a template for site-direct mutagenesis (whole plasmid amplification) using four sets of primers, see Table 3.1 and Section 2.12. The resulting constructs, see Table 2.3 encoded LecA with additional lysine residues at the *N*- or *C*- terminus.

Table 3.1: Primer sequences for increasing LecA lysine content (Synthesised by IDT, Belgium)

Name	Primer Sequence (5' → 3')	Change
LecAKF	P-TAAAAGCTTAATTAGCTGAGCTTGGACTCCTGT	-
LecA3KR	P- CTTCTTCTTGGACTGATCCTTTCCAATATTGACACT	3 lysine insertion
LecA5KR	P- CTTCTTCTTCTTCTTGGACTGATCCTTTCCAATATTGACACTGAA	5 lysine insertion
LecA3KHF	P-TCGCATCACCATCACCATCACGGATCCATG	-
LecA3KHR	P- CTTCTTCTTCATAGTTAATTTCTCCTCTTTAATGAA	3 lysine ins/del*
LecAH3KF	P-TCCATGGCTTGGAAAGGTGAGGTTCTGGC	-
LecAH3KR	P- CTTCTTCTTTCCGTGATGGTGATGGTGATGCGATCC	3 lysine insertion

Notes: Non-binding nucleotides are in bold.
 * Insertion and deletion. 6 nucleotides before the His₆ tag were replaced with 9 nucleotides encoding lysine.
 P- denotes phosphorylation at the 5' end.

The pLecA3KH plasmid encodes LecA3KH which contains three lysine residues before the *N*-terminus His₆ tag. The pLecAH3K plasmid encodes LecAH3K which contains three lysine residues between the *N*-terminus His₆ tag and LecA. The pLecA3K plasmid encodes LecA3K which contains three lysine residues at the *C*-terminus. The pLecA5K plasmid encodes LecA5K which contains five lysine residues at the *C*-terminus. The

protein sequences of these four LecA variants are compared in Fig. 3.31 to unaltered LecA.

```

LecA -MRGSHHHHHHG---SMAWKGEVLANNEAGQVTSIIYNPGDVITIVAAGWASYGP
LecA3KH MKKKSHHHHHHG---SMAWKGEVLANNEAGQVTSIIYNPGDVITIVAAGWASYGP
LecAH3K -MRGSHHHHHHGKKKSMAWKGEVLANNEAGQVTSIIYNPGDVITIVAAGWASYGP
LecA3K -MRGSHHHHHHG---SMAWKGEVLANNEAGQVTSIIYNPGDVITIVAAGWASYGP
LecA5K -MRGSHHHHHHG---SMAWKGEVLANNEAGQVTSIIYNPGDVITIVAAGWASYGP

LecA TQKWGPQGDREHPDQGLICHDAFCGALVMKIGNSGTIPVNTGLFRWVAPNNVQGA
LecA3KH TQKWGPQGDREHPDQGLICHDAFCGALVMKIGNSGTIPVNTGLFRWVAPNNVQGA
LecAH3K TQKWGPQGDREHPDQGLICHDAFCGALVMKIGNSGTIPVNTGLFRWVAPNNVQGA
LecA3K TQKWGPQGDREHPDQGLICHDAFCGALVMKIGNSGTIPVNTGLFRWVAPNNVQGA
LecA5K TQKWGPQGDREHPDQGLICHDAFCGALVMKIGNSGTIPVNTGLFRWVAPNNVQGA

LecA ITLIYNDVPGTYGNNSGSFSVNIKDKQS-----
LecA3KH ITLIYNDVPGTYGNNSGSFSVNIKDKQS-----
LecAH3K ITLIYNDVPGTYGNNSGSFSVNIKDKQS-----
LecA3K ITLIYNDVPGTYGNNSGSFSVNIKDKQSKKK--
LecA5K ITLIYNDVPGTYGNNSGSFSVNIKDKQSKKKKK

```

Fig. 3.31: Multiple protein sequence alignment of LecA variants. The inserted lysine (K) residues (red) and the start methionine (M) of LecA (green) are highlighted. Alignment generated using ClustalW.

Each new plasmid construct was transformed into *E. coli* KRX cells after which a small scale expression was completed for 10 clones for each LecA variant to screen for expression, as described in Section 2.20. Fig. 3.32 shows the expression check and the IMAC purification of LecA5K. The new plasmid constructs were purified and sequenced by Eurofins Genomics. Full nucleotide sequence data can be found in Appendix D.

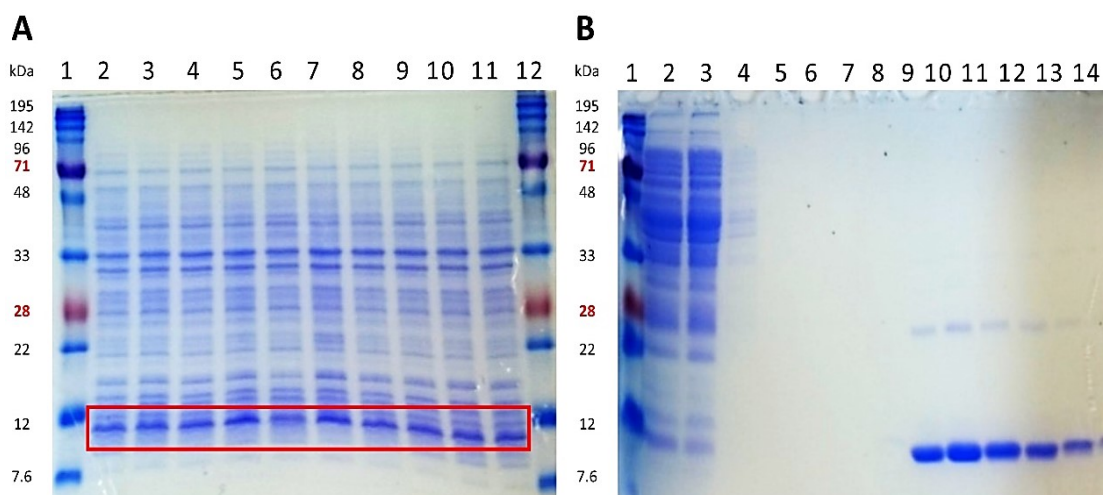


Fig. 3.32: Expression check and purification of LecA5K. **A)** Analysis by 15 % SDS-PAGE of the expression of LecA5K. *E. coli* KRX cells transformed with pLecA5K plasmid were grown in 8 mL TB cultures with ampicillin and IPTG both at 100 µg/mL. Culture volume harvested was determined using a spectrophotometer, see Section 2.20. In lanes 1 and 12; Expedeon prestained dual-colour marker (Fig. 2.5), Lanes 2-11; Clones 1-10 expressing LecA5K. The red box highlights the LecA5K protein bands **B)** Analysis by 15 % SDS-PAGE of the IMAC purification of LecA5K from clone 4 (lane 5 in gel A). Three imidazole wash steps, 30 mL of 20 mM, 20 mL of 40 mM and 10 mL of 80 mM were completed before eluting with 250 mM imidazole. In Lane 1; Expedeon prestained dual-colour marker (Fig. 2.5), Lane 2; filtered lysate, Lane 3; unbound filtered lysate, Lane 4; Wash 1 (20 mM), Lane 5; Wash 2 (40 mM), Lane 6; Wash 3 (80 mM), Lane 7 - 14; 1 mL elution fractions (250 mM).

The LecA5K expression check yielded similar results as the LecA5K protein bands were nearly identical across all clones. Clone 5 in lane 6, see Fig 3.32 gel A, produced the least LecA5K. Clone 4, lane 5, was selected for the large scale expression of LecA5K. The purification from this clone is shown in Fig. 3.32 gel B. This purification of LecA5K shows that the additional lysine residues did not interfere with IMAC purification. LecA5K was concentrated in the elution fractions 9 to 14. A protein that was approximately twice the size of LecA5K was co-purified. This may be a LecA5K dimer. In *P. aeruginosa* LecA forms a tetrameric structure where monomers interact with their C-termini. The additional lysine residues at the C-terminus may have encouraged dimerization. Fig. 3.33 shows the 3D structure of LecA5K.

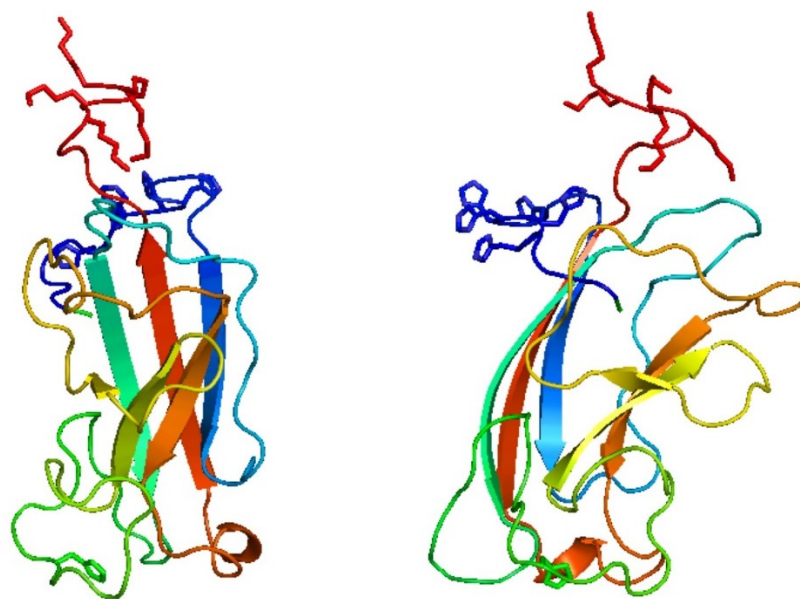


Fig. 3.33: Two horizontal views of the 3D structure of LecA5K represented in cartoon format. The *N*- and *C*- termini are green and orange respectively. The His₆ tag side chains are shown in blue. The side chains of the five added lysine residues are shown in red at the *C*-terminus. A histidine side chain is shown in green, His50, is a key residue involved in galactose binding (lower part of image). It forms a hydrogen bond with the hydroxyl group on carbon 6 of galactose. This 3D structure was generated by the I-TASSER tool, see Section 2.14. These images were made using open-source PyMOL 1.3.

The four LecA lysine variants were successfully expressed and purified using IMAC. They were analysed by SDS-PAGE with unmodified LecA and with the EGFP_LecA fusion protein, see Fig. 3.34. As LecA is a relatively small protein, 12.7 kDa, an additional SDS-PAGE gel with a low range protein ladder was ran to check for the presence of co-purified small proteins that may have completely passed through previous gels.

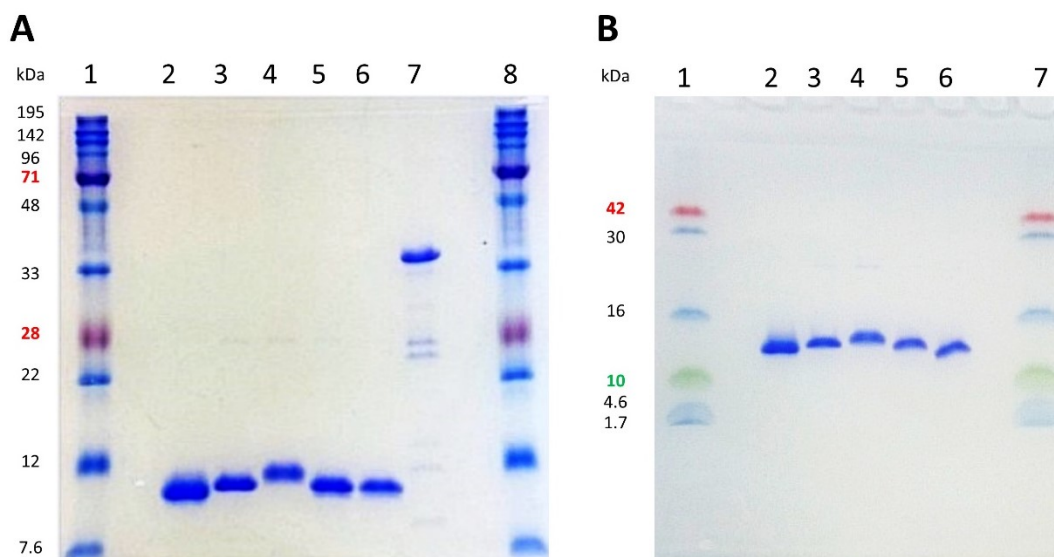


Fig. 3.34: SDS-PAGE analysis of purified and biotinylated LecA variants with broad and low range protein markers. A) Analysis by 15 % SDS-PAGE of all LecA variants. In lanes 1 and 8; Expedeon prestained dual-colour marker (Fig. 2.5), Lane 2; LecA, Lane 3; LecA3K, Lane 4; LecA5K, Lane 5; LecA3KH, Lane 6; LecAH3K, Lane 7; EGFP_LecA(not biotinylated). **B)** Analysis by 15 % SDS-PAGE of LecA variants with a low range protein marker. In lanes 1 and 7; CST prestained low range protein marker, (Fig. 2.5), Lane 2; LecA, Lane 3; LecA3K, Lane 4; LecA5K, Lane 5; LecA3KH, Lane 6; LecAH3K.

Fig. 3.34 shows that the four LecA variants with added lysine were successfully purified. The subtle addition of 3 lysine residues and 5 lysine residues at the C-terminus of LecA, lanes 3 and 4 in gel A and B, resulted in an obvious size shift when the proteins were resolved on 15 % acrylamide gels. The addition of lysine residues directly before or after the His₆ tag did not negatively impact their purification. Lanes 5 and 6 in both gels show that LecA3KH and LecAH3K were successfully purified. The EGFP_LecA fusion protein, lane 7 gel A, was not as pure as the other proteins. Co-purified proteins are visible which are sized between the 22-28 kDa protein markers. These proteins were present in the EGFP_LecA elution fractions, see Fig. 3.30, and were concentrated along with EGFP_LecA during the buffer exchanging process. The biotinylation of LecA was assessed by ELLA, see Fig. 3.35.

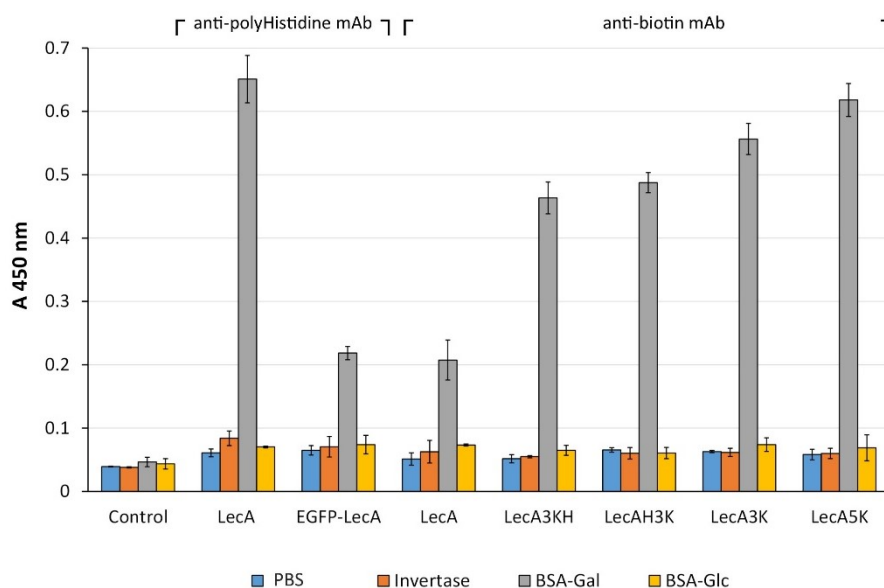


Fig. 3.35: ELLA analysis of LecA and biotinylated LecA variants. An ELLA was completed as per Section 2.25 using recombinant LecA proteins. LecA was probed with anti-polyHistidine and anti-biotin mAbs. EGFP-LecA was detected with an anti-polyHistidine mAb only as it was not biotinylated. LecA3KH, LecAH3K, Lec3K and Lec5K were detected with an anti-biotin mAb. Error bars were calculated from the standard deviation of three replicates.

The addition of extra lysine residues to either termini of LecA resulted in its increased detection with an anti-biotin mAb while retaining its galactose binding ability. These biotinylated LecA variants were also assessed on the flow cytometer where their detection (fluorescent intensity) after binding to the CHO cell surface differed. This flow cytometry data is presented in Section 5.8. EGFP-LecA was detected with the anti-polyHistidine mAb as it was not biotinylated. Its absorbance value was ~0.2 while LecA had an absorbance value of ~0.65. This absorbance difference could be due to the size difference between LecA, 12.7 kDa, and the EGFP-LecA fusion protein, 41.4 kDa. All lectins added to the ELLA plate were at 5 µg/mL. For every 1 mole of EGFP-LecA added there was 3.25 moles of LecA added therefore a greater signal would be expected with more galactose binding sites and His₆ tags available in the LecA sample. The size difference between LecA and the LecA with added lysine is not as significant as they differ by only 1, 3 or 5 amino acids. As expected, LecA5K produced the strongest signal as it had the greatest biotin binding potential with 5 lysine residues added. Its

absorbance value was similar to, but slightly lower than, LecA detected with an anti-polyHistidine mAb. LecA5K was subsequently used in fluorescent microscopy and flow cytometry analysis of CHO cells, Chapters 4 and 5.

3.5.6 ELLA analysis of LecA5K and RCA I with competing and non-competing monosaccharides

Recombinant LecA5K was premixed with its specific monosaccharide, galactose, and separately with a highly similar monosaccharide, glucose, before being adding to a plate to which glycoproteins, including BSA-Gal, have been attached. The plant lectin RCA I which is also a galactose binding lectin was also assessed by ELLA for comparison. Galactose is an epimer of glucose, the only difference is the orientation of the hydroxyl group on the fourth carbon, see Fig. 1.1. The inhibition of these lectins with this pair of stereoisomers was determined using ELLA, see Fig. 3.36 and Fig. 3.37.

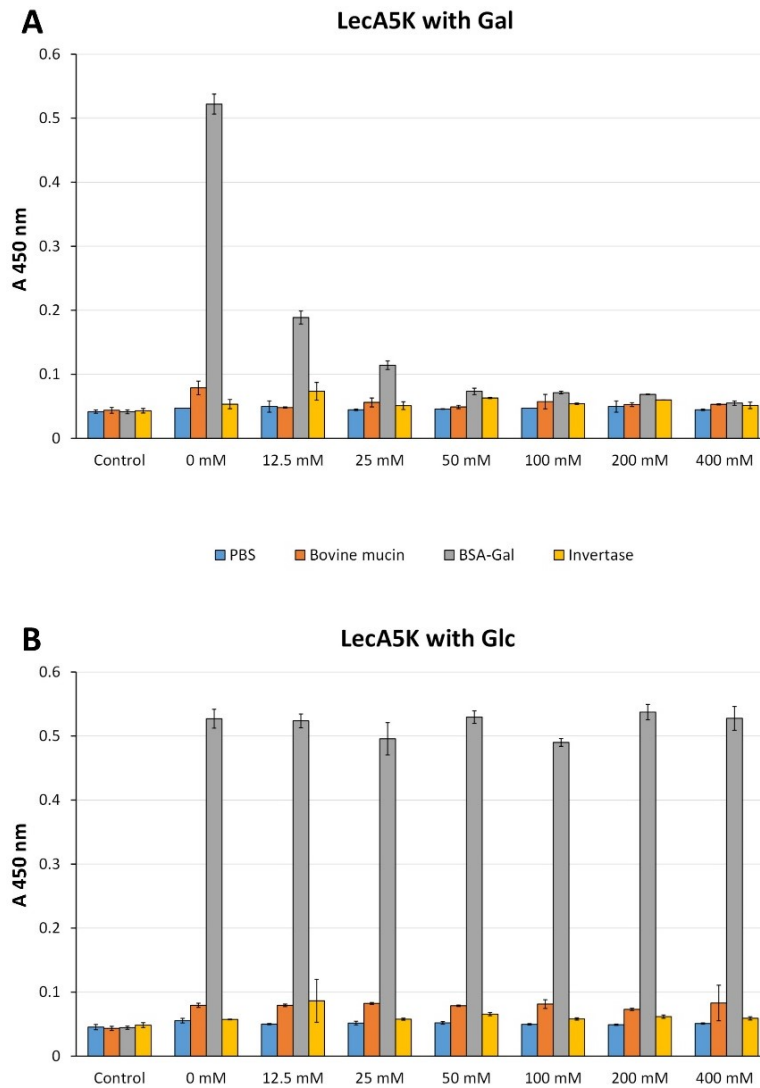


Fig. 3.36: ELLA analysis of LecA5K with Gal and Glc monosaccharides. An ELLA was completed as per Section 2.25 using biotinylated LecA5K. **A)** LecA5K premixed with galactose, 0 - 400 mM. **B)** LecA5K premixed with glucose, 0 - 400 mM. LecA5K binding was detected with an anti-biotin mAb. Error bars were calculated from the standard deviation of three replicates.

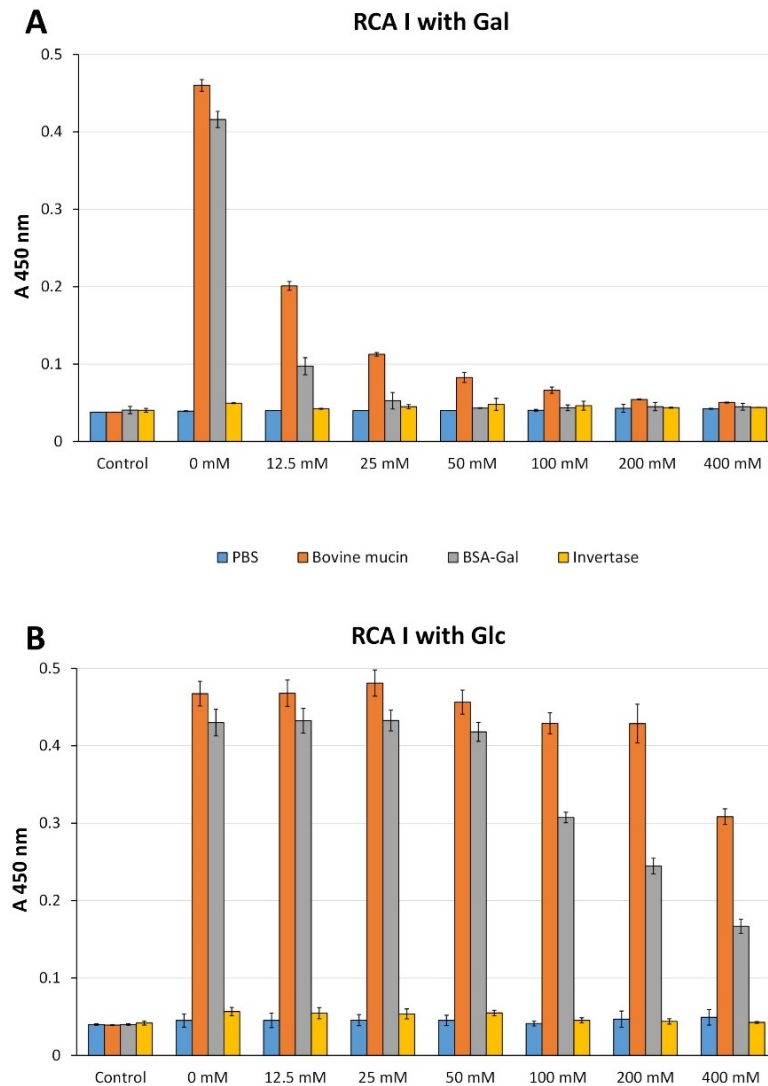


Fig. 3.37: ELLA analysis of RCA I with Gal and Glc monosaccharides. An ELLA was completed as per Section 2.25 using biotinylated RCA I. **A)** RCA I premixed with galactose, 0 - 400 mM. **B)** RCA I premixed with glucose, 0 - 400 mM. RCA I binding was detected with an anti-biotin mAb. Error bars were calculated from the standard deviation of three replicates.

LecA5K inhibition with galactose, see Fig. 3.36, was similar to RCA I inhibition with galactose. Both lectins were nearly completely inhibited by 50 mM galactose. LecA5K did not bind bovine mucin like RCA I. However, RCA I is a galactose and a GalNAc binder. LecA5K was not inhibited by glucose as absorbance values remained the same as the glucose concentration increased to 400 mM. RCA I was partially inhibited by 100 mM, 200 mM and 400 mM glucose. RCA I binding to BSA-Gal was more affected

by the addition of glucose. Neither lectin bound invertase which consists of predominantly high-mannose type glycans.

3.6 Confirmation of recombinant lectin biotinylation

To confirm that the recombinant lectins were successfully purified and biotinylated prior to being used as probes on live cells, a western blot was completed, see Section 2.21. Two identical acrylamide gels were loaded; one stained with coomassie blue stain to detect all proteins, and the second gel was used in a western blot where it was subsequently probed with an anti-biotin antibody conjugated to HRP, see Fig. 3.38.

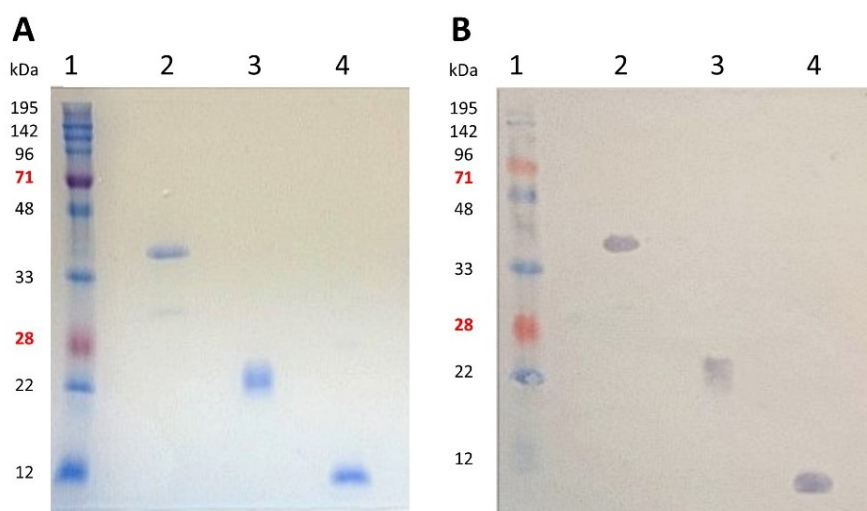


Fig. 3.38: SDS-PAGE and western blot analysis of biotinylated recombinant lectins. **A)** Analysis by 15 % SDS-PAGE of recombinant biotinylated lectins. **B)** Western blot from identical SDS-PAGE gel probed with an anti-biotin antibody conjugated to HRP. In both A and B lanes 1; Expedeon prestained dual-colour marker (Fig. 2.5), Lane 2; biotinylated AAL-2, Lane 3; biotinylated GafD, Lane 4; biotinylated LecA5K.

3.7 Discussion

The terminal GlcNAc specific lectin, AAL-2, was cloned, expressed and purified successfully. The IMAC purification gels in Fig. 3.3, 3.4 and 3.11 show that AAL-2 was strongly expressed in *E. coli* KRX cells. However, the initial purifications of the AAL-2 protein resulted in elution fractions with a number of contaminating proteins. The cloning strategies used to rectify this problem; included (i) switching the His₆ tag to the C-terminus, (ii) the insertion of a spacer between the His₆ tag and the AAL-2 protein and (iii) fusing AAL-2 to EGFP had mixed results. The 30 amino acid spacer between the His₆ tag and AAL-2 increased the interaction between the His₆ tag on the protein and the nickel on the resin. Without this spacer AAL-2 starts being released when the imidazole concentration increases to 40 mM, see Fig. 3.4 lane 5. However, with the spacer the His₆ tag remains bound to the nickel even when the imidazole concentration increased to 80 mM, shown in Fig. 3.9 gel A lane 5. In fact, AAL-2 is not detected in this gel until the third 1 mL elution fraction after 250 mM imidazole is added. The AAL-2 3D structure in Fig 3.10 image B shows that the spacer extends the His₆ tag away from the rest of the protein. The His₆ tag on the C-terminus of AAL-2 appears partially available from the 3D structure generated by the I-TASSER tool, see Fig. 3.10 image C. However, this protein was not successfully purified. Fig 3.9 gel B shows that the protein was not captured by the column but flowed through the resin and was detected in the unbound sample in lane 3.

AAL-2 with an N-terminal His₆ tag without a spacer was successfully expressed and purified, see Fig 3.11. Changing the imidazole concentration in the wash steps resulted in purer AAL-2 fractions than were achieved by switching the His₆ tag to the C-terminus or introducing a spacer at the N-terminus of the protein. Altering the purification protocol of a protein should be first completed after experiencing purification difficulties prior to cloning which requires more time and materials.

For a recombinant lectin to be successfully utilised as a cell surface glycan probe it is important that it is labelled in a stable way. Purified AAL-2 was successfully biotinylated. This was shown in Fig. 3.15 where anti-polyHistidine and anti-biotin mAbs yield similar results during ELLA analysis. The specificity of AAL-2 binding was clearly demonstrated in Fig. 3.16 where a low GlcNAc concentration, 12.5 mM,

significantly reduced binding but a high GalNAc concentration, 400 mM, had little effect. This recombinant GlcNAc binder may be more useful than similar commercial plant GlcNAc binders, such as WGA and GSL II. They were both similarly inhibited with GlcNAc and uninhibited with GalNAc, Fig. 3.17 and Fig. 3.18. AAL-2 may be a superior GlcNAc probe for a variety of reasons.

- WGA did not bind BSA-GlcNAc at all, see Fig. 3.17. WGA binds preferentially to GlcNAc dimers and trimers and GlcNAc residues in complex *N*-glycans. BSA-GlcNAc is more akin to *O*-GlcNAc and *O*-glycans and was therefore bound only by AAL-2 and GSL II.
- WGA may also interact with glycoproteins through their sialic acid residues, although this can be reduced when its succinylated form is used.
- WGA may require salt and/or acid for complete elution. Free GlcNAc was able to inhibit WGA during ELLA analysis. However, this additional requirement may be needed in other applications. For sequential live cell staining this elution requirement will adversely affect live cells.
- GSL II binding is broader than that of AAL-2, i.e. it bound bovine mucin, BSA-GlcNAc and invertase.
- GSL II has lower affinity for GlcNAc than AAL-2. Its binding was completely reduced with the addition of 25 mM GlcNAc. While this may be useful in certain applications, e.g. sequential probing of live cells, it is a negative in many others, e.g. lectin affinity chromatography.

A second terminal GlcNAc specific lectin, GafD1-178, was also expressed and purified successfully. GafD1-178 is a more specific GlcNAc binding probe than AAL-2. It is specific for β terminal GlcNAc residues. GafD1-178 has the greatest affinity for GlcNAc- β 1-3Gal. The elution fractions from its IMAC purification, gel B Fig. 3.20, show that other proteins were not co-purified. Its purification is simplified as cell lysis is not required as the protein is translocated out of the cytoplasm. GafD1-178 was successfully biotinylated, see Fig. 3.21, as similar absorbance values were observed after it was probed with anti-polyHistidine and anti-biotin mAbs during ELLA analysis. GafD1-178 binding specificity was demonstrated by ELLA, Fig. 3.22. GafD1-178 binding gradually decreased with increasing GlcNAc. Increasing free GalNAc had no effect on GafD1-178 binding to BSA-GlcNAc.

A galactose specific lectin, LecA, from *P. aeruginosa* was expressed and successfully purified. Initial labelling efforts were ineffective. As commercial plant lectins and other recombinant lectins used in this work were all biotinylated, so all lectins could be labelled in an identical fashion with a fluorescent streptavidin conjugate, DyLight488, cloning strategies were devised to enhance the lysine content of LecA so as to achieve an appropriate level of biotinylation, i.e. (i) similar ELLA results when a lectin is detected with anti-polyHistidine and anti-biotin mAbs and (ii) sufficient fluorescent intensity signal when using the flow cytometer so stained and unstained cell samples are clearly distinguished. Initially a directly labelled EGFP-LecA fusion protein was produced. This was achieved by inserting the LecA coding sequence after the EGFP sequence in the pQE-30_EGFP plasmid, see Fig. 3.27.

The new plasmid construct, pEGFP_LecA, was initially confirmed using plasmid restriction analysis using AccI and by completing small scale expressions to check for the correct fusion protein size, see Fig. 3.28 and Fig. 3.29, prior to large scale expression, 200 mL, and purification using IMAC, Fig. 3.30. Fusing LecA to EGFP did not prevent it from binding BSA-Gal, although a reduction in binding was observed, see ELLA in Fig. 3.35. This could be caused by the reduced His₆ tag availability as the EGFP-LecA protein is much larger than LecA, 3.25 times, and all lectin samples were calculated in µg/mL prior to their addition to the plate.

Site-directed mutagenesis was used to amplify the pQE-30_LecA plasmid with primers encoding additional lysine residues. Four LecA variants were made; LecA3KH, LecAH3K, LecA3K and LecA5K. All were successfully expressed and purified, see Fig. 3.34. Inserting lysine residues directly before and after the His₆ tag, LecA3KH and LecAH3K, did not affect His₆ tag availability during IMAC purification. All four variants were biotinylated to a greater degree than unmodified LecA, see Fig 3.35, as expected. The samples probed with LecA5K, with 5 lysine residues added, had the largest absorbance value after detection with an anti-biotin mAb, see Fig 3.35. The 3D structure of LecA5K, generated by the I-TASSER tool Fig. 3.33, showed that the C-terminus with added lysine was extended away from the protein and at the opposite end to the galactose binding site so there was, presumably, minimal interference with LecA5K binding.

The galactose specificity of LecA5K was clearly demonstrated by ELLA, see Fig 3.36. LecA5K was nearly fully inhibited by 50 mM galactose. The addition of glucose had no inhibitory effects. LecA5K inhibition with galactose was similar to that of the galactose binding plant lectin RCA I, see Fig. 3.37. However, RCA I also bound bovine mucin unlike LecA5K. RCA I has a broader glycan specificity as it can tolerate GalNAc residues unlike LecA5K.

Fig. 3.38 shows the SDS-PAGE and the western blot analysis of the recombinant lectins produced and biotinylated; AAL-2, GafD1-178 and LecA5K. All three lectins were strongly detected by the anti-biotin mAb. The binding specificity of these recombinant lectins was demonstrated with the addition of GlcNAc or galactose. Galactose and GlcNAc specific lectins are useful probes when assessing live cells. Increased galactosylation of cell surfaces, e.g. granulocytes and lymphocytes, is associated with the progression of apoptosis (Heyder et al. 2003). Additionally, increased GlcNAc on cell surfaces indicates incomplete *N*-glycan synthesis or sialic acid cleavage which are both indicators for cell stress and a marker for apoptosis (Batisse et al. 2004). The recombinant lectins produced here can, through their specific binding, clearly distinguish between pairs of stereoisomers. This is difficult for other glycan analysis methods like conventional mass spectrometry as stereoisomers have identical masses (Yang et al. 2016). Similarly, certain HPLC formats, e.g. high pH (13.0) anion-exchange (AE), can finely resolve glycans, although the basic conditions may lead to the epimerisation of certain monosaccharides, e.g. GlcNAc to ManNAc (Gohlke 2002).

The work presented in this chapter demonstrates the relative ease at which recombinant lectins may be produced consistently in bacterial systems. Of equal importance is the amenability of these lectins to alteration through a variety of cloning strategies, e.g. fusing to a fluorescent protein, site-directed mutagenesis, inserting additional residues or switching the position of the His₆ tag. This consistency and plasticity allows for the potential generation of novel glycan probes for a broad range of applications that surpass those of commercial plant lectins.

Chapter 4

**Investigating CHO DP-12 lectin cytotoxicity
and cell surface glycosylation using lectins and
fluorescent microscopy**

4.1 Overview

The probing of live CHO DP-12 cells with lectins is described in this chapter. The recombinant lectins, produced and purified in Chapter 3, and commercial plant and fungal lectins are used to establish a qualitative cell surface glycan profile for these cells. Lectin binding can be very specific, discriminating between α - and β - linked monosaccharides, which provides information about cell surface glycosylation through their binding or absence of binding. Initially, lectin cytotoxicity was assessed using a colourimetric assay dependant on cell metabolic activity. A resazurin-based assay was used for this. Fluorescent microscopy was used to assess lectin binding to live CHO DP-12 cells. The lectins, which were biotinylated, were premixed with a fluorescent streptavidin conjugate, DyLight488, and then added to cells. The work presented in this chapter is from live cell analysis only. Cells were not fixed prior to or after probing with lectins. Cell fixation and permeabilisation are required when probes need to access intracellular targets. This is not required for cell surface glycan analysis. To demonstrate lectin specificity, free monosaccharides were used to competitively inhibit lectin binding. Additionally, fluorescently labelled EGFP-LecA, produced in Chapter 3, was also used and compared to biotinylated and DyLight488 labelled LecA5K.

4.2 Determining lectin toxicity

A cell viability assay was used to determine the cytotoxic effect of lectins on CHO DP-12 cells. The FluoroFire-Blue ProViaTox assay, described in Section 2.28.1, was used. This is a resazurin-based assay which results in the reduction, and subsequent fluorescence, of a dye in the presence of metabolically active cells, see Fig. 4.1. Cells that have decreased metabolic activity, due to the addition of lectin, will reduce less dye. It is important to assess the potential cytotoxic effect of certain lectins, over a short period of time, on CHO cells. It is already well established that the long exposure of CHO cells to certain lectins is cytotoxic (Ripka and Stanley 1986). A variety of lectin resistant CHO clones have been utilised in the past few decades in identifying glycosylation pathways, genes involved in glycosylation and the functional roles of glycans (North et al. 2009; Patnaik and Stanley 2006). These lectin resistant CHO cell lines could be established due to the relative plastic nature of CHO and how the addition

of certain lectins would select for glycosyltransferase knockouts, essential in order for the cells to keep proliferating.

Before cells were incubated with lectins, the optimal seeding cell concentration was determined. It is important that the cells are seeded within a concentration range that is high enough to produce a signal that is detectable by the assay but also not too high so as to exceed the linear range of the assay. A 1 in 2 serial dilution of cells was assayed in triplicate to identify a suitable cell seeding concentration, Fig. 4.1.

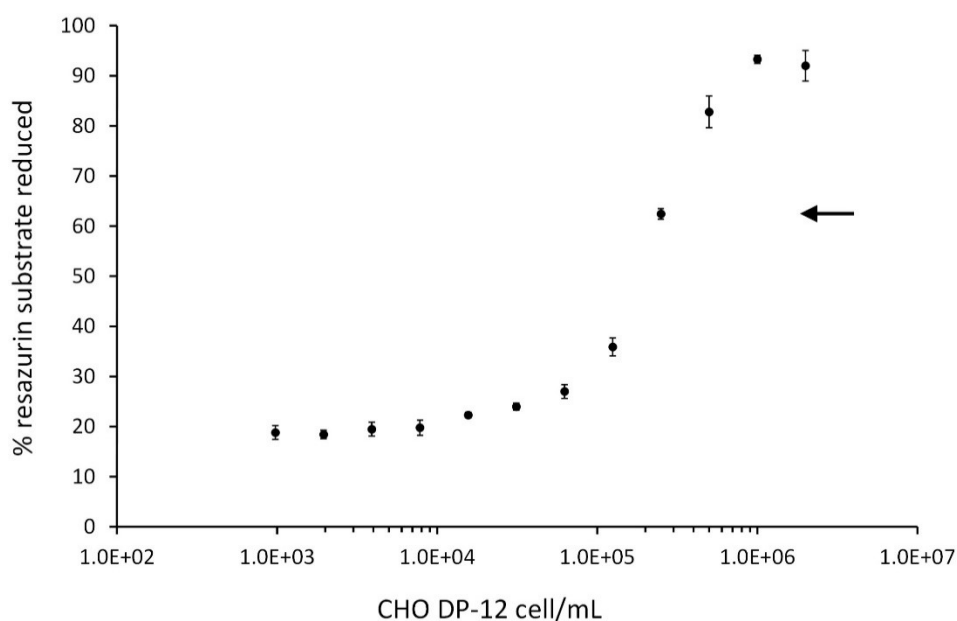


Fig. 4.1: Determining optimum seeding concentration. A 1 in 2 serial dilution from 2.0×10^6 to 9.8×10^2 cells/mL was assayed in triplicate using the FluoroFire-Blue ProViaTox assay, see Section 2.28.1. A 100 μ L cell suspension was added to each well followed by 20 μ L of PBS and 10 μ L of resazurin reagent. The plate was incubated at 37 $^{\circ}$ C for 4 h and read at 570 nm and 600 nm. The % of reagent reduced was calculated using the absorbance readings in the equations described in the assay technical manual, see Section 2.28.1. The 2.5×10^5 cells/mL sample is indicated by the arrow. Error bars were calculated from the standard deviation of three replicates.

The serial dilution of CHO DP-12 cells resulted in an S-shape curve when the percentage of resazurin reagent reduced was plotted against cell concentration on a logarithmic scale. The linear range of the assay was reached at a greater cell

concentration than suggested in the technical manual. The manufacturer suggests that the assay is sensitive to cell concentrations as low as 1.25×10^3 cells/mL. However, a CHO DP-12 cell concentration of 1.6×10^4 cells/mL was required for the percentage of resazurin reagent reduced to noticeably increase. The linear range for CHO DP-12 cells in this assay was between 6.25×10^4 cells/mL and 5×10^5 cells/mL. The 2.5×10^5 cells/mL sample, indicated by the arrow in Fig. 4.1, was deemed a suitable cell seeding concentration as it is above the midpoint of the linear range of the assay.

Recombinant lectins produced in Chapter 3 and commercial plant and fungal lectins, with similar binding specificities, were assessed for their cytotoxic effects towards CHO DP-12 cells. Cells were incubated with lectin, up to $50 \mu\text{g/mL}$, and their metabolic activity was assessed using the FluoroFire-Blue ProViaTox assay, see Fig. 4.2. This assay was completed as described in Section 2.28.1.

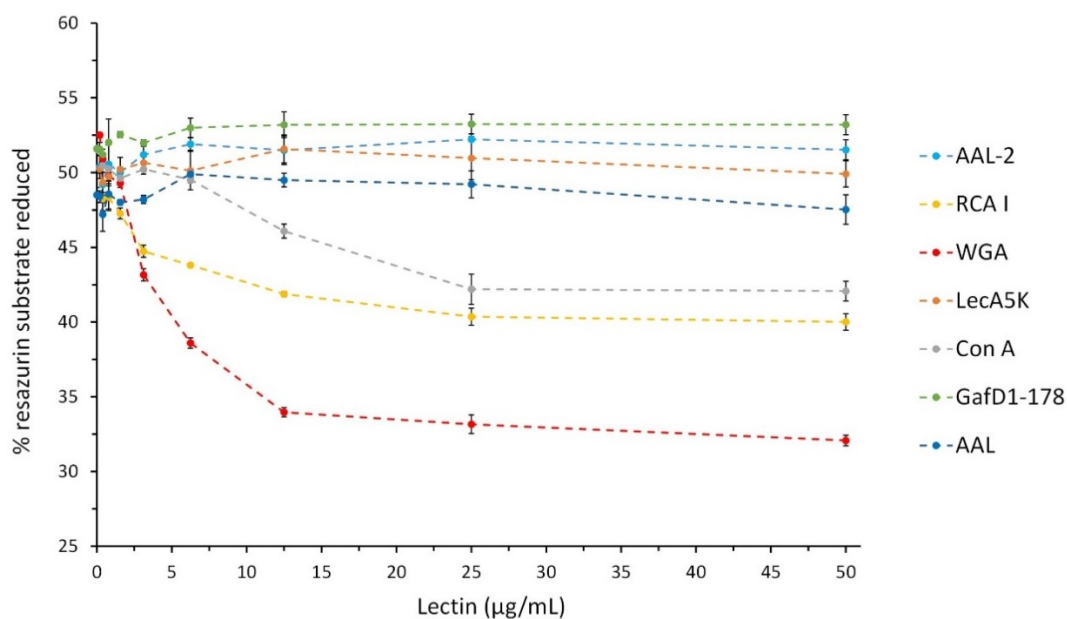


Fig. 4.2: CHO DP-12 cell lectin toxicity. A 1 in 2 serial dilution of lectin, 50 to 0 $\mu\text{g/mL}$, was incubated with CHO DP-12 cells in triplicate. A $100 \mu\text{L}$ cell suspension, 2.5×10^5 cells/mL, was added to each well followed by $20 \mu\text{L}$ of PBS containing lectin and $10 \mu\text{L}$ of reagent. The plate was incubated at $37 \text{ }^\circ\text{C}$ for 4 h and read at 570 nm and 600 nm. The % of reagent reduced was calculated, see Section 2.28.1. The lectins used were recombinant *Agrocybe aegerita* lectin 2 (AAL-2), *Ricinus communis* agglutinin I (RCA), wheat germ agglutinin (WGA), recombinant LecA5K, recombinant GafD1-178, ConcanavalinA (Con A) and *Aleuria aurantia* lectin (AAL). Error bars were calculated from the standard deviation of three replicates.

It is important to determine lectin cytotoxicity prior to probing cells with them. Therefore any change in cell viability can be attributed to the cell environment or sample preparation, i.e. lectin cytotoxicity can be eliminated as a variable or appropriately noted. Some of the lectins used were cytotoxic, i.e. WGA, RCA I and Con A, as less reagent was reduced due to reduced metabolic activity. The three recombinant lectins, AAL-2, GafD1-178 and LecA5K, produced no measurable cytotoxic effect, i.e. the percentage of reagent reduced was consistent across all lectin concentrations, even above recommended probing concentrations, i.e. 50 µg/mL. The decrease in cell viability of cells incubated with RCA I or WGA was noticeable with a relatively low lectin concentration, 3.25 µg/mL. AAL, a fucose specific fungal lectin, was the only non-recombinant lectin which did not adversely affect CHO DP-12 cells.

4.3 CHO DP-12 cell surface glycoanalysis using lectins and fluorescent microscopy

The cells that were prepared for glycoanalysis were adherently grown CHO DP-12 cells. They were cultured as described in Section 2.27.3. To prepare cells for lectin probing, cells were removed from T75 tissue culture flasks 48 hours prior to analysis using trypsin and seeded into 6 well cell culture plates. Cells were seeded at 1.5×10^5 cells/well in 3 mL of complete medium. A 48 hour incubation period prior to analysis allowed the cells to proliferate and fully adapt to the 6-well plate. The cell concentration used, 5×10^4 cells/mL or 1.5×10^5 cells/well, typically resulted in approximately 75 % confluency of the 6-well plate after 48 hours incubation. This level of confluency is ideal as cells are completely acclimatised and attached to the 6-well plate but also still growing in a monolayer.

A Nikon Eclipse Ti inverted fluorescent microscope was used to observe lectin binding to the CHO DP-12 cell surface. A Hoechst nuclear stain, NucBlue (ThermoFisher R37605), was used to counterstain the cells. NucBlue is excited by ultraviolet light at 350 nm and has an emission maximum at 461 nm. The dye is cell-permeable and binds to the minor groove of double stranded DNA. NucBlue fluorescence is detected in the DAPI filter of the microscope. This stain is important as it colocalises the lectin binding

observed. DyLight488 streptavidin conjugate (Pierce 21832), which emits green fluorescence, was premixed with biotinylated lectins, both prepared at 5 µg/mL. DyLight488 is excited by light at 493 nm and has an emission maximum at 518 nm, see Fig. 1.18 for excitation and emission spectra. DyLight 488 fluorescence is detected in the FITC channel. The full protocol for sample preparation is described in Section 2.28.2. A bright-field image, white light illumination, of the cells was initially obtained to observe the spread of cells attached to the plate. A well of unprobed cells served as the negative control on each plate. This control is important for determining the appropriate fluorescent microscope and imaging software settings. A long exposure time and/or high light intensity may produce cellular autofluorescence. This negative control is therefore vital as it ensures that light detected in the FITC channel is correctly attributed to lectin binding only and not due to cellular autofluorescence.

Lectins were selected that are known to bind to the residues commonly found in glycans. Table 1.1 and Fig. 1.1 show the relatively small number of monosaccharides that are the building blocks for eukaryotic glycans. The lectins and their binding specificities used in this chapter are described in Table 4.1. The specificity of lectin binding was demonstrated by competitive inhibition, i.e. premixing the DyLight488 and lectin with a competitive free monosaccharide. This was completed for all lectins except MAL II which requires sialic acid for inhibition. Sialic acid causes adverse cellular effects due to its low pH(<5.0) and interpretable images cannot be obtained after its addition. A brightfield image of CHO DP-12 cells is shown in Fig. 4.3. Lectin binding to the CHO DP-12 cell surface is shown in Fig. 4.4 to Fig. 4.13. These images were captured at 100x to 400x magnification. Images obtained in the DAPI and FITC channels are overlaid to validate that the fluorescence detected, i.e. lectin binding, is from the cells and not from lectin adhering to the plate surface. Two additional controls, other than monosaccharide competitive inhibition, are shown in Fig. 4.5. These were (i) the addition of DyLight488 to cells without lectin; this control is to check if DyLight488 adheres to cells or the plate and if the washing steps are sufficient to remove it. (ii) Cells were also probed with unlabelled lectin, AAL-2, to demonstrate that the fluorescence is from DyLight488 labelled lectins and that cellular autofluorescence is not detected in the FITC channel.

Table 4.1: Lectin panel for fluorescent microscopic analysis of CHO DP-12 cells

Lectin	Binding specificity	Competing monosaccharide*
<i>commercial plant and fungal lectins</i>		
Con A	Core α -Mannose	α -Methylmannoside α -Methylglucoside
GSL II	α - or β - GlcNAc	-
RCA I	Galactose or GalNAc	Galactose
LCA	α -Mannose	α -Methylmannoside α -Methylglucoside
AAL	α 1,6-Fucose	L-Fucose
UEA I	α 1,2-Fucose	-
MAL II**	α 2,3-NeuNAc	-
WGA	GlcNAc and NeuNAc	GlcNAc
<i>recombinant lectins</i>		
AAL-2	α - or β - GlcNAc	GlcNAc
GafD1-178	β - GlcNAc	-
LecA5K	Galactose	Galactose
EGFP-LecA	Galactose	Galactose
LecB	Fucose	Fucose

* Competing free monosaccharides were added at concentrations recommended by the supplier (Vector Laboratories)

** MAL II was not inhibited due to the low pH of sialic acid

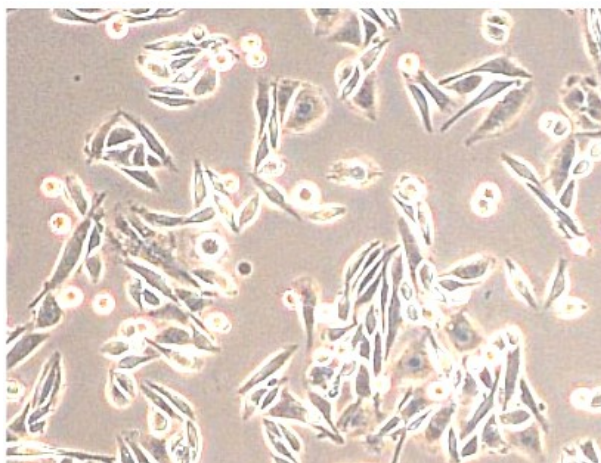


Fig. 4.3: Brightfield image of CHO DP-12 cells. Cells were seeded into 6-well plates at 1.5×10^5 cells/well and incubated for 48 hours. Cells are unprobed and are overlaid with 500 μ L of TBS. The image was captured with a Nikon Eclipse Ti inverted fluorescent microscope (400x magnification).

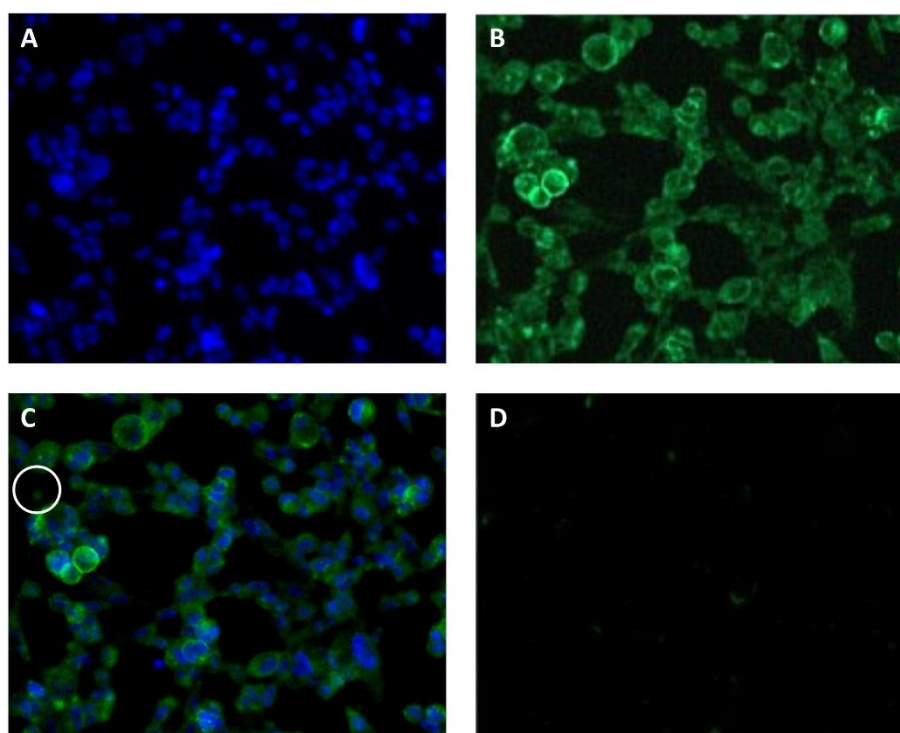


Fig. 4.4: CHO DP-12 cells probed with AAL. A) Nuclear stain. B) Cells shown in A probed with AAL labelled with DyLight488. C) Merged image of A and B. D) AAL labelled with DyLight488 and premixed with 0.2 M fucose. A region where lectin binding is detected without corresponding fluorescence from the nuclear stain is circled. The image was captured at 400x magnification.

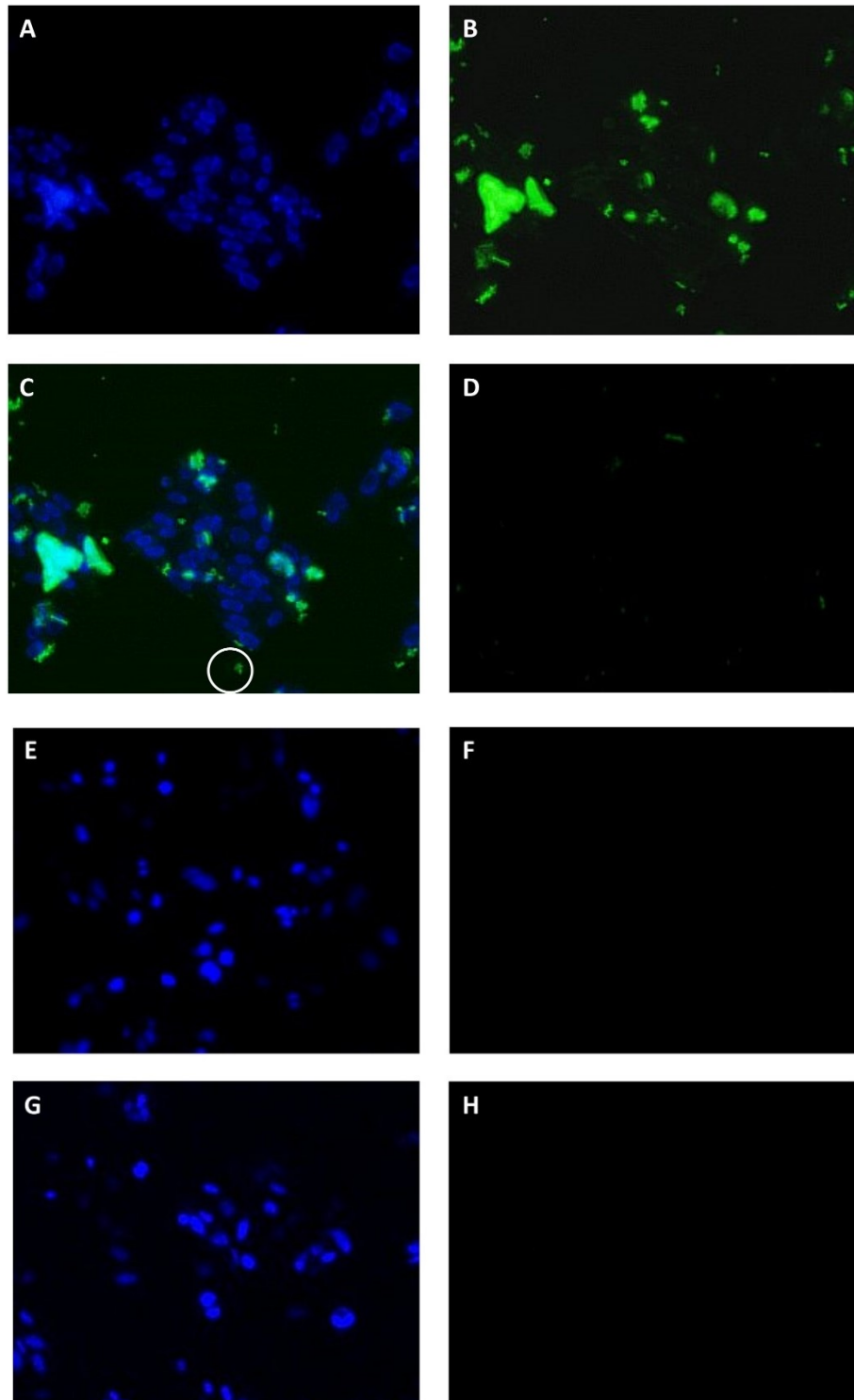


Fig. 4.5: CHO DP-12 cells probed with recombinant AAL-2. **A)** Nuclear stain. **B)** AAL-2 labelled with DyLight488. **C)** Merged image of A and B. **D)** AAL-2 labelled with DyLight488 and premixed with 0.4 M GlcNAc. **E)** Nuclear stain. **F)** Cells shown in E probed with AAL-2 without DyLight488. **G)** Nuclear stain. **H)** Cells shown in G probed with DyLight488 without lectin. A region where lectin binding is detected without corresponding fluorescence from the nuclear stain is circled. The image was captured at 400x magnification.

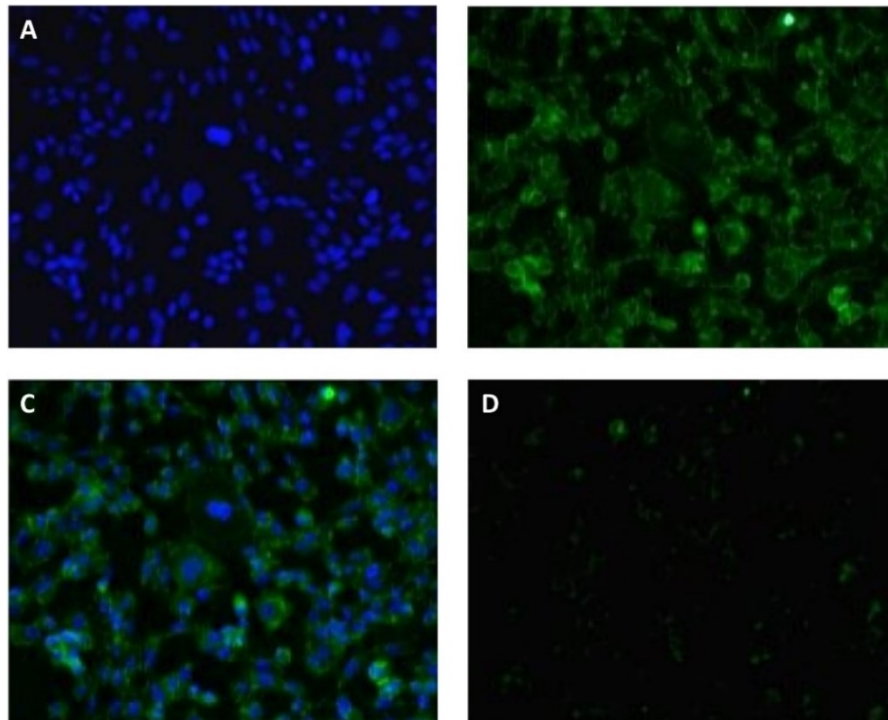


Fig. 4.6: CHO DP-12 cells probed with Con A. **A)** Nuclear stain. **B)** Con A labelled with DyLight488. **C)** Merged image of A and B. **D)** Con A labelled with DyLight488 and premixed with 0.2 M α -methylmannoside and 0.2 M α -methylglucoside (100x). The image was captured at 100x magnification.

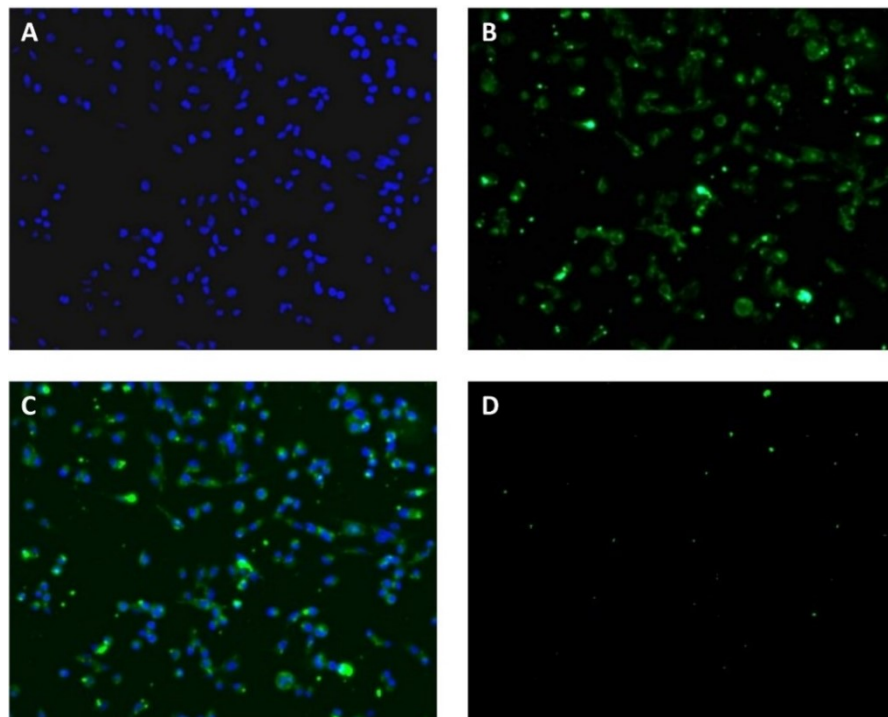


Fig. 4.7: CHO DP-12 cells probed with LCA. **A)** Nuclear stain. **B)** LCA labelled with DyLight488. **C)** Merged image of A and B. **D)** LCA labelled with DyLight488 and premixed with 0.2 M α -methylmannoside and 0.2 M α -methylglucoside. The image was captured at 100x magnification.

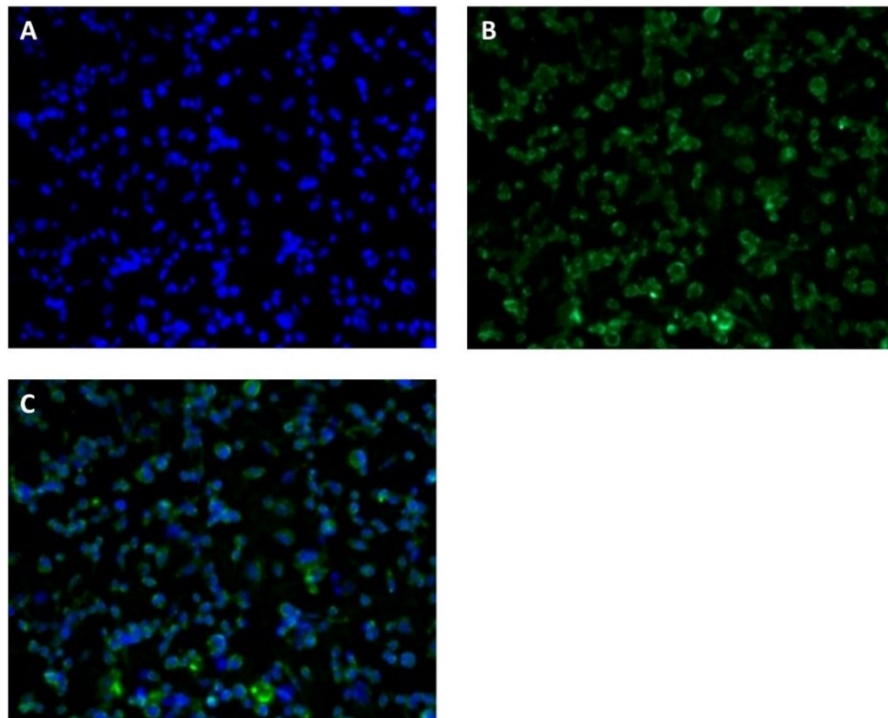


Fig. 4.8: CHO DP-12 cells probed with MAL II. A) Nuclear stain. B) MAL II labelled with DyLight488. C) Merged image of A and B. The image was captured at 100x magnification.

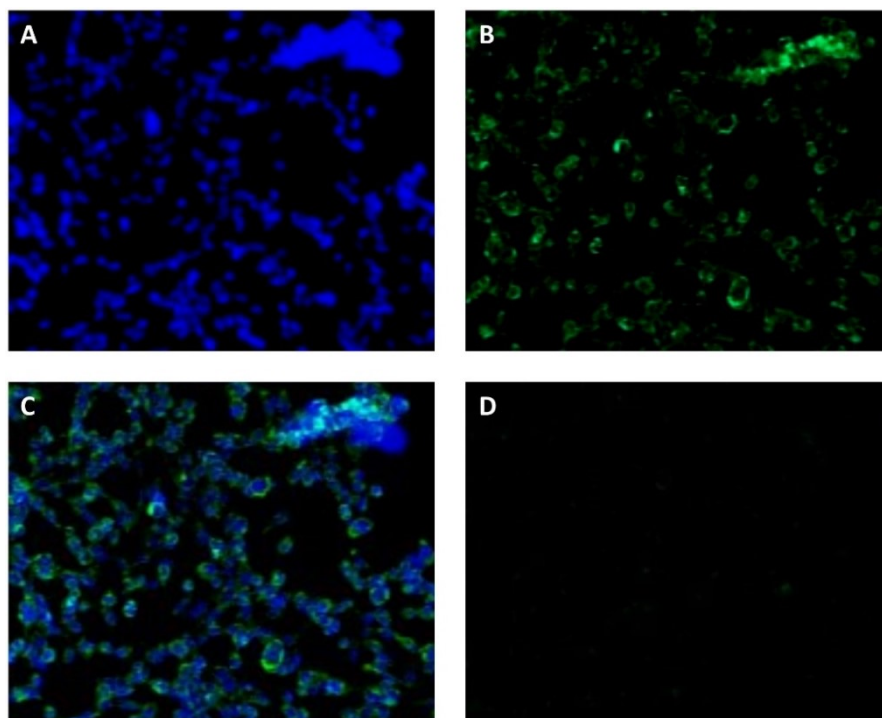


Fig. 4.9: CHO DP-12 cells probed with recombinant LecB. A) Nuclear stain. B) LecB labelled with DyLight488. C) Merged image of A and B. D) LecB labelled with DyLight488 and premixed with 0.2 M fucose. The image was captured at 100x magnification.

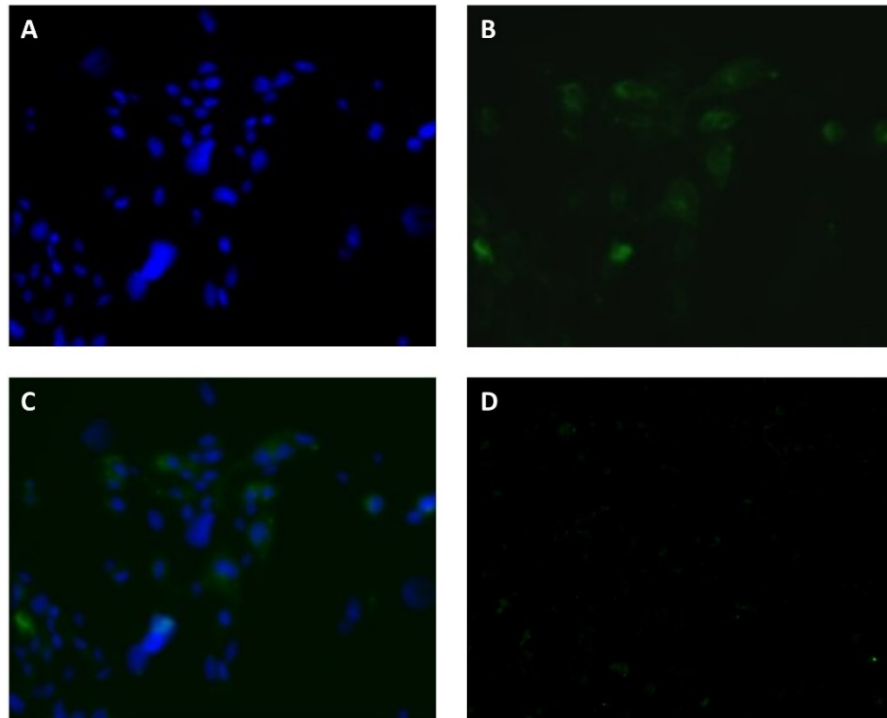


Fig. 4.10: CHO DP-12 cells probed with recombinant EGFP-LecA. A) Nuclear stain. B) EGFP-LecA. C) Merged image of A and B. D) EGFP-LecA premixed with 0.4 M galactose. The image was captured at 400x magnification.

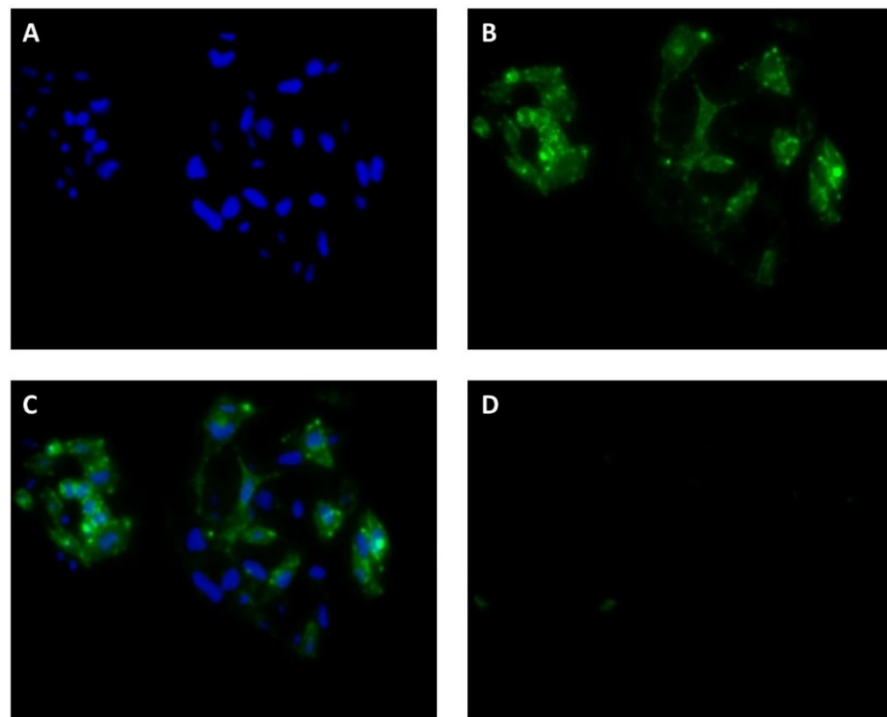


Fig. 4.11: CHO DP-12 cells probed with recombinant LecA5K. A) Nuclear stain. B) LecA5K labelled with DyLight488. C) Merged image of A and B. D) LecA5K labelled with DyLight488 and premixed with 0.4 M galactose. The image was captured at 400x magnification.

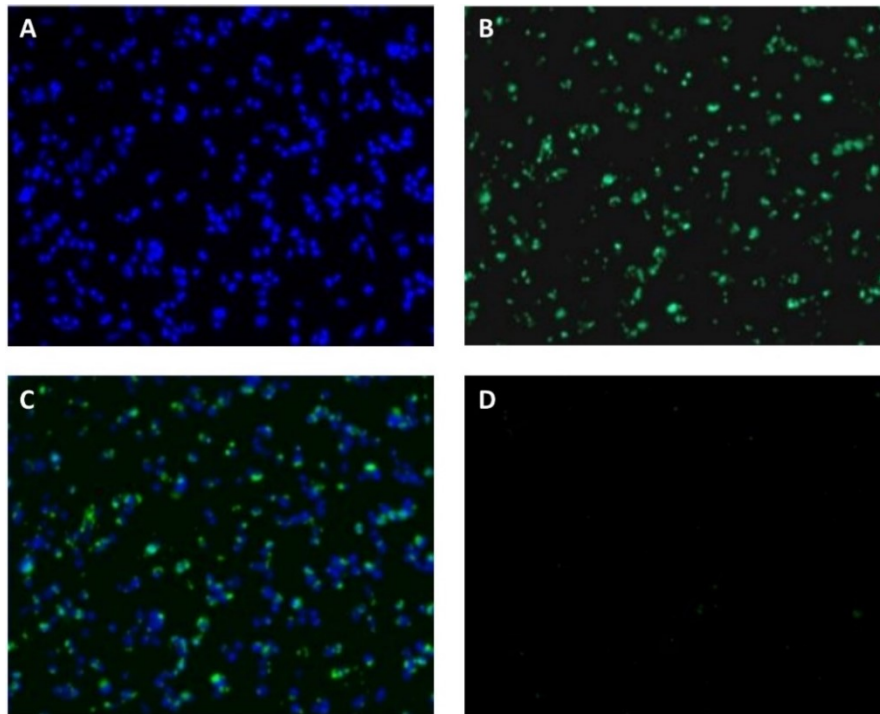


Fig. 4.12: CHO DP-12 cells probed with RCA I. A) Nuclear stain. B) RCA I labelled with DyLight488. C) Merged image of A and B. D) RCA I labelled with DyLight488 and premixed with 0.2 M galactose. The image was captured at 100x magnification.

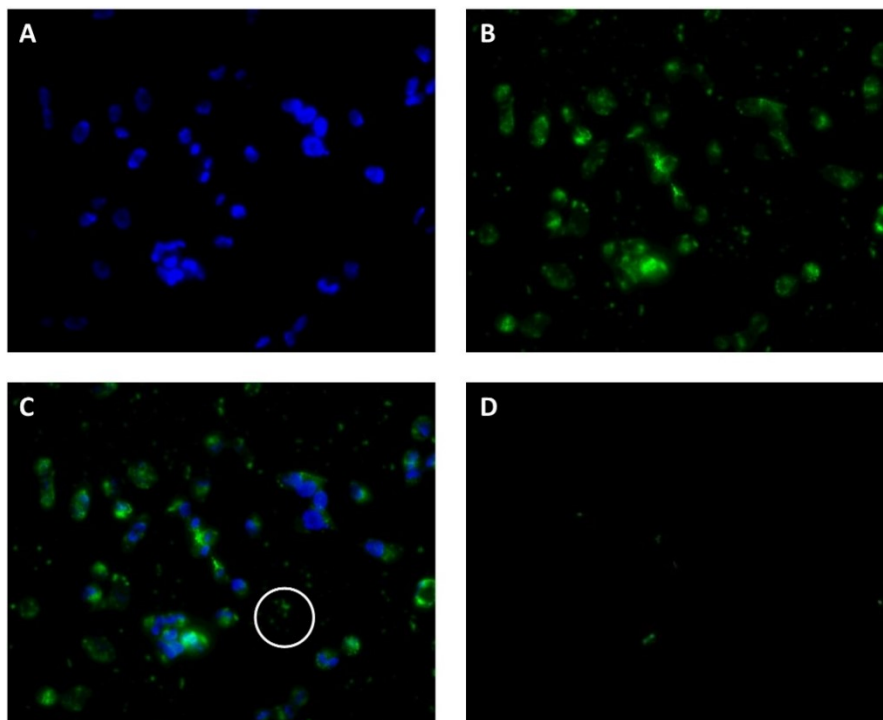


Fig. 4.13: CHO DP-12 cells probed with WGA. A) Nuclear stain. B) WGA labelled with DyLight488. C) Merged image of A and B. D) WGA labelled with DyLight488 and premixed with 0.5 M GlcNAc. A region where lectin binding is detected without corresponding fluorescence from the nuclear stain is circled. The image was captured at 400x magnification.

Lectin binding to cells was observed for AAL, AAL-2, ConA, LCA, MAL II, LecA5K, EGFP-LecA, RCA I and WGA. Lectin binding was significantly if not fully reduced for all lectins with the addition of free monosaccharides. The extra controls shown in Fig. 4.5 show that free DyLight will not stick to cells or the plate, i.e. the well washing steps are adequate. Additionally, unlabelled lectin did not alter cellular autofluorescence. The merged images clearly show the overlap between the fluorescence from the nuclear stain and the DyLight488 labelled lectins. However, additional fluorescence was detected from spots on the plate which did not correspond to attached cells, i.e. fluorescence from the nuclear stain was not detected in these regions. Some of these areas are circled, see Fig. 4.4, Fig. 4.5 and Fig. 4.13. Glycosylated proteins in the cell culture medium, which adhered to the plate, may have caused this.

Binding was not detectable with all lectins. UEA I, GSL II and GafD1-178 did not bind to the CHO surface, see Fig. 4.14, Fig. 4.15 and Fig. 4.16.

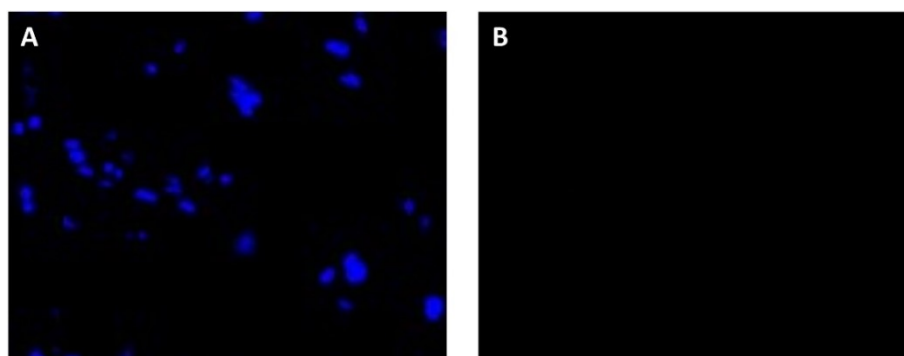


Fig. 4.14: CHO DP-12 cells probed with UEA I. A) Nuclear stain. B) UEA I labelled with DyLight488. The image was captured at 400x magnification.

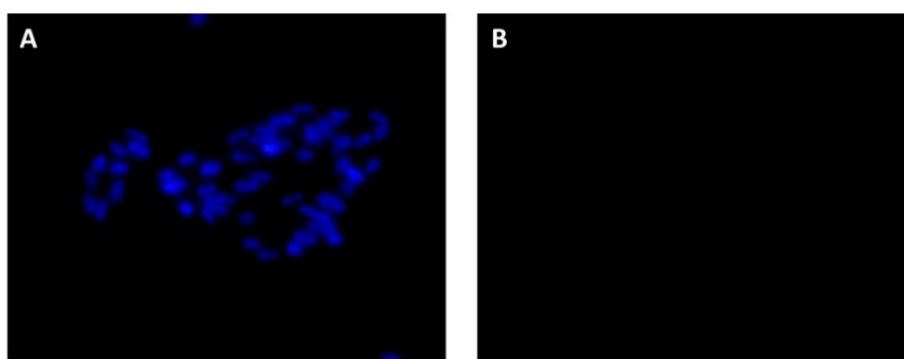


Fig. 4.15: CHO DP-12 cells probed with GSL II. A) Nuclear stain. B) GSL II labelled with DyLight488. The image was captured at 400x magnification.

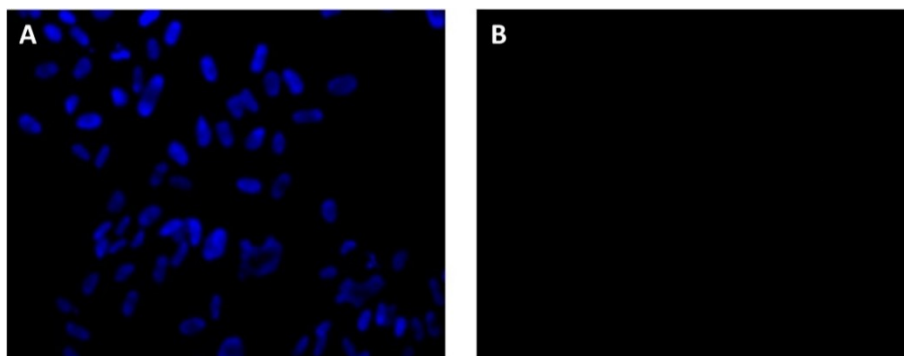


Fig. 4.16: CHO DP-12 cells probed with recombinant GafD1-178. A) Nuclear stain. B) GafD1-178 labelled with DyLight488. The image was captured at 400x magnification.

4.4 Discussion

The FluoroFire-Blue ProViaTox assay was used to investigate the cytotoxicity of a panel of lectins. Significant cytotoxicity differences were observed among the lectins tested. In the absence of lectin, cells reduced approximately 50 % of the resazurin substrate during the incubation period. Recombinant lectins AAL-2, LecA5K and GafD1-178 were shown to be non-toxic to CHO DP-12 cells. Cells incubated with the highest recombinant lectin concentration tested, 50 $\mu\text{g}/\text{mL}$, had reduced between 49 to 53 % of the resazurin substrate. The fucose specific fungal lectin, AAL, was also non-toxic to the CHO DP-12 cells as the percentage of the reagent reduced remained constant across increasing lectin concentrations.

Incubating CHO cells with Con A, RCA I and WGA caused a decrease in the reduction of resazurin substrate. WGA was the most cytotoxic of the lectins tested. WGA at 6.25 $\mu\text{g}/\text{mL}$ had reduced 38 % of the resazurin substrate which reduced to 32 % at 50 $\mu\text{g}/\text{mL}$. The cytotoxicity of WGA, a GlcNAc and sialic acid binder, is well known. Schwarz et al. (1998) investigated its toxicity in pancreatic cells and concluded that cells exposed to WGA had condensed chromatin, nuclear fragmentation and released DNA, all of which are hallmarks of apoptosis. The process of WGA toxicity include the initial binding to sialic acid and GlcNAc followed by internalization and relocation to the nucleus. RCA I, a terminal galactose binder, also reduced less reagent with increasing lectin. WGA has also been used to generate lectin resistant CHO cell lines from the

CHO K1 cell line, which is the parental cell line for the CHO DP-12 cells used here (Zhang et al. 2013; Stanley and Sundaram 2014). CHO cells which have developed WGA resistance have been shown to lack glycosyltransferase activity for the transfer of GlcNAc to α -mannose residues. Cells without this *N*-acetylglucosaminyltransferase activity (GlcNAc-T) contain glycans which terminate in mannose and obviously lack the glycan capping sequence, GlcNAc-Gal-Sialic acid. Additionally, Stanley and Sundaram (2014) determined the WGA concentration at which only 10 % of cells survived, 4 μ g/mL, using an MTT assay. The seeding CHO DP-12 concentration for investigating lectin toxicity was determined by the serial dilution of CHO cells, see Fig. 4.1. The chosen concentration, 2.5×10^5 cells/mL, was selected as it was above the midpoint of the linear range of the assay. FluoroFire-Blue ProViaTox assay, from Molecutools, was not as sensitive as expected as a concentration of 1.6×10^4 cells/mL was required for the percentage of reagent reduced to increase above baseline values.

The diversity of the CHO DP-12 glycocalyx is clearly shown by the lectin binding observed in Fig. 4.4 to Fig. 4.13. Fluorescence differences were observed for two fucose binders, AAL and UEA I which bind α 1-6-fucose and α 1-2-fucose respectively. Strong AAL binding was observed, see Fig. 4.4, which was significantly reduced by 0.2 M fucose. The first GlcNAc residue in complex *N*-glycans, attached to asparagine, is commonly fucosylated. This GlcNAc residue may have α 1-6 and/or α 1-2 linked fucose. The fluorescence from AAL binding shows the prevalence of fucosylated complex *N*-glycans at the CHO cell surface. UEA I binding was not observed, see Fig. 4.14. Glycolipids and *O*-glycans, on erythrocytes and endothelial cells, may contain α 1,2-fucose. The P^k antigen is a glycolipid commonly found on fibroblast cells however its structure, Gal α 1,4Gal β 1,4G1 does not contain α 1,2-fucose (Pourazar 2007).

Two α -mannose binders, Con A and LCA, produced similar results, see Fig. 4.6 and Fig. 4.7. LCA binding is known to be enhanced if the core oligosaccharide is fucosylated, according to the supplier (Vector Laboratories). Premixing the lectins with 0.2 M α -methylmannoside and 0.2 M α -methylglucoside did not fully inhibit lectin binding, although it was noticeably reduced. MAL II binding, see Fig. 4.8, was clearly observed. Minimal non-cellular fluorescence was visible from cells probed with MAL II, i.e. the fluorescence from the nuclear stain and lectin binding completely overlapped.

This lectin binding confirms the abundance of complex *N*-glycans capped with α 2-3-sialic acid on the CHO cell surface. MAL II binding was not inhibited with sialic acid due to the latter's low pH.

WGA binding to cells was clearly detected, see Fig. 4.13, and inhibited by the presence of 0.5 M GlcNAc. However, it produced the least clean image with much fluorescence from non-cellular artefacts on the cell culture plate. The region circled in Fig. 4.13 image C shows this high background fluorescence which was even more noticeable when the cells were viewed through the microscope eyepiece. This fluorescence from non-cell objects was also detected from cells probed with AAL and AAL-2, see the circled regions in Fig. 4.4 image C and Fig. 4.5 image C respectively. Foetal bovine serum in the CHO cell culture medium is a possible reason for this. Excess DyLight488 will not adhere to the plate as demonstrated by the control in Fig. 4.5 image H. However, the abundance of glycosylated proteins in the culture medium, from serum and from excreted proteins, may attach to the plate during the 48 hour incubation period. This unwanted fluorescence does not remove the validity of lectin binding to the CHO cell surface. However, fluorescence from the nuclear counterstain must also be observed from the same region on the plate in order to confirm lectin binding to the cell surface. It is important to note that the DME/Ham's F12 (D8437) medium used here does contain a low level of biotin, 0.0035 mg/L (Sigma 2015). While this may adhere to the 6-well plate during the incubation period, it is presumably at too low a concentration or it is removed during the wash steps as no fluorescence was detected when only DyLight488 was added to the well, see control in Fig. 4.5 image H.

The recombinant lectins produced in Chapter 3 were appropriately biotinylated as determined by ELLA analysis. The results reported in this chapter agree with this and confirm that they are suitable probes for investigating live cell surface glycosylation. Cells probed with AAL-2 are shown in Fig. 4.5. Strong binding was observed although some cells appeared to have little or no bound AAL-2, the region directly above the circle in Fig. 4.5 image C shows cells, as indicated by nuclear stain, which have not been bound by AAL-2. AAL-2 specificity is clearly shown with the almost complete reduction in fluorescence in the sample with 0.5 M GlcNAc. Two LecA labelling methods, direct protein fusion with EGFP and indirect labelling with biotin and

DyLight488, were compared, see Fig. 4.10 and Fig. 4.11. Both lectins bound to the CHO cell surface and were subsequently detected in the FITC channel. Both lectins were also successfully inhibited by competing galactose. LecA5K was however, noticeably more fluorescent. This probe presumably has many DyLight488 fluorophores conjugated per protein and therefore may outshine the EGFP-LecA fusion. The EGFP-LecA fusion is over three times the size of LecA5K. Logically this size difference could reduce fluorescence as a result of steric hindrance. However, while LecA5K is smaller than its EGFP fusion equivalent it is actually larger once it is bound by the DyLight488 streptavidin conjugate. The average molecular weight of DyLight488 streptavidin is 60 kDa (BioLegend 2017). It is possible that the difference in fluorescence observed between these two probes is due to their concentration difference, i.e. their molarity is not the same as the lectin probing concentration used was 5 $\mu\text{g}/\text{mL}$ regardless of lectin molecular weight. This is a likely explanation of the binding differences observed between these two probes in the ELLA analysis reported in the previous chapter, see Section 3.5.5, and it also a likely explanation of their binding differences observed on live CHO cells here. EGFP, although attached to the *N*-terminus at the opposite end to the LecA galactose binding site, may have slightly altered LecA folding and therefore affected LecA affinity and/or binding. This is a concern when fluorescent fusion proteins are generated (Snapp 2005). The fucose specific recombinant lectin, LecB, was observed binding the CHO cell surface, see Fig. 4.9, in a similar fashion to AAL, see Fig. 4.4. It was inhibited with 0.2 M fucose and little background fluorescence was detected.

Competitive free monosaccharides were added to demonstrate the specificity of lectin binding. Most of the lectins were successfully inhibited. Some lectins are not fully inhibited with free monosaccharides alone, even at high concentrations. For example WGA generally requires salt and/or acid for complete inhibition (Vector Labs 2017). The complete inhibition of WGA and MAL II binding may have been achieved using fixed cells. However, fixing cells may lead to other problems such as the alteration and internalisation of cell surface glycans and/or lectin internalisation and subsequent binding to intracellular glycans. These problems may increase or decrease the fluorescence signal observed (Holmes et al. 2001). The two additional controls shown in Fig. 4.5, cells probed with unlabelled AAL-2 and with lectin free DyLight488, were

successfully completed. Unlabelled AAL-2 did not alter cellular autofluorescence and free DyLight488 did not adhere to cells or the cell culture plate yielding a false positive fluorescence signal. Therefore all green fluorescence observed is from lectin binding primarily to CHO cell surfaces but also, to a much lesser extent, to proteins stuck to the cell culture plate.

Lectin binding was not observed after CHO cells were probed with recombinant GafD1-178 or GSL II, both of which are terminal GlcNAc binders, see Fig. 4.15 and Fig. 4.16. Binding was not expected from these lectins. Healthy cells, generally, do not have exposed α - or β -linked GlcNAc on the non-reducing terminal of oligosaccharides whereas cells undergoing apoptosis will display these residues (Franz et al. 2006). However, dying cells, i.e. those going through anoikis, are not present on the plate as cells were seeded at an appropriate density in fresh medium. Additionally, any such cells would only be present at a very low concentration and would ultimately be removed during the washing steps.

Fluorescent microscopy has been successfully used to qualitatively assess CHO cell surface glycans using a combination of recombinant lectins, produced in the previous chapter, and commercial plant and fungal lectins. It is important to note that fluorescence from one lectin cannot be accurately compared to that from another lectin due to biotinylation differences, i.e. stronger fluorescence from AAL probed cells than from MAL II probed cells does not necessarily mean that there is more fucose than sialic acid present on the cell surface. Nevertheless, the work presented in the previous chapter, where the specificity of lectin binding was clearly demonstrated, has been built on with the fluorescent microscopic analysis shown here and has confirmed the applicability of recombinant lectins for live cell glycoanalysis.

Chapter 5

Investigating CHO DP-12 cell surface glycosylation using lectin probes and flow cytometry

5.1 Overview

This chapter describes the probing of live CHO DP-12 cells with lectins and the subsequent analysis completed by flow cytometry. A panel of lectins was used to probe CHO DP-12 cells which were initially grown adherently. Cells were adapted to suspension culture and their cell surface glycans were again analysed with a panel of lectins using a flow cytometer. A variety of conditions were assessed to optimise the cell sample preparation prior to flow cytometry analysis. These conditions included; the method for the removal of adherent cells from tissue culture flasks, the lectin probing concentration and the lectin probing temperature. Lectin binding was competitively inhibited with free monosaccharides. This was previously completed using ELLA (Chapter 3) and during the fluorescent microscopic analysis of live CHO DP-12 cells (Chapter 4). The specificity of lectin binding was confirmed using competing free monosaccharides but also with non-competitive free monosaccharides. Additionally, for recombinant lectins, binding was also evaluated in the presence of BSA linked monosaccharides.

The changing chemical composition of cell culture medium may drastically alter cell physiology, protein synthesis and glycosylation. This has been discussed in the introduction chapter, see Section 1.11.2. Here, CHO DP-12 cells were treated with spent medium, i.e. nutrient depleted medium, and cell surface glycosylation was investigated with lectins. Following this, CHO DP-12 cells were treated with cell culture medium in which only one component was altered, i.e. glutamine, ammonia or sodium butyrate concentrations, from the standard cell culture medium described in Section 2.4. After these treatments the cells were once again probed with a panel of lectins and binding was analysed by flow cytometry. Recombinant IgG1, produced by CHO DP-12 cells, was purified from treated culture medium using Protein A/G. It was subsequently glycoanalysed by ELLA to determine if there was a correlation between lectin binding to the cell surface and the recombinant product.

5.2 Adapting adherent CHO DP-12 cells to serum-free suspension culture

CHO DP-12 is an adherent cell line. It was subcultured adherently in T75 flasks in medium containing serum, see Sections 2.4 and 2.27.3. Cell stocks were cryopreserved

in serum, see Section 2.27.6. Foetal bovine serum is a rich source of undefined components such as attachment factors, micronutrients, growth factors and hormones which would otherwise be absent from basal medium. However, as animal-derived serum is not completely defined it is a potential source of pathogens in cell culture. For recombinant protein production serum composition is an issue as it varies from batch to batch. A batch of serum may be derived from a large number of animals. Serum is also expensive and recent consumption increases means global demand may soon exceed supply (Karnieli et al. 2017). CHO cells generally adhere to culture flasks during growth, however they may be adapted to suspension culture. This allows high cell density cultures to be reached thereby improving product yields (Miki and Takagi 2014).

A standard DME/F12 medium was used for the adherent subculture of CHO DP-12. BalanCD CHO Growth A, a more expensive and chemically-defined medium which is optimised for the production of recombinant proteins in CHO, was used for CHO DP-12 suspension cultures. The composition of both media is described in Section 2.4. The BalanCD CHO Growth A product insert recommends two methods for adapting CHO cells from serum-supplemented medium to serum-free medium, i.e. direct adaption and sequential adaption (IrvineSci 2017). Adaption from serum-supplemented to serum-free medium and from adherent to suspension culture were attempted simultaneously. CHO DP-12 cells were passaged adherently three times after revival from liquid nitrogen stored stocks before being seeded into 5 mL suspension cultures. For the direct adaption the cells were switched from adherent serum-supplemented medium to serum-free suspension medium, see Section 2.4. For the sequential adaption the cells were switched from adherent serum-supplemented medium to a 3:1 mix of serum-supplemented to serum-free medium. Cells were seeded into 5 mL cultures in triplicate and cell viability was measured daily to determine to optimum adaptation method. The result of these two adaption methods is displayed in Fig. 5.1.

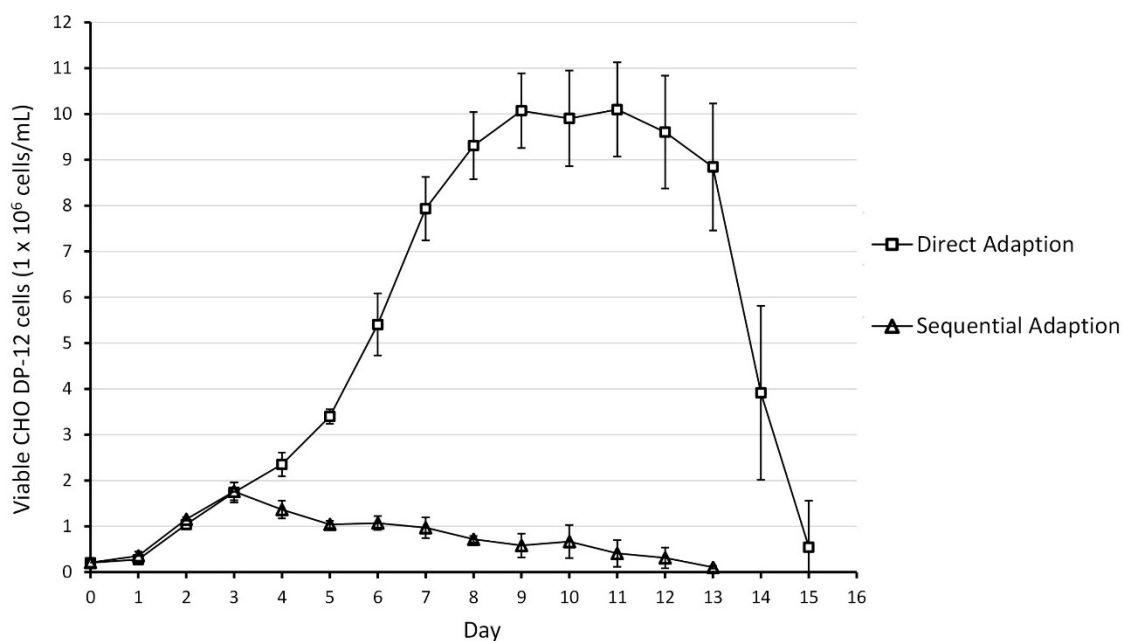


Fig. 5.1: Adapting CHO DP-12 cells from adherent serum-supplemented culture to suspension serum-free culture. Adherent CHO DP-12 cells were seeded in to 5 mL suspension cultures at 3×10^5 viable cells/mL into serum-free suspension medium (direct adaption) and into a 3:1 mix of serum-supplemented to serum-free medium (sequential adaption), see Section 2.4. An orbital shaker was used at 200 rpm to maintain the suspension culture, see Section 2.27.3 Fig. 2.9. The viable cell concentration was determined using the ADAM cell counter, see Section 2.27.5. Error bars were calculated from the standard deviation of three replicates.

The cells that were switched directly from serum-supplemented to serum-free medium thrived. They achieved a high cell culture density, reaching 10×10^6 viable cells/mL by day 9. The viable cell concentration was similar for both methods until day 4 when the sequentially adapted viable cell concentration dropped significantly. There was a 22.5 % drop in the viable cell concentration observed from day 3 to day 4. These cells did not recover but further declined on day 5 and onwards. It was possible to change the adherent serum-supplemented culture to a suspension serum-free culture simultaneously. The direct adaption method was subsequently used to generate suspension cultures each time a fresh CHO DP-12 stock was revived and initially passaged 3 times adherently.

5.3 Determining an appropriate lectin probing concentration

CHO DP-12 cells were not fixed prior to lectin probing and analysis by the flow cytometer. Some lectins are cytotoxic as shown by the FluoroFire-Blue ProViaTox assay in Fig. 4.3. It is important that an appropriate lectin probing concentration is used so the fluorescent signal may be distinguished from unprobed/unstained cells, i.e. peak separation is observed. Secondly, it is a waste of lectin if it is used at a certain concentration when equivalent results could be obtained at a lower concentration. Additionally, published methods for live cell lectin binding analysis using a flow cytometer vary in terms of lectin probing concentration and total cell number probed. Stanley and Sundaram (2014) recommended the lectin range 5 - 20 $\mu\text{g}/\text{mL}$ whereas Tao et al. (2008) used a broader range, 2.5 - 40 $\mu\text{g}/\text{mL}$. Three lectins, AAL, AAL-2 and RCA I at 1 - 20 $\mu\text{g}/\text{mL}$, were used to probe CHO DP-12 cells. Fig. 5.2 shows the binding observed and Fig. 5.3 shows the corresponding SSC-A versus FSC-A dotplots.

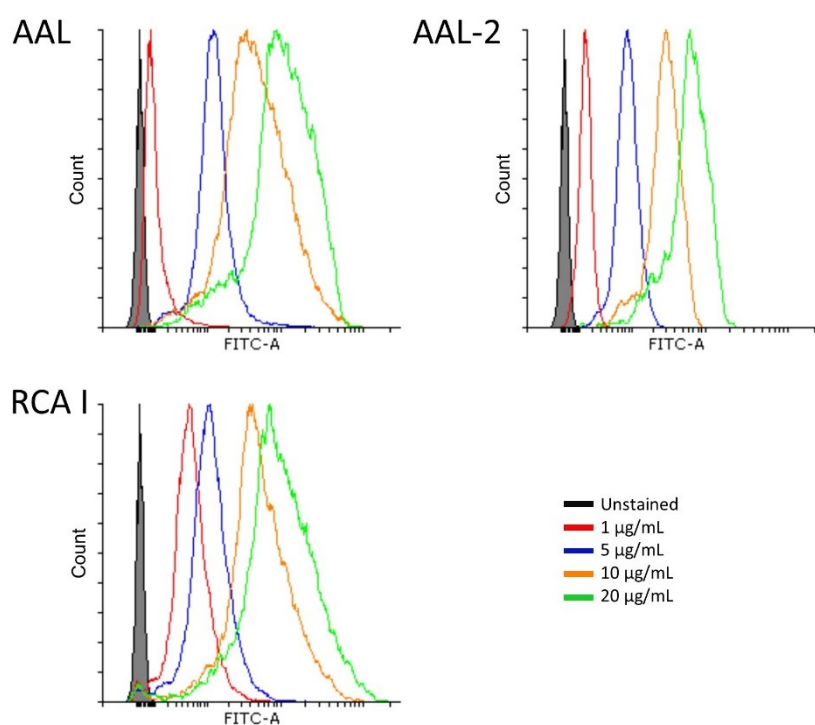


Fig. 5.2: Determining an appropriate lectin probing concentration. Overlay histograms of suspension adapted CHO DP-12 cells are shown. Cells were probed with lectin (1 - 20 $\mu\text{g}/\text{mL}$) as described in Section 2.28.3.1. The data analysis and gating strategy is explained in Section 2.28.3.3. Fucose specific AAL, recombinant GlcNAc specific AAL-2 and galactose specific RCA I lectins were used.

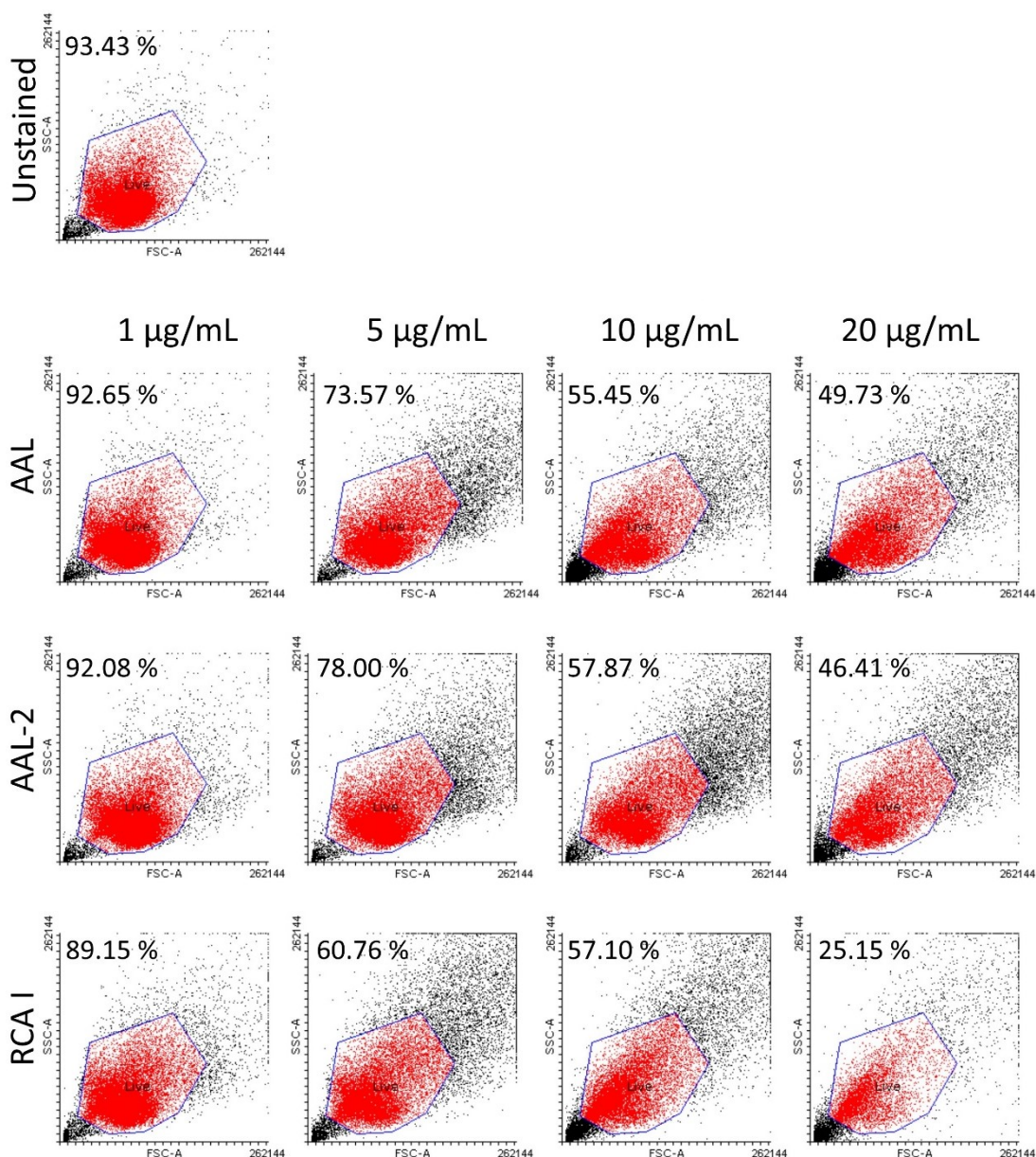


Fig. 5.3: Dotplots of suspension CHO DP-12 cells probed with lectins. SSC-A versus FSC-A dotplots were gated. The percentage of cells within the live gate is shown on each dotplot. Suspension adapted CHO DP-12 cells were probed with lectin (1 - 20 µg/mL) as described in Section 2.28.3.1. The data analysis and gating strategy is explained in Section 2.28.3.3. Fucose specific AAL, recombinant GlcNAc specific AAL-2 and galactose specific RCA I lectins were used.

Significant lectin binding differences were observed for the four lectin concentrations tested. The fluorescence observed in the FITC channel increased, as expected, with increasing lectin concentration, see Fig. 5.2. The peak shape also changed with increasing lectin. This was particularly noticeable for cells probed with AAL and RCA

I at 10 and 20 $\mu\text{g}/\text{mL}$ where the peak broadened and symmetry was lost. Probing cells with lectin at 5 $\mu\text{g}/\text{mL}$ was deemed appropriate. At this lectin concentration the fluorescence observed was separated from the unstained sample. Additionally, although this concentration did reduce the number of cells in the live gate, it was not significant. 73.57 %, 78.00% and 60.76 % of cells probed with AAL, AAL-2 and RCA I, respectively, at 5 $\mu\text{g}/\text{mL}$ remained in the live gate. The data corresponding to Fig. 5.2 and Fig. 5.3, including mean fluorescence intensity values (MFI), is tabulated in Appendix E.

5.4 Determining an appropriate cell number to probe

The number of cells to aliquot per sample for lectin probing was investigated. The number of cells probed and the fluorescence observed will, naturally, also depend on the lectin probing concentration. The objective is to find a balance between the fluorescent signal, minimising lectin toxicity and probing an appropriate number of cells so as to obtain sufficient data. A minimum of 10,000 events were recorded on the cytometer for each sample. However, a far greater number of cells are required for each sample to (i) ensure a visible cell pellet is formed when the samples are centrifuged before and after washing/probing and (ii) to fine-tune the flow cytometer settings, i.e. pre-running samples before recording events to correctly adjust the voltages. A flow cytometry protocol by Stanley and Sundaram (2014) recommends 5×10^5 cells/sample. Life science vendors BioLegend and BD Biosciences recommend $5\text{-}10 \times 10^5$ cells/sample and 10×10^5 cells/sample respectively (BioLegend 2010; BD 2013).

Recombinant AAL-2 and *Galanthus nivalis* lectin (GNL) were used to probe $5\text{-}9 \times 10^5$ CHO DP-12 cells per sample. AAL-2 and GNL were selected as their binding to the CHO cell surface generates narrow normal distributed peaks therefore subtle fluorescence intensity differences are more noticeable. This result is displayed in Fig. 5.4 with corresponding MFI values tabulated in Appendix E.

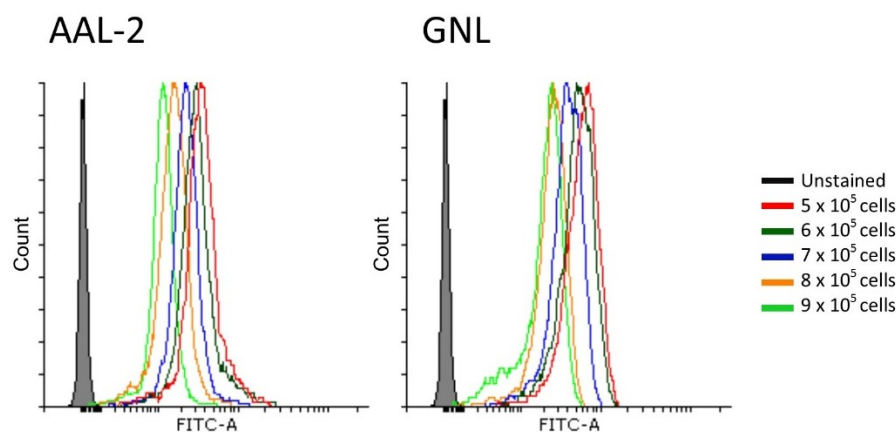


Fig. 5.4: Determining an appropriate cell number per sample. Overlay histograms of suspension adapted CHO DP-12 cells are shown. Cells were aliquoted ($5\text{-}9 \times 10^5$ cells/tube) and probed with lectin ($5 \mu\text{g}/\text{mL}$) as described in Section 2.28.3.1. The data analysis and gating strategy is explained in Section 2.28.3.3. Recombinant GlcNAc specific AAL-2 and mannose specific GNL lectins were used.

As expected the fluorescent intensity from lectin binding decreased with an increase in cell number. The cell pellet from 5×10^5 cells was easily dislodged from the bottom of the microcentrifuge tube, during supernatant removal, leading to cell loss. This was not an issue with the larger cell numbers probed. For all subsequent flow cytometry experiments, 7×10^5 cells were aliquoted per sample.

5.5 Determining an appropriate temperature for probing cells with lectins

This protocol parameter was assessed because flow cytometry staining methods frequently recommend probing cells on ice or at room temperature (BD 2013). Additionally, the optimal binding temperature is not the same for each lectin, even if they are from the same organism, e.g. Gilboa-Garber and Sudakevitz (1999) showed that the peak hemagglutinating activity for LecA (PA-IL) and LecB (PA-IIL), both from *P. aeruginosa*, is achieved at $4 \text{ }^\circ\text{C}$ and $42 \text{ }^\circ\text{C}$ respectively. As lectin binding was previously assessed by ELLA analysis, in which lectins are used at ambient temperatures, cells were probed with lectin and incubated at $4 \text{ }^\circ\text{C}$ or at room temperature ($\sim 20 \text{ }^\circ\text{C}$). The lectin binding differences observed is shown in Fig. 5.5.

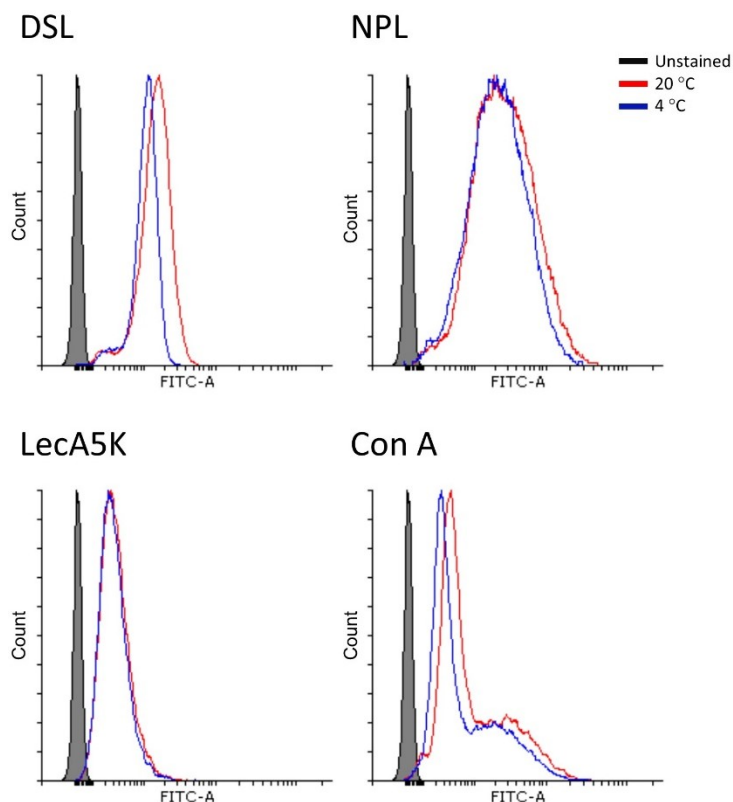


Fig. 5.5: Determining an appropriate cell lectin probing temperature. Overlay histograms of suspension adapted CHO DP-12 cells are shown. Cells were prepared as described in Section 2.28.3.1 and incubated for 30 minutes at 20 °C or 4 °C. The data analysis and gating strategy is explained in Section 2.28.3.3. Recombinant galactose specific LecA5K, GlcNAc specific *Datura stramonium* lectin (DSL) and mannose specific *Narcissus pseudonarcissus* lectin (NPL) and concanavalin A (Con A) lectins were used.

Although binding was clearly evident at both temperatures an increased signal was observed from cells probed with lectins at room temperature, ~20 °C. For all subsequent flow cytometry experiments, cells were probed at this temperature which is also more convenient to work with. The MFI values corresponding to Fig. 5.5 is tabulated in Appendix E.

5.6 Detaching adherent CHO DP-12 cells from tissue culture flasks

Trypsin (EC 3.4.21.4) is commonly used to detach adherent cells from culture surfaces. This serine protease alters the cell membrane by cleaving surface proteins which may lead to cell dysregulation and even cell death due to the up regulation of apoptosis-related proteins (Sigma 2014; Huang et al. 2010). Trypsin solutions for cell culture often contain EDTA. The removal of cells by these solutions is two pronged, (i) trypsin cleaves proteins directly after arginine and lysine residues at the C-terminus (Rodriguez et al. 2008) and (ii) EDTA chelates calcium which cell adhesion molecules (CAMs), e.g. integrins, require for binding to other cells and to surfaces (Zhang and Chen 2012). Trypsinising cells may be altering the cell surface glycosylation profile which is subsequently detected by lectins. To investigate this three additional cell removal methods were used; cell scraper (mechanical), cell dissociation solution (CDS, non-enzymatic) and EDTA. Cells were probed with a panel of 5 lectins, see Table 5.1 and Fig. 5.6.

Table 5.1: Comparison of MFI from trypsinised cells with cells removed using a scraper, CDS and EDTA

20,000 events recorded for each sample. Full data shown in Appendix E.

% MFI change compared to trypsinised cells			
Lectin	Scraper	CDS	EDTA
AAL-2	14.68	8.85	-8.41
Con A	59.61	-3.00	-24.40
DSL	-8.26	-18.49	-27.48
MAL II	1.03	26.96	-5.61
RCA I	63.35	-26.19	4.16

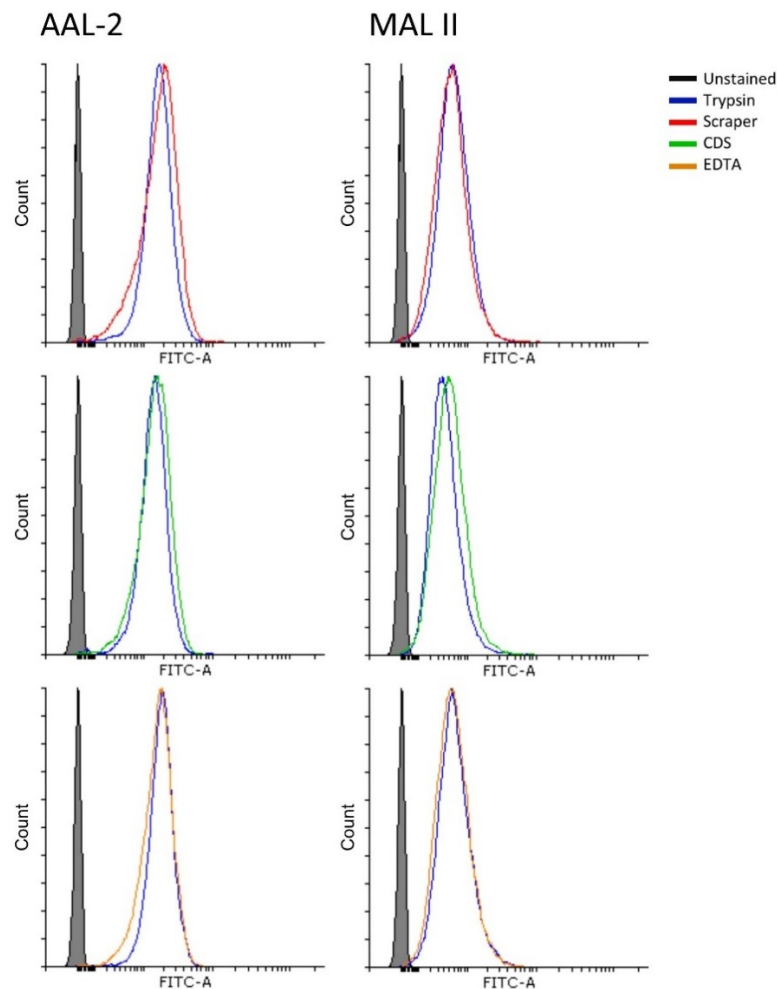


Fig. 5.6: Comparison of cell detachment methods using AAL-2 and MAL II. Overlay histograms of adherent CHO DP-12 cells are shown. Cells were removed from T75 tissue culture flasks using trypsin-EDTA (Sigma T4174), cell scraper, cell dissociation solution (Sigma C5914) and 10 mM EDTA. For each solution, 5 mL was added to a T75 tissue culture flask and incubated for 5 minutes at 37 °C. Cells were prepared as described in Section 2.28.3.1. The data analysis and gating strategy is explained in Section 2.28.3.3. Recombinant AAL-2 and sialic acid binding MAL II were used.

It can be seen that lectin binding was not identical for all cell preparation methods used. Cells removed from tissue culture flasks with CDS and EDTA had reduced lectin binding for 3 out of 5 and 4 out of 5 of the lectins tested, see Table 5.1. For the cells removed mechanically, an increase in AAL-2 (14.68 %), Con A (59.61 %) and RCA I (63.35 %) binding was observed when compared to trypsinised cells. For subsequent adherent cell preparations for lectin probing and flow cytometry analysis, cells were removed from tissue culture flasks using a cell scraper.

5.7 Lectin binding differences between adherent and suspension CHO DP-12 cell surfaces

Table 5.2: Comparison of MFI from lectins probing adherent and suspension adapted CHO DP-12 cells

20,000 events recorded for each sample. Full data shown in Appendix F.

Lectin	Adherent	Suspension	% change
Unstained	8.09	8.15	0.78
AAL	1575.49	1039.31	-34.03
AAL-2	1761.63	1461.46	-17.04
Con A	4961.77	2916.62	-41.22
DBA	35.88	38.08	6.11
DSL	2051.25	2069.47	0.89
ECL	2341.18	1327.09	-43.32
GafD1-178	9.88	7.39	-25.16
GNL	1364.42	1352.12	-0.90
GSL I	126.38	108.93	-13.80
GSL I B4	182.07	129.73	-28.75
GSL II	33.32	15.88	-52.32
HPA	32.03	22.01	-31.27
Jacalin	4395.63	2968.49	-32.47
LCA	5271.05	4852.08	-7.95
LecA5K	406.10	974.57	139.98
LecB	96.12	119.62	24.45
MAL I	4174.70	2321.59	-44.39
MAL II	1625.69	1496.06	-7.97
NPL	2575.78	2231.79	-13.35
PNA	753.92	266.69	-64.63
RCA I	2875.69	2620.98	-8.86
SBA	166.35	88.35	-46.89
SNA	937.69	104.42	-88.86
WGA	2929.20	4377.19	49.43

Table 5.2 displays the results of adherent and suspension adapted CHO DP-12 cells probed with a panel of 24 lectins. Reduced lectin binding was observed with suspension

adapted cells for all lectins except LecA5K, LecB, and WGA where increases of 139.98 %, 24.45 % and 49.43 % were observed and DSL and GNL where no difference was detected. The size difference between both cell populations was noticeable when performing cells counts with a haemocytometer, see Section 2.27.4, and on SSC-A versus FSC-A dotplots. The forward and side scatter differences between these cell populations are shown in Fig. 5.7.

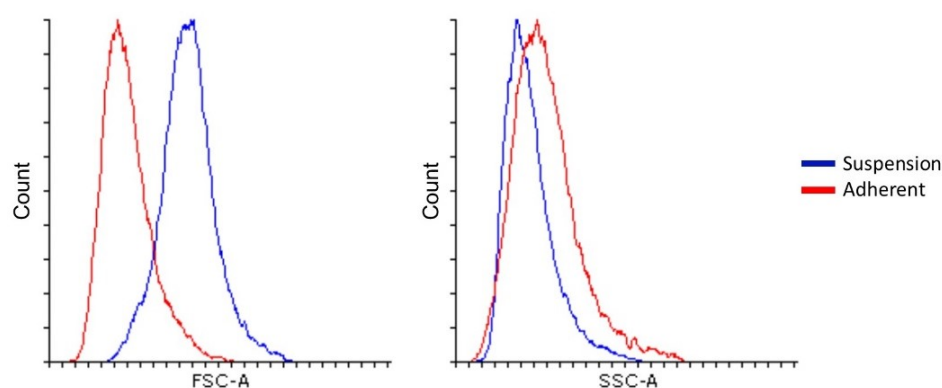


Fig. 5.7: FSC-A and SSC-A comparison of adherent and suspension adapted CHO DP-12 cells. Overlay histograms of CHO DP-12 cells are shown where forward scatter (FSC-A) and side scatter (SSC-A) are compared. Both cell samples are the unstained cell samples in Table 5.2. Cells were prepared as described in Section 2.28.3.1. The data analysis and gating strategy is explained in Section 2.28.3.3. Additional data for these cell samples is shown in Appendix F.

5.8 Comparison of LecA variants binding to the CHO DP-12 cell surface

LecA variants were generated by inserting lysine residues at the *N*- or *C*- termini of the LecA protein sequence. A LecA fusion protein, with EGFP, was also produced. This work is described in Chapter 3, see Fig. 3.34 for SDS-PAGE analysis of purified LecA lectins and Fig. 3.35 for their comparison by ELLA. Here, all six LecA lectins were assessed for their ability to detect galactose on the CHO DP-12 cell surface, see Fig 5.8. Binding had been previously observed for other galactose binding lectins, ECL, GSL I B4 and RCA, see Table 5.2.

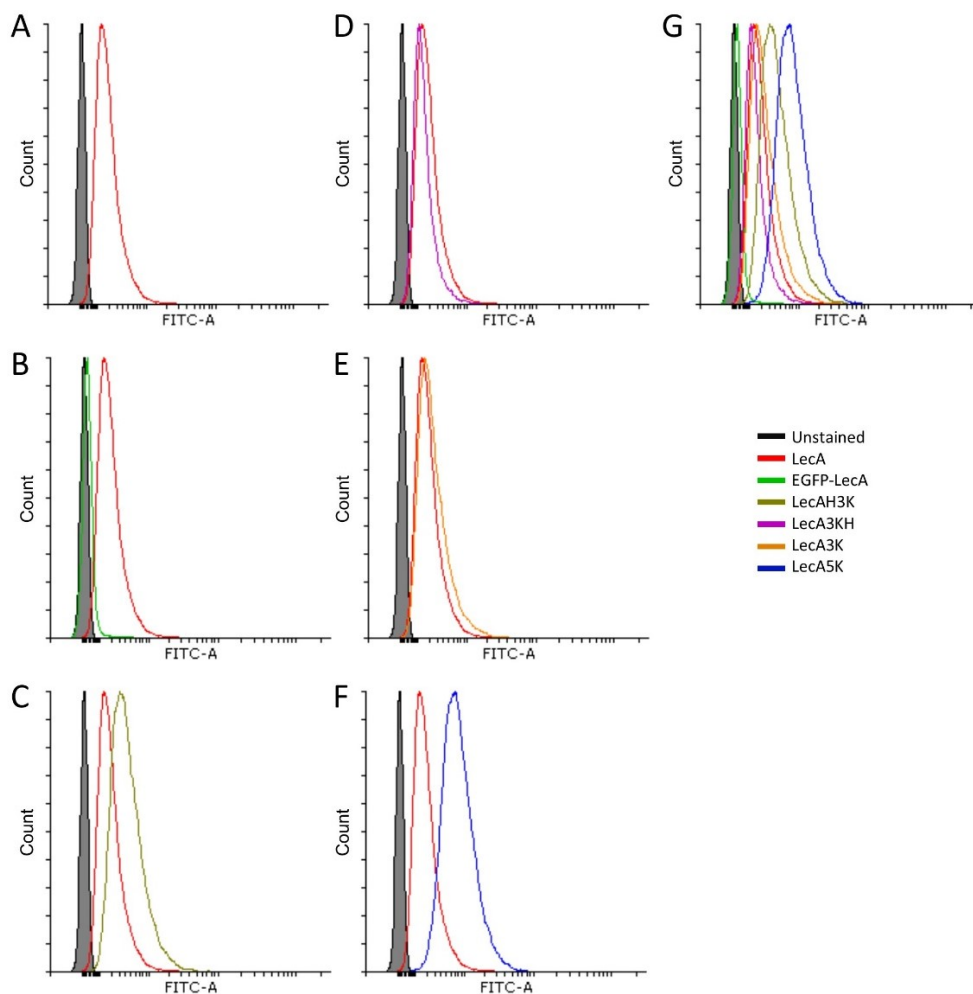


Fig. 5.8: Comparison of LecA and LecA variants binding suspension adapted CHO DP-12 cells. Overlay histograms of CHO DP-12 cells are shown where unmodified LecA is compared directly with each variant. All lectins were biotinylated except EGFP-LecA. Unstained and LecA probed cells are shown in A-G. **B)** EGFP-LecA. **C)** LecAH3K. **D)** LecA3KH. **E)** LecA3K. **F)** LecA5K. **G)** All lectins. Cells were prepared as described in Section 2.28.3.1. The data analysis and gating strategy is explained in Section 2.28.3.3.

The MFI values corresponding to Fig. 5.8 is tabulated in Appendix F. Unmodified LecA is not biotinylated sufficiently to observe peak separation from an unstained cell sample, i.e. the signal-to-noise ratio is too low. Directly labelling LecA with EGFP did not resolve this. Both LecAH3K and LecA5K provided complete peak separation from an unstained sample. LecA5K was used for all subsequent flow cytometry experiments as it resulted in a 3.25-fold increase in MFI when compared with LecA.

5.9 Assessing the specificity of lectin binding to live CHO DP-12 cells

The binding specificities of recombinant lectins produced in Chapter 3 were assessed by ELLA. Here, recombinant lectins and commercial plant and fungal lectins were assessed by premixing with competitive monosaccharides prior to probing live CHO DP-12 cells. It is important to assess lectin binding, and inhibition, to the CHO cell surface on the flow cytometer as live cell samples are inherently more complex and diverse than the glycoproteins used during ELLA analysis. For Fig. 5.9 to Fig. 5.23 all cells were prepared as described in Section 2.28.3.1. The data analysis and gating strategy is explained in Section 2.28.3.3. Additional data for these histograms is shown in Appendix G.

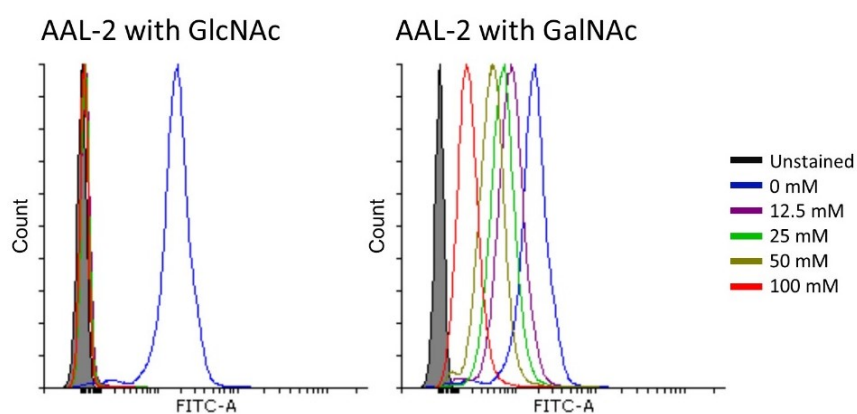


Fig. 5.9: AAL-2 inhibition check with competitive/non-competitive monosaccharide gradient. Overlay histograms of suspension adapted CHO DP-12 cells probed with recombinant AAL-2 with free GlcNAc or GalNAc.

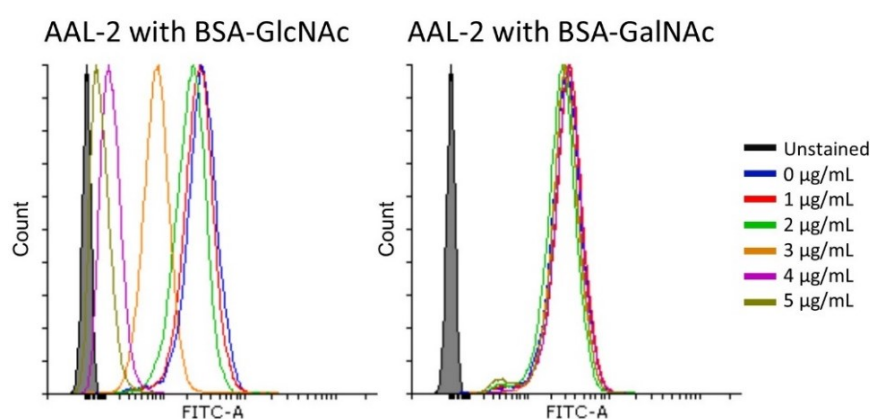


Fig. 5.10: AAL-2 inhibition check with competitive/non-competitive BSA-linked monosaccharide gradient. Overlay histograms of suspension adapted CHO DP-12 cells probed with recombinant AAL-2 with BSA-GlcNAc or BSA-GalNAc.

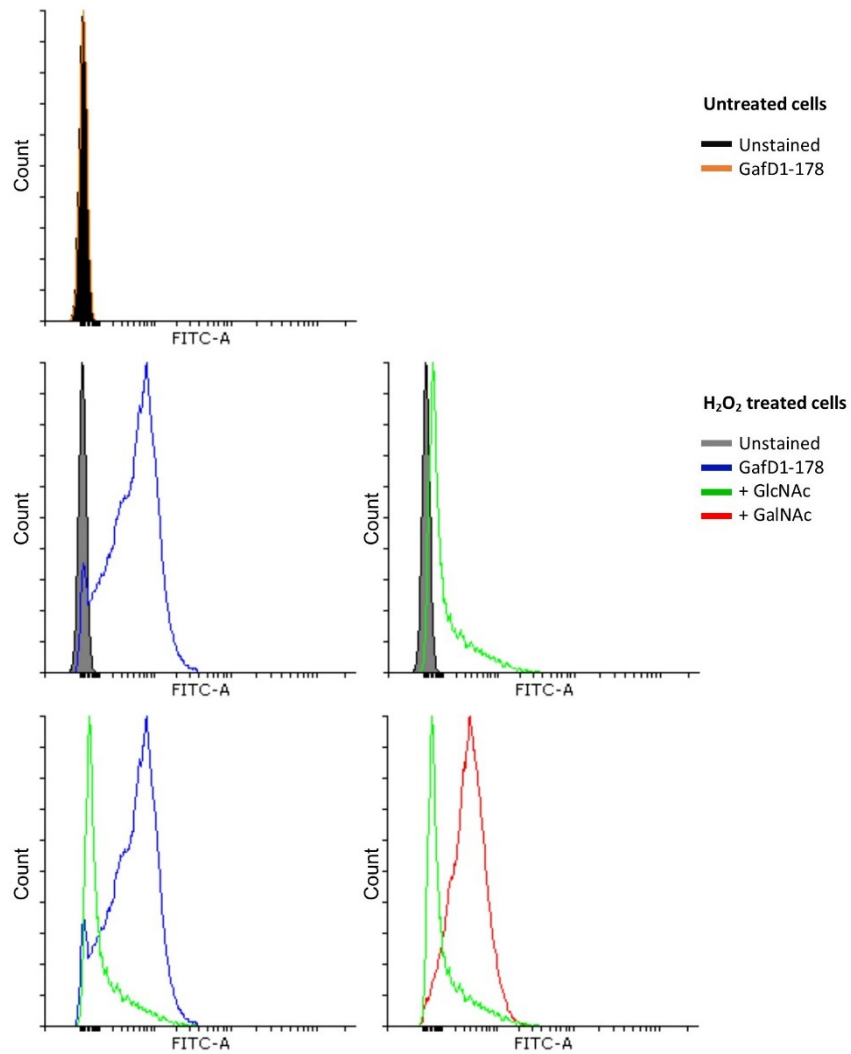


Fig. 5.11: GafD1-178 inhibition check with competitive/non-competitive monosaccharides. Overlay histograms of suspension adapted CHO DP-12 cells probed with recombinant GafD1-178 with 100 mM GlcNAc or 100 mM GalNAc. GafD1-178 does not bind healthy CHO DP-12 cells, top histogram. A CHO cell suspension was spiked with H₂O₂ (0.489 mM) 5 hours prior cell sample preparation to induce apoptosis.

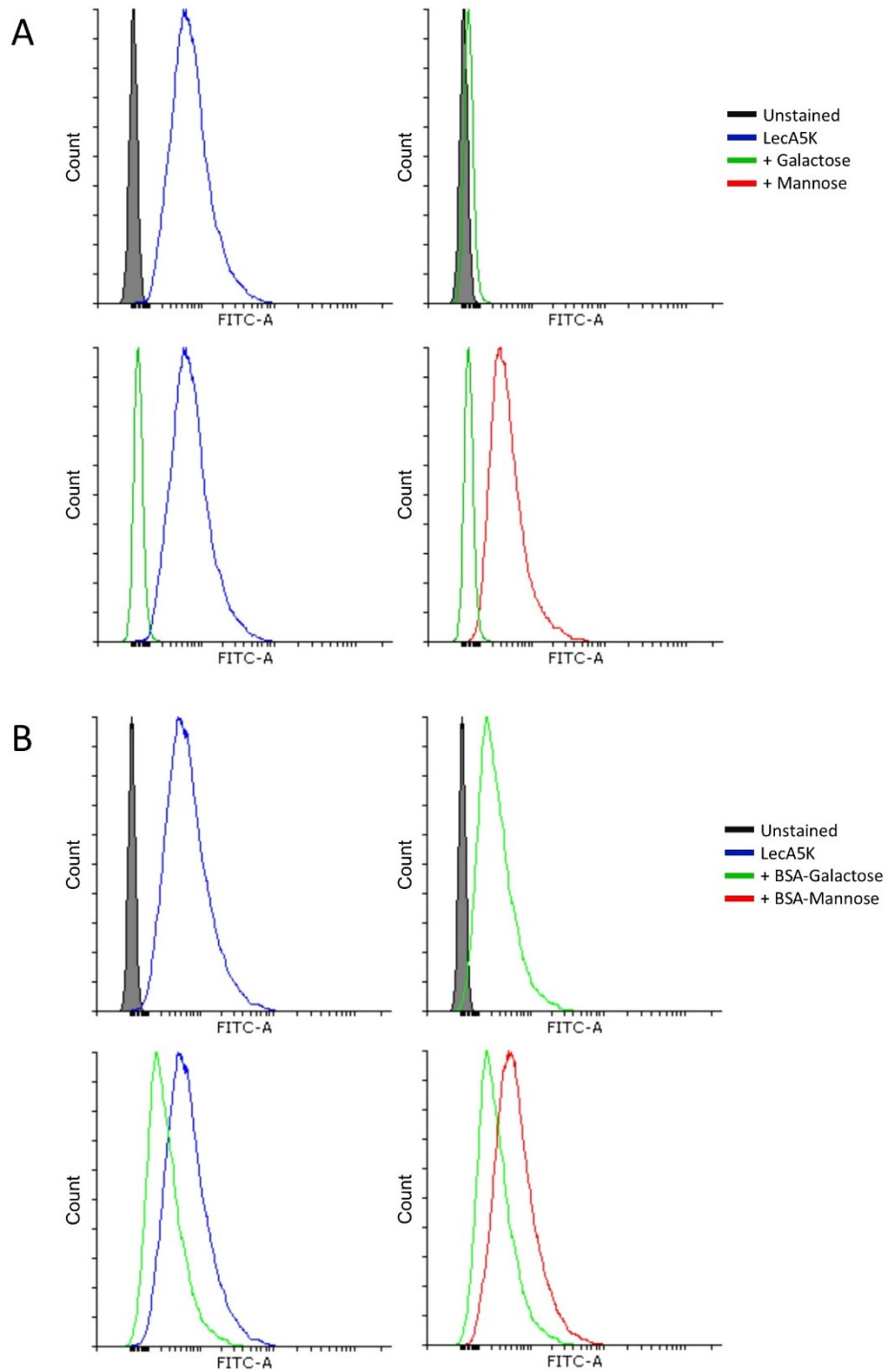


Fig. 5.12: LecA5K inhibition check with competitive/non-competitive monosaccharides. A) Overlay histograms of suspension adapted CHO DP-12 cells probed with recombinant LecA5K with 100 mM galactose or 100 mM mannose. B) Overlay histograms of suspension adapted CHO DP-12 cells probed with recombinant LecA5K with 5 μg/mL BSA-galactose or 5 μg/mL BSA-mannose.

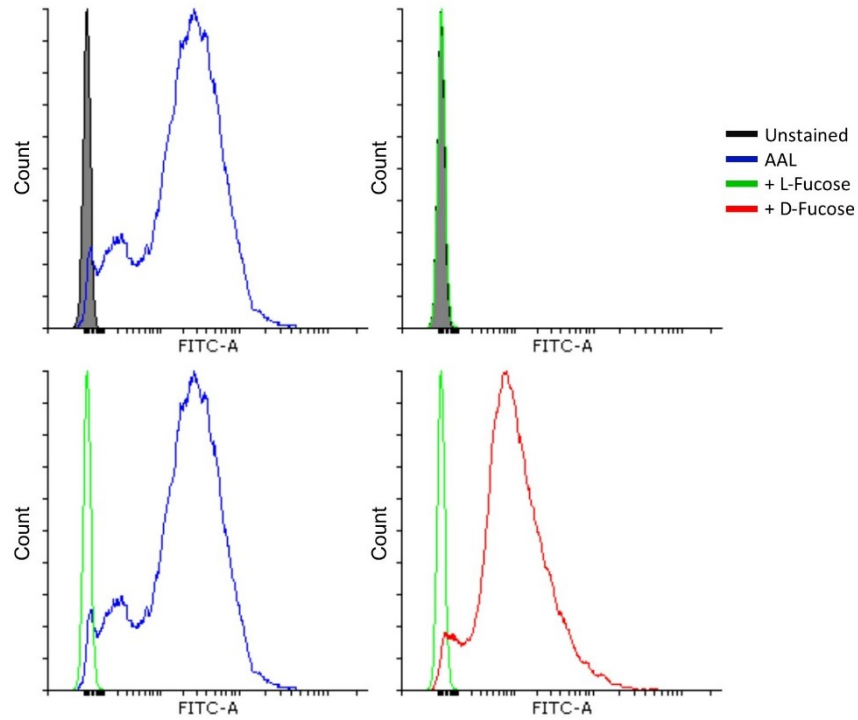


Fig. 5.13: AAL inhibition check with competitive/non-competitive monosaccharides. Overlay histograms of suspension adapted CHO DP-12 cells probed with AAL with 200 mM L-fucose or 200 mM D-fucose.

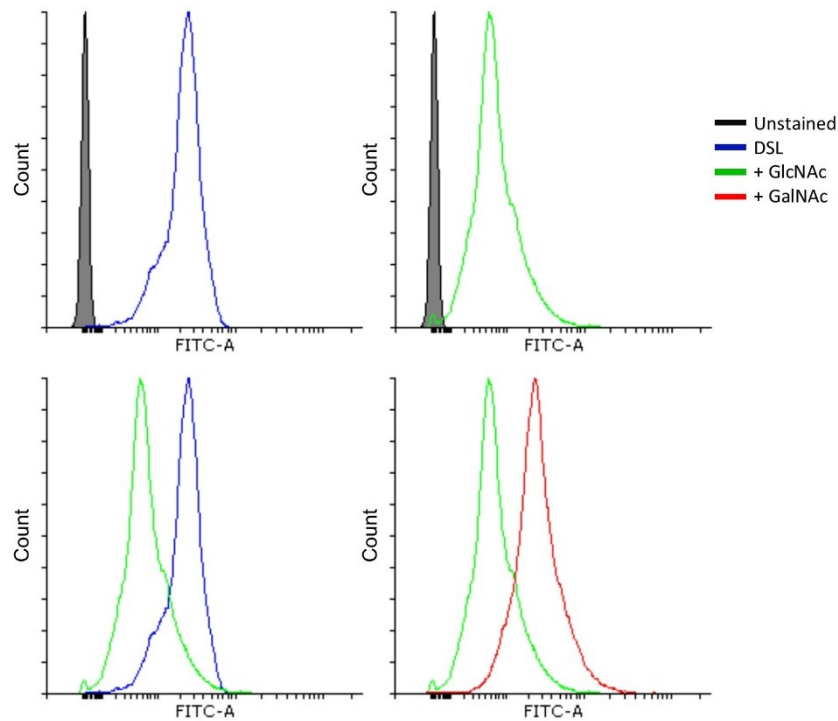


Fig. 5.14: DSL inhibition check with competitive/non-competitive monosaccharides. Overlay histograms of suspension adapted CHO DP-12 cells probed with DSL with 400 mM GlcNAc or 400 mM GalNAc.

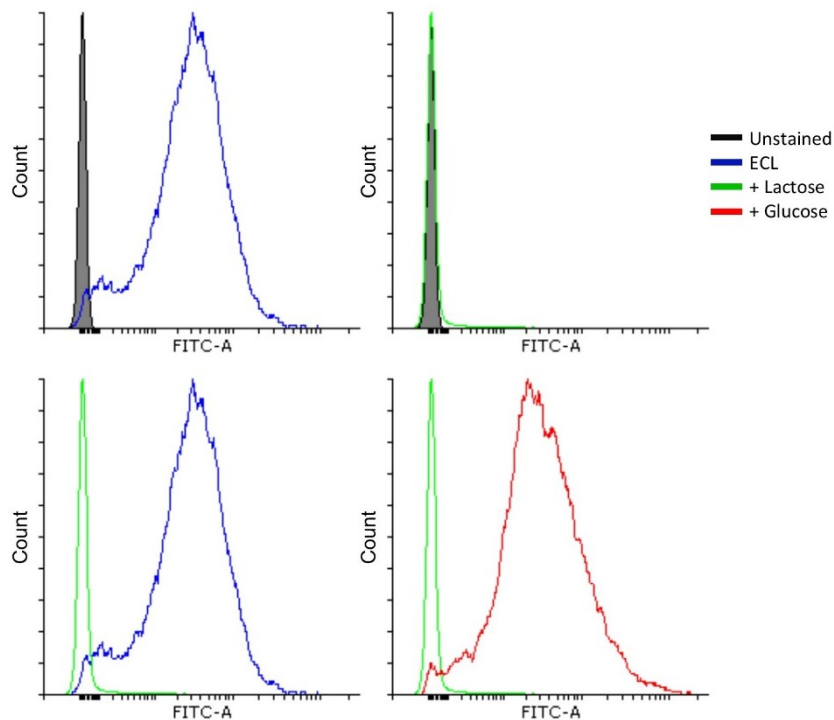


Fig. 5.15: ECL inhibition check with competitive/non-competitive monosaccharides. Overlay histograms of suspension adapted CHO DP-12 cells probed with ECL with 200 mM lactose or 200 mM glucose.

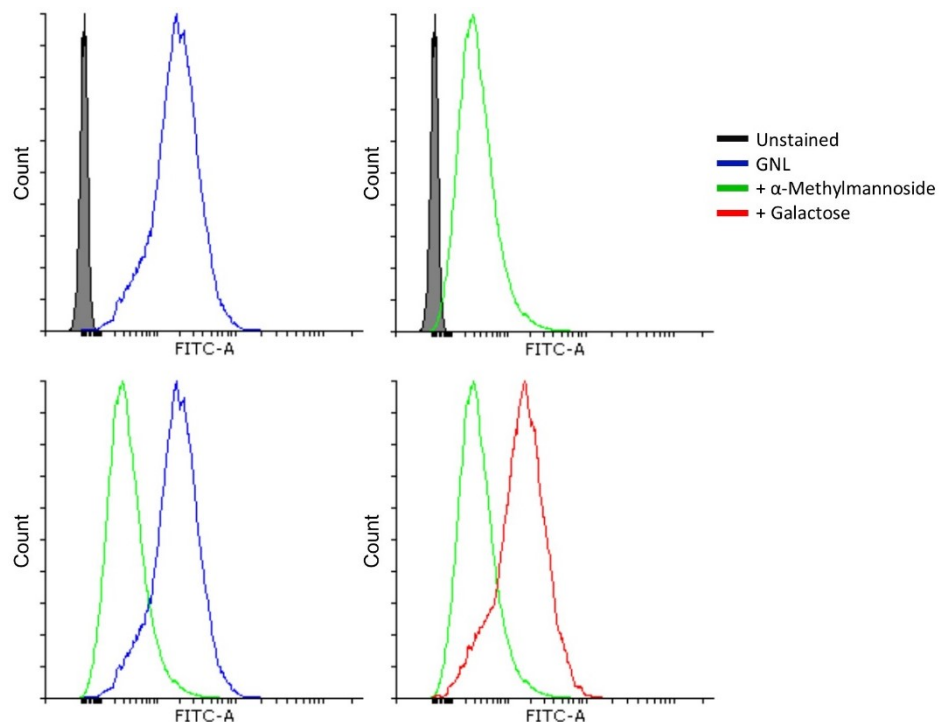


Fig. 5.16: GNL inhibition check with competitive/non-competitive monosaccharides. Overlay histograms of suspension adapted CHO DP-12 cells probed with GNL with 200 mM α -methylmannoside or 200 mM galactose.

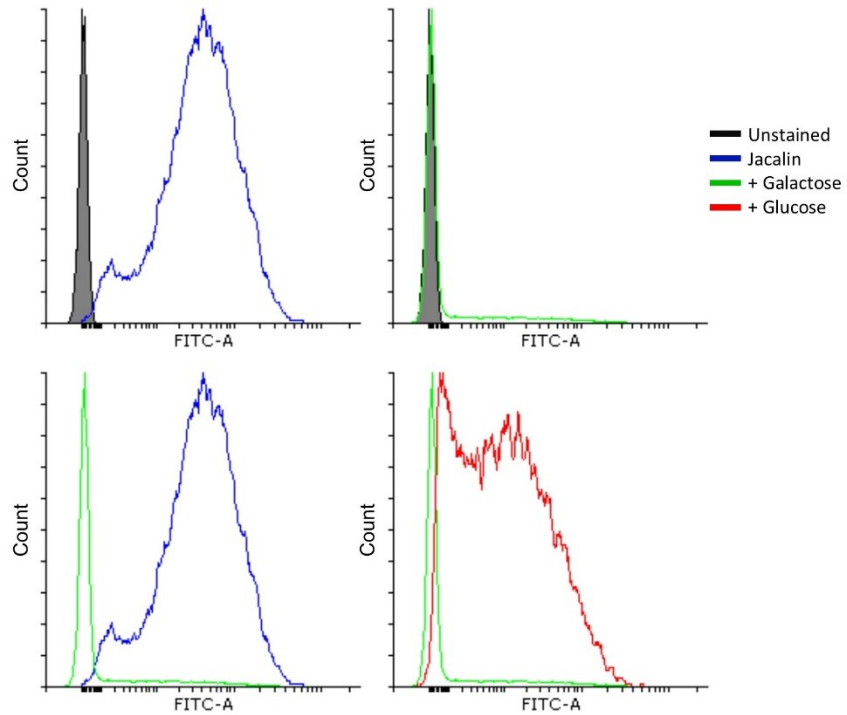


Fig. 5.17: Jacalin inhibition check with competitive/non-competitive monosaccharides. Overlay histograms of suspension adapted CHO DP-12 cells probed with Jacalin with 800 mM galactose or 800 mM glucose.

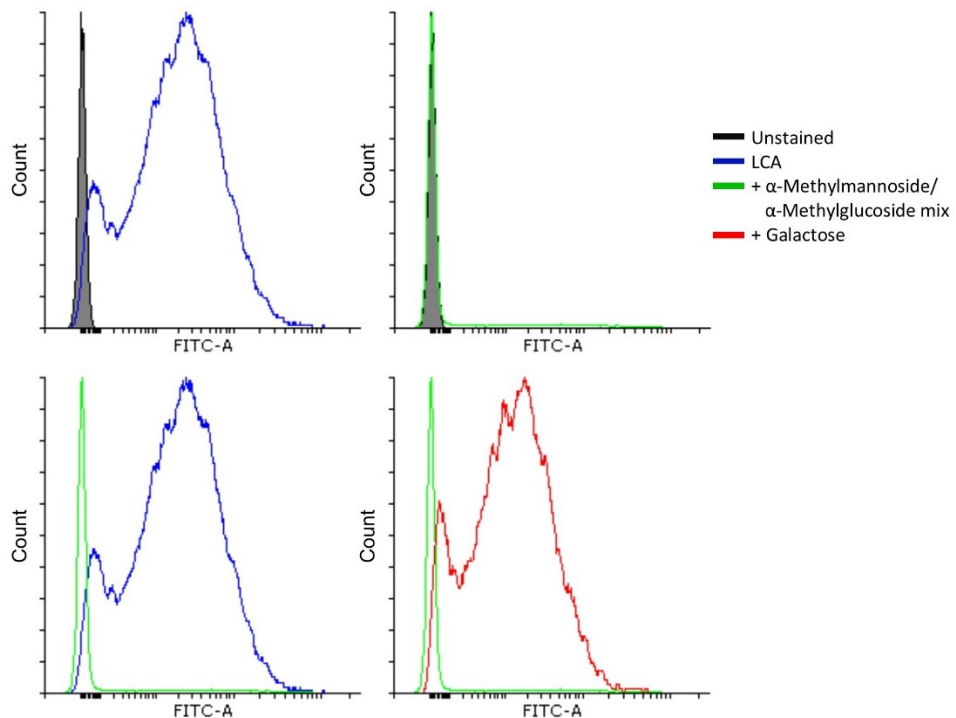


Fig. 5.18: LCA inhibition check with competitive/non-competitive monosaccharides. Overlay histograms of suspension adapted CHO DP-12 cells probed with LCA with 200 mM α -methylmannoside/ α -methylglucoside mix or 200 mM galactose.

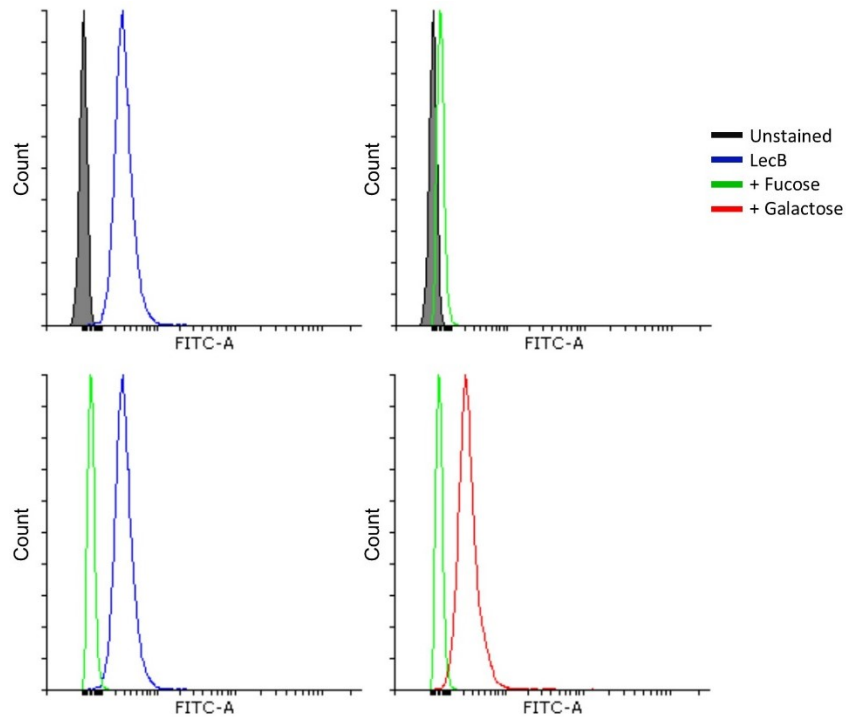


Fig. 5.19: LecB inhibition check with competitive/non-competitive monosaccharides. Overlay histograms of suspension adapted CHO DP-12 cells probed with LecB with 200 mM fucose or 200 mM galactose.

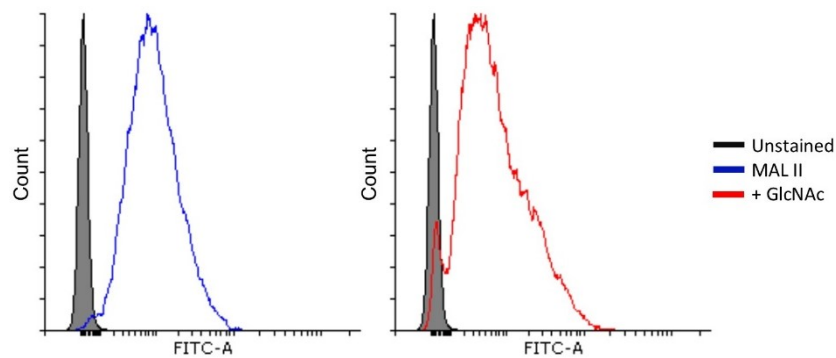


Fig. 5.20: MAL II inhibition check with non-competitive monosaccharide. Overlay histograms of suspension adapted CHO DP-12 cells probed with sialic acid binding MAL II with 200 mM GlcNAc.

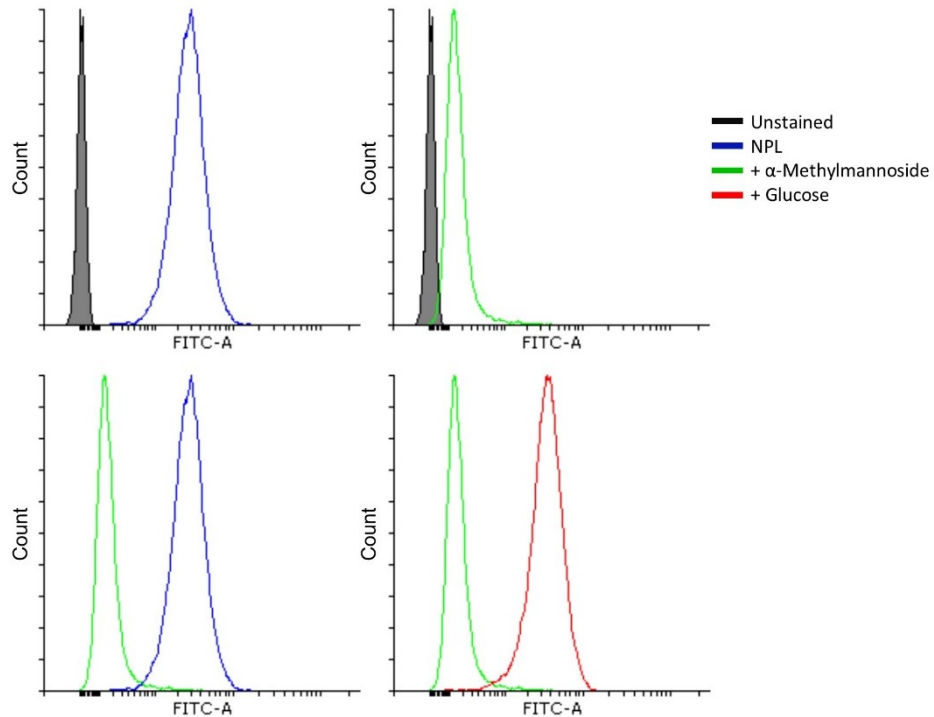


Fig. 5.21: NPL inhibition check with competitive/non-competitive monosaccharides. Overlay histograms of suspension adapted CHO DP-12 cells probed with NPL with 400 mM α -methylmannoside or 400 mM glucose.

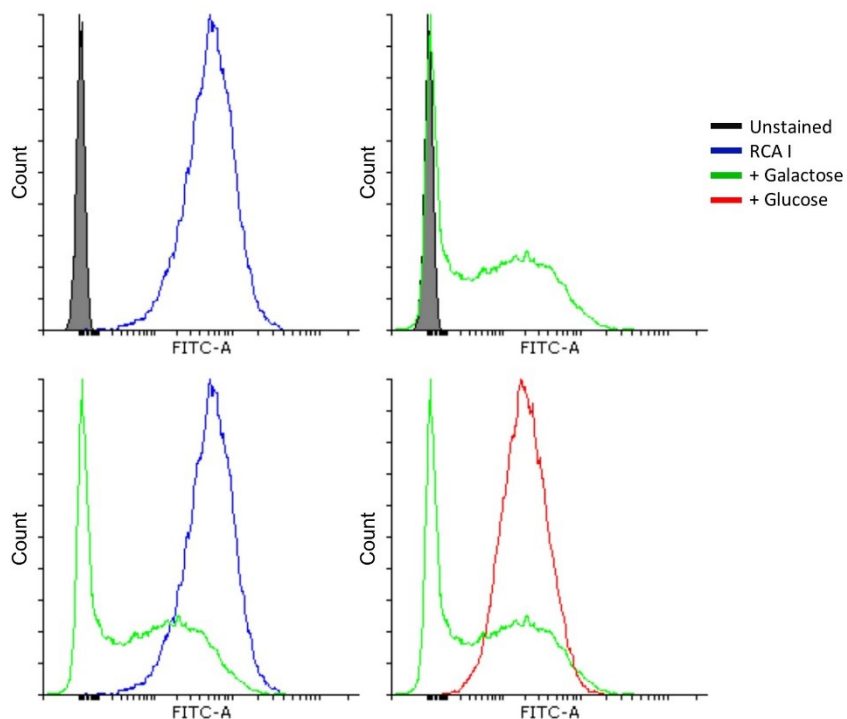


Fig. 5.22: RCA I inhibition check with competitive/non-competitive monosaccharides. Overlay histograms of suspension adapted CHO DP-12 cells probed with RCA I with 200 mM galactose or 200 mM glucose.

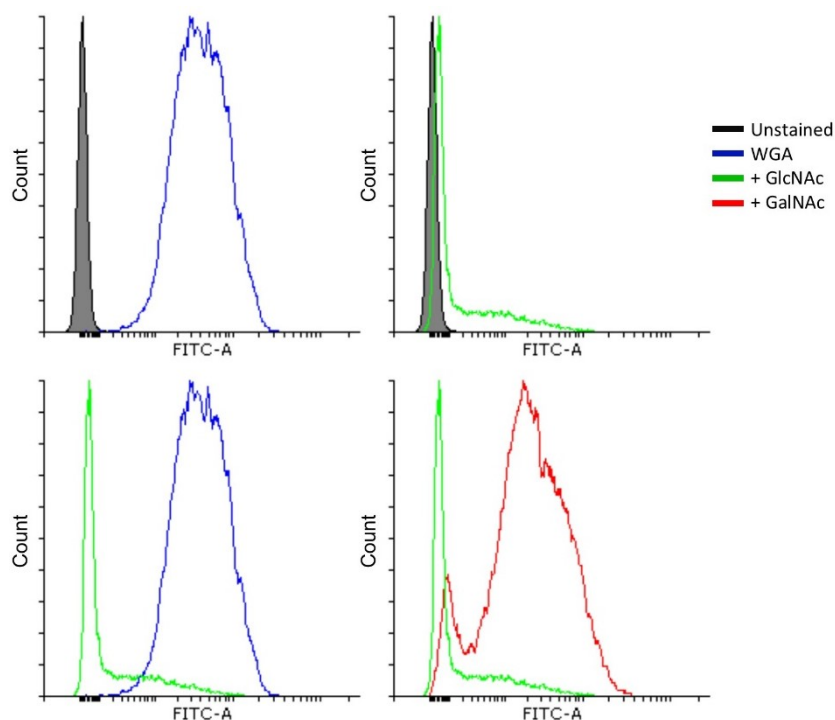


Fig. 5.23: WGA inhibition check with competitive/non-competitive monosaccharides. Overlay histograms of suspension adapted CHO DP-12 cells probed with WGA with 400 mM GlcNAc or 400 mM GalNAc.

These lectin inhibition studies demonstrate the specificity of lectin binding and how similar monosaccharides are distinguished. For many lectins, binding was not reduced in the presence of non-competitive monosaccharides. This was observed for LecA5K, AAL, DSL, ECL, GNL, LCA, LecB, MAL II, NPL and RCA I. When AAL-2, Jacalin and WGA were mixed with a non-competitive free monosaccharide, reduced binding was observed. For AAL-2, see Fig. 5.9, each GlcNAc concentration tested, 12.5 mM to 100 mM, fully inhibited binding. Free GalNAc also inhibited AAL-2 although to a lesser extent. Additional AAL-2 inhibition studies were completed with BSA-linked monosaccharides to further assess its binding, see Fig. 5.10. AAL-2 binding was reduced with BSA-GlcNAc but not with BSA-GalNAc. Jacalin was inhibited with 0.8 M galactose, see Fig. 5.17, but its epimer, glucose, did not exhibit a similar effect. MAL II is a sialic acid binding lectin. Sialic acid was not used to demonstrate the specificity of MAL II binding as its low pH leads to cell death. However, MAL II binding was not compromised with the addition of 200 mM GlcNAc, see Fig. 5.20.

5.10 Effect of spent medium on CHO DP-12 cell surface glycosylation

The composition of culture medium may severely affect cell growth, protein synthesis and protein glycosylation (Hossler et al. 2009). This was discussed at length in the introduction chapter, see Section 1.11.2. CHO DP-12 suspension adapted cells were treated with nutrient depleted medium and probed with a panel of lectins. The objective of this experiment was to determine if lectin binding differences between treated and untreated cells are observed prior to assessing specific cell culture medium changes, e.g. glutamine free medium. Spent medium was collected from CHO DP-12 suspension cultures on day 9 (1×10^7 viable cells/mL) which had been seeded at 3×10^5 viable cells/mL. These cultures were at the end of stationary growth phase but still viable, > 97 %, as determined by the trypan blue exclusion method, see Section 2.27.4.

5 mL CHO DP-12 suspension cultures, 4×10^6 viable cells/mL, were centrifuged at 250 g for 5 min to pellet the cells. The supernatant was removed and the cells were resuspended in spent medium. Following a 24 h incubation period, cells were probed with a panel of lectins and analysed by flow cytometry. After this 24 h spent medium treatment, additional cells were reseeded back into fresh fully supplemented suspension medium, as described in Section 2.4, and incubated for 72 h. Following this, cells were again probed with a panel of lectins and analysed by flow cytometry. The result of this experiment is summarised in Table 5.3.

Table 5.3: Comparison of MFI from lectin binding suspension adapted CHO DP-12 cells treated and untreated with spent medium

10,000 events recorded for each sample in triplicate, average tabulated. Full data shown in Appendix H. Cells were treated for 24 h with spent medium and probed with lectins. Additional cells were reseeded in fresh medium after treatment and analysed after 72 h.

Lectin	Untreated	Treated 24 h	% MFI change	Untreated	Treated 24 h + 72 h	% MFI change
Unstained	6.81	6.05	-11.14	3.99	3.66	-8.31
AAL	1498.92	1095.44	-26.92	1525.26	1042.34	-31.66
AAL-2	2016.01	1402.25	-30.44	2040.63	1569.21	-23.10
DSL	1668.68	1331.32	-20.22	2001.95	1765.73	-11.80
ECL	2480.32	1912.61	-22.89	3315.81	2652.74	-20.00
GSL I B4	37.04	138.33	273.50	48.42	54.77	13.11
HPA	41.50	138.76	234.40	23.86	22.33	-6.42
Jacalin	3129.16	2208.09	-29.44	6905.70	4640.08	-32.81
LCA	2706.31	1851.73	-31.58	1748.40	1186.68	-32.13
LecA5K	366.04	1204.50	229.07	537.78	711.17	32.24
MAL II	1211.61	681.03	-43.79	1284.44	1060.89	-17.40
PNA	283.40	2498.44	781.58	185.97	223.61	20.24
RCA I	3515.66	2817.95	-19.85	6432.83	5589.53	-13.11
SBA	93.08	793.48	752.48	277.81	229.27	-17.47
WGA	6315.45	4565.84	-27.70	6944.84	6162.94	-11.26

Fig. 5.24 to Fig. 5.31 display histograms and bar charts of relative MFI values for cells probed with recombinant AAL-2, recombinant LecA5K, MAL II and PNA which are specific for GlcNAc, Gal, α 2-3-NeuNAc and β 1-3-GalNAc respectively. Relative MFI values are calculated from normalising the untreated MFI value to 1. Additional data can be found in Appendix H.

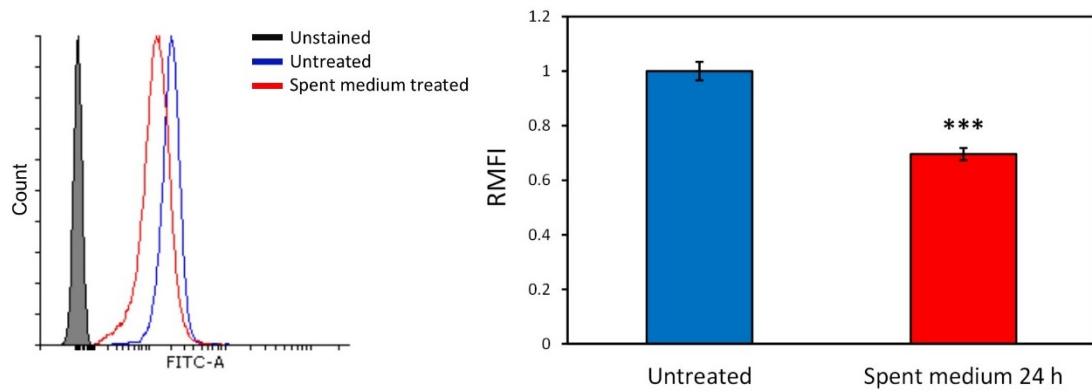


Fig. 5.24: CHO DP-12 cells probed with AAL-2 following spent medium treatment. Overlay histogram and corresponding bar chart of RMFI of suspension CHO DP-12 cells probed with recombinant AAL-2 after a 24 h treatment with 9-day spent medium. A 30.44 % reduction in AAL-2 binding was observed and found to be statistically significant as determined by a standard Student's *t*-test, (p-value < 0.001, n=3).

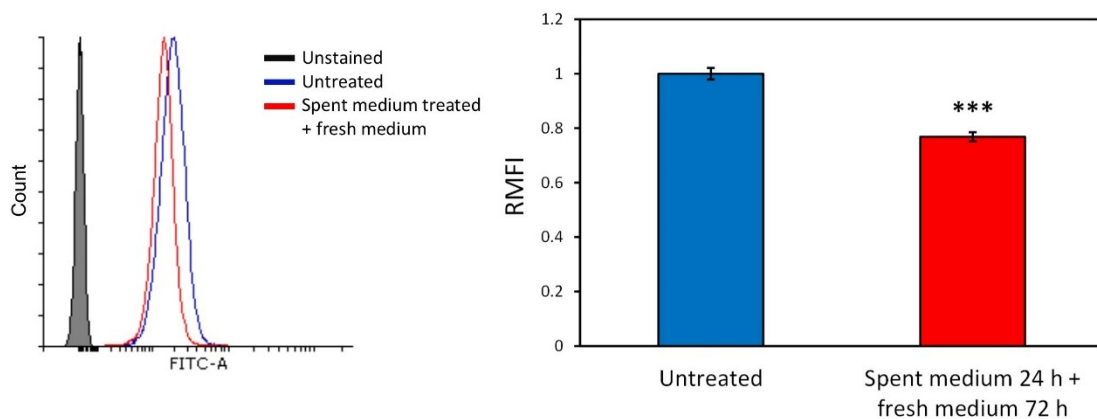


Fig. 5.25: CHO DP-12 cells probed with AAL-2 after spent medium and fresh medium treatments. Overlay histogram and corresponding bar chart of RMFI of suspension CHO DP-12 cells probed with recombinant AAL-2 after a 24 h treatment with 9-day spent medium followed by a 72 h fresh medium treatment. A 23.10 % reduction in AAL-2 binding was observed and found to be statistically significant as determined by a standard Student's *t*-test, (p-value < 0.001, n=3).

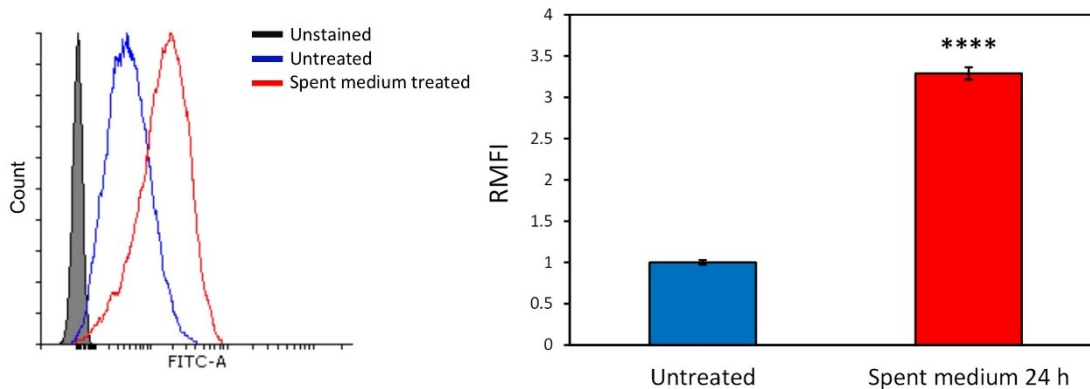


Fig. 5.26: CHO DP-12 cells probed with LecA5K following spent medium treatment. Overlay histogram and corresponding bar chart of RMFI of suspension CHO DP-12 cells probed with recombinant LecA5K after a 24 h treatment with 9-day spent medium. A 229 % increase in LecA5K binding was observed and found to be statistically significant as determined by a standard Student's *t*-test, (p-value < 0.0001, n=3).

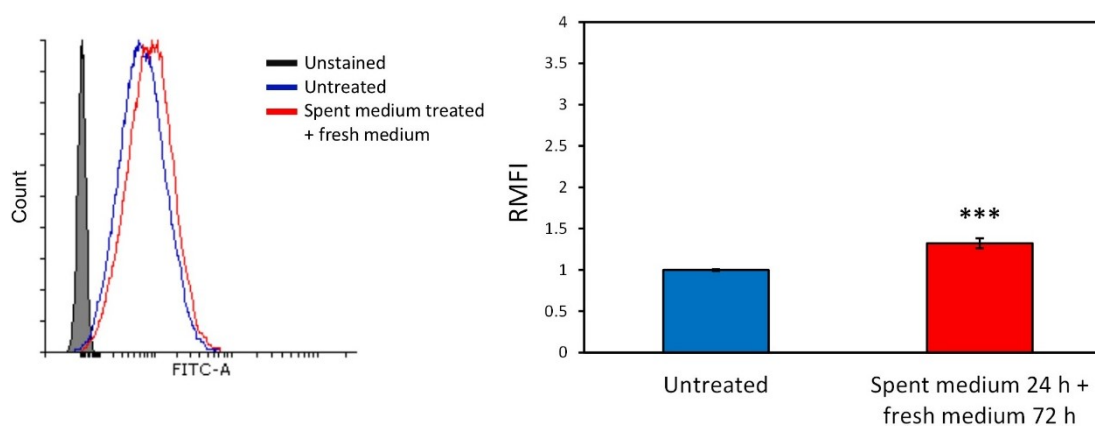


Fig. 5.27: CHO DP-12 cells probed with LecA5K after spent medium and fresh medium treatments. Overlay histogram and corresponding bar chart of RMFI of suspension CHO DP-12 cells probed with recombinant LecA5K after a 24 h treatment with 9-day spent medium followed by a 72 h fresh medium treatment. A 32.24 % increase in LecA5K binding was observed and found to be statistically significant as determined by a standard Student's *t*-test, (p-value < 0.001, n=3).

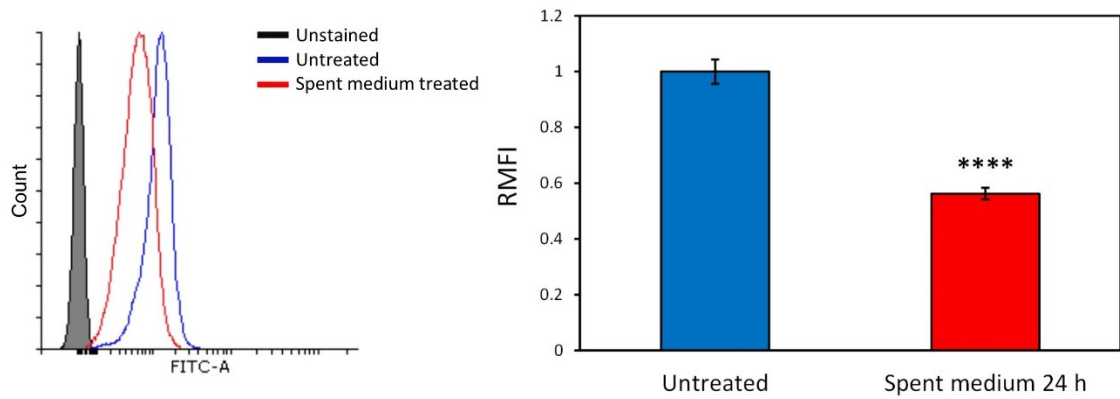


Fig. 5.28: CHO DP-12 cells probed with MAL II following spent medium treatment. Overlay histogram and corresponding bar chart of RMFI of suspension CHO DP-12 cells probed with MAL II after a 24 h treatment with 9-day spent medium. A 43.79 % reduction in MAL II binding was observed and found to be statistically significant as determined by a standard Student's *t*-test, (p-value < 0.0001, n=3).

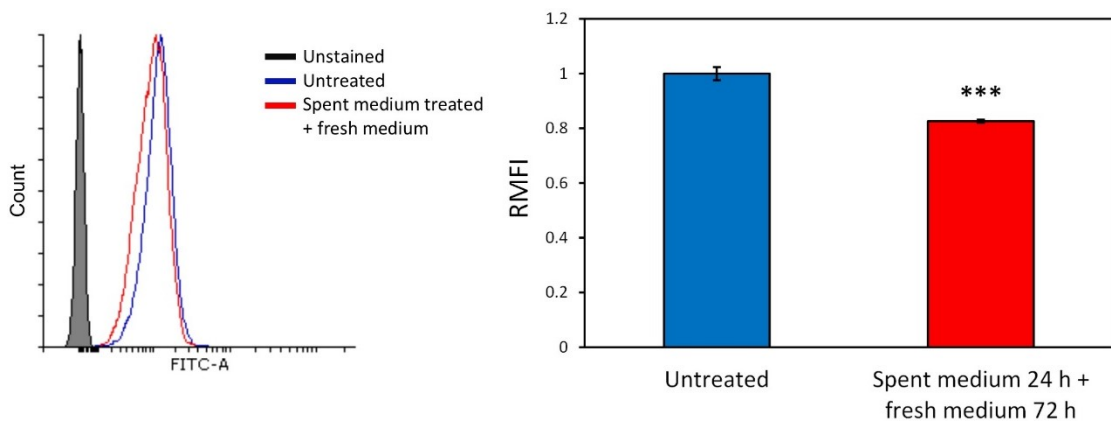


Fig. 5.29: CHO DP-12 cells probed with MAL II after spent medium and fresh medium treatments. Overlay histogram and corresponding bar chart of RMFI of suspension CHO DP-12 cells probed with MAL II after a 24 h treatment with 9-day spent medium followed by a 72 h fresh medium treatment. A 17.4 % reduction in MAL II binding was observed and found to be statistically significant as determined by a standard Student's *t*-test, (p-value < 0.001, n=3).

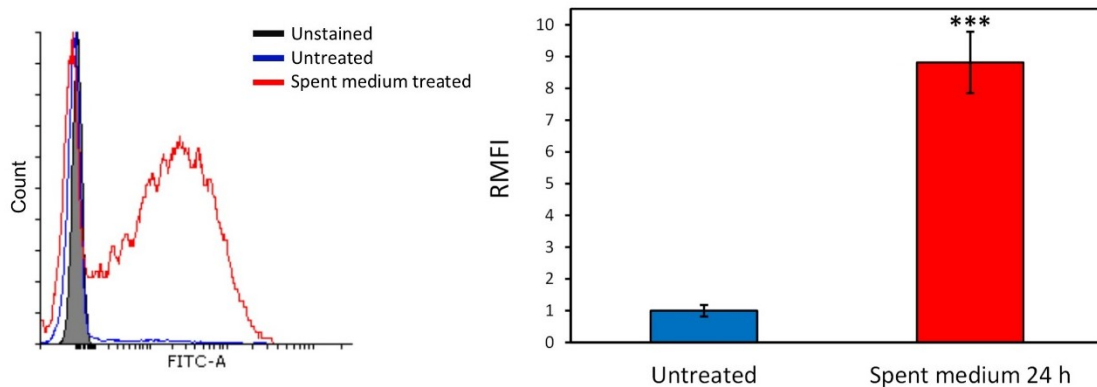


Fig. 5.30: CHO DP-12 cells probed with PNA following spent medium treatment. Overlay histogram and corresponding bar chart of RMFI of suspension CHO DP-12 cells probed with PNA after a 24 h treatment with 9-day spent medium. A 781 % increase in PNA binding was observed and found to be statistically significant as determined by a standard Student's *t*-test, (p-value < 0.001, n=3).

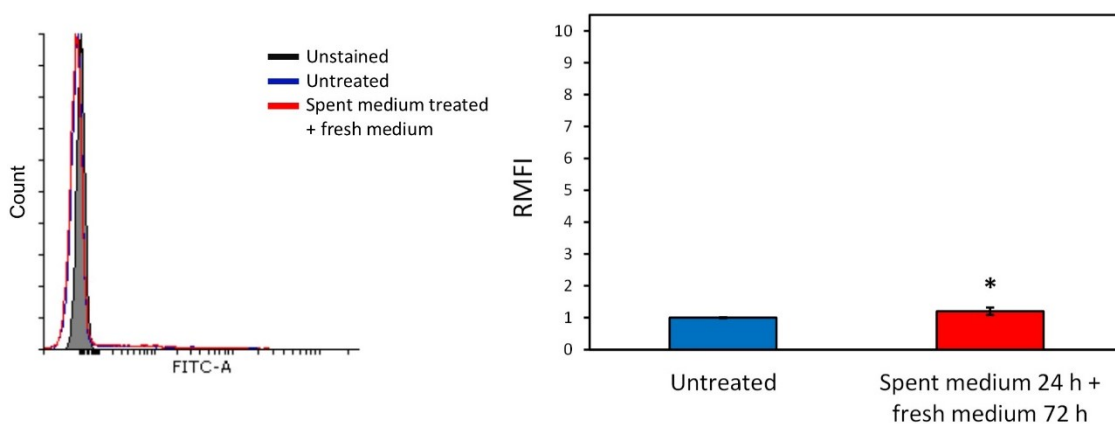


Fig. 5.31: CHO DP-12 cells probed with PNA after spent medium and fresh medium treatments. Overlay histogram and corresponding bar chart of RMFI of suspension CHO DP-12 cells probed with PNA after a 24 h treatment with 9-day spent medium followed by a 72 h fresh medium treatment. A 20.24 % increase in PNA binding was observed and found to be statistically significant as determined by a standard Student's *t*-test, (p-value < 0.05, n=3).

Significant lectin binding differences were observed between spent medium treated and untreated cells, e.g. PNA binding increased over 700 %. Other lectins which had increased binding included GSL I B4, HPA, recombinant LecA5K, and SBA. The remaining lectins all had decreased binding to treated cells, see Table 5.3. A regression back to MFI values more similar to those of untreated cells was observed when the cells

were incubated with fresh medium following spent medium treatment, e.g. LecA5K, PNA and WGA. The large increase in binding observed from the galactophilic lectins LecA5K and PNA was nearly fully reversed when the cells were reseeded in fresh medium. An increase in terminal galactose should coincide with a decrease in terminal sialic acid on glycans on the cell surface. This was observed as MAL II binding decreased after spent medium treatment. These results show that nutrient depleted medium can influence cell surface glycosylation. In the following sections a single parameter in cell culture growth medium is altered at a time.

5.11 Effect of reduced L-glutamine on CHO DP-12 cell surface glycosylation

The impact of nutrient depleted medium on cell surface glycosylation was presented in the previous section which established that glycosylation changes do occur when cells are nutrient deprived but also that they are detectable by lectins. In this section a single cell culture medium parameter, glutamine concentration, was altered. L-Glutamine depletion has been previously linked with altered glycosylation on recombinant proteins, see introductory Section 1.11.2. During the development of tissue culture medium in the 1950s, L-glutamine was required at 10- to 100-fold in excess of other amino acids for cell survival and proliferation *in vitro* (Newsholme et al. 2003).

Irvine Scientific, which supply chemically-defined medium optimised for the production of recombinant proteins in CHO, recommend a 4-8 mM L-glutamine concentration in culture (IrvineSci 2017). Their BalanCD CHO Growth A Medium was used supplemented with 4 mM L-glutamine as described in Section 2.4. The supernatant was removed from 5 mL CHO DP-12 suspension cultures (4×10^6 viable cells/mL) and the cells were resuspended in fresh glutamine free medium, as described in Section 2.4. Following a 48 h incubation period, cells were probed with a panel of lectins and analysed by flow cytometry. After this 48 h glutamine free treatment, additional cells were reseeded back into fresh fully supplemented suspension medium with glutamine (4 mM), as described in Section 2.4, and incubated for 72 h. Following this, cells were

again probed with a panel of lectins and analysed by flow cytometry. The result of this experiment is summarised in Table 5.4

Table 5.4: Comparison of MFI from lectin binding suspension adapted CHO DP-12 cells treated and untreated with L-glutamine free medium

10,000 events recorded for each sample in triplicate, average tabulated. Full data shown in Appendix I. Cells were treated for 48 h with L-glutamine free medium (0 mM) and probed with lectins. Additional cells were reseeded in fresh medium (4 mM L-glut) after treatment and analysed after 72 h.

Lectin	Untreated	Treated 48 h	% MFI change	Untreated	Treated 24 h + 72 h	% MFI change
Unstained	4.50	6.53	45.10	5.56	4.54	-18.36
AAL	899.48	937.45	4.22	1221.45	1042.88	-14.62
AAL-2	1939.73	2324.82	19.85	2058.33	1567.19	-23.86
DSL	1334.09	1475.33	10.59	1624.07	1284.02	-20.94
ECL	3926.23	3995.16	1.76	3193.44	2130.32	-33.29
GafD1-178	23.91	25.55	6.85	21.23	23.03	8.48
GNL	1432.46	1707.87	19.23	1373.28	1221.94	-11.02
GSL I B4	223.96	681.36	204.23	91.80	40.97	-55.37
HPA	243.35	346.92	42.56	24.90	23.21	-6.79
Jacalin	5209.20	4075.47	-21.76	3952.75	2373.98	-39.94
LCA	4335.50	4212.26	-2.84	3225.37	2550.14	-20.94
LecA5K	1279.07	3712.31	190.23	287.95	363.09	26.10
LecB	540.76	649.80	20.16	129.78	135.87	4.69
MAL II	1104.36	1077.16	-2.46	1075.88	963.32	-10.46
NPL	811.28	1002.86	23.61	3376.25	2890.63	-14.38
PNA	944.25	2375.86	151.61	142.43	206.01	44.65
RCA I	4915.97	5052.18	2.77	4472.31	3716.28	-16.90
SBA	854.50	813.35	-4.82	772.63	713.75	-7.62
WGA	5541.35	5445.93	-1.72	6095.27	6651.32	9.12

Fig. 5.32 to Fig. 5.39 display histograms and bar charts of relative MFI values for cells probed with recombinant LecA5K, MAL II, PNA and RCA I. Additional data can be found in Appendix I.

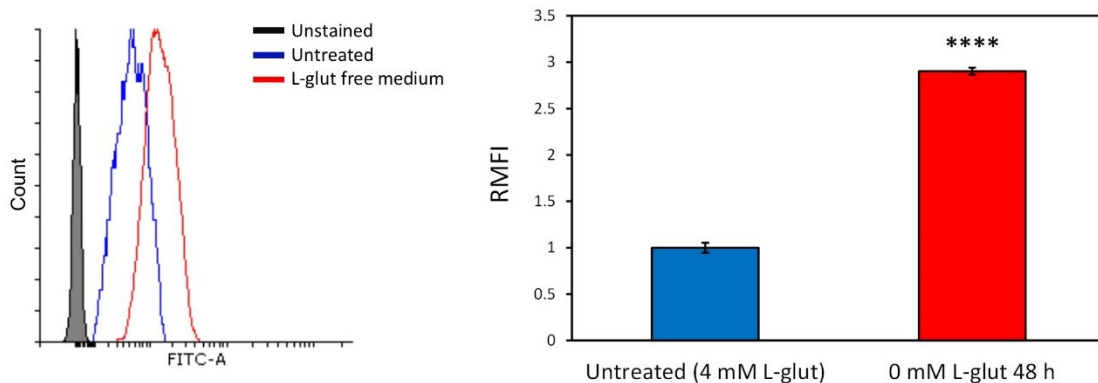


Fig. 5.32: CHO DP-12 cells probed with LecA5K following L-glutamine free medium treatment. Overlay histogram and corresponding bar chart of RMFI of suspension CHO DP-12 cells probed with recombinant LecA5K after a 48 h treatment with L-glutamine free (0 mM) medium. A 190 % increase in LecA5K binding was observed and found to be statistically significant as determined by a standard Student's *t*-test, (p-value < 0.0001, n=3).

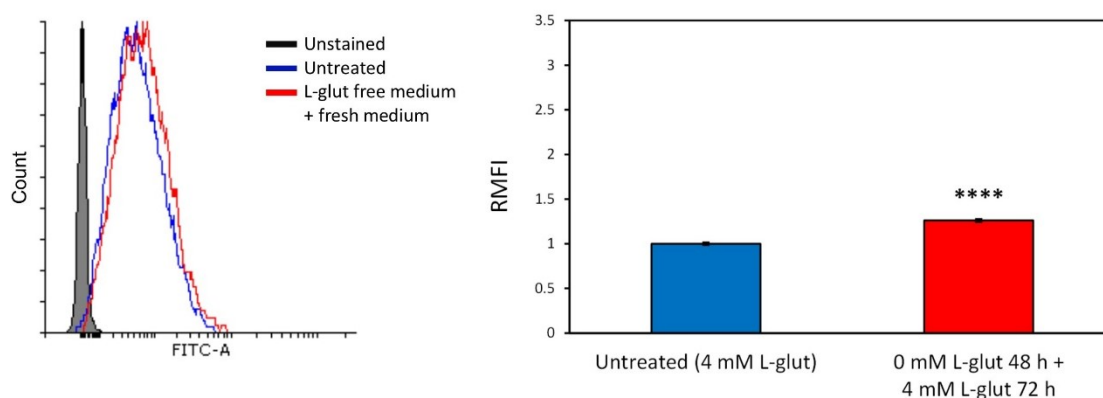


Fig. 5.33: CHO DP-12 cells probed with LecA5K following L-glutamine free medium and fresh medium treatments. Overlay histogram and corresponding bar chart of RMFI of suspension CHO DP-12 cells probed with recombinant LecA5K after a 48 h treatment with L-glutamine free (0 mM) medium followed by a 72 h fresh medium treatment (4 mM L-glut). A 26.10 % increase in LecA5K binding was observed and found to be statistically significant as determined by a standard Student's *t*-test, (p-value < 0.0001, n=3).

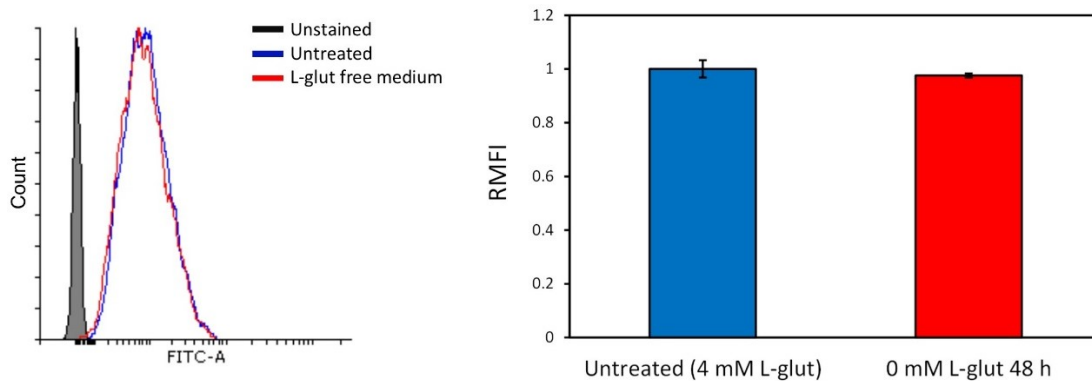


Fig. 5.34: CHO DP-12 cells probed with MAL II following L-glutamine free medium treatment. Overlay histogram and corresponding bar chart of RMFI of suspension CHO DP-12 cells probed with MAL II after a 48 h treatment with L-glutamine free (0 mM) medium. A 2.46 % decrease in MAL II binding was observed and found to be statistically insignificant as determined by a standard Student's *t*-test, (p -value > 0.05, $n=3$).

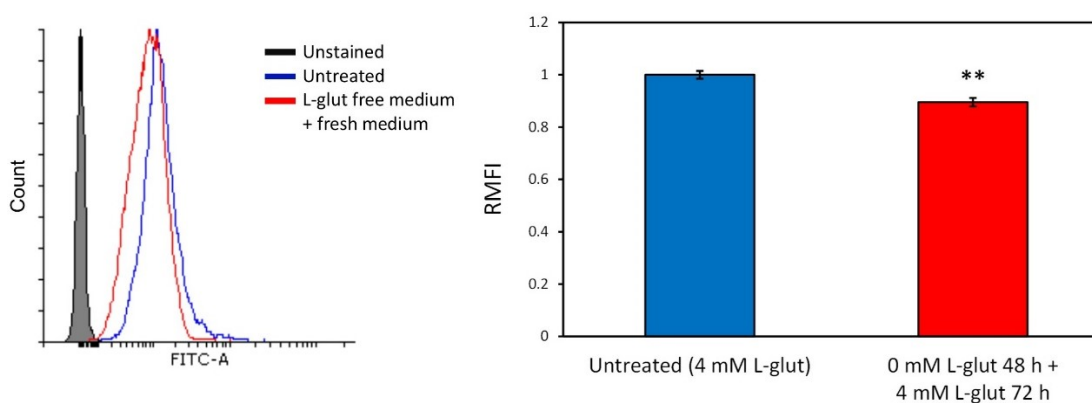


Fig. 5.35: CHO DP-12 cells probed with MAL II following L-glutamine free medium and fresh medium treatments. Overlay histogram and corresponding bar chart of RMFI of suspension CHO DP-12 cells probed with MAL II after a 48 h treatment with L-glutamine free (0 mM) medium followed by a 72 h fresh medium treatment (4 mM L-glut). A 10.46 % decrease in MAL II binding was observed and found to be statistically significant as determined by a standard Student's *t*-test, (p -value < 0.01, $n=3$).

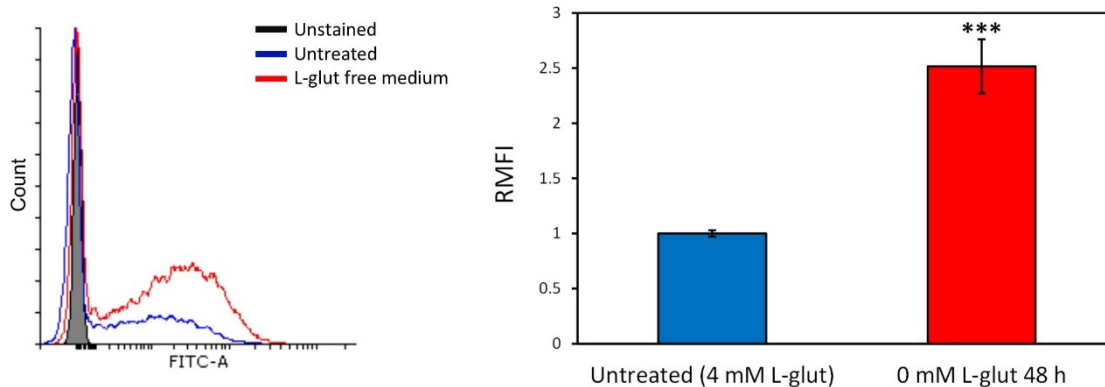


Fig. 5.36: CHO DP-12 cells probed with PNA following L-glutamine free medium treatment. Overlay histogram and corresponding bar chart of RMFI of suspension CHO DP-12 cells probed with PNA after a 48 h treatment with L-glutamine free (0 mM) medium. A 151 % increase in PNA binding was observed and found to be statistically significant as determined by a standard Student's *t*-test, (p-value < 0.001, n=3).

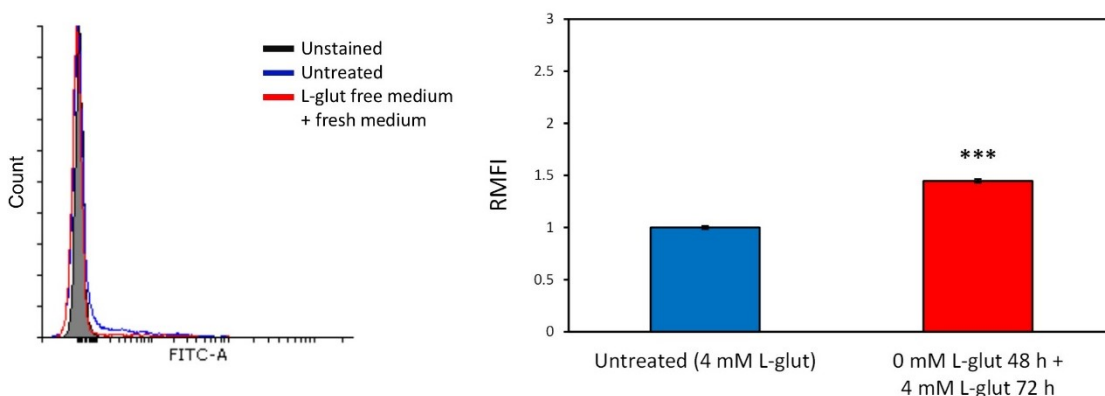


Fig. 5.37: CHO DP-12 cells probed with PNA following L-glutamine free medium and fresh medium treatments. Overlay histogram and corresponding bar chart of RMFI of suspension CHO DP-12 cells probed with PNA after a 48 h treatment with L-glutamine free (0 mM) medium followed by a 72 h fresh medium treatment (4 mM L-glut). A 44.65 % increase in PNA binding was observed and found to be statistically significant as determined by a standard Student's *t*-test, (p-value < 0.001, n=3).

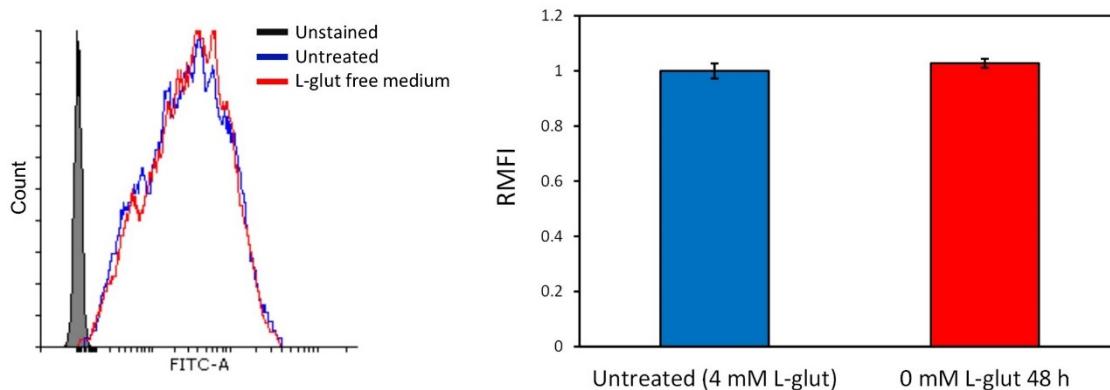


Fig. 5.38: CHO DP-12 cells probed with RCA I following L-glutamine free medium treatment. Overlay histogram and corresponding bar chart of RMFI of suspension CHO DP-12 cells probed with RCA I after a 48 h treatment with L-glutamine free (0 mM) medium. A 2.77 % increase in RCA I binding was observed and found to be statistically insignificant as determined by a standard Student's *t*-test, (p -value > 0.05 , $n=3$).

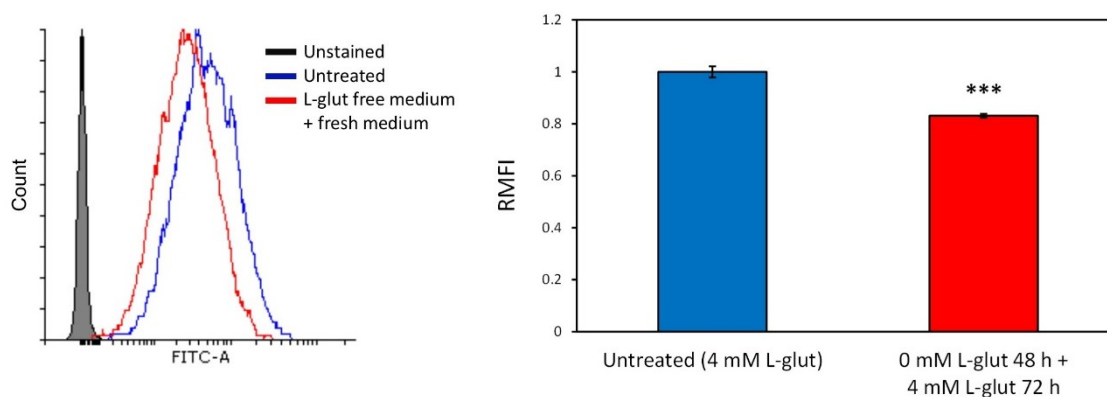


Fig. 5.39: CHO DP-12 cells probed with RCA I following L-glutamine free medium and fresh medium treatments. Overlay histogram and corresponding bar chart of RMFI of suspension CHO DP-12 cells probed with RCA I after a 48 h treatment with L-glutamine free (0 mM) medium followed by a 72 h fresh medium treatment (4 mM L-glut). A 10.46 % decrease in RCA I binding was observed and found to be statistically significant as determined by a standard Student's *t*-test, (p -value < 0.001 , $n=3$).

There was a noticeable increase in LecA5K and PNA binding to cells after 48 h in L-glut free medium, 190 % and 151 %. The change in LecA5K and PNA is similar to what was observed when cells were treated with spent medium. However, many other lectins, such as ECL, LCA, MAL II and RCA, had a delayed change in binding, i.e. little difference after 48 h in L-glut free medium but a greater change observed following an additional 72 h in medium containing L-glut.

5.12 Effect of ammonia on CHO DP-12 cell surface glycosylation

L-Glutamine is an essential component of cell culture medium. However, when metabolised it generates an unwanted by product, ammonia, see introductory Section 1.11.2. One mole of L-glutamine is metabolised to one to two moles of ammonia. Ammonia may alter glycosylation by increasing the cellular pH and decreasing glycosyltransferase efficiency. To investigate the effect of ammonia on CHO cell surface glycosylation, cells from 5 mL CHO DP-12 suspension cultures (4×10^6 viable cells/mL) were pelleted and resuspended in fresh medium, as described in Section 2.4, spiked with 10 mM ammonium chloride (NH_4Cl). Following a 48 h incubation period, cells were probed with a panel of lectins and analysed by flow cytometry. After this ammonium treatment additional cells were reseeded back into fresh fully supplemented suspension medium without ammonium, as described in Section 2.4, and incubated for 72 h. Following this, cells were again probed with a panel of lectins and analysed by flow cytometry. The result of this experiment is summarised in Table 5.5.

Table 5.5: Comparison of MFI from lectin binding suspension adapted CHO DP-12 cells treated and untreated with 10 mM NH₄Cl

10,000 events recorded for each sample in triplicate, average tabulated. Full data shown in Appendix J. Cells were treated for 48 h with NH₄Cl spiked medium (10 mM) and probed with lectins. Additional cells were reseeded in fresh medium after treatment and analysed after 72 h.

Lectin	Untreated	Treated 48 h	% MFI change	Untreated	Treated 24 h + 72 h	% MFI change
Unstained	4.53	3.64	-19.52	4.89	4.98	1.79
AAL	971.14	982.48	1.17	1488.98	1083.05	-27.26
AAL-2	1174.58	1218.81	3.77	2259.13	1597.31	-29.30
DSL	1176.74	852.87	-27.52	2086.56	1606.24	-23.02
ECL	1652.74	1765.79	6.84	1823.65	1039.05	-43.02
GafD1-178	59.47	65.82	10.67	16.95	14.50	-14.48
GNL	1453.59	1510.30	3.90	2196.09	1818.02	-17.22
GSL I B4	153.58	172.99	12.64	162.89	84.31	-48.24
HPA	147.76	136.90	-7.35	40.98	31.31	-23.59
Jacalin	2878.45	3141.76	9.15	5302.18	3283.84	-38.07
LCA	3855.91	3325.15	-13.76	3215.87	1822.89	-43.32
LecA5K	1569.28	1352.45	-13.82	1054.54	983.10	-6.77
LecB	544.78	687.47	26.19	124.41	108.22	-13.01
MAL II	1075.82	944.19	-12.24	1154.93	1009.43	-12.60
NPL	2628.84	3652.55	38.94	4281.84	3595.03	-16.04
PNA	894.83	1436.73	60.56	474.78	347.25	-26.86
RCA I	4231.91	3651.48	-13.72	5270.78	4352.19	-17.43
SBA	778.10	864.15	11.06	94.71	99.58	5.14
WGA	4069.84	3827.96	-5.94	7540.77	6964.80	-7.64

Fig. 5.40 to Fig. 5.46 display histograms and bar charts of relative MFI values for cells probed with recombinant AAL-2, LCA and recombinant LecA5K. Additional data can be found in Appendix J.

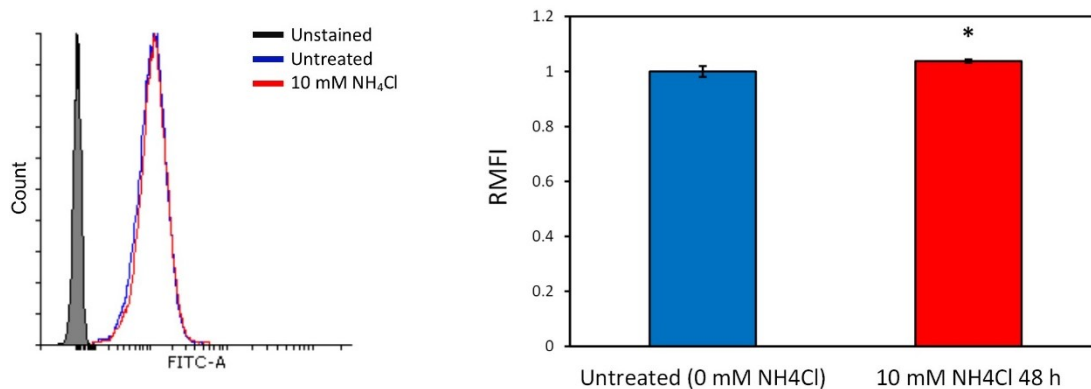


Fig. 5.40: CHO DP-12 cells probed with AAL-2 following NH₄Cl treatment. Overlay histogram and corresponding bar chart of RMFI of suspension CHO DP-12 cells probed with recombinant AAL-2 after a 48 h treatment with medium containing 10 mM NH₄Cl. A 3.77 % increase in AAL-2 binding was observed and found to be statistically significant as determined by a standard Student's *t*-test, (p-value < 0.05, n=3).

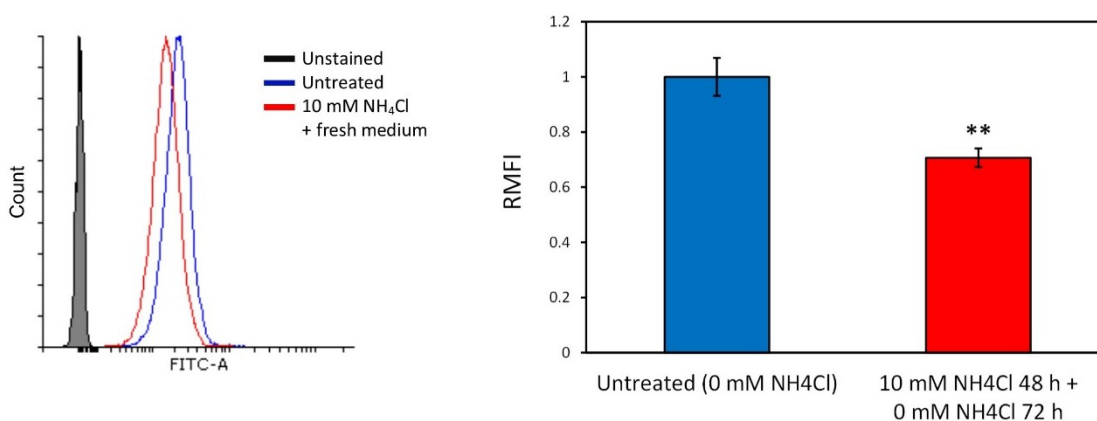


Fig. 5.41: CHO DP-12 cells probed with AAL-2 following NH₄Cl and fresh medium treatments. Overlay histogram and corresponding bar chart of RMFI of suspension CHO DP-12 cells probed with recombinant AAL-2 after a 48 h treatment with medium containing 10 mM NH₄Cl followed by a 72 h fresh medium treatment (0 mM NH₄Cl). A 29.30 % decrease in AAL-2 binding was observed and found to be statistically significant as determined by a standard Student's *t*-test, (p-value < 0.01, n=3).

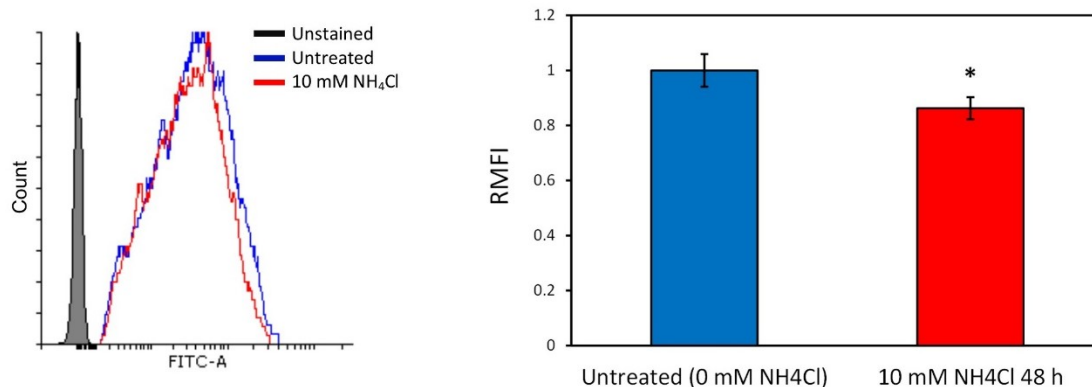


Fig. 5.42: CHO DP-12 cells probed with LCA following NH₄Cl treatment. Overlay histogram and corresponding bar chart of RMFI of suspension CHO DP-12 cells probed with LCA after a 48 h treatment with medium containing 10 mM NH₄Cl. A 13.76 % decrease in LCA binding was observed and found to be statistically significant as determined by a standard Student's *t*-test, (p-value < 0.05, n=3).

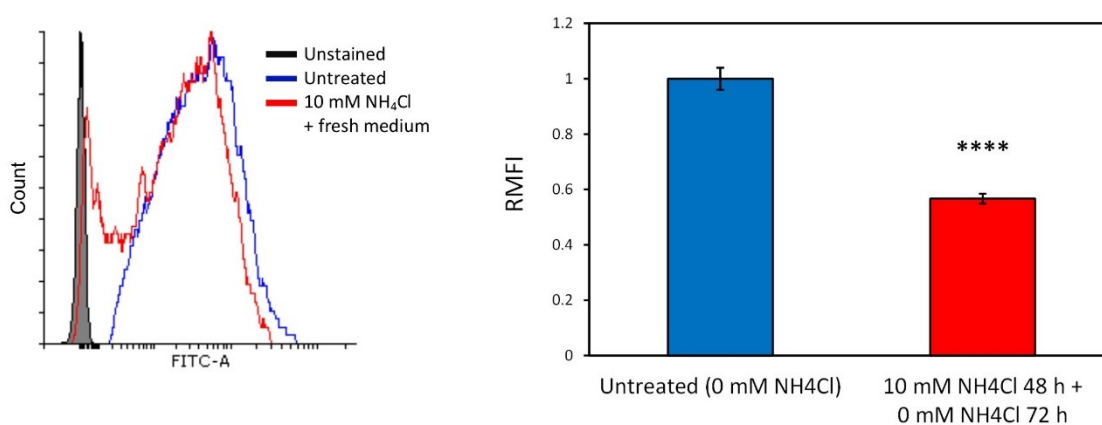


Fig. 5.43: CHO DP-12 cells probed with LCA following NH₄Cl and fresh medium treatments. Overlay histogram and corresponding bar chart of RMFI of suspension CHO DP-12 cells probed with LCA after a 48 h treatment with medium containing 10 mM NH₄Cl followed by a 72 h fresh medium treatment (0 mM NH₄Cl). A 43.32 % decrease in LCA binding was observed and found to be statistically significant as determined by a standard Student's *t*-test, (p-value < 0.0001, n=3).

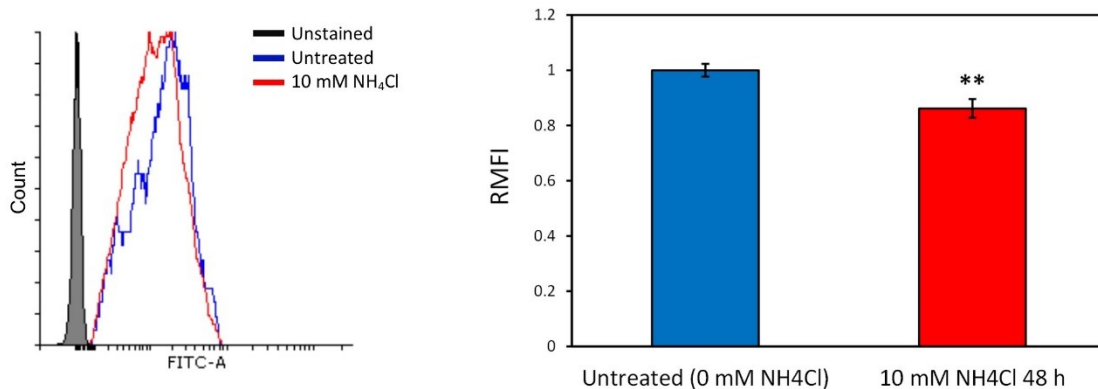


Fig. 5.44: CHO DP-12 cells probed with LecA5K following NH₄Cl treatment. Overlay histogram and corresponding bar chart of RMFI of suspension CHO DP-12 cells probed with recombinant LecA5K after a 48 h treatment with medium containing 10 mM NH₄Cl. A 13.82 % decrease in LecA5K binding was observed and found to be statistically significant as determined by a standard Student's *t*-test, (*p*-value < 0.01, *n*=3).

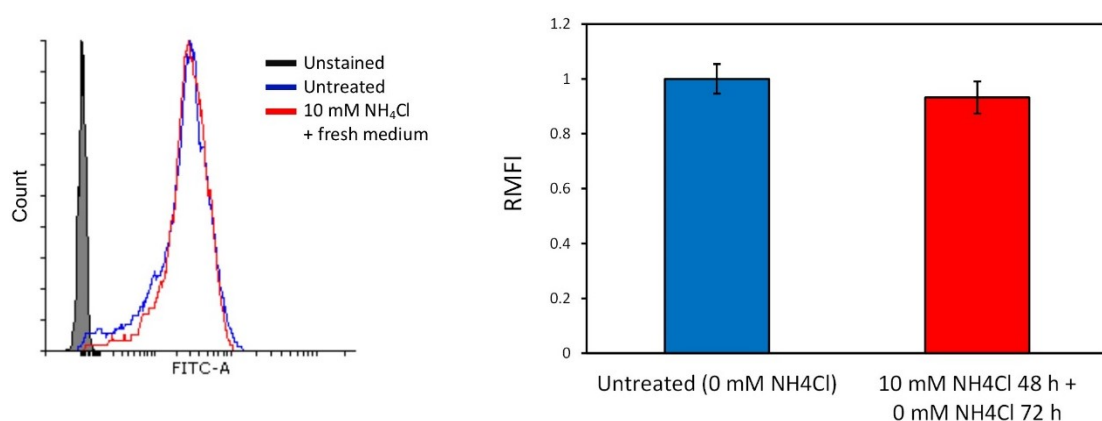


Fig. 5.45: CHO DP-12 cells probed with LecA5K following NH₄Cl and fresh medium treatments. Overlay histogram and corresponding bar chart of RMFI of suspension CHO DP-12 cells probed with recombinant LecA5K after a 48 h treatment with medium containing 10 mM NH₄Cl followed by a 72 h fresh medium treatment (0 mM NH₄Cl). A 6.77 % decrease in LecA5K binding was observed and found to be statistically insignificant as determined by a standard Student's *t*-test, (*p*-value > 0.05, *n*=3).

Here, increased ammonia was shown to alter glycosylation. Lectin binding differences were observed after cells were treated with 10 mM NH₄Cl for 48 h. However, these differences were not as striking as those observed after spent medium or reduced L-glut treatment. The most significant decrease and increase in lectin binding was from DSL, 27.52 %, and PNA, 60.56 %, directly after NH₄Cl treatment. Some lectins, LCA for example, had reduced binding to NH₄Cl treated cells, -13.82 %, which decreased further, -43.32 %, after cells were transferred into fresh NH₄Cl free medium, shown in Fig. 5.42 and Fig. 5.43. This pattern was observed for many lectins, i.e. reseeding treated cells in fresh medium did not produce similar lectin binding patterns to untreated cells.

5.13 Effect of sodium butyrate on CHO DP-12 cell surface glycosylation

The three previous sections identified CHO cell surface glycosylation changes, detectable by lectins, due to depleted nutrients or unwanted by product accumulation. In this section the effect of sodium butyrate (NaBu), a compound commonly added to boost recombinant protein yields was investigated (Chen et al. 2011). While increasing protein yields, cell viability and protein glycosylation may be also effected, see Section 1.11.2. Here, a panel of lectins were used to assess CHO DP-12 cell surface glycosylation changes induced by the addition of NaBu. Cells from 5 mL CHO DP-12 suspension cultures (2×10^6 viable cells/mL) were pelleted and resuspended in fresh medium, as described in Section 2.4, containing 3 mM NaBu. Following a 96 h incubation period, cells were probed with a panel of lectins and analysed by flow cytometry. After this NaBu treatment additional cells were reseeded back into fresh fully supplemented suspension medium without NaBu, as described in Section 2.4, and incubated for 96 h. Following this, cells were again probed with a panel of lectins and analysed by flow cytometry. The result of this experiment is summarised in Table 5.6.

Table 5.6: Comparison of MFI from lectin binding suspension adapted CHO DP-12 cells treated and untreated with 3 mM NaBu

10,000 events recorded for each sample in triplicate, average tabulated. Full data shown in Appendix K. Cells were treated for 96 h with 3 mM NaBu and probed with lectins. Additional cells were reseeded in fresh medium after treatment and analysed after 96 h.

Lectin	Untreated	Treated 96 h	% MFI change	Untreated	Treated 96 h + 96 h	% MFI change
Unstained	5.19	5.67	9.38	5.87	6.28	6.98
AAL	3131.88	2557.01	-18.36	4867.63	4089.80	-15.98
AAL-2	1356.71	1584.28	16.77	4073.29	3837.45	-5.79
DSL	1144.29	1306.32	14.16	1442.62	1653.26	14.60
ECL	2040.09	2215.62	8.60	4276.34	4089.01	-4.38
GafD1-178	9.12	30.80	237.56	21.72	36.96	70.16
GNL	1077.88	1732.37	60.72	1126.17	1675.22	48.75
GSL I B4	78.84	182.25	131.16	142.78	244.52	71.25
HPA	26.94	60.03	122.84	47.26	81.94	73.38
Jacalin	2783.16	3294.86	18.39	6215.14	4306.35	-30.71
LCA	1998.20	1723.68	-13.74	3233.45	3384.43	4.67
LecA5K	776.57	1689.40	117.55	1387.84	2645.99	90.66
LecB	92.20	173.92	88.63	612.85	602.45	-1.70
MAL II	1278.37	1099.95	-13.96	1628.38	1695.14	4.10
NPL	2314.31	2665.22	15.16	2918.00	2982.09	2.20
PNA	825.11	584.40	-29.17	3137.64	2490.57	-20.62
RCA I	5672.72	4165.80	-26.56	6008.24	5113.35	-14.89
SBA	406.31	391.35	-3.68	755.38	545.75	-27.75
WGA	6222.89	4431.51	-28.79	7087.36	5867.90	-17.21

Fig. 5.46 to Fig. 5.53 displays the histograms and bar charts of relative MFI values for cells probed with recombinant AAL-2, recombinant LecA5K, MAL II and RCA I. Additional data is shown in Appendix K.

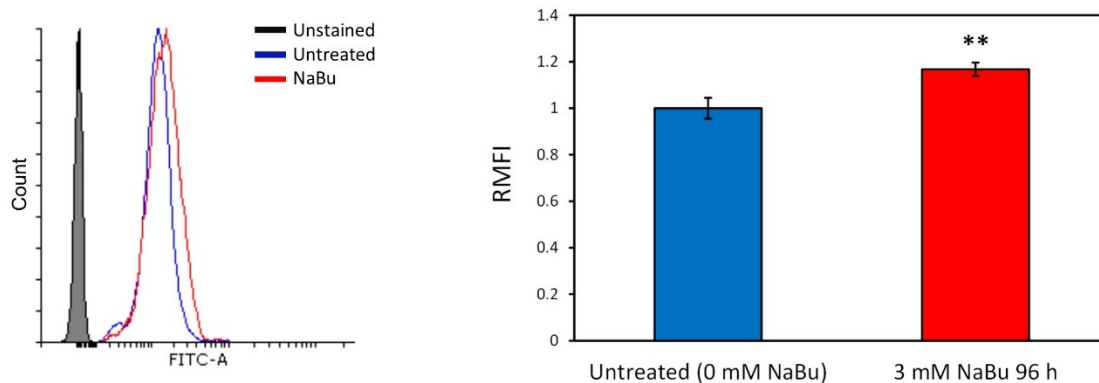


Fig. 5.46: CHO DP-12 cells probed with AAL-2 following NaBu treatment. Overlay histogram and corresponding bar chart of RMFI of suspension CHO DP-12 cells probed with recombinant AAL-2 after a 96 h treatment with medium containing 3 mM NaBu. A 16.77 % increase in AAL-2 binding was observed and found to be statistically significant as determined by a standard Student's *t*-test, (p -value < 0.01, $n=3$).

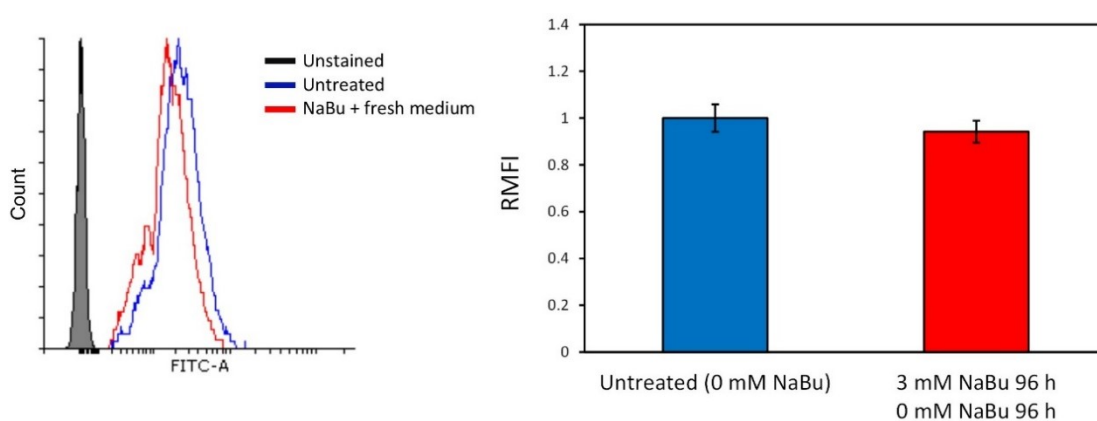


Fig. 5.47: CHO DP-12 cells probed with AAL-2 following NaBu and fresh medium treatments. Overlay histogram and corresponding bar chart of RMFI of suspension CHO DP-12 cells probed with recombinant AAL-2 after a 96 h treatment with medium containing 3 mM NaBu followed by a 96 h fresh medium treatment (0 mM NaBu). A 5.79 % decrease in AAL-2 binding was observed and found to be statistically insignificant as determined by a standard Student's *t*-test, (p -value > 0.05, $n=3$).

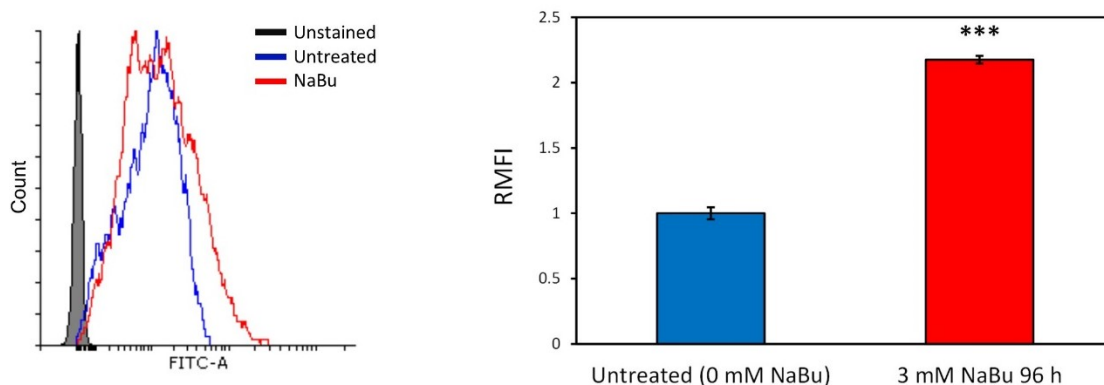


Fig. 5.48: CHO DP-12 cells probed with LecA5K following NaBu treatment. Overlay histogram and corresponding bar chart of RMFI of suspension CHO DP-12 cells probed with recombinant LecA5K after a 96 h treatment with medium containing 3 mM NaBu. A 117 % increase in LecA5K binding was observed and found to be statistically significant as determined by a standard Student's *t*-test, (p -value < 0.001, $n=3$).

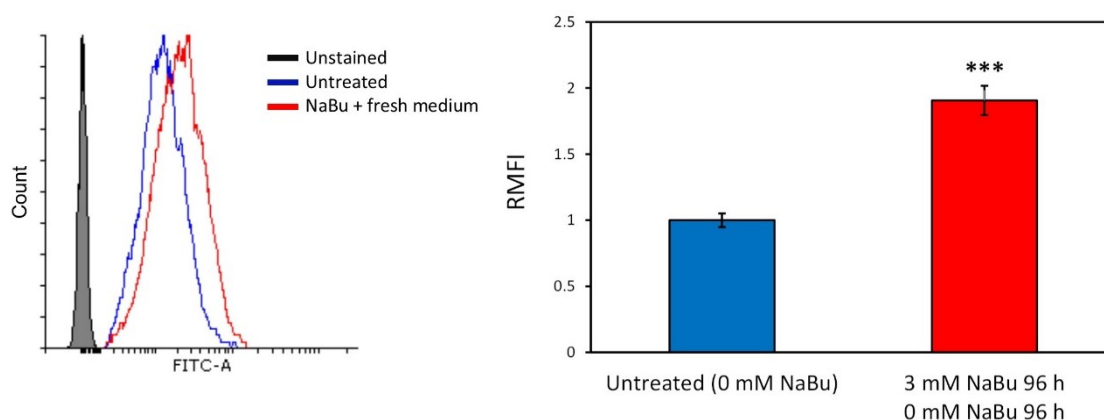


Fig. 5.49: CHO DP-12 cells probed with LecA5K following NaBu and fresh medium treatments. Overlay histogram and corresponding bar chart of RMFI of suspension CHO DP-12 cells probed with recombinant LecA5K after a 96 h treatment with medium containing 3 mM NaBu followed by a 96 h fresh medium treatment (0 mM NaBu). A 90.66 % increase in LecA5K binding was observed and found to be statistically significant as determined by a standard Student's *t*-test, (p -value < 0.001, $n=3$).

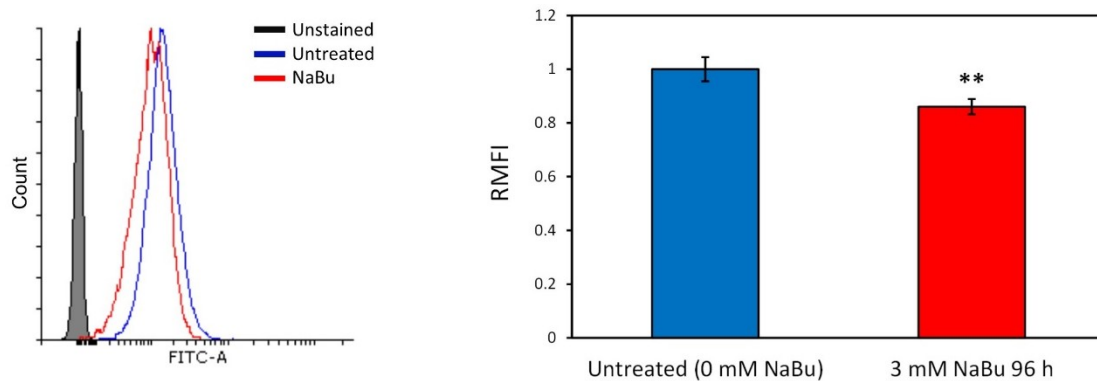


Fig. 5.50: CHO DP-12 cells probed with MAL II following NaBu treatment. Overlay histogram and corresponding bar chart of RMFI of suspension CHO DP-12 cells probed with MAL II after a 96 h treatment with medium containing 3 mM NaBu. A 13.96 % decrease in MAL II binding was observed and found to be statistically significant as determined by a standard Student's *t*-test, (p-value < 0.01, n=3).

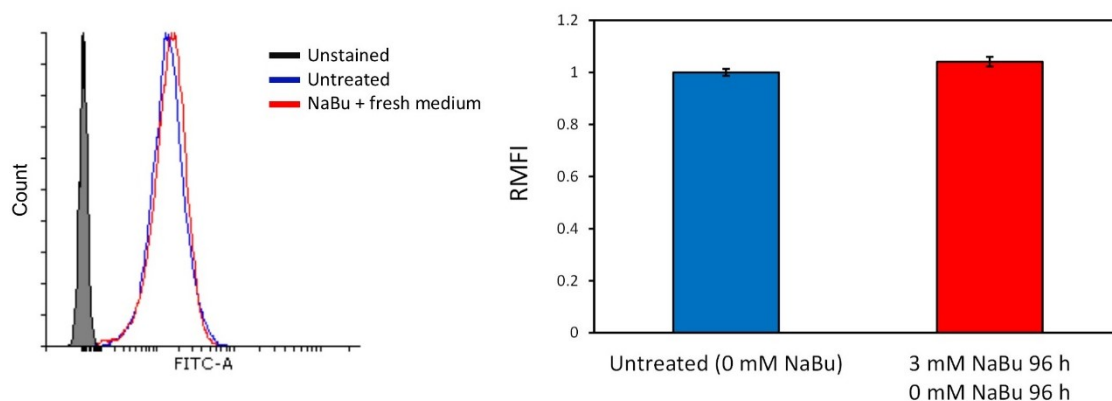


Fig. 5.51: CHO DP-12 cells probed with MAL II following NaBu and fresh medium treatments. Overlay histogram and corresponding bar chart of RMFI of suspension CHO DP-12 cells probed with MAL II after a 96 h treatment with medium containing 3 mM NaBu followed by a 96 h fresh medium treatment (0 mM NaBu). A 4.10 % increase in MAL II binding was observed and found to be statistically insignificant as determined by a standard Student's *t*-test, (p-value > 0.05, n=3).

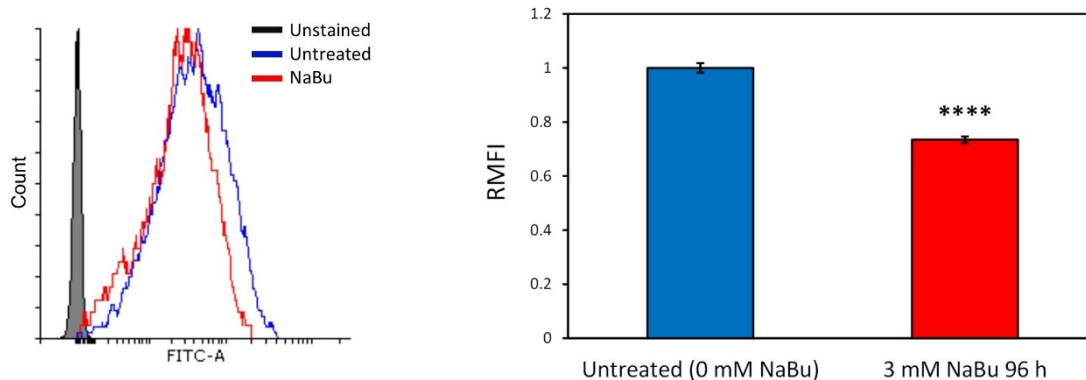


Fig. 5.52: CHO DP-12 cells probed with RCA I following NaBu treatment. Overlay histogram and corresponding bar chart of RMFI of suspension CHO DP-12 cells probed with RCA I after a 96 h treatment with medium containing 3 mM NaBu. A 26.56 % decrease in RCA I binding was observed and found to be statistically significant as determined by a standard Student's *t*-test, (p-value < 0.0001, n=3).

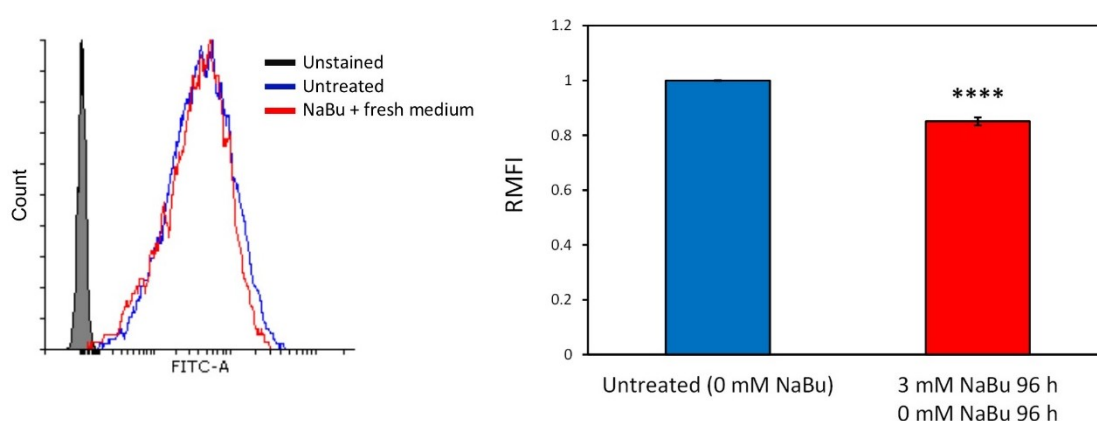


Fig. 5.53: CHO DP-12 cells probed with RCA I following NaBu and fresh medium treatments. Overlay histogram and corresponding bar chart of RMFI of suspension CHO DP-12 cells probed with RCA I after a 96 h treatment with medium containing 3 mM NaBu followed by a 96 h fresh medium treatment (0 mM NaBu). A 14.89 % decrease in RCA I binding was observed and found to be statistically significant as determined by a standard Student's *t*-test, (p-value < 0.0001, n=3).

Lectin binding differences were observed after cells were treated with 3 mM NaBu for 96 h. A decrease in MAL II binding, 13.96 %, was reversed when the cells were reseeded in NaBu free medium. This is similar to what Rodriguez et al. (2005) observed

from β -IFN expressed by CHO cells. They detected a decrease in the occurrence of disialylated glycans, from 36.5 % to 21.2 %, in a batch culture supplemented with 1 mM NaBu. An increase in LecA5K binding, 117 %, remained largely unreversed, 90.66 %, upon the reseeded of treated cells in NaBu free medium.

5.14 Purification and glycoanalysis of recombinant IgG1 from an untreated CHO DP-12 culture

CHO DP-12 cells co-express light and heavy chains of the murine recombinant IgG1 which inhibits interleukin 8 mediated human neutrophil chemotaxis. The purification of IgG1 from CHO DP-12 cultures was completed for two key reasons, (i) to confirm that the cells are in fact CHO DP-12 cells and are expressing anti-IL-8 IgG1 and (ii) to complete ELLA analysis on purified IgG1 from treated CHO DP-12 cell cultures. It is of vital importance that cell line authentication is completed to add a level of confidence to any scientific research. There are a variety of vendors which offer authentication services for human cell lines, e.g. Eurofins Genomics and LGC Standards. However, such services are not available for CHO cell lines (Almeida et al. 2016). IgG1 is a 146 kDa glycoprotein. The expression of IgG1 is maintained by the addition of methotrexate, 200 nM, in cell culture media. IgG1 was purified from untreated CHO DP-12 suspension cultures as described in Section 2.18. The supernatant was pre-concentrated, as described in Section 2.22, prior to IgG1 purification. The result of this purification is shown in Fig. 5.54.

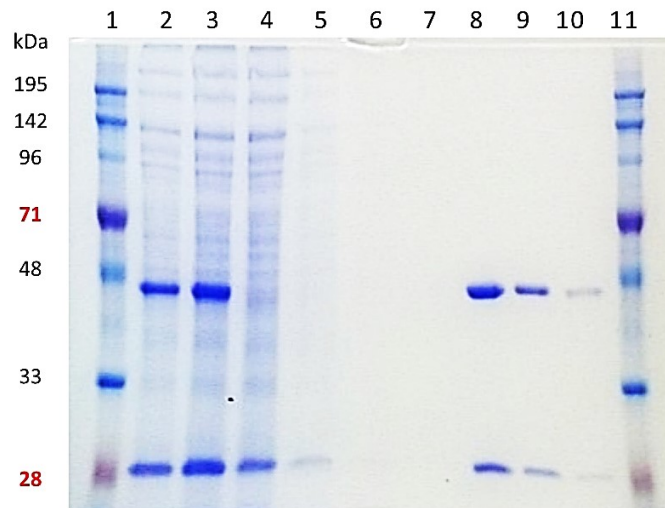


Fig. 5.54: Purification of recombinant IgG1 using Protein A/G. Analysis by 15 % SDS-PAGE of IgG1 purification from suspension adapted CHO DP-12 cultures. Purification described in Section 2.22. In Lanes 1 and 11; Expedeon prestained dual-colour marker (Fig. 2.5), Lane 2; neat CHO DP-12 supernatant, Lane 3; concentrated CHO DP-12 supernatant, Lane 4; unbound supernatant, Lanes 5-7; Wash 1-3 (PBS), Lanes 8-10; elution fractions 1-3 (0.1 M glycine pH 2.5).

Elution fractions 1, 2 and 3 from Fig. 5.54 were pooled and quantified using the BCA assay, see Section 2.23.1. To confirm that the eluted protein is IgG1 and does not contain contaminant proteins a western blot was completed using an anti-IgG mAb peroxidase-conjugate as described in Section 2.21. Two identical SDS-PAGE gels were run where 2 μ g of IgG1 was loaded three times in non-denaturing, mild denaturing and strong denaturing conditions. See SDS-PAGE gel and western blot analysis in Fig. 5.55. An indirect ELISA was completed, as described in Section 2.26, to assess IgG1 specificity, see Fig. 5.56.

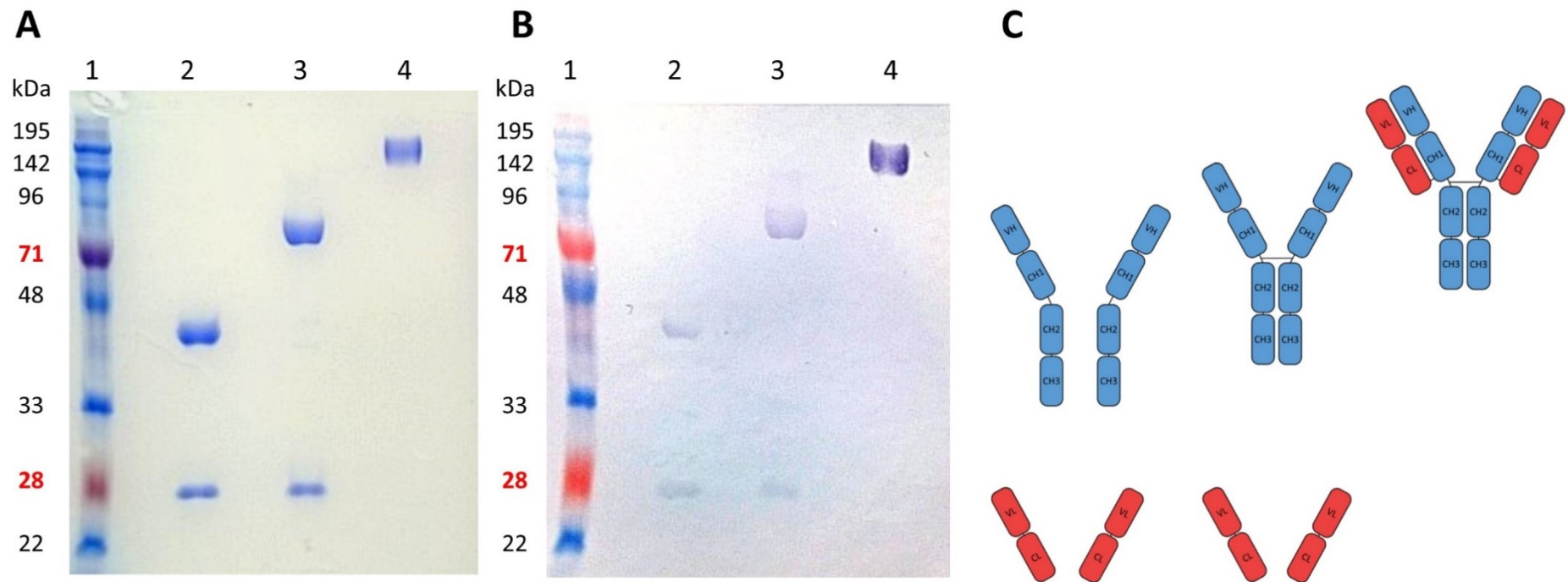


Fig. 5.55: SDS-PAGE and western blot analysis of purified IgG1. Analysis by 15 % SDS-PAGE (A) and western blot (B) of purified IgG1 from suspension adapted CHO DP-12 cultures. Western blot completed using anti-IgG (H+L) peroxidase-conjugate as described in Section 2.21. In both A and B Lane 1; Expedeon prestained dual-colour marker (Fig. 2.5), Lane 2; strong denaturation - IgG1 in 10x SDS-PAGE sample buffer, see Section 2.5, and boiled for 5 min, Lane 3; mild denaturation - IgG1 in 10x SDS-PAGE sample buffer not boiled, Lane 4; non-denaturation - IgG1 loaded in 20 % glycerol. C) A schematic of the separation of heavy and light antibody chains corresponding to lanes 2, 3 and 4 in images A and B. Image created using Microsoft Publisher 15.0.

The purified IgG1 was prepared in 3 different denaturing conditions which resulted in four differently sized bands on the gel and western blot in Fig. 5.55. These were; (i) whole IgG1 ~146 kDa, (ii) heavy chain dimer ~90 kDa, (iii) heavy chain monomer ~45 kDa and (iv) light chain monomer ~28 kDa. An indirect ELISA was completed using purified IgG1 and an anti-IgG peroxidase conjugate antibody to demonstrate its specificity, see Fig. 5.56.

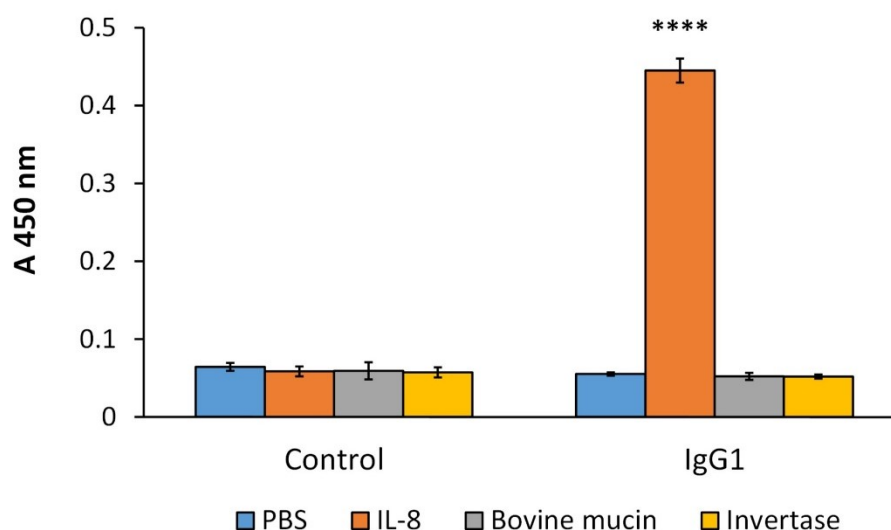


Fig. 5.56: ELISA analysis of purified IgG1. An indirect ELISA was completed as per Section 2.26 using purified IgG1 as the primary antibody and anti-IgG (H+L) as the secondary antibody. IgG1 binding IL-8 was observed and found to be statistically significant as determined by a standard Student's *t*-test, (p -value < 0.0001). Error bars were calculated from the standard deviation of three replicates.

The *N*-glycan at position Asn297 on the IgG1 heavy chain is located in the hinge region, see Fig. 1.25. Due to this location, lectins may have reduced or no access to the glycan. Purified IgG1 was heat treated, 40-90 °C, for 30 min prior to adding to a 96-well plate to partially denature the protein and make the glycans more accessible. To determine which temperature is most appropriate for opening the hinge region of IgG1 for lectin binding during ELLA analysis, two lectins, mannose specific Con A and fucose specific AAL, were used. A direct ELISA was also completed on one row of the 96-well plate, i.e. anti-IgG mAb was added instead of a lectin, which served as an added control. Fig. 5.57 displays the result of this ELLA/ELISA.

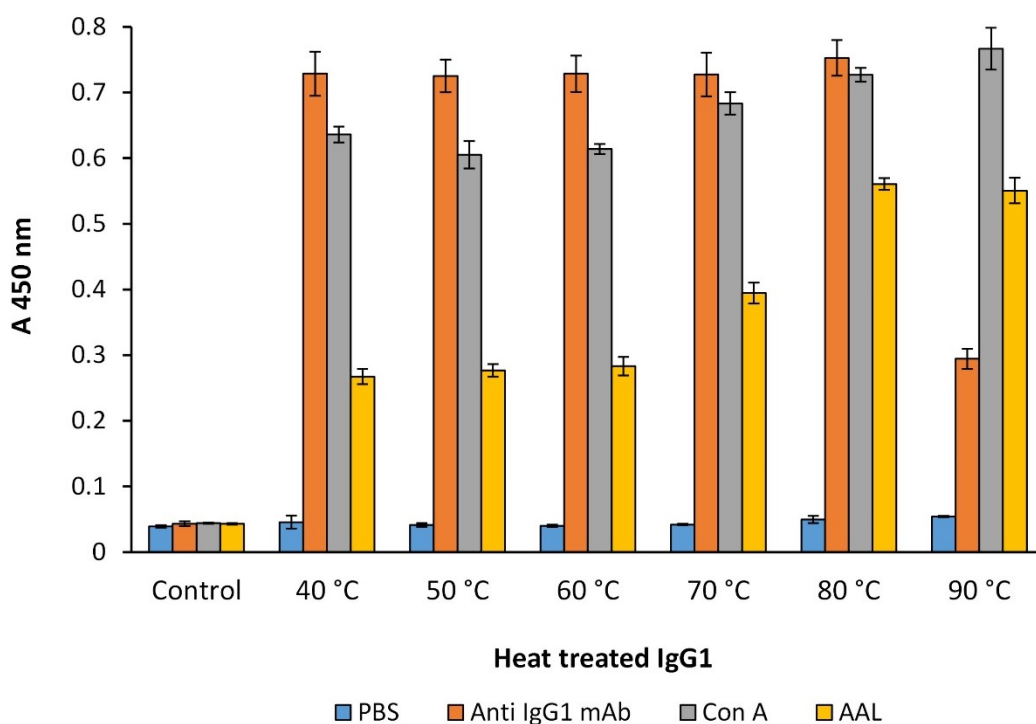


Fig. 5.57: ELLA and ELISA analysis of heat treated IgG1. An ELLA and a direct ELISA were completed as per Sections 2.25 and 2.26 using purified IgG1. Immunoglobulin G1 was heated for 30 min before adding to 96-well plate. Error bars were calculated from the standard deviation of three replicates.

5.15 Purification and glycoanalysis of recombinant IgG1 from CHO DP-12 cultures treated with spent medium, reduced L-glut, NH₄Cl or NaBu

The supernatant from suspension adapted CHO DP-12 cultures, which were treated with spent medium, L-glut free medium, ammonia or NaBu in Sections 5.10, 5.11, 5.12 and 5.13, were collected for IgG1 purification and subsequent glycoanalysis by ELLA. Immunoglobulin G1 was purified from 12 different CHO DP-12 cultures, described in Table 5.7. All supernatants were pre-concentrated on PEG prior to purification using Protein A/G columns, as described in Section 2.18, see purified IgG1 in Fig. 5.58. Immunoglobulin G1 was not purified from cultures directly after spent medium treatment as the existing IgG1 could not be accounted for. The IgG1 purified from each sample was then glycoanalysed by a panel of lectins, see ELLA result in Fig. 5.59 and 5.60.

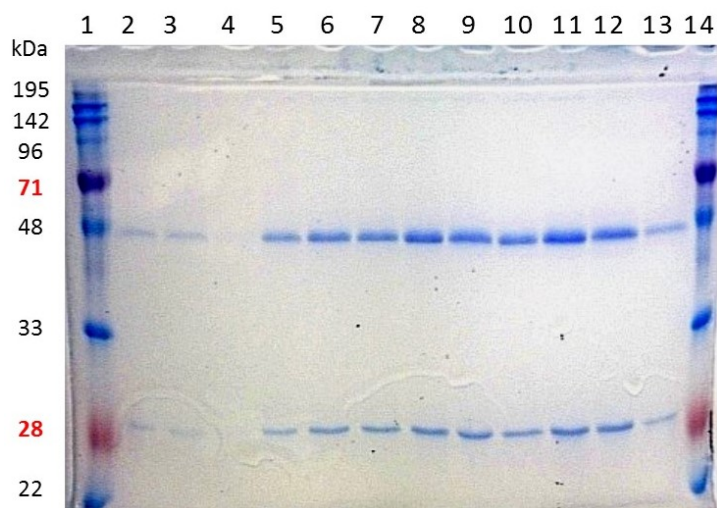


Fig. 5.58: Purification of recombinant IgG1 from 12 treated CHO DP-12 cultures. Analysis by 15 % SDS-PAGE of IgG1 purification, as described in Section 2.22, from treated suspension adapted CHO DP-12 cultures. In Lanes 1 and 14; Expedeon prestained dual-colour marker (Fig. 2.5), Lane 2-13; purified IgG1 from CHO cultures treated with spent medium, reduced L-glutamine, NH_4Cl or NaBu addition. Samples described in Table 5.7.

Table 5.7: Purified recombinant IgG1 samples and corresponding flow cytometry sections and treatments

IgG1 Sample	Lane in Fig. 5.58	Corresponding Section	Treatment
1	2	5.10	Untreated
2	3	5.10	Spent medium 24 h + 72 h fresh medium
3	4	-	Spent medium 48 h + 72 h fresh medium*
4	5	5.11	Untreated
5	6	5.11	0 mM L-glut 48 h
6	7	5.11	0 mM L-glut 48 h + 72 h fresh medium (4 mM)
7	8	5.12	Untreated
8	9	5.12	10 mM NH_4Cl 48 h
9	10	5.12	10 mM NH_4Cl 48 h + 72 h fresh medium (0 mM)
10	11	5.13	Untreated
11	12	5.13	3 mM NaBu 96 h
12	13	5.13	3 mM NaBu 96 h + 96 h fresh medium (0 mM)

* Flow cytometry data not presented in this work

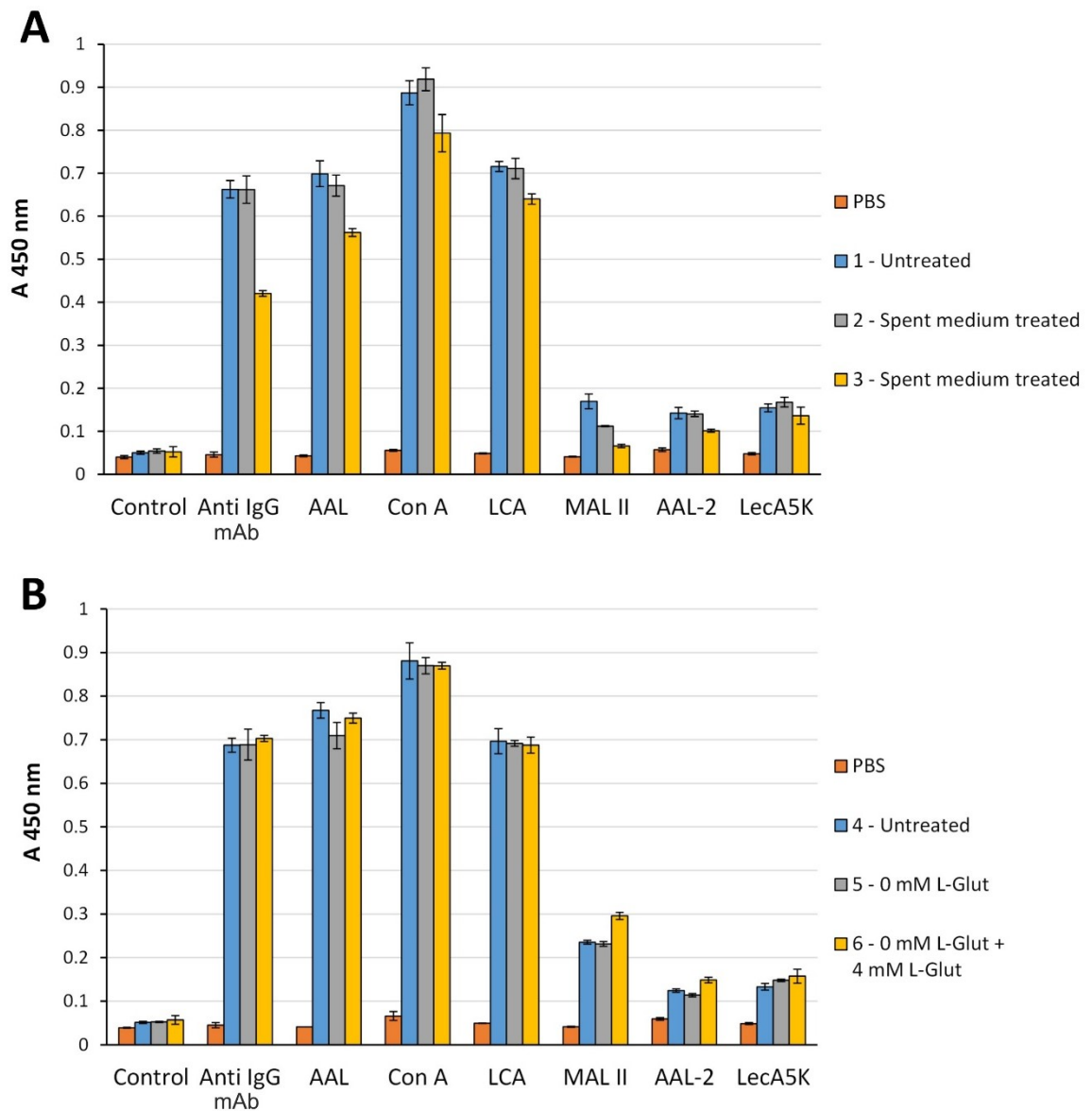


Fig. 5.59: ELLA and ELISA analysis of purified IgG1 from treated cultures. An ELLA and an indirect ELISA were completed as per Sections 2.25 and 2.26 using purified IgG1. Immunoglobulin G1 was heated for 30 min at 80 °C before adding to plate. **A)** IgG1 from CHO DP-12 cells treated with spent medium. **B)** IgG1 from CHO DP-12 cells treated with L-glut free medium. Samples described in Table 5.7. Error bars were calculated from the standard deviation of three replicates.

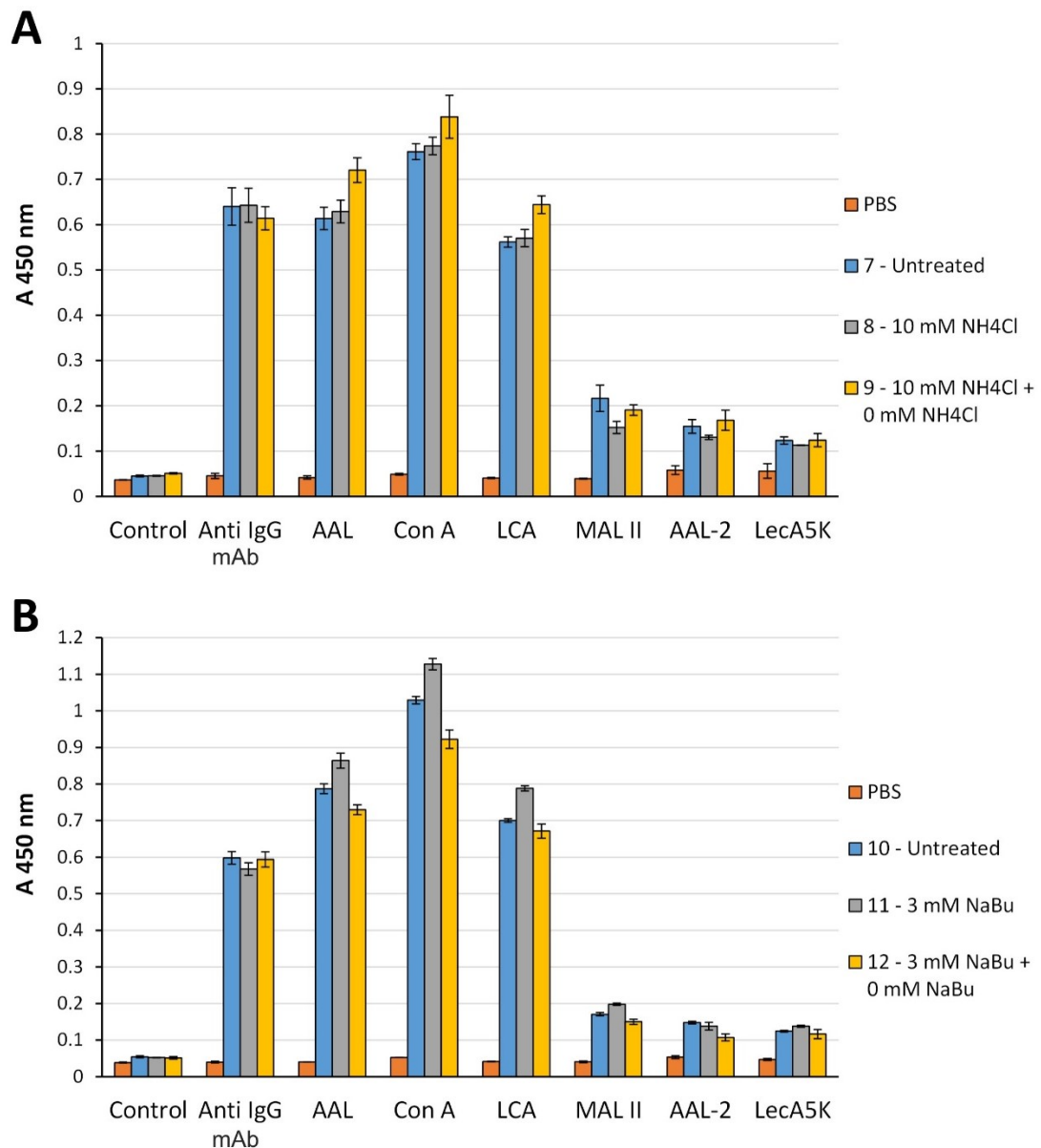


Fig. 5.60: ELLA and ELISA analysis of purified IgG1 from treated cultures. An ELLA and an indirect ELISA were completed as per Sections 2.25 and 2.26 using purified IgG1. Immunoglobulin G1 was heated for 30 min at 80 °C before adding to plate. **A)** IgG1 from CHO DP-12 cells treated with NH₄Cl. **B)** IgG1 from CHO DP-12 cells treated with NaBu. Samples described in Table 5.7. Error bars were calculated from the standard deviation of three replicates.

Subtle IgG1 glycan differences were detected, e.g. increased LCA binding to IgG1 from NaBu treated cells, Fig. 5.60 image B. However, LCA binding to the CHO cell surface decreased after the same treatment. Similarly, when CHO cells were treated with L-glut

free medium MAL II binding to the cell surface did not change, see Fig. 5.34. When these treated cells were reseeded in fresh medium and analysed 72 h later a 10.46 % decrease in MAL II binding was observed, see Fig. 5.35. When the IgG1 from these cells were analysed with MAL II, no change was observed for the former but the latter had increased MAL II binding, see Fig. 5.59 image B. A strong correlation between the glycosylation on the CHO DP-12 cell surface and secreted product, IgG1, was not found by ELLA analysis.

5.16 Discussion

To prepare live CHO DP-12 cells for lectin probing and subsequent analysis by a flow cytometer, a variety of parameters were assessed. However, adapting adherent CHO DP-12 cells to suspension culture was initially completed. Typically three steps are required to adapt CHO cells to serum-free high cell density suspension cultures. The protocol outlined by Sinacore et al. (2000) recommends (i) seeding cells in spinner/shaker tubes in serum supplemented medium, (ii) the gradual reduction of serum in the medium and finally (iii) using a chemically defined medium to achieve high cell density cultures. A similar protocol was also suggested by Rodrigues et al. (2013) for CHO K1 cells, the cell line from which CHO DP-12 is derived. They define high cell density cultures as those with $\geq 4.0 \times 10^6$ viable cells/mL. Here the direct and sequential adaption methods recommended by IrvineSci (2017) were attempted. The direct method, i.e. simultaneously switching cells from adherent culture to suspension culture and from serum-supplemented to serum-free, proved to be most appropriate, see Fig. 5.1. A high cell density suspension culture was achieved by day 5 of the direct adaption method which ultimately reached a plateau by day 9 at $\sim 10 \times 10^6$ viable cells/mL. This direct adaption method was then used to generate all CHO DP-12 suspension cultures.

The lectin probing concentration and cell number per sample were assessed. These two parameters are clearly linked, i.e. an increased cell number per sample will reduce the lectin:cell ratio. Due to toxicity of some lectins, primarily plant lectins, see cytotoxicity assay in Section 4.2, it was necessary to identify a suitable lectin probing concentration. Lectins are used at 5 $\mu\text{g/mL}$ during ELLA analysis so lectin concentrations above and

below this value were assessed using AAL, AAL-2 and RCA I. At 1 $\mu\text{g}/\text{mL}$ the fluorescent signal from lectin binding was not clearly separated from an unstained cell sample, see Fig. 5.2. Clear separation was achieved with 5, 10 and 20 $\mu\text{g}/\text{mL}$. However, lectin concentration had an inverse relationship with the percentage of cells in the live gate, see Fig. 5.3. Approximately 70 % of cells probed with lectin at 5 $\mu\text{g}/\text{mL}$ remained in the live gate. This dropped to 56 % and 40 % when the lectin concentration increased to 10 $\mu\text{g}/\text{mL}$ and 20 $\mu\text{g}/\text{mL}$. A lectin probing concentration of 5 $\mu\text{g}/\text{mL}$ was shown to be suitable for live cell lectin staining. This concentration was then used to determine an appropriate cell number to aliquot per sample. Fig. 5.4 shows the result of probing $5-9 \times 10^5$ cells/sample with recombinant AAL-2 and GNL. As anticipated, the fluorescent signal decreased as the lectin became more dilute with a higher cell number. Even so, all of the cell samples aliquoted and probed with lectin resulted in a strong signal clearly separated from an unstained cell sample. The pellet from the 5×10^5 cell sample was not stable during the wash steps. A larger cell number per sample helped reduce cell loss and form a more stable pellet. For live cell lectin staining of CHO DP-12 cells, 7×10^5 cells aliquoted per sample is suitable.

Lectin binding temperature was investigated due to different temperatures recommended in flow cytometry protocols (BD 2013). Fig. 5.5 shows that lectin binding increased with temperature for the four lectins tested. There was a 0.7 %, 3.38 %, 30.52 % and a 30.82 % increase in MFI for lectins LecA5K, NPL, Con A and DSL respectively, when incubated with cells at 20 °C as opposed to 4 °C. It is often recommended to keep cells on ice while probing with lectin or antibody as it will help reduce cell clumping (BD 2013; Stanley and Sundaram 2014). However, Holmes et al. (2001) acknowledge that higher temperatures, ~ 20 °C, may be required for certain probes. Cell clumping was not an issue here for cells probed at room temperature.

Four different methods for removing adherent cells from tissue culture flasks were assessed. Trypsin is routinely used for sub-culturing cells. However, as trypsin cleaves proteins, it may be reducing the glycan content at the CHO cell surface prior to lectin probing. Due to the aggressiveness of this protease, e.g. it is extensively used in MS-based proteomic techniques for degrading proteins to peptides Olsen et al. (2004), it may be an inappropriate method of cell removal. Increased lectin binding was

observed for cells removed with a cell scraper as opposed to trypsin, CDS or 10 mM EDTA, see Table 5.1 and Fig. 5.6. Unexpectedly however, there was greater variation in lectin binding between the three non-enzymatic methods than between any one of them and trypsin. If trypsinising cells was removing surface glycans, which it appears to be doing, then all non-enzymatic methods of cell removal should be more similar. The inconsistency observed here was not an issue as suspension cells were used for the majority of the subsequent experiments in this chapter.

When comparing lectin binding between adherent and suspension adapted CHO DP-12 cells, adherent cells were removed using a cell scraper. The surface glycosylation of CHO cells from adherent and suspension cultures were assessed using a panel of 24 lectins, see Table 5.2. Significant differences were observed, e.g. AAL, Con A, ECL, Jacalin, and PNA had reduced MFIs of 34.03 %, 41.22 %, 43.32 %, 32.47 % and 64.63 % respectively. Increased binding was observed for LecA5K, 139.98 %, and WGA, 49.43 %. The mean FSC-A for suspension adapted cells was 78.16 % larger than that for adherent cells. However, the mean SSC-A for adherent cells was 17.52 % larger, see Fig. 5.7. These differences in FSC-A and SSC-A could partially explain the variation in lectin binding observed. The FSC light is light diffracted along the same plane as the laser beam and it is proportional to the cell surface area, i.e. size. The SSC light is both refracted and reflected light collected at 90 ° to the laser beam and is proportional to the internal complexity and granularity of the cell (Adan et al. 2017). There are a plethora of additional factors that may explain cell surface differences between adherent and suspension adapted cells. When cells are adapted to serum-free suspension culture there is an increase in actin filament expression and certain membrane proteins, e.g. integrins, are rearranged in order to compensate for the interruption to cell surface protein signalling caused by serum withdrawal (Walther et al. 2015).

Fig. 5.8 compares the binding of LecA and all LecA lysine and EGFP variants, generated in Section 3.5.5, to CHO DP-12 cells. LecA has a low lysine content, 4 residues, which results in insufficient biotinylation and therefore it is not clearly distinguished from the unstained cell sample. Fusing EGFP to LecA did not produce a usable probe for the flow cytometer. While fusing EGFP, 27 kDa, to LecA may have

steric consequences and interfere with LecA folding, as reported by Snapp (2005), the ELLA analysis of this protein, see Section 3.5.5, suggests it remained functional. However, two of the five LecA variants produced, resulted in an increase in the LecA binding signal observed. 78.74 % of cells probed with LecA are in the positive gate with a MFI of 217.64, see Fig. 5.8 image A. Whereas 99 % of cells probed with LecAH3K or LecA5K are in the positive gate with MFIs of 512.13 or 925.95, see Fig. 5.8 images C and F. The LecA probe was successfully altered, i.e. the generation of the LecA5K variant had an improved signal, 3.25-fold, which was clearly separated from the unstained cell sample.

Competing free monosaccharides were premixed with lectins prior to incubation with cells to demonstrate the specificity of lectin binding. Most of the lectins were successfully inhibited, see Fig. 5.9 to Fig. 5.23. Some lectins were not fully inhibited with free monosaccharides alone, even at high concentrations. For example WGA was not completely inhibited with the addition of 400 mM GlcNAc as it generally requires salt and/or acid for complete inhibition (Vector Labs 2017). The inhibiting concentrations recommended by the supplier of the lectins, Vector Laboratories, were used during this assessment.

The complete inhibition of AAL-2 was achieved with 12.5 mM GlcNAc, see Fig. 5.9. Surprisingly, GalNAc also inhibited AAL-2 although to a lesser extent. A second AAL-2 inhibition check was completed, see Fig. 5.10, using BSA linked monosaccharides instead of free monosaccharides. Here, increasing BSA-GlcNAc gradually reduced AAL-2 binding whereas increasing BSA-GalNAc did not have a similar effect. The BSA linked monosaccharides are akin to glycoproteins as the monosaccharides are presented on a protein rather than free in solution. The specificity of AAL-2 binding was previously shown by ELLA, see Fig. 3.16. This specificity was clearly demonstrated again here as AAL-2 binding was not reduced with the addition of BSA-GalNAc, even at 5 μ g/mL. GafD1-178 was partially inhibited with free GlcNAc, see Fig. 5.11. Apoptosis was induced in CHO DP-12 cells with the addition of H₂O₂ (0.489 mM) prior to probing as GafD1-178 will not bind healthy cells. LecA5K inhibition was assessed using free monosaccharides and BSA linked monosaccharides, see Fig. 5.12. In contrast to AAL-2, LecA5K was fully inhibited with free galactose but

BSA-galactose only partially reduced binding. Free mannose or BSA-mannose did not reduce binding.

AAL, ECL, Jacalin and LCA were fully inhibited when premixed with their competitive monosaccharides, 200 mM D-fucose, 200 mM lactose, 800 mM galactose and 200 mM α -methylmannoside/ α -methylglucoside mix in Fig. 5.13, Fig. 5.15, Fig. 5.17 and Fig. 5.18 respectively. DSL, GNL, NPL, RCA I and WGA were not fully inhibited when premixed with their competitive monosaccharides in Fig. 5.14, Fig. 5.16, Fig. 5.21, Fig. 5.22 and Fig. 5.23 respectively, although reduced binding was observed. Lectin binding was not inhibited by the addition of highly similar monosaccharides, 'non-competitive', for all lectins tested, Fig. 5.9 to Fig. 5.23, which again demonstrates the selective nature of lectins and how suitable they are for probing complex targets such as the CHO DP-12 glycocalyx.

CHO DP-12 cells were treated with spent medium, from day 9 of a batch culture, to stress the cells, i.e. induce glycocalyx changes, and determine if lectin binding is altered. The glycocalyx is involved in many interactions with other cells and proteins and changes to it may be informative as to the state of the cell, see Section 1.3.4. Spent medium was collected from high cell density cultures, $\sim 1 \times 10^7$ viable cells/mL 9 days after seeding at 3×10^5 viable cells/mL. These cultures are deprived of nutrients and also contain accumulated by products such as ammonia. In a study by Reinhart et al. (2015) they assessed eight chemically defined CHO culture media in batch culture expressing IgG from CHO DG44. They found that with BalanCD CHO, also used in this work, they achieved the highest cell concentration ($\sim 9 \times 10^6$ cells/mL), second highest IgG concentration (~ 800 mg/L) and highest ammonium accumulation (~ 175 mg/L or 9.7 mM) out of the eight media evaluated in batch mode.

Fig. 5.24 to Fig. 5.31 displays histograms and bar charts for cells probed with recombinant AAL-2, recombinant LecA5K, MAL II and PNA after treatment with spent medium for 48 h. LecA5K binding increased 229 %. This large increase was nearly completely reversed after treated cells were cultured in fresh medium for 72 h, i.e. this increase had reduced to 32.24 %. This clearly demonstrates the sensitivity of the glycocalyx to the cellular environment. In Fig. 5.28 and Fig. 5.29 the change in MAL II

binding is shown, i.e. a 43.79 % decrease in binding after spent medium treatment which reduced to 17.4 % following the addition of complete medium. This was an important observation. MAL II is a sialic acid binder, α 2-3-NeuNAc, and a decrease in its binding indicates that the glycans have a reduced level of sialylation. In complex *N*-glycans, removing terminal sialic acid exposes a galactose residue, see Fig. 1.6, and increased LecA5K binding is therefore expected. A dramatic increase, 781 %, in PNA binding is shown in Fig. 5.30. Similar to LecA5K binding, this increase had reduced to 20.24 % after incubation with fresh medium, see Fig. 5.31. PNA discriminates between sialylated and non-sialylated T-antigen, Gal β 1-3GalNAc, and so a decrease in MAL II binding is also expected to coincide with an increase in PNA binding, which was observed (Chacko and Appukuttan 2001).

An additional experiment was completed where the cells from the suspension CHO DP-12 culture from which the spent medium was collected, i.e. fed 9 days previously, was compared to cells which were last fed 4 days previously. The MFI values from this experiment is shown in Appendix K. The lectin binding profile for these two cultures differ only slightly, e.g. the greatest difference observed was a 13.7 % decrease in LecA5K binding. This emphasizes that the change in lectin binding to spent medium treated cells is caused by the sudden change in the cellular environment, i.e. decrease in nutrient availability and increased ammonia, to which the cells have not acclimatised.

L-Glutamine is an essential component in cell culture media where it is a carbon and nitrogen source and a precursor for peptide and protein synthesis (Rao and Samak 2011). Research by Wong et al. (2005) clearly illustrates the effect of low glutamine in CHO cell culture. They reported a 10-fold increase in IFN- γ production when glutamine was low, 0.3 mM, which they attribute to reduced ammonia and lactate accumulation. However when glutamine concentrations were very low, < 0.1 mM, high cell density cultures were not achieved and there was a decrease in glycan sialylation and an increase in hybrid and high-mannose glycans on IFN- γ . Here, CHO DP-12 cells were treated with L-glut free medium, for 48 h, and probed with a panel of lectins. The lectin binding observed is reported in Table 5.4. Fig. 5.32 shows the 190 % increase in LecA5K binding which was statistically significant (p-value < 0.0001, n=3). This increase was reduced to 26.10 % following the incubation in fresh medium, see Fig. 5.33. This is

similar to what was observed with PNA. A 151 % increase in binding after L-glut free medium treatment, see Fig. 5.36, which reduced to 44.65 % following the addition of fresh medium, see Fig. 5.37. These results are similar to what was observed when cells were treated with spent medium. The glycosylation changes observed here could be caused by altered metabolic pathways due to L-glut depletion. Wahrheit et al. (2014) studied the impact of L-glut limitation on the growth and metabolism of CHO cells grown in a variety of batch and fed-batch modes and found that pyruvate and glucose uptake were significantly lower in L-glut free cultures. Fan et al. (2015) reported that when glucose consumption rates in CHO cells are high, more mature glycans patterns are typically observed.

When L-glut is metabolised to glutamate, ammonia is released. L-glut is also commonly degraded in cell culture media resulting in the equimolar increase of ammonia. This degradation in cell culture media is pH, temperature and phosphate concentration dependant (Ahn and Antoniewicz 2012). Ammonia has a negative effect on cell growth and viability, which is cell line dependent (Jagusic et al. 2016). Ammonia concentrations as low as 2 mM has been shown to effect the synthesis of O-linked glycans and N-linked glycans, particularly the addition of sialic acid (Andersen and Goochee 1995; Yang and Butler 2000). Butler (2006) proposed two mechanisms to explain how ammonia influences glycosylation. Firstly, ammonia is incorporated into glucosamine and the UDP-GlcNAc/UTP ratio is increased. UDP-GlcNAc competes with CMP-NANA for transport into the Golgi and the result is less substrate available for sialylation. Secondly, ammonia raises the pH which effects both nucleotide sugar transport and the efficiency of sialyltransferases in the Golgi (Gawlitzeck et al. 2000). As previously mentioned, Reinhart et al. (2015) measured 9.7 mM ammonia in batch cultures of CHO DG44 cells. A higher ammonia concentration, 13 mM, was recorded by Altamirano et al. (2000) in batch cultures of CHO TF70R cells, although they had supplemented the medium with fructose and galactose. Lectin binding to CHO DP-12 surfaces was altered after the cells were reseeded in medium containing 10 mM NH₄Cl, see Table 5.5. Lectin binding patterns did not resemble the untreated cells, even after a 72 h incubation with NH₄Cl free medium. This is similar to what was observed with cells treated with L-glut free medium. The metabolic shock to the cells, that is 10 mM NH₄Cl, may not be rectified for several passages. There was, presumably, a high

ammonia concentration in the spent medium that was used to treat cells in Section 5.10. This ammonia would have accumulated slowly intracellularly as the cells grew and metabolised all available L-glut which may have very different physiological consequences to a large amount of NH₄Cl added exogenously in fresh medium.

Sodium butyrate addition may not only improve product yields but also alter the glycosylation of glycoproteins produced in CHO as reported by Lamotte et al. (1999). Mimira et al. (2001) reported that the addition of 2 mM NaBu to CHO-K1 cells did not alter the glycosylation or glycoform ratios of two IgG3 antibodies but the IgG titer increased significantly, 2-4 fold. It seems that effect of NaBu supplementation varies and therefore must be assessed for each glycoprotein. In Section 5.13 CHO DP-12 cells were treated with 3 mM NaBu, see Table 5.6. The largest increase in binding, 237.56 %, was observed using recombinant GafD1-178. This increase is not as noteworthy as it seems when the percentage of cells in the negative and positive gates are considered, i.e. less than 4 % of counted events were in the positive gate. A big fluctuation in MFI from a low number of events, without considering the number of cells in the gates, can lead to a misinterpretation of the data. The α -mannose binder, GNL, had increased binding, 60.72 %, to cells treated with 3 mM NaBu. This increase was greater than that observed for cells treated with L-glut free media, 19.23 %, or 10 mM NH₄Cl, 3.90 %. Additionally, GNL binding remained higher, 48.75 %, for cells treated with 3 mM NaBu even after a 96 h incubation in NaBu free medium. A large increase in LecA5K binding was also observed, 117 %, which decreased slightly, 90.66 %, when cells were reseeded in fresh medium with 0 mM NaBu. The decrease in MAL II binding, 13.96 %, was completely reversed, no statistical difference found between treated and untreated, upon reseeded the cells in fresh medium, see Fig. 5.50 and Fig. 5.51.

The purification of IgG1 using Protein A/G was successfully completed, see Fig. 5.54. The heavy and light chains, ~45 kDa and ~28 kDa, are clearly visible in the neat and concentrated supernatant in lanes 2 and 3. The Protein A/G captured all the IgG1 as it was not observed in the unbound fraction in lane 4. The captured IgG1 was eluted with the addition of 0.1 M glycine at pH 2.5 in lanes 8, 9 and 10. The purified IgG1 was shown to be specific for IL-8, see Fig. 5.56 p-value < 0.0001 n=3. To complete ELLA analysis on purified IgG1 the ELLA protocol described in Section 2.25 had to be

modified slightly. Initial efforts resulted in little or no lectin binding to purified IgG1, with the exception of Con A, data not shown. Immunoglobulin G1 contains an *N*-glycan at Asn297 on each heavy chain which is not easily accessed by lectins. There may be additional glycans in the antigen binding region although these are not conserved, i.e. only 10-20 % of IgGs have *N*-glycan sites here (Vidarsson et al. 2014). Purified IgG1 was treated for 30 min at various temperatures to separate the heavy chains and allow increased lectin access to the hinge region, see Fig. 5.57. This was successfully completed. Con A binding increased by 14.3 % when IgG1 was treated at 80 °C instead of 40 °C. AAL binding also increased, 109 %, over the same temperatures. Preheating purified IgG1 at 80 °C for 30 min prior to immobilising on a 96-well plate dramatically increased lectin access to the glycans. An anti-IgG mAb was included as an additional control which bound identically to IgG1 treated at 40-80 °C. Anti-IgG mAb binding dropped significantly, 60.9 %, when IgG1 was heated at 90 °C. In subsequent ELLAs for IgG1, the samples were heated treated at 80 °C for 30 min. At this temperature lectin binding was greatly improved but the IgG1 was still detected by the anti-IgG antibody. The latter was essential in order to ascribe a change in lectin binding to a change in the glycosylation of IgG1 and not to increased or reduced IgG1 in the well.

Immunoglobulin G1 was successfully purified from the supernatant of all treated CHO DP-12 cultures in Sections 5.10 to 5.13, see Fig. 5.58 and Table 5.7. The purified IgG1 was then quantified using a BCA assay, described in Section 2.23.1, and analysed by ELLA, see Fig. 5.59 and Fig. 5.60. Overall a correlation between lectin binding to the CHO DP-12 cell surface and IgG1 product was not found. The correlation between the CHO cell surface and product glycosylation was previously reported by Grainger and James (2013), particularly during stationary phase growth. There are a variety of reasons which could explain why this was not observed here; (i) the cells were analysed after being treated and the supernatant was collected at the same time. However, this supernatant will also contain IgG1 that was produced prior to the cells responding to the particular treatment and (ii) glycosylation changes to IgG1 may be infrequent and therefore only account for a relatively small fraction of the total IgG1 pool, which would make their detection more difficult.

Flow cytometry has been successfully used here to quantitatively assess CHO DP-12 cell surface glycans using a combination of recombinant lectins, produced in chapter 3, and commercial plant and fungal lectins. The binding observed was directly dependent on the cellular environment as a variety of lectins, most notably AAL-2, LecA5K, MAL II and PNA, had altered binding when cells were treated which was lessened upon the removal of the same treatment. The usefulness of recombinant lectins for live cell glycoanalysis is clearly demonstrated in this chapter.

Chapter 6

General Discussion

6.1 Discussion

The work presented here assesses the suitability of recombinant lectin probes for investigating the cell surface glycosylation of a mammalian cell line, CHO DP-12, in unison with fluorescent based techniques such as fluorescent microscopy and flow cytometry. The initial part of this work, aim 1, involved expressing and purifying recombinant lectins using IMAC, presented in Chapter 3. Due to the initial difficulties encountered while purifying AAL-2, see Section 3.3.2, a number of variations were cloned. This involved using a variety of molecular cloning techniques to isolate the DNA sequence encoding AAL-2 and insert it into other vectors so as to generate AAL-2 with a His₆ tag at the C-terminus and to introduce a spacer between the His₆ tag at the N-terminus at the start of the AAL-2 protein, see Section 3.3.3. This work was completed without knowing the structure of AAL-2, i.e. it was unknown whether the termini are exposed and if a His₆ tag would be accessible to Ni-charged IMAC resin. These attempts, including generating an EGFP-AAL-2 fusion protein, did not improve the purification of AAL-2 using IMAC. However, AAL-2 was successfully purified when the imidazole concentration in the wash buffers was optimised, see Section 3.3.4. This GlcNAc specific probe was appropriately biotinylated and its binding specificity was demonstrated by ELLA. An attempt was made to generate novel lectin probes through the mutagenesis of AAL-2. This work was again attempted prior to having structural information and binding pocket information about AAL-2 which ultimately proved to be unfruitful, see Appendix B.

The *P. aeruginosa* galactophilic lectin, LecA, was successfully expressed, purified and directly labelled with biotin. Initial efforts to biotinylate LecA were unsuccessful, see Fig. 3.25, due to the relatively low number of available amine groups which are found on the N-terminus and on lysine side chains. Four LecA variants were produced to incorporate additional lysine residues at either terminus to improve its biotinylation. All four variants had an increased signal compared to unmodified LecA when assessed with the anti-biotin mAb, see ELLA Fig. 3.35. However, when assessed by flow cytometry only 2 of the variants, LecAH3K and LecA5K, were superior to unmodified LecA, see Fig. 5.8. An EGFP-LecA fusion protein was also generated and successfully purified. This was produced to directly label the lectin with a fluorescent protein which would remove the need to biotinylate the lectin probe. A strong signal was not detected from

this fusion protein binding to CHO DP-12 cells by the flow cytometer although it was shown to be active and galactose specific by ELLA, see Fig. 3.35, and by fluorescent microscopy, see Fig. 4.10. This work shows the relative ease at which lectin probes can be altered through a combination of molecular techniques to enhance labelling and/or their purification using chromatographic methods. After the purification of recombinant lectin probes, their binding specificities were clearly demonstrated by ELLA. AAL-2 was inhibited with GlcNAc whereas its epimer, GalNAc did not reduce AAL-2 binding to bovine mucin or BSA-GlcNAc, see Fig. 3.16. A similar preference for GlcNAc only was shown by GafD1-178, see Fig. 3.22. LecA5K was fully inhibited by 50 mM Gal whereas 400 mM Glc did not reduce its binding as shown by ELLA, see Fig. 3.36. A cytotoxicity assay was completed, see Fig. 4.2, which confirmed that the recombinant lectins produced here are not toxic like some commercial plant lectins, e.g. Con A, RCA I and WGA all reduced CHO DP-12 cell viability.

Following the purification and characterisation of these lectin probes they were then used in conjunction with commercial plant and fungal lectins to glycoanalyse the surface of live cells using fluorescent microscopy and flow cytometry. The primary monosaccharides involved in eukaryotic glycosylation are shown in Fig. 1.2 and Table 1.1. A lectin panel was used which would be sufficient for detecting these glycan building blocks. Fluorescent microscopy was initially used to assess lectin binding qualitatively. This work is presented in Chapter 4. The binding specificities of these lectins were assessed again here using free monosaccharides. The cell surface is inherently more complex than an immobilised glycoprotein on a 96-well plate. These inhibition checks again verified the specificity of lectin binding while demonstrating that the recombinant lectins produced are appropriate for live cell glycoanalysis. However, some issues arose using the fluorescent microscope. Primarily strong fluorescent signal from non-cell artefacts on the plate, see Fig. 4.4 and Fig. 4.5. These regions can be ignored if a nuclear counterstain is not detected. However these artefacts may inflate the fluorescence attributed to lectin binding to the cell surface when they are adjacent to cells.

Flow cytometry was used to assess lectin binding to the CHO DP-12 cell surface, see Chapter 5. This quantitative method resolves some of the issues encountered when using

fluorescent microscopy, primarily the low number of cells analysed and high fluorescence from non-cell artefacts. However, a separate issue was faced here where the combined effect of lectin binding and centrifugation during cell preparation negatively impacted cell viability. To overcome this it was important to determine a suitable lectin probing concentration to achieve a sufficient lectin binding signal while minimising lectin toxicity. A lectin probing concentration of 5 $\mu\text{g}/\text{mL}$ at room temperature ($\sim 20\text{ }^\circ\text{C}$) was shown to be optimal, see Section 5.3, where typically a minimum of 60 % of cells remained in the live gate. It was necessary to optimise cell preparation due to the harsh conditions reported in some published protocols (Stanley and Sundaram 2014). They suggested three 10 min centrifugation steps at 800 g prior to incubation with lectin, up to 20 $\mu\text{g}/\text{mL}$, for up to 60 min followed by another 5 min centrifugation step at 1,000 g for preparing CHO cells. Here, these conditions were found to be harsh and caused unwanted and avoidable cell death. It was therefore essential that the cell preparation was optimised prior to probing cells with a large panel of lectins.

Flow cytometry is a quantitative technique; however, when comparing lectin binding to various cell samples, only those analysed during the same experiment were compared. This was done for a variety of reasons; (i) to add confidence to the results by eliminating variables, i.e. a single lectin mix was prepared and split between cell samples therefore lectin incubation time and cell preparation are identical as they are completed together and (ii) slight variation or drift in the flow cytometer from day to day, e.g. other users may have calibrated the instrument for cell cycle analysis between visits to the cytometer. Only comparing lectin binding patterns between cell samples analysed on the same day restricts the total number of lectins that can be used due to the constraints of working with live cells. However, a lectin panel of 15-20 lectins was typically used which is more than sufficient for glycoanalysing the CHO DP-12 cell surface.

Lectin binding profiles for adherent and suspension adapted CHO DP-12 cells were compared, see Table 5.2. Large differences in lectin binding were observed. Cell surface changes, as cells adapt to suspension culture, e.g. loss of cell surface attachment factors, and the change in cell surface area, see Fig. 5.7, could explain the differences observed. Lectin specificity checks with inhibiting sugars were completed using the flow

cytometer. These had been previously done using the fluorescent microscope however many lectins were only partially inhibited with the addition of a competing free monosaccharide. The inhibition checks completed using the flow cytometer, shown in Fig. 5.9 to Fig. 5.23, clearly show the monosaccharide discriminating power of lectins.

The major *N*- and *O*-glycans on the CHO cell surface have been comprehensively reported by North et al. (2009). They digested glycoproteins with trypsin prior to PNGase F treatment to release *N*-glycans. The release of *O*-glycans was completed using reductive elimination. The glycans were separated and analysed by MALDI-TOF tandem MS. The glycoprofile reported by North et al. (2009) was extensive, ranging from high mannose glycans, Man₉GlcNAc₂, to complex *N*-glycans, containing over 20 *N*-acetylglucosamine (Galβ1-4GlcNAc) units.

Here, a variety of cell treatments were investigated to determine if there were significant changes to lectin binding patterns as a result. Initially spent medium was used, see Section 5.10, which resulted in increased LecA5K (229 %) and PNA (781 %) binding and decreased MAL II (43 %) binding. When cells were treated with reduced L-glut, increased NH₄Cl or NaBu, lectin binding profiles changed. The changes observed were not the same for each of the medium treatments investigated. Recombinant lectins were shown to be suitable and appropriate probes for investigating cell surface glycans. The recombinant LecA5K was particularly informative as increased binding was observed for cells treated with spent medium, L-glut free medium or following treatment with NaBu which was subsequently reversed when the cells were reseeded in fresh medium. Where an increase in LecA5K binding was observed so was a decrease in MAL II binding. This result is to be expected as a decrease in sialic acid will naturally expose galactose residues leading to increased binding from galactophilic lectins.

Grainger and James (2013) have shown that variation in cell surface glycans, particularly outer-branch residues such as galactose, is cell line specific after they assessed six CHO cell lines, derived from CHO K1SV cells, all secreting the same IgG4 mAb. Similar work by Davies et al. (2013) has shown that cell surface glycosylation is clone specific, again particularly outer-branch residues, such as galactose, are more prone to variation. The work presented by Grainger and James (2013) and Davies et al.

(2013) has been built on here where the profiles of exposed cell surface glycans, again particularly galactophilic lectins, have been shown to change dramatically when cells are stressed through changing chemical conditions, i.e. depleted nutrient availability and increased ammonia. Low glutamine levels in cell culture has been shown to negatively impact the intracellular concentration of UTP (Fan et al. 2015). Similarly, work by Kochanowski et al. (2008), using CHO cells, has shown that glycosylation processes, particularly *N*-glycosylation, is affected by UTP concentration as it is a precursor molecule for the synthesis of activated sugars, e.g. UDP-GlcNAc and UDP-Glc. The changes in lectin binding observed here, particularly LecA5K, MAL II and PNA in Sections 5.10 and 5.11, could be explained by the intracellular UTP concentration being influenced by reduced nutrient availability.

Although there are many published reports on CHO cells focusing on optimising mAb production, there is however a scarcity of literature about glycosylation changes, to both cell and product, due to altered medium composition. Reinhart et al. (2015) has investigated the impact of various CHO cell culture media combinations on IgG yields and IgG glycans. Variation in IgG glycans was found between the eight commercially available media tested, e.g. undesirable high mannose glycans (Man₅GlcNAc₂) fluctuated between 3 % and 9 % of total IgG glycans. As such a variation was observed between the different culture media used it is therefore logical to assume nutrient depleted medium will have a similar if not greater effect on product glycosylation.

Mass spectrometry analysis of glycans is routinely completed to evaluate CHO cell engineering efforts to improve mAb glycosylation, e.g. increase sialylation (Lin et al. 2015). In upstream cell line development and clonal selection settings, this analysis is ideal as it is the most comprehensive. However, it is not as suited to providing information pertaining to the cell or product glycosylation in a timely fashion. Glycan analysis using MS based techniques has been discussed in the introduction chapter, see Section 1.5.2. The main disadvantage with this technique is the time required for sample preparation, i.e. protein digestion and glycan release, prior to glycan interrogation which may require in excess of 72 h. In addition, commonly used glycosidases, e.g. PNGase F, may not be able to cleave all *N*-glycans due to steric hindrance. Both these issues are

not a concern during glycan analysis using lectins where protein digestion and glycan release are not required.

Here, recombinant IgG1 was purified from CHO DP-12 cultures. An initial indirect ELISA showed that it was specific for IL-8 and that the cells were indeed CHO DP-12 as presumed. Immunoglobulin G1 was also purified from treated CHO DP-12 cultures to investigate a potential correlation between changes in lectin binding to IgG and the cell surface. No such correlation was found. Subtle changes are suggested, i.e. increased Con A and LCA binding to IgG from cells treated with 3 mM NaBu, see Fig. 5.60. However, the variation observed within a sample, in triplicate, is as great as the variation between samples and so these differences are not significant. There are many possible explanations for this including (i) a low percentage of IgG with altered glycans which makes detection difficult and (ii) lectin inaccessibility to glycans, although here, the IgG was heat treated to allow for increased lectin access, see Fig. 5.57, but perhaps this needs to be further optimised.

There are many areas of this work which could be further explored. Initially, the recombinant lectin library could be expanded through site-directed and random mutagenesis of LecA to generate non-toxic lectins, not only with a different binding specificity but those that are more stable which would ultimately expand the potential applications of these lectins, i.e. pH stable lectins are beneficial for lectin affinity chromatography (LAC) applications as they can withstand column cleaning conditions. This mutagenesis work would take considerable time as there are numerous ways in which lectin activity could be adversely affected. Additionally, more sensitive automated systems, such as the previously mentioned Pall FortéBio OctetRED96 in Section 1.9 which can quantitatively assess the binding kinetics of protein-glycan interactions, could be used in unison with lectin probes to rapidly glycoprofile a glycoprotein, e.g. mAb, at various points throughout the bioreactor campaign. This instrument may then establish if there is any correlation between cell surface and product glycans. Lastly, some of the cell culture treatments completed here could be repeated in a pilot sized bioreactor, ~5 L, to confirm if similar lectin binding patterns are obtained in a batch culture more akin to large scale manufacturing.

In summary the principal objectives of this work, see Section 1.12, were successfully achieved. Recombinant lectins were expressed, purified and their labelling was enhanced using site-directed mutagenesis. These novel lectins were characterised for their specificity by ELLA and shown to be suitable non-toxic probes for investigating cell surface glycosylation. The response of CHO DP-12 cell cultures to adverse cell culture medium treatments was such that lectin binding was significantly altered for many of the lectins used and in fact partially or completely reversible upon removal of the insult. The data obtained from lectin binding is obviously not as detailed as that from MS based techniques, see Section 1.5.2. However, the speed at which lectins can provide information regarding cell surface glycosylation is unparalleled, i.e. cells from a suspension culture may be isolated, washed, probed for 30 min with lectins and analysed by flow cytometry all within 60 min. This work has demonstrated how appropriate lectins are for assessing cell surface glycans.

References

-A-

Absolute antibody 2017. *Antibody structure IgG* [Online]. Available from: <http://absoluteantibody.com/antibody-resources/antibody-overview/antibody-structure/> [Accessed 12 April 2017].

Adan, A., Alizada, G., Kiraz, Y., Baran, Y. and Nalbant, A. 2017. Flow cytometry: Basic principles and applications. *Critical Reviews in Biotechnology*, 37(2), pp.163-176.

Ahn, W.S. and Antoniewicz, M.R. 2012. Towards dynamic metabolic flux analysis in CHO cell cultures. *Biotechnology Journal*, 7(1), pp.61-74.

Almeida, J.L., Cole, K.D. and Plant, A.L. 2016. Standards for cell line authentication and beyond. *PLoS Biology*, 14(6), pp.e1002476.

Altamirano, C., Paredes, C., Cairo, J.J. and Godia, F. 2000. Improvement of CHO cell culture medium formulation: Simultaneous substitution of glucose and glutamine. *Biotechnology Progress*, 16(1), pp.69-75.

Andersen, D.C. and Goochee, C.F. 1995. The effect of ammonia on the O-linked glycosylation of granulocyte colony-stimulating factor produced by chinese hamster ovary cells. *Biotechnology and Bioengineering*, 47(1), pp.96-105.

Andersen, D.C. and Krummen, L. 2002. Recombinant protein expression for therapeutic applications. *Current Opinion in Biotechnology*, 13(2), pp.117-123.

Anthony, R.M., Nimmerjahn, F., Ashline, D.J., Reinhold, V.N., Paulson, J.C. and Ravetch, J.V. 2008. Recapitulation of IVIG anti-inflammatory activity with a recombinant IgG fc. *Science (New York, N.Y.)*, 320(5874), pp.373-376.

Anthony, R.M., Kobayashi, T., Wermeling, F. and Ravetch, J.V. 2011. Intravenous gammaglobulin suppresses inflammation through a novel TH2 pathway. *Nature*, 475(7354), pp.110-113.

Arey, B.J. 2012. Chapter 12: The Role of Glycosylation in Receptor Signaling *IN: Petrescu, S. (ed.) Glycosylation*. Rijeka: InTech, pp.273-286.

Arnold, J.N., Wormald, M.R., Sim, R.B., Rudd, P.M. and Dwek, R.A. 2007. The impact of glycosylation on the biological function and structure of human immunoglobulins. *Annual Review of Immunology*, 25, pp.21-50.

Auriti, C., Prencipe, G., Moriondo, M., Bersani, I., Bertaina, C., Mondini, V. and Inglese, R. 2017. Mannose-binding lectin: Biologic characteristics and role in the susceptibility to infections and ischemia-reperfusion related injury in critically ill neonates. *Journal of Immunology Research*, 2017(7045630), pp.1-11.

Azuma, Y., Taniguchi, A. and Matsumoto, K. 2000. Decrease in cell surface sialic acid in etoposide-treated jurkat cells and the role of cell surface sialidase. *Glycoconjugate Journal*, 17(5), pp.301-306.

-B-

Baneyx, F. 1999. Recombinant protein expression in escherichia coli. *Current Opinion in Biotechnology*, 10(5), pp.411-421.

Banga, A.K. 2015. *Therapeutic Peptides and Proteins: Formulation, Processing, and Delivery Systems*. 3rd ed. Florida: CRC Press.

Bapu, D., Runions, J., Kadhim, M. and Brooks, S.A. 2016. N-acetylgalactosamine glycans function in cancer cell adhesion to endothelial cells: A role for truncated O-glycans in metastatic mechanisms. *Cancer Letters*, 375(2), pp.367-374.

Barondes, S.H. 1988. Bifunctional properties of lectins: Lectins redefined. *Trends in Biochemical Sciences*, 13(12), pp.480-482.

Batisse, C., Marquet, J., Greffard, A., Fleury-Feith, J., Jaurand, M.C. and Pilatte, Y. 2004. Lectin-based three-color flow cytometric approach for studying cell surface glycosylation changes that occur during apoptosis. *Cytometry. Part A: The Journal of the International Society for Analytical Cytology*, 62(2), pp.81-88.

BD 2013. *BD protocol cell surface staining* [Online]. Available from: https://wwwbdbiosciences.com/documents/BD_Protocol_CellSurface_Staining_StemCell.pdf [Accessed 22 May 2017].

BD 2017. *Fitc annexin V apoptosis detection kit i* [Online]. Available from: <http://www.bdbiosciences.com/eu/applications/research/apoptosis/apoptosis-kits-sets/fitc-annexin-v-apoptosis-detection-kit-i/p/556547> [Accessed 03 April 2017].

Beckman 2017. *Moflo astrios eq* [Online]. Available from: <http://www.beckman.com/coulter-flow-cytometry/instruments/cell-sorters/moflo-astrios-eq> [Accessed 1 April 2017].

Beer, A., Andre, S., Kaltner, H., Lensch, M., Franz, S., Sarter, K., Schulze, C., Gaipf, U.S., Kern, P., Herrmann, M. and Gabius, H.J. 2008. Human galectins as sensors for apoptosis/necrosis-associated surface changes of granulocytes and lymphocytes. *Cytometry. Part A: The Journal of the International Society for Analytical Cytology*, 73(2), pp.139-147.

Behr, J.R. and Sasisekharan, R. 2007. Integrated approach to glycan structure-function relationships IN: Sansom, C. and Markman, O. (eds.) *Glycobiology*. Bloxham: Scion, pp.78-92.

Berg, J.M., Tymoczko, J.L. and Stryer, L. 2002. *Biochemistry*. 5th ed. New York: WH Freeman.

BioLegend 2010. *BioLegend surface staining flow protocol* [Online]. Available from: https://www.biolegend.com/media_assets/support_protocol/BioLegend_Surface_Staining_Flow_Protocol.pdf [Accessed 21 May 2017].

BioLegend 2016. *DyLight 488 streptavidin* [Online]. Available from: <https://www.biolegend.com/en-us/products/dyLight-488-streptavidin-6793> [Accessed 20 May 2017].

Blanchard, B., Nurisso, A., Hollville, E., Tétaud, C., Wiels, J., Pokorná, M., Wimmerová, M., Varrot, A. and Imberty, A. 2008. Structural basis of the preferential binding for globo-series glycosphingolipids displayed by pseudomonas aeruginosa lectin I. *Journal of Molecular Biology*, 383(4), pp.837-853.

Bondos, S.E. and Bicknell, A. 2003. Detection and prevention of protein aggregation before, during, and after purification. *Analytical Biochemistry*, 316(2), pp.223-231.

Boraston, A., Bouckaert, J. and Imberty, A. 2011. *f17g/gafd* [Online]. Available from: <http://www.functionalglycomics.org/CFGparadigms/index.php/F17G/GafD> [Accessed 05 April 2017].

Bork, K., Horstkorte, R. and Weidemann, W. 2009. Increasing the sialylation of therapeutic glycoproteins: The potential of the sialic acid biosynthetic pathway. *Journal of Pharmaceutical Sciences*, 98(10), pp.3499-3508.

Bushnell, T. 2015. *How to create the right flow cytometry antibody panel every time* [Online]. Available from: <https://expertcytometry.com/flow-cytometry-antibody-panel/> [Accessed 02 April 2017].

Butler, M. 2006. Optimisation of the cellular metabolism of glycosylation for recombinant proteins produced by mammalian cell systems. *Cytotechnology*, 50(1-3), pp.57-76.

Byrne, B., Donohoe, G.G. and O'Kennedy, R. 2007. Sialic acids: Carbohydrate moieties that influence the biological and physical properties of biopharmaceutical proteins and living cells. *Drug Discovery Today*, 12(7-8), pp.319-326.

-C-

Campbell, C.T. and Yarema, K.J. 2005. Large-scale approaches for glycobiology. *Genome Biology*, 6(11), pp.236-236.

Caramelo, J.J. and Parodi, A.J. 2015. A sweet code for glycoprotein folding. *FEBS Letters*, 589(22), pp.3379-3387.

Chacko, B.K. and Appukuttan, P.S. 2001. Peanut (*Arachis hypogaea*) lectin recognizes α -linked galactose, but not N-acetyl lactosamine in N-linked oligosaccharide terminals. *International Journal of Biological Macromolecules*, 28(5), pp.365-71.

Chandler, K.B. and Costello, C.E. 2016. Glycomics and glycoproteomics of membrane proteins and cell-surface receptors: Present trends and future opportunities. *Electrophoresis*, 37(11), pp.1407-1419.

Chen, F., Ye, Z., Zhao, L., Liu, X., Fan, L. and Tan, W.S. 2012. Correlation of antibody production rate with glucose and lactate metabolism in Chinese hamster ovary cells. *Biotechnology Letters*, 34(3), pp.425-432.

Chen, F., Kou, T., Fan, L., Zhou, Y., Ye, Z., Zhao, L. and Tan, W. 2011. The combined effect of sodium butyrate and low culture temperature on the production, sialylation, and biological activity of an antibody produced in CHO cells. *Biotechnology and Bioprocess Engineering*, 16(6), pp.1157-1165.

Chung, B., Jeong, Y., Choi, O. and Kim, J. 2001. Effect of Sodium Butyrate on Glycosylation of Recombinant Erythropoietin *IN*: Lindner-Olsson, E., Chatzissavidou, N. and Lüllau, E. (eds.) *Animal Cell Technology: From Target to Market: Proceedings of the 17th ESACT Meeting Tylösand, Sweden, June 10-14, 2001*. Dordrecht: Springer Netherlands, pp.207-209.

Cohen, M., Hurtado-Ziola, N. and Varki, A. 2009. ABO blood group glycans modulate sialic acid recognition on erythrocytes. *Blood*, 114(17), pp.3668-3676.

Cohen, S.N., Chang, A.C.Y., Boyer, H.W. and Helling, R.B. 1973. Construction of biologically functional bacterial plasmids *in vitro*. *Proceedings of the National Academy of Sciences of the United States of America*, 70(11), pp.3240-3244.

Comer, F.I., Vosseller, K., Wells, L., Accavitti, M.A. and Hart, G.W. 2001. Characterization of a mouse monoclonal antibody specific for O-linked N-acetylglucosamine. *Analytical Biochemistry*, 293(2), pp.169-177.

Corfield, A.P. and Berry, M. 2015. Glycan variation and evolution in the eukaryotes. *Trends in Biochemical Sciences*, 40(7), pp.351-359.

Crespo, H., Guadalupe Cabral, M., Teixeira, A.V., Lau, J.T.Y., Trindade, H. and Videira, P.A. 2008. Effect of sialic acid loss on dendritic cell maturation. *Immunology*, 128(1), pp.e621-e631.

Crespo, H., Lau, J.T.Y. and Videira, P.A. 2013. Dendritic cells: A spot on sialic acid. *Frontiers in Immunology*, 4(491), pp.1-15.

-D-

D'Alessandris, C., Andreozzi, F., Federici, M., Cardellini, M., Brunetti, A., Ranalli, M., Del Guerra, S., Lauro, D., Del Prato, S., Marchetti, P., Lauro, R. and Sesti, G. 2004. Increased O-glycosylation of insulin signaling proteins results in their impaired activation and enhanced susceptibility to apoptosis in pancreatic beta-cells. *FASEB Journal: Official Publication of the Federation of American Societies for Experimental Biology*, 18(9), pp.959-961.

D'Angelo, G., Capasso, S., Sticco, L. and Russo, D. 2013. Glycosphingolipids: Synthesis and functions. *FEBS Journal*, 280(24), pp.6338-6353.

Davies, S.L., Lovelady, C.S., Grainger, R.K., Racher, A.J., Young, R.J. and James, D.C. 2013. Functional heterogeneity and heritability in CHO cell populations. *Biotechnology and Bioengineering*, 110(1), pp.260-274.

Dekkers, G., Plomp, R., Koeleman, C.A., Visser, R., von Horsten, H.H., Sandig, V., Rispens, T., Wuhrer, M. and Vidarsson, G. 2016. Multi-level glyco-engineering techniques to generate IgG with defined fc-glycans. *Scientific Reports*, 6, pp.36964.

Dell, A., Galadari, A., Sastre, F. and Hitchen, P. 2010. Similarities and differences in the glycosylation mechanisms in prokaryotes and eukaryotes vol. 2010, article ID 148178, 14 pages, 2010. *International Journal of Microbiology*, 2010(148178), pp.1-14.

Dotan, N., Altstock, R.T., Schwarz, M. and Dukler, A. 2006. Anti-glycan antibodies as biomarkers for diagnosis and prognosis. *Lupus*, 15(7), pp.442-450.

Durocher, Y. and Butler, M. 2009. Expression systems for therapeutic glycoprotein production. *Current Opinion in Biotechnology*, 20(6), pp.700-707.

-E-

Edelman, G.M., Cunningham, B.A., Reeke, G.N., Becker, J.W., Waxdal, M.J. and Wang, J.L. 1972. The covalent and three-dimensional structure of concanavalin A. *Proceedings of the National Academy of Sciences of the United States of America*, 69(9), pp.2580-2584.

Eklund, E.A. and Freeze, H.H. 2005. Essentials of glycosylation. *Seminars in Pediatric Neurology*, 12(3), pp.134-143.

Ellgaard, L. and Helenius, A. 2003. Quality control in the endoplasmic reticulum. *Nature Reviews. Molecular Cell Biology*, 4(3), pp.181-191.

EMA 1999. *European medicines agency remicade* [Online]. Available from: http://www.ema.europa.eu/docs/en_GB/document_library/EPAR_-_Product_Information/human/000240/WC500050888.pdf [Accessed 14 April 2017].

EMA 2012. *Elelyso assessment report* [Online]. Available from: http://www.ema.europa.eu/docs/en_GB/document_library/EPAR_-_Public_assessment_report/human/002250/WC500135112.pdf [Accessed 05 February 2017].

EMA 2015a. *European medicines agency avastin* [Online]. Available from: http://www.ema.europa.eu/docs/en_GB/document_library/EPAR_-_Scientific_Discussion/human/000582/WC500029262.pdf [Accessed 15 August 2016].

EMA 2015b. *European medicines agency raptiva* [Online]. Available from: http://www.ema.europa.eu/docs/en_GB/document_library/EPAR_-_Scientific_Discussion/human/000542/WC500057849.pdf [Accessed 15 August 2016].

EMA 2016. *Flixabi assessment report* [Online]. Available from: http://www.ema.europa.eu/docs/en_GB/document_library/EPAR_-_Public_assessment_report/human/004020/WC500208358.pdf [Accessed 11 April 2017].

Engvall, E. and Perlmann, P. 1971. Enzyme-linked immunosorbent assay (ELISA). Quantitative assay of immunoglobulin G. *Immunochemistry*, 8(9), pp.871-874.

Esser, A.K., Miller, M.R., Huang, Q., Meier, M.M., Beltran-Valero, d.B., Stipp, C.S., Campbell, K.P., Lynch, C.F., Smith, B.J., Cohen, M.B. and Henry, M.D. 2012. Loss of LARGE2 disrupts functional glycosylation of α -dystroglycan in prostate cancer. *The Journal of Biological Chemistry*, 288(4), pp.2132-2142.

-F-

Fan, Y., Jimenez Del Val, I., Muller, C., Lund, A.M., Sen, J.W., Rasmussen, S.K., Kontoravdi, C., Baycin-Hizal, D., Betenbaugh, M.J., Weilguny, D. and Andersen, M.R. 2015. A multi-pronged investigation into the effect of glucose starvation and culture duration on fed-batch CHO cell culture. *Biotechnology and Bioengineering*, 112(10), pp.2172-2184.

Fan, Y., Jimenez Del Val, I., Muller, C., Wagtberg Sen, J., Rasmussen, S.K., Kontoravdi, C., Weilguny, D. and Andersen, M.R. 2015. Amino acid and glucose metabolism in fed-batch CHO cell culture affects antibody production and glycosylation. *Biotechnology and Bioengineering*, 112(3), pp.521-535.

Ferrini, J., Martin, M., Taupiac, M. and Beaumelle, B. 1995. Expression of functional ricin B chain using the baculovirus system. *European Journal of Biochemistry*, 233(3), pp.772-777.

Fox, J.L. 2012. First plant-made biologic approved. *Nature Biotechnology*, 30(6), pp.472-472.

Franz, S., Frey, B., Sheriff, A., Gaipf, U.S., Beer, A., Voll, R.E., Kalden, J.R. and Herrmann, M. 2006. Lectins detect changes of the glycosylation status of plasma membrane constituents during late apoptosis. *Cytometry.Part A : The Journal of the International Society for Analytical Cytology*, 69(4), pp.230-239.

Freeze, H.H. 2013. Understanding human glycosylation disorders: Biochemistry leads the charge. *The Journal of Biological Chemistry*, 288(10), pp.6936-6945.

Freeze, H.H., Eklund, E.A., Ng, B.G. and Patterson, M.C. 2015. Neurological aspects of human glycosylation disorders. *Annual Review of Neuroscience*, 38, pp.105-125.

-G-

Galili, U. 2013. Anti-gal: An abundant human natural antibody of multiple pathogenesis and clinical benefits. *Immunology*, 140(1), pp.1-11.

Gasparini, R., Panatto, D., Bragazzi, N.L., Lai, P.L., Bechini, A., Levi, M., Durando, P. and Amicizia, D. 2015. How the knowledge of interactions between meningococcus and the human immune system has been used to prepare effective neisseria meningitidis vaccines. *Journal of Immunology Research*, 2015, pp.1-26.

Gawlitzeck, M., Ryll, T., Lofgren, J. and Sliwkowski, M.B. 2000. Ammonium alters *N*-glycan structures of recombinant TNFR-IgG: Degradative versus biosynthetic mechanisms. *Biotechnology and Bioengineering*, 68(6), pp.637-646.

Gemeiner, P., Mislovičová, D., Tkáč, J., Švitel, J., Pätoprstý, V., Hrabárová, E., Kogan, G. and Kožár, T. 2009. Lectinomics: II. A highway to biomedical/clinical diagnostics. *Biotechnology Advances*, 27(1), pp.1-15.

Gerlach, J.Q., Sharma, S., Leister, K.J. and Joshi, L. 2012. A Tight-Knit Group: Protein Glycosylation, Endoplasmic Reticulum Stress and the Unfolded Protein Response *IN*: Agostinis, P. and Afshin, S. (eds.) *Endoplasmic Reticulum Stress in Health and Disease*. 1st ed. Netherlands: Springer, pp.23-39.

Geyer, H. and Geyer, R. 2006. Strategies for analysis of glycoprotein glycosylation. *Biochimica Et Biophysica Acta*, 1764(12), pp.1853-1869.

Gilboa-Garber, N. and Sudakevitz, D. 1999. The hemagglutinating activities of pseudomonas aeruginosa lectins PA-IL and PA-IIL exhibit opposite temperature profiles due to different receptor types. *FEMS Immunology and Medical Microbiology*, 25(4), pp.365-369.

Gohlke, M. 2002. Separation of *N*-Glycans by HPLC *IN*: Kannicht, C. (ed.) *Posttranslational Modifications of Proteins*. 1st ed. New Jersey: Humana Press, pp.45-61.

Grainger, R.K. and James, D.C. 2013. CHO cell line specific prediction and control of recombinant monoclonal antibody *N*-glycosylation. *Biotechnology and Bioengineering*, 110(11), pp.2970-2983.

Gronemeyer, P., Ditz, R. and Strube, J. 2014. Trends in Upstream and Downstream Process Development for Antibody Manufacturing. *Bioengineering*, 1(4), pp.188-212.

Groves, J.A., Lee, A., Yildirim, G. and Zachara, N.E. 2013. Dynamic O-GlcNAcylation and its roles in the cellular stress response and homeostasis. *Cell Stress & Chaperones*, 18(5), pp.535-558.

Gu, J., Isaji, T., Sato, Y., Kariya, Y. and Fukuda, T. 2009. Importance of N-glycosylation on alpha5beta1 integrin for its biological functions. *Biological & Pharmaceutical Bulletin*, 32(5), pp.780-785.

Gu, J., Isaji, T., Xu, Q., Kariya, Y., Gu, W., Fukuda, T. and Du, Y. 2012. Potential roles of N-glycosylation in cell adhesion. *Glycoconjugate Journal*, 29(8), pp.599-607.

Guo, H.B., Lee, I., Kamar, M., Akiyama, S.K. and Pierce, M. 2002. Aberrant N-glycosylation of beta1 integrin causes reduced alpha5beta1 integrin clustering and stimulates cell migration. *Cancer Research*, 62(23), pp.6837-6845.

Gupta, G., Surolia, A. and Sampathkumar, S.G. 2010. Lectin microarrays for glycomic analysis. *Omics : A Journal of Integrative Biology*, 14(4), pp.419-436.

-H-

Hallgren, P., Lundblad, A. and Svensson, S. 1975. A new type of carbohydrate-protein linkage in a glycopeptide from normal human urine. *The Journal of Biological Chemistry*, 250(14), pp.5312-5314.

Hamilton, S.R. and Gerngross, T.U. 2007. Glycosylation engineering in yeast: The advent of fully humanized yeast. *Current Opinion in Biotechnology*, 18(5), pp.387-392.

Hanahan, D. 1985. Techniques for transformation of *E. coli*. *IN: Anonymous DNA Cloning*. 1st ed. Ireland: IRL Press Oxford,

Hara, Y., Kanagawa, M., Kunz, S., Yoshida-Moriguchi, T., Satz, J.S., Kobayashi, Y.M., Zhu, Z., Burden, S.J., Oldstone, M.B. and Campbell, K.P. 2011. Like-acetylglucosaminyltransferase (LARGE)-dependent modification of dystroglycan at thr-317/319 is required for laminin binding and arenavirus infection. *Proceedings of the National Academy of Sciences of the United States of America*, 108(42), pp.17426-17431.

Hardman, K.D. and Ainsworth, C.F. 1972. Structure of concanavalin A at 2.4-Å resolution. *Biochemistry*, 11(26), pp.4910-4919.

Hart, G.W., Slawson, C., Ramirez-Correa, G. and Lagerlof, O. 2011. Cross talk between O-GlcNAcylation and phosphorylation: Roles in signaling, transcription, and chronic disease. *Annual Review of Biochemistry*, 80, pp.825-858.

Hart, G.W., Housley, M.P. and Slawson, C. 2007. Cycling of O-linked beta-N-acetylglucosamine on nucleocytoplasmic proteins. *Nature*, 446(7139), pp.1017-1022.

Harvey, D.J., Wing, D.R., Küster, B. and Wilson, I.B.H. 2000. Composition of N-linked carbohydrates from ovalbumin and co-purified glycoproteins. *Journal of the American Society for Mass Spectrometry*, 11(6), pp.564-571.

Harwood, K.R. and Hanover, J.A. 2014. Nutrient-driven O-GlcNAc cycling – think globally but act locally. *Journal of Cell Science*, 127(9), pp.1857-1867.

Hayter, P.M., Curling, E.M., Baines, A.J., Jenkins, N., Salmon, I., Strange, P.G., Tong, J.M. and Bull, A.T. 1992. Glucose-limited chemostat culture of Chinese hamster ovary cells producing recombinant human interferon-gamma. *Biotechnology and Bioengineering*, 39(3), pp.327-335.

Hendrick, V., Winnepenninckx, P., Abdelkafi, C., Vandeputte, O., Cherlet, M., Marique, T., Renemann, G., Loa, A., Kretzmer, G. and Werenne, J. 2001. Increased productivity of recombinant tissular plasminogen activator (t-PA) by butyrate and shift of temperature: A cell cycle phases analysis. *Cytotechnology*, 36(1-3), pp.71-83.

Hennet, T. 2012. Diseases of glycosylation beyond classical congenital disorders of glycosylation. *Biochimica Et Biophysica Acta (BBA) - General Subjects; Glycoproteomics*, 1820(9), pp.1306-1317.

Heyder, P., Gaipf, U.S., Beyer, T.D., Voll, R.E., Kern, P.M., Stach, C., Kalden, J.R. and Herrmann, M. 2003. Early detection of apoptosis by staining of acid-treated apoptotic cells with FITC-labeled lectin from narcissus pseudonarcissus. *Cytometry. Part A : The Journal of the International Society for Analytical Cytology*, 55(2), pp.86-93.

Holmes, K., Lantz, L.M., Fowlkes, B.J., Schmid, I. and Giorgi, J.V. 2001. Preparation of cells and reagents for flow cytometry. *Current Protocols in Immunology*, Chapter 5, pp.Unit 5.3.

Hossler, P., Khattak, S.F. and Li, Z.J. 2009. Optimal and consistent protein glycosylation in mammalian cell culture. *Glycobiology*, 19(9), pp.936-949.

Hsu, K. and Mahal, L.K. 2009. Sweet tasting chips: Microarray-based analysis of glycans. *Current Opinion in Chemical Biology*, 13(4), pp.427-432.

Huang, H., Hsing, H., Lai, T., Chen, Y., Lee, T., Chan, H., Lyu, P., Wu, C., Lu, Y., Lin, S., Lin, C., Lai, C., Chang, H., Chou, H. and Chan, H. 2010. Trypsin-induced proteome alteration during cell subculture in mammalian cells. *Journal of Biomedical Science*, 17(1), pp.36.

Hudgin, R.L., Pricer, W.E., Jr, Ashwell, G., Stockert, R.J. and Morell, A.G. 1974. The isolation and properties of a rabbit liver binding protein specific for asialoglycoproteins. *The Journal of Biological Chemistry*, 249(17), pp.5536-5543.

-I-

Ihara, Y., Inai, Y., Ikezaki, M., Matsui, I.L., Manabe, S. and Ito, Y. 2014. C-Mannosylation: A Modification on Tryptophan in Cellular Proteins *IN: Endo, T., Seeberger, P.H., Hart, G.W., Wong, C. and Taniguchi, N. (eds.) Glycoscience: Biology and Medicine*. Tokyo: Springer Japan, pp.1-8.

Imberty, A., Wimmerová, M., Mitchell, E.P. and Gilboa-Garber, N. 2004. Structures of the lectins from *Pseudomonas aeruginosa*: Insights into the molecular basis for host glycan recognition. *Microbes and Infection*, 6(2), pp.221-228.

Ip, W.K., Takahashi, K., Ezekowitz, R.A. and Stuart, L.M. 2009. Mannose-binding lectin and innate immunity. *Immunological Reviews*, 230(1), pp.9-21.

IrvineSci 2015. *BalanCD CHO growth A* [Online]. Available from: http://www.irvinesci.com/uploads/technical-documentations/40960_BalanCD_CHO_Growth_A_Rev1_WEB.pdf [Accessed 20 May 2017].

-J-

Jagusic, M., Forcic, D., Brgles, M., Kutle, L., Santak, M., Jergovic, M., Kotarski, L., Bendelja, K. and Halassy, B. 2016. Stability of minimum essential medium functionality despite l-glutamine decomposition. *Cytotechnology*, 68(4), pp.1171-1183.

Jayapal, K., Wlaschin, K., Hu, W. and Yap, M. 2007. Recombinant protein therapeutics from CHO cells - 20 years and counting. *Chemical Engineering Progress*, 103, pp.40-47.

Jenkins, N., Parekh, R.B. and James, D.C. 1996. Getting the glycosylation right: Implications for the biotechnology industry. 14(8), pp.975-981.

Jiang, S., Chen, Y., Wang, M., Yin, Y., Pan, Y., Gu, B., Yu, G., Li, Y., Wong, B., Liang, Y. and Sun, H. 2012. A novel lectin from agrocybe aegerita shows high binding selectivity for terminal N-acetylglucosamine. *Biochemical Journal*, 443, pp.369-378.

JIC - John Innes Centre 2016. *Fluorescence microscopy* [Online]. Available from: https://www.jic.ac.uk/microscopy/more/T5_6.htm [Accessed 25 March 2017].

JM109 *Stratagene - Genotypes of bacterial strains* [Online]. Available from: http://www.genomics.agilent.com/files/Mobio/Strains_Genotypes_of_Bacterial_Strains_2pgs.pdf [Accessed November 23 2016].

Johnson, M.B. and Criss, A.K. 2013. Fluorescence microscopy methods for determining the viability of bacteria in association with mammalian cells. *Journal of Visualized Experiments*, 79(e50729), pp.1-9.

Julenius, K., Johansen, M.B., Zhang, Y., Brunak, S. and Gupta, R. 2009. Prediction of Glycosylation Sites in Proteins *IN*: von der Lieth, C.W., Lütteke, T. and Frank, M. (eds.) *Bioinformatics for Glycobiology and Glycomics*. John Wiley & Sons, Ltd, pp.163-192.

-K-

Kadam, R.U., Bergmann, M., Garg, D., Gabrieli, G., Stocker, A., Darbre, T. and Reymond, J. 2013. Structure-based optimization of the terminal tripeptide in glycopeptide dendrimer inhibitors of pseudomonas aeruginosa biofilms targeting LecA. *Chemistry - A European Journal*, 19(50), pp.17054-17063.

Kaneko, Y., Nimmerjahn, F. and Ravetch, J.V. 2006. Anti-inflammatory activity of immunoglobulin G resulting from fc sialylation. *Science*, 313(5787), pp.670-673.

Karnieli, O., Friedner, O.M., Allickson, J.G., Zhang, N., Jung, S., Fiorentini, D., Abraham, E., Eaker, S.S., Yong, T.K., Chan, A., Griffiths, S., When, A.k., Oh, S. and Karnieli, O. 2017. A consensus introduction to serum replacements and serum-free media for cellular therapies. *Cytotherapy*, 19(2), pp.155-169.

Karsten, C.M., Pandey, M.K., Figge, J., Kilchenstein, R., Taylor, P.R., Rosas, M., McDonald, J.U., Orr, S.J., Berger, M., Petzold, D., Blanchard, V., Winkler, A., Hess, C., Reid, D.M., Majoul, I.V., Strait, R.T., Harris, N.L., Kohl, G., Wex, E., Ludwig, R., Zillikens, D., Nimmerjahn, F., Finkelman, F.D., Brown, G.D., Ehlers, M. and Kohl, J. 2012. Anti-inflammatory activity of IgG1 mediated by fc galactosylation and association of fc γ RIIB and dectin-1. *Nature Medicine*, 18(9), pp.1401-1406.

Kelley, B.D. 2001. Biochemical engineering: Bioprocessing of therapeutic proteins. *Current Opinion in Biotechnology*, 12(2), pp.173-174.

Kelley, B. 2009. Industrialization of mAb production technology: The bioprocessing industry at a crossroads. *Mabs*, 1(5), pp.443-452.

Kentzer, E.J., Buko, A., Menon, G. and Sarin, V.K. 1990. Carbohydrate composition and presence of a fucose-protein linkage in recombinant human pro-urokinase. *Biochemical and Biophysical Research Communications*, 171(1), pp.401-406.

- Keogh, D., Thompson, R., Larragy, R., McMahon, K., O'Connell, M., O'Connor, B. and Clarke, P. 2014. Generating novel recombinant prokaryotic lectins with altered carbohydrate binding properties through mutagenesis of the PA-IL protein from *Pseudomonas aeruginosa*. *Biochimica Et Biophysica Acta (BBA) - General Subjects*, 1840(6), pp.2091-2104.
- Kim, H.J., Lee, S.J. and Kim, H. 2008. Antibody-based enzyme-linked lectin assay (ABELLA) for the sialylated recombinant human erythropoietin present in culture supernatant. *Journal of Pharmaceutical and Biomedical Analysis*, 48(3), pp.716-721.
- Kim, J.Y., Kim, Y.G. and Lee, G.M. 2012. CHO cells in biotechnology for production of recombinant proteins: Current state and further potential. *Applied Microbiology and Biotechnology*, 93(3), pp.917-930.
- Kim, N.S. and Lee, G.M. 2000. Overexpression of bcl-2 inhibits sodium butyrate-induced apoptosis in Chinese hamster ovary cells resulting in enhanced humanized antibody production. *Biotechnology and Bioengineering*, 71(3), pp.184-193.
- Kinoshita, M., Murakami, E., Oda, Y., Funakubo, T., Kawakami, D., Kakehi, K., Kawasaki, N., Morimoto, K. and Hayakawa, T. 2000. Comparative studies on the analysis of glycosylation heterogeneity of sialic acid-containing glycoproteins using capillary electrophoresis. *Journal of Chromatography A*, 866(2), pp.261-271.
- Kobata, A. and Amano, J. 2005. Altered glycosylation of proteins produced by malignant cells, and application for the diagnosis and immunotherapy of tumours. *Immunology and Cell Biology*, 83(4), pp.429-439.
- Kochanowski, N., Blanchard, F., Cacan, R., Chirat, F., Guedon, E., Marc, A. and Goergen, J.L. 2008. Influence of intracellular nucleotide and nucleotide sugar contents on recombinant interferon-gamma glycosylation during batch and fed-batch cultures of CHO cells. *Biotechnology and Bioengineering*, 100(4), pp.721-733.
- Krishnamoorthy, L. and Mahal, L.K. 2009. Glycomic analysis: An array of technologies. *ACS Chemical Biology*, 4(9), pp.715-732.

KRX Promega - bacterial strains for protein expression [Online]. Available from: <https://www.promega.com/-/media/files/resources/product-guides/proteomics/bacterial-strains-for-protein-expression.pdf?la=en> [Accessed November 23 2016].

Kugelberg, E., Gollan, B. and Tang, C.M. 2008. Mechanisms in neisseria meningitidis for resistance against complement-mediated killing. *Vaccine*, 26(6), pp.I34-I39.

-L-

Laemmli, U.K. 1970. Cleavage of structural proteins during the assembly of the head of bacteriophage T4. *Nature*, 227(5259), pp.680-685.

Lagassé, H.D., Alexaki, A., Simhadri, V.L., Katagiri, N.H., Jankowski, W., Sauna, Z.E. and Kimchi-Sarfaty, C. 2017. Recent advances in (therapeutic protein) drug development. *F1000research*, 6, pp.113.

Laine, R.A. 1997. Information capacity of the carbohydrate code. *Pure and Applied Chemistry*, 69(9), pp.1867-1873.

Laken, H.A. and Leonard, M.W. 2001. Understanding and modulating apoptosis in industrial cell culture. *Current Opinion in Biotechnology*, 12(2), pp.175-179.

Lam, S.K. and Ng, T.B. 2011. Lectins: Production and practical applications. *Applied Microbiology and Biotechnology*, 89(1), pp.45-55.

Lamotte, D., Buckberry, L., Monaco, L., Soria, M., Jenkins, N., Engasser, J. and Marc, A. 1999. Na-butyrate increases the production and α 2,6-sialylation of recombinant interferon- γ expressed by α 2,6-sialyltransferase engineered CHO cells. *Cytotechnology*, 29(1), pp.55-64.

Lauc, G., Huffman, J.E., Pucic, M., Zgaga, L., Adamczyk, B., Muzinic, A., Novokmet, M., Polasek, O., Gornik, O., Kristic, J., Keser, T., Vitart, V., Scheijen, B., Uh, H.W., Molokhia, M., Patrick, A.L., McKeigue, P., Kolcic, I., Lukic, I.K., Swann, O., van Leeuwen, F.N., Ruhaak, L.R., Houwing-Duistermaat, J.J., Slagboom, P.E., Beekman, M., de Craen, A.J., Deelder, A.M., Zeng, Q., Wang, W., Hastie, N.D., Gyllensten, U., Wilson, J.F., Wuhrer, M., Wright, A.F., Rudd, P.M., Hayward, C., Aulchenko, Y., Campbell, H. and Rudan, I. 2013. Loci associated with *N*-glycosylation of human immunoglobulin G show pleiotropy with autoimmune diseases and haematological cancers. *PLoS Genetics*, 9(1), pp.e1003225.

Lauc, G., Kristic, J. and Zoldos, V. 2014. Glycans - the third revolution in evolution. *Frontiers in Genetics*, 5, pp.145.

Lebendiker, M. and Danieli, T. 2014. Production of prone-to-aggregate proteins. *FEBS Letters*, 588(2), pp.236-246.

Lee, D.Y., Hayes, J.J., Pruss, D. and Wolffe, A.P. 1993. A positive role for histone acetylation in transcription factor access to nucleosomal DNA. *Cell*, 72(1), pp.73-84.

Lee, J.S. and Lee, G.M. 2012. Effect of sodium butyrate on autophagy and apoptosis in Chinese hamster ovary cells. *Biotechnology Progress*, 28(2), pp.349-357.

Lee, J.S., Wee, T.L. and Brown, C.M. 2014. Calibration of wide-field deconvolution microscopy for quantitative fluorescence imaging. *Journal of Biomolecular Techniques: JBT*, 25(1), pp.31-40.

Leroy, J.G. 2006. Congenital disorders of *N*-glycosylation including diseases associated with *O*- as well as *N*-glycosylation defects. *Pediatric Research*, 60(6), pp.643-656.

Li, F., Vijayasankaran, N., Shen, A., Kiss, R. and Amanullah, A. 2010. Cell culture processes for monoclonal antibody production. *Mabs*, 2(5), pp.466-477.

Liebming, E., Huttner, S., Vavra, U., Fischl, R., Schoberer, J., Grass, J., Blaukopf, C., Seifert, G.J., Altmann, F., Mach, L. and Strasser, R. 2009. Class I α -mannosidases are required for *N*-glycan processing and root development in *Arabidopsis thaliana*. *The Plant Cell*, 21(12), pp.3850-3867.

Lin, N., Mascarenhas, J., Sealover, N.R., George, H.J., Brooks, J., Kayser, K.J., Gau, B., Yasa, I., Azadi, P. and Archer-Hartmann, S. 2015. Chinese hamster ovary (CHO) host cell engineering to increase sialylation of recombinant therapeutic proteins by modulating sialyltransferase expression. *Biotechnology Progress*, 31(2), pp.334-346.

Lingwood, C.A. 2011. Glycosphingolipid functions. *Cold Spring Harbor Perspectives in Biology*, 3(7), pp.1-26.

Lira-Navarrete, E., Valero-González, J., Villanueva, R., Martínez-Júlvez, M., Tejero, T., Merino, P., Panjekar, S. and Hurtado-Guerrero, R. 2011. Structural insights into the mechanism of protein O-fucosylation. *Plos One*, 6(9), pp.e25365.

Liu, B., Spearman, M., Doering, J., Lattova, E., Perreault, H. and Butler, M. 2014. The availability of glucose to CHO cells affects the intracellular lipid-linked oligosaccharide distribution, site occupancy and the N-glycosylation profile of a monoclonal antibody. *Journal of Biotechnology*, 170, pp.17-27.

Liu, H., Saxena, A., Sidhu, S.S. and Wu, D. 2017. Fc engineering for developing therapeutic bispecific antibodies and novel scaffolds. *Frontiers in Immunology*, 8, pp.38.

Lodish, H., Berk, A., Zipursky, S.L., Matsudaira, P., Baltimore, D. and Darnell, J. 2000. *Molecular Cell Biology*. 4th ed. New York: W. H. Freeman.

Lombard, J. 2016. The multiple evolutionary origins of the eukaryotic N-glycosylation pathway. *Biology Direct*, 11(1), pp.36.

Loris, R., Tielker, D., Jaeger, K. and Wyns, L. 2003. Structural basis of carbohydrate recognition by the lectin LecB from *Pseudomonas aeruginosa*. *Journal of Molecular Biology*, 331(4), pp.861-870.

-M-

Ma, J. and Hart, G.W. 2014. O-GlcNAc profiling: From proteins to proteomes. *Clinical Proteomics*, 11(1), pp.1-16.

Mahajan, P.B. 2016. Recent advances in application of pharmacogenomics for biotherapeutics. *The AAPS Journal*, 18(3), pp.605-611.

- Manning, J.C., Romero, A., Habermann, F.A., Garcia Caballero, G., Kaltner, H. and Gabius, H.J. 2017. Lectins: A primer for histochemists and cell biologists. *Histochemistry and Cell Biology*, 147(2), pp.199-222.
- Matsuda, A., Kuno, A., Ishida, H., Kawamoto, T., Shoda, J. and Hirabayashi, J. 2008. Development of an all-in-one technology for glycan profiling targeting formalin-embedded tissue sections. *Biochemical and Biophysical Research Communications*, 370(2), pp.259-263.
- McCoy, J.P.J., Varani, J. and Goldstein, I.J. 1983. Enzyme-linked lectin assay (ELLA): Use of alkaline phosphatase-conjugated *griffonia simplicifolia* B4 isolectin for the detection of α -D-galactopyranosyl end groups. *Analytical Biochemistry*, 130(2), pp.437-444.
- Meesmann, H.M., Fehr, E.M., Kierschke, S., Herrmann, M., Bilyy, R., Heyder, P., Blank, N., Krienke, S., Lorenz, H.M. and Schiller, M. 2010. Decrease of sialic acid residues as an eat-me signal on the surface of apoptotic lymphocytes. *Journal of Cell Science*, 123(Pt 19), pp.3347-3356.
- Merckel, M.C., Tanskanen, J., Edelman, S., Westerlund-Wikström, B., Korhonen, T.K. and Goldman, A. 2003. The structural basis of receptor-binding by escherichia coli associated with diarrhea and septicemia. *Journal of Molecular Biology*, 331(4), pp.897-905.
- Mescher, M.F. and Strominger, J.L. 1976. Purification and characterization of a prokaryotic glucoprotein from the cell envelope of halobacterium salinarium. *The Journal of Biological Chemistry*, 251(7), pp.2005-2014.
- Miki, H. and Takagi, M. 2014. Design of serum-free medium for suspension culture of CHO cells on the basis of general commercial media. *Cytotechnology*, 67(4), pp.689-697.
- Mimura, Y., Lund, J., Church, S., Dong, S., Li, J., Goodall, M. and Jefferis, R. 2001. Butyrate increases production of human chimeric IgG in CHO-K1 cells whilst maintaining function and glycoform profile. *Journal of Immunological Methods*, 247(1-2), pp.205-216.

Mitra, N., Sharon, N. and Surolia, A. 2003. Role of N-linked glycan in the unfolding pathway of erythrina corallodendron lectin. *Biochemistry*, 42(42), pp.12208-12216.

Miyoshi, E., Moriwaki, K. and Nakagawa, T. 2008. Biological function of fucosylation in cancer biology. *Journal of Biochemistry*, 143(6), pp.725-729.

Morelle, W. and Michalski, J. 2007. Analysis of protein glycosylation by mass spectrometry. 2(7), pp.1585-1602.

Mulagapati, S., Koppolu, V. and Raju, T.S. 2017. Decoding of O-linked glycosylation by mass spectrometry. *Biochemistry*, 56(9), pp.1218-1226.

Munkley, J. and Elliott, D.J. 2016. Hallmarks of glycosylation in cancer. *Oncotarget*, 7(23), pp.35478-35489.

-N-

Nascimento, K.S., Cunha, A.I., Nascimento, K.S., Cavada, B.S., Azevedo, A.M. and Aires-Barros, M. 2012. An overview of lectins purification strategies. *Journal of Molecular Recognition*, 25(11), pp.527-541.

NCBI *ALG13*, *UDP-N-acetylglucosaminyltransferase subunit [homo sapiens (human)]* [Online]. Available from: <https://www.ncbi.nlm.nih.gov/gene/79868> [Accessed 07 March 2017 2017].

Neubert, P. and Strahl, S. 2016. Protein O-mannosylation in the early secretory pathway. *Current Opinion in Cell Biology*, 41, pp.100-108.

Newsholme, P., Lima, M.M.R., Procopio, J., Pithon-Curi, T., Doi, S.Q., Bazotte, R.B. and Curi, R. 2003. Glutamine and glutamate as vital metabolites. *Brazilian Journal of Medical and Biological Research*, 36, pp.153-163.

Nicolson, G.L. 1974. The interactions of lectins with animal cell surfaces. *International Review of Cytology*, 39, pp.89-190.

Nikon 2017. *Eclipse-ti-S - inverted-microscopes* [Online]. Available from: https://www.nikoninstruments.com/en_EU/Products/Inverted-Microscopes/Eclipse-Ti-S [Accessed 25 March 2017].

North, S.J., Huang, H., Sundaram, S., Jang-Lee, J., Etienne, A.T., Trollope, A., Chalabi, S., Dell, A., Stanley, P. and Haslam, S.M. 2009. Glycomics profiling of chinese hamster ovary cell glycosylation mutants reveals N-glycans of a novel size and complexity. *The Journal of Biological Chemistry*, 285(8), pp.5759-5775.

Nothhaft, H. and Szymanski, C.M. 2010. Protein glycosylation in bacteria: Sweeter than ever. *Nature Reviews Microbiology*, 8(11), pp.765-778.

NRC - National Research Council (US) Committee on Assessing the Importance and Impact of Glycomics and Glycosciences 2012. *Transforming Glycoscience: A Roadmap for the Future*. Washington (DC): National Academies Press (US).

-O-

O'Connell, T. 2016. *Development of new methods to study cell surface glycosylation*. PhD. Dublin City University.

O'Connell, T.M., King, D., Dixit, C.K., O'Connor, B., Walls, D. and Ducree, J. 2014. Sequential glycan profiling at single cell level with the microfluidic lab-in-a-trench platform: A new era in experimental cell biology. *Lab on a Chip*, 14(18), pp.3629-3639.

O'Connor, B., Monaghan, D. and Cawley, J. 2017. Lectin Affinity Chromatography (LAC) *IN*: Walls, D. and Loughran, S. (eds.) *Protein Chromatography*. 2nd ed. New York: Humana Press, pp.411-420.

Ogawa, M., Furukawa, K. and Okajima, T. 2014. Extracellular O-linked $\hat{\text{I}}^2$ -N-acetylglucosamine: Its biology and relationship to human disease. *World Journal of Biological Chemistry*, 5(2), pp.224-230.

Ohba, H., Bakalova, R. and Muraki, M. 2003. Cytoagglutination and cytotoxicity of wheat germ agglutinin isolectins against normal lymphocytes and cultured leukemic cell lines—relationship between structure and biological activity. *Biochimica Et Biophysica Acta (BBA) - General Subjects*, 1619(2), pp.144-150.

Ohtsubo, K. and Marth, J.D. 2006. Glycosylation in cellular mechanisms of health and disease. *Cell*, 126(5), pp.855-867.

Oliveira, C., Teixeira, J.A. and Domingues, L. 2013. Recombinant lectins: An array of tailor-made glycan-interaction biosynthetic tools. *Critical Reviews in Biotechnology*, 33(1), pp.66-80.

Olsen, J.V., Ong, S.E. and Mann, M. 2004. Trypsin cleaves exclusively C-terminal to arginine and lysine residues. *Molecular & Cellular Proteomics: MCP*, 3(6), pp.608-614.

Ozturk, S.S., Riley, M.R. and Palsson, B.O. 1992. Effects of ammonia and lactate on hybridoma growth, metabolism, and antibody production. *Biotechnology and Bioengineering*, 39(4), pp.418-431.

-P-

PALL 2017. *The octet RED96 system* [Online]. Available from: <http://www.fortebio.com/octet-RED96.html> [Accessed 20 April 2017].

Patnaik, S.K. and Stanley, P. 2006. Lectin-Resistant CHO glycosylation mutants. *Methods in Enzymology*, 416, pp.159-182.

Peumans, W.J. and Van Damme, E.J.M. 1995. Lectins as plant defense proteins. *Plant Physiology*, 109(2), pp.347-352.

Planinc, A., Bones, J., Dejaegher, B., Van Antwerpen, P. and Delporte, C. 2016. Glycan characterization of biopharmaceuticals: Updates and perspectives. *Analytica Chimica Acta*, 921, pp.13-27.

Porath, J., Carlsson, J., Olsson, I. and Belfrage, G. 1975. Metal chelate affinity chromatography, a new approach to protein fractionation. *Nature*, 258, pp.598-599.

Pourazar, A. 2007. Red cell antigens: Structure and function. *Asian Journal of Transfusion Science*, 1(1), pp.24-32.

Praissman, J.L. and Wells, L. 2014. Mammalian O-mannosylation pathway: Glycan structures, enzymes, and protein substrates. *Biochemistry*, 53(19), pp.3066-3078.

Precopio, M.L., Betts, M.R., Parrino, J., Price, D.A., Gostick, E., Ambrozak, D.R., Asher, T.E., Douek, D.C., Harari, A., Pantaleo, G., Bailer, R., Graham, B.S., Roederer, M. and Koup, R.A. 2007. Immunization with vaccinia virus induces polyfunctional and phenotypically distinctive CD8(+) T cell responses. *The Journal of Experimental Medicine*, 204(6), pp.1405-1416.

Pucic, M., Knezevic, A., Vidic, J., Adamczyk, B., Novokmet, M., Polasek, O., Gornik, O., Supraha-Goreta, S., Wormald, M.R., Redzic, I., Campbell, H., Wright, A., Hastie, N.D., Wilson, J.F., Rudan, I., Wuhrer, M., Rudd, P.M., Josic, D. and Lauc, G. 2011. High throughput isolation and glycosylation analysis of IgG-variability and heritability of the IgG glycome in three isolated human populations. *Molecular & Cellular Proteomics: MCP*, 10(10), pp.M111.010090.

-Q-

Qin, H., Cheng, K., Zhu, J., Mao, J., Wang, F., Dong, M., Chen, R., Guo, Z., Liang, X., Ye, M. and Zou, H. 2017. Proteomics analysis of O-GalNAc glycosylation in human serum by an integrated strategy. *Analytical Chemistry*, 89(3), pp.1469-1476.

-R-

Rademacher, T.W., Parekh, R.B. and Dwek, R.A. 1988. Glycobiology. *Annual Review of Biochemistry*, 57, pp.785-838.

Radhakrishnan, P., Dabelsteen, S., Madsen, F.B., Francavilla, C., Kopp, K.L., Steentoft, C., Vakhrushev, S.Y., Olsen, J.V., Hansen, L., Bennett, E.P., Woetmann, A., Yin, G., Chen, L., Song, H., Bak, M., Hlady, R.A., Peters, S.L., Opavsky, R., Thode, C., Qvortrup, K., Schjoldager, K.T., Clausen, H., Hollingsworth, M.A. and Wandall, H.H. 2014. Immature truncated O-glycophenotype of cancer directly induces oncogenic features. *Proceedings of the National Academy of Sciences of the United States of America*, 111(39), pp.E4066-E4075.

Rao, R. and Samak, G. 2011. Role of glutamine in protection of intestinal epithelial tight junctions. *Journal of Epithelial Biology & Pharmacology*, 5(1), pp.47-54.

Reinhart, D., Damjanovic, L., Kaisermayer, C. and Kunert, R. 2015. Benchmarking of commercially available CHO cell culture media for antibody production. *Applied Microbiology and Biotechnology*, 99(11), pp.4645-4657.

Ren, X.M., Li, D.F., Jiang, S., Lan, X.Q., Hu, Y., Sun, H. and Wang, D.C. 2015. Structural basis of specific recognition of non-reducing terminal *N*-acetylglucosamine by an *Agrocybe aegerita* lectin. *PloS One*, 10(6), pp.e0129608.

Reuel, N.F., Mu, B., Zhang, J., Hinckley, A. and Strano, M.S. 2012. Nanoengineered glycan sensors enabling native glycoprofiling for medicinal applications: Towards profiling glycoproteins without labeling or liberation steps. *Chemical Society Reviews*, 41(17), pp.5744-5779.

Reuter, G. and Gabius, H.J. 1999. Eukaryotic glycosylation: Whim of nature or multipurpose tool? *Cellular and Molecular Life Sciences: CMLS*, 55(3), pp.368-422.

Ripka, J. and Stanley, P. 1986. Lectin-resistant CHO cells: Selection of four new pea lectin-resistant phenotypes. *Somatic Cell and Molecular Genetics*, 12(1), pp.51-62.

Riss, T.L., Moravec, R.A., Niles, A.L., Duellman, S., Benink, H.A., Worzella, T.J. and Minor, L. 2013. Cell Viability Assays *IN*: Sittampalam, G.S., Coussens, N.P., Brimacombe, K., Grossman, A., Arkin, M., Auld, D., Austin, C., Baell, J., Bejcek, B., Chung, T.D.Y., Dahlin, J.L., Devanaryan, V., Foley, T.L., Glicksman, M., Hall, M.D., Hass, J.V., Inglese, J., Iversen, P.W., Kahl, S.D., Lal-Nag, M., Li, Z., McGee, J., McManus, O., Riss, T., Trask, J., Weidner, J.R., Xia, M. and Xu, X. (eds.) *Assay Guidance Manual*. Bethesda: Eli Lilly & Company and the National Center for Advancing Translational Sciences.

Rodrigues, M.E., Costa, A.R., Henriques, M., Cunnah, P., Melton, D.W., Azeredo, J. and Oliveira, R. 2013. Advances and drawbacks of the adaptation to serum-free culture of CHO-K1 cells for monoclonal antibody production. *Applied Biochemistry and Biotechnology*, 169(4), pp.1279-1291.

Rodriguez, J., Spearman, M., Huzel, N. and Butler, M. 2005. Enhanced production of monomeric interferon-beta by CHO cells through the control of culture conditions. *Biotechnology Progress*, 21(1), pp.22-30.

Rodriguez, J., Gupta, N., Smith, R.D. and Pevzner, P.A. 2008. Does trypsin cut before proline? *Journal of Proteome Research*, 7(1), pp.300-305.

Rosano, G.L. and Ceccarelli, E.A. 2014. Recombinant protein expression in escherichia coli: Advances and challenges. *Frontiers in Microbiology*, 5, pp.172.

-S-

Sack, U., Tárnok, A. and Rothe, G. 2006. *Cellular Diagnostics: Basic Principles, Methods and Clinical Applications of Flow Cytometry*. 1st ed. Germany: Karger.

Sarter, K., Mierke, C., Beer, A., Frey, B., Führrohr, B.G., Schulze, C. and Franz, S. 2007. Sweet clearance: Involvement of cell surface glycans in the recognition of apoptotic cells. *Autoimmunity*, 40(4), pp.345-348.

Scanlan, C.N., Burton, D.R. and Dwek, R.A. 2008. Making autoantibodies safe. *Proceedings of the National Academy of Sciences*, 105(11), pp.4081-4082.

Schäffer, C. and Messner, P. 2017. Emerging facets of prokaryotic glycosylation. *FEMS Microbiology Reviews*, 41(1), pp.49-91.

Schellekens, H. and Moors, E. 2010. Clinical comparability and European biosimilar regulations. *Nature Biotechnology*, 28(1), pp.28-31.

Schneider, M., Marison, I.W. and von Stockar, U. 1996. The importance of ammonia in mammalian cell culture. *Journal of Biotechnology*, 46(3), pp.161-185.

Schwarz, F. and Aebi, M. 2011. Mechanisms and principles of N-linked protein glycosylation. *Current Opinion in Structural Biology*, 21(5), pp.576-582.

Schwarz, R.E., Wojciechowicz, D.C., Picon, A.I., Schwarz, M.A. and Paty, P.B. 1998. Wheatgerm agglutinin-mediated toxicity in pancreatic cancer cells. *British Journal of Cancer*, 80(11), pp.1754-1762.

Seidenfaden, R., Krauter, A., Schertzinger, F., Gerardy-Schahn, R. and Hildebrandt, H. 2003. Polysialic acid directs tumor cell growth by controlling heterophilic neural cell adhesion molecule interactions. *Molecular and Cellular Biology*, 23(16), pp.5908-5918.

Sethuraman, N. and Stadheim, T.A. 2006. Challenges in therapeutic glycoprotein production. *Current Opinion in Biotechnology*, 17(4), pp.341-346.

Sharon, N. and Lis, H. 2004. History of lectins: From hemagglutinins to biological recognition molecules. *Glycobiology*, 14(11), pp.53R-62R.

Shental-Bechor, D. and Levy, Y. 2008. Effect of glycosylation on protein folding: A close look at thermodynamic stabilization. *Proceedings of the National Academy of Sciences*, 105(24), pp.8256-8261.

Sheridan, C. 2007. Commercial interest grows in glycan analysis. 25(2), pp.145-146.

Shi, X. and Jarvis, D.L. 2007. Protein N-glycosylation in the baculovirus-insect cell system. *Current Drug Targets*, 8(10), pp.1116-1125.

Shields, R.L., Lai, J., Keck, R., O'Connell, L.Y., Hong, K., Meng, Y.G., Weikert, S.H. and Presta, L.G. 2002. Lack of fucose on human IgG1 N-linked oligosaccharide improves binding to human fcγ₃ RIII and antibody-dependent cellular toxicity. *The Journal of Biological Chemistry*, 277(30), pp.26733-26740.

Shilova, N., Huflejt, M.E., Vuskovic, M., Obukhova, P., Navakouski, M., Khasbiullina, N., Pazynina, G., Galanina, O., Bazhenov, A. and Bovin, N. 2015. Natural antibodies against sialoglycans. *Topics in Current Chemistry*, 366, pp.169-181.

Sigma. 2013. *Invertase glycoprotein standard* [Online]. Available from: <https://www.sigmaaldrich.com/content/dam/sigmaaldrich/docs/Sigma/Bulletin/i0408bul.pdf> [Accessed 11 October 2016].

Sigma 2014. *Removal of adherent cells* [Online]. Available from: <http://www.sigmaaldrich.com/technical-documents/protocols/biology/removal-of-adherent-cells.html> [Accessed 22 may 2017].

Sigma 2015. *Dulbecco's modified eagle's Medium/Ham's nutrient mixture F-12 formulation* [Online]. Available from: <https://www.sigmaaldrich.com/content/dam/sigmaaldrich/docs/Sigma/Formulation/d8062for.pdf> [Accessed 12 April 2017].

Sigma. 2017. *Alkaline β -elimination* [Online]. Available from: <http://www.sigmaaldrich.com/life-science/molecular-biology/molecular-biology-products.html?TablePage=19365078> [Accessed 13 March 2017].

Sinacore, M.S., Drapeau, D. and Adamson, S.R. 2000. Adaptation of mammalian cells to growth in serum-free media. *Molecular Biotechnology*, 15(3), pp.249-257.

Singh, H. and Sarathi, S.P. 2012. Insight of lectins- A review. *International Journal of Scientific & Engineering Research*, 3(4), pp.1-9.

Skropeta, D. 2009. The effect of individual N-glycans on enzyme activity. *Bioorganic & Medicinal Chemistry*, 17(7), pp.2645-2653.

Sleytr, U.B. and Thorne, K.J. 1976. Chemical characterization of the regularly arranged surface layers of *Clostridium thermosaccharolyticum* and *Clostridium thermohydrosulfuricum*. *Journal of Bacteriology*, 126(1), pp.377-383.

Smith, P.K., Krohn, R.I., Hermanson, G.T., Mallia, A.K., Gartner, F.H., Provenzano, M.D., Fujimoto, E.K., Goeke, N.M., Olson, B.J. and Klenk, D.C. 1985. Measurement of protein using bicinchoninic acid. *Analytical Biochemistry*, 150(1), pp.76-85.

Snapp, E. 2005. Design and use of fluorescent fusion proteins in cell biology. *Current Protocols in Cell Biology*, Unit-21.4.

Solis, D., Bovin, N.V., Davis, A.P., Jimenez-Barbero, J., Romero, A., Roy, R., Smetana, K., Jr and Gabius, H.J. 2015. A guide into glycosciences: How chemistry, biochemistry and biology cooperate to crack the sugar code. *Biochimica Et Biophysica Acta*, 1850(1), pp.186-235.

Spearmann, M., Rodriguez, J., Huzel, N., Sunley, K. and Butler, M. 2007. Effect of Culture Conditions on Glycosylation of Recombinant beta-Interferon in CHO Cells IN: Smith, R. (ed.) *Cell Technology for Cell Products*. 1st ed. Netherlands: Springer, pp.71-85.

Spring, K.R. and Davidson, M.W. 2016. *Introduction to fluorescence microscopy* [Online]. Available from: <https://www.microscopyu.com/techniques/fluorescence/introduction-to-fluorescence-microscopy> [Accessed 25 March 2017].

Stanley, P. 2011. Golgi glycosylation. *Cold Spring Harbor Perspectives in Biology*, 3(4), pp.1-13.

Stanley, P. and Sundaram, S. 2014. Rapid assays for lectin toxicity and binding changes that reflect altered glycosylation in mammalian cells. *Current Protocols in Chemical Biology*, 6(2), pp.117-133.

Sterner, E., Flanagan, N. and Gildersleeve, J.C. 2016. Perspectives on anti-glycan antibodies gleaned from development of a community resource database. *ACS Chemical Biology*, 11(7), pp.1773-1783.

Stirnemann, J., Belmatoug, N., Camou, F., Serratrice, C., Froissart, R., Caillaud, C., Levade, T., Astudillo, L., Serratrice, J., Brassier, A., Rose, C., Billette, d.V. and Berger, G.M. 2017. A review of gaucher disease pathophysiology, clinical presentation and treatments. *International Journal of Molecular Sciences*, 18(2), 441, pp.1-30.

Street, J.C., Delort, A.M., Braddock, P.S. and Brindle, K.M. 1993. A $1\text{H}/15\text{N}$ n.m.r. study of nitrogen metabolism in cultured mammalian cells. *Biochemical Journal*, 291, pp.485-492.

Sung, Y.H., Song, Y.J., Lim, S.W., Chung, J.Y. and Lee, G.M. 2004. Effect of sodium butyrate on the production, heterogeneity and biological activity of human thrombopoietin by recombinant Chinese hamster ovary cells. *Journal of Biotechnology*, 112(3), pp.323-335.

Swiech, K., Picanco-Castro, V. and Covas, D.T. 2012. Human cells: New platform for recombinant therapeutic protein production. *Protein Expression and Purification*, 84(1), pp.147-153.

-T-

Takahashi, K. and Ezekowitz, B. 2005. The role of the mannose-binding lectin in innate immunity. *Clinical Infectious Diseases*, 41(7), pp.440-444.

Tanskanen, J., Saarela, S., Tankka, S., Kalkkinen, N., Rhen, M., Korhonen, T.K. and Westerlund-Wikström, B. 2000. The gaf fimbrial gene cluster of *escherichia coli* expresses a full-size and a truncated soluble adhesin protein. *Journal of Bacteriology*, 183(2), pp.512-519.

Tao, S.C., Li, Y., Zhou, J., Qian, J., Schnaar, R.L., Zhang, Y., Goldstein, I.J., Zhu, H. and Schneck, J.P. 2008. Lectin microarrays identify cell-specific and functionally significant cell surface glycan markers. *Glycobiology*, 18(10), pp.761-769.

Tashima, Y. and Stanley, P. 2014. Antibodies that detect O-linked beta-D-N-acetylglucosamine on the extracellular domain of cell surface glycoproteins. *The Journal of Biological Chemistry*, 289(16), pp.11132-11142.

Taylor, M.E. and Drickamer, K. 2006. *Introduction to glycobiology*. 2nd ed. Oxford: Oxford University Press.

Thermo 2017. *ThermoFisher - fluorescein (FITC)* [Online]. Available from: <https://www.thermofisher.com/ie/en/home/life-science/cell-analysis/fluorophores/fluorescein.html> [Accessed 31 March 2017].

Thompson, R., Creavin, A., O'Connell, M., O'Connor, B. and Clarke, P. 2011. Optimization of the enzyme-linked lectin assay for enhanced glycoprotein and glycoconjugate analysis. *Analytical Biochemistry*, 413(2), pp.114-122.

Timal, S., Hoischen, A., Lehle, L., Adamowicz, M., Huijben, K., Sykut-Cegielska, J., Paprocka, J., Jamroz, E., van Spronsen, F.J., Korner, C., Gilissen, C., Rodenburg, R.J., Eidhof, I., Van den Heuvel, L., Thiel, C., Wevers, R.A., Morava, E., Veltman, J. and Lefeber, D.J. 2012. Gene identification in the congenital disorders of glycosylation type I by whole-exome sequencing. *Human Molecular Genetics*, 21(19), pp.4151-4161.

Trummer, E., Fauland, K., Seidinger, S., Schriebl, K., Lattenmayer, C., Kunert, R., Vorauer-Uhl, K., Weik, R., Borth, N., Katinger, H. and Muller, D. 2006. Process parameter shifting: Part II. biphasic cultivation-A tool for enhancing the volumetric productivity of batch processes using epo-fc expressing CHO cells. *Biotechnology and Bioengineering*, 94(6), pp.1045-1052.

Tsao, Y.S., Cardoso, A.G., Condon, R.G., Voloch, M., Lio, P., Lagos, J.C., Kearns, B.G. and Liu, Z. 2005. Monitoring Chinese hamster ovary cell culture by the analysis of glucose and lactate metabolism. *Journal of Biotechnology*, 118(3), pp.316-327.

-U-

Upreti, R.K., Kumar, M. and Shankar, V. 2003. Bacterial glycoproteins: Functions, biosynthesis and applications. *Proteomics*, 3(4), pp.363-379.

-V-

Varki, A. 2011. Evolutionary forces shaping the golgi glycosylation machinery: Why cell surface glycans are universal to living cells. *Cold Spring Harbor Perspectives in Biology*, 3(6), pp.1-14.

Varki, A., Cummings, R.D., Esko, J.D., Freeze, H.H., Stanley, P., Bertozzi, C.R., Hart, G.W. and Etzler, M.E. 2009. *Essentials of glycobiology*. 2nd ed. New York: Cold Spring Harbor Laboratory Press.

Vasudevan, D. and Haltiwanger, R.S. 2014. Novel roles for O-linked glycans in protein folding. *Glycoconjugate Journal*, 31(0), pp.417-426.

Vector Labs 2016. *Biotinylated wheat germ agglutinin (WGA)* [Online]. Available from: <https://vectorlabs.com/biotinylated-wheat-germ-agglutinin-wga.html> [Accessed 20 May 2017].

Vidarsson, G., Dekkers, G. and Rispen, T. 2014. IgG subclasses and allotypes: From structure to effector functions. *Frontiers in Immunology*, 5, pp.520.

Villacres, C., Tayi, V.S., Lattova, E., Perreault, H. and Butler, M. 2015. Low glucose depletes glycan precursors, reduces site occupancy and galactosylation of a monoclonal antibody in CHO cell culture. *Biotechnology Journal*, 10(7), pp.1051-1066.

-W-

Wahrheit, J., Nicolae, A. and Heinzle, E. 2014. Dynamics of growth and metabolism controlled by glutamine availability in Chinese hamster ovary cells. *Applied Microbiology and Biotechnology*, 98(4), pp.1771-1783.

Walsh, G. 2000. Biopharmaceutical benchmarks. 18(8), pp.831-833.

Walsh, G. 2009. *Post-translational modification of protein biopharmaceuticals*. Weinheim: Wiley-VCH.

Walsh, G. 2014. Biopharmaceutical benchmarks 2014. *Nature Biotechnology*, 32(10), pp.992-1000.

Walsh, G. and Jefferis, R. 2006. Post-translational modifications in the context of therapeutic proteins. *Nature Biotechnology*, 24(10), pp.1241-1252.

Walther, C.G., Whitfield, R. and James, D.C. 2015. Importance of interaction between integrin and actin cytoskeleton in suspension adaptation of CHO cells. *Applied Biochemistry and Biotechnology*, 178, pp.1286-1302.

Wang, P., Wang, H., Gai, J., Tian, X., Zhang, X., Lv, Y. and Jian, Y. 2016. Evolution of protein N-glycosylation process in Golgi apparatus which shapes diversity of protein N-glycan structures in plants, animals and fungi. *Scientific Reports*, 7, pp.40301.

Weichert, H. and Becker, M. 2013. Online glucose-lactate monitoring and control in cell culture and microbial fermentation bioprocesses. *BMC Proceedings*, 7(6), pp.1-2.

Wells, L. 2013. The o-mannosylation pathway: Glycosyltransferases and proteins implicated in congenital muscular dystrophy. *The Journal of Biological Chemistry*, 288(10), pp.6930-6935.

Westerlund-Wikström, B. and Korhonen, T.K. 2005. Molecular structure of adhesin domains in *Escherichia coli* fimbriae. *International Journal of Medical Microbiology*, 295(6), pp.479-486.

Westgeest, K.B., Bestebroer, T.M., Spronken, M.I.J., Gao, J., Couzens, L., Osterhaus, A.D.M.E., Eichelberger, M., Fouchier, R.A.M. and de Graaf, M. 2015. Optimization of an enzyme-linked lectin assay suitable for rapid antigenic characterization of the neuraminidase of human influenza A(H3N2) viruses. *Journal of Virological Methods*, 217, pp.55-63.

Wilkerson, M.J. 2012. Principles and applications of flow cytometry and cell sorting in companion animal medicine. *The Veterinary Clinics of North America. Small Animal Practice*, 42(1), pp.53-71.

Wingfield, P.T. 2015. Overview of the purification of recombinant proteins. *Current Protocols in Protein Science / Editorial Board, John E. Coligan ... [Et Al.]*, 80, pp.6.1.1-6.1.35.

Wong, A.W., Scales, S.J. and Reilly, D.E. 2007. DNA internalized via caveolae requires microtubule-dependent, Rab7-independent transport to the late endocytic pathway for delivery to the nucleus. *The Journal of Biological Chemistry*, 282(31), pp.22953-22963.

Wong, D.C.F., Tin Kam Wong, K., Tang Goh, L., Kiat Heng, C. and Gek Sim Yap, M. 2005. Impact of dynamic online fed-batch strategies on metabolism, productivity and *N*-glycosylation quality in CHO cell cultures. *Biotechnology and Bioengineering*, 89(2), pp.164-177.

-X-

Xu, X., Nagarajan, H., Lewis, N.E., Pan, S., Cai, Z., Liu, X., Chen, W., Xie, M., Wang, W., Hammond, S., Andersen, M.R., Neff, N., Passarelli, B., Koh, W., Fan, H.C., Wang, J., Gui, Y., Lee, K.H., Betenbaugh, M.J., Quake, S.R., Famili, I., Palsson, B.O. and Wang, J. 2011. The genomic sequence of the Chinese hamster ovary (CHO)-K1 cell line. *Nature Biotechnology*, 29(8), pp.735-741.

-Y-

Yamada, K., Hyodo, S., Matsuno, Y., Kinoshita, M., Maruyama, S., Osaka, Y., Casal, E., Lee, Y.C. and Kakehi, K. 2007. Rapid and sensitive analysis of mucin-type glycans using an in-line flow glycan-releasing apparatus. *Analytical Biochemistry*, 371(1), pp.52-61.

Yang, H., Shi, L., Zhuang, X., Su, R., Wan, D., Song, F., Li, J. and Liu, S. 2016. Identification of structurally closely related monosaccharide and disaccharide isomers by PMP labeling in conjunction with IM-MS/MS. *Scientific Reports*, 6, pp.28079.

Yang, M. and Butler, M. 2002. Effects of ammonia and glucosamine on the heterogeneity of erythropoietin glycoforms. *Biotechnology Progress*, 18(1), pp.129-138.

Yasukawa, Z., Sato, C. and Kitajima, K. 2005. Inflammation-dependent changes in α 2,3-, α 2,6-, and α 2,8-sialic acid glycotopes on serum glycoproteins in mice. *Glycobiology*, 15(9), pp.827-837.

Yoon, S.K., Choi, S.L., Song, J.Y. and Lee, G.M. 2005. Effect of culture pH on erythropoietin production by chinese hamster ovary cells grown in suspension at 32.5 and 37.0 degrees C. *Biotechnology and Bioengineering*, 89(3), pp.345-356.

Yue, T. and Haab, B.B. 2009. Microarrays in glycoproteomics research. *Clinics in Laboratory Medicine*, 29(1), pp.15-29.

-Z-

Zhang, P., Chan, K.F., Haryadi, R., Bardor, M. and Song, Z. 2013. CHO Glycosylation Mutants as Potential Host Cells to Produce Therapeutic Proteins with Enhanced Efficacy *IN: Zhong, J.J. (ed.) Future Trends in Biotechnology*. Berlin Heidelberg: Springer, pp.63-87.

Zhang, K. and Kaufman, R.J. 2006. The unfolded protein response: A stress signaling pathway critical for health and disease. *Neurology*, 66(2 Suppl 1), pp.S102-9.

Zhang, K. and Chen, J. 2012. The regulation of integrin function by divalent cations. *Cell Adhesion & Migration*, 6(1), pp.20-29.

Zhang, L., Luo, S. and Zhang, B. 2015. Glycan analysis of therapeutic glycoproteins. *Mabs*, 8(2), pp.205-215.

Zhang, Y. 2008. I-TASSER server for protein 3D structure prediction. *BMC Bioinformatics*, 9(1), pp.40.

Appendix A

Nucleotide and protein sequences for AAL-2 with *N*-terminal His₆ tag, *N*-terminal His₆ tag with linker, *C*-terminal His₆ tag and EGFP fusion

A.1 AAL-2 with an *N*- terminal His₆ tag from pQE-30_AAL-2 plasmid, Table 2.2

Nucleotide sequence

ATGAGAGGATCG**CATCACCATCACCATCAC**GGATCC**ATG**ACCTCTAACGTTATCACC
CAGGACCTGCCGATCCCGGTTGCTTCTCGTGGTTTTCGCTGACATCGTTGGTTTTCGGT
CTGGACGGTGTGTTATCGGTCGTAACGCTGTAAACCTGCAGCCGTTCCCTGGCTGTT
AAAAACTTCGCTCAGAACGCTGGTGGTTGGCTGACCACCAAACACGTTCTGTCTGATC
GCTGACACCACCGGTACCGGTAAAGGTGACATCGTTGGTTTCGGTAACGCTGGTGT
TACGTTTCTGTAAACAACGGTAAAAACACCTTCGCTGACCCGCCGAAAATGGTTATC
GCTAACTTCGGTTACGACGCTGGTGGTTGGCGTGTGAAAAACACCTGCGTTACCTG
GCTGACATCCGTAAAATCGGTCGTGCTGACATCATCGGTTTCGGTGAAAAGGTGTT
CTGGTTTCTCGTAACAACGGTGGTCTGAACCTTCGGTCCGGCTACCCTGGTTCTGAAA
GACTTCGGTTACGACGCTGGTGGTTGGCGTCTGGACCGTCACCTGCGTTTCCTGGCT
GACGTTACCGGTAACGGTCACCTGGACATCGTTGGTTTTCGGTGACAAACACGTTTTC
ATCTCTCGTAACAACGGTGACGGTACCTTCGCTCCGGCTAAATCTGTTATCGACAAC
TTCTGCATCGACGCTGGTGGTTGGAAAATCGGTGACCACCCGCGTTTTCGTTGCTGAC
CTGACCGGTGACGGTACCGCTGACATCATCGGTTGCGGTAAAGCTGGTTGCTGGGTT
GCTCTGAACAACGGTGGTGGTGTTCGGTCAGGTAAACTGGTTATCAACGACTTC
GGTACCGACAAAGGTTGGCAGGCTGCTAAACACCCGCGTTTCATCGCTGACCTGACC
GGTAACGGTCGTGGTGACGTTGTTGGTTTTCGGTAACGCTGGTGTTCGTTGCTCTG
AACAACGGTGACGGTACCTTCCAGTCTGCTAAACTGGTTCTGAAAGACTTCGGTGT
CAGCAGGGTTGGACCGTTTTCTAAACACCGTCGTTTTCGTTGTTGACCTGACCGGTGAC
GGTTGCGCTGACATCATCGGTTTCGGTGAAAAGAAACCCTGGTTTCTTACAACGAC
GGTAAAGGTAACCTTCGGTCCGGTTAAAGCTCTGACCAACGACTTCTCTTCTCTGGT
GGTAAATGGGCTCCGGAAACCACCGTTTGCTGGATGGCTAACCTGGACTCTTCTCGT
CAC**TAA**

Highlighted regions: Starting codon (green), *N*-terminus His₆ tag is (blue), First codon
in the AAL-2 sequence (green underlined), Stop codon (red)

Translated protein sequence

MRGSHHHHHHGS**M**TSNVITQDLPIPVASRGFADIVGFGLDGVVIGRNAVNLPFLAV
KNFAQNAGGWLTTKHVRLIADTTGTGKGDIVGFGNAGVYVSVNNGKNTFADPPKMVI
ANFGYDAGGWRVEKHLRYLADIRKIGRADIIGFGEKGVLVSRNNGGLNFGPATLVLK
DFGYDAGGWRLDRHLRFLADVTGNHGLDIVGFGDKHVFI SRNNGDGT FAPAKSVI DN
FCIDAGGWKIGDHPRFVADLTGDGTADIIIGCGKAGCWVALNNGGGVFGQVKLVINDF
GTDKGWQAAKHPRFIADLTGNRGRDVGFGNAGVYVALNNGDGT FQS AKLV LKDFGV
QQGWTVSKHRRFVVDLTGDGCADIIGFGEKETLVSYNDGKGNFGPVKALTNDFSFSG
GKWAPETTVCWMANLDSSRH-

A.2 AAL-2 with a 30 amino acid linker and an N- terminal His₆ tag from pAAL-2_NL plasmid, Table 2.3 and construction Fig. 3.4

Nucleotide sequence

ATG**AGAGGATCG****CATCACCATCACCATCAC****TCTGCTGGTCTGGTTCCGCGTGGTTCT**
ACCGCTATCGGTATGGGTTCTGGTGACGACGACGACAAATCTCCGATGGGTTACCGT
GGATCCATGACCTCTAACGTTATCACCCAGGACCTGCCGATCCCGGTTGCTTCTCGT
GGTTTCGCTGACATCGTTGGTTTCGGTCTGGACGGTGTGTTATCGGTCGTAACGCT
GTTAACCTGCAGCCGTTCCCTGGCTGTTAAAACTTCGCTCAGAACGCTGGTGGTTGG
CTGACCACCAAACACGTTTCGTCTGATCGCTGACACCACCGGTACCGGTAAAGGTGAC
ATCGTTGGTTTCGGTAACGCTGGTGTTCAGTTTCTGTTAACAACGGTAAAAACACC
TTCGCTGACCCGCCGAAAATGGTTATCGCTAACTTCGGTTACGACGCTGGTGGTTGG
CGTGTGAAAAACACCTGCGTTACCTGGCTGACATCCGTAAAATCGGTCGTGCTGAC
ATCATCGGTTTCGGTGAAAAAGGTGTTCTGGTTTCTCGTAACAACGGTGGTCTGAAC
TTCGGTCCGGCTACCCTGGTTCGAAAGACTTCGGTTACGACGCTGGTGGTTGGCGT
CTGGACCGTACCTGCGTTTCCCTGGCTGACGTTACCGGTAACGGTCACCTGGACATC
GTTGGTTTCGGTGACAAACACGTTTTTCATCTCTCGTAACAACGGTGACGGTACCTTC
GCTCCGGCTAAATCTGTTATCGACAACCTTCTGCATCGACGCTGGTGGTTGGAAAATC
GGTGACCACCCGCGTTTCGTTGCTGACCTGACCGGTGACGGTACCGCTGACATCATC
GGTTGCGGTAAAGCTGGTTGCTGGGTGCTCTGAACAACGGTGGTGGTGTTCGCGT
CAGGTTAAACTGGTTATCAACGACTTCGGTACCGACAAAGGTTGGCAGGCTGCTAAA
CACCCGCGTTTCATCGCTGACCTGACCGGTAACGGTCGTGGTGACGTTGTTGGTTTC
GGTAACGCTGGTGTTCAGTTGCTCTGAACAACGGTGACGGTACCTTCCAGTCTGCT
AAACTGGTTCTGAAAGACTTCGGTGTTCAGCAGGGTTGGACCGTTTCTAAACACCGT
CGTTTCGTTGTTGACCTGACCGGTGACGGTTGCGCTGACATCATCGGTTTCGGTGAA
AAAGAAACCCTGGTTTCTTACAACGACGGTAAAGGTAACCTTCGGTCCGGTTAAAGCT
CTGACCAACGACTTCTCTTTCTCTGGTGGTAAATGGGCTCCGGAAACCACCGTTTGC
TGGATGGCTAACCTGGACTCTTCTCGTCAC**TAA**

Highlighted regions: Starting codon (green), N-terminus His₆ tag is (blue), 90 nucleotide linker (black underlined), First codon in the AAL-2 sequence (green underlined), Stop codon (red)

Translated protein sequence

MRGSHHHHHHSAGLVPRGSTAIGMGS**GDDDDKSPMGYRGS****M**TSNVITQDLPIPVASR
GFADIVGFGLDGVVIGRNAVNLPFLAVKNFAQNAGGWLTTKHVRLIADTTGTGKGD
IVGFGNAGVYVSVNNGKNTFADPPKMVIANFGYDAGGWRVEKHLRYLADIRKIGRAD
IIGFGEKGVLSRNNGGLNFGPATLVLKDFGYDAGGWRLDRHLRFLADVTGNHGLDI
VGFGDKHVFI SRNNGDGFAPAKSVINDFCIDAGGWKIGDHPRFVADLTGDGTADII
GCGKAGCWVALNNGGGVFGQVKLVINDFGTDKGWQA AKHPRFIADLTGNRGRDVG
FNAGVYVALNNGDGTFS AKLVKDFGVQQGWTVSKHRRFVVDLTGDGCADIIGFGE
KETLVSYNDGKGNFGPVKALTNDFSFSGGKWAPETTVCWMANLDSSRH-

A.3 AAL-2 with a C-terminal His₆ tag from pAAL-2_CT plasmid, Table 2.3 and construction Fig. 3.6

Nucleotide sequence

ATGACCTCTAACGTTATCACCCAGGACCTGCCGATCCCGGTTGCTTCTCGTGGTTTC
GCTGACATCGTTGGTTTCGGTCTGGACGGTGTGTTATCGGTCGTAACGCTGTTAAC
CTGCAGCCGTTCCCTGGCTGTTAAAACTTCGCTCAGAACGCTGGTGGTTGGCTGACC
ACCAAACACGTTTCGTCTGATCGCTGACACCACCGGTACCGGTAAAGGTGACATCGTT
GGTTTCGGTAACGCTGGTGTTCACGTTTCTGTAAACAACGGTAAAAACACCTTCGCT
GACCCGCCGAAAATGGTTATCGCTAACTTCGGTTACGACGCTGGTGGTTGGCGTGTT
GAAAAACACCTGCGTTACCTGGCTGACATCCGTAATAATCGGTCGTGCTGACATCATC
GGTTTCGGTGAAAAGGTGTTCTGGTTTCTCGTAACAACGGTGGTCTGAACTTCGGT
CCGGCTACCCTGGTTCTGAAAGACTTCGGTTACGACGCTGGTGGTTGGCGTCTGGAC
CGTCACCTGCGTTTCCTGGCTGACGTTACCGGTAACGGTCACCTGGACATCGTTGGT
TTCGGTGACAAACACGTTTTTCATCTCTCGTAACAACGGTGACGGTACCTTCGCTCCG
GCTAAATCTGTTATCGACAACCTTCTGCATCGACGCTGGTGGTTGGAAAATCGGTGAC
CACCCGCGTTTTCGTTGCTGACCTGACCGGTGACGGTACCGCTGACATCATCGGTTGC
GGTAAAGCTGGTTGCTGGGTTGCTCTGAACAACGGTGGTGGTGTTCGGTCAGGTT
AAACTGGTTATCAACGACTTCGGTACCGACAAAGGTTGGCAGGCTGCTAAACACCCG
CGTTTCATCGCTGACCTGACCGGTAACGGTTCGTGGTGACGTTGTTGGTTTTCGGTAAC
GCTGGTGTTCACGTTGCTCTGAACAACGGTGACGGTACCTTCCAGTCTGCTAAACTG
GTTCTGAAAGACTTCGGTGTTCAGCAGGGTTGGACCGTTTTCTAAACACCGTCGTTTC
GTTGTTGACCTGACCGGTGACGGTTGCGCTGACATCATCGGTTTTCGGTGAAAAGAA
ACCCTGGTTTTCTTACAACGACGGTAAAGGTAACCTTCGGTCCGGTTAAAGCTCTGACC
AACGACTTCTCTTTCTCTGGTGGTAAATGGGCTCCGGAAACCACCGTTTTGCTGGATG
GCTAACCTGGACTCTTCTCGTCACAGATCTCATCACCATCACCATCACATAA

Highlighted regions: First codon in the AAL-2 sequence (green underlined), Last codon in AAL-2 sequence (black underlined), C-terminus His₆ tag is (blue), Stop codon (red)

Translated protein sequence

MTSNVITQDLPIPVASRGFADIVGFGLDGVVIGRNAVNLPFLAVKNFAQNAGGWLT
TKHVRLIADTTGTGKGDIVGFNAGVYVSVNNGKNTFADPPKMVIANFGYDAGGWRV
EKHLRYLADIRKIGRADIIGFGEKGVLSRNNGLNFGPATLVLKDFGYDAGGWRLD
RHLRFLADVTDGNHLDIVGFGDKHVFI SRNNGDGT FAPAKSVIDNFCIDAGGWKIGD
HPRFVADLTGDGTADIIGCGKAGCWVALNNGGVFGQVKLVINDFGTDKGWQAAKHP
RFIADLTGNRGRDVVGFNAGVYVALNNGDGT FQSAKLVLKDFGVQQGWTVSKHRRF
VVDLTGDGCADIIGFGEKETLVSYNDGKGNFGPVKALTNDFFSFGGKWAPETTVCWM
ANLDSSRHRSHHHHHH-

A.4 EGFP-AAL-2 fusion with a His₆ tag at the EGFP N-terminus from pEGFP_AAL-2 plasmid, Table 2.3 and construction Fig. 3.5

Nucleotide sequence

ATGAGAGGATCG**CATCACCATCACCATCAC**GGATCTATGAGTAAAGGAGAAGAACTT
TTCAGTGGAGTTGTCCCAATTCTTGTGTAATTAGATGGTGATGTTAATGGGCACAAA
TTTTCTGTCAGTGGAGAGGGTGAAGGTGATGCAACATACGGAAAACCTTACCCTTAAA
TTTATTTGCACTACTGGAAAACCTGTTCCATGGCCAACACTTGTCACTACTCTC
ACTTATGGTGTTCATGCTTTGCGAGATACCCAGATCATATGAAACAGCATGACTTT
TTCAAGAGTGCCATGCCCGAAGGTTATGTACAGGAAAGAACTATATTTTTCAAAGAT
GACGGGAACTACAAGACACGTGCTGAAGTCAAGTTTGAAGGTGATACCCTTGTTAAT
AGAATCGAGTTAAAAGGTATTGATTTTAAAGAAGATGGAAACATTCTTGGACACAAA
TTGGAATACAACCTATAACTCACACAATGTATACATCATGGCAGACAAAACAAAAGAAT
GGAATCAAAGTTAACTTCAAAAATTAGACACAACATTGAAGATGGAAGCGTTCAACTA
GCAGACCATTATCAACAAAATACTCCAATTGGCGATGGCCCTGTCCTTTTACCAGAC
AACCATTACCTGTCCACACAATCTGCCCTTTCGAAAGATCCCAACGAAAAGAGAGAC
CACATGGTCCTTCTTGAGTTTGTAAACAGCTGCTGGGATTACACATGGCATGGATGAA
CTATACAAAGGATCCATGACCTCTAACGTTATCACCCAGGACCTGCCGATCCCGGTT
GCTTCTCGTGGTTTTCGCTGACATCGTTGGTTTTCGGTCTGGACGGTGTGTTATCGGT
CGTAACGCTGTTAACCTGCAGCCGTTCCCTGGCTGTTAAAAACTTCGCTCAGAACGCT
GGTGGTTGGCTGACCACCAAACACGTTTCGTCTGATCGCTGACACCACCGGTACCGGT
AAAGGTGACATCGTTGGTTTTCGGTAACGCTGGTGTTCGTTTTCTGTTAACAACGGT
AAAAACACCTTCGCTGACCCGCCGAAAATGGTTATCGCTAACTTCGGTTACGACGCT
GGTGGTTGGCGTGTGAAAAACACCTGCGTTACCTGGCTGACATCCGTAAAATCGGT
CGTGCTGACATCATCGTTTTCGGTGAAAAGGTGTTCTGGTTTTCTCGTAACAACGGT
GGTCTGAACTTCGGTCCGGCTACCCTGGTTCTGAAAGACTTCGGTTACGACGCTGGT
GGTTGGCGTCTGGACCGTCACCTGCGTTTTCTGGCTGACGTTACCGGTAACGGTCAC
CTGGACATCGTTGGTTTTCGGTGACAAACACGTTTTTCATCTCTCGTAACAACGGTGAC
GGTACCTTCGCTCCGGCTAAATCTGTTATCGACAACCTTCTGCATCGACGCTGGTGGT
TGAAAAATCGGTGACCACCCGCGTTTTCGTTGCTGACCTGACCGGTGACGGTACCGCT
GACATCATCGGTTGCGGTAAAGCTGGTTGCTGGGTTGCTCTGAACAACGGTGGTGGT
GTTTTCGGTGAGGTTAAACTGGTTATCAACGACTTCGGTACCGACAAAGGTTGGCAG
GCTGCTAAACACCCGCGTTTTCATCGCTGACCTGACCGGTAACGGTTCGTGGTGACGTT
GTTGGTTTTCGGTAACGCTGGTGTTCGTTGCTCTGAACAACGGTACGGTACCTTC
CAGTCTGCTAAACTGGTTCTGAAAGACTTCGGTGTTCAGCAGGGTTGGACCGTTTTCT
AAACACCGTTCGTTTTCGTTGTTGACCTGACCGGTGACGGTTGCGCTGACATCATCGGT
TTCGGTGAAAAGAAACCCTGGTTTTCTTACAACGACGGTAAAGGTAACCTTCGGTCCG
GTAAAGCTCTGACCAACGACTTCTCTTTCTCTGGTGGTAAATGGGCTCCGGAAACC
ACCGTTTGCTGGATGGCTAACCTGGACTCTTCTCGTCAC**TAA**

Highlighted regions: Starting codon (green underlined), N-terminus His₆ tag is (blue), EGFP sequence (green), First codon in the AAL-2 sequence (orange underlined), Stop codon (red), Translated protein sequence (EGFP-AAL-2 fusion)

Translated protein sequence

MRGSHHHHHHGSMSKGEELFTGVVPIVVELDGDVNGHKFSVSGEGEGDATYGKLT
LKFICTTGKLPVPWPTLVTTLYGVQCFARYPDHMKQHDFFKSAMPEGYVQERTIFFKD
DGNKTRAEVVKFEGDTLVNRIELKIDFKEDGNILGHKLEYNNSHNVYIMADKQKN
GIKVNFKIRHNIEDGSVQLADHYQONTPIGDGPVLLPDNHYLSTQSALSKDPNEKRD
HMLLEFVTAAGITHGMDELYKGSMTSNVITQDLPIPVASRGFADIVGFGLDG
VIGRNAVNLQPFLAVKNFAQNAGGWLTTKHVRLIADTTGTGKGDIVGFGNAGVYVSVNNG
KNTFADPPKMVIANFGYDAGGWRVEKHLRYLADIRKIGRADIIGFGEKGVLSR
NNGGLNFGPATLVLKDFGYDAGGWRDLRHLRFLADVTGNGHLDIVGFGDKHVFIS
RNNGDGTFAPAKSVIDNFCIDAGGWKIGDHPRFVADLTGDGTADIIGCGKAGC
WVALNNGGGVFGQVKLVINDFGTDKGWQAAKHPRFIADLTGNRGDVGFGNAGVY
VALNNGDGTFAQSAKLVLKDFGVQQGWTVSKHRRFVVDLTGDGCADIIGFGEK
ETLVSYNNGKGNFGPVKALTNDFSFSGGKWAPETTVCCWMANLDSSRH-

Appendix B

Mutagenesis of AAL-2

B.1 Mutagenesis of AAL-2

Site-directed mutagenesis was used to alter the AAL-2 coding sequence. Residues in the AAL-2 protein thought to be involved in GlcNAc binding were modified using 4 primers, see Table 2.4, and a whole vector amplification strategy. Producing an AAL-2 variant which has lost its GlcNAc binding ability could be used as an added control in live cell staining for example, i.e. to investigate if the lectin is interacting with or adhering to the cell surface by any other means. Alternatively an AAL-2 variant with reduced affinity for GlcNAc would be useful in many applications, such as sequential lectin probing of cells/glycoproteins where lectins with lower affinities are more easily removed and for lectin affinity chromatography (LAC) applications where a lectin with an altered affinity may identify previously missed glycoforms.

B.2 AAL-2 BLAST search

The structure of AAL-2 and the key residues required for GlcNAc binding were not known prior to June 2015 (Ren *et al.* 2015). A protein BLAST search was completed to identify similar protein sequences and to gain information about AAL-2. Another mushroom lectin *Psathyrella velutina* lectin (PVL), which also binds GlcNAc, has 60 % sequence similarity with AAL-2, Fig B.1. The residues in PVL involved with GlcNAc binding were identified from the Protein Data bank (Protein ID: 2C4D). There are 41 amino acids that form polar interactions with GlcNAc at 6 sites. 30 of these amino acid residues are present in AAL-2.

AAL-2	5	VITQDLPIPVASRGFADIVGFGLDGVVIGRNAVNLPFLAVKNFAQNAGG	54
		: . : : :::	
PVL	4	VISQALPVPTRIPGVADLVGFGNGGVYIIRNSLLIQVVKVINNFYDAGG	53
AAL-2	55	WLTTKHVRLIADTTGTGKGDIVGFGNAGVYVSVNNGKNTFADPPKMVIAN	104
		. .	
PVL	54	WRVEKHVRLIADTTGDNQPDVVGFGENGVWISTNNGNNTFVDPPKMVLAN	103
AAL-2	105	FGYDAGGWRVEKHLRFLADIRKIGRADIIGFGEKGVLSRNNGLNFGPA	154
		. .	
PVL	104	FAYAAGWRVEKHIREMADLRKTGRADIVGFGDGGIYISRNNGGGQFAPA	153
AAL-2	155	TLVLKDFGYDAGGWRLDRHLRFLADVTGNHGLDIVGFGDKHVFISRNGD	204
		. .	
PVL	154	QLALNINFGY-AQWRLDRLRFLADVTGDGLLDVVGFGENQVYIARNSGN	202
AAL-2	205	GTFAPAKSVIDNFCIDAGGWKIGDHPRFVADLTGDGTADIIGCGKAGCWV	254
		. .	
PVL	203	GTFQPAQAVVNNFCIGAGGWTTISAHPRVVADLTGDRKADILGFVAGVYT	252
AAL-2	255	ALNNGGGVFGQVKLVINDFGTDKQWQAAKHPRFIADLTGNRGRDVGFGN	304
		: .	
PVL	253	SLNNGNGTFGAVNLVLKDFGVNSGWVREKHVRCVSSLTNKKVGDIIIGFD	302
AAL-2	305	AGVYVALNNGDGTQSAKLVLKDFGVQGWTVSKHRRFVVDLTGDGCADI	354
		. .	
PVL	303	AGVYVALNNGNGTFGPVKRVIDNFGYNQGWVRVDKHPRFVVDLTGDGCADI	352
AAL-2	355	IGFGEKETLVSyndGKGNFGPvkALtNDFsFSGGkwApETtVcWmANL	402
		: .	
PVL	353	VGFGENSVWACMNKGDGTGPIQLIDDMTVSKG-WTLQKTVRYAANL	399

Fig B.1: The alignment of AAL-2 and PVL protein sequences. AAL-2 shares 60 % sequence similarity with the PVL. The alignment was completed using the EMBOSS Water tool available from the European Bioinformatics Institute (www.ebi.ac.uk/Tools/psa/emboss_water/). The PVL residues involved with GlcNAc binding are shown in bold and are shaded when also present in the AAL-2 sequence.

B.3 Site-directed mutagenesis of AAL-2

Alanine substitution is a commonly used technique to determine functional residues. Substituting an amino acid with alanine removes the side chain atoms, past the β -carbon, and the functionality of the protein can be altered or lost if it is a key residue (Morrison and Weiss 2001). Two of the presumed GlcNAc binding sites of AAL-2, as identified from PVL similarity, were mutated to knockout binding. Two rounds of SDM were used to change 10 nucleotides in the AAL-2 coding sequence. Fig. B.2 shows the primer sequences and the change in the AAL-2 coding sequence.

```

1   ATG ACC TCT AAC GTT ATC ACC CAG GAC CTG CCG ATC CCG GTT GCT TCT CGT 51
52  GGT TTC GCT GAC ATC GTT GGT TTC GGT CTG GAC GGT GTT GTT ATC GGT CGT 102
                                     CGA CAA TTT TTG AAG CGA GTC TTG
103 AAC GCT GTT AAC CTG CAG CCG TTC CTG GCT GTT AAA AAC TTC GCT CAG AAC 153
    CGA CGA CGA GCG CTG ACC ACC AAA CAC GTT CGT CTG ATC GC
154 GCT GGT GGT TGG CTG ACC ACC AAA CAC GTT CGT CTG ATC GCT GAC ACC ACC 204
205 GGT ACC GGT AAA GGT GAC ATC GTT GGT TTC GGT AAC GCT GGT GTT TAC GTT 255
256 TCT GTT AAC AAC GGT AAA AAC ACC TTC GCT GAC CCG CCG AAA ATG GTT ATC 306
307 GCT AAC TTC GGT TAC GAC GCT GGT GGT TGG CGT GTT GAA AAA CAC CTG CGT 357
358 TAC CTG GCT GAC ATC CGT AAA ATC GGT CGT GCT GAC ATC ATC GGT TTC GGT 408
409 GAA AAA GGT GTT CTG GTT TCT CGT AAC AAC GGT GGT CTG AAC TTC GGT CCG 459
460 GCT ACC CTG GTT CTG AAA GAC TTC GGT TAC GAC GCT GGT GGT TGG CGT CTG 510
511 GAC CGT CAC CTG CGT TTC CTG GCT GAC GTT ACC GGT AAC GGT CAC CTG GAC 561
562 ATC GTT GGT TTC GGT GAC AAA CAC GTT TTC ATC TCT CGT AAC AAC GGT GAC 612
                                     GC CGA TTT AGA CAA TAG CTG TTG AAG ACG TAA CTG CGA
613 GGT ACC TTC GCT CCG GCT AAA TCT GTT ATC GAC AAC TTC TGC ATC GAC GCT 663
    GCT GCT GCT AAA ATC GGT GAC CAC CCG CGT TTC GTT GC
664 GGT GGT TGG AAA ATC GGT GAC CAC CCG CGT TTC GTT GCT GAC CTG ACC GGT 714
715 GAC GGT ACC GCT GAC ATC ATC GGT TGC GGT AAA GCT GGT TGC TGG GTT GCT 765
766 CTG AAC AAC GGT GGT GGT GTT TTC GGT CAG GTT AAA CTG GTT ATC AAC GAC 816
817 TTC GGT ACC GAC AAA GGT TGG CAG GCT GCT AAA CAC CCG CGT TTC ATC GCT 867
868 GAC CTG ACC GGT AAC GGT CGT GGT GAC GTT GTT GGT TTC GGT AAC GCT GGT 918
919 GTT TAC GTT GCT CTG AAC AAC GGT GAC GGT ACC TTC CAG TCT GCT AAA CTG 969
970 GTT CTG AAA GAC TTC GGT GTT CAG CAG GGT TGG ACC GTT TCT AAA CAC CGT 1020
1021 CGT TTC GTT GTT GAC CTG ACC GGT GAC GGT TGC GCT GAC ATC ATC GGT TTC 1071
1072 GGT GAA AAA GAA ACC CTG GTT TCT TAC AAC GAC GGT AAA GGT AAC TTC GGT 1122
1123 CCG GTT AAA GCT CTG ACC AAC GAC TTC TCT TTC TCT GGT GGT AAA TGG GCT 1173
1174 CCG GAA ACC ACC GTT TGC TGG ATG GCT AAC CTG GAC TCT TCT CGT CAC TAA 1224

```

Fig B.2: Whole vector amplification strategy for the generation of pAAL-2_MT.

The AAL-2 sequence was amplified with the whole pQE-30 sequence using two primers, AAL-2 FP1 and AAL-2 RP1 (Table 2.4). A second round of SDM was completed using AAL-2 FP2 and AAL-2 RP2 primers (Table 2.4). The reverse primers are shown in blue and the forward primers are shown in red. The nucleotides in bold were mutated following amplification with these primers. The underlined codons are the two sets of three codons that were mutated, G53A, G54A, W55A and G222A, G223A, W224A. A silent mutation was incorporated into the reverse primer AAL-2 RP2, I219I, to avoid primer hairpin formation.

The first round of SDM was completed using primers AAL-2 FP1 and AAL-2 RP1. Following this a DpnI digest was completed to remove the template plasmid. The plasmid containing the mutated AAL-2 was ligated and competent *E. coli* JM109 cells

were transformed with it. A plasmid purification was completed to obtain fresh plasmid to serve as the template during the second round of SDM using primers AAL-2 FP2 and AAL-2 RP2. A DpnI digest and plasmid ligation were completed again and the plasmid was transformed into competent *E. coli* KRX cells. A plasmid purification was again completed and the mutagenesis was confirmed after the plasmid was sequenced, see Section 2.13.

	1				50
AAL-2	MRGSHHHHHH	GSMKGEELM	TSNVITQDLP	IPVASRGFAD	IVGFGLDGVV
AAL-2mut	MRGSHHHHHH	GSMKGEELM	TSNVITQDLP	IPVASRGFAD	IVGFGLDGVV
	51				100
AAL-2	IGRNAVNLQP	FLAVKNFAQN	AGGW LTTKHV	RLIADTTGTG	KGDIVGFGNA
AAL-2mut	IGRNAVNLQP	FLAVKNFAQN	AAAA LTTKHV	RLIADTTGTG	KGDIVGFGNA
	101				150
AAL-2	GVYVSVNNGK	NTFADPPKMV	IANFGYDAGG	WRVEKHLRYL	ADIRKIGRAD
AAL-2mut	GVYVSVNNGK	NTFADPPKMV	IANFGYDAGG	WRVEKHLRYL	ADIRKIGRAD
	151				200
AAL-2	IIGFGEKGVL	VSRNNGGLNF	GPATLVLKDF	GVDAGGWRLD	RHLRFLADVT
AAL-2mut	IIGFGEKGVL	VSRNNGGLNF	GPATLVLKDF	GVDAGGWRLD	RHLRFLADVT
	201				250
AAL-2	GNGHLDIVGF	GDKHVFISRN	NGDGTAFAPAK	SVIDNFCIDA	GGW KIGDHPR
AAL-2mut	GNGHLDIVGF	GDKHVFISRN	NGDGTAFAPAK	SVIDNFCIDA	AAA KIGDHPR
	251				300
AAL-2	FVADLTGDGT	ADIIGCGKAG	CWVALNNGGG	VFGQVKLVIN	DFGTDKGWQA
AAL-2mut	FVADLTGDGT	ADIIGCGKAG	CWVALNNGGG	VFGQVKLVIN	DFGTDKGWQA
	301				350
AAL-2	AKHPRFIADL	TGNRGDVVG	FGNAGVYVAL	NNGDGTQSA	KLVLKDFGVQ
AAL-2mut	AKHPRFIADL	TGNRGDVVG	FGNAGVYVAL	NNGDGTQSA	KLVLKDFGVQ
	351				400
AAL-2	QGWTVSKHRR	FVVDLTGDGC	ADIIGFGEKE	TLVSYNDGKG	NFGPVKALTN
AAL-2mut	QGWTVSKHRR	FVVDLTGDGC	ADIIGFGEKE	TLVSYNDGKG	NFGPVKALTN
	401		426		
AAL-2	DFSFSGGKWA	PETTVCWMAN	LDSSRH		
AAL-2mut	DFSFSGGKWA	PETTVCWMAN	LDSSRH		

Fig B.3: AAL-2 and AAL-2_{mut} protein sequence alignment. The emboldened residues highlight sequence differences. Alignment completed using Multalin version 5.4.1.

B.4 Expression of mutated AAL-2

The pAAL-2_MT plasmid containing the mutated AAL-2 coding sequence, AAL-2_{mut}, was inserted into competent *E. coli* KRX cells for expression in 200 mL TB medium, see Section 2.15. The cells were lysed by a cell disruptor and the resulting lysate was passed through two Ni-charged IMAC columns, one containing Profinity IMAC resin (Bio-rad) and the other containing IMAC-Sepharose resin (GE Healthcare). Fig. B.4 shows the protein fractions from these purifications.

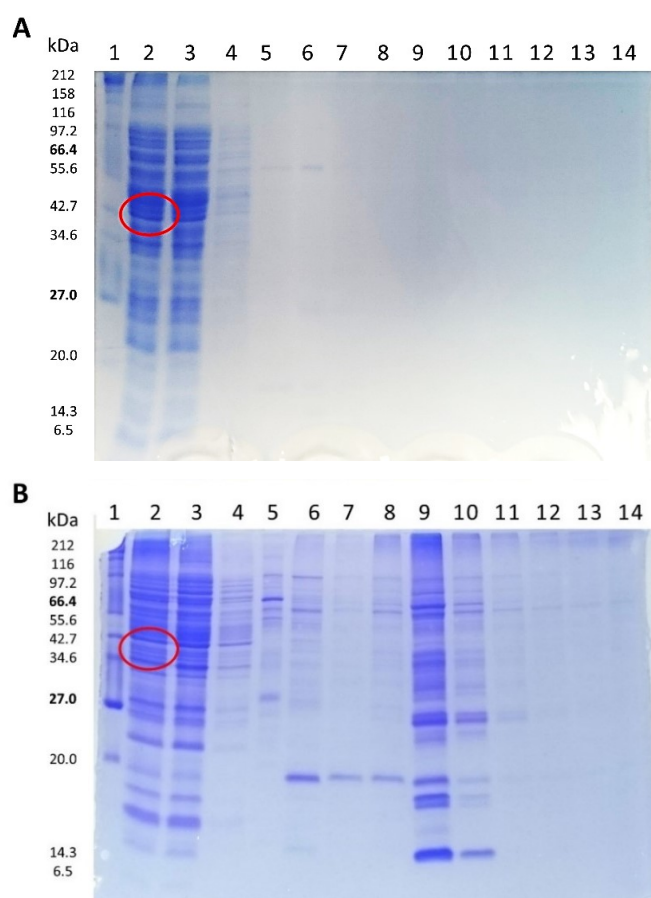


Fig B.4: IMAC purification of AAL-2_{mut}. **A)** Attempted purification of AAL-2_{mut} from a 200 mL TB culture using Profinity IMAC resin (Bio-rad). **B)** Attempted purification of AAL-2_{mut} from a 200 mL TB culture using IMAC-Sepharose resin (GE Healthcare). Three imidazole wash steps, 20 mL of 20 mM, 20 mL of 50 mM and 10 mL of 80 mM were completed before eluting with 250 mM imidazole. In both images Lane 1; NEB protein ladder (Fig. 2.5), Lane 2; filtered lysate, Lane 3; unbound filtered, Lane 4; Wash 1 (20 mM), Lane 5; Wash 2 (50 mM), Lane 6; Wash 3 (80 mM), Lanes 7 - 14; 1 mL elution fractions 1-8.

B.5 Binding sites of AAL-2

The mutagenesis of AAL-2 to alter binding affinity/specificity was not attempted again. The publication by Ren et al. (2015) presented the AAL-2 structure and its six GlcNAc binding sites, Fig. B.5. Due to the large number of binding sites and the many residues involved in glycan interactions, AAL-2 is not an ideal lectin to use as template for the generation of novel lectin probes.

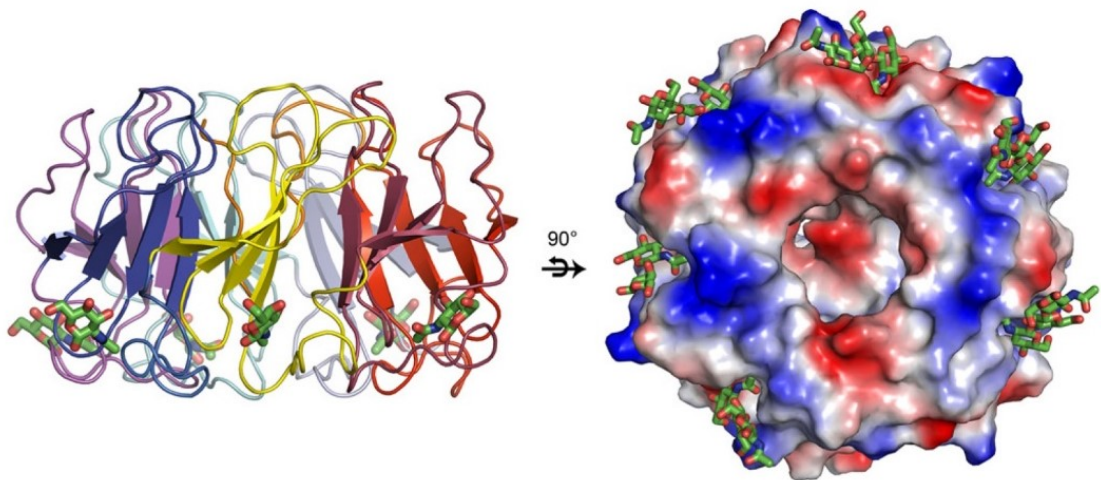


Fig. B.5: The six GlcNAc binding pockets of AAL-2. Horizontal and vertical views of the AAL-2 lectin in cartoon format (left) and surface electrostatic potential diagram (right) with the binding pockets occupied by GlcNAc β 1-3Gal β 1-4GlcNAc represented in stick format. Image modified from Ren et al. (2015).

Appendix C

IMAC purification of LecA

C.1 IMAC resin saturation

A standard 200 mL TB expression culture of LecA (12.7 kDa) was completed, see Section 2.15, using *E. coli* KRX cells containing the pQE-30_LecA plasmid. The cells were lysed by a cell disruptor and the resulting lysate was passed through a 2 mL Ni-charged IMAC-Sepharose (GE Healthcare), see Section 2.17. Fig. C.1 gel A shows the wash and elution fractions from this purification. A second purification was completed, Fig. C.1 gel B using less filtered lysate to reduce protein precipitation and gel smearing.

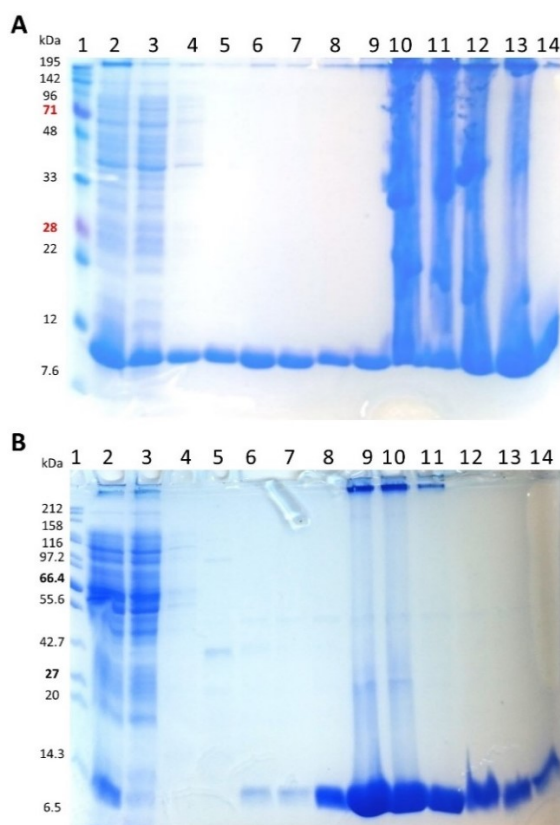


Fig. C.1: IMAC purification of LecA. Analysis by 15 % SDS-PAGE of *N*-terminally His₆ tagged LecA in *E. coli* KRX. Three imidazole wash steps, 20 mL of 20 mM, 20 mL of 40 mM and 10 mL of 80 mM were completed before eluting with 250 mM imidazole. **A)** All filtered lysate loaded. **B)** 25 % of filtered lysate loaded. In both gels Lane 1; Protein markers (Fig. 2.5), Lane 2; filtered lysate, Lane 3; unbound filtered lysate, Lane 4; Wash 1 (20 mM), Lane 5; Wash 2 (40 mM), Lane 6; Wash 3 (80 mM), Lane 7 - 14; 1 mL elution fractions (250 mM).

LecA was strongly expressed and fully saturated the Ni-charged column. Fig. C.1 gel A shows a large LecA band in the unbound fraction in lane 3. IMAC-Sepharose FastFlow resin can bind up to 40 mg per mL. The LecA band in the flow through indicates that the 80 mg resin capacity, 2 mL, was surpassed. The smearing in lanes 10 to 13 indicate that the protein capacity of the polyacrylamide has been reached. Smearing makes it impossible to detect unwanted proteins in the same lanes. Lanes 5 to 9 in gel A indicates that unwanted proteins have been removed but it does not mean that the later fractions contain pure LecA. Gel B shows the purification of LecA with a reduced filtered lysate loading volume, ~ 25 % of that loaded in gel A, although it was from a second expression culture which may differ slightly in cell concentration and therefore LecA concentration. The IMAC resin was not saturated as a large LecA (12.7 kDa) band was not observed in lane 4. The concentration of LecA in elution fractions 3, 4 and 5, (lanes 9, 10 and 11) was high which caused protein aggregation and did not allow all the sample loaded to pass from the stacking gel into the resolving gel. Loading less filtered lysate may prevent gel smearing all the while still achieving relatively pure fractions of the desired protein.

Appendix D

Nucleotide and protein sequences for EGFP-LecA fusion, LecA and LecA with additional lysine residues

D.1 EGFP-LecA with an *N*-terminus His₆ tag from pEGFP_LecA plasmid, Table 2.2, and constructed in Fig. 3.26

Nucleotide sequence

ATGAGAGGATCGCATCACCATCACCATCACGGATCTATGAGTAAAGGAGAAGAACTT
TTCACTGGAGTTGTCCCAATTCTTGTTGAATTAGATGGTGATGTTAATGGGCACAAA
TTTTCTGTCAGTGGAGAGGGTGAAGGTGATGCAACATACGGAAAACCTTACCCTTAAA
TTTATTTGCACTACTGGAAAACCTACCTGTTCCATGGCCAACACTTGTCACTACTCTC
ACTTATGGTGTTCATGCTTTGCGAGATACCCAGATCATATGAAACAGCATGACTTT
TTCAAGAGTGCCATGCCCGAAGGTTATGTACAGGAAAGAACTATATTTTTCAAAGAT
GACGGAACTACAAGACACGTGCTGAAGTCAAGTTTGAAGGTGATACCCTTGTTAAT
AGAATCGAGTTAAAAGGTATTGATTTTAAAGAAGATGGAAACATTCTTGACACAAA
TTGGAATACAACATAACTCACACAATGTATACATCATGGCAGACAAAACAAAAGAAT
GGAATCAAAGTTAACTTCAAAAATTAGACACAACATTGAAGATGGAAGCGTTCAACTA
GCAGACCATTATCAACAAAATACTCCAATTGGCGATGGCCCTGTCCTTTTACCAGAC
AACCATTACCTGTCCACACAATCTGCCCTTTCGAAAGATCCCAACGAAAAGAGAGAC
CACATGGTCCTTCTTGAGTTTGTAAACAGCTGCTGGGATTACACATGGCATGGATGAA
CTATACAAAGGATCCATGAGAGGATCGCATCACCATCACCATCACGGATCCATGGCT
TGGAAGGTGAGGTTCTGGCTAATAACGAAGCAGGGCAGGTAACGTCGATTATCTAC
AATCCGGGCGATGTCATTACCATCGTCGCCGCCGGTTGGGCCAGTTACGGACCTACC
CAGAAATGGGGGCCGCAGGGCGATCGGGAGCATCCGGACCAAGGGCTGATCTGCCAC
GATGCGTTTTGTGGTGGCTGGTCATGAAGATTGGCAACAGCGGAACCATTCGGGTC
AATACCGGTTGTTCCGTTGGGTTGCACCCAATAATGTCCAGGGTGCAATCACTCTT
ATCTACAACGACGTGCCCGGAACCTATGGCAATAACTCCGGCTCGTTCAGTGTCAAT
ATTGGAAGGATCAGTCC**TAA**

Highlighted regions: Starting codon (green underlined), *N*-terminus His₆ tag (blue), EGFP sequence (green), First codon in the LecA sequence (orange underlined), Stop codon (red)

Translated protein sequence

MRGSHHHHHHGSMSKGEELFTGVVPIVVELDGDVNGHKFSVSGEGEGDATYGLTLK
FICTTGKLPVPWPTLVTTLTYGVCFARYPDHMKQHDFFKSAMPEGYVQERTIFFKD
DGNYKTRAEVKFEGDTLVNRIELKGIDFKEDGNILGHKLEYNYNSHNVYIMADKQKN
GIKVNFKIRHNIEDGSVQLADHYQQNTPIGDGPVLLPDNHYLSTQSALSKDPNEKRD
HMLLEFVTAAGITHGMDELYKGSMMAWKGEVLANNEAGQVTSIIYNPGDVITIVAA
GWASYGPTQKWGPQGDREHPDQGLICHDAFCGALVMKIGNSGTIPVNTGLFRWVAPN
NVQGAITLIYNDVPGTYGNNSGSFSVNIGKDQS -

D.2 LecA with an *N*-terminal His₆ tag from pQE-30_LecA plasmid, Table 2.2

Nucleotide sequence

```
ATGAGAGGATCGCATCACCATCACCATCACGGATCCATGGCTTGGAAAGGTGAGGTT
CTGGCTAATAACGAAGCAGGGCAGGTAACGTCGATTATCTACAATCCGGGCGATGTC
ATTACCATCGTCGCCCGCGGTTGGGCCAGTTACGGACCTACCCAGAAATGGGGGCCG
CAGGGCGATCGGGAGCATCCGGACCAAGGGCTGATCTGCCACGATGCGTTTTGTGTT
GCGCTGGTCATGAAGATTGGCAACAGCGGAACCATTCCGGTCAATACCGGGTTGTTC
CGTTGGGTTGCACCCAATAATGTCCAGGGTGCAATCACTCTTATCTACAACGACGTG
CCCGGAACCTATGGCAATAACTCCGGCTCGTTCAGTGTCAATATTGGAAAGGATCAG
TCCTAA
```

Highlighted regions: Starting codon (green), *N*-terminus His₆ tag is (blue), First codon in the LecA sequence (green underlined), Stop codon (red)

Translated protein sequence

```
MRGSHHHHHHGSMAWKGEVLANNEAGQVTSIIYNPGDVITIVAAGWASYGPTQKWGP
QGDREHPDQGLICHDAFCGALVMKIGNSGTIPVNTGLFRWVAPNNVQGAITLIYNDV
PGTYGNNSGSFSVNIGKDQS -
```

D.3 LecA3KH with an *N*-terminal His₆ tag from pLecA3KH plasmid, Table 2.3

Nucleotide sequence

```
ATGAAGAAGAAGTCGCATCACCATCACCATCACGGATCCATGGCTTGGAAAGGTGAG
GTTCTGGCTAATAACGAAGCAGGGCAGGTAACGTCGATTATCTACAATCCGGGCGAT
GTCATTACCATCGTCGCCCGCGGTTGGGCCAGTTACGGACCTACCCAGAAATGGGGG
CCGCAGGGCGATCGGGAGCATCCGGACCATGGGCTGATCTGCCACGATGCGTTTTGT
GGTGCCTGGTCATGAAGATTGGCAACAGCGGAACCATTCCGGTCAATACCGGGTTG
TTCCGTTGGGTTGCACCCAATAATGTCCAGGGTGCAATCACTCTTATCTACAACGAC
GTGCCCCGAACCTATGGCAATAACTCCGGCTCGTTCAGTGTCAATATTGGAAAGGAT
CAGTCCTAA
```

Highlighted regions: Starting codon (green), inserted lysine codons (bold), *N*-terminus His₆ tag is (blue), First codon in the LecA sequence (green underlined), Stop codon (red)

Translated protein sequence

```
MKKKSHHHHHHGSMAWKGEVLANNEAGQVTSIIYNPGDVITIVAAGWASYGPTQKWG
PQGDRHPDQGLICHDAFCGALVMKIGNSGTIPVNTGLFRWVAPNNVQGAITLIYND
VPGTYGNNSGSFSVNIGKDQS -
```

D.4 LecAH3K with an *N*-terminal His₆ tag from pLecAH3K plasmid, Table 2.3

ATGAGAGGATCG**CATCACCATCACCATCAC**GGAA**AAGAAGAAG**TCC**ATG**GCTTGGAAA
GGTGAGGTTCTGGCTAATAACGAAGCAGGGCAGGTAACGTCGATTATCTACAATCCG
GGCGATGTCATTACCATCGTCGCCGCCGGTTGGGCCAGTTACGGACCTACCCAGAAA
TGGGGGCCGCAGGGCGATCGGGAGCATCCGGACCATGGGCTGATCTGCCACGATGCG
TTTTGTGGTGCCTGGTCATGAAGATTGGCAACAGCGGAACCATTCGGTCAATACC
GGTTGTTCCGTTGGGTTGCACCCAATAATGTCCAGGGTGCAATCACTCTTATCTAC
AACGACGTGCCCGGAACCTATGGCAATAACTCCGGCTCGTTCAGTGTCAATATTGGA
AAGGATCAGTCC**TAA**

Highlighted regions: Starting codon (green), *N*-terminus His₆ tag is (blue), inserted lysine codons (bold), First codon in the LecA sequence (green underlined), Stop codon (red)

Translated protein sequence

MRGSHHHHHHG**KKK**SM**AW**KGEVLANNEAGQVTSIIYNPGDVITIVAAGWASYGPTQK
WGPQGDREHPDQGLICHDAFCGALVMKIGNSGTIPVNTGLFRWVAPNNVQGAILIY
NDVPGTYGNNSGSFVSNIKQDS-

D.5 LecA3K with an *N*-terminal His₆ tag from pLecA3K plasmid, Table 2.3

Nucleotide sequence

ATGAGAGGATCG**CATCACCATCACCATCAC**GGATCC**ATG**GCTTGGAAAGGTGAGGTT
CTGGCTAATAACGAAGCAGGGCAGGTAACGTCGATTATCTACAATCCGGGCGATGTC
ATTACCATCGTCGCCGCCGGTTGGGCCAGTTACGGACCTACCCAGAAATGGGGCCG
CAGGGCGATCGGGAGCATCCGGACCAAGGGCTGATCTGCCACGATGCGTTTTGTGGT
GCGCTGGTCATGAAGATTGGCAACAGCGGAACCATTCGGTCAATACCGGGTTGTTC
CGTTGGGTTGCACCCAATAATGTCCAGGGTGCAATCACTCTTATCTACAACGACGTG
CCCGGAACCTATGGCAATAACTCCGGCTCGTTCAGTGTCAATATTGGAAAGGATCAG
TCC**AAGAAGAAGTAA**

Highlighted regions: Starting codon (green), *N*-terminus His₆ tag is (blue), First codon in the LecA sequence (green underlined), inserted lysine codons (bold), Stop codon (red)

Translated protein sequence

MRGSHHHHHHGS**M**AWKGEVLANNEAGQVTSIIYNPGDVITIVAAGWASYGPTQKWGP
QGDREHPDQGLICHDAFCGALVMKIGNSGTIPVNTGLFRWVAPNNVQGAILIYNDV
PGTYGNNSGSFVSNIKQDS**KKK**-

D.6 LecA5K with an *N*-terminal His₆ tag from pLecA5K plasmid, Table 2.3

Nucleotide sequence

ATGAGAGGATCG**CATCACCATCACCATCAC**GGATCC**ATG**GCTTGGAAAGGTGAGGTT
CTGGCTAATAACGAAGCAGGGCAGGTAACGTCGATTATCTACAATCCGGGCGATGTC
ATTACCATCGTCGCCCGCGTTGGGCCAGTTACGGACCTACCCAGAAATGGGGGCCG
CAGGGCGATCGGGAGCATCCGGACCAAGGGCTGATCTGCCACGATGCGTTTTGTGTT
GCGCTGGTCATGAAGATTGGCAACAGCGGAACCATCCGGTCAATACCGGGTTGTTC
CGTTGGGTTGCACCCAATAATGTCCAGGGTGCAATCACTCTTATCTACAACGACGTG
CCCGGAACCTATGGCAATAACTCCGGCTCGTTCAGTGTCAATATTGGAAAGGATCAG
TCC**AAGAAGAAGAAGTAA**

Highlighted regions: Starting codon (green), *N*-terminus His₆ tag is (blue), First codon in the LecA sequence (green underlined), inserted lysine codons (bold), Stop codon (red)

Translated protein sequence

MRG**S****HHHHHH**G**S**MAWKGEVLANNEAGQVTSIIYNPGDVITIVAAGWASYGPTQKWGP
QGDREHPDQGLICHDAFCGALVMKIGNSGTIPVNTGLFRWVAPNNVQGAIITLIYNDV
PGTYGNNSGSFSVNIGKDQ**S****KKKKK**-

Appendix E

Flow cytometry data for optimising cell preparation for lectin probing

Table E.1: Flow cytometry data for determining an appropriate lectin probing concentration, see Fig. 5.2 and Fig. 5.3

20,000 events recorded for each sample

Sample	Cells in Live Gate (%)	Negative (%)	Positive (%)	MFI
Unstained	93.43	99.99	0.01	4.84
AAL 1 µg/mL	92.65	78.66	21.34	43.07
AAL 5 µg/mL	73.57	0.33	99.67	1196.73
AAL 10 µg/mL	55.45	7.90	92.08	4183.59
AAL 20 µg/mL	49.73	4.38	95.62	11069.41
AAL-2 1 µg/mL	92.08	0.46	99.54	261.52
AAL-2 5 µg/mL	78.00	0.07	99.93	1818.57
AAL-2 10 µg/mL	57.87	0.14	99.86	3897.47
AAL-2 20 µg/mL	46.41	0.34	99.66	6571.27
RCA 1 µg/mL	89.15	1.95	98.05	395.27
RCA 5 µg/mL	60.76	2.54	97.46	1391.80
RCA 10 µg/mL	57.10	1.67	98.33	3575.94
RCA 20 µg/mL	25.15	0.95	99.05	5749.80

Table E.2: Flow cytometry data for determining an appropriate cell number per sample, see Fig. 5.4

10,000 events recorded for each sample in triplicate, average tabulated

Sample (Cell #)	Cells in Live Gate (%)	Negative (%)	Positive (%)	MFI
Unstained (7×10^5)	88.92	99.97	0.03	8.76
AAL-2 (5×10^5)	83.92	0.13	99.87	3055.41
AAL-2 (6×10^5)	85.9	0.09	99.91	2733.83
AAL-2 (7×10^5)	84.49	0.07	99.93	2480.04
AAL-2 (8×10^5)	83.63	0.14	99.86	2324.88
AAL-2 (9×10^5)	90.04	0.14	99.86	1812.76
DSL (5×10^5)	72.51	0.01	99.99	4759.30
DSL (6×10^5)	73.6	0.04	99.96	4373.18
DSL (7×10^5)	76.07	0.01	99.99	4019.94
DSL (8×10^5)	81.45	0.05	99.95	3457.86
DSL (9×10^5)	70.8	0.06	99.94	3303.32

Table E.3: Flow cytometry data for determining an appropriate cell lectin probing temperature, see Fig. 5.5

20,000 events recorded for each sample in triplicate, average tabulated

Sample	Cells in Live Gate (%)	Negative (%)	Positive (%)	MFI
Unstained (20 °C)	87.47	99.98	0.02	5.72
Con A (20 °C)	83.63	1.17	98.83	1878.12
DSL (20 °C)	68.47	0.10	99.90	1629.07
LecA5K (20 °C)	87.70	0.22	99.78	405.85
NPL (20 °C)	70.07	0.18	99.82	3999.71
Unstained (4 °C)	87.36	99.81	0.19	6.56
Con A (4 °C)	86.27	1.17	98.83	1438.89
DSL (4 °C)	72.28	0.10	99.90	1245.35
LecA5K (4 °C)	88.06	1.90	98.10	402.68
NPL (4 °C)	61.80	0.15	99.85	3868.76

Table E.4: Flow cytometry data for comparing trypsin and cell scraper for cell detachment, see Fig. 5.6

20,000 events recorded for each sample

Sample	Cells in Live Gate (%)	Negative (%)	Positive (%)	MFI
Unstained (Trypsin)	88.97	100.00	0.00	0.53
AAL-2 (Trypsin)	71.08	0.30	99.70	1725.83
Con A (Trypsin)	57.91	10.57	89.41	3080.92
DSL (Trypsin)	68.70	0.85	99.15	701.19
MAL II (Trypsin)	72.23	0.93	99.07	643.20
RCA I (Trypsin)	63.82	8.79	91.21	1914.66
Unstained (Scraper)	74.35	99.97	0.03	2.92
AAL-2 (Scraper)	67.34	0.51	99.49	1979.15
Con A (Scraper)	60.24	16.99	82.97	4917.35
DSL (Scraper)	68.64	1.60	98.40	643.25
MAL II (Scraper)	67.38	1.12	98.88	649.80
RCA I (Scraper)	61.78	14.59	85.41	3127.53

Table E.5: Flow cytometry data for comparing trypsin and cell dissociation solution for cell detachment, see Fig. 5.6

20,000 events recorded for each sample

Sample	Cells in Live Gate (%)	Negative (%)	Positive (%)	MFI
Unstained (Trypsin)	93.84	100.00	0.00	0.44
AAL-2 (Trypsin)	77.22	0.53	99.47	1528.46
Con A (Trypsin)	59.37	2.86	97.14	2431.53
DSL (Trypsin)	62.47	0.24	99.76	1230.13
MAL II (Trypsin)	79.27	0.50	99.50	486.57
RCA I (Trypsin)	68.87	13.49	86.50	2473.79
Unstained (CDS)	88.53	99.99	0.01	1.71
AAL-2 (CDS)	73.42	0.19	99.81	1663.67
Con A (CDS)	68.32	5.00	95.00	2358.61
DSL (CDS)	68.38	0.84	99.16	1002.64
MAL II (CDS)	76.79	0.80	99.20	617.74
RCA I (CDS)	69.63	25.47	74.53	1825.92

Table E.6: Flow cytometry data for comparing trypsin and 10 mM EDTA solution for cell detachment, see Fig. 5.6

20,000 events recorded for each sample

Sample	Cells in Live Gate (%)	Negative (%)	Positive (%)	MFI
Unstained (Trypsin)	94.09	100.00	0.00	0.56
AAL-2 (Trypsin)	71.49	0.13	99.87	1981.86
Con A (Trypsin)	64.57	9.33	90.67	3492.85
DSL (Trypsin)	62.56	0.20	99.80	1189.00
MAL II (Trypsin)	76.52	0.38	99.62	734.43
RCA I (Trypsin)	62.95	3.80	96.20	1702.42
Unstained (EDTA)	77.96	99.95	0.05	2.15
AAL-2 (EDTA)	65.32	0.15	99.85	1815.27
Con A (EDTA)	64.78	31.53	68.45	2640.62
DSL (EDTA)	65.15	0.91	99.09	862.27
MAL II (EDTA)	68.64	0.50	99.50	693.26
RCA I (EDTA)	61.53	8.41	91.59	1773.30

Appendix F

Flow cytometry data for CHO DP-12 adherent and suspension culture comparison

Table F.1: Flow cytometry data for adherent CHO DP-12 cells probed with lectin panel, summarised in Table 5.2

20,000 events recorded for each sample

Lectin	Cells in Live Gate (%)	Negative (%)	Positive (%)	MFI
Unstained	91.90	100.00	0.00	8.09
AAL	79.97	7.52	92.48	1575.49
AAL-2	76.26	0.09	99.91	1761.63
Con A	60.31	26.89	73.08	4961.77
DBA	94.08	98.95	1.05	35.88
DSL	65.03	0.22	99.78	2051.25
ECL	72.81	1.06	98.94	2341.18
GafD1-178	92.74	99.89	0.11	9.88
GNL	88.55	0.11	99.89	1364.42
GSL I	93.88	97.10	2.90	126.38
GSL I B4	93.03	98.43	1.57	182.07
GSL II	92.88	75.71	24.29	33.32
HPA	93.10	92.42	7.58	32.03
Jacalin	62.70	12.15	87.85	4395.63
LCA	59.20	1.57	98.43	5271.05
LecA5	85.05	10.09	89.91	406.10
LecB	89.43	66.14	33.86	96.12
MAL I	60.24	2.18	97.82	4174.70
MAL II	75.92	1.78	98.22	1625.69
NPL	85.54	0.05	99.95	2575.78
PNA	94.15	74.60	25.40	753.92
RCA I	58.44	4.40	95.59	2875.69
SBA	94.30	98.72	1.28	166.35
SNA	92.69	97.91	2.09	937.69
WGA	52.57	5.75	94.25	2929.20

Table F.2: Flow cytometry data for suspension adapted CHO DP-12 cells probed with lectin panel, summarised in Table 5.2

20,000 events recorded for each sample

Lectin	Cells in Live Gate (%)	Negative (%)	Positive (%)	MFI
Unstained	86.50	99.98	0.02	8.15
AAL	78.57	6.98	93.02	1039.31
AAL-2	79.26	0.04	99.96	1461.46
Con A	66.10	29.99	69.99	2916.62
DBA	88.12	98.39	1.60	38.08
DSL	74.86	0.05	99.95	2069.47
ECL	76.79	1.08	98.92	1327.09
GafD1-178	93.45	99.58	0.42	7.39
GNL	83.03	0.17	99.83	1352.12
GSL I	86.79	97.66	2.34	108.93
GSL I B4	88.32	98.32	1.68	129.73
GSL II	89.26	91.18	8.82	15.88
HPA	91.86	98.83	1.17	22.01
Jac	65.99	13.03	86.97	2968.49
LCA	57.68	0.60	99.40	4852.08
LecA5	80.67	0.91	99.09	974.57
LecB	86.84	41.08	58.92	119.62
MAL I	64.28	1.64	98.36	2321.59
MAL II	72.71	0.75	99.25	1496.06
NPL	77.51	0.30	99.70	2231.79
PNA	93.74	89.59	10.39	266.69
RCA I	62.66	0.18	99.82	2620.98
SBA	93.29	95.21	4.79	88.35
SNA	92.82	98.89	1.11	104.42
WGA	58.10	0.44	99.56	4377.19

Table F.3: Flow cytometry data for unstained adherent and suspension adapted CHO DP-12, corresponding to Fig. 5.7 and Fig. H.1.

20,000 events recorded for each sample

Sample	Cells in Live Gate (%)	Mean FSC-A (% change)	Mean SSC-A (% change)
Adherent	91.69	59977.45	69086.22
Suspension	91.12	106856.13 (+78.16)	56981.26 (-17.52)

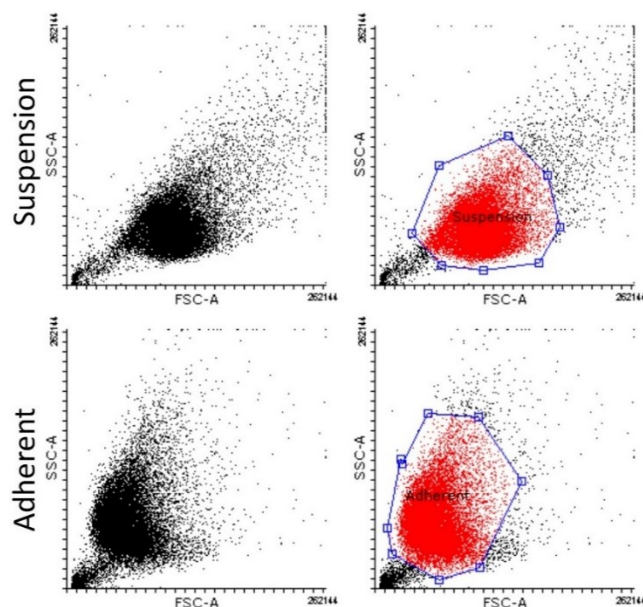


Fig. F.1: Gated and ungated dotplots of adherent and suspension adapted CHO DP-12 cells. SSC-A versus FSC-A dotplots of unprobed cells corresponding to Table H.3 and Fig. 5.7. Cells were prepared as described in Section 2.28.3.1. The data analysis and gating strategy is explained in Section 2.28.3.3.

Table F.4: Flow cytometry data for assessing LecA and LecA variants, corresponding to Fig. 5.8

20,000 events recorded for each sample

Lectin	Cells in Live Gate (%)	Negative (%)	Positive (%)	MFI
Unstained	86.16	99.98	0.02	6.32
LecA	84.91	21.26	78.74	217.64
EGFP-LecA	86.97	96.65	3.35	220.89
LecA3KH	85.94	46.52	53.48	153.89
LecAH3K	82.18	0.88	99.12	512.13
LecAK3	83.42	13.48	86.52	293.09
LecAK5	83.07	0.08	99.92	925.95

Appendix G

Flow cytometry data for lectin inhibition checks

Table G.1: Flow cytometry data for suspension CHO DP-12 cells probed with recombinant AAL-2 and GafD1-178, corresponding to Fig. 5.9, Fig. 5.10 and Fig. 5.11

20,000 events recorded for each sample

Sample	Cells in Live Gate (%)	Negative (%)	Positive (%)	MFI
Unstained	92.14	100.00	0.00	1.93
AAL-2	84.08	1.68	98.32	1886.10
AAL-2 + 12.5 mM GlcNAc	91.62	97.29	2.71	52.31
AAL-2 + 25 mM GlcNAc	92.62	97.81	2.19	51.85
AAL-2 + 50 mM GlcNAc	92.50	97.96	2.04	58.33
AAL-2 + 100 mM GlcNAc	91.40	97.75	2.25	51.22
AAL-2 + 12.5 mM GalNAc	89.18	1.37	98.63	1049.64
AAL-2 + 25 mM GalNAc	90.10	0.54	99.46	787.11
AAL-2 + 50 mM GalNAc	90.14	2.91	97.09	569.50
AAL-2 + 100 mM GalNAc	90.86	24.20	75.80	208.08
Unstained	86.62	99.98	0.02	5.73
AAL-2	85.56	0.07	99.93	3117.47
AAL-2 + 1 ug/mL BSA-GlcNAc	85.99	0.05	99.95	2835.09
AAL-2 + 2 ug/mL BSA-GlcNAc	89.47	0.03	99.97	2234.10
AAL-2 + 3 ug/mL BSA-GlcNAc	89.77	0.07	99.93	902.66
AAL-2 + 4 ug/mL BSA-GlcNAc	89.49	16.03	83.97	193.03
AAL-2 + 5 ug/mL BSA-GlcNAc	89.36	56.32	43.68	100.49
AAL-2 + 1 ug/mL BSA-GalNAc	82.58	0.04	99.96	3318.55
AAL-2 + 2 ug/mL BSA-GalNAc	87.39	0.02	99.98	2893.48
AAL-2 + 3 ug/mL BSA-GalNAc	82.15	0.02	99.98	3014.07
AAL-2 + 4 ug/mL BSA-GalNAc	85.97	0.02	99.98	3262.52
AAL-2 + 5 ug/mL BSA-GalNAc	86.43	0.02	99.98	2961.68
Unstained (Untreated)	92.35	99.99	0.01	6.10
GafD (Untreated)	82.06	97.6	2.4	7.93
Unstained (H ₂ O ₂ treated)	90.83	99.94	0.06	5.18
GafD (H ₂ O ₂ treated)	66.07	1.43	98.57	424.58
GafD + 0.1 M GlcNAc (H ₂ O ₂ treated)	67.60	33.10	66.90	260.69
GafD + 0.1 M GalNAc (H ₂ O ₂ treated)	55.17	1.70	98.30	382.99

Table G.2: Flow cytometry data for suspension CHO DP-12 cells probed with recombinant LecA5K, AAL, DSL, ECL, GNL, and Jacalin corresponding to Fig. 5.12 to Fig. 5.17

20,000 events recorded for each sample

Sample	Cells in Live Gate (%)	Negative (%)	Positive (%)	MFI
Unstained	88.88	99.95	0.05	7.73
LecA5K	81.45	0.36	99.64	862.76
LecA5K + 0.1 M Gal	87.51	99.18	0.82	31.76
LecA5K + 0.1 M Man	82.70	1.83	98.17	506.80
Unstained	82.78	99.99	0.01	12.64
LecA5K	82.50	1.76	98.24	768.62
LecA5K + 5 ug/mL BSA-Gal	83.12	18.71	81.29	351.77
LecA5K + 5 ug/mL BSA-Man	84.43	2.45	97.55	737.41
Unstained	82.90	99.99	0.01	8.75
AAL	67.95	6.04	93.96	2645.84
AAL 0.2 M L-Fuc	83.79	99.68	0.32	20.17
AAL 0.2 M D-Fuc	67.36	4.95	95.04	1092.09
DSL	67.24	0.24	99.76	2443.96
DSL 0.4 M GlcNAc	69.52	0.34	99.66	1465.35
DSL 0.4 M GalNAc	67.69	0.11	99.89	2384.46
ECL	70.74	3.16	96.84	4422.84
ECL 0.2 M Lac	86.63	95.60	4.40	43.03
ECL 0.2 M Glu	67.69	1.24	98.76	2756.93
Unstained	90.11	99.98	0.02	8.17
GNL	81.98	0.16	99.84	2200.79
GNL 0.2 M α -Methylmannoside	89.57	4.01	95.99	428.47
GNL 0.2 M Gal	78.31	0.38	99.62	1895.86
Unstained	90.97	99.99	0.01	4.36
Jacalin	76.98	0.68	99.32	4895.73
Jacalin 0.8 M Gal	90.93	79.79	20.21	870.32
Jacalin 0.8 M Glc	82.24	9.93	90.07	2277.46

Table G.3: Flow cytometry data for suspension CHO DP-12 cells probed with LCA, LecB, MAL II, NPL, RCA I, and WGA corresponding to Fig. 5.18 to Fig. 5.23

20,000 events recorded for each sample

Sample	Cells in Live Gate (%)	Negative (%)	Positive (%)	MFI
Unstained	88.25	99.98	0.02	4.83
LCA	76.89	6.74	93.26	3777.54
LCA 0.2 M α -Methylmannoside/ α -Methylglucoside	95.58	84.49	15.51	1390.58
LCA 0.2 M Glc	92.04	58.10	41.89	2703.62
Unstained	91.78	100.00	0.00	3.23
LecB	90.00	0.40	99.60	305.78
LecB 0.2 M Fuc	87.35	0.38	99.62	43.02
LecB 0.2 M Gal	84.57	0.34	99.66	303.18
Unstained	83.83	99.99	0.01	7.92
MAL II	79.22	1.43	98.57	1165.61
MAL I 0.2 M GlcNAc	76.87	8.66	91.34	1063.74
Unstained	90.97	99.99	0.01	4.36
NPL	80.42	0.01	99.99	3053.72
NPL 0.4 M α -Methylmannoside	92.44	7.55	92.45	194.47
NPL 0.4 M Glc	84.53	0.01	99.99	3818.80
RCA I	66.64	0.06	99.94	6374.08
RCA I 0.2 M Gal	82.22	32.83	67.15	1706.15
RCA I 0.2 M Glc	83.48	0.04	99.96	3474.61
Unstained	83.83	99.99	0.01	7.92
WGA	66.75	0.06	99.94	4647.64
WGA 0.4 M GlcNAc	78.46	66.72	33.28	468.28
WGA 0.4 M GalNAc	62.68	6.49	93.51	3125.72

Appendix H

Flow cytometry data for spent medium treated cells

Table H.1: Flow cytometry data for suspension CHO DP-12 cells untreated (24 h) and probed with lectin panel, corresponding to Table 5.3 and Fig. 5.24 to Fig. 5.31

10,000 events recorded for each sample in triplicate, average tabulated

Lectin	Cells in Live Gate (%)	Negative (%)	Positive (%)	MFI
Unstained	88.99	99.99	0.01	6.81
AAL	80.07	0.61	99.39	1498.92
AAL-2	91.84	0.00	100.00	2016.01
DSL	89.19	0.06	99.94	1668.68
ECL	72.34	19.88	80.12	2480.32
GafD1-178	89.67	99.51	0.49	16.61
GNL	81.11	0.08	99.92	1641.82
GSL I B4	89.82	99.27	0.73	37.04
GSL II	88.64	99.47	0.53	11.99
HPA	89.33	94.07	5.93	41.50
Jacalin	77.52	0.73	99.27	3129.16
LCA	76.94	5.81	94.19	2706.31
LecA5K	87.41	6.93	93.07	366.04
LecB	88.79	0.61	99.39	314.01
MAL II	88.27	0.05	99.95	1211.61
NPL	79.37	0.07	99.93	2623.15
PNA	87.12	89.65	10.23	283.40
RCA I	76.61	0.08	99.92	3515.66
SBA	91.29	90.89	8.72	93.08
SNA	90.39	96.90	3.08	19.84
WGA	65.39	0.07	99.93	6315.45

Table H.2: Flow cytometry data for suspension CHO DP-12 cells spent medium treated (24 h) and probed with lectin panel, corresponding to Table 5.3 and Fig. 5.24 to Fig. 5.31

10,000 events recorded for each sample in triplicate, average tabulated

Lectin	Cells in Live Gate (%)	Negative (%)	Positive (%)	MFI
Unstained	86.74	99.99	0.01	6.05
AAL	72.39	1.82	98.18	1095.44
AAL-2	76.77	0.02	99.98	1402.25
DSL	72.70	0.09	99.91	1331.32
ECL	60.16	20.52	79.47	1912.61
GafD1-178	83.56	99.84	0.16	15.54
GNL	67.82	0.08	99.92	1487.19
GSL I B4	81.71	92.61	7.39	138.33
GSL II	76.95	92.55	7.45	36.17
HPA	78.65	53.85	46.15	138.76
Jacalin	68.97	5.71	94.29	2208.09
LCA	67.39	14.02	85.98	1851.73
LecA5K	73.90	1.32	98.68	1204.50
LecB	82.54	0.81	99.19	269.20
MAL II	80.80	0.21	99.79	681.03
NPL	54.10	0.15	99.85	2822.64
PNA	72.95	25.68	73.92	2498.44
RCA I	64.79	0.57	99.43	2817.95
SBA	78.80	63.70	36.28	793.48
SNA	84.28	97.61	2.39	22.55
WGA	54.89	0.15	99.85	4565.84

Table H.3: Flow cytometry data for suspension CHO DP-12 cells spent medium treated (T) and untreated (U) for 24 h followed by 72 h fresh medium and probed with lectin panel, corresponding to Table 5.3 and Fig. 5.24 to Fig. 5.31

10,000 events recorded for each sample in triplicate, average tabulated

Lectin	Cells in Live Gate (%)	Negative (%)	Positive (%)	MFI
Unstained (U)	88.09	100.00	0.00	3.99
AAL (U)	76.77	0.22	99.78	1525.26
AAL-2 (U)	84.64	0.08	99.92	2040.63
DSL (U)	80.52	0.15	99.85	2001.95
ECL (U)	66.84	13.01	86.99	3315.81
GSL I B4 (U)	91.72	97.67	2.33	48.42
HPA (U)	91.38	97.26	2.74	23.86
Jacalin (U)	47.61	3.20	96.80	6905.70
LCA (U)	78.47	35.88	64.11	1748.40
LecA5K (U)	85.57	4.13	95.87	537.78
MAL II (U)	85.69	0.07	99.93	1284.44
PNA (U)	90.77	93.68	6.23	185.97
RCA I (U)	60.20	0.25	99.75	6432.83
SBA (U)	90.29	85.93	14.07	277.81
WGA (U)	66.93	0.13	99.87	6944.84
Unstained (T)	87.91	100.00	0.00	3.66
AAL (T)	80.01	0.29	99.71	1042.34
AAL-2 (T)	83.40	0.03	99.97	1569.21
DSL (T)	80.11	0.02	99.98	1765.73
ECL (T)	69.57	10.09	89.91	2652.74
GSL I B4 (T)	84.55	97.84	2.16	54.77
HPA (T)	84.96	98.21	1.79	22.33
Jacalin (T)	54.83	2.78	97.22	4640.08
LCA (T)	69.40	38.29	61.71	1186.68
LecA5K (T)	72.93	2.03	97.97	711.17
MAL II (T)	75.38	0.08	99.92	1060.89
PNA (T)	79.54	91.90	8.03	223.61
RCA I (T)	56.85	0.14	99.86	5589.53
SBA (T)	81.14	87.83	12.17	229.27
WGA (T)	45.93	0.17	99.83	6162.94

Appendix I

Flow cytometry data for cells treated with L-glut free medium

Table I.1: Flow cytometry data for suspension CHO DP-12 cells untreated (48 h) and probed with lectin panel, corresponding to Table 5.4 and Fig. 5.32 to Fig. 5.39

10,000 events recorded for each sample in triplicate, average tabulated

Lectin	Cells in Live Gate (%)	Negative (%)	Positive (%)	MFI
Unstained	92.91	99.99	0.01	4.50
AAL	88.28	0.11	99.89	899.48
AAL-2	67.59	0.09	99.91	1939.73
DSL	89.46	0.05	99.95	1334.09
ECL	72.82	17.15	82.85	3926.23
GafD1-178	66.14	87.31	12.69	23.91
GNL	87.31	0.06	99.94	1432.46
GSL I B4	93.71	75.51	24.49	223.96
HPA	94.07	46.68	53.32	243.35
Jacalin	62.99	5.65	94.35	5209.20
LCA	75.86	16.70	83.30	4335.50
LecA5K	60.19	5.42	94.58	1279.07
LecB	73.09	22.64	77.36	540.76
MAL II	86.94	0.19	99.81	1104.36
NPL	90.04	0.17	99.83	811.28
PNA	92.74	60.30	39.57	944.25
RCA I	58.98	0.37	99.63	4915.97
SBA	93.62	61.87	38.13	854.50
WGA	56.11	1.03	98.97	5541.35

Table I.2: Flow cytometry data for suspension CHO DP-12 cells treated (0 mM L-glut 48 h) and probed with lectin panel, corresponding to Table 5.4 and Fig. 5.32 to Fig. 5.39

10,000 events recorded for each sample in triplicate, average tabulated

Lectin	Cells in Live Gate (%)	Negative (%)	Positive (%)	MFI
Unstained	92.90	99.98	0.02	6.53
AAL	87.81	0.14	99.86	937.45
AAL-2	77.10	0.10	99.90	2324.82
DSL	91.59	0.02	99.98	1475.33
ECL	63.99	9.28	90.72	3995.16
GafD1-178	64.70	90.37	9.63	25.55
GNL	83.55	0.04	99.96	1707.87
GSL I B4	93.65	46.82	53.17	681.36
HPA	91.38	34.01	65.99	346.92
Jacalin	62.06	11.74	88.26	4075.47
LCA	66.49	12.62	87.37	4212.26
LecA5K	46.21	0.64	99.36	3712.31
LecB	75.29	5.35	94.65	649.80
MAL II	79.12	0.24	99.76	1077.16
NPL	81.72	0.15	99.85	1002.86
PNA	92.01	34.22	65.77	2375.86
RCA I	60.09	0.47	99.53	5052.18
SBA	92.14	57.30	42.63	813.35
WGA	55.78	0.97	99.03	5445.93

Table I.3: Flow cytometry data for suspension CHO DP-12 cells untreated (48 h + 72 h) and probed with lectin panel, corresponding to Table 5.4 and Fig. 5.32 to Fig. 5.39

10,000 events recorded for each sample in triplicate, average tabulated

Lectin	Cells in Live Gate (%)	Negative (%)	Positive (%)	MFI
Unstained	88.56	99.97	0.03	5.56
AAL	84.60	0.54	99.46	1221.45
AAL-2	84.76	0.05	99.95	2058.33
DSL	86.88	0.12	99.88	1624.07
ECL	71.24	13.78	86.20	3193.44
GafD1-178	89.23	97.19	2.80	21.23
GNL	86.76	0.07	99.93	1373.28
GSL I B4	90.51	93.68	6.31	91.80
HPA	90.16	94.25	5.75	24.90
Jacalin	74.81	0.99	99.01	3952.75
LCA	71.92	0.65	99.35	3225.37
LecA5K	87.58	12.67	87.32	287.95
LecB	89.87	14.11	85.88	129.78
MAL II	88.69	0.04	99.96	1075.88
NPL	80.96	0.02	99.98	3376.25
PNA	90.88	87.52	12.45	142.43
RCA I	70.54	0.04	99.96	4472.31
SBA	90.47	74.18	25.79	772.63
WGA	63.57	0.06	99.94	6095.27

Table I.4: Flow cytometry data for suspension CHO DP-12 cells treated (0 mM L-glut 48 h + 4 mM L-glut 72 h) and probed with lectin panel, corresponding to Table 5.4 and Fig. 5.32 to Fig. 5.39

10,000 events recorded for each sample in triplicate, average tabulated

Lectin	Cells in Live Gate (%)	Negative (%)	Positive (%)	MFI
Unstained	90.45	99.97	0.03	4.54
AAL	80.70	0.34	99.66	1042.88
AAL-2	87.10	0.02	99.98	1567.19
DSL	75.70	0.04	99.96	1284.02
ECL	71.16	9.28	90.71	2130.32
GafD1-178	88.13	98.96	1.04	23.03
GNL	81.36	0.05	99.95	1221.94
GSL I B4	90.30	97.17	2.83	40.97
HPA	87.95	95.97	4.03	23.21
Jacalin	70.49	0.52	99.48	2373.98
LCA	72.58	0.72	99.28	2550.14
LecA5K	87.46	8.27	91.73	363.09
LecB	87.70	15.30	84.70	135.87
MAL II	83.50	0.07	99.93	963.32
NPL	70.28	0.05	99.95	2890.63
PNA	89.07	92.21	7.76	206.01
RCA I	70.91	0.02	99.98	3716.28
SBA	86.50	86.35	13.63	713.75
WGA	54.48	0.03	99.97	6651.32

Appendix J

Flow cytometry data for cells treated with 10 mM NH₄Cl

Table J.1: Flow cytometry data for suspension CHO DP-12 cells untreated (48 h) and probed with lectin panel, corresponding to Table 5.5 and Fig. 5.40 to Fig. 5.45

10,000 events recorded for each sample in triplicate, average tabulated

Lectin	Cells in Live Gate (%)	Negative (%)	Positive (%)	MFI
Unstained	84.21	99.99	0.01	4.53
AAL	83.92	0.19	99.80	971.14
AAL-2	62.89	0.07	99.93	1174.58
DSL	85.65	0.12	99.88	1176.74
ECL	69.16	12.06	87.93	1652.74
GafD1-178	78.49	78.07	21.87	59.47
GNL	80.19	2.39	97.60	1453.59
GSL I B4	86.93	80.92	19.03	153.58
HPA	86.93	51.03	48.95	147.76
Jacalin	63.17	2.46	97.53	2878.45
LCA	56.43	14.56	85.44	3855.91
LecA5K	49.24	8.73	91.26	1569.28
LecB	56.20	18.99	81.01	544.78
MAL II	75.69	0.43	99.57	1075.82
NPL	64.12	17.56	82.43	2628.84
PNA	88.33	68.31	31.55	894.83
RCA I	51.56	3.37	96.62	4231.91
SBA	91.12	53.83	46.17	778.10
WGA	47.42	0.56	99.44	4069.84

Table J.2: Flow cytometry data for suspension CHO DP-12 cells treated (10 mM NH₄Cl 48 h) and probed with lectin panel, corresponding to Table 5.5 and Fig. 5.40 to Fig. 5.45

10,000 events recorded for each sample in triplicate, average tabulated

Lectin	Cells in Live Gate (%)	Negative (%)	Positive (%)	MFI
Unstained	83.37	99.99	0.01	3.64
AAL	75.12	0.32	99.68	982.48
AAL-2	68.65	0.11	99.89	1218.81
DSL	41.39	0.39	99.61	852.87
ECL	67.03	6.01	93.99	1765.79
GafD1-178	70.76	76.02	23.98	65.82
GNL	72.63	0.11	99.89	1510.30
GSL I B4	82.91	73.37	26.57	172.99
HPA	78.06	54.74	45.24	136.90
Jacalin	54.06	1.70	98.30	3141.76
LCA	60.39	16.56	83.44	3325.15
LecA5K	56.90	9.39	90.61	1352.45
LecB	39.35	12.58	87.42	687.47
MAL II	72.58	2.31	97.69	944.19
NPL	49.29	0.11	99.89	3652.55
PNA	80.71	46.66	53.24	1436.73
RCA I	48.15	0.86	99.14	3651.48
SBA	78.87	46.24	53.75	864.15
WGA	38.87	0.81	99.19	3827.96

Table J.3: Flow cytometry data for suspension CHO DP-12 cells untreated (48 h + 72 h) and probed with lectin panel, corresponding to Table 5.5 and Fig. 5.40 to Fig. 5.45

10,000 events recorded for each sample in triplicate, average tabulated

Lectin	Cells in Live Gate (%)	Negative (%)	Positive (%)	MFI
Unstained	89.85	100.00	0.00	4.89
AAL	83.02	0.15	99.85	1488.98
AAL-2	88.10	0.05	99.95	2259.13
DSL	87.31	0.01	99.99	2086.56
ECL	85.67	2.34	97.66	1823.65
GafD1-178	92.69	98.50	1.50	16.95
GNL	84.25	0.07	99.93	2196.09
GSL I B4	92.77	89.12	10.81	162.89
HPA	92.76	88.91	11.09	40.98
Jacalin	65.20	1.89	98.11	5302.18
LCA	70.64	24.47	75.52	3215.87
LecA5K	71.17	1.40	98.60	1054.54
LecB	87.97	28.97	71.03	124.41
MAL II	88.46	0.06	99.94	1154.93
NPL	74.15	0.02	99.98	4281.84
PNA	90.90	77.88	21.55	474.78
RCA I	66.56	0.08	99.92	5270.78
SBA	91.93	89.50	10.48	94.71
WGA	64.86	0.03	99.97	7540.77

Table J.4: Flow cytometry data for suspension CHO DP-12 cells treated (10 mM NH₄Cl 48 h + 0 mM NH₄Cl 72 h) and probed with lectin panel, corresponding to Table 5.5 and Fig. 5.40 to Fig. 5.45

10,000 events recorded for each sample in triplicate, average tabulated

Lectin	Cells in Live Gate (%)	Negative (%)	Positive (%)	MFI
Unstained	92.40	99.87	0.13	4.98
AAL	78.45	0.11	99.89	1083.05
AAL-2	85.13	0.04	99.96	1597.31
DSL	84.94	0.04	99.96	1606.24
ECL	73.58	1.30	98.70	1039.05
GafD1-178	88.71	99.27	0.73	14.50
GNL	75.62	0.10	99.90	1818.02
GSL I B4	86.23	95.33	4.67	84.31
HPA	88.18	95.39	4.61	31.31
Jacalin	58.04	4.78	95.21	3283.84
LCA	76.85	23.47	76.52	1822.89
LecA5K	67.60	0.38	99.62	983.10
LecB	85.87	39.47	60.53	108.22
MAL II	83.18	0.13	99.87	1009.43
NPL	66.92	0.06	99.94	3595.03
PNA	86.66	82.47	17.52	347.25
RCA I	65.49	0.11	99.89	4352.19
SBA	86.43	88.68	11.31	99.58
WGA	59.01	0.05	99.95	6964.80

Appendix K

Flow cytometry data for cells treated with 3 mM NaBu

Table K.1: Flow cytometry data for suspension CHO DP-12 cells untreated (96 h) and probed with lectin panel, corresponding to Table 5.6 and Fig. 5.46 to Fig. 5.53

10,000 events recorded for each sample in triplicate, average tabulated

Lectin	Cells in Live Gate (%)	Negative (%)	Positive (%)	MFI
Unstained	94.14	99.98	0.02	5.19
AAL	77.69	2.41	97.59	3131.88
AAL-2	94.82	0.05	99.95	1356.71
DSL	93.94	0.52	99.48	1144.29
ECL	86.58	7.71	92.29	2040.09
GafD1-178	94.41	99.54	0.46	9.12
GNL	93.75	0.35	99.65	1077.88
GSL I B4	94.67	93.87	6.13	78.84
HPA	94.57	96.32	3.68	26.94
Jacalin	86.86	1.42	98.58	2783.16
LCA	91.14	31.94	68.06	1998.20
LecA5K	80.42	11.02	88.98	776.57
LecB	94.52	57.96	42.04	92.20
MAL II	93.86	0.08	99.92	1278.37
NPL	88.30	0.08	99.92	2314.31
PNA	95.19	64.91	35.09	825.11
RCA I	68.70	0.25	99.75	5672.72
SBA	95.15	75.27	24.73	406.31
WGA	75.31	0.68	99.32	6222.89

Table K.2: Flow cytometry data for suspension CHO DP-12 cells treated (3 mM NaBu 96 h) and probed with lectin panel, corresponding to Table 5.6 and Fig. 5.46 to Fig. 5.53

10,000 events recorded for each sample in triplicate, average tabulated

Lectin	Cells in Live Gate (%)	Negative (%)	Positive (%)	MFI
Unstained	70.57	99.18	0.82	5.67
AAL	56.73	6.78	93.22	2557.01
AAL-2	69.12	0.08	99.92	1584.28
DSL	69.44	0.27	99.73	1306.32
ECL	59.87	3.35	96.65	2215.62
GafD1-178	70.09	97.10	2.90	30.80
GNL	71.48	0.30	99.70	1732.37
GSL I B4	67.42	91.12	8.88	182.25
HPA	71.27	81.45	18.55	60.03
Jacalin	57.46	1.55	98.45	3294.86
LCA	60.21	39.25	60.75	1723.68
LecA5K	76.98	9.29	90.71	1689.40
LecB	64.81	14.50	85.50	173.92
MAL II	59.10	0.38	99.62	1099.95
NPL	55.68	0.37	99.63	2665.22
PNA	64.46	78.82	21.16	584.40
RCA I	43.67	1.12	98.88	4165.80
SBA	63.84	70.30	29.66	391.35
WGA	45.74	1.52	98.48	4431.51

Table K.3: Flow cytometry data for suspension CHO DP-12 cells untreated (96 h + 96 h) and probed with lectin panel, corresponding to Table 5.6 and Fig. 5.46 to Fig. 5.53

10,000 events recorded for each sample in triplicate, average tabulated

Lectin	Cells in Live Gate (%)	Negative (%)	Positive (%)	MFI
Unstained	92.61	99.95	0.05	5.87
AAL	77.02	1.18	98.82	4867.63
AAL-2	77.40	0.08	99.92	4073.29
DSL	92.55	0.02	99.98	1442.62
ECL	77.65	11.84	88.16	4276.34
GafD1-178	92.75	98.34	1.66	21.72
GNL	91.80	0.04	99.96	1126.17
GSL I B4	91.78	91.00	9.00	142.78
HPA	94.26	89.68	10.32	47.26
Jacalin	75.33	4.45	95.55	6215.14
LCA	86.92	27.24	72.74	3233.45
LecA5K	73.39	7.85	92.15	1387.84
LecB	66.88	19.32	80.68	612.85
MAL II	90.73	0.05	99.95	1628.38
NPL	83.02	0.02	99.98	2918.00
PNA	92.60	30.96	68.98	3137.64
RCA I	71.03	0.12	99.88	6008.24
SBA	90.87	60.08	39.78	755.38
WGA	68.53	0.11	99.89	7087.36

Table K.4: Flow cytometry data for suspension CHO DP-12 cells treated (3 mM NaBu 96 h + 0 mM NaBu 96 h) and probed with lectin panel, corresponding to Table 5.6 and Fig. 5.46 to Fig. 5.53

10,000 events recorded for each sample in triplicate, average tabulated

Lectin	Cells in Live Gate (%)	Negative (%)	Positive (%)	MFI
Unstained	69.81	98.82	1.18	6.28
AAL	53.03	1.65	98.35	4089.80
AAL-2	12.09	1.04	98.96	3837.45
DSL	68.22	0.06	99.94	1653.26
ECL	43.56	6.75	93.25	4089.01
GafD1-178	67.87	96.41	3.59	36.96
GNL	67.83	0.34	99.66	1675.22
GSL I B4	68.30	92.65	7.34	244.52
HPA	66.92	65.76	34.24	81.94
Jacalin	49.43	7.32	92.68	4306.35
LCA	54.01	21.09	78.91	3384.43
LecA5K	76.57	1.95	98.05	2645.99
LecB	53.70	11.98	88.02	602.45
MAL II	65.35	0.10	99.90	1695.14
NPL	60.84	0.19	99.81	2982.09
PNA	66.58	38.36	61.54	2490.57
RCA I	49.18	0.35	99.65	5113.35
SBA	68.53	88.87	11.12	545.75
WGA	48.71	0.32	99.68	5867.90

Table K.5: Comparison of MFI from lectin binding suspension adapted CHO DP-12 cells fed 4 and 9 days previously and probed with lectin panel

Lectin	4 day	9 day	% MFI change
Unstained	5.07	5.89	16.17
AAL	1003.55	963.30	-4.01
AAL-2	1935.46	1813.57	-6.30
GNL	971.73	1088.41	12.01
Jacalin	3471.66	3205.31	-7.67
LCA	2106.44	1853.18	-12.02
LecA5K	657.04	567.03	-13.70
MAL II	832.14	740.12	-11.06
PNA	265.21	302.03	13.88
RCA	4452.28	4200.31	-5.66
WGA	5836.50	5222.24	-10.52